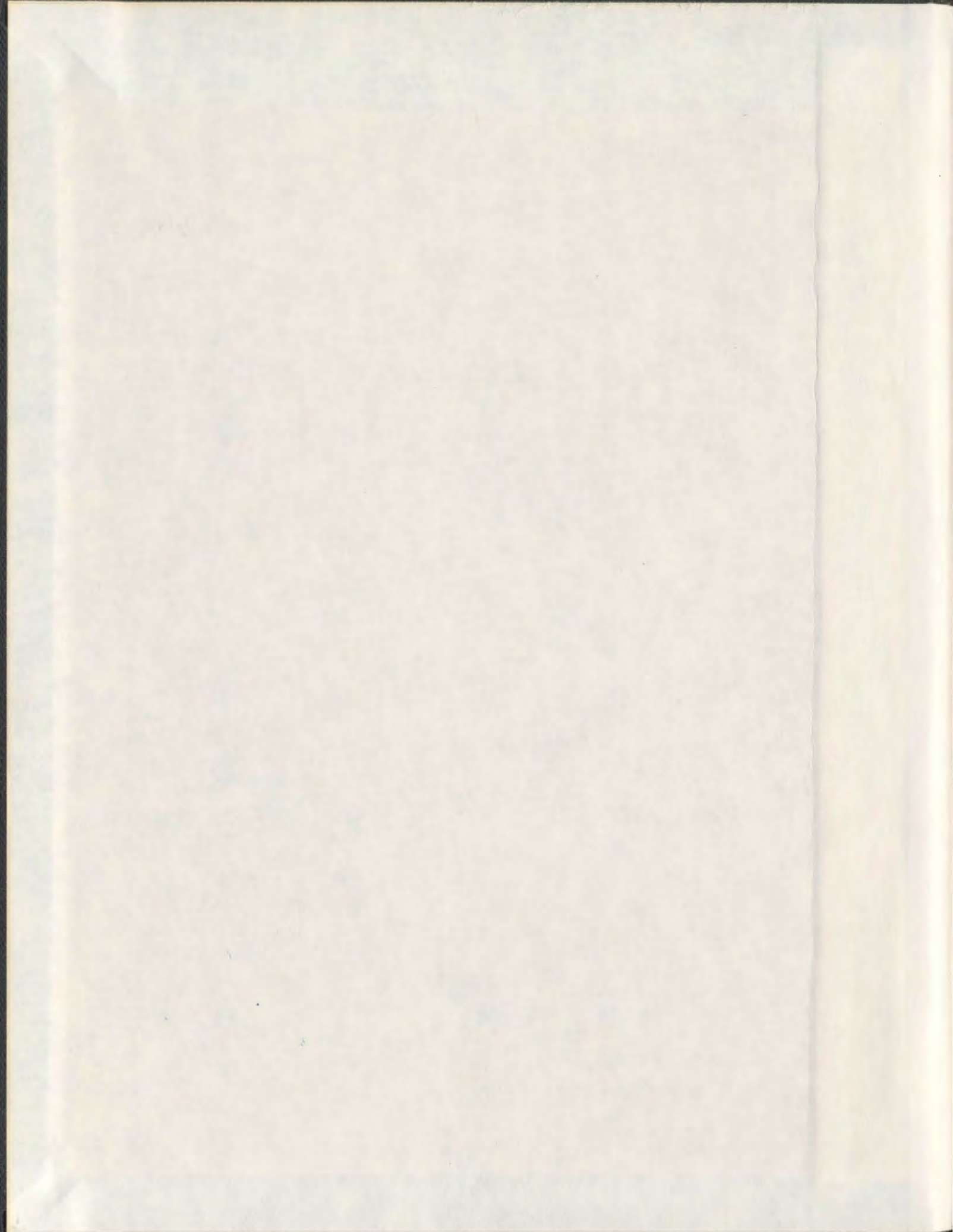


**SYNTHESIS, CHARACTERIZATION AND REACTIVITY
OF AMINE-PHENOLATE COMPLEXES TOWARDS
THE PREPARATION OF ALIPHATIC POLYESTERS**

NDUKA IKPO



Synthesis, Characterization and Reactivity of Amine-phenolate Complexes

Towards the Preparation of Aliphatic Polyesters

by

© Nduka Ikpo

A Thesis submitted to the School of Graduate Studies
in partial fulfillment of the requirements for the degree of

Doctor of Philosophy

Department of Chemistry

Memorial University of Newfoundland

December 2012

St. John's Newfoundland

ABSTRACT

Biodegradable polymers such as poly(ϵ -caprolactone) (PCL), polylactide (PLA) and polycarbonate (PC) are important materials in commodity, biomedical and pharmaceutical applications. This is due to their biodegradable, biocompatible and permeable properties, and the fact that the monomers can be sourced from annually renewable feedstocks. One of the most important methods in producing these polymers is ring-opening polymerization (ROP) initiated by metal complexes.

Many metal complexes are effective initiators for the ROP of small ring monomers; however, some undergo side reactions during polymerization that lead to low molecular weight polymers and decrease the level of control in polymer formation. Ligand design and catalyst design using main group and early transition metals have played a vital role in the development of this area. In view of this, Li, Zn, Al, Ti, and Zr complexes bearing various N-, and O-mixed donor monoanionic piperazinyl- and morpholinyl-based phenolate ligands were synthesized in this project. The complexes were fully characterized by elemental analysis, NMR spectroscopy, and X-ray crystallography. In addition, using Brookhart's acid, cationic zinc complex was synthesized and characterized using ^1H , ^{13}C , ^{19}F and ^{11}B NMR spectroscopy.

The ROP reactions of *rac*-LA and ϵ -CL using Zn alkyl and alkoxide complexes were performed. Data showed that polymerization occurred immediately using the alkoxide complexes; however, for the alkyl complexes, polymerization was possible only in the presence of alcohol. In addition, microwave irradiation (MW) was found to reduce reaction time significantly while maintaining control of the polymerization reaction.

Furthermore, the Al and Li complexes are active for the ROP of ϵ -CL in the presence of benzyl alcohol (BnOH), while the Li complexes are also active in the absence of BnOH. Polymerization kinetics were monitored by observing the degree of conversion of ϵ -CL to PCL by ^1H NMR spectroscopy. The observed rates and activation energies are related to the steric effects and the outersphere substituents of the complexes. The polymers were analyzed by GPC, MALDI-TOF MS, DSC and TGA. Preliminary investigations into the copolymerization of epoxides with CO_2 using Zn and Al complexes were promising; however, further experiments are required to optimize the reaction method.

ACKNOWLEDGEMENTS

First, I offer my sincere gratitude to my supervisor, Dr. Francesca Kerton for giving me the opportunity to join her research group and for her valuable guidance, suggestions, expertise, continuous encouragement and support throughout the course of this study. I would also thank Dr. Francesca Kerton for the useful comments and revisions during the writing of this thesis, which made it possible for me to complete this thesis. My special thanks to Dr. Chris Kozak for his useful suggestions and support in the lab and group meetings. I would want to use this opportunity to express my profound gratitude to my supervisory committee members: Dr. Chris Kozak, Dr. Dave Thompson and Dr. Louise Dawe for their useful discussion and suggestions throughout the period of my studies.

My thanks also go to all the MUN Chemistry Department staff, especially Brian Power and the Mech Shop people for always helping to fix our numerous problems with glassware and machines and equipment. My gratitude to people in Chemistry main office, especially Viola Martin (late), Mary Flinn, Rosalind Collins and Ebony Penney. A special thanks to Dr. Louise Dawe for solving all the crystal structures contained in this thesis. I would also extend my thanks to C-CART (Centre for Chemical Analysis, Research and Training): Dr. Celine Schneider, Dr. Brent Myron, Julie Collins and Linda Windsor for their knowledge and advice with instrumentation (NMR, DSC, TGA and MALDI-TOF MS).

I would like to thank all the present and past members of Green Chemistry and Catalysis group, especially the undergraduates and Christian Hoffmann whose help contributed to the successful completion of my study. I also thank Justin, Rebecca,

Hassan and Khalid for many helpful discussions and encouragement. Special thanks to Dr. Pawel Horeglad (University of Warsaw) for advice on tacticity calculations. I especially thank Katalin for always having a willing ear and a word of encouragement. Thanks to Jenna and Samantha for proof-reading parts of my thesis. My gratitude goes to the Bauers family (Larry, Shelly, Katie and Sam) for their hospitality and support

I would also like to thank NSERC (Dr. Kerton's Discovery Grant), Department of Chemistry, School of Graduate Studies (SGS), Graduate Students' Union (GSU) and Memorial University for funding. My regards and gratitude go to those who supported me in any respect during the course of this study.

I offer my profound and earnest gratitude to my mother, siblings and my parents' in-law for their understanding, patience, support and encouragement during the period of this research work and special thanks to my friend Nkeiru for her encouragement. I thank my God through whom all things are possible and without whose mercy I don't believe I would be at this point in my life.

Lastly, my sincere and profound gratitude go to my wife Amaka. She has borne the brunt of my stress and shared the highs and lows that came across throughout the period of this study. No amount of gift or word can express my heartfelt appreciation for the patience, word of prayers, and encouragement she has shown to me. She has been my source of inspiration. Amaka, you are the best.

Dedicated to

Amarachi and Chigozirim Ikpo

Table of Contents

Abstract	ii
Acknowledgements	iv
Table of Contents	vii
List of Tables	xv
List of Figures	xviii
List of Schemes	xxiv
List of Abbreviations	xxvi
List of Appendices	xxxii
Chapter 1. Literature Review.....	1-94
1.1 Introduction	1
1.2 Biodegradable Polymers	3
1.3 History/Background of Biodegradable Polyester Development	4
1.4 General Synthesis of Biodegradable Polyesters	5
1.4.1 Polycondensation (Step-Growth) Polymerization	6
1.4.2 Ring-Opening Polymerization (Chain-Growth Mechanism)	7
1.4.3 Ring-opening Polymerization Mechanism	8
1.5 Microwave Assisted Ring-Opening Polymerization	14
1.6 Polylactides (PLAs).....	15

1.6.1	PLA Microstructures (Stereochemistry)	17
1.6.2	Mechanisms for the Synthesis of Stereocontrolled PLAs.....	19
1.6.3	Determination of PLA Tacticity	20
1.7	Poly(ϵ -caprolactone) (PCL)	23
1.8	Kinetics of Ring-Opening Polymerization	25
1.8.1	Nuclear Magnetic Resonance Spectroscopy for Kinetic Studies.....	26
1.8.2	Activation Energy (E_a) Determination.....	28
1.8.3	Enthalpy (ΔH^\ddagger) and Entropy (ΔS^\ddagger) of Activation	28
1.9	Single Site Metal Initiators for ROP of Cyclic Esters.....	29
1.9.1	Chemistry of Li, Zn and Al.....	30
1.9.2	Single-Site Initiators Supported by N-,N-Donor Ligands	31
1.9.3	Single-Site Initiators Supported by N-,O-donor ligands.....	34
1.9.4	Single-Site Initiators Supported by Monanionic N-,O-Donor Ligands	38
1.9.5	Lithium Complexes Used for the ROP of Cyclic Esters.....	42
1.9.6	Al, Zn, and Li Amine-Phenolate Complexes Used for ROP of ϵ -CL.....	45
1.10	Reactions Using Carbon Dioxide as a Feedstock	55
1.11	Synthesis of Polycarbonate and/or Cyclic Carbonates <i>via</i> Reaction of CO ₂ and Epoxides	56
1.12	Catalysts for Copolymerization and Coupling of Epoxides and CO ₂	62

1.12.1	Aluminum Catalysts for Copolymerization Reactions of Epoxides and CO ₂ .	62
1.12.2	Zinc Catalysts for Copolymerization of Epoxides and CO ₂	66
1.12.3	Aluminum and Zinc Catalysts for Coupling of Epoxides and CO ₂	75
1.13	Titanium and Zirconium Amine-Phenolate Complexes	82
1.14	Objectives and Outline of the Thesis.....	83
1.15	References.....	85
1.16	Co-Authorship Statement	95
Chapter 2. Synthesis and Characterization of Amine-phenol Ligands		99-119
2.1	Introduction	100
2.2	Results and Discussion.....	102
2.2.1	Morpholinyl Phenol Ligands	105
2.2.2	2,6-Dimethyl Morpholinyl Phenol Ligands	107
2.2.3	Homopiperazinyl Bis(phenol) Lgand	108
2.3	Conclusions	109
2.4	Experimental Section	110
2.4.1	General Procedures	110
2.4.2	Single Crystal X-ray Diffraction Studies	111
2.4.3	Synthetic procedures	112

2.5	References	118
Chapter 3. Zinc Complexes of Piperazinyl-Amine Phenolate Ligands: Synthesis, Characterization and Ring-Opening Activity		
120-174		
3.1	Introduction	121
3.2	Results and Discussion.....	123
3.3	Synthesis and Characterization of Zinc Aminephenolate Complexes	125
3.4	X-ray Crystallographic Analysis of Zinc Complexes	129
3.5	Polymerization of Cyclic Esters	137
3.5.1	Ring-Opening Polymerization of <i>rac</i> -Lactide	137
3.5.2	Ring-Opening Polymerization of ϵ -Caprolactone.....	148
3.6	Reactivity of Complexes towards CO ₂ and Cyclohexene Oxide Coupling	150
3.7	Conclusions	153
3.8	Experimental Section	154
3.8.1	General Considerations	154
3.8.2	Crystallographic Procedures	155
3.8.3	Synthetic Procedures.....	159
3.8.4	Polymerization Procedures	167
3.9	References	170

Chapter 4. Aluminum Methyl and Chloro Complexes bearing Monoanionic Amine-Phenolate Ligands: Synthesis, Characterization and Use in Polymerization ..175-231

4.1	Introduction	176
4.2	Results and Discussion	179
4.2.1	Synthesis and solid-state structures	179
4.3	Ring-Opening Polymerization of ϵ -Caprolactone	187
4.4	End-group Analysis	193
4.4.1	NMR Spectroscopy	193
4.4.2	MALDI-TOF Mass Spectrometry	195
4.5	Kinetic Studies of ϵ -CL Polymerization	198
4.6	Thermal Properties Studies	207
4.6.1	Thermalgravimetric Analysis (TGA)	207
4.6.2	Differential Scanning Calorimetry (DSC)	208
4.7	Copolymerization of Carbon Dioxide and Epoxides using Compounds 4.4 and 4.5	210
4.8	Conclusions	214
4.9	Experimental Section	215
4.9.1	General Considerations	215
4.9.2	Single Crystal X-ray Diffraction Studies	217

4.9.3	Synthetic Procedures.....	220
4.10	Polymerization Procedures	223
4.10.1	Typical ROP of ϵ -CL Procedure.....	223
4.10.2	Representative Copolymerization Procedure.....	224
4.11	References.....	225
Chapter 5. Ring-Opening Polymerization of ϵ-Caprolactone by Lithium Piperazinyl-Amine Phenolate Complexes: Synthesis, Characterization and Kinetic Studies.....		
.....		232-264
5.1	Introduction	233
5.2	Results and Discussion.....	235
5.2.1	Synthesis and Solid-State Structures	235
5.3	Polymerization Studies.....	239
5.3.1	Ring-Opening Polymerization of ϵ -Caprolactone.....	239
5.3.2	Kinetic Studies of ϵ -Caprolactone Polymerization.....	243
5.3.3	NMR Spectroscopy Analysis of Polycaprolactone.....	249
5.3.4	MALDI-TOF MS Analysis.....	251
5.4	Conclusions	254
5.5	Experimental Section	255
5.5.1	General Considerations.....	255

5.5.2	Single Crystal X-ray Diffraction Studies	256
5.5.3	Synthetic procedures	258
5.5.4	Polymerization Procedure	260
5.6	References	261
Chapter 6. Synthesis and Structure of Lithium, Titanium, Zirconium and Zinc Amine-Phenolate Complexes		265-291
6.1	Introduction	266
6.2	Results and Discussion	267
6.2.1	Synthesis of amine-phenolate titanium alkoxide	267
6.2.2	Synthesis of Amine-Phenolate Zirconium Amide Complex	270
6.2.3	Synthesis of Amine-Bis(phenolate) Titanium Complex	271
6.2.4	Synthesis of Amine-Bis(phenolate) Lithium Complex	274
6.2.5	Synthesis of Cationic Zinc Complex	278
6.3	Conclusion	280
6.4	Experimental Section	281
6.4.1	General Considerations	281
6.4.2	X-ray Crystallographic Studies	282
6.4.3	Synthetic Procedures	284
6.5	References	289

Chapter 7. Conclusion	291-295
7.1 Summary	292
Apendices.....	296

List of Tables

Table 1.1. <i>rac</i> -LA tetrad probabilities based on Bernoullian statistics.....	22
Table 1.2. Comparison of the activity of various metal complexes used for catalytic ROP of LA	51
Table 1.3. Comparison of the activity of various metal complexes used for catalytic ROP of ϵ -CL	54
Table 1.4. Comparison of the activity of various metal catalysts for copolymerization of CO ₂ and epoxides.....	73
Table 1.5. Comparison of activity of various metal catalysts for the coupling of CO ₂ and epoxides	81
Table 2.1. Some amine-phenol ligands independently reported by other research groups	102
Table 2.2. Summary of crystal data for compounds [L8]H and [L11]H ₂	112
Table 3.1. Ring-opening polymerization of <i>rac</i> -LA initiated by complexes 3.2-3.5, 3.7 in toluene.....	140
Table 3.2. Bulk polymerization of <i>rac</i> -LA initiated by 3.5 and 3.6 at 130 °C	147
Table 3.3. Details of the ROP of ϵ -CL initiated by complexes 3.2-3.5 and 3.7 in toluene	149
Table 3.4. Reaction of cyclohexene oxide (CHO) with CO ₂ in the presence of Zn complexes and co-catalysts.....	152
Table 3.5. Summary of crystal data for compounds [L2]H, 3.1-3.5.....	157
Table 3.6. Summary of crystal data for compounds 3.6 and 3.7	158

Table 4.1. τ values for compounds 4.1-4.4	182
Table 4.2. Polymerization of ϵ -CL initiated by compounds 4.1-4.5 in the presence and absence of BnOH	190
Table 4.3. A comparison of rate constants for the ROP of ϵ -CL initiated by various aluminum and metal complexes in toluene.....	204
Table 4.4. A comparison of activation energy for the ROP of ϵ -CL initiated by various aluminum and metal complexes.....	206
Table 4.5. A comparison of activation parameters for ϵ -CL polymerization initiated by Al complexes 4.1-4.3	207
Table 4.6. Melting point, ΔH_m and crystallinity of PCL obtained with compound 4.2 /BnOH and compound 4.4	210
Table 4.7. Coupling reactions of SO and CO ₂ using compound 4.5 and PPnCl.....	210
Table 4.8. Copolymerization of CHO/CO ₂ using 4.1, 4.4 and 4.5 as catalysts ^[a]	214
Table 4.9. Summary of crystal data for compounds 4.1-4.4	219
Table 5.1. Polymerization of ϵ -CL using complexes 5.1-5.3 in the presence and absence of BnOH.....	241
Table 5.2. A comparison of rate of constants for ϵ -CL polymerization by various metal alkoxides	245
Table 5.3. Summary of crystal data for compounds 5.1 and 5.3	257
Table 6.1. Selected bond lengths (Å) and angles (°) for compound 6.3	273
Table 6.2. Selected bond lengths (Å) and angles (°) for compound 6.4	277
Table 6.3. Summary of crystal data for compounds 6.1-6.4	283

List of Figures

Figure 1.1. Intramolecular (top) and intermolecular transesterification reactions in the ROP of LA.....	13
Figure 1.2. Stereoisomers of lactide	17
Figure 1.3. Microstructures of polylactide that can be obtained from <i>rac</i> - or <i>meso</i> -LA...	18
Figure 1.4. ¹ H NMR spectrum showing the methine and methyl features of racemic PLA	20
Figure 1.5. Homonuclear decoupled ¹ H NMR spectrum of the methine region of PLA...	21
Figure 1.6. Methine and methylene proton resonances of monomer and polymer for reaction samples from a ROP reaction of <i>rac</i> -LA (left) and ϵ -CL (right).	27
Figure 1.7. Single-site initiators supported by N-donor ligands for the ROP of cyclic esters	32
Figure 1.8. Schematic structure of tapered isotactic PLA.....	35
Figure 1.9. Chiral aluminum initiators bearing salen and salan ligands for the ROP of lactide.....	36
Figure 1.10 Achiral aluminum initiators bearing salen and salan ligands for the ROP of lactide.....	38
Figure 1.11. Single-site zinc complexes supported by half salen ligands for the ROP of lactide.....	40
Figure 1.12. Single-site initiators supported by monoanionic N-,O-donor ligands for the ROP of lactide.....	41
Figure 1.13. Bisphenolate hexalithium alkoxide complex for the ROP of cyclic esters. ...	43

Figure 1.14. Amine bis(phenolate) tetralithium complexes for the ROP of cyclic esters .	44
Figure 1.15 Monoanionic aminophenolate dinuclear lithium complexes for the ROP of cyclic esters.....	45
Figure 1.16. Aluminum complexes supported by amine-phenolate ligands used for the ROP of ϵ -CL	47
Figure 1.17. Li and Zn complexes bearing amine-bis(phenolate) ligand used for the ROP of ϵ -CL	50
Figure 1.18. Chemical transformation of CO_2 into commodity chemicals.....	56
Figure 1.19. Reaction coordinate diagram of coupling reaction of CO_2 and PO.....	60
Figure 1.20. Reaction coordinate diagram of coupling reaction of CO_2 and CHO	61
Figure 1.21. Porphyrinato aluminum catalysts for copolymerization of CO_2 and epoxides	63
Figure 1.22. Proposed mechanism for copolymerization of CO_2 and epoxides involving bimetallic complexes	64
Figure 1.23. Salen aluminum catalysts for the copolymerization of CHO and CO_2	66
Figure 1.24. Zinc-bis(phenoxide) complexes for the copolymerization of CHO and CO_2	67
Figure 1.25. β -diiminate-zinc catalysts for epoxide and CO_2 copolymerization.....	69
Figure 1.26. Bimetallic zinc complexes bearing amine-phenolate ligands for copolymerization of epoxides and CO_2	72
Figure 1.27. Aluminum salen complexes for the cycloaddition reaction of CO_2 and epoxides	76

Figure 1.28. Bimetallic aluminum salen complexes for cycloaddition reaction of CO ₂ with epoxides	77
Figure 1.29. Zinc complexes for the synthesis of cyclic carbonates from CO ₂ and epoxides	80
Figure 1.30. Amine bis(phenolate) titanium and zirconium alkoxide complexes for olefin polymerization	82
Figure 2.1. ¹ H NMR spectrum of [L4]H.....	106
Figure 2.2. MALDI-TOF mass spectrum of [L4]H.....	106
Figure 2.3. Molecular structure of [L8]H.	108
Figure 2.4. Molecular structure of [L11]H ₂	109
Figure 3.1. Molecular structure of [L2]H	124
Figure 3.2. Ball and stick representation of [L5]H.....	125
Figure 3.3. The methylene region of variable temperature ¹ H NMR spectra of compound 3.4 in C ₅ D ₅ N	129
Figure 3.4. Molecular structure of complex 3.1	130
Figure 3.5. Molecular structure of complex 3.2	132
Figure 3.6. Molecular structure of complex 3.3	133
Figure 3.7. Ball and stick representation of complex 3.4	134
Figure 3.8. Molecular structure of complex 3.5	135
Figure 3.9. Molecular structure of complex 3.6	136
Figure 3.10. Molecular structure of complex 3.7	137

Figure 3.11. Plots of M_n and PDI vs. monomer conversion for compound 3.3 / ^t BuOH initiated ROP of LA.....	138
Figure 3.12. Typical homonuclear decoupled ¹ H NMR spectrum of the methine region of PLA prepared by compound 3.3 / ^t BuOH.....	142
Figure 3.13. Section of the ¹ H NMR spectrum (CDCl ₃) of PLA sample prepared with complex 3.3 / ^t BuOH.....	144
Figure 3.14. First-order plot of LA consumption in a reaction with complex 3.7 /BnOH conducted at 60 °C	145
Figure 3.15. Plots of ln([LA] ₀ /[LA] _t) vs time for solventless polymerization of <i>rac</i> -LA initiated by complex 3.5 and 3.6	148
Figure 3.16. First-order plots of ε-CL consumption in ROP reactions conducted at 70 °C with complex 3.7 /BnOH and 3.2 /BnOH.....	150
Figure 4.1. Some previously reported piperazinyl and morpholinyl aminephenolate based complexes	178
Figure 4.2. Molecular structure of complex 4.1	183
Figure 4.3. Molecular structure of complex 4.2	184
Figure 4.4. Molecular structure of complex 4.3	185
Figure 4.5. Molecular structure of complex 4.4	186
Figure 4.6. Ball and stick representation of complex 4.5	187
Figure 4.7. ¹ H NMR spectra of compound 4.2 and of a 1:1 reaction of complex 4.2 with BnOH in tol- <i>d</i> ₈	188
Figure 4.8. Typical ¹ H NMR spectrum of PCL prepared using complex 4.1 /BnOH	194

Figure 4.9. ¹ H NMR spectrum of PCL prepared using complex 4.4	195
Figure 4.10. MALDI-TOF mass spectrum of PCL prepared using 4.2 /BnOH.....	197
Figure 4.11. MALDI-TOF mass spectrum of PCL initiated by complex 4.4	198
Figure 4.12. Semilogarithmic plots of ln[ε-CL] ₀ /[ε-CL] _t vs. time for the ROP of ε-CL at different monomer molar ratios initiated with complex 4.2	199
Figure 4.13. Relationship between M_n^{GPC} of the polymer and initial mole ratio [CL] ₀ /[4.2 /BnOH] ₀ for the polymerization of ε-CL initiated by 4.2 /BnOH.....	200
Figure 4.14. Semilogarithmic plots of ln[ε-CL] ₀ /[ε-CL] vs time for the ROP of ε-CL at different temperatures initiated with complex 4.3 /BnOH.....	201
Figure 4.15. Semilogarithmic plots of ln[CL] ₀ /[CL] _t vs time for observed rate constant comparison between complexes (4.1-4.3)/BnOH, 4.4 and 4.5 at 80 °C	202
Figure 4.16. Arrhenius plot of ln(k_{obs}) vs 1/T for the ROP of ε-CL initiated by 4.3 /BnOH.	204
Figure 4.17. TGA thermogram of the PCL sampled obtained using complexes 4.1 /BnOH and 4.4	208
Figure 4.18. DSC thermogram of PCL samples obtained by complexes 4.2 /BnOH and 4.4	209
Figure 4.19. ¹ H NMR spectrum of the copolymerization of CHO and CO ₂	212
Figure 4.20. Possible key ionic intermediate in CO ₂ -epoxide copolymerization facilitated by complex 4.5	213
Figure 5.1. Molecular structure of complex 5.1	237
Figure 5.2. Molecular structure of complex 5.3	238

Figure 5.3. Variable temperature ^1H NMR spectrum of the methylene region of complex 5.3	239
Figure 5.4. Effect of monomer concentration on the time of polymer conversion.....	242
Figure 5.5. Semilogarithmic plots of $\ln[\epsilon\text{-CL}]_0/[\epsilon\text{-CL}]_t$ vs time at different monomer molar ratios using complexes 5.1 and 5.3/BnOH	243
Figure 5.6. Semilogarithmic plots of $\ln[\epsilon\text{-CL}]_0/[\epsilon\text{-CL}]_t$ vs Time for the ROP of $\epsilon\text{-CL}$ at different temperatures using complexes 5.1 and 5.1/BnOH	244
Figure 5.7. Arrhenius plots of $\ln(k_{\text{obs}})$ vs $1/T$ for the ROP of $\epsilon\text{-CL}$ using complexes 5.1 and 5.1/BnOH	249
Figure 5.8. Typical ^1H NMR spectra of PCL synthesized with complexes 5.3 and 5.2/BnOH	250
Figure 5.9. ^{13}C NMR spectra for PCL initiated by complexes 5.3 and 5.2/BnOH	251
Figure 5.10. MALDI-TOF mass spectrum of PCL prepared using complex 5.3	252
Figure 5.11. MALDI-TOF mass spectrum of PCL formed using 5.2/BnOH	253
Figure 6.1. Molecular structure of complex 6.1	269
Figure 6.2. Molecular structure of complex 6.2	271
Figure 6.3. Molecular structure of complex 6.3	273
Figure 6.4. Solution-state ^7Li NMR spectrum of complex 6.4 in C_6D_6	274
Figure 6.5. ORTEP structure of complex 6.4	276
Figure 6.6. The ladder-like core of 6.4 showing its transoid-cisoidal geometry	277
Figure 6.7. ^1H NMR spectrum of $[\text{H}(\text{OEt}_2)_2]^+[\{3,5\text{-(CF}_3)_2\text{C}_6\text{H}_3\}_4\text{B}]^-$	279
Figure 6.8. ^1H NMR spectrum of complex 6.6	280

List of Schemes

Scheme 1.1. Structures of 6-hydroxycaproic, lactic and glycolic acid	5
Scheme 1.2. Synthesis of aliphatic polyesters <i>via</i> polycondensation polymerization	6
Scheme 1.3. Initiation step in the cationic mechanism for the ROP of ϵ -CL	9
Scheme 1.4. Structure of tin(II) octanoate, zinc(II) lactate, aluminum(III) isopropoxide.	10
Scheme 1.5. Coordination-insertion ring-opening polymerization mechanism.	11
Scheme 1.6. Life cycle of polylactide (PLA).....	16
Scheme 1.7. Synthesis of ϵ -caprolactone <i>via</i> Baeyer-Villiger oxidation process.....	23
Scheme 1.8. Synthesis of ϵ -caprolactone from renewable resources	24
Scheme 1.9. Industrial synthesis of polycarbonate of phosgene	57
Scheme 1.10. General catalytic reaction of epoxides and CO ₂ generating polycarbonate, cyclic carbonate and/or poly(ethercarbonate)	58
Scheme 1.11. Possible reaction pathways for the catalytic reaction of CO ₂ with epoxides	59
Scheme 1.12. Synthesis of aluminum calix[4]arene catalyst for copolymerization of CO ₂ and epoxides.....	64
Scheme 1.13. Proposed mechanism for the synthesis of cyclic carbonate using bimetallic complex with Bu ₄ NBr as co-catalyst	78
Scheme 1.14. Synthesis of amine mono(phenolate) zirconium alkoxide complex	83
Scheme 2.1. Procedure for preparation of amine-phenol ligands.	103
Scheme 2.2. Proposed mechanism of Mannich condensation.	104

Scheme 3.1. Synthetic procedure for the synthesis of piperazinyl amine-phenolate zinc complexes	126
Scheme 3.2. Synthesis of a morpholinyl amine-phenolate zinc complex.....	126
Scheme 4.1. Synthesis of methyl and chloro Al aminephenolate complexes.....	180
Scheme 5.1. Synthesis of amine-phenolate lithium complexes	235
Scheme 5.2. Proposed mechanism for catalytic ROP of ϵ -CL using Li aminephenolate complexes	247
Scheme 6.1. Synthetic procedure for the synthesis of amine-phenolate titanium and zirconium complexes.	268
Scheme 6.2. Synthetic procedure for Ti and Li amine-bis(phenolate) complexes	272
Scheme 6.3. Synthesis of cationic amine-phenolate zinc complex (6.6).....	278

List of Abbreviations and Symbols

(°):	degree
Å:	Angstrom (10^{-10} m)
BDI:	β -diketiminat
BnOH:	benzyl alcohol
bp:	boiling point
BPA:	bisphenol A
br:	broad
BuLi:	butyllithium
C ₅ D ₅ N:	deuterated pyridine
C ₆ D ₆ :	deuterated benzene
C ₇ D ₈ :	deuterated toluene
CaH ₂ :	calcium hydride
calcd:	calculated
Cat.:	catalyst
CDCl ₃ :	deuterated chloroform
CH ₂ Cl ₂ :	dichloromethane
CHC:	cyclohexene carbonate
CHCl ₃ :	chloroform
CHO:	cyclohexene oxide
<i>cis</i> :	on the same side
Cl ⁻ :	chloride ion

ϵ -CL:	ϵ -caprolactone
cm:	centimetre (10^{-2} m)
D,L-LA:	D,L-lactide
d:	doublet
D ₂ O:	deuterium oxide
Da:	dalton
DHBA:	2,5-dihydroxybenzoic acid
D-LA:	D-lactide
DMAP:	(4-dimethylamino)pyridine
DSC:	differential scanning calorimetry
E_a :	activation energy
EDBP:	2,2'-ethylidene-bis(4,6-di- <i>tert</i> -butylphenol)
ESI:	electrospray ionization
<i>et al.</i> :	and co-workers
Et:	ethyl
Et ₂ O:	diethyl ether
EtOH:	ethanol
g:	gram
GOF:	goodness of fit
GPC:	gel permeation chromatography
h:	hour
HSBA:	Hard and soft acids and bases

Hz:	hertz
<i>i</i> :	isotactic
<i>in situ</i> :	in the reaction mixture
^{<i>i</i>} Pr:	isopropyl
<i>J</i> :	coupling constant
K:	kelvin
<i>k</i> _{app} :	apparent rate constant
<i>k</i> _{obs} :	observed rate constant
LA:	lactide
L-LA:	L-lactide
L _n :	ligand
<i>m/z</i> :	mass-to-charge ratio
M:	molar (mols L ⁻¹)
<i>meso</i> -LA:	<i>meso</i> -lactide
<i>m</i> :	meta
<i>m</i> :	multiplet (in NMR)
MALDI-TOF:	matrix assisted laser desorption/ionization time-of-flight
Me:	methyl
MeOH:	methanol
mg:	milligram (10 ⁻³ g)
MHz:	megahertz (10 ⁶ Hz)
min:	minute

mL:	millilitre (10 L)
mmol:	millimole (10^{-3} mol)
M_n :	number average molecular weight
mp:	melting point
MS:	mass spectrometry
M_w :	weight average molecular weight
NMR:	nuclear magnetic resonance
<i>o</i> :	ortho
OH:	hydroxyl ion
OR:	alkoxide
ORTEP:	Oak Ridge thermal-ellipsoid plot program
O ^t Bu:	tert-butoxide
<i>p</i> :	para
PC:	propylene carbonate
PCHC:	poly(cyclohexene carbonate)
PCHO:	poly(cyclohexene oxide)
PCL:	poly(caprolactone)
PDI:	polydispersity index
PE:	poly(ethene)
PGA:	polyglycolide
Ph:	phenyl
PLA:	poly(lactic acid) or polylactide

P_m :	probability of meso enchainment
PO:	propylene oxide
PPC:	poly(propylene carbonate)
ppm:	parts per million
PPNCl:	bis(triphenylphosphoranylidene)iminium chloride
PPO:	poly(propylene oxide)
PPPs	polyether polycarbonate polyols
P_r :	probability of racemic enchainment
q:	quartet (NMR)
R:	alkyl moiety
<i>rac</i> :	racemic
ROP:	ring-opening polymerization
RT:	room temperature
s:	singlet (in NMR)
salan:	N,N'-bis(phenolato)-1,2-diaminoethane
salen:	N,N'-bis(salicylaldehyde)ethylenediamine)
SC:	styrene carbonate
SO:	styrene oxide
T:	temperature (°C)
t:	time
t:	triplet (in NMR)
^t Am:	tertiary amyl

TBABr:	tetrabutylammonium bromide
^t Bu:	tertiary-butyl
TFPP:	tetra(pentafluorophenyl)porphyrin
T_g :	glass transition temperature
T_m :	melting temperature
TGA:	thermal gravimetric analysis
THF:	tetrahydrofuran
TMS:	tetramethylsilane
TOF:	turnover frequency
TON:	turnover number
TPB:	tris(pyrazolyl)borate
TPP:	meso-tetra-phenylporphyrinato(2-)
<i>trans</i> :	on the other side
vs.:	versus
X_c	crystallinity
VT:	variable temperature
δ :	chemical shift
μL :	microlitre (10^{-6} L)

List of Appendices

Appendix A: NMR Spectroscopy

Figure A1.1. ^1H NMR spectrum of [L1]H.....	297
Figure A1.2. ^{13}C NMR spectrum of [L1]H.....	298
Figure A1.3. ^1H NMR spectrum of [L2]H.....	299
Figure A1.4. ^{13}C NMR spectrum of [L2]H.....	300
Figure A1.5. ^1H NMR spectrum of [L3]H.....	301
Figure A1.6. ^{13}C NMR spectrum of [L3]H.....	302
Figure A1.7. ^{13}C NMR spectrum of [L4]H.....	303
Figure A1.8. ^1H NMR spectrum of [L5]H.....	304
Figure A1.9. ^{13}C NMR spectrum of [L5]H.....	305
Figure A1.10. ^1H NMR spectrum of [L6]H.....	306
Figure A1.11. ^{13}C NMR spectrum of [L6]H.....	307
Figure A1.12. ^1H NMR spectrum of [L7]H.....	308
Figure A1.13. ^{13}C NMR spectrum of [L7]H.....	309
Figure A1.14. ^1H NMR spectrum of [L8]H.....	310
Figure A1.15. ^{13}C NMR spectrum of [L8]H.....	311
Figure A1.16. ^1H NMR spectrum of [L9]H.....	312
Figure A1.17. ^{13}C NMR spectrum of [L9]H.....	313
Figure A1.18. ^1H NMR spectrum of [L10]H.....	314
Figure A1.19. ^{13}C NMR spectrum of [L10]H.....	315
Figure A1.20. ^1H NMR spectrum of [L11]H ₂	316

Figure A1.21. ^{13}C NMR spectrum of [L11]2H.....	317
Figure A1.22. ^1H NMR spectrum of 3.1 ($\text{C}_5\text{D}_5\text{N}$, 500 MHz, 343 K).....	318
Figure A1.23. ^{13}C NMR spectrum of 3.1 ($\text{C}_5\text{D}_5\text{N}$, 125 MHz, 298 K).....	319
Figure A1.24. ^1H NMR spectrum of 3.2 ($\text{C}_5\text{D}_5\text{N}$, 500MHz, 343 K).....	320
Figure A1.25. ^{13}C NMR spectrum of 3.2 ($\text{C}_5\text{D}_5\text{N}$, 125MHz, 298 K).....	321
Figure A1.26. ^1H NMR spectrum of 3.3 ($\text{C}_5\text{D}_5\text{N}$, 500 MHz, 358 K).....	322
Figure A1.27. ^{13}C NMR spectrum of 3.3 ($\text{C}_5\text{D}_5\text{N}$, 125 MHz, 298K).....	323
Figure A1.28. ^{13}C NMR spectrum of 3.4 ($\text{C}_5\text{D}_5\text{N}$, 125 MHz, 298 K).....	324
Figure A1.29. ^1H NMR spectrum of 3.5 ($\text{C}_5\text{D}_5\text{N}$, 500 MHz, 343 K).....	325
Figure A1.30. ^{13}C NMR spectrum of 3.5 ($\text{C}_5\text{D}_5\text{N}$, 125 MHz, 298 K).....	326
Figure A1.31. ^1H NMR spectrum of 3.6 ($\text{C}_5\text{D}_5\text{N}$, 500 MHz, 358 K).....	327
Figure A1.32. ^{13}C NMR spectrum of 3.6 (C_6D_6 , 125 MHz, 298 K).....	328
Figure A1.33. ^1H NMR spectrum of 3.7 ($\text{C}_5\text{D}_5\text{N}$, 500 MHz, 313 K).....	329
Figure A1.34. ^{13}C NMR spectrum of 3.7 ($\text{C}_5\text{D}_5\text{N}$, 125 MHz, 298 K).....	330
Figure A1.35. ^1H NMR spectrum of 4.1 ($\text{C}_5\text{D}_5\text{N}$, 300 MHz, 298 K).....	331
Figure A1.36. ^{13}C NMR spectrum of 4.1 (C_7D_8 , 125 MHz, 298 K).....	332
Figure A1. 37. ^{27}Al NMR spectrum of 4.1 ($\text{C}_5\text{D}_5\text{N}$, 78.22 MHz, 298 K).....	333
Figure A1.38. ^1H NMR spectrum of 4.2 ($\text{C}_5\text{D}_5\text{N}$, 500 MHz, 328 K).....	334
Figure A1.39. ^{13}C NMR spectrum of 4.2 ($\text{C}_5\text{D}_5\text{N}$, 125 MHz, 298 K).....	335
Figure A1.40. ^{27}Al NMR spectrum of 4.2 ($\text{C}_5\text{D}_5\text{N}$, 78.22 MHz, 298 K).....	336
Figure A1.41. ^1H NMR spectrum of 4.3 (C_6D_6 , 500 MHz, 343 K).....	337
Figure A1.42. ^{13}C NMR spectrum of 4.3 (C_6D_6 , 125 MHz, 298 K).....	338

Figure A1.43. ^{27}Al NMR spectrum of 4.3 (C_6D_6 , 78.22 MHz, 298 K)	339
Figure A1.44. ^1H NMR spectrum of 4.4 ($\text{C}_5\text{D}_5\text{N}$, 300 MHz, 298 K)	340
Figure A1.45. ^{13}C NMR spectrum of 4.4 ($\text{C}_5\text{D}_5\text{N}$, 125 MHz, 298 K)	341
Figure A1.46. ^{27}Al NMR spectrum of 4.4 ($\text{C}_5\text{D}_5\text{N}$, 78.22 MHz, 298 K)	342
Figure A1.47. ^1H NMR spectrum of 4.5 ($\text{C}_5\text{D}_5\text{N}$, 300 MHz, 298 K)	343
Figure A1.48. ^{13}C NMR spectrum of 4.5 ($\text{C}_5\text{D}_5\text{N}$, 125 MHz, 298 K)	344
Figure A1.49. ^{27}Al NMR spectrum of 4.5 ($\text{C}_5\text{D}_5\text{N}$, 78.22 MHz, 298 K)	345
Figure A1.50. Variable temperature ^1H NMR spectra of 5.1 ($\text{C}_5\text{D}_5\text{N}$, 500 MHz)	346
Figure A1.51. ^{13}C NMR spectrum of 5.1 ($\text{C}_5\text{D}_5\text{N}$, 125 MHz, 298K)	347
Figure A1. 52. ^7Li NMR spectrum of 5.1 ($\text{C}_5\text{D}_5\text{N}$, 116 MHz, 298 K)	348
Figure A1.53. Variable temperature ^1H NMR spectra of 5.2 ($\text{C}_5\text{D}_5\text{N}$, 500MHz)	349
Figure A1.54. ^{13}C NMR spectrum of 5.2 ($\text{C}_5\text{D}_5\text{N}$, 125 MHz, 298 K)	350
Figure A1.55. ^7Li NMR spectrum of 5.2 ($\text{C}_5\text{D}_5\text{N}$, 116 MHz, 298 K)	351
Figure A1.56. ^{13}C NMR spectrum of 5.3 ($\text{C}_5\text{D}_5\text{N}$, 125 MHz, 298 K)	352
Figure A1.57. ^1H NMR spectrum of 6.1 (C_6D_6 , 500 MHz, 298 K)	354
Figure A1.58. ^1H NMR spectrum of 6.2 ($\text{C}_5\text{D}_5\text{N}$, 500 MHz, 313 K)	356
Figure A1.59. ^1H NMR spectrum of 6.4 (C_6D_6 , 500 MHz, 298 K)	357
Figure A1.60. ^{13}C NMR spectrum of 6.4 (C_6D_6 , 125 MHz, 298 K)	358
Figure A1.61. Typical ^1H NMR spectra showing the conversion of LA to PLA with time mediated by 5.6 at 130 °C (Bulk polymerization)	359
Figure A1.62. Typical ^1H NMR spectra showing the conversion of CL to PCL mediated by 5.1 at 60 °C	360

Figure A1.63. GPC traces of polymer samples prepared using (a) 4.1 /BnOH and (b) 4.4	361
--	-----

Appendix B: MALDI-TOF Mass Spectrometry

Figure B1.1. MALDI-TOF mass spectrum of [L1]H	362
Figure B1.2. MALDI-TOF mass spectrum of [L2]H	362
Figure B1.3. MALDI-TOF mass spectrum of [L3]H	363
Figure B1.4. MALDI-TOF mass spectrum of [L5]H	363
Figure B1.5. MALDI-TOF mass spectrum of [L6]H	364
Figure B1.6. MALDI-TOF mass spectrum of [L8]H	364
Figure B1.7. MALDI-TOF mass spectrum of [L11]H ₂	365
Figure B1.8. MALDI-TOF mass spectrum of PCL prepared using 4.1 /BnOH.....	366
Figure B1.9. MALDI-TOF mass spectrum of PCL prepared using 4.3 /BnOH.....	367
Figure B1.10. MALDI-TOF mass spectrum of PCL initiated by 5.1 in THF	368
Figure B1.11. MALDI-TOF mass spectrum of PCL initiated by 5.1 in toluene	369
Figure B1.12. MALDI-TOF mass spectrum of PCL initiated by 5.1 /BnOH in toluene..	370
Figure B1.13. MALDI-TOF mass spectrum OF PCL initiated by 5.2 /BnOH in toluene	371
Figure B1.14. MALDI-TOF mass spectrum of PCL prepared using 5.3 /BnOH in toluene	372

Appendix C: Kinetic Plots

Figure C1.1. Semilogarithmic plots of $\ln[\text{CL}]_0/[\text{CL}]_t$ vs time for ROP of CL at different monomer molar ratios initiated with 4.1 /BnOH	373
Figure C1.2. Semilogarithmic plots of $\ln[\text{CL}]_0/[\text{CL}]_t$ vs time for ROP of CL at different monomer molar ratios initiated with 4.3 /BnOH	373
Figure C1.3. Plot of M_n^{GPC} of polymer vs initial mole ratio $[\text{CL}]_0/[\text{4.1/BnOH}]_0$ for ROP of CL initiated by 4.1 /BnOH at 80 °C.....	374
Figure C1.4. Plot of M_n^{GPC} of polymer vs initial mole ratio $[\text{CL}]_0/[\text{4.3/BnOH}]_0$ for ROP of CL initiated by 4.3 /BnOH at 80 °C.....	374
Figure C1.5. Semilogarithmic plots of $\ln[\text{CL}]_0/[\text{CL}]_t$ vs time for ROP of CL initiated with 4.1 /BnOH at different temperature.	375
Figure C1.6 Semilogarithmic plots of $\ln[\text{CL}]_0/[\text{CL}]_t$ vs time for ROP of CL initiated by 4.2 /BnOH at different temperature	375
Figure C1.7. Arrhenius plot of $\ln(k_{\text{obs}})$ vs $1/T$ for ROP of CL initiated by 4.1 /BnOH ...	376
Figure C1.8. Arrhenius plot of $\ln(k_{\text{obs}})$ vs $1/T$ for ROP of CL initiated by 4.2 /BnOH	377
Figure C1.9. Eyring plot of $\ln(k_{\text{obs}}/T)$ vs $1/T$ for ROP of CL initiated by 4.1 /BnOH.....	377
Figure C1.10. Eyring plot of $\ln(k_{\text{obs}}/T)$ vs $1/T$ for ROP of CL initiated by 4.2 /BnOH.....	378
Figure C1. 11. Eyring plot for $\ln(k_{\text{obs}}/T)$ vs $1/T$ for ROP of CL initiated by 4.3 /BnOH .	378
Figure C1.12. Semilogarithmic plot of $\ln[\text{CL}]_0/[\text{CL}]_t$ vs time for ROP OF CL initiated by 5.3 at different temperature.....	379
Figure C1.13. Semilogarithmic plot of $\ln[\text{CL}]_0/[\text{CL}]_t$ vs time for ROP of CL initiated by 5.3 /BnOH at different temperature	379

Figure C1.14. Arrhenius plot of $\ln(k_{\text{obs}})$ vs time for ROP of CL initiated by 5.3	380
Figure C1.15. Arrhenius plot of $\ln(k_{\text{obs}})$ vs time for ROP of CL initiated by 5.3/BnOH .	380

Appendix D: Summary of R and R^2 Values

Table D1. 1. Activation parameters obtained from polymerization initiated by Al methyl complexes	381
Table D1.2. Summary of R and R^2 values of polymerization initiated by 4.1/BnOH	381
Table D1.3. Summary of R and R^2 values of polymerization initiated by 4.2/BnOH	381
Table D1.4. Summary of R and R^2 values of polymerization initiated by 4.3/BnOH	382

CHAPTER 1

Literature Review

Chapter 1

Literature Review

1.1 Introduction

Polymers are an invaluable class of materials in our everyday lives and find use in many domestic and industrial areas. This has caused the demand for man-made polymeric materials to grow enormously over the last six decades. Among the many commercial synthetic polymers available, polyolefins derived from petrochemical feedstocks are by far the most important and widely used class of materials due to monomer availability and low cost.¹ The success of synthetic polymers can be attributed to the unique combination of properties including hardness, lightness, weather resistance, processability, rigidity and toughness.²

Despite the numerous advantages of polyolefins, two drawbacks concerned with their manufacture and use need to be solved. Namely, the use of depleting resources in their production and the ultimate fate of these large scale commodity polymers in the environment. The widespread use of polymers has created environmental problems; despite increased popularity of plastic recycling, the disposal of these non-degradable materials has led to serious pollution.³ In addition, the ultimate formation of greenhouse gases if the polymers are disposed of *via* incineration could have unpredictable and irreversible consequences on the global climate.⁴ Therefore, biodegradable polymers are receiving a great deal of attention and emerging as environmentally friendly alternatives. For these reasons, a tremendous amount of scientific research aimed at the synthesis of

biodegradable polymers has been undertaken and impressive advances have been achieved. The main classes of biodegradable polymers being studied in academia are polyesters (section 1.2).

Polycarbonates form a commercially important class of polymers due to their attractive properties, including strength, lightness, durability, high transparency, heat resistance, biodegradability and good electrical insulation as well as being easily processed and coloured. Thus, these materials have been widely used in optical media, the automotive industry, the medical and health industries, components of electrical/electronic devices and reusable bottles.⁵ The production of aliphatic polycarbonates using carbon dioxide (CO₂) as a feedstock is economically and environmentally appealing, especially with the growing safety and toxicity concerns associated with the production of conventional polycarbonate from bis(phenol) A (BPA) and phosgene.⁶ CO₂ is a ubiquitous chemical in the natural environment and also the main by-product of many industrial processes. With increasing concerns about the environmental impact of increasing CO₂ levels in the environment, the chemical fixation of CO₂ has attracted attention as a potential carbon source in new materials.^{6,7} Carbon dioxide are formed in steel mills, in the cement industry, in steam power plant and in fermentation processes. There are already several industrial processes that use CO₂ as a starting material including the synthesis of urea, cyclic carbonates, carbamic acids and derivatives.⁸ The quantity of CO₂ consumed by these processes will not be able to significantly decrease the amount of CO₂ generated from human activities (including transportation, energy generation and manufacturing). But this approach potentially

affords access to more environmentally friendly routes to producing chemicals otherwise obtained from reagents harmful to the environment.⁶ In addition to the aforementioned commercial applications of CO₂, several interesting processes involving CO₂ chemical fixation are under investigation and the most promising processes include methanol synthesis and transformation of CO₂ and oxiranes (epoxides) into valuable polycarbonates and/or cyclic carbonates. CO₂ is generally considered as a green, environmentally benign feedstock, as it is cheap, non-toxic and renewable. Nonetheless, CO₂ is a challenging feedstock to use because it is relatively inert with a Gibbs energy of formation of -394.01 kJ mol⁻¹.^{8,9} The use of reactive species such as oxiranes is one way to overcome the unfavourable thermodynamics.

1.2 Biodegradable Polymers

Among the classes of biodegradable polymers, linear aliphatic polyesters, especially polylactide (PLA), polyglycolide (PGL) and polycaprolactone (PCL) are particularly attractive. This can be attributed not only to the fact that they maintain many of the desirable properties of traditional plastics, but they are also biocompatible and bio-assimilable. They degrade ultimately to innocuous components (water and CO₂) by naturally-occurring microorganisms such as bacteria, fungi or algae.^{1,10} These polymers are primarily used where biocompatibility is important. However, their physico-chemical properties (toughness, tensile strength, glass transition temperature, permeability, decomposition temperature, melting temperature, etc.) are also important in determining the applications for these polymers. Both of these properties (degradability and physical behaviour) depend on the polymer's structure, including linkers between ester groups and

stereochemistry where applicable (section 1.6.1). In light of the benefits biodegradable polymers offer through their desirable properties, their applications range from commodity polymer materials such as carrier bags, compostable waste bags, film packaging for food, rigid packaging (containers or bottles) or biodegradable mulching films to biomaterials, for example drug/gene delivery systems or tissue/bone engineering substrates (orthopedic screws and pins, sutures, scaffold for soft tissue regeneration, implants etc.).¹¹

1.3 History/Background of Biodegradable Polyester Development

Polyesters, including those described above, have been known for many years, in fact reports dating as far back as the sixteenth century described the self-condensation of lactic acid to yield solid materials.¹² However, the development of high molecular weight polyesters started as part of the pioneering work of Carothers and co-workers on polymerization of oligomeric lactides in 1932.¹³ They observed rapid polymerization of ϵ -caprolactone and lactide at 250-275 °C without using a catalyst. The resulting polymer had an apparent molecular weight of about 3000 g mol⁻¹. Similarly, polymerization could be performed at a lower temperature (~150 °C) in the presence of potassium carbonate. Unfortunately, the polymers were abandoned for further development, as they had low melting temperatures and poor hydrolytic stability properties, and thus, were not considered useful for long-term industrial uses.

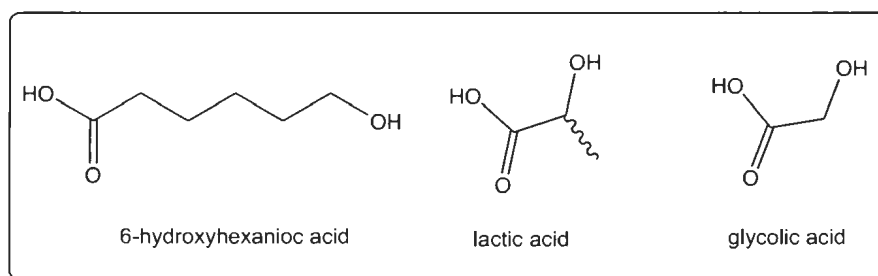
A few decades after Carothers' work, the very hydrolytic instability of the polymer which gives rise to biodegradation was recognized to be an important feature of such aliphatic polyesters. It has enabled their application as both biomedical and commodity

degradable materials such as resorbable surgical sutures, stents and fibers. As a consequence, there is increasing demands for sustainable biopolymer production. PLA is now produced on a 300 million pound per annum scale by Natureworks LLC, a joint venture between Cargill and Teijin Limited, and on a smaller scale by other business enterprises in Europe and Japan, proving that manufacture of PLA is economically viable.^{10,14}

1.4 General Synthesis of Biodegradable Polyesters

Polyesters such as polycaprolactone, polylactide and polyglycolide can be prepared by two different polymerization methods namely:

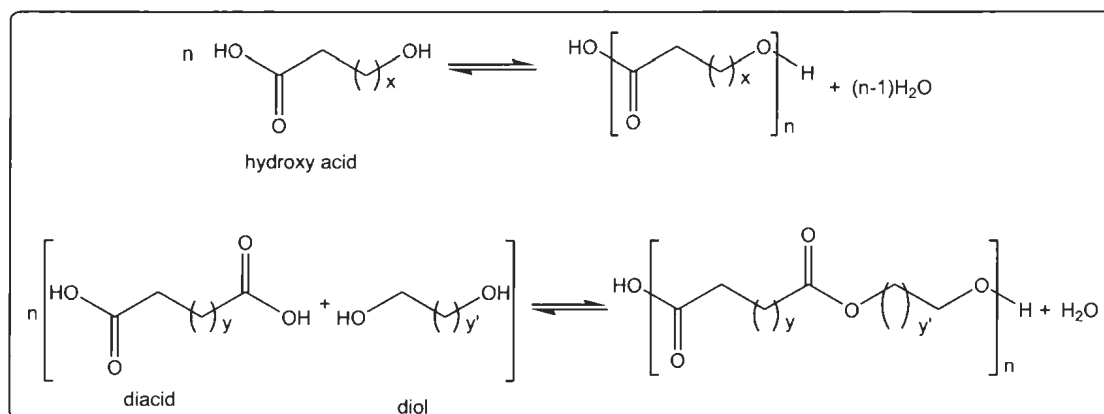
- (a) Polycondensation (Step-growth) polymerization of acids such as 6-hydroxycaproic (6-hydroxyhexanoic) acid, lactic (2-hydroxypropionic) acid and glycolic acid (Scheme 1.1)
- (b) Ring-opening polymerization (ROP) (Chain-growth) of cyclic esters such as caprolactone, lactide and glycolide.



Scheme 1.1. Structures of 6-hydroxycaproic, lactic and glycolic acid

1.4.1 Polycondensation (Step-Growth) Polymerization

Polyesters are typically prepared from condensation reactions between difunctional monomers such as self-condensation of hydroxy acids, diacids with diols or by interchange reaction of diesters with diols as shown in Scheme 1.2.^{11,15}



Scheme 1.2. Synthesis of aliphatic polyesters *via* polycondensation polymerization; $x = 4$, $y = 16$ and $y' = 2$ for 6-hydroxyhexanoic acid, octadecanedioic acid and propane-1,3-diol.

Although the step-growth polymerization method is less expensive than ROP, it suffers from some major drawbacks, including (1) difficulty in removal of the by-product (water) (2) high temperatures and (3) long reaction times. The condensation reaction is an equilibrium reaction, thus, it is not easy to drive the reaction to completion because of the difficulty of removing the by-product (water) from the polymerization medium and this leads to the production of low molecular weight polymers. Furthermore, the harsh reaction conditions (high temperature and long reaction time) generally required for step growth polymerization favour side reactions, which in turn result in polymeric materials

with ill-defined microstructures, limited access to specific end-groups and the inability to prepare well-defined copolymers.^{11,16} It is worth noting that high molecular weight PLA has been achieved by an azeotropic distillation process established by Mitsui Chemicals, in which a boiling solvent (e.g. diphenyl ether, bp 130 °C) along with a catalyst are used and water is continuously removed by Soxhlet extraction through molecular sieves.^{16,17}

1.4.2 Ring-Opening Polymerization (Chain-Growth Mechanism)

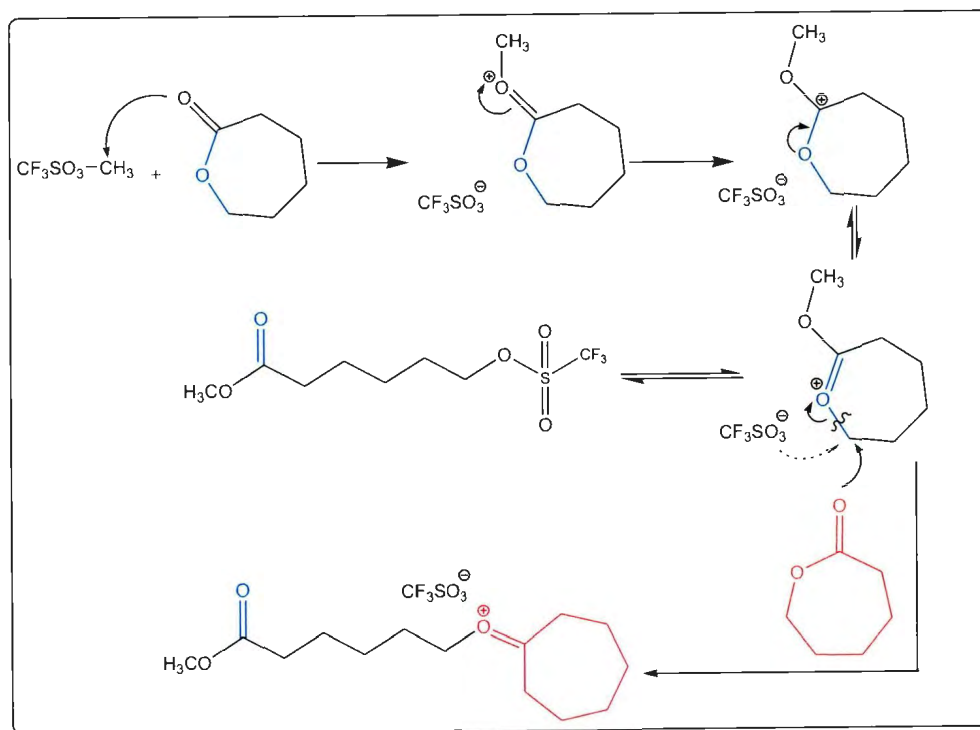
Ring-opening polymerization (ROP) of cyclic esters, unlike the direct condensation route, provides the opportunity to synthesize high molecular weight polymers under mild conditions. The possibility of manipulation of the chemistry of polymers through altering the monomer to initiator ratio and careful selection of initiators and co-initiators results in polymers with controlled architecture and tailor-made properties. This makes ROP the most efficient method for the production of well-defined polyesters. Therefore, it is no surprise that ROP is the most commonly studied and commercially used method for the production of PLA and PCL.^{3,12,14,18} The production of polyesters through ROP has been successfully conducted in solution, bulk, melt and suspension phases. The thermodynamic driving force for ROP of cyclic esters such as ϵ -caprolactone, δ -valerolactone, β -butyrolactone and the cyclic diesters, lactide and glycolide is the relief of ring strain, which enables the entropy, unfavorable in all polymerizations, to be overcome.^{18,19,20}

1.4.3 Ring-Opening Polymerization Mechanism

The ROP of cyclic esters can proceed through several different reaction mechanisms, often dependent on the initiator type, including anionic,¹⁴ cationic,^{4,15} activated monomer²¹⁻²³ and coordination-insertion mechanism.²⁴⁻²⁸ The cationic mechanism will be briefly discussed, and then the discussion will focus on mechanisms that have been widely seen in ROP using ligand-supported metal complexes i.e. the coordination-insertion mechanism.

1.4.3.1 Cationic Ring-Opening Polymerization

The cationic ROP of cyclic esters has been shown to occur in the presence of alkylating agents, acylating agents, Lewis acids and protic acids as the catalyst (e.g. triethyloxonium tetrafluoroborate, borontrifluoride, methyl triflate, ZnCl_2 , AlCl_3 , trifluoroacetic acid and hydrochloric acid and).^{14,29} The proposed mechanism for cationic ROP (Scheme 1.3) consists of an initiation step, a propagation step and a termination step. The initiation step involves the activation of the monomer by methylation or protonation of one of the exocyclic oxygens of the monomer carbonyls, resulting in the formation of a positively charged species (carbenium ion) (Scheme 1.3). Nucleophilic attack by a second monomer leads to a ring opening of the carbenium ion bond (O-CH) to generate another electrophilic carbenium ion. The propagation step occurs by subsequent attacks by additional monomers until the polymerization is terminated by addition of a monofunctional nucleophile such as water.^{4,15} The pitfall of this method is that it is difficult to control and often low molecular weight polymers are obtained.³⁰

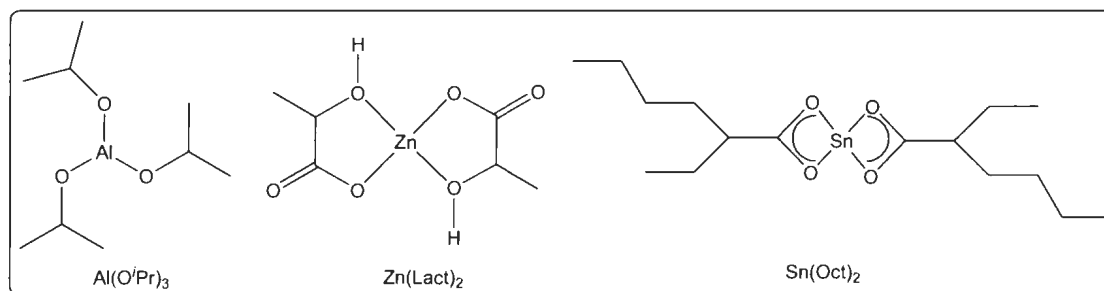


Scheme 1.3. Initiation step in the cationic mechanism for the ROP of ε-CL.^{15,31}

1.4.3.2 Coordination-Insertion Ring-Opening Polymerization

Among the various ROP mechanisms, coordination–insertion is the most widely studied and accepted method for the synthesis of high molecular weight polyesters, which has been supported theoretically by density functional theory (DFT) calculations and experimentally by analysis of the resulting polymer.²⁴⁻²⁸ This method enables good control over the polymer molecular weight, molecular weight distributions, and results in no epimerization reactions. Additionally, it allows for the preparation of stereoregular polymers with well defined end-groups (e.g. polylactide or polymers of functionalized ε-caprolactone).^{32,33}

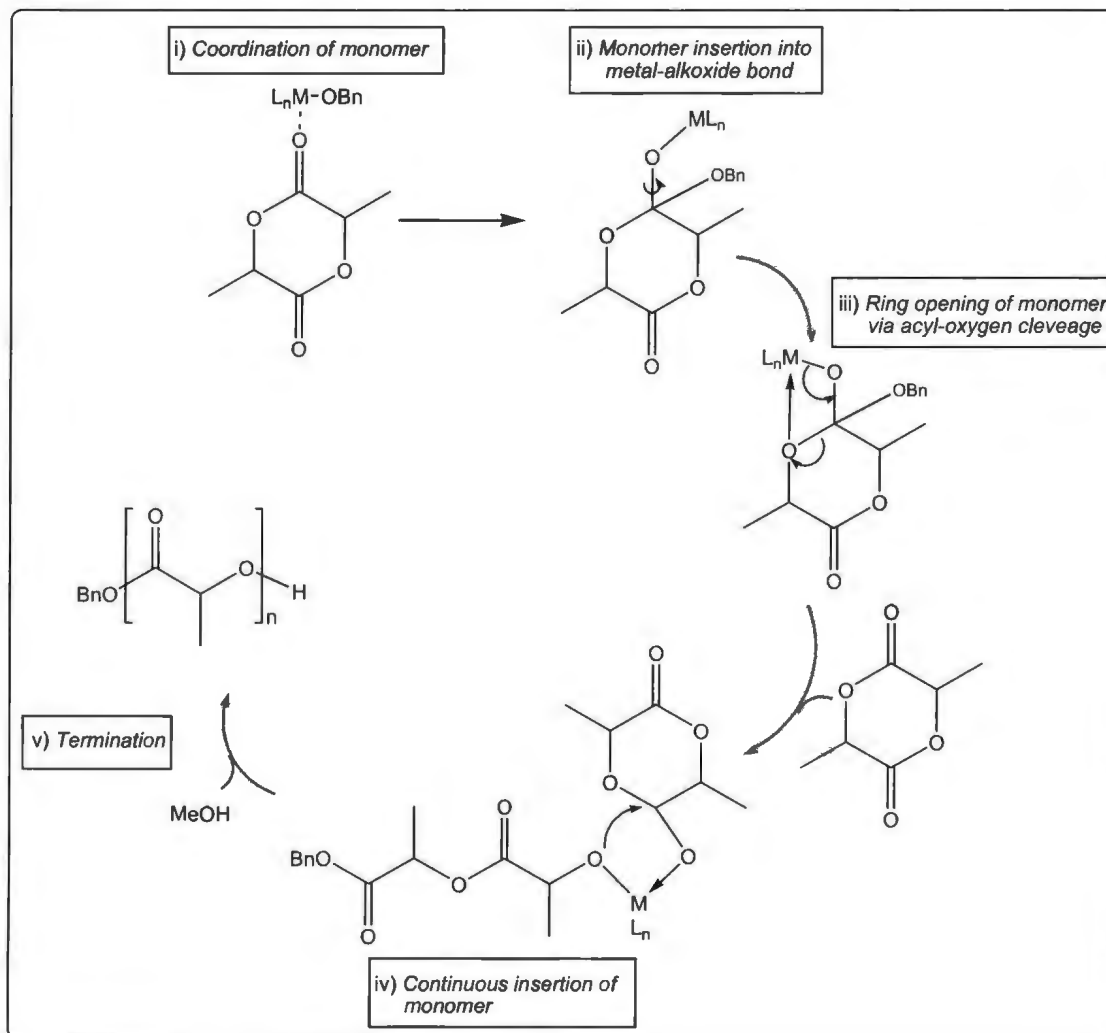
The first generation active initiators widely used for coordination-insertion ROP of cyclic esters were based on simple metal alkoxides with empty *p*, *d* or *f* orbitals of favourable energy. The complexes possess a covalent bond between the metal atom and the oxygen atom, and thus, react as coordination catalysts and not anionic initiators. The use of these complexes (aluminium(III) isopropoxide $[\text{Al}(\text{O}^i\text{Pr})_3]$, zinc(II) lactate $[\text{Zn}(\text{Lact})_2]$ and tin(II) bis{2-ethylhexanoate} $[\text{Sn}(\text{Oct})_2]$ (tin(II) octanoate)) (Scheme 1.4) contributed immensely to a better understanding of the coordination-insertion mechanism.^{1,30,33,34}



Scheme 1.4. Structure of tin(II) octanoate, zinc(II) lactate, aluminum(III) isopropoxide

The polymerization mechanism (Scheme 1.5) involves (i) coordination of the monomer molecule to the Lewis acidic metal centre through the exocyclic oxygen of the monomer, (ii) monomer insertion into metal alkoxide bond, (iii) ring opening of the monomer *via* acyl-oxygen cleavage and (iv) continuous insertions of monomer and finally (v) termination by hydrolysis of the propagating chain.³⁵ The coordination of the monomer increases the nucleophilicity of the metal alkoxide region of the initiator and weakens the carbonyl $\text{C}=\text{O}$ bond thereby rendering the monomer carbonyl group more susceptible to nucleophilic attacks (increased electrophilicity of the carbonyl group) of the metal alkoxide. Thus, the acyl-oxygen bond is broken and the resulting chain is inserted into the

metal-oxygen bond of the initiator. The polymerization propagates as additional monomer molecules are opened and inserted into the metal-oxygen bond until the polymerization is terminated e.g. by addition of a protic alcohol such as methanol.



Scheme 1.5. Coordination-insertion ring-opening polymerization mechanism.

Zinc(II) lactate,³⁶ aluminum(III) isopropoxide³⁷ and tin(II) octanoate³⁸ complexes have been demonstrated to be efficient initiators in the ROP of cyclic esters, but generally

need elevated temperatures or long reaction times. These catalysts suffer from several drawbacks in terms of their use in ROP including a propensity towards side-reactions such as transesterification, equilibria phenomena (ligand exchange) and multiple nuclearities (they do not always act as single-site initiators). These lead to limited control over polymer molecular weight thereby broadening the molecular weight distribution and can cause changes in the microstructure of the resulting polymer.^{35,39} Transesterification reactions result from the exchange of ester groups between different chains and this leads to redistribution of monomer sequences in the polymer chain. Multiple nuclearity can be defined as a process whereby multiple active metal sites exist in the catalyst structure, thereby initiating more than one type of growing polymer chain from metal centres within the catalyst system.

Transesterification can occur as: (a) intramolecular (back-biting) and/or (b) intermolecular transesterification. In intramolecular transesterification, cyclic macromolecules and short chain polymers are generated leading to a decrease in the average molecular weight. Intermolecular transesterification involves a random polymer chain-ends exchange when two growing polymer chains approach each other causing a broadening of molecular weight distribution (Figure 1.1).^{4,26} It is worth noting that transesterification is influenced by factors such as temperature, reaction time, type of initiator and nature of monomer.

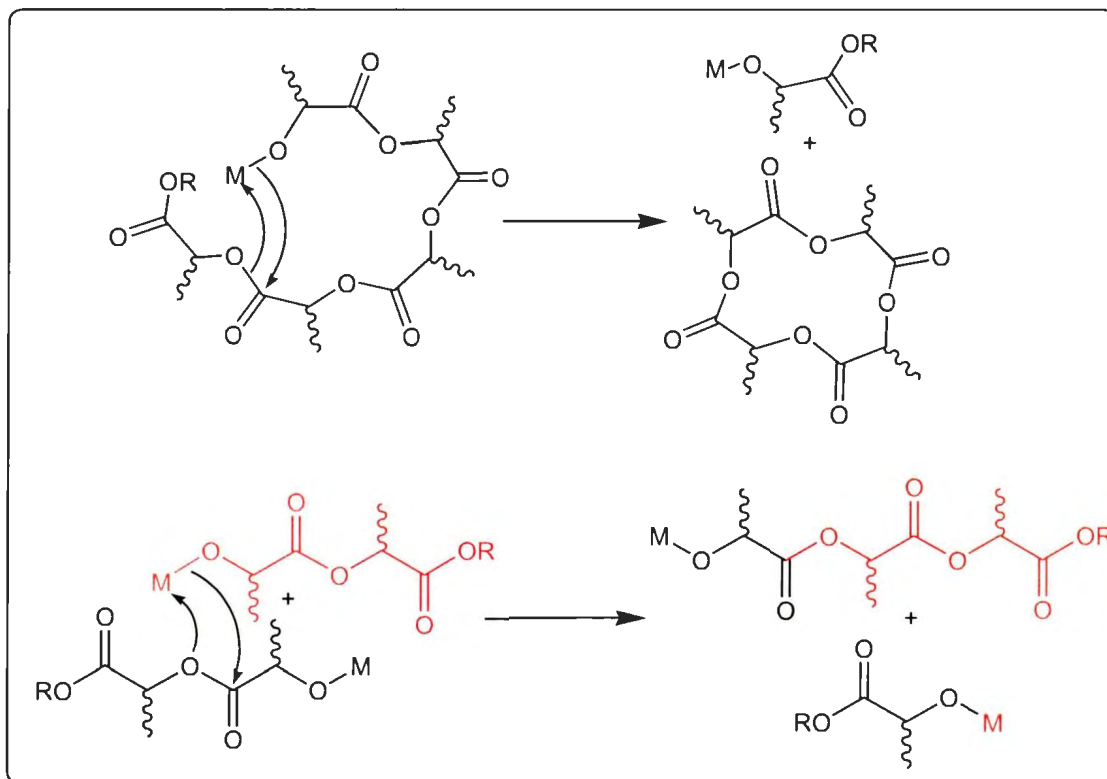


Figure 1.1. Intramolecular (top) and intermolecular transesterification reactions in the ROP of LA.¹⁸

These undesirable side reactions can be attributed to the homoleptic nature of the early catalyst systems e.g. $\text{Al}(\text{iOPr})_3$, and in order to obviate these problems, major research efforts have been focused towards obtaining initiator systems well-suited to promote living polymerization. A living polymerization is defined as “A chain polymerization from which chain transfer and chain termination are absent. In many cases, the rate of chain initiation is fast compared with the rate of chain propagation, so that the number of kinetic-chain carriers is essentially constant throughout the polymerization”.⁴⁰

1.5 Microwave Assisted Ring-Opening Polymerization

Microwaves are electromagnetic radiation with frequencies between 300 GHz and 300 MHz (with a wavelength in the range of 1 mm to 1 m).⁴¹ Most commercial microwave ovens produce a microwave wavelength of 12.25 cm, which corresponds to a frequency of 2.45 GHz in order to avoid interferences with telecommunication devices.⁴¹ The use of microwave irradiation as an alternative to conductive heating systems has become a well-established technique to promote and enhance chemical reactions.^{42,43} As an environmentally friendly process, microwave irradiation offers a number of merits over conventional heating, including instantaneous and rapid bulk heating, direct heating, high temperature homogeneity, higher yields, shorter reaction times and reduction of side reactions.⁴¹

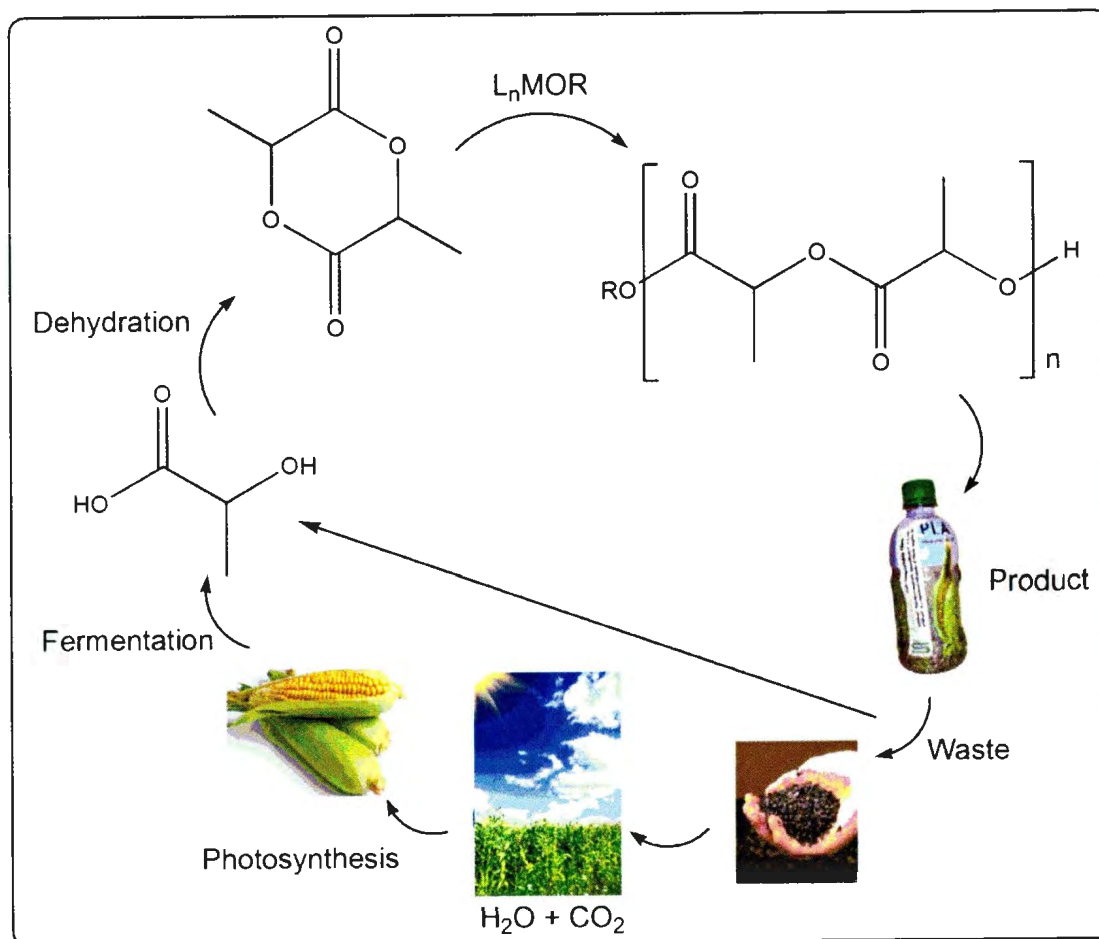
Microwave irradiation has been employed in polymerizations such as polycondensations, free- and controlled-radical polymerization and ring-opening polymerization.⁴³ However, the focus of this section will be on some of the coordination-insertion ROP of cyclic esters carried out using microwave irradiation.

Albert and co-workers in 1996 reported the first microwave coordination-insertion ROP of lactones in which they compared the thermal- and microwave-activated polymerizations of ϵ -caprolactone at 180 °C in the presence of titanium tetrabutylate. However, the results did not indicate any substantial improvement relating to the use of microwave irradiation.⁴⁴ Fang *et al.* studied the ROP of ϵ -caprolactone and ϵ -caprolactam using tin(II) bis(2-ethylhexanoate) and an aliphatic alcohol (1,4-butanediol) as catalyst and initiator at low forward power, applying variable frequency (2.4 to 7.0 GHz) microwave

irradiation. They found that caprolactone and ϵ -caprolactam both exhibited effective absorption of microwaves to induce fast chemical reactions, and PCL with M_w of 8600-9900 g mol^{-1} was produced after 2 h of irradiation. Comparative analysis of this polymer with that produced by conventional heating after 12 h revealed that the microwave produced PCL had equivalent glass transition (T_g), melting temperature (T_m) and thermal stability.^{45,46} Sivalingam *et al.*⁴⁷ studied the kinetics of microwave ROP of ϵ -CL in bulk using a zinc catalyst at 350 W with different heating periods (30-50 s). In their experiments, they set up two models for both conventional and microwave heating processes, and the activation energies determined from temperature dependent rate coefficients for pure conventional heating, thermally aided catalytic polymerization and microwave-aided catalytic polymerization were 24.3 kcal mol^{-1} , 13.4 kcal mol^{-1} and 5.7 kcal mol^{-1} respectively. These data suggested that microwave irradiation increased the polymerization rate by lowering the activation energy.

1.6 Polylactides (PLAs)

Polylactides are linear aliphatic polyesters composed of lactide repeat units and can be synthesized by ring-opening polymerization of lactide. PLA is an attractive polymer family because in addition to being thermoplastic, biodegradable, compostable, and produced from annually renewable resources such as corn and sugar beets, it shows mechanical and barrier behaviour comparable to traditional polymers like polystyrene (PS) and polyethylene terephthalate (PET).⁴⁸ PLA is readily compostable as shown in Scheme 1.6, thus, making it a sustainable environmentally friendly plastic.



Scheme 1.6. Life cycle of polylactide (PLA).¹⁸

Lactide is the cyclic dimer of lactic acid which can be obtained by fermentation of glucose. LA molecules possess two stereogenic centres resulting in three distinct stereoisomers (Figure 1.2); (*S,S*)-LA (L-LA), (*R,R*)-LA (D-LA) and (*R,S*)-LA (*meso*-LA). The equimolar mixture of D-LA and L-LA is known as *rac*-LA (DL-LA).⁴⁹

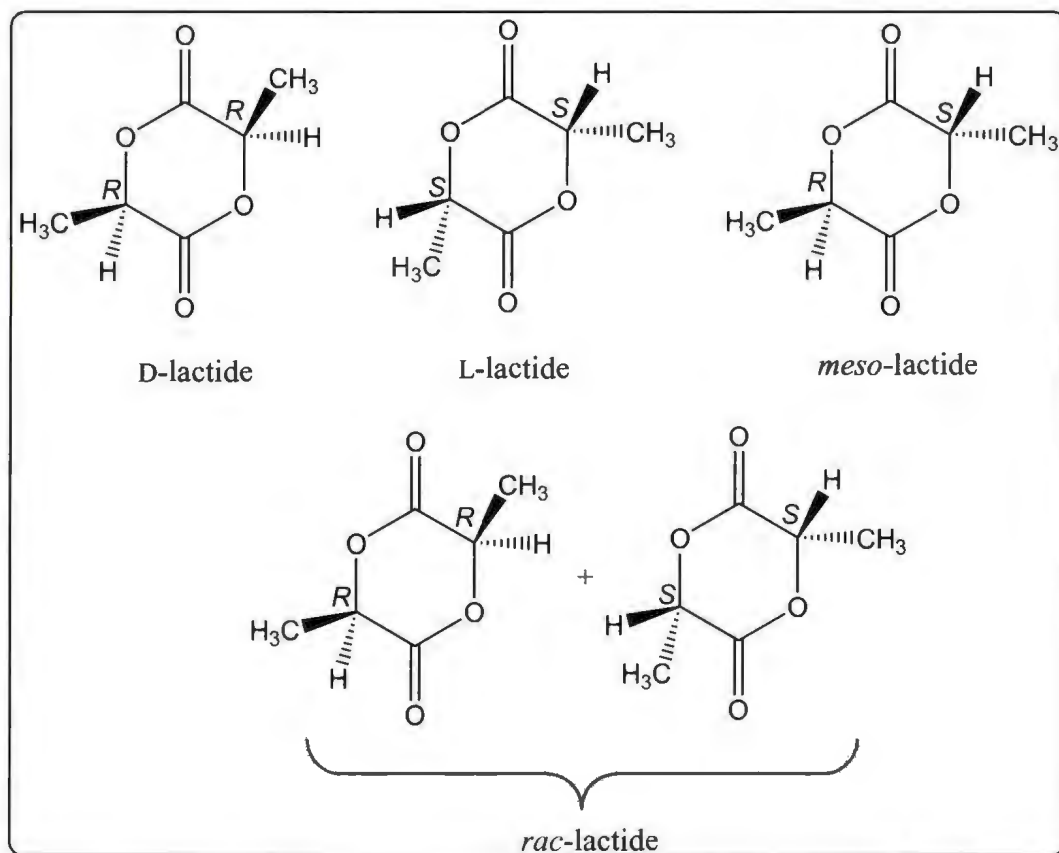


Figure 1.2. Stereoisomers of lactide

1.6.1 PLA Microstructures (Stereochemistry)

The physical and mechanical properties of PLA, including its thermal resistance, melting temperature, mechanical strength, and degradation rate, critically depend on the alignment of *R* and *S* stereogenic centres along the polymer chain (Figure 1.3).³⁵ Stereocontrolled ROP of *rac*-LA or *meso*-LA can afford PLA with a variety of microstructures. ROP of D-LA or L-LA can lead to stereocontrolled homopolymers (e.g. poly-D-lactide) if epimerization does not occur in the polymerization process. The ROP of *rac*-LA can yield either isotactic PLA where adjacent stereocenters are of the same stereochemistry or heterotactic PLA in which alternate polyaddition of D-LA and L-LA is

obtained along the growing polymer chain. The ROP of *meso*-LA can also afford heterotactic or syndiotactic PLA where the adjacent stereocenters are of opposite configuration (Figure 1.3). Polymers often form that partially obey stereocontrol e.g. heterotactic enriched PLA.

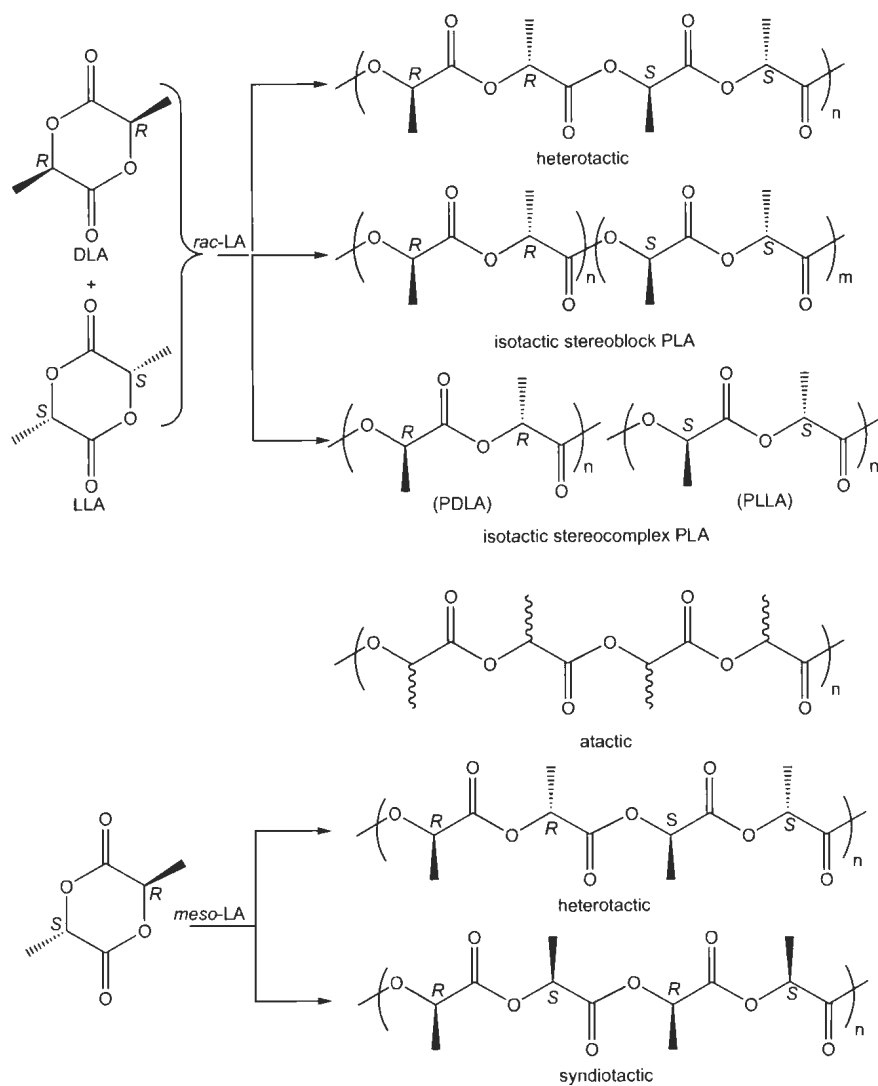


Figure 1.3. Microstructures of polylactide that can be obtained from *rac*- or *meso*-LA.

1.6.2 Mechanisms for the Synthesis of Stereocontrolled PLAs

The preparation of stereoregular PLAs using a variety of metal complexes as single-site initiators involves two different mechanisms *viz*: (a) Chain-end control and (b) Enantiomorphic site-control mechanism.

(a) The chain-end control mechanism is where the insertion of the incoming *rac*-LA or cleavage site of the monomer in *meso*-LA polymerization is determined by the chirality in the last repeating unit along the propagating chain.^{35,49} If the chiral centre of the last unit is repeated, then isotactic PLA is obtained from *rac*-LA polymerization and heterotactic PLA will be obtained from *meso*-LA polymerization. If the chiral centre of the last unit favours *racemic* enchainment (*S,S*) i.e. insertion through the opposite chiral centre, then heterotactic (monomer alternating after each ring-opening event) PLA forms from *rac*-LA polymerization, while syndiotactic (alternating *S* and *R* stereocenters) will be obtained from the polymerization of *meso*-LA.

(b) The enantiomorphic site-control mechanism is where the orientation of the next inserted monomer in *rac*-LA polymerization or the cleavage site of the monomer in *meso*-LA polymerization is controlled by the chirality of the surrounding ligand of the initiator. Therefore, under enantiomorphic site-control mechanism, only isotactic or syndiotactic PLA can be obtained from the polymerization of *rac*- or *meso*-LA respectively. It is worth noting that atactic means absence of stereoregularity in a polymer sample (Figure 1.3).³⁵

As a consequence of their stereoregularity, isotactic and syndiotactic polymers are crystalline materials with a melting temperature (T_m) of around 180 °C and 152 °C

respectively. Mixtures of poly(L-LA){PLLA} and poly(D-LA){PDLA} form stereocomplexes with melting temperature (T_m) values up to 220 °C. On the other hand, heterotactic PLAs based on *rac*-LA and *meso*-LA form amorphous polymers that show no melting temperature.^{35,49}

1.6.3 Determination of PLA Tacticity

Tacticity of a polymer sample can be determined using ^{13}C NMR and homonuclear decoupled ^1H NMR analysis. In the ^1H NMR of a PLA sample, there are two sets of signals for the methine and methyl protons. The methine and methyl resonances couple and are observed as a number of overlapping quartet and doublets respectively (Figure 1.4).

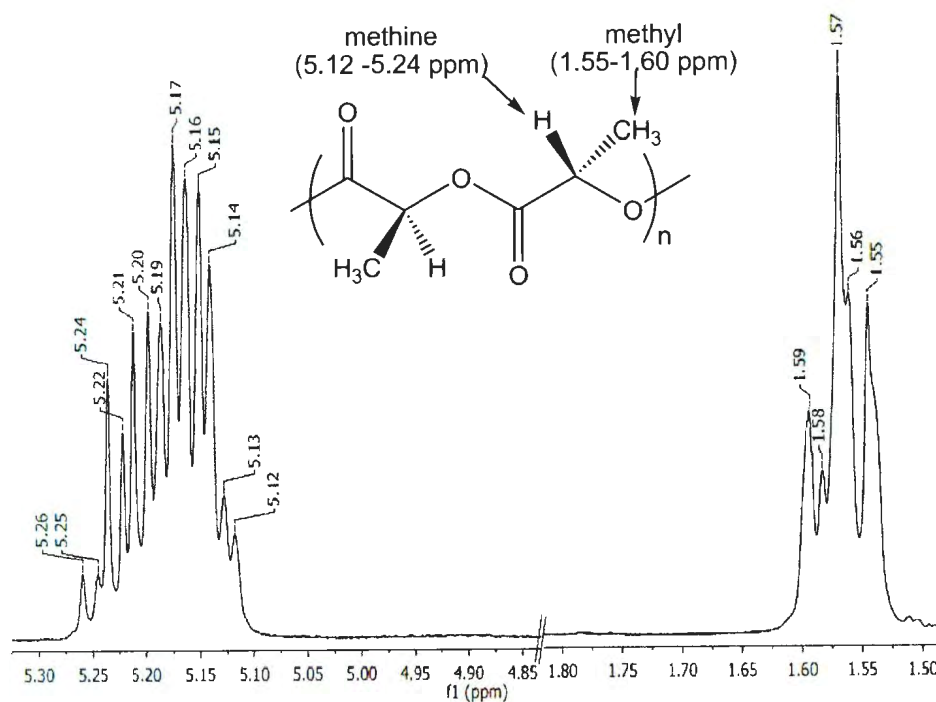


Figure 1.4. ^1H NMR spectrum showing the methine and methyl features of racemic PLA

In order to simplify the signals, homonuclear decoupling of the methyl signal is carried out resulting in singlet resonances in the methyl region. The homonuclear decoupling experiment consists of applying lower power continuous wave irradiation at the methyl resonance, which eliminates spin-spin coupling relaxation processes with the methine protons. In the absence of the coupling to the methyl protons, the overlapping quartets in the methine region are reduced to manageable splitting patterns, which correspond to different tetrad sequences: *rrr*, *rmr*, *mmm*, *rrm*, *mmr*, *mrr* and *rmm* as shown in Figure 1.5.

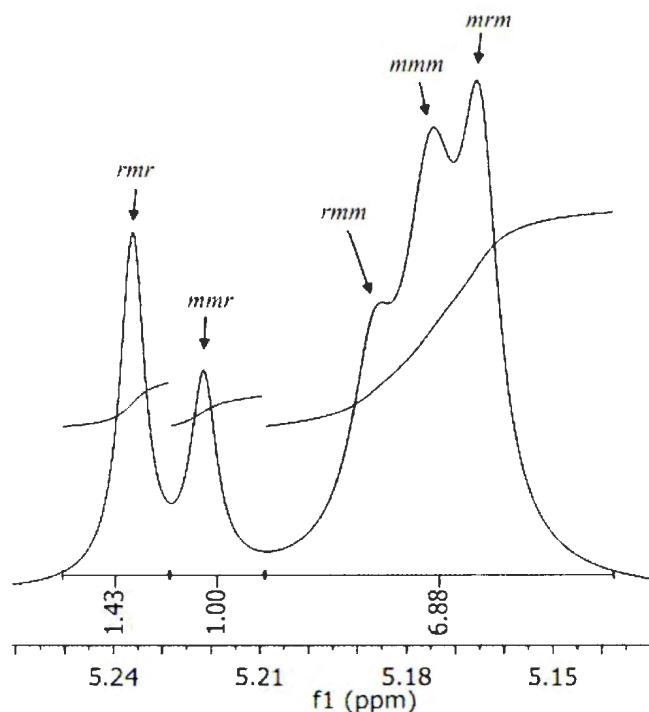


Figure 1.5. Homonuclear decoupled ^1H NMR spectrum of the methine region of PLA.

The chirality of each newly inserted monomer may be identical or opposite to the last repeating unit of the growing polymer chain, thus adaptation of Bovey formalism

provides a method for describing the tacticities of the polymer such that identical or opposite sequences are described by ‘*i*’ (isotactic) or ‘*s*’ (syndiotactic) respectively. These can also be referred to as *meso* (*m*) and *racemic* (*r*) respectively.^{50,51} Two adjacent units in a polymer molecule make a diad, therefore a tetrad can be assigned to four consecutive repeating units. At the tetrad stereosequence level, the homonuclear decoupled ¹H NMR spectrum of PLA synthesized using *rac*-LA can exhibit five resonances corresponding to *rmr*, *mmr*, *rmm*, *mmm* and *mrmm* tetrads. Only two stereosequences (*rmr* and *rrm/mrr*) can be observed for PLA obtained from *meso*-LA.⁵² In addition, homonuclear decoupled ¹H NMR spectra of syndiotactic and isotactic PLA contain only one resonance corresponding to *rrr* or *mmm* stereosequence, whereas, heterotactic PLA contains two peaks *rmr* (*SRRS*) and *mrmm* (*SSRR*) respectively. By analysing the relative integration of the tetrad, it is possible to determine both the overall microstructure of the polymer and the mechanism by which stereoselectivity is occurring.⁵⁰ The degree of stereoregularity in LA polymerization is expressed as the probability of *racemic* (P_r) or *meso* (P_m) enchainment. The probability can be calculated based on Bernoullian Statistics (Table 1.1) from the deconvoluted homonuclear decoupled ¹H NMR spectrum of a polymer sample

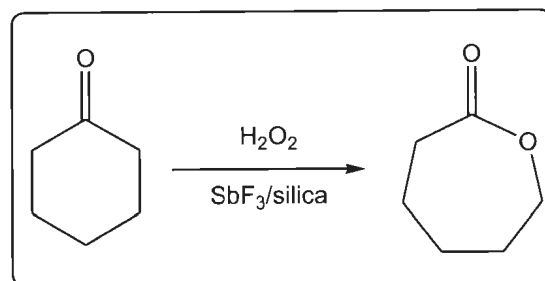
Table 1.1. *rac*-LA tetrad probabilities based on Bernoullian statistics⁵¹

tetrad	probability
	<i>rac</i> -LA
[<i>mmm</i>]	$P_m^2 + P_r P_m / 2$
[<i>mmr</i>]	$P_r P_m / 2$
[<i>rmm</i>]	$P_r P_m / 2$
[<i>rmr</i>]	$P_r^2 / 2$
[<i>mrmm</i>]	$(P_r^2 + P_r P_m) / 2$

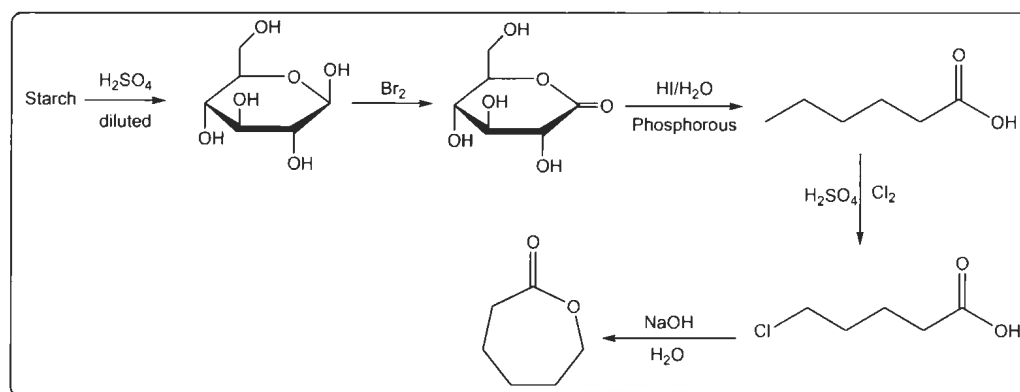
For ROP of *rac*- or *meso*-lactide, P_r or $P_m = 0.5$ signifies atactic polymer, whereas for *rac*-lactide $P_r = 1.00$ ($P_m = 0.00$) and $P_m = 1.00$ ($P_r = 0.00$) describes perfect heterotactic and isotactic polymers respectively. In the case of ROP of *meso*-lactide $P_r = 1.00$ ($P_m = 0.00$) and $P_m = 1.00$ ($P_r = 0.00$) describe perfect syndiotactic and heterotactic polymers respectively.⁵⁰

1.7 Poly(ϵ -caprolactone) (PCL)

Lactones are named based on the acid molecule from which they are prepared (for example propio 3 carbon, valero 5 carbon, capro 6 carbon). This is usually preceded by a Greek prefix such as α , β , γ , etc, which indicates the number of carbons and position of the first carbon after the carbonyl carbon in the ring, then followed with the lactone suffix. Polycaprolactone (PCL) is an aliphatic polyester composed of hexanoate repeat units and can be synthesized by polymerization of a relatively cheap monomer ϵ -caprolactone. The monomer is mainly produced by the Baeyer-Villiger oxidation of cyclohexanone with peracids or hydrogen peroxide as shown in Scheme 1.7. Furthermore, there have been reports about the potential availability of ϵ -caprolactone from starch (Scheme 1.8), making polycaprolactone a polymer with high industrial potential.³³



Scheme 1.7. Synthesis of ϵ -caprolactone *via* Baeyer-Villiger oxidation process

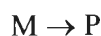


Scheme 1.8. Synthesis of ϵ -caprolactone from renewable resources

Polycaprolactone is a semi-crystalline polymer with a degree of crystallinity which can reach 69% but which tends to decrease with increasing molecular weight. PCL has a glass transition temperature well below room temperature ($-60\text{ }^{\circ}\text{C}$), low tensile strength ($\sim 23\text{ MPa}$), but extremely high elongation at breakage ($>700\%$).^{15,53} The polymer is highly processible as it is soluble in a wide range of solvents, while having exceptional blend-compatibility. It is non-toxic, has high permeability to many drugs and undergoes hydrolytic degradation. However, the rate of degradation is rather slow (2-3 years). As a consequence, extensive research into its potential applications in biomedical and other fields has been performed. Applications studied include its use as a long term drug/vaccine delivery vehicle (in particular, for contraceptive delivery),⁵³⁻⁵⁵ as scaffolds in tissue engineering,⁵⁶⁻⁵⁸ in microelectronics,⁵⁹ as adhesives⁶⁰ and in packaging.¹¹ Therefore, it is of immense importance to develop synthetic methods for the polymerization of this monomer in order to control its molecular weight, and co-monomer incorporation, which are the major parameters that control the polymer composition.

1.8 Kinetics of Ring-Opening Polymerization

Monitoring the change in the concentration of a reactant with time as a reaction progresses provides vital information about the way the reaction proceeds. In most cases, the monitoring of the reaction entails determining the the amount of product formed or the amount of reactant consumed. For example, a reaction of a reagent M (monomer) being converted to product P (polymer) is depicted below:



From this, the rate of reaction could be determined as the decrease in monomer concentration or the increase in the polymer concentration respectively, where [M] and [P] are the concentration of monomer and polymer as shown in Equation 1.1 and Equation 1.2:

$$\text{Rate} = -d[M]/dt \quad \text{Equation 1.1}$$

$$\text{Rate} = d[P]/dt \quad \text{Equation 1.2}$$

Assuming the polymerization to be first-order with respect to monomer, and that the concentration of the initiator is constant, then

$$\text{Rate} = k[M] \quad \text{Equation 1.3}$$

When Equation 1.1 and Equation 1.3 are combined

$$\text{Rate} = -d[M]/dt = k[M] \quad \text{Equation 1.4}$$

Integration of Equation 1.4 will afford

$$\ln[M]_t - \ln[M]_0 = -kt \quad \text{Equation 1.5}$$

[M]_t is concentration of monomer at time t, [M]₀ is concentration of monomer at time zero and *k* is the observed rate constant calculated from the slope of linear dependence of

$\ln([M]_0/[M]_t)$ versus time.⁶¹ Therefore, from Equation 1.5, a plot of natural logarithm of $([M]_0/[M]_t)$ versus time should be linear. The timescale of a reaction usually determines which analytical technique can be used to monitor the kinetics of such a reaction. It is comparatively simple to monitor the kinetics of a reaction occurring over minutes, hours and days as opposed to reactions occurring at femtoseconds ($1 \text{ fs} = 10^{-15} \text{ s}$), which require highly specialized techniques. Luckily the observable reaction time for most polymerization reactions is in the range of minutes to days. This implies that a number of techniques could be useful for monitoring progression of polymerization reactions, including UV, IR, NMR and Raman spectroscopy. However, in this work, polymerization kinetics were determined by manual sampling using ^1H NMR spectroscopy, which enabled the determination of catalytic observed rate constants and associated activation parameters as a function of ligand substituent. These data, in conjunction with MALDI-TOF MS analysis, provide mechanistic knowledge and insights into the catalyzed ROP reactions.

1.8.1 Nuclear Magnetic Resonance Spectroscopy for Kinetic Studies

The ring strain inherent with cyclic esters leads to significantly different chemical shifts between the monomer and polymer signals in ^1H NMR spectra. For example, the methine protons of LA and PLA give a quartet and multiplet resonances located in the ranges from 4.99-5.06 ppm and 5.12-5.26 ppm, respectively. The ϵ -methylene protons of CL and PCL give rise to triplets located at 4.21-4.25 ppm and 4.04-4.08 ppm respectively (Figure 1.6). The complete separation in the ^1H NMR spectrum of the monomer resonances from the relevant resonances of the polymer enables kinetic data to be

obtained with minimal error originating from overlapping of peaks. Integration of the methine or the methylene protons of the monomer relative to that of the polymer for samples withdrawn at pre-determined intervals during the polymerization allows for the calculation of percentage conversion by a ratio of polymer/total monomer and polymer peak areas.

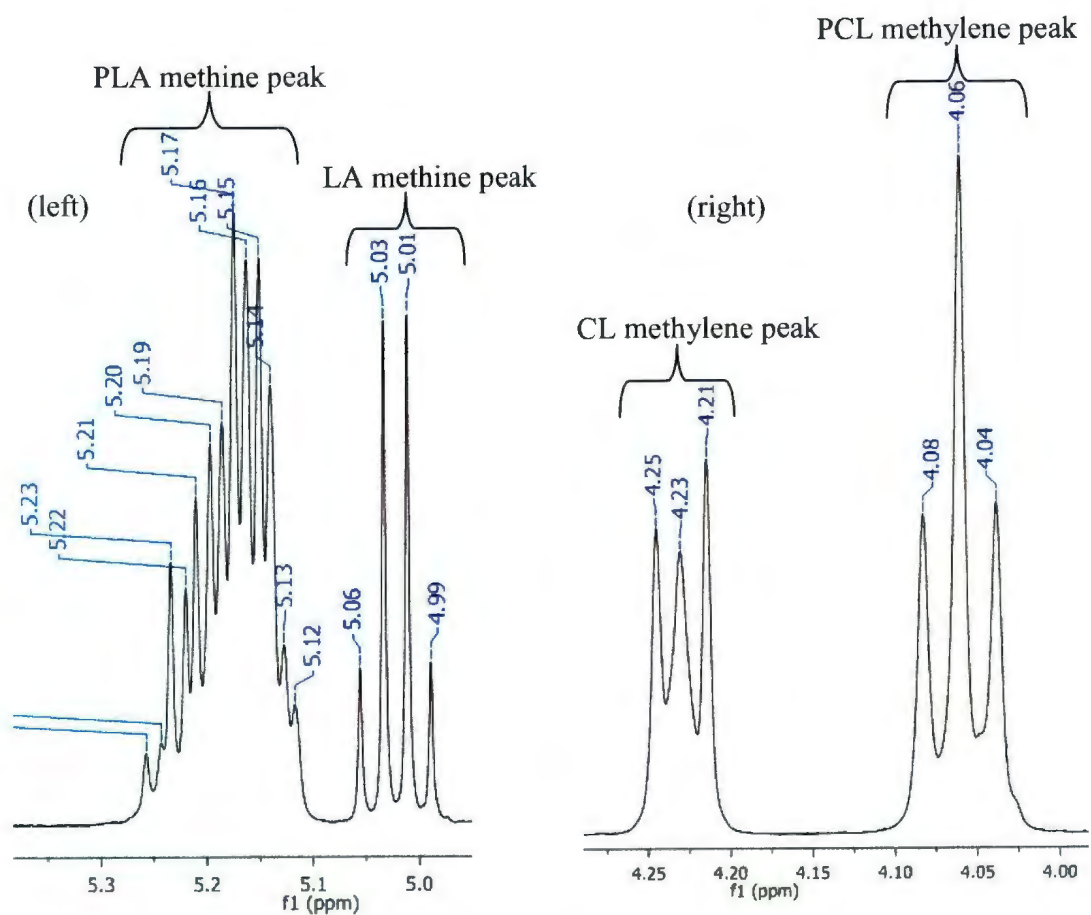


Figure 1.6. Methine and methylene proton resonances of monomer and polymer for reaction samples from a ROP reaction of *rac*-LA (left) and ϵ -CL (right).

1.8.2 Activation Energy (E_a) Determination

Activation energy can be defined as the minimum energy required to initiate a chemical reaction. For any reaction with non-zero activation energy, the rate constant is dependent on temperature. The Arrhenius equation describes the relationship between the rate constant and temperature, where A is the Arrhenius coefficient, R is the molar gas constant and T is the temperature.

$$k = Ae^{(-E_a/RT)} \text{ or } \ln k = \ln A - (E_a/RT) \quad \text{Equation 1.6}$$

Hence, from Equation 1.6, activation energy (E_a) can be determined by a plot of the natural logarithm of observed rate constant (k) versus the reciprocal of the polymerization temperature, which should be linear with a slope of $-E_a/R$ and a y-intercept of $\ln A$.⁶¹

1.8.3 Enthalpy (ΔH^\ddagger) and Entropy (ΔS^\ddagger) of Activation

The Eyring equation (equation 1.7) is generally used in mechanistic research to interpret the temperature dependence of rate constants.

$$\ln(k/T) = -(\Delta H^\ddagger/R) \cdot 1/T + \ln(k_B/h) + \Delta S^\ddagger/R \quad \text{Equation 1.7}$$

$$\begin{aligned} \text{Where } R &= \text{Universal gas constant} = 8.3144 \text{ [J mol}^{-1} \text{ K}^{-1}] \\ K_B &= \text{Boltzmann's constant} = 1.381 \times 10^{-23} \text{ [J K}^{-1}] \\ h &= \text{Planck constant} = 6.626 \times 10^{-34} \text{ [J s]} \end{aligned}$$

According to the Eyring equation, the plot of natural logarithm of observed rate constant divided by the reaction temperature ($\ln k/T$) versus the inverse of the temperature ($1/T$) should produce a straight line. The ΔH^\ddagger is obtained from the slope and ΔS^\ddagger from the

intercept. Comparison between the Arrhenius equation and Eyring equation shows that E_a and ΔH^\ddagger on one hand and $\ln A$ and ΔS^\ddagger on the other are analogous quantities.⁶²

1.9 Single Site Metal Initiators for ROP of Cyclic Esters

The desired characteristics, such as controlled molecular weight, narrow molecular weight distributions, end-group control, and well-defined stereochemistry of a polymer can be achieved through construction of a well-defined ancillary ligand environment around the metal centre. The ligands exert steric hindrance in the coordination environment of the metal centre thereby decreasing the occurrence of side reactions while affording control over polymer formulations and microstructures. These types of catalysts are often referred to as “single site” catalysts and they have general formula L_nM-R , where L_n is n equivalents of a ligand set bound to the metal and therefore adjusts the reactivity of the active metal centre (M) during the polymerization reaction and R is a group that can initiate the ring-opening polymerization.⁶³ Multidentate anionic ligands with O-, N- or N-/O-mixed donor atom sets such as phenolate, guanidinate, β -diketiminato (BDI), salen, bis(phenolate) and salan are the widely used ligands in main group and transition metal chemistry. This is primarily because they are easily tunable, thus allowing for convenient variation of the steric and electronic properties around the metal centre and making them less susceptible to ligand redistribution. It is also pertinent to consider the nature of the metal for biomedical applications, as there is concern that remnants of the catalyst are not entirely removed from the polymer.³² Therefore, searching for suitable metal complexes of high activity based on biocompatible metals has been an important research topic. As a consequence, a large number of single-site

catalysts have been developed in the past three decades based on biocompatible metals supported by various ligand sets. Among these metals, Li, Mg, Ca, Zn and Al have attracted much attention due to their lack of colour, low toxicity, low cost, ready availability and their polymerization properties in term of reactivity and selectivity. Of particular relevance to the work in this thesis are Li, Zn and Al, therefore their chemistry will be discussed briefly here before proceeding with well-defined and single-site catalysts for ROP of cyclic esters.

1.9.1 Chemistry of Li, Zn and Al

Lithium is from the most electropositive group in the periodic table, its chemistry is dominated by an oxidation state of +1 (M^+) and its binding in lithium(I) complexes is predominantly electrostatic. Thus, its coordination number is determined mainly by the number of binding sites of the ligand.⁶⁴

Zinc has an electronic configuration of $[Ar] 3d^{10}3s^2$ and its chemistry is dominated by the +2 oxidation state. Zn shows similarities to Mg as many of their compounds are isomorphous, and like Mg it exhibits “hard” behaviour in complexing readily with O-donor ligands. Having a filled d shell, it also shares a feature more readily associated with transition elements in its tendency to form a large number of stable complexes, not only with O-donor ligands but with N- and S- ligands and with halides, pseudohalides and cyanide. The filled d shell confers no crystal field stabilization on Zn^{2+} , therefore the coordination number and stereochemistry of a particular compound depends only on the size of the Zn^{2+} cation and the steric requirements of the ligand.⁶⁵

Aluminum possesses amphoteric behaviour, a [Ne] $3s^23p^1$ configuration and combines with almost all non-metallic elements in the common oxidation state of +3, M^{3+} ion. The Al^{3+} ion is the most Lewis acidic among group 13 metals, it exhibits exceptional affinity for oxygen and in term of polarizability is considered a “hard” acceptor/acid.⁶⁶

These cations are redox-inactive and this feature is doubtless important in the ring-opening polymerization where they are inert toward β -hydrogen abstraction within the growing chain polymer.

1.9.2 Single-Site Initiators Supported by N-,N-Donor Ligands

Historically, tetraphenylporphyrin (TPP) aluminum complexes synthesized by Inoue and co-workers were the first N-donor supported catalytic systems (Figure 1.7) developed for ROP of CL and LA. The polymerizations using these catalysts exhibited living characteristics such as linear increase of M_n with monomer conversion and narrow polydispersities. However, the reaction rates were slow, for example complex **1.1** polymerized D-LA with 94% conversion only after 96 h at 100 °C in dichloromethane to give a polymer with M_n 16,400 g mol⁻¹ (M_n calc = 13500 g mol⁻¹) and molecular weight distribution of 1.12.⁶⁷ The methoxide **1.2** exhibited similar behaviour, but the ethyl **1.3** and chloride **1.4** were inactive for the ROP of LA and CL.⁶⁸ Furthermore, in the presence of alcohol such as methanol (MeOH), these complexes efficiently initiated the ROP of ϵ -CL leading to polymers with narrow molecular weight distribution ($M_w/M_n < 1.15$). However, in absence of alcohol, the polymerization is less controlled with $M_w/M_n = 1.5$.⁶⁹

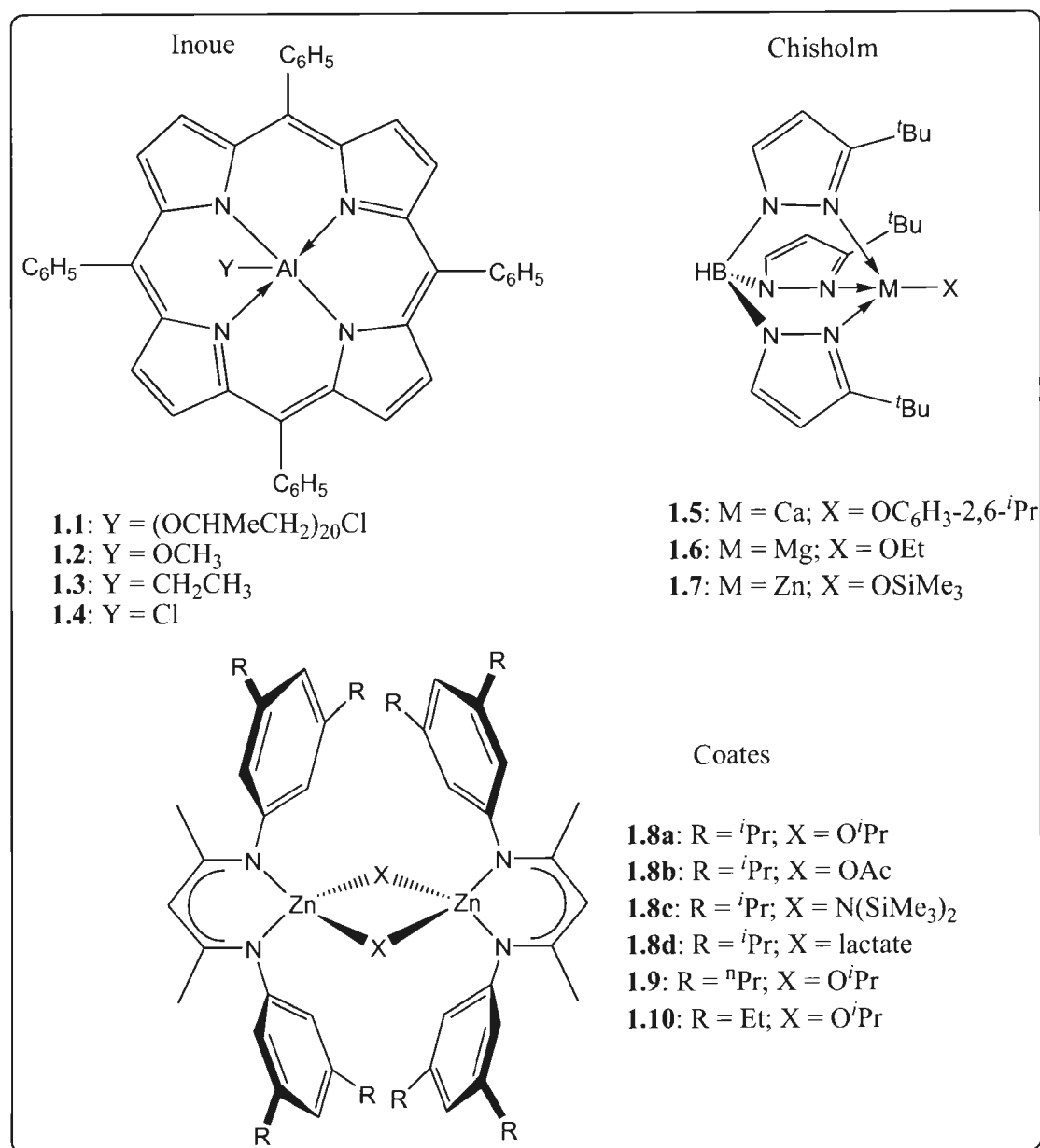


Figure 1.7. Single-site initiators supported by N-donor ligands for the ROP of cyclic esters

Tris(pyrazolyl)borate (TPB) metal complexes are important initiator systems in the history of ROP of cyclic esters, they confer the required steric hindrance around the metal

centre and thereby inhibit aggregation. Chisholm and co-workers synthesized a series of complexes of Mg, Ca and Zn supported by tris(pyrazolyl)borate ligands (Figure 1.7). The polymerization of 100 equivalent of *rac*-LA using complex **1.5** proceeded with up to 90% conversion in 60 seconds at room temperature using THF as the solvent.^{70,71} The polymerization of *rac*-LA using **1.6** afforded a linear relationship between M_n and LA monomer conversion, together with low polydispersities ($M_w/M_n = 1.10-1.25$).^{72,73} The zinc complex **1.7** is less active than the magnesium analogs (**1.6**). For example, at room temperature, **1.6** showed 90% conversion of 500 equivalents of *rac*-LA in 60 minutes in DCM, whereas, **1.7** requires 6 days to reach about the same conversion under identical conditions.⁷³ It was also found that the Ca complex exhibited good heteroselectivity in *rac*-lactide polymerization in THF ($P_s = 0.9$), which decreased when CH_2Cl_2 was used as the solvent. The enhanced ROP rate for Ca compared with Zn and Mg was attributed to the polarity difference within the initiating M-OR bond.⁷⁴

Numerous complexes based on bidentate N-donor ligands have been investigated for lactide ROP. Out of these, β -diketiminato ligands have attracted the greatest amount of attention due to the outstanding stereochemical control and activity shown by their metal complexes. Coates *et al.* reported a series of Zn complexes supported by β -diketiminato ligands and they found the complexes to act as single-site living initiators for the polymerization of *rac*-lactide and *meso*-lactide. The dinuclear (β -diketiminato)Zn isopropoxide complex **1.8** (Figure 1.7) achieved 95% conversion of 200 equivalents of *rac*-LA within 20 minutes at room temperature to highly heterospecific PLA with narrow polydispersity ($M_w/M_n = 1.10$) and a P_r value up to 0.90. The P_r value was improved to

0.94 at 0 °C after 2 h.⁷⁵ It was observed that the substituents on the β -diketiminato ligand play a crucial role in controlling the stereoselectivity and the rate of polymerization. For instance, changing the *i*Pr groups of **1.8** to *n*Pr (**1.9**) or Et (**1.10**) leads to a drop in heterotacticity to $P_r = 0.76$ and $P_r = 0.79$ respectively at 20 °C. In addition, the nature of the initiating group (X) on **1.8** significantly influenced both the molecular weight and the polydispersity of the polymers: the alkoxide groups (**1.8a** and **1.8d**) gave predictable M_n and narrow PDI (1.10 and 1.14), but acetate (**1.8b**), and amide (**1.8c**) complexes gave polymers with broad polydispersities (PDI = 2.95 and 2.07) and higher than expected molecular weights, probably due to slow rates of initiation *vs.* propagation.⁷⁶

1.9.3 Single-Site Initiators Supported by N-,O-donor ligands

A number of complexes supported by chelating N-,O- mixed donor ligands have been shown to be stereoselective in the polymerization of lactide through an enantiomeric site-control mechanism. Spassky *et al.* were the first to show that an aluminum alkoxide complex supported by a chiral binaphthyl Schiff-base ligand **1.11** and **1.12** (Figure 1.9) mediated a highly stereocontrolled polymerization of *rac*-lactide to furnish, at less than 50% conversion, predominantly isotactic PLA with P_m value of 0.88.^{49,77} At higher conversions, both enantiomers of *rac*-LA were polymerized affording (*RR*)- and (*SS*)-enriched polymers with narrow molecular weight distributions. Analysis of the resulting polymer revealed the microstructure of the polymer to be a tapered stereoblock (Figure 1.8) (where the monomer composition varied from *R*-units alone to *S*-units alone over the length of the polymer chain), which exhibited a high melting temperature (T_m) of 187 °C.

This is higher than that of enantiopure isotactic (*S*)-PLA or (*R*)-PLA, which have T_m between 170 and 180 °C.^{78,79}



Figure 1.8. Schematic structure of tapered isotactic PLA

Ovitt and Coates showed that the same catalyst with an isopropoxide initiating unit (**1.12**) afforded syndiotactic PLA from *meso*-lactide.⁸⁰ Radano and coworkers later reported that by using a racemic mixture of **1.12** in ROP of *rac*-lactide, enantiomerically pure PDLA and PLLA were produced.⁸¹ However, Coates *et al.* demonstrated that the actual structure of the resulting polymer was a stereoblock copolymer with a melting temperature of 179 °C.⁸² Furthermore, Majerska and Duda showed that using **1.12**, a true PLLA-PDLA stereoblock copolymer could be prepared via a ligand exchange mechanism. This mechanism entailed initiation from one enantiomer of the catalyst, while addition of the opposite enantiomer at 50% lactide conversion afforded a stereoblock copolymer through chain transfer.⁸³

Feijen and co-workers demonstrated the effects of slight changes in the backbone of the salen ligand toward the stereocontrol of polymers by using a diaminocyclohexane moiety in the salen ligand, **1.13** (Figure 1.9) for *rac*-LA polymerization. This complex, in contrast to Spassky's catalyst **1.11**, exhibited stereocontrol by preferential polymerization of L-LA over D-LA in toluene and bulk polymerization affording highly isotactic stereoblock PLA materials with high thermal stability ($T_m = 183.5$ °C) and P_m values of 0.93 and 0.88 respectively.^{84,85} The same group also reported *meso*-LA polymerization

using chiral aluminium salen complexes in the presence of isopropanol (**1.14a–c**, Figure 1.9). This occurred in a controlled manner ($M_{n,exp} = 6000\text{--}7000 \text{ g mol}^{-1}$ and $M_w/M_n = 1.09\text{--}1.12$) and produced syndiotactically biased PLAs ($P_r = 0.64, 0.69$ and 0.70 , respectively).⁸⁶

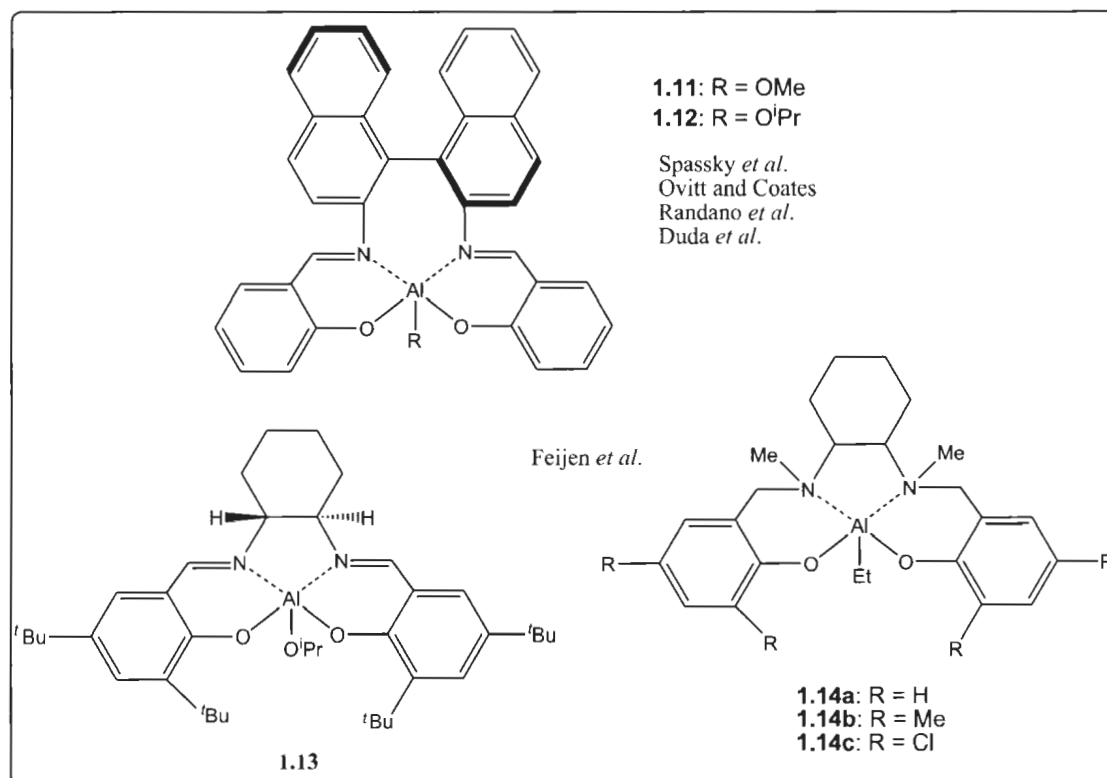


Figure 1.9. Chiral aluminum initiators bearing salen and salan ligands for the ROP of lactide.

In addition, several achiral salen-based catalysts have also been shown to exhibit very high levels of stereocontrol in the ROP of lactide. Nomura and co-workers found that *in situ* generated aluminum alkoxides from the achiral Schiff-base aluminum ethyl complexes (**1.15a–c**, Figure 1.10) and alcohol exhibited a very high level of stereocontrol

for the ROP of *rac*-lactide through a chain-end control mechanism. Investigation of the effects of the variation of both the imine spacer (ligand backbone) and the phenoxy substituents of the complexes on the kinetic and stereocontrol of the ROP of *rac*-LA revealed that the longer and less rigid imine spacer (propyl group) in combination with the most sterically hindering *ortho*-substituents (**1.15b**) afforded the greatest level of stereocontrol. It furnished PLA materials with an isotacticity ($P_m = 0.91$) higher than that of PLA obtained with a complex containing a shorter and more rigid ethylene diimine bridge (**1.15a**).⁸⁷ Further polymerizations conducted by the Nomura group employing a Schiff base aluminum complex with a flexible $-\text{CH}_2\text{C}(\text{Me})_2\text{CH}_2-$ imine spacer and more bulky $^t\text{BuMe}_2\text{Si}$ substituents at the *ortho* position of the phenol groups (**1.15c**) afforded stereoblock PLA from *rac*-lactide with a P_m value of 0.98 and T_m of 210 °C.⁸⁸ Gibson and co-workers independently reported extensive work on the effect of variation of the ligand substituents of various aminophenol (salan-base) aluminum alkoxide complexes (Figure 1.10) generated by *in situ* alcoholysis of the respective salan-base aluminum ethyl complexes using benzyl alcohol. Results of the polymerization of *rac*-LA conducted at 70 °C in toluene revealed that by variation of the ligand substituents, the stereoselectivity could be manipulated such that tacticities of PLA ranging from $P_r = 0.21$ to $P_r = 0.96$ could be obtained. It was found that electron withdrawing phenoxy substituents increased the rate of polymerization, while a longer amine spacer enhanced stereocontrol.⁸⁹

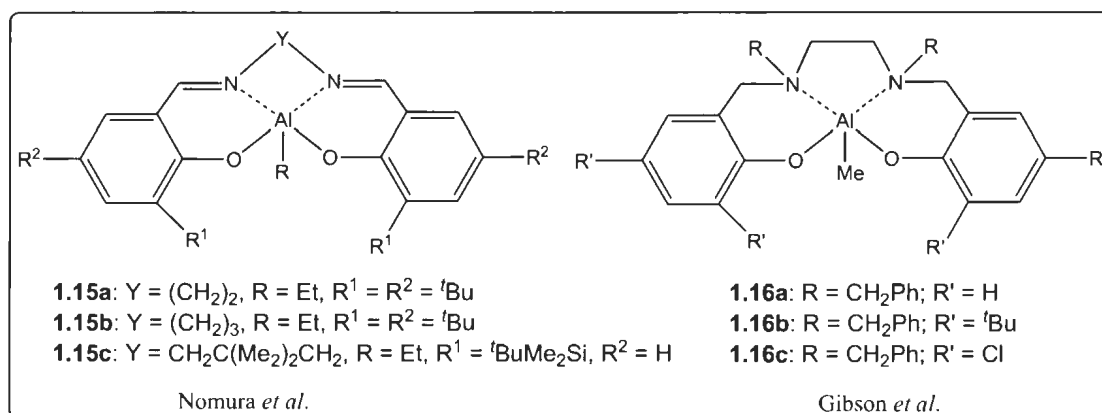


Figure 1.10 Achiral aluminum initiators bearing salen and salan ligands for the ROP of lactide

1.9.4 Single-Site Initiators Supported by Monanionic N,O-Donor Ligands

The research described in this thesis focuses on zinc, lithium and aluminum complexes stabilized by monoanionic aminephenolate ligands for the ROP of cyclic esters. Thus, the following section will discuss a literature overview of some of the metal catalysts supported by phenolate and related ligands employed for polymerization of cyclic esters.

Chisholm *et al.* described zinc complexes of a half salen ligand bearing amide or phenoxide initiating groups (**1.17a** and **1.17b**, Figure 1.11), which catalyzed the polymerization of both L-LA and *rac*-LA in benzene at room temperature affording 90% conversion in 3 h and 72 h respectively. The lower rate for the complex with the phenoxide initiating unit (**1.17b**) was attributed to the steric demands of the 2,6-*tert*-butylphenoxide used.⁹⁰

Lin and co-workers synthesized a series of zinc complexes supported by NNO-tridentate Schiff-base ligands (**1.18a-d**, Figure 1.11) for ROP of *rac*-LA. The

polymerization was well controlled (PDI = 1.07-1.26) and it was observed that the tacticity of the polymer was significantly influenced by the ligand used. For instance, changing the ligand from a less steric to a sterically bulkier ligand at 25 °C resulted in an increase in P_r from 0.59 to 0.74. For the zinc complex bearing bulkier *tert*-butyl substituents on the phenoxy group, polymers with narrower molecular weight distribution (PDI = 1.13) and better stereochemical control ($P_r = 0.74$) were obtained. However the activity of the complex was reduced, requiring 6 h to reach 98% conversion of the monomer. Reduction of steric hindrance led to a reduction in heterospecificity as the analogue of this complex with no alkyl substituents on the phenoxy group exhibited weak stereoselectivity furnishing heterotactic PLA with a P_r value of 0.59 under identical reaction conditions. Furthermore, modification of the ligand by increasing the steric hindrance and introducing electron donating groups on the imine carbon significantly enhanced the rate of reaction, thus leading to ROP of L-LA at 0 °C in 4 minutes and conversions of 100% to afford PLAs with narrow molecular weight distributions.^{91,92}

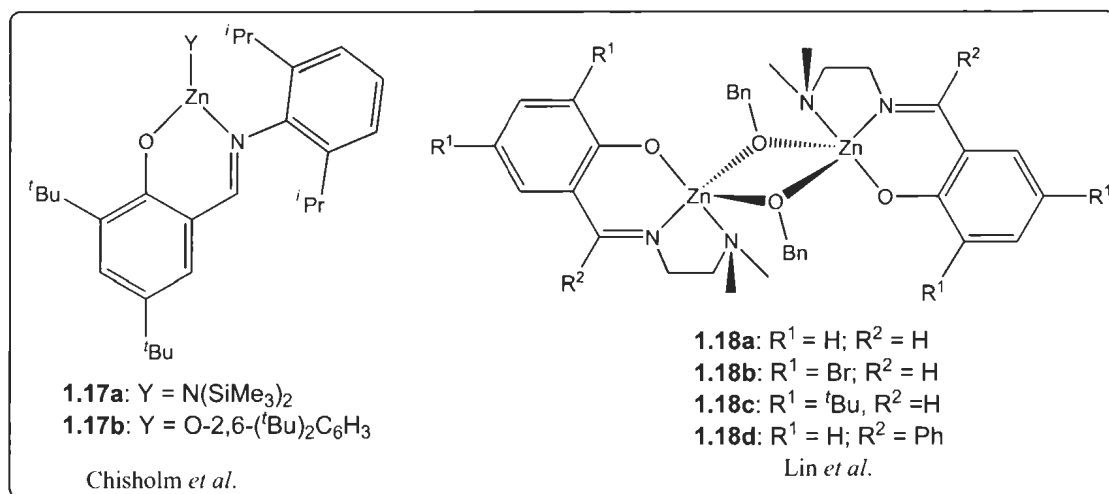


Figure 1.11. Single-site zinc complexes supported by half salen ligands for the ROP of lactide

Hillmyer and Tolman described the synthesis of a dizinc monoethoxide complex (**1.19**, Figure 1.12) bearing a phenoxy based ancillary, which possessed two ethylenediamine units bonded at the *ortho* sites of the phenoxy ring. They successfully used the complex for rapid polymerization of *rac*-LA in dichloromethane to give atactic PLA (90% conversion, 30 minutes and room temperature). The complex afforded polymer with a narrow molecular weight distribution (PDI = 1.19) and exhibited living catalyst behavior.⁹³ Inspired by these promising results, the same group further investigated an alkoxo bridged bimetallic complex (**1.20**, Figure 1.12), which was reported to be highly active for the polymerization of *rac*-LA in dichloromethane and room temperature. High conversions and narrow molecular weight distributions (PDI = 1.34-1.42) were obtained over a wide range of monomer-to-catalyst ratios. Even at a ratio of 1500, conversion of 93% was observed in 18 minutes to afford polymer with high

molecular weight (130 kg mol^{-1}).⁹⁴ This feat makes it the most active zinc-based catalyst for lactide polymerization, however, no stereochemical control was observed.

Sobota and co-workers reported the synthesis of hetero- (**1.21**) and homoleptic (**1.22**) zinc complexes (supported by an aminophenolate ligand (Figure 1.12)). The complexes efficiently initiated the ROP of L-LA at room temperature in dichloromethane with the heteroleptic zinc alkoxide complex reaching 98% conversion in 2 h, while the homoleptic analogue in the presence of benzyl alcohol as co-catalyst achieved near quantitative conversion in 1 h. Both complexes afforded PLAs with narrow molecular weight distributions (PDI = 1.09 and 1.16 respectively).⁹⁵

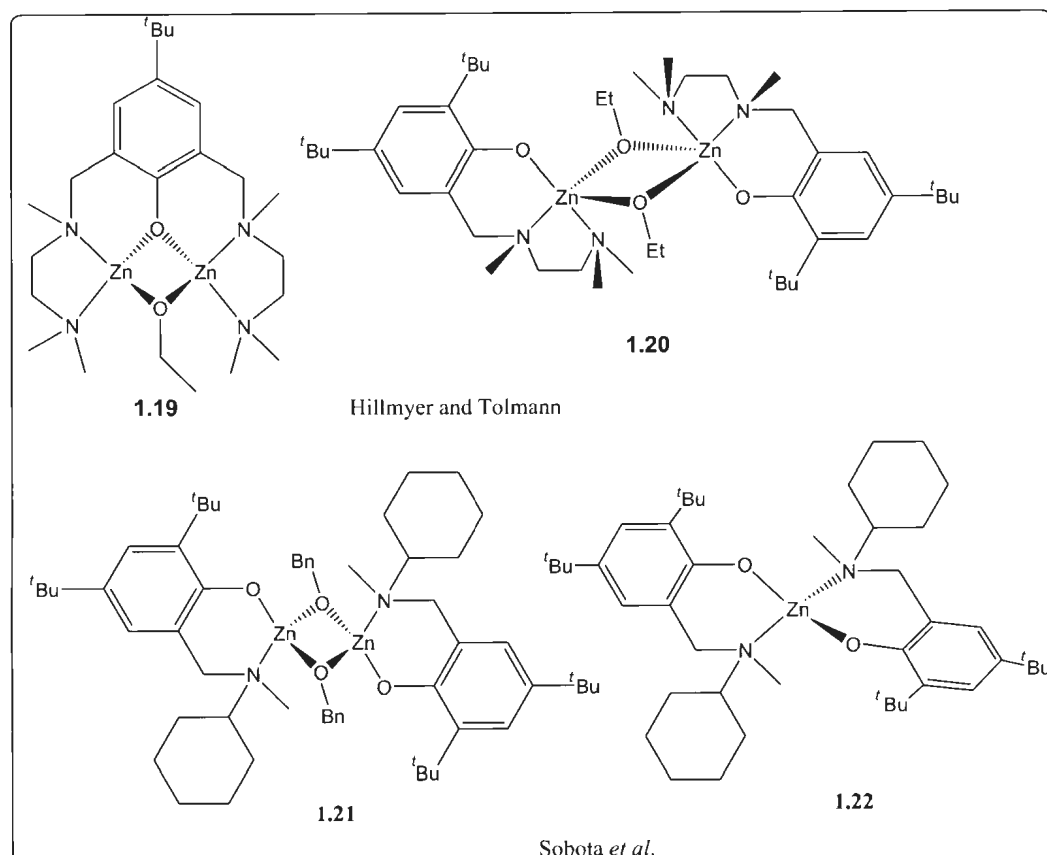


Figure 1.12. Single-site initiators supported by monoanionic N-,O-donor ligands for the ROP of lactide

1.9.5 Lithium Complexes Used for the ROP of Cyclic Esters

In an effort to develop efficient and biocompatible catalysts for the preparation of PCL and PLA, several alkali metal complexes such as lithium complexes have been employed and found to be active for the ring-opening polymerization of cyclic esters.

Xie *at al.* reported that lithium chloride effectively initiated the ROP of lactide in the presence of ethylene glycol and methyl α -D-glucopyranoside as co-initiator affording PLA with high polydispersity indices (>2.2).⁹⁶ Kricheldorf and Kasperczyk described the use of butyllithium and lithium *tert*-butoxide respectively as efficient initiators for ROP of lactide.⁹⁷⁻⁹⁹ These compounds are effective initiators, but due to their highly basic nature the polymerization reactions were not controlled, which led to side reactions that resulted in polymers with very broad molecular weight distributions.

In order to circumvent the inherent side reactions, Lin and co-workers adopted the strategy of introducing the bulky ligand [2,2-ethylidene-bis(4,6-di-*tert*-butylphenol)] (EDBP-H₂) to provide steric hindrance around the active lithium ions. By the reaction of EDBP-H₂ and ⁿBuLi, the cage-like lithium complex (**1.23**) was obtained from which lithium alkoxide (**1.24**) can be subsequently prepared by alcoholysis as shown in Figure 1.13. The lithium alkoxide (**1.24**) was found to be efficient initiator for the ROP of L-lactide in dichloromethane at 25 °C, reaching completion within 1 h. The reaction rate decreases with decrease in temperature, for example, at 0 °C, the polymerization reached completion within 6 h. However, the PLA obtained at 0 °C had a narrower molecular weight distribution (1.11) than that obtained at room temperature (1.43).¹⁰⁰

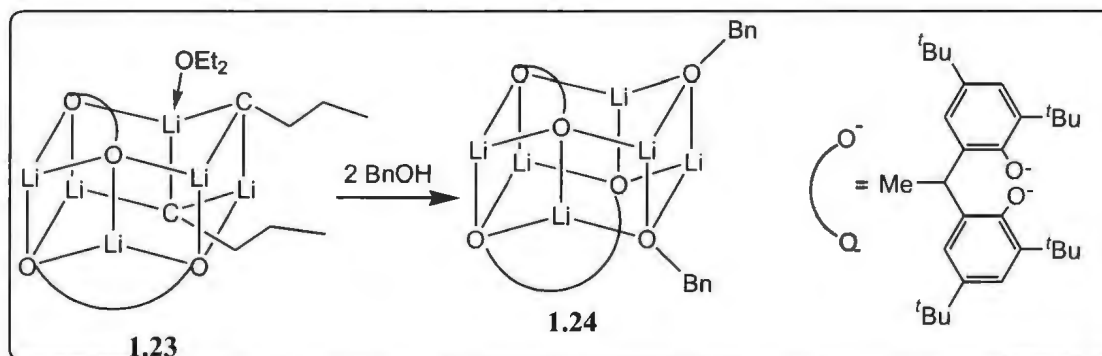


Figure 1.13. Bisphenolate hexalithium alkoxide complex for the ROP of cyclic esters.

As part of continuing efforts to develop efficient catalysts/initiators for ring-opening polymerization of cyclic esters, Chen *et al.* reported the synthesis of tetranuclear lithium complexes bearing multidentate amine bis(phenolate) ligands (**1.25a-c**, Figure 1.14) and their catalytic activities toward ROP of L-lactide.¹⁰¹ Poor conversions and poor PDI values were observed for the complexes. The addition of benzyl alcohol as co-initiator allowed efficient catalytic activities to be achieved (conversion above 93% within 20 minutes).

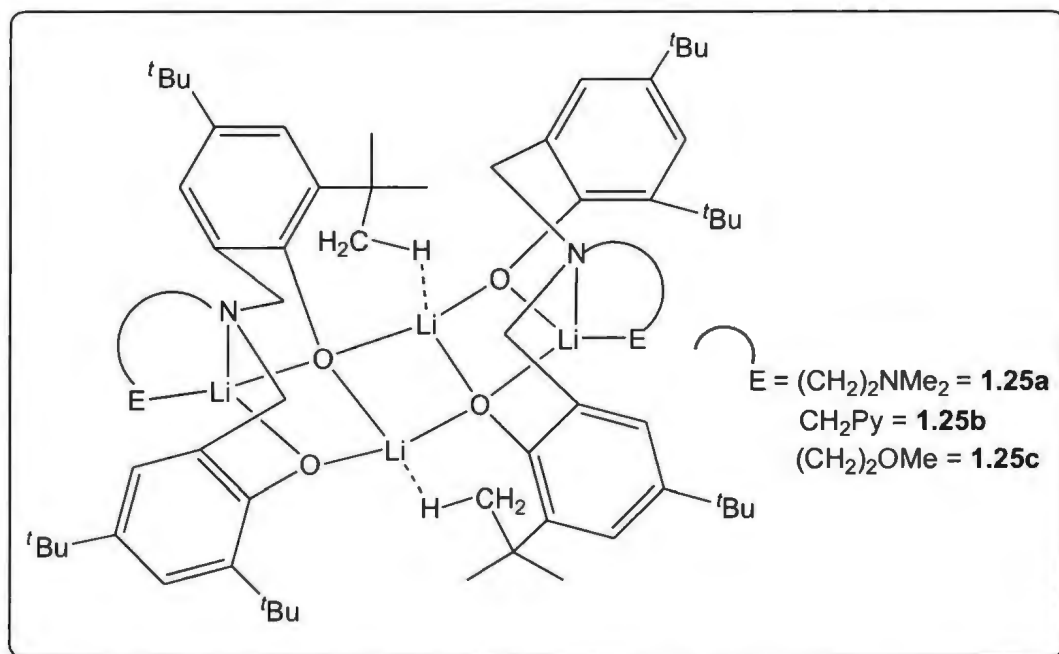


Figure 1.14. Amine bis(phenolate) tetralithium complexes for the ROP of cyclic esters

Chen and co-workers also described the synthesis of lithium complexes bearing mono-anionic aminephenolate ligands (**1.26a-d**, Figure 1.15), which is relevant to the work in this thesis. They found that the complexes demonstrated efficient activity in catalyzing ring-opening polymerization of L-lactide in the presence of benzyl alcohol, with living character at 26.5 °C. Relating to structure/activity relationships, they observed that the complexes with pendant amine functionalities (**1.26c**) exhibited higher rates of reaction than those with pendant methoxy or thioether functionalities.¹⁰²

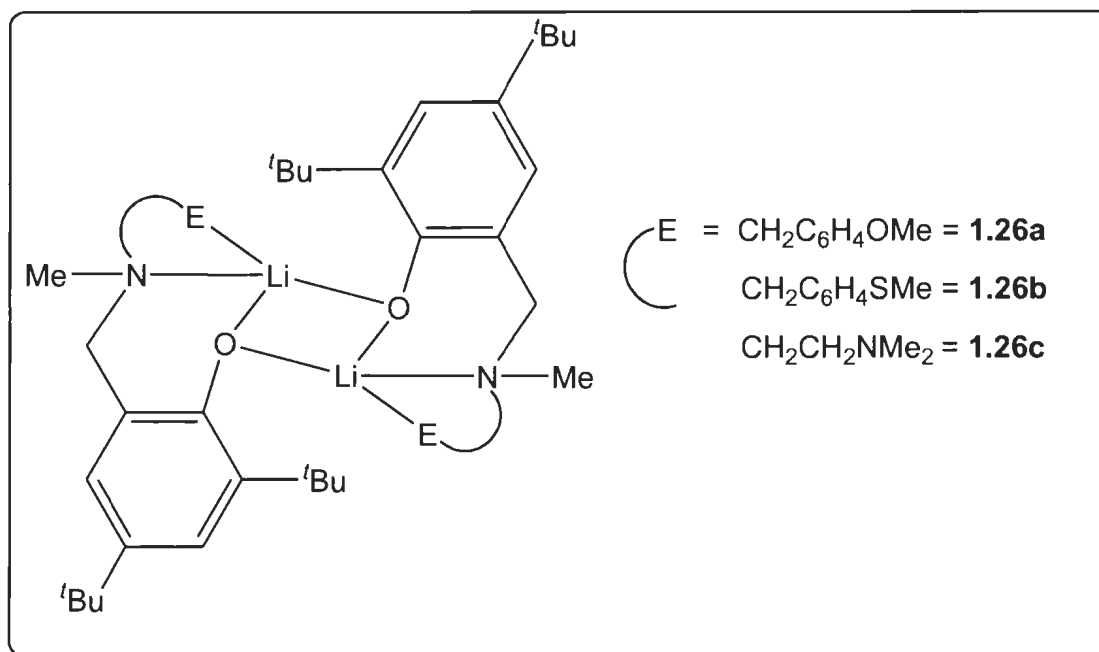


Figure 1.15 Monoanionic aminophenolate dinuclear lithium complexes for the ROP of cyclic esters

1.9.6 Al, Zn, and Li Amine-Phenolate Complexes Used for ROP of ϵ -CL

Chen *et al.* reported the use of monomeric five-coordinate aluminum complexes supported by dianionic amine bis(phenolate) ligands (**1.27a** and **b**, Figure 1.16) to catalyze the polymerization of ϵ -caprolactone. The polymerization reactions were carried out in toluene at 50 °C and evidence for controlled “living” polymerization was given by the narrow molecular weight distributions, the linear relationship between the number-average molecular weight (M_n) and the monomer-to-initiator ratio ($[\epsilon\text{-CL}]_0/[\text{Al}]_0$). This was corroborated by the resumption experiment (addition of another portion of ϵ -CL monomer after the polymerization of the first addition had gone to completion), which led

to an incremental increase in molecular weight from the first polymer ($M_n = 8.77 \text{ kg mol}^{-1}$ for **1.27a**; 11.7 kg mol^{-1} for **1.27b**) to the final polymer ($M_n = 20.3 \text{ kg mol}^{-1}$ for **1.27a**; 21.6 kg mol^{-1} for **1.27b**).¹⁰³

In 2005, Nomura and co-workers reported a systematic investigation of ligand substituents for the polymerization of ϵ -CL using Al salicylaldimine complexes (**1.28a-c**, Figure 1.16). The polymerization of ϵ -CL was carried out at $25 \text{ }^\circ\text{C}$ in the presence of benzyl alcohol (BnOH). They noted that no reaction took place in the absence of BnOH and that a complex having a sterically demanding imine moiety enhanced the polymerization. For example, the best polymerization result was obtained by **1.28a** (the complex with the sterically demanding 2,4,6-tri-*tert*-butylphenylimine moiety and a methyl substituent at the 3- and 5-positions of the salicylidene moiety). This complex afforded nearly quantitative conversion of CL within 10 min to give PCL with narrow polydispersity ($M_w/M_n = 1.16$).¹⁰⁴

Recently, amine-bis(phenolate) aluminum complexes bearing a piperazine (**1.29**)¹⁰⁵ or homopiperazine (**1.30**)¹⁰⁶ backbone have been reported to be active for the ROP of ϵ -CL. The dimeric aluminum complex **1.29** was reported to show high catalytic activity by polymerizing 2000 equiv of ϵ -CL to 96% yield within 12 h at $20 \text{ }^\circ\text{C}$ in the presence of 1 equiv of BnOH.¹⁰⁵ Complex **1.30** initiated the polymerization of 300 equivalents of ϵ -CL at $130 \text{ }^\circ\text{C}$ and up to 97% conversion can be achieved within 30 minutes to afford PCL with reasonable PDI (1.54).¹⁰⁶

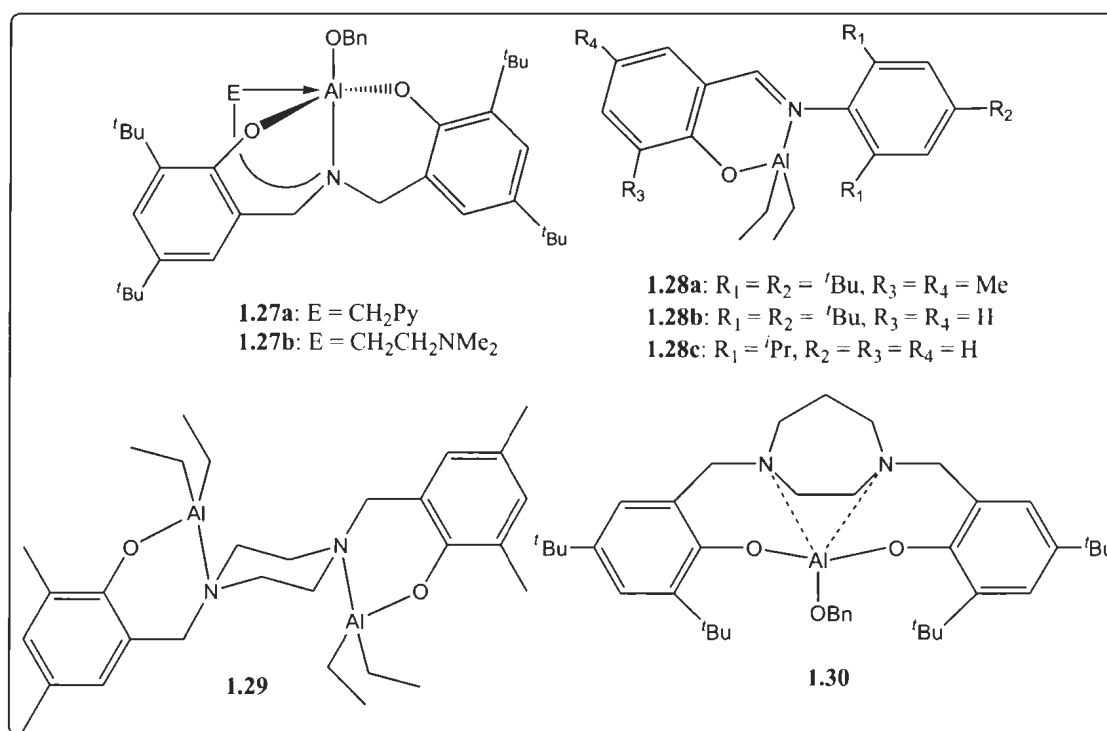


Figure 1.16. Aluminum complexes supported by amine-phenolate ligands used for the ROP of ϵ -CL

Silvernail *et al.* reported the synthesis of amine-bis(phenolate) zinc complex **1.31** (Figure 1.17) and its application for the controlled ROP of ϵ -CL in the presence of BnOH at 25 °C using THF as the solvent. It was observed that low [CL]₀/[Zn]₀ ratios and high monomer concentration was necessary to achieve >85% monomer conversion, narrow PDIs (1.08-1.24), and predictable molecular weights in reasonable reaction times. From the kinetic study, they found that the overall data support an activated-monomer mechanism for the polymerization of ϵ -CL that involves equilibria among various monomeric forms of **1.31-S** (S = THF, BnOH, and CL).¹⁰⁷

Darensbourg *et al.* synthesized zinc complexes bearing pendant arm tridentate Schiff base ligands (**1.32a** and **b**, Figure 1.17), which were found to be active catalysts for the ROP of ϵ -CL, providing polymers with the expected molecular weights and with low PDI. The polymerizations carried out in C_6D_6 at ambient temperature were found to be first-order in monomer concentrations, affording the rate constants of $2.17 \times 10^{-3} M^{-1} s^{-1}$ for **1.32a** and $2.90 \times 10^{-3} M^{-1} s^{-1}$ for **1.32b**. They also conducted the polymerization reaction in the melt at 110 °C and a pseudoliving character for the ROP was observed as evidenced in the linear relationship between M_n and the monomer/initiator ratio. However, the PDIs were rather broad (1.23-1.56). In addition, the molecular weights of the PCL were not in agreement with their expected theoretical values, which suggest the existence of transesterification occurring during the polymerization process.¹⁰⁸

Recently, Shaver *et al.* examined the structure/activity relationships of aluminum initiators coordinated to a single tridentate Schiff base ligand (**1.33a-c**, Figure 1.17) in ϵ -CL polymerization. They conducted the polymerizations in monomer:catalyst ratios of 100:1 in toluene at room temperature. The complexes initiated the polymerization of ϵ -CL. However, polydispersities (PDIs = 1.71-1.79) were high and observed molecular weights were higher than expected from monomer conversion. Thus, none of the catalysts were effective at controlling the polymerization.¹⁰⁹

Liang and co-workers reported the synthesis and utilization of an amine-bis(phenolate) lithium complex (**1.34**, Figure 1.17) for the ROP of ϵ -CL in the presence and absence of alcohol at room temperature to give high molecular weight PCL with narrow PDIs. They observed that the presence of benzyl alcohol effectively increases the

ROP rates, though at the expense of slightly wider molecular weight distributions. For example, in the presence of BnOH, the conversion was 69% and the PDI of the polymer was 1.18 after 12 h, while in the presence of BnOH, the conversion was 96% and the PDI was 1.24 under identical reaction conditions.¹¹⁰

It is worth noting that there are only a few publications regarding amine-mono(phenolate) lithium complexes as polymerization initiators for cyclic esters. Thus, the field of monoanionic aminephenolates is relatively unexplored in comparison with the analogous dianionic bis(phenolate)s discussed earlier (Sections 1.9.5 and 1.9.6).

The ROP activity for the complexes reported in the literature and discussed in this introductory Chapter is summarized in Table 1.2. It is clear that some complexes (e.g. **1.5**, **1.6**, **1.8** and **1.18** for LA; **1.28**, **1.29** and **1.31** for CL polymerization) exhibit high activity and good control, whereas other complexes perform ROP at a much slower rate and with less control over molecular weight distribution and stereochemistry.

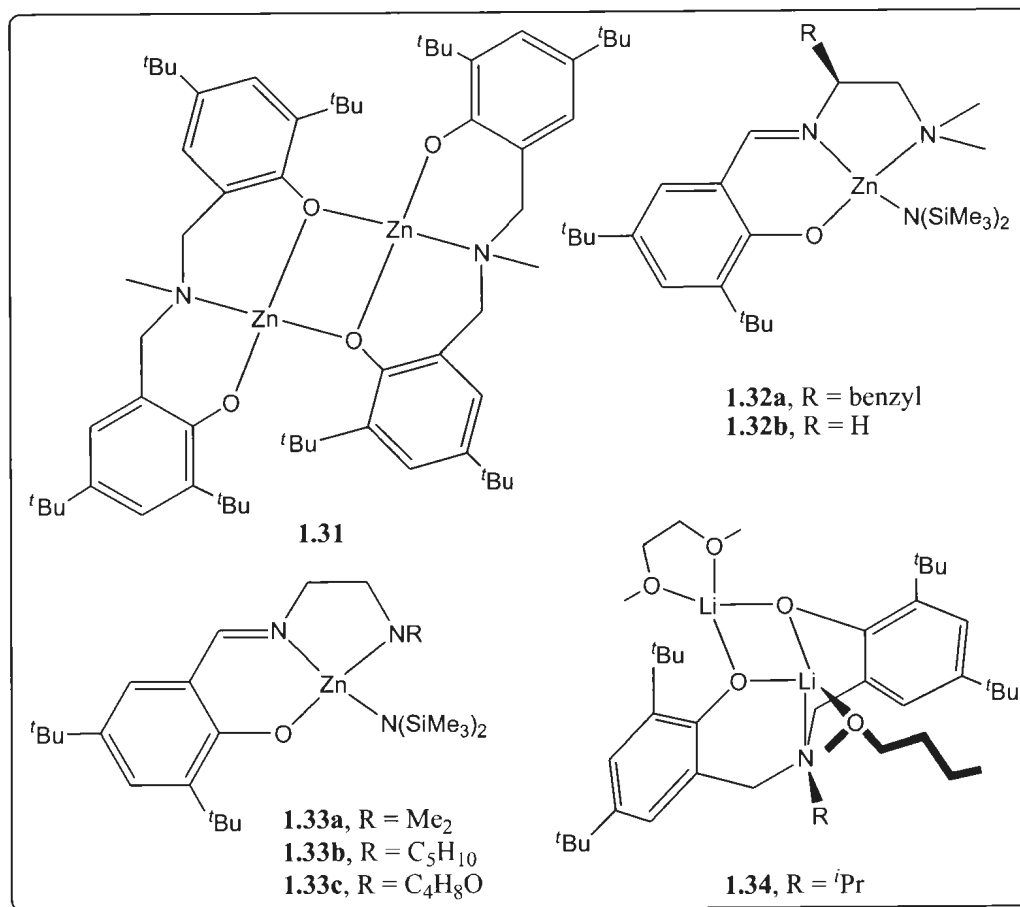


Figure 1.17. Li and Zn complexes bearing amine-bis(phenolate) ligand used for the ROP of ϵ -CL

Table 1.2. Comparison of the activity of various metal complexes used for catalytic ROP of LA

Initiator	Ligand	Monomer (equiv)	Conditions	Conv. (%)	M_n^a (kg mol ⁻¹)	M_w/M_n	P_r	Ref
1.1-Al	TPP	D-LA (100)	100 °C, 96 h, DCM	94	16.4	1.12		68
1.3-Al				0				69
1.4-Al	TPP	D-LA (100)	100 °C, DCM	0				69
1.5-Ca	TPB	<i>rac</i> -LA (200)	25 °C, 60 s, THF	90	40.1	1.68	0.90	71,72
1.6-Mg	TPB	<i>rac</i> -LA (500)	25 °C, 60 min, DCM	90				73,74
			$k_{\text{obs}} = 3.9 \times 10^{-2} \text{ min}^{-1}$					
1.7-Zn	TPB	<i>rac</i> -LA (500)	25 °C, 6 d, DCM	90				74
			$k_{\text{obs}} = 7.8 \times 10^{-4} \text{ min}^{-1}$					
1.8a-Zn	BDI	<i>rac</i> -LA (200)	25 °C, 20 min, DCM	95	37.9	1.10	0.90	76
		<i>rac</i> -LA (200)	0 °C, 2 h, DCM	95	38.8		0.94	76
1.8b-Zn		<i>rac</i> -LA (200)	20 °C, 70 h, DCM	92	61.4	2.07	0.94	76
1.8c-Zn		<i>rac</i> -LA (200)	20 °C, 10 h, DCM	34	38.8	2.95		77
1.8d-Zn		<i>rac</i> -LA (200)	20 °C, 20 min, DCM	97	30.5	1.14		77
1.9-Zn	BDI	<i>rac</i> -LA (200)	20 °C, 19 h, DCM	97	35.8	1.18	0.76	77
1.10-Zn		<i>rac</i> -LA (200)	20 °C, 8 h, DCM	97	42.5	1.09	0.79	77

^a M_n determined from GPC, TPP = tetraphenylporphyrin, TPB = tris(pyrazolyl)borate, BDI = β -diketiminate

Table 1.2. continued

Initiator	Ligand	Monomer (equiv)	Conditions	Conv. (%)	M_n (kg mol ⁻¹)	M_w/M_n	P_r	Ref
1.11-Al	SalenBinap	<i>rac</i> -LA (75)	70 °C, 12 d, toluene	98	12.7	1.27		78
1.12-Al	SalenBinap	<i>meso</i> -LA (100)	70 °C, 40 h, toluene	94	12.0 (13.5)	1.05	0.96	80
<i>rac</i> - 1.12-Al	SalenBinap	<i>meso</i> -LA (100)	70 °C, 40 h, toluene	98	13.6 (15.0)	1.07	0.80	82
	SalenBinap	<i>rac</i> -LA (100)	80 °C, 7.5 h, THF	93	3.40 (3.10)	1.10		83
1.13-Al	SalenBinap	<i>rac</i> -LA (62)	70 °C, 12 d, toluene	85	7.70 (7.60)	1.06	0.93	84
		<i>rac</i> -LA (200)	130 °C, 2d, bulk	95	24.9 (27.3)	1.37	0.88	85
1.14-Al / ^{<i>i</i>} PrOH	Salen	<i>meso</i> -LA (100)	70 °C, toluene,					
			(a) 23 h	97	5.79 (7.01)	1.12	0.64	
			(b) 27 h	94	5.86 (6.74)	1.10	0.69	86
			(c) 27 h	83	4.38 (5.99)	1.09	0.70	
1.15-Al /BnOH	Salen	<i>rac</i> -LA (100)	70 °C, toluene,					
			(a) 72 h	19	5.30	1.07	0.79	87
			(b) 14 h	95	22.4	1.06	0.92	
			(c) 27 h	83	20.2	1.08	0.93	88
1.16-Al /BnOH	Salan	<i>rac</i> -LA(100)	70 °C, toluene,					
			(a) 21 h	98	21.2	1.08	0.21	89
			$k_{app} = 7.98 \times 10^{-6} \text{ s}^{-1}$					
			(b) 120 h	77	11.3	1.05	0.61	
			$k_{app} = 3.4 \times 10^{-6} \text{ s}^{-1}$					
			(c) 21 h	94	17.8	1.06	0.96	
			$k_{app} = 37.8 \times 10^{-6} \text{ s}^{-1}$					

Table 1.2. continued

Initiator	Ligand	Monomer (equiv)	Conditions	Conv. (%)	M_n (kg mol ⁻¹)	M_w/M_n	P_r	Ref
1.17-Zn	Salen	<i>rac</i> -LA (20)	25 °C, benzene, (a) 3 h (b) 72 h	90 90				
1.18-Zn	Salen	<i>rac</i> -LA (100)	25 °C, DCM, (a) 4 h (b) 4 h (c) 6 h	97 95 98	6.30 10.7 10.5	1.26 1.07 1.13	0.59 0.65 0.74	91
1.19-Zn	Amine-phenolate	<i>meso</i> -LA (100) <i>rac</i> -LA (300)	0 °C, (d) 4 min, DCM 25 °C, 30 min, DCM $k_{app} = 9 \times 10^{-4} \text{ s}^{-1}$	100 90	17.4 20.6	1.12 1.19		92 93
1.20-Zn	Amine-penolate	<i>rac</i> -LA (1500)	25 °C, 18 min, DCM	93	130	1.34		94
1.21-Zn	Amine-penolate	L-LA (100)	25 °C, 2 h, DCM	98	14.2	1.09		95
1.22-Zn/BnOH	Amine-penolate	L-LA (100)	25 °C, 1 h, DCM	99	14.4	1.16		95
1.24-Li	Bisphenolate	L-LA (150)	25 °C, 1 h, DCM 0 °C, 6 h, DCM	99 98	12.8 9.70	1.43 1.11		100
1.25-Li/BnOH	Amine- bisphenolate	L-LA (100)	26.5 °C, toluene, (a) 20 min (b) 25 min (c) 35 min	93 94 88	20.0 18.9 20.1	1.18 1.15 1.15		101
1.26-Li/BnOH	Amine-phenolate	L-LA (500)	26.5 °C, 5 min, DCM	93	5.60	1.19		102

Table 1.3. Comparison of the activity of various metal complexes used for catalytic ROP of ϵ -CL

Initiator	Ligand	Monomer (equiv)	Conditions	Conv. (%)	M_n (kg mol ⁻¹)	M_w/M_n	Ref
1.27a -Al	Amine- bis(phenolate)	ϵ -CL (50)	50 °C, toluene, 2 h	93	20.3	1.04	103
1.27b -Al	Amine- bis(phenolate)	ϵ -CL (50)	50 °C, toluene, 30 min	99	21.6	1.04	103
1.28a -Al	Half salen	ϵ -CL (100)	25 °C, toluene, 10 min	96	29.8	1.16	104
1.28b -Al	Half salen	ϵ -CL (100)	25 °C, toluene, 60 min	86	26.1	1.18	104
1.28c -Al	Half salen	ϵ -CL (100)	25 °C, toluene, 24 h	97	26.6	1.19	104
1.29 -Al/BnOH	Amine- bis(phenolate)	ϵ -CL (2000)	20 °C, DCM, 12 h	96	13.8	1.28	105
1.30 -Al	Amine- bis(phenolate)	ϵ -CL (300)	130 °C, melt, 30 min.	97	73.1	1.54	106
1.31 -Zn/BnOH	Amine- bis(phenolate)	ϵ -CL (50)	25 °C, 4 h, THF	91	1.70	1.24	107
1.32a -Zn	Half salen	ϵ -CL (200)	110 °C, melt, 1 h	99	13.6	1.55	108
1.33b -Zn	Half salen	ϵ -CL (100)	25 °C, 2 h, toluene	72	25.2	1.72	109
1.34 -Li	Amine- bis(phenolate)	ϵ -CL (100)	25 °C, 12 h, toluene	96	11.0	1.24	110

1.10 Reactions Using Carbon Dioxide as a Feedstock

Considering the steadily increasing concentration of CO₂ in the atmosphere, its utilization in synthetic chemistry is very attractive, particularly on an industrial scale. In the last four decades, considerable research has been performed to find technological routes to transform CO₂ into molecules such as urea, salicylic acids, cyclic carbonates and polymers in an economic way.^{111,112} Figure 1.18 outlines some reactions that utilize CO₂ to produce organic chemicals or intermediates for the chemical industry. For example, Bayer MaterialScience in 2011 started a new pilot plant at Chempark Leverkusen, Germany for a catalytic process in which CO₂ is used as a reactant to produce polyether polycarbonate polyols (PPPs), a feedstock for making polyurethanes.¹¹³

Also CO₂ can be converted *via* chemical, photochemical and electrochemical processes into energy storage chemicals, such as syngas, formic acid, methane, ethylene, methanol, and dimethyl ether (DME).^{114,115} Considerable research is being conducted in many directions to further the economic viability of these processes.^{116,117} For example, Carbon Recycling International (CRI) developed the world's first commercial scale plant in Iceland that utilizes hydrogen (H₂) and CO₂ to produce about five million litres of renewable methanol per annum. The CO₂ feedstock and renewable power for the electrolysis of water to produce hydrogen are both supplied by the nearby geothermal power plant.¹¹⁸

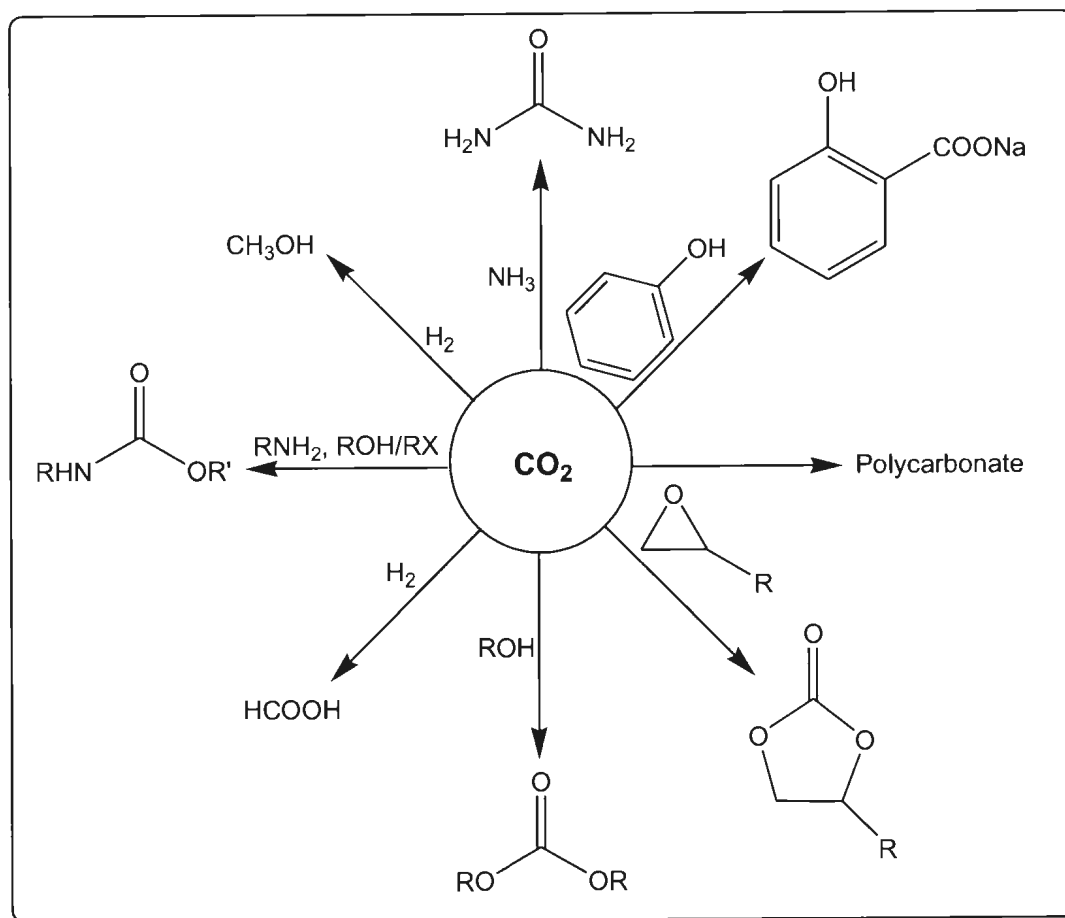
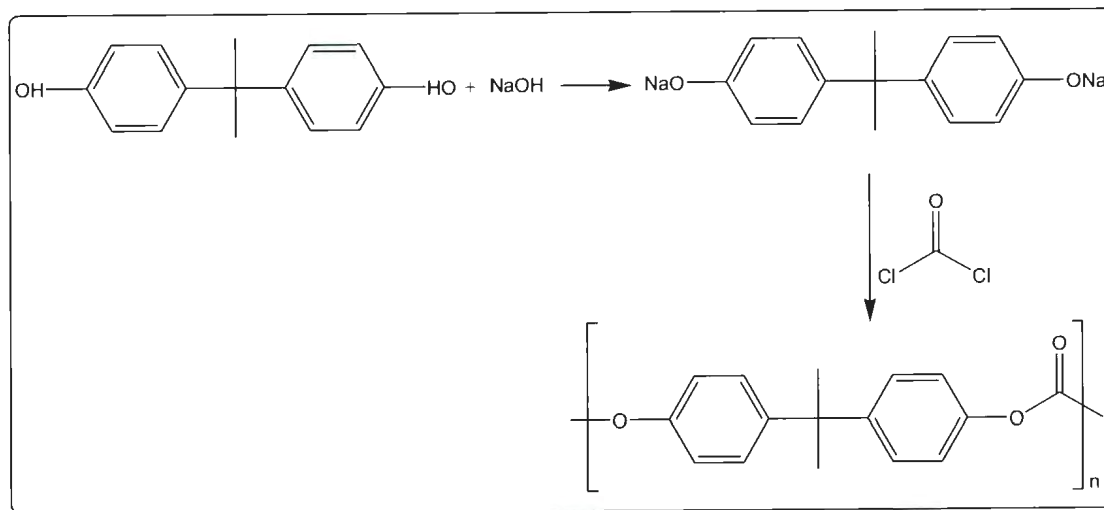


Figure 1.18. Chemical transformation of CO₂ into commodity chemicals

1.11 Synthesis of Polycarbonate and/or Cyclic Carbonates *via* Reaction of CO₂ and Epoxides

In 1969, Inoue and co-workers discovered that a mixture of ZnEt₂ and H₂O was active for catalyzing the alternating copolymerization of propylene oxide (PO) and CO₂. An optimum 1:1 ratio of ZnEt₂/H₂O gave the best yields of methanol-insoluble PPC, with an activity of 0.12 h⁻¹ at 80 °C and 20–50 atm CO₂.^{119,120}

This new discovery by Inoue provided a beneficial utilization of CO₂ and an environmentally friendly alternative route to the production of polycarbonate in contrast to the conventional route which uses large amounts of hazardous phosgene and bis(phenol) A (BPA) (Scheme 1.9).^{6,121}

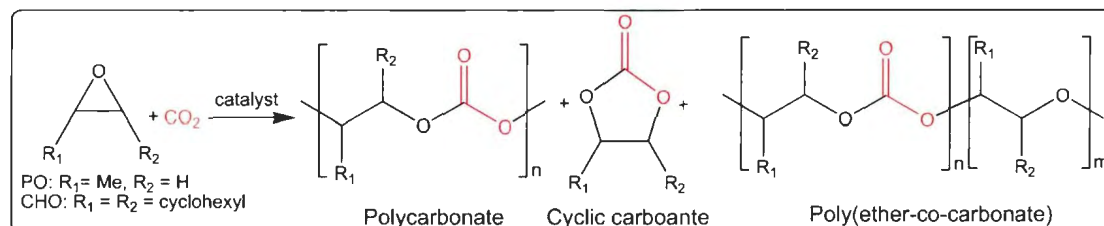


Scheme 1.9. Industrial synthesis of polycarbonate of phosgene [Poly(oxycarbonyloxy-1,4-phenylenedimethylmethylene-1,4-phenylene)]¹²¹

Following this discovery, Inoue developed other heterogeneous catalysts based upon a combination of ZnEt₂ and several dihydric sources such as resorcinol, dicarboxylic acids and primary amines for copolymerization of propylene oxide and CO₂.¹²²⁻¹²⁵ However, the polymerization reactions with the catalysts could not be well controlled and usually resulted in polymers of wide polydispersities and unpredictable molecular weights. As a consequence, several homogenous catalysts have been developed for this reaction.

The homogeneous copolymerization of CO₂ and epoxides can be mediated by various Lewis acidic metal halides, carboxylate or alkoxide/aryloxide complexes and it is proposed to occur *via* a coordination-insertion mechanism.⁷ Besides the alternating

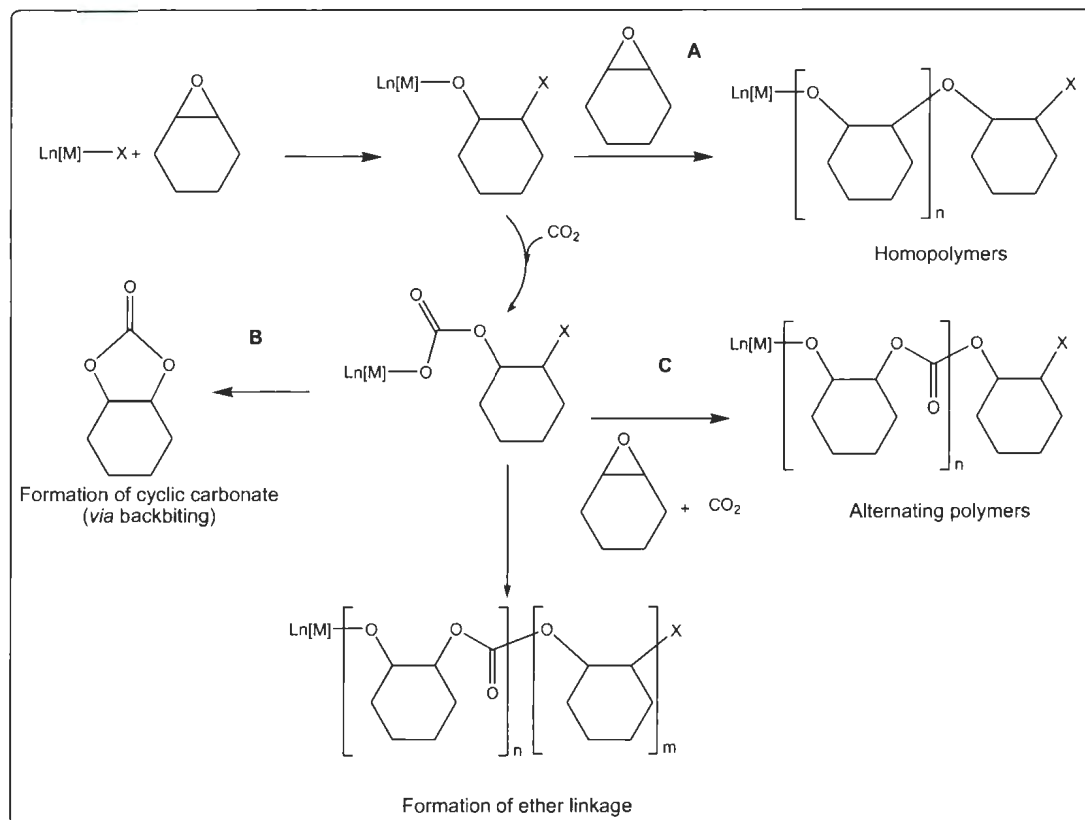
copolymerization of epoxides/ CO_2 to polycarbonate, the reaction can also yield other products such as cyclic carbonate and/or poly(ether-co-carbonate) (Scheme 1.10).



Scheme 1.10. General catalytic reaction of epoxides and CO_2 generating polycarbonate, cyclic carbonate and/or poly(ethercarbonate) [PO = propylene oxide; CHO = cyclohexene oxide]

The metal complex initiates the ring-opening of the epoxide by coordination of the monomer to the metal centres followed by attack at a methine carbon by a nucleophilic group (nucleophilic axial/leaving group or added co-catalyst e.g. chloride ion), which leads to the formation of a metal-bound alkoxide (Scheme 1.11).^{5,6} Consecutive epoxide ring-opening and insertion into the metal-alkoxide bond leads to homopolymerization to form polyether (Pathway A). On the other hand, CO_2 insertion into the metal-alkoxide bond forms a metal-bound carboxylate followed by subsequent production of cyclic carbonate through a back-biting process (Pathway B). Furthermore, if the CO_2 insertion were rapid and the epoxide ring opening were slow, it could be followed by multiple repetitions of the series of the reaction, leading to consecutive alternating enchainment of epoxide and CO_2 to form polycarbonate with only carbonate linkage (100% carbonate) (Pathway C).^{6,7} However, if CO_2 insertion were the rate limiting step and epoxide

opening were more rapid, the polymers would have a high percentage of ether linkages as a result of consecutive addition of epoxide.



Scheme 1.11. Possible reaction pathways for the catalytic reaction of CO₂ with epoxides

Darensbourg *et al.*¹²⁶ have extensively studied the effect of temperature on the rates of polycarbonate versus cyclic carbonate formation in which both propylene oxide and cyclohexene oxide were used. It was found that for reactions involving PO and CO₂, the formation of cyclic propylene carbonate (CPC) is favoured over poly(propylene) carbonate (PPC) formation. This is as a result of (CPC) being more thermodynamically stable than polycarbonates (PPC) and therefore its formation is favoured especially at higher temperatures as shown in Figure 1.19. For the reaction between CHO and CO₂, the

formation of cyclic cyclohexene carbonate (CHC) does not compete significantly with chain growth because there is a greater energy barrier to surmount (Figure 1.20), and therefore copolymer formation is more facile for this CHO compared with PO.

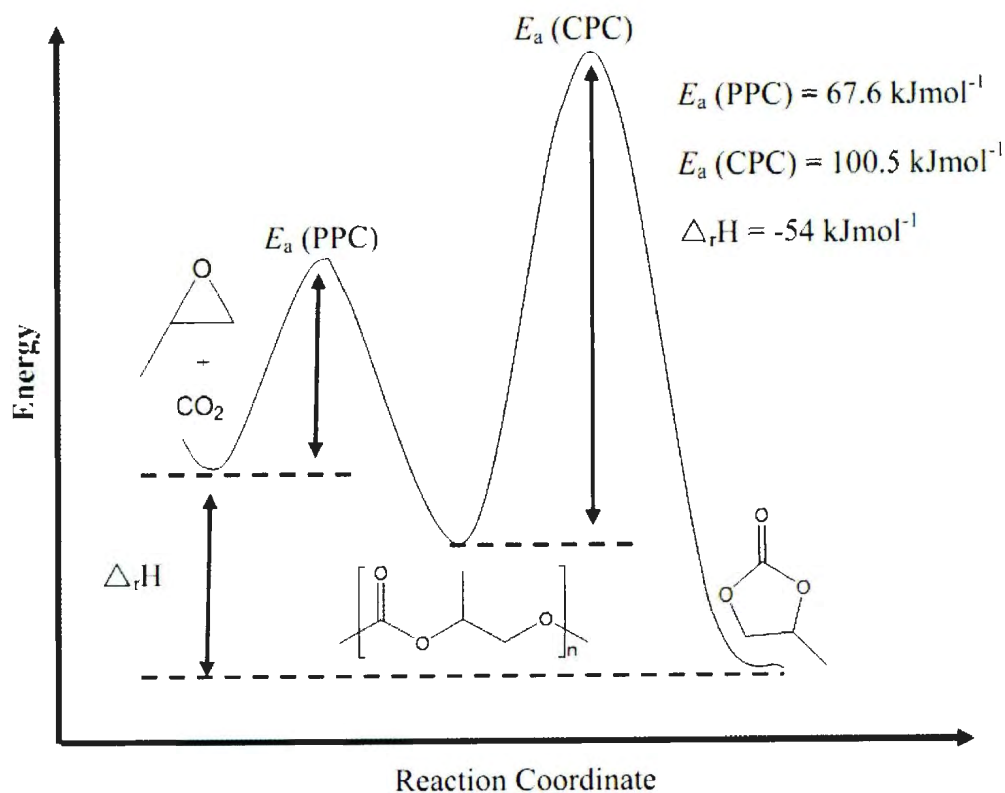


Figure 1.19. Reaction coordinate diagram of coupling reaction of CO_2 and PO

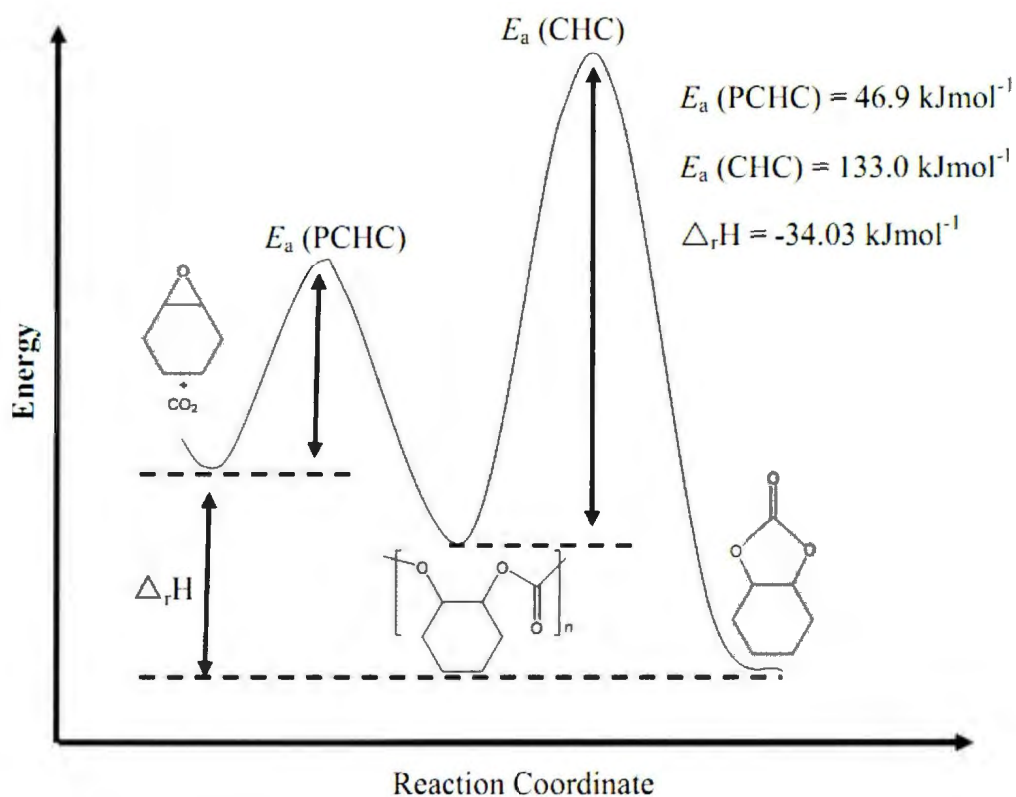


Figure 1.20. Reaction coordinate diagram of coupling reaction of CO₂ and CHO

Thus, a reaction favouring the formation of only one desired product (either cyclic carbonate or polycarbonate) can be achieved by slightly changing the catalyst and/or co-catalyst structures or by manipulation of the reaction conditions (temperature, CO₂ pressure, and co-catalyst loading). For example, since cyclic carbonates are thermodynamically more stable than polycarbonates, carrying out the reaction of CO₂ and epoxides at elevated temperatures can increase the selectivity towards the formation of cyclic carbonates. While decreasing the reaction temperature can enhance the selectivity towards the polycarbonates. It should be noted that the choice of monomer is also of crucial importance.

1.12 Catalysts for Copolymerization and Coupling of Epoxides and CO₂

In the past few decades, there have been a number of fascinating developments in the field of catalysts for carbon dioxide copolymerization with epoxides, especially with metal (Zn, Al, Cr, and Co) complexes supported by sterically demanding ligands such as phenoxides, salens, porphyrins, and diketiminates.

1.12.1 Aluminum Catalysts for Copolymerization Reactions of Epoxides and CO₂

Inoue and co-workers were the first to explore single-site catalysts based on aluminum complexes supported by a tetraphenylporphyrin (TPP) ligand framework (**1.31a** and **b**, Figure 1.21) for the copolymerization reaction of epoxides and CO₂ in 1978.¹²⁷ The complexes were reported to be active for the homopolymerization of propylene oxide as well as for the copolymerization of CO₂ and epoxides. The aluminum alkoxide complex (**1.31a**) copolymerized PO and CO₂ giving poly(propylene carbonate) ($M_n = 3900 \text{ g mol}^{-1}$; $M_w/M_n = 1.15$), but with low incorporation of CO₂ (40% carbonate) and a reaction time of 19 days.^{127,128} On the other hand, the chloride complex (**1.31b**) did not react with CO₂. However, improvements were achieved when **1.31b** in combination with a quaternary phosphonium or ammonium salt (EtPh₃PBr or Et₄NBr) as the co-catalyst was used for copolymerization of PO and CHO respectively. This feat significantly increased the percentage of carbonate linkage content, affording in a living manner completely alternating copolymers with moderate molecular weights and narrow polydispersities (PPC: $M_n = 3500 \text{ g mol}^{-1}$, PDI = 1.09, TOF = 0.18 h^{-1} and PCHC: $M_n = 6200 \text{ g mol}^{-1}$, PDI = 1.06, TOF = 0.30 h^{-1}).¹²⁹ Although propylene carbonate could not be avoided as a by-

product (*ca* 20% yield relative to converted propylene oxide), cyclohexene carbonate was not observed. Furthermore, the “living” nature of the polymerization was illustrated by synthesis of several AB- and ABA-type block copolymers incorporating poly(propylene oxide) (PPO) and poly(propylene carbonate) (PPC) segments.¹²⁹

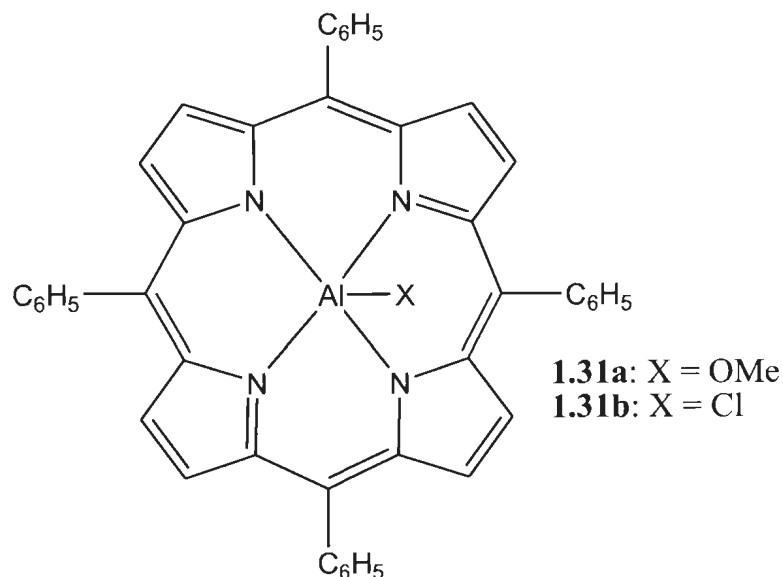
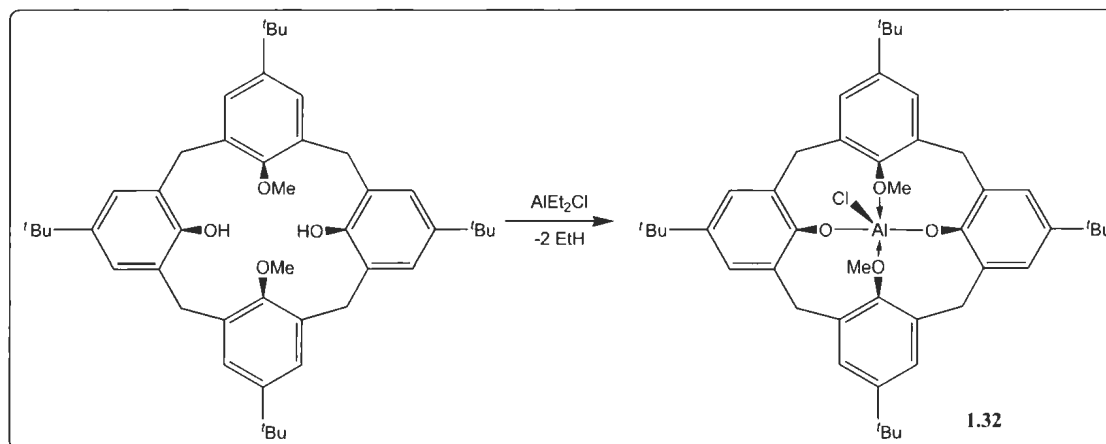


Figure 1.21. Porphyrinato aluminum catalysts for copolymerization of CO₂ and epoxides

In 1998, Kuran *et al.*¹³⁰ reported the activity of an aluminum calix[4]arene complex synthesized from 25,27-dimethoxy-26,28-dihydroxy-*p*-*tert*-butylcalix[4]arene (dmcaH₂) and diethylaluminum chloride, as illustrated in Scheme 1.12, for the copolymerization of epoxides and CO₂. The complex **1.32** [(dmca)AlCl] was found to be active for the alternating copolymerization of CO₂ with PO or CHO, affording copolymers with a low percentage of carbonate linkage. In addition, cyclic carbonates were obtained as by-products relative to the epoxides. Kuran proposed a mechanism involving the participation of bimetallic complexes (Figure 1.22) in the alternating copolymerization, emphasizing that the backside nucleophilic attack, proved by the inversion of the

configuration of the carbon atom of the cleaved epoxide C–O bond during polymerization, is possible only if a bimolecular reaction has occurred.



Scheme 1.12. Synthesis of aluminum calix[4]arene catalyst for copolymerization of CO₂ and epoxides

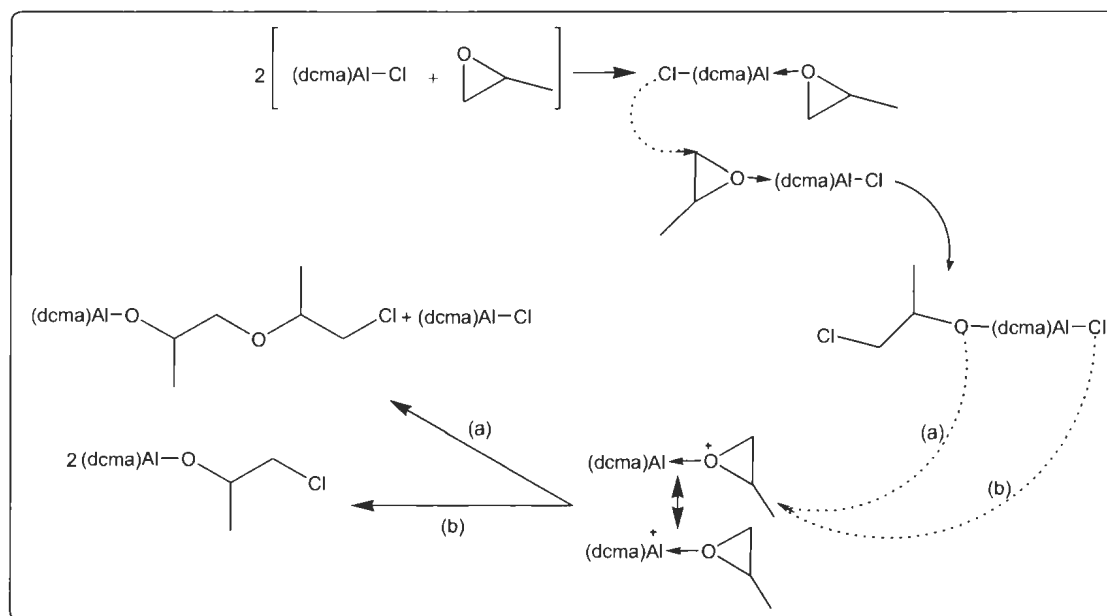
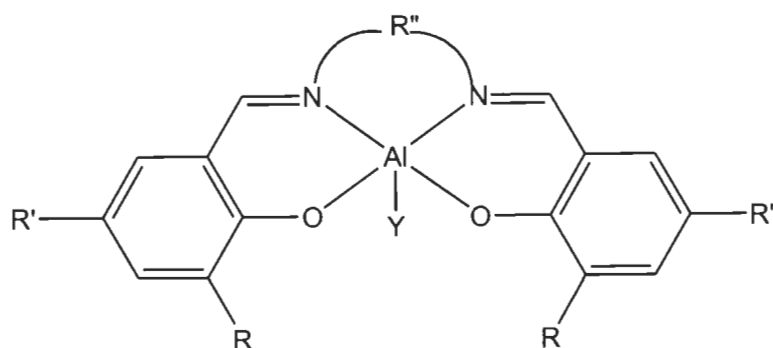


Figure 1.22. Proposed mechanism for copolymerization of CO₂ and epoxides involving bimetallic complexes.¹³⁰

Chisholm *et al.*, using porphyrinato aluminum complexes, conducted an extensive investigation into the mechanism of the ring opening of PO in the copolymerization of PO/CO₂ and found a first order dependence on [Al], which supports the theory of involvement of a monometallic species in the mechanism. They equally determined that the roles of the co-catalyst (in this case DMAP) involved promoting the insertion of CO₂ into the Al-alkoxide bond and labilization of the carboxylate ligand towards ring opening of PO.¹³¹ This explained why, in the absence of added co-catalyst, (TPP)Al catalyst induced the homopolymerization of PO, whereas when co-catalyst was added alternating copolymerization of PO and CO₂ occurred, which is kinetically favored.

Darensbourg *et al.* reported the synthesis of an array of Schiff-base aluminum complexes (Figure 1.23) which were utilized along with both ionic and neutral bases as cocatalysts (e.g. DMAP, Bu₄NCl, Bu₄NN₃, and Bu₄NOAc) for the copolymerization of carbon dioxide and cyclohexene oxide at 80 °C, 35 bar CO₂ for 8 h. They studied the reactivity of these complexes for this process as substituents on the diimine backbone and phenolate rings were altered. It was observed that for this aluminum system electron-withdrawing groups on the salen ligands were needed to generate the most active catalyst toward production of polycarbonates from CO₂ and cyclohexene oxide. For example, only cyclic carbonate was produced when **1.33a**, possessing electron donating ^tBu substituents in the 3 and 5 positions of the phenolate rings, was used in the presence of PPnCl as co-catalyst. Removal of the ^tBu groups from the phenolate ring (reduction of electron donating ability), and employing **1.33b** as a catalyst with PPnCl provided

poly(cyclohexene carbonate) in good yield but with a sizable quantity of cyclic carbonate. However, the introduction of strongly electron-withdrawing nitro groups in the 5-position (**1.33c**), in combination with Bu_4NCl as co-catalyst, offered the most active catalyst/co-catalyst system for the copolymerization of CHO and CO_2 to afford alternating copolymers with TOF value of 35.4 h^{-1} .¹³²



1.33a: $\text{R} = \text{R}' = \text{'Bu}$, $\text{R}'' = -\text{C}_6\text{H}_{10}-$, $\text{Y} = \text{Et}$

1.33b: $\text{R} = \text{R}' = \text{H}$, $\text{R}'' = -\text{C}_6\text{H}_{10}-$, $\text{Y} = \text{Cl}$

1.33c: $\text{R} = \text{'Bu}$, $\text{R}' = \text{NO}_2$, $\text{R}'' = -\text{C}_2\text{H}_4-$, $\text{Y} = \text{Cl}$

Darensbourg *et al.*

Figure 1.23. Salen aluminum catalysts for the copolymerization of CHO and CO_2

1.12.2 Zinc Catalysts for Copolymerization of Epoxides and CO_2

Zinc-based catalysts were the first and most widely used active species for the alternating copolymerization of epoxides and CO_2 . Although most of the zinc catalysts are heterogeneous, the development of a series of zinc phenoxide derivatives (Figure 1.24) as catalysts by Darensbourg and co-workers was a significant breakthrough as the first discrete zinc complexes (**1.34a-d**) for the copolymerization of epoxides and CO_2 .¹³³ This discovery prompted the rapid advances currently being experienced in the field of copolymerization of epoxides and CO_2 . For example, **1.34a** copolymerizes CHO and CO_2

at 80 °C and 55 bar CO₂ to give a copolymer containing 91% syndiotactic polycarbonate linkages (and 9% polyether) with good activity (>350g polymer/g [Zn] in 69 h). However, the polymerization is not well-controlled as the reactions produced polymers with very high polydispersity indices ($M_w/M_n = 2.5-4.5$). Variation of the base as well as the substituents on the phenolate ligands showed that **1.34d** is approximately 4 times more active.¹³⁴ In 2000, the fluorinated complex **1.35** was reported to be an effective catalyst for the copolymerization of cyclohexene oxide and CO₂, and the homopolymerization of cyclohexene oxide. In the case of the copolymerization process (80 °C and 55 bar CO₂), the polycarbonate copolymer that was produced is completely alternating, with no polyether linkages. However, the homopolymerization of cyclohexene oxide to afford polyether in the presence of **1.35** as catalyst is much more facile than the copolymerization process. This observation led to the conclusion that epoxide ring-opening by a metal-bound alkoxide functionality from the growing polymer chain is much faster than by the corresponding carbonate functionality.¹³⁵

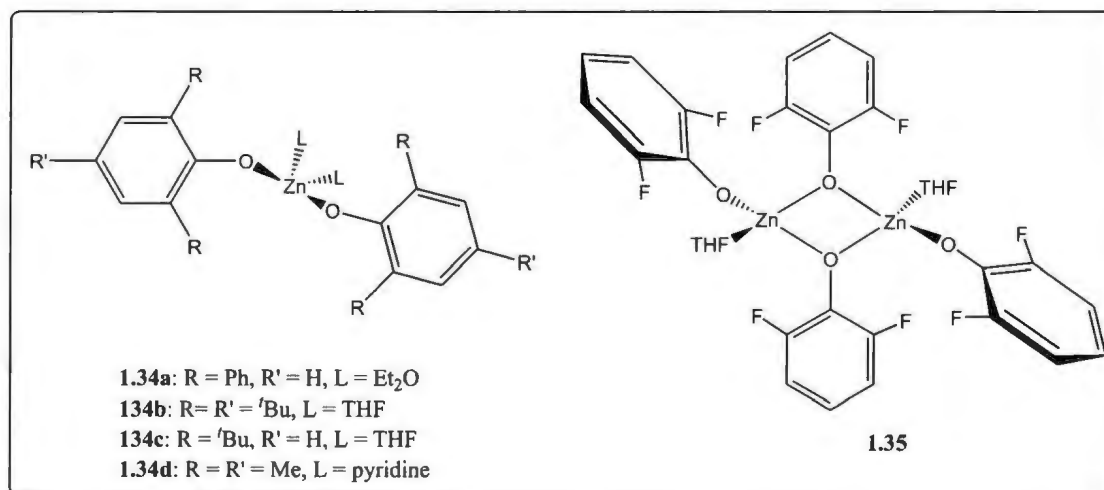


Figure 1.24. Zinc-bis(phenoxide) complexes for the copolymerization of CHO and CO₂

The next major breakthrough in zinc catalyst-design for the copolymerization process came from Coates and co-workers who described a highly active, living epoxide-CO₂ copolymerization system of β -diiminate (BDI) zinc catalysts (Figure 1.25). **1.36a** and **1.36b** catalyzed the alternating copolymerization of CHO and CO₂ at 50 °C and 6.9 bar CO₂ to give a copolymer containing 95% polycarbonate linkages, low molecular weight distribution of 1.07-1.14 and with good activity (TOF = 224 h⁻¹ and 239 h⁻¹ respectively). However, the less bulky **1.36c** and **1.36d** were inactive, which revealed that the substituents on the ancillary β -diketiminato ligand play a crucial role in determining the activity of these catalysts.^{136,137} Furthermore, a subtle change of (**1.36b**) R₁ = H, R₂ = R₃ = Et to (**1.36f**) R₁ = CN, R₂ = Me and R₃ = *i*Pr respectively increased the TOF from 239 h⁻¹ to 2290 h⁻¹ under the same reaction conditions.¹³⁸ They also noted that the bimetallics were poor catalysts for the copolymerization of PO/CO₂, while the monomeric species was very active for the copolymerization of PO/CO₂ to PPC at 6.9 bar and 25 °C with a TOF of 235 h⁻¹.¹³⁸ The work of the Coates group sheds more light on the field of epoxide/CO₂ copolymerization and gave momentum towards the possibility of designing highly efficient well-defined catalysts for copolymerization process.

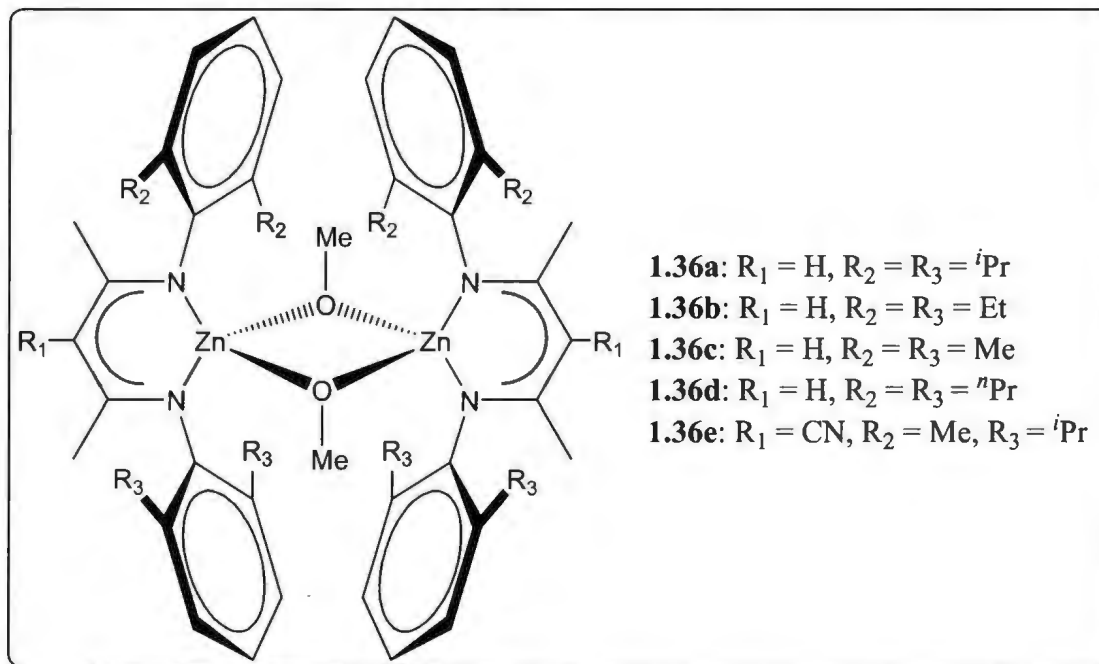


Figure 1.25. β -diiminate-zinc catalysts for epoxide and CO_2 copolymerization

In 2005, Xiao *et al.* reported the synthesis of Trost's dinuclear zinc complexes bearing multidentate semi azacrown ether (**1.37a-f**, Figure 1.26) and their application to the alternating copolymerization of CHO and CO_2 . Complex **1.37a** showed excellent activity affording PCHC in 99% conversion with >99% carbonate linkage at CO_2 pressure of 20 bar, 60 °C, 5 mol% of catalyst loading, 2 mol% EtOH additive and for 6 h. The copolymer exhibited relatively narrow polydispersity ($M_w/M_n = 1.35$) and molecular weight with $M_n = 19.2 \text{ kg mol}^{-1}$.¹³⁹ A systematic investigation of the effects of alcohol additives, CO_2 pressure, ligand substituents and catalyst loading on the activity and selectivity for polycarbonate formation was performed. It was found that addition of 0.4 equivalents of EtOH relative to ligand was optimal, affording a copolymer with $M_n = 23.0 \text{ kg mol}^{-1}$ ($M_w/M_n = 1.43$) in 95% yield as opposed to addition of two equivalents that

rendered the catalyst inactive. Their investigation on catalyst loading revealed that increasing the catalyst loading from 0.1 to 0.5 mol% increased the conversion from 57% to 80% and simultaneously decreased TOF from 142 h⁻¹ to 80 h⁻¹, while selectivity and PDI essentially remained unchanged (92% and 94% carbonate linkage; $M_w/M_n = 1.28$ and 1.30 respectively). It was found that the nature of substituent groups (Ar or R) on the ligand influenced the yield and chemoselectivities of the resulting copolymers. For example, **1.37a** afforded a copolymer with >99% conversion and >99% carbonate linkage, however, the introduction of electron donating groups at the α,α -diaryl moieties of the ligand (**1.37b** and **1.37c**) slightly lowered yield to 79% and 71% respectively, while placing strongly electron withdrawing group at the same position (**1.37d** and **1.37e**) afforded polymers with ill-controlled chemoselectivity of 22% carbonate linkage. Modifications to the bridging phenolic part of the ligand backbone by introduction of NO₂ group (**1.37f**) led to an unsatisfactory yield (41%) and relatively broad molecular weight distribution ($M_w/M_n = 1.94$).

In 2009, the bimetallic zinc complex (**1.38a**, Figure 1.26), bearing a macrocyclic ancillary ligand was shown to catalyze the highly alternating copolymerization of CHO and CO₂.¹⁴⁰ Furthermore, **1.38a** could operate under much milder conditions (1 bar CO₂, 80–100 °C and a 0.1% catalyst loading) with a turnover number (TON) in the range of 430–530 and a TOF in the range of 18–25 h⁻¹. The polycarbonates produced exhibited narrow molecular weight distributions (<1.21), and no ether linkages. However, small amounts (<6%) of cyclic carbonate, the yield of which increased slightly with increasing temperature, were obtained.

Investigation of the steric and electronic influence of the substituents on the structure and the activity of the dimetallic zinc complex in copolymerisation reactions was carried out.¹⁴¹ It was found that **1.38c** is less active than **1.38a** and **1.38b** giving TOF of 6 h⁻¹, which was attributed to the electron-donating effect of the methoxy substituent resulting in a decrease in zinc Lewis acidity and a simultaneous decrease in binding and activation of CHO and CO₂. The alkyl substituents on **1.38a** (TOF = 9.2 h⁻¹) and **1.38b** (TOF = 8.3 h⁻¹) at 80 °C, did not exert any significant electronic influence on the Lewis acidity of the zinc centers and as a result are more active. In addition, the authors suggest that any steric effect was minimal as the substitution is quite far from the active site, however, they also noted that this slight difference in sterics improved the solubility of **1.38a** in CHO. In 2011, the Williams group reported a detailed kinetic study, which revealed that the experimentally determined activation energies (E_a) using **1.38a** for the formation of PCHC and CHC are 96.8 ± 1.6 and 137.5 ± 6.4 kJ mol⁻¹ respectively.¹⁴² The determined E_a values are somewhat higher than values determined for CHO/CO₂ copolymerization using a Cr salen based catalyst (PCHC: 46.9 kJ mol⁻¹ and CHC: 133.0 kJ mol⁻¹)¹²⁶ and a dinuclear magnesium catalyst (PCHC: 45.3 kJ mol⁻¹ and CHC: 127.2 kJ mol⁻¹).¹⁴³ This high E_a for PCHC formation explains the relative high temperatures (>60 °C) required for the catalysts **1.38a-c**.

The copolymerization activities for the complexes reported in the literature and discussed in this introductory Chapter are summarized in Table 1.4. It can be seen that among the complexes, **1.36a, b, d** exhibited unprecedented high activity and good polymerization control.

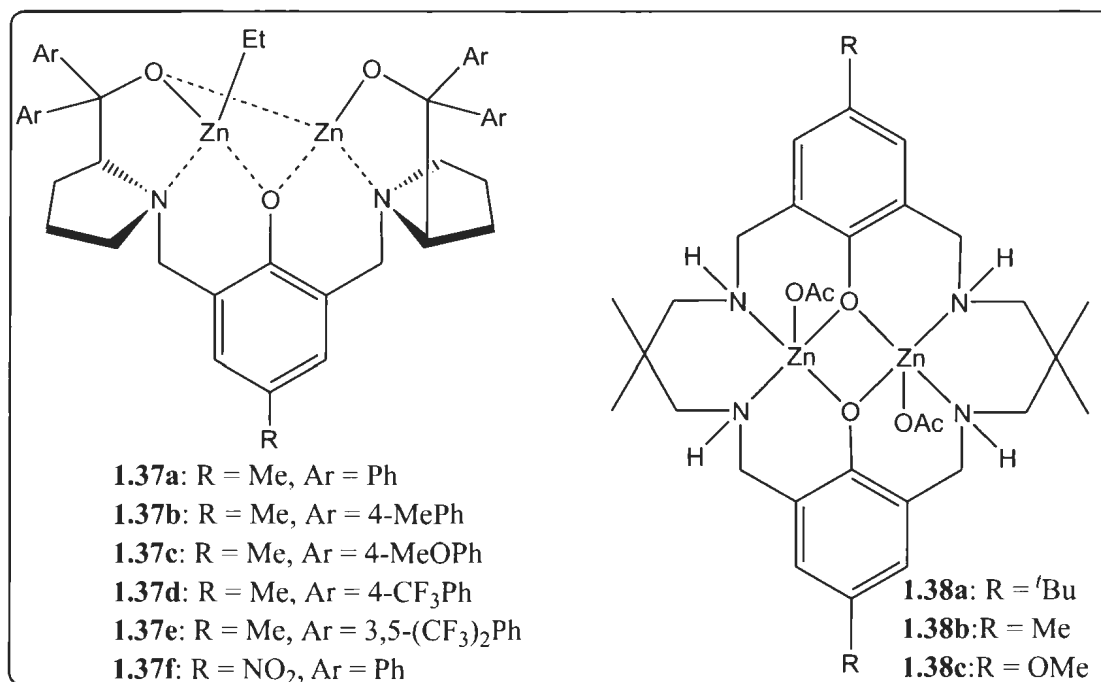


Figure 1.26. Bimetallic zinc complexes bearing amine-phenolate ligands for copolymerization of epoxides and CO₂

Unfortunately, it should be noted that the properties of polycarbonates produced so far from CO₂ are inferior to the conventional polycarbonates from bisphenol-A. The glass transition temperature T_g which is *ca* 35 °C lower than the conventional polycarbonates, should be improved to make it more industrially feasible. Nonetheless, milestones have been achieved in the past decade, and efforts are ongoing to bring this environmentally friendly process to industrial practicality. For example, Lee has developed Co-salen complexes which are being industrially applied,^{144,145} but for biomedical and other applications Co impurities could be a problem, so Zn and Al catalysts are highly desirable.

Table 1.4. Comparison of the activity of various metal catalysts for copolymerization of CO₂ and epoxides

Catalyst/ ligand	Co- catalyst	Conditions	Monomer (equiv.)	Conv (%)	%-CO ₃ linkage	Cyclic car- bonate (%)	<i>M_n</i> (kg mol ⁻¹)	<i>M_w</i> / <i>M_n</i>	TOF (h ⁻¹)	Ref
1.31a -Al/ TPP	none	20 °C, 19 d, 8 bar CO ₂	PO	No data	40	No data	3.90	1.15	No data	127, 128
1.31b -Al/ TPP	EtPh ₃ PBr	RT, 14 d, 49 bar CO ₂ , DCM	PO (100)	>99	>99	20	3.50	1.09	0.18	129
1.31b -Al/ TPP	EtPh ₃ PBr	RT, 14 d, 49 bar CO ₂ , DCM	CHO (100)	100	100	No data	6.20	1.06	0.30	129
1.32 -Al/ dmca	none	35 °C, 168 h, 60 bar CO ₂ , toluene	PO (100)	38	13	14	5.62	No data	No data	130
1.32 -Al/ dmca	none	35 °C, 264 h, 60 bar CO ₂ , toluene	CHO (50)	26	18	4	1.93	No data	No data	130
1.31b -Al/ TPP	DMAP	25 °C, 40 h, 50 bar CO ₂	PO (1500)	No data	48	No data	No data	No data	No data	131
1.33c -Al/ Salen	Bu ₄ NCl	80 °C, 8 h, 35 bar CO ₂	CHO	No data	96	3	No data	No data	35.4	132

Table 1.4. continued.....

Catalyst/ ligand	Co- catalyst	Conditions	Monomer (equiv.)	Conv (%)	%-CO ₃ linkage	Cyclic carbonate yield (%)	M_n (kg mol ⁻¹)	M_w/M_n	TOF (h ⁻¹)	Ref
1.34a -Zn/ diphenoxide	none	80 °C, 69 h, 55 bar CO ₂	CHO	65	91	No data	3.80	4.5	No data	133
1.35 -Zn/ diphenoxide	none	80 °C, 55 bar CO ₂	CHO	No data	No data	No data	42.0	6.0	16.5	135
1.36a -Zn/ BDI	none	50 °C, 2 h, 8 bar CO ₂	CHO	No data	96	No data	31.0	1.11	247	137
1.36b -Zn/ BDI	none	50 °C, 2 h, 8 bar CO ₂	CHO	No data	96	No data	22.0	1.12	235	137
1.36e -Zn/ BDI	none	50 °C, 2 h, 8 bar CO ₂	CHO	No data	96	No data	22.0	1.12	235	138
1.37a -Zn/ Amine- phenolate	EtOH	60 °C, 6 h, 20 bar CO ₂	CHO	99	99	No data	19.2	1.35	No data	139
1.38 -Zn/ Amine- phenolate	none	100 °C, 24 h, 1 bar CO ₂	CHO (1000)	>99	>99	No data	3.07	1.21	25	140

1.12.3 Aluminum and Zinc Catalysts for Coupling of Epoxides and CO₂

In 2004, Lu and co-workers reported the use of Schiff-base aluminum complexes (**1.39a-h**, Figure 1.27) in combination with a quaternary ammonium salt $n\text{-Bu}_4\text{NX}$ ($X = \text{Cl, Br, I}$) at 6 bar CO₂ and ambient temperature to induce the coupling reaction of CO₂ and epoxides, affording cyclic carbonate in good yield.¹⁴⁶ During their investigation, it was found that variation of the substituent groups on the aromatic ring (**1.39a-c**), the leaving group (**1.39d-f**) and/or diamine backbone (**1.39g, 1.39h**) played a crucial role in designing efficient catalysts for the cycloaddition reaction of epoxides and CO₂. For example, **1.39a** in conjunction with $n\text{-Bu}_4\text{NI}$ exhibited the highest catalytic activity (TOF = 84.2 h⁻¹) of all the catalysts and was close to ten times more active than complex **1.39c** (TOF = 8.9 h⁻¹) based on TOF. Furthermore, they discovered that the Schiff-base aluminum complexes in combination with 18-crown-6 and KI catalyzed the coupling of (*S*)-propylene oxide and CO₂ to give (*S*)-propylene carbonate. In this reaction, complexes **1.39a** and **1.39d-f** were found to be more effective catalysts (TOF = 59.7-62.3 h⁻¹) and their activities are at least five times greater than for **1.39c** (TOF = 10.1 h⁻¹). Lu *et al.* attributed that the better activities could be due to the high electrophilicity and the more accessible coordination site available for the epoxide within these complexes.¹⁴⁹

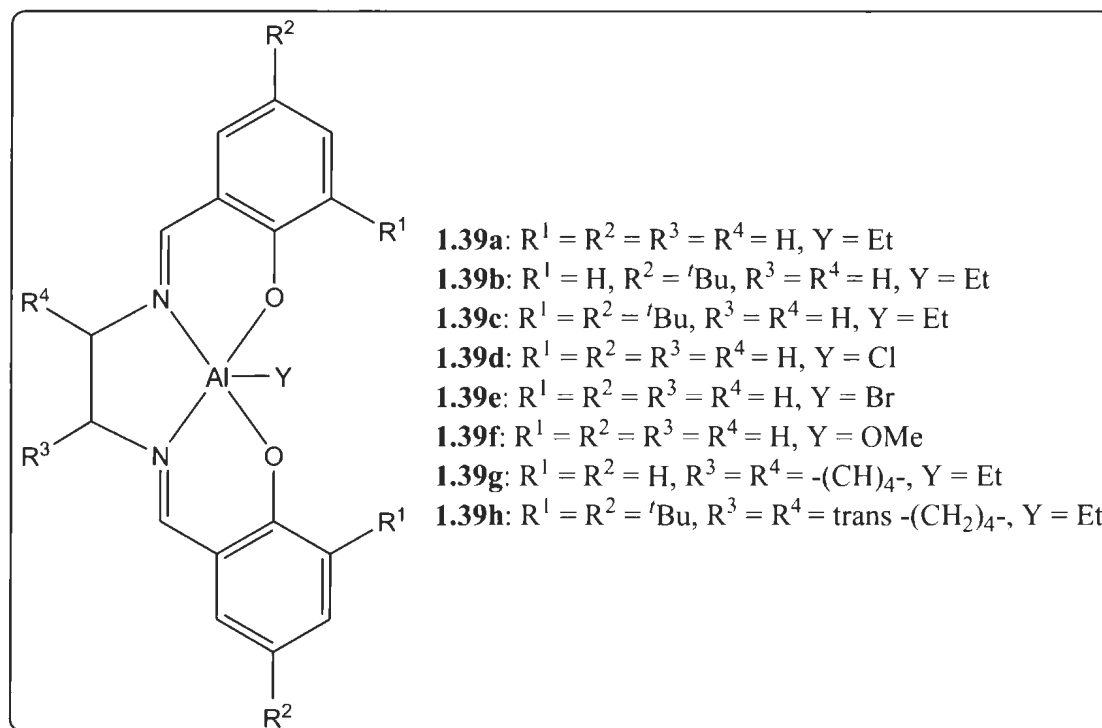


Figure 1.27. Aluminum salen complexes for the cycloaddition reaction of CO_2 and epoxides

North *et al.* reported the synthesis of a series of bimetallic Al–O–Al bridged salen complexes (Figure 1.28) and their utilization in combination with $n\text{-Bu}_4\text{NBr}$ to catalyze the formation of styrene carbonates from the reaction of CO_2 with styrene oxide.¹⁴⁸ They conducted the cycloaddition reactions under exceptionally mild conditions (25 °C, 1 bar CO_2) and the bimetallic complexes displayed high catalytic activity. However, no conversion was observed in the absence of either the catalyst or co-catalyst. They found that the loading of the catalyst and co-catalyst affects the conversion.¹⁴⁹ For example, reducing the amount of complex **1.40a** from 1.0 mol% to 0.1 mol% had no effect on the conversion (85%), but simultaneous reduction of the amount of the two components to

0.1 mol% dramatically reduced the conversion from 86 to 27%. Increasing the catalyst and co-catalyst load from 0.1 to 2.5 mol% increased the conversion from 27 to 98%. The influence of the halide within the tetrabutylammonium salt co-catalyst was investigated and the order of catalytic effectiveness was found to be Br > I > Cl > F. The variation of the substituents on the aromatic rings (**1.40b-g**) was carried out to investigate their electronic and steric influence on the catalytic activity. However, no trend was apparent, but it was observed that when the ^tBu groups were gradually removed from the aromatic rings (**1.40a-c**), the conversion decreased from 62 to 28%. North attributed this result to the decreasing solubility of the catalyst (**1.40c** did not fully dissolve in the reaction mixture) rather than a steric effect.

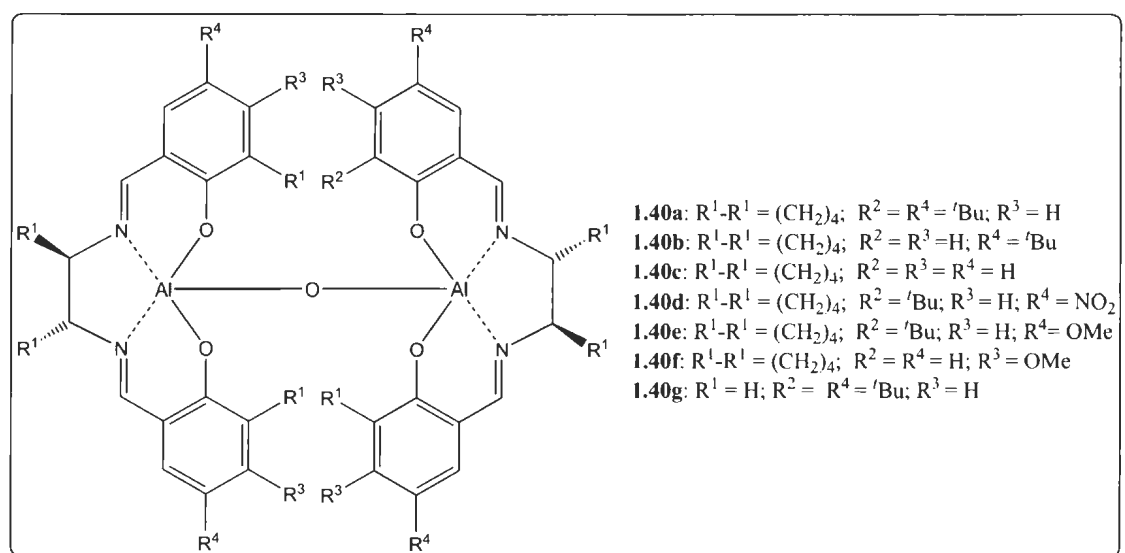
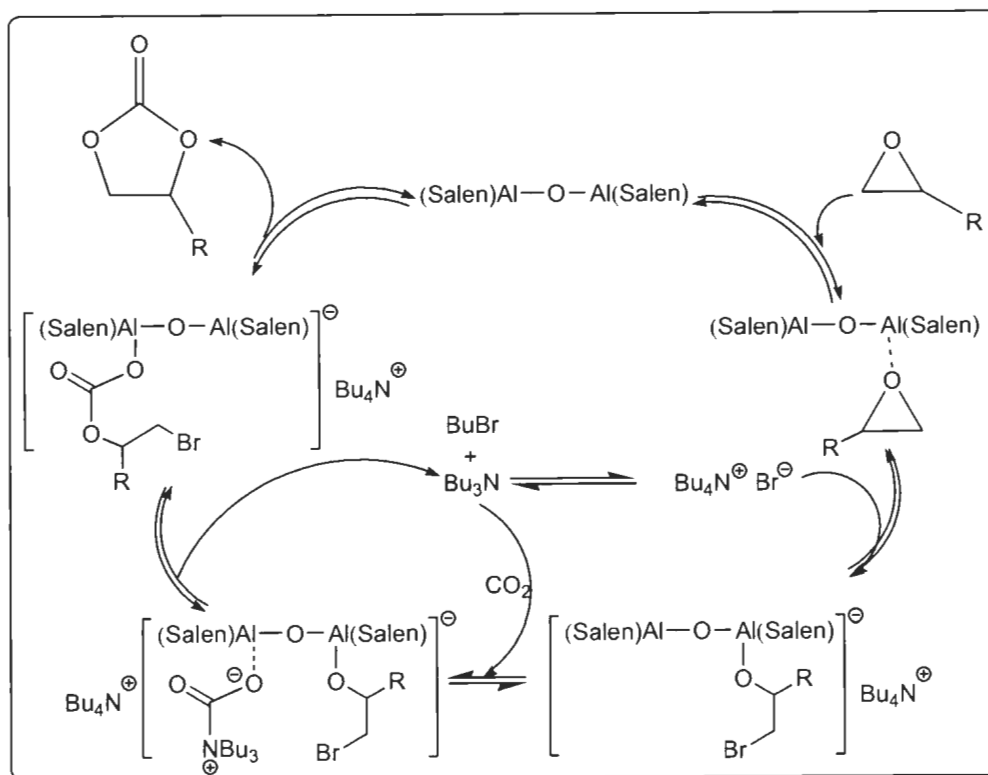


Figure 1.28. Bimetallic aluminum salen complexes for cycloaddition reaction of CO₂ with epoxides

Based on the experimental evidence, a mechanism was proposed (Scheme 1.13), and the key feature is the simultaneous activation of epoxide and CO_2 by the two neighbouring metal centres, which promotes the intramolecular nucleophilic attack of the alkoxide to the carbon atom of the activated CO_2 molecule. This explains the exceptionally high levels of catalytic activity observed with the bimetallic complexes compared to monometallic salen complexes.¹⁴⁹ It has been suggested that in this mechanism the co-catalyst, Bu_4NBr , plays a second role besides the ring opening of the epoxide by the bromide. Bu_4NBr can decompose to tributylamine (Bu_3N), which can form a carbamate salt with CO_2 ($\text{Bu}_3\text{N}^+\text{-CO}_2^-$) and this salt can coordinate more easily to the second Al-centre compared to CO_2 alone.^{149,150}



Scheme 1.13. Proposed mechanism for the synthesis of cyclic carbonate using bimetallic complex with Bu_4NBr as co-catalyst

In 2003, Shi *et al.* explored the catalytic performance of zinc complexes bearing binaphthyldiamino Schiff base ligand **1.41a-c** (Figure 1.29) in the coupling reaction of CO₂ and epoxides. The complexes were found to efficiently catalyze the formation of cyclic carbonates of terminal epoxides.¹⁵¹ They found that the presence of organic base such as DMAP (4dimethylaminopyridine), Et₃N, DBU (1,5-diazabicyclo[5.4.0]undec-5-ene), DABCO (1,4-diazabicyclo-[2.2.2]octane), or pyridine (0.2 mol%) was crucial to promote the reaction. The best catalyst system involved the combination of unsubstituted binaphthyldiamino salen-type zinc complex **1.41a** (0.1 mol%) and Et₃N (0.2 mol%), under the optimized reaction conditions of 100 °C and 35 bar CO₂ in a reaction period of 2 h. **1.41a** afforded cyclic carbonates such as propylene, butylene, epichlorohydrin, or phenylethylene carbonates, in high yields (89-100%).

More recently, zinc tetraphenylporphyrin complexes with quaternary onium salts (**1.42a** and **1.42b**, Figure 1.29) were reported to exhibit high catalytic activity towards the cycloaddition of CO₂ to CHO.¹⁵² These complexes were designed to act as a bifunctional catalysts. The proposed mechanism involves nucleophilic attack by the halide ion on the less-hindered side of the epoxide, along with concurrent activation of the epoxide by coordination of the Zn(II) ion. The oxyanion generated from ring-opening then attacks CO₂ to give a CO₂-adduct, which leads to the formation of the cyclic carbonate and regeneration of the catalyst. Furthermore, **1.42b** afforded cyclic carbonate in good yield (80%) under the reaction conditions of 120 °C, 10 bar CO₂, 0.005% catalyst load and for 3 h, while **1.42a** afforded only 24% yield under the same conditions. This indicates that

the quaternary ammonium bromide co-catalyst is better than quaternary phosphonium bromide for this catalyst-system.

However, it should be noted that by contrast the Zn catalyst systems (**1.41** and **1.42**) are outperformed by the Al-salen-based catalysts (**1.39** and **1.40**) regarding reaction temperature and pressure.

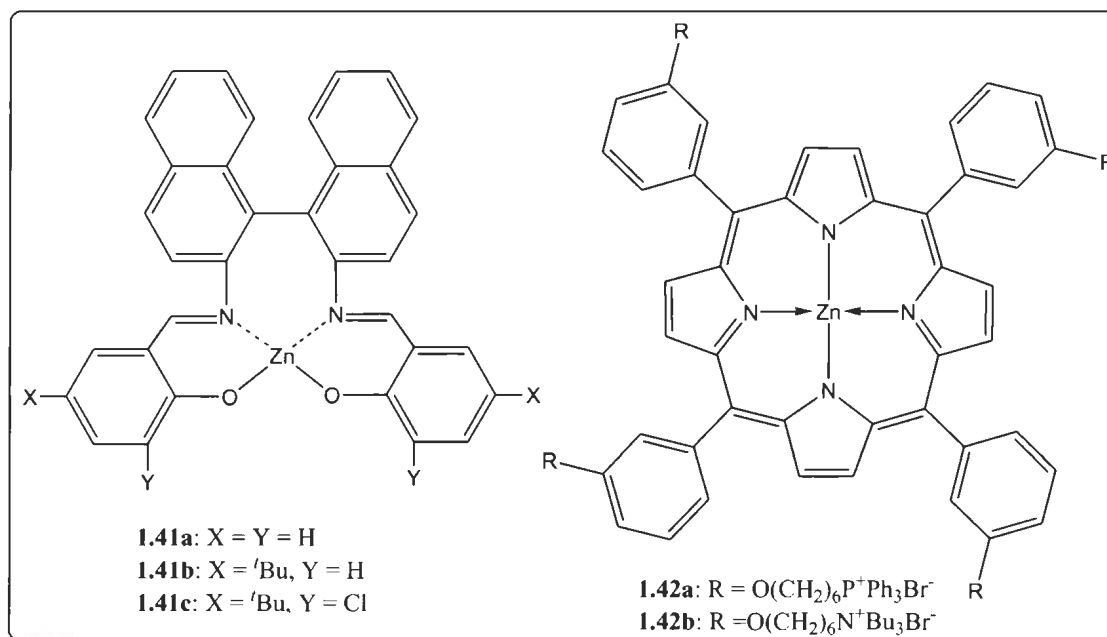


Figure 1.29. Zinc complexes for the synthesis of cyclic carbonates from CO₂ and epoxides

The coupling reaction activities for the complexes reported in the literature and discussed in this introductory chapter are summarized in Table 1.5. It can be seen that complexes e.g. **1.39** and **1.40** show better activity with regards to the reaction conditions, whereas other complexes can perform the same reaction but under more harsh reaction conditions.

Table 1.5. Comparison of activity of various metal catalysts for the coupling of CO₂ and epoxides

Catalyst/ ligand	Co-catalyst	Conditions	Monomer (equiv)	Conv (%)	TOF (h ⁻¹)	TON	Ref
1.39a -Al/ salen	n-Bu ₄ NI	35 °C, 8 h, 6 bar CO ₂	PO (800)	No data	84.2	No data	146
1.39e -Al/ salen	18-crown-6-KI	25 °C, 8 h, 6 bar CO ₂	PO (800)	No data	62.3	No data	147
1.40a -Al/ salen	Bu ₄ NBr	25 °C, 24 h, 1 bar CO ₂	SO	98	No data	No data	149
1.41a -Zn/ salen	Et ₃ N	100 °C, 2 h, 35 bar CO ₂	PO (100)	90 (yield)	450	901	151
1.42b -Zn/ TPP	none	120 °C, 3 h, 10 bar CO ₂	Epoxyhexane	80	No data	No data	152

1.13 Titanium and Zirconium Amine-Phenolate Complexes.

Early transition metal complexes bearing phenolate ligands exhibit amazing reactivity in enantioselective transformations,¹⁵³ olefin polymerization, lactide and caprolactone polymerization.^{6,154-157} Kol and co-workers introduced a series of amine bis(phenolate) Group IV metal complexes with additional side-arm and *ortho/para* substituents of varying steric and electronic nature (Figure 1.30) for olefin polymerization.¹⁵⁸⁻¹⁶¹

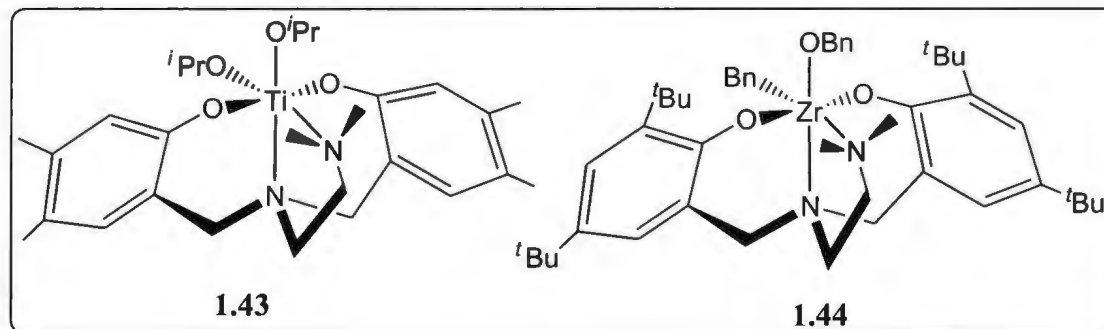
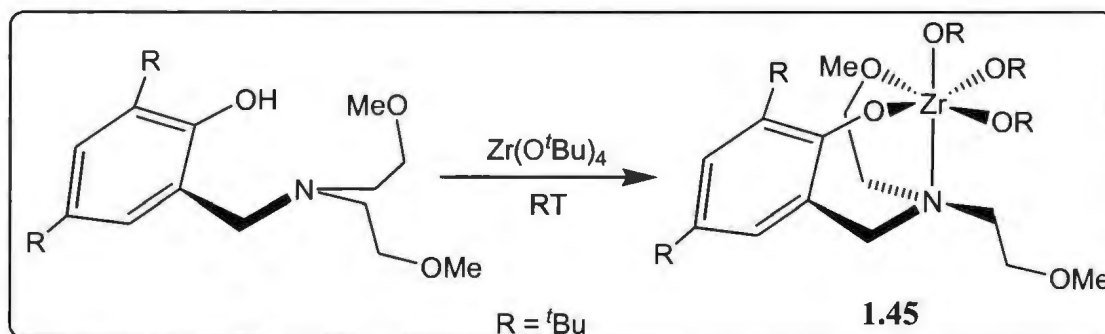


Figure 1.30. Amine bis(phenolate) titanium and zirconium alkoxide complexes for olefin polymerization

To further advance their work in ligand design for group IV metals, Kol and co-workers introduced in 2005 monoanionic amine mono(phenolate) ligands that possessed two neutral side-arms. Reactions of these ligands with group IV metal alkoxides such as $\text{Ti}(\text{O}^i\text{Pr})_4$ and $\text{Zr}(\text{O}^t\text{Bu})_4$ at room temperature (Scheme 1.14) afforded the new complexes in high yield.¹⁶²



Scheme 1.14. Synthesis of amine mono(phenolate) zirconium alkoxide complex

1.14 Objectives and Outline of the Thesis

Despite the fact that some excellent initiators have been reported for the polymerization of cyclic esters and copolymerization of CO₂/epoxide in the literature, the search for new catalysts that can generate well-defined polyesters and aliphatic polycarbonate is still vital. Improving the performance and versatility of metal catalysts is an important research goal that may be achieved through understanding the mechanism(s) of the ROP process and applying that knowledge to catalyst design and development. Thus, the aims of the research described in this thesis are to: (a) synthesize families of related potentially biocompatible catalyst systems; (b) apply these systems in the ring-opening polymerization of cyclic esters and copolymerization of CO₂ and epoxides.

Regarding catalyst design, this investigation is focused on the identification of parameters influencing the catalyst properties through modification of the substituents on the ligands. Besides this, the influence of the outersphere substituents of the amine unit

within the ligand (amine compared with ether) will also be assessed. The elucidation of polymerization mechanisms is also an objective of the research.

Chapter 2 provides an overview of the synthesis and characterization of the series of ligands used in this thesis to prepare the zinc, aluminum, lithium and group IV metal complexes. In Chapter 3, the synthesis and molecular structures of a series of zinc complexes bearing monoanionic amine mono(phenolate) ligands are described. The catalytic activities of the *in situ* generated and isolated zinc alkoxides toward the ROP of *rac*-lactide and ϵ -caprolactone in solution and in bulk conditions are described. Chapter 4 introduces the preparation and characterization of a series of aluminum methyl and chloro complexes. The catalytic activity of these aluminum complexes toward the ROP of ϵ -caprolactone and copolymerization of epoxides and CO₂ is described. The synthesis and characterization of trimetallic lithium complexes bearing piperazinyl based amine phenolate ligands and their catalytic activity toward the ROP of ϵ -caprolactone in the presence and absence of benzyl alcohol is described in Chapter 5. In Chapter 6, the synthesis and molecular structures of group IV metal complexes, lithium aggregates and attempted cationic zinc complex synthesis are described.

1.15 References

1. M. J.-L. Tschan, E. Brule, P. Haquette and C. M. Thomas, *Polym. Chem.*, **2012**, *3*, 836.
2. S. Mecking, *Angew. Chem. Int. Ed.* **2004**, *43*, 1078.
3. C. M. Thomas, *Chem. Soc. Rev.* **2010**, *39*, 165.
4. O. Dechy-Cabaret, B. Martin-Vaca and D. Bourissou, *Chem. Rev.* **2004**, *104*, 6147.
5. C.-X. Miao, J.-Q. Wang and L.-N. He, *Open Org. Chem. J.*, **2008**, *2*, 68.
6. X.-B. Lu and D. J. Darensbourg, *Chem. Soc. Rev.*, **2012**, *41*, 1462.
7. M. R. Kember, A. Buchard and C. K. Williams, *Chem. Commun.*, **2011**, *47*, 141.
8. E. Quaranta and M. Anesta, The Chemistry of N-CO₂ Bonds: Synthesis of Carbamic acids and Their Derivatives, Isocyanates, and Ureas. In *Carbon Dioxide as Chemical Feedstock*; M. Anesta, Ed.; Wiley-VCH Verlag GmbH & Co. KGaA, Weinheim. **2010**, pp 121-159.
9. M. H. Chisholm and Z. Zhou, *J. Mater. Chem.*, **2004**, *14*, 3081.
10. C. A. Wheaton, P. G. Hayes and B. J. Ireland, *Dalton Trans.*, **2009**, 4832.
11. S. M. Guillaume and J.-F. Carpentier, *Catal. Sci. Technol.*, **2012**, *2*, 898.
12. A. Sodergard and M. Stolt, *Prog. Poly. Sci.*, **2002**, *27*, 1123.
13. W. H. Carothers, G. L. Dorough and F. J. vanNatta, *J. Am. Chem. Soc.*, **1932**, *54*, 761.
14. P. Gupta and V. Kumar, *Eur. Polym. J.*, **2007**, *43*, 4053.
15. M. Labet and W. Thielemans, *Chem. Soc. Rev.*, **2009**, *38*, 3484.
16. C. Jérôme, and P. Lecomte, *Adv. Drug Delivery Rev.*, **2008**, *60*, 1056.
17. Y. Cheng, S. Deng, P. Chen and R. Ruan, *Front. Chem. China*, **2009**, *4*, 259.
18. R. H. Platel, L. M. Hodgson and C. K. Williams, *Polymer Rev.*, **2008**, *48*, 11.
19. A. P. Dove, *Chem. Commun.*, **2008**, 6446.

20. S. Strandman, J. E. Gautrot and X. X. Zhu, *Polym. Chem.*, **2011**, *2*, 791.
21. M. S. Kim, K. S. Seo, G. Khang and H. B. Lee, *Macromol. Rapid Commun.*, **2005**, *26*, 643.
22. S. J. Penczek, *Polym. Sci., Part A: Polym. Chem.*, **2000**, *38*, 1919.
23. D. Bourissou, B. Martin-Vaca, A. Dumitrescu, M. Graullier and F. Lacombe, *Macromolecules*, **2005**, *38*, 9993.
24. E. L. Marshall, V. C. Gibson and H. S Rzepa, *J. Am. Chem. Soc.*, **2005**, *127*, 6048.
25. M. Ryner, K. Stridsberg, A. C. Albertsson, H. von Schenck and M. Svensson, *Macromolecules*, **2001**, *34*, 3881.
26. P. Dubois, C. Jacobs, R. Jerome and P. Teyssie, *Macromolecules*, **1991**, *24*, 2266.
27. H. R. Kricheldorf, M. Berl and N. Scharnagl, *Macromolecules*, **1988**, *21*, 286.
28. A. Kowalski, A. Duda and S. Penczek, *Macromolecules*, **2000**, *33*, 7359.
29. H. R. Kricheldorf. *Chemosphere*, **2001**, *43*, 49.
30. C. Wang, H. Li and X. Zhao, *Biomaterials*, **2004**, *25*, 5797.
31. A. Khanna, Y. Sudha, S. Pillai and S. Rath, *J. Mol. Model.*, **2008**, *14*, 367.
32. A.-C. Albertsson, and I. K. Varma, *Biomacromolecules*, **2003**, *4*, 1466.
33. A. Arbaoui and C. Redshaw, *Polym. Chem.*, **2010**, *1*, 801.
34. R. E. Drumright, P. R. Gruber and E. Henton, *Adv. Mater.*, **2000**, *12*, 1841.
35. P. J. Dijkstra, H. Du and J. Feijen, *Polym. Chem.*, **2011**, *2*, 520.
36. G. Schwach, J. Coudane, R. Engel and M. Vert, *Polym. Int.*, **1998**, *46*, 177.
37. H. R. Kricheldorf, I. Kreiser-Saunders and A. Stricker, *Macromolecules*, **2000**, *33*, 702.
38. P. Dubois, R. Jerome, and P. Teyssie, *Makromol. Chem. Macromol. Symp.*, **1991**, *42*, 103.
39. J. H. Khan, F. Schuea and G. A. George, *Polym. Int.*, **2009**, *58*, 296.

40. D. McNaught and A. Wilkinson, *Compendium of Chemical Terminology: IUPAC Recommendations*. Blackwell Science: Oxford, **1997**.
41. C. O. Kappe, D. Dallinger and S. Murphree, *Practical Microwave Synthesis for Organic Chemists*, Wiley-VCH Verlag GmbH & Co. KGaA, Weinheim. **2009**, pp 11-162.
42. C. O. Kappe, B. Pieber and D. Dallinger, *Angew. Chem. Int. Ed.* **2012**, *51*, 2.
43. M. Iannelli, Microwave Heating as a Tool for sustainable Polymer Chemistry. In *Microwave Heating as a Tool for sustainable Chemistry*, N. E. Leadbeater, Ed.; CRC Press, Taylor & Francis Group, New York, **2010**, pp 60-65; S. Sinnwell and H. Ritter, *Aust. J. Chem.* **2007**, *60*, 729.
44. H. Albert, H. Warth, R. Muelhaupt and R. Janda, *Macromol. Chem. Phys.* **1996**, *197*, 1633.
45. X. M. Fang, S. J. Huang and D. A. Scola, *Polym. Mater. Sci. Eng.*, **1998**, *79*, 518.
46. X. M. Fang, C. D. Simone, E. Vaccaro, S. J. Huang and D. A. Scola, *J. Polym. Sci., Part A: Polym. Chem.*, **2002**, *40*, 2264.
47. G. Sivalingam, N. Agarwal and G. Madras, *J. Appl. Polym. Sci.*, **2004**, *91*, 1450.
48. R. A. Auras, B. Harte, S. Selke and R. Hernandez, *J. Plast. Film Sheeting*, **2003**, *19*, 123.
49. J.-C. Buffet and J. Okuda, *Polym. Chem.*, **2011**, *2*, 2758.
50. M. J. Stanford and A. P. Dove, *Chem. Soc. Rev.*, **2010**, *39*, 486.
51. H. L. Frisch, C. L. Mallows, and F. A. Bovey, *J. Chem. Phys.*, **1966**, *45*, 1565.; F. A. Bovey and P. A. Mirau, *NMR of Polymers*, Academic Press, San Diego, **1996**.
52. M. T. Zell, B. E. Padden, A. J. Paterick, K. A. M. Thakur, R. T. Kean, M. A. Hillmyer and E. J. Munson, *Macromolecules*, **2002**, *35*, 7700.
53. L. S. Nair, and C. T. Laurencin, *Prog. Polym. Sci.*, **2007**, *32*, 762.
54. Y. Ikada and H. Tsuji, *Macromol. Rapid Commun.*, **2000**, *21*, 117.
55. V. R. Sinha, K. Bansal, K. Kaushik, R. Kumria and A. Trehan, *Int. J. Pharm.*, **2004**, *278*, 1.

56. C. X. F. Lam, S. H. Teoh and D. W. Hutmacher, *Polym. Int.*, **2007**, *56*, 718.
57. J. Pena, T. Corrales, I. Izquierdo-Barba, A. L. Doadrio and M. Vallet-Regi, *Polym. Degrad. Stab.*, **2006**, *91*, 1424.
58. M. J. Jenkins, K. L. Harrison, M. M. C. G. Silva, M. J. Whitaker, K. M. Shakesheff and S. M. Howdle, *Eur. Polym. J.*, **2006**, *42*, 3145.
59. J. L. Hedrick, T. Magbitang, E. F. Connor, T. Glauser, W. Volksen, C. J. Hawker, V. Y. Lee and R. D. Miller, *Chem.–Eur. J.*, **2002**, *8*, 3308.
60. P. Joshi and G. Madras, *Polym. Degrad. Stab.*, **2008**, *93*, 1901.
61. K. M. Stridsberg, M. Ryner and A. C. Albertsson, Controlled Ring Opening Polymerization: Polymers with Controlled Architecture. In *Advances in Polymer Science*; A. C. Albertsson, Ed.; Springer-Verlag: Berlin, **2002**, *157*, pp 41-65.
62. F. Tudos and P. K. David, *Polym. Degrad. Stab.*, **1995**, *50*, 159; G. Lente, I. Fabian and A. J. Poe, *New J. Chem.*, **2005**, *29*, 759.
63. G. W. Coates, *J. Chem. Soc., Dalton Trans.*, **2002**, 467.
64. U. Olsher, *Chem. Rev.*, **1991**, *91*, 137.
65. N. N. Greenwood and A. Earnshaw, 'Chemistry of the Elements', 2nd edn., Butterworth-Heinemann, Oxford, **1997**, Chap. 29.
66. N. N. Greenwood and A. Earnshaw, 'Chemistry of the Elements', 2nd edn., Butterworth-Heinemann, Oxford, **1997**, Chap. 7.
67. L. Trofimoff, T. Aida and S. Inoue, *Chem. Lett.* **1987**, 991.
68. T. Yasuda, T. Aida and S. Inoue, *Bull. Chem. Soc. Jpn.* **1986**, *59*, 3931.
69. M. Endo, T. Aida and S. Inoue, *Macromolecules*, **1987**, *20*, 2982.
70. M. H. Chisholm, J. C. Gallucci and K. Phomphrai, *Chem. Commun.*, **2003**, 48.
71. M. H. Chisholm, J. C. Gallucci and K. Phomphrai, *Inorg. Chem.*, **2004**, *43*, 6717.
72. M. H. Chisholm and N. W. Eilerts, *Chem. Commun.*, **1996**, 853.
73. M. H. Chisholm, N. W. Eilerts, J. C. Huffman, S. S. Iyer, M. Pacold and K. Phomphrai, *J. Am. Chem. Soc.*, **2000**, *122*, 11845.

74. M. H. Chisholm, *Inorg. Chim. Acta.*, **2009**, *362*, 4284.
75. M. Cheng, A. B. Attygalle, E. B. Lobkovsky and G. W. Coates, *J. Am. Chem. Soc.*, **1999**, *121*, 11583.
76. B. M. Chamberlain, M. Cheng, D. R. Moore, T. M. Ovitt, E. B. Lobkovsky and G. W. Coates, *J. Am. Chem. Soc.*, **2001**, *123*, 3229.
77. Leborgne, V. Vincens, M. Joulgard and N. Spassky, *Makromol. Chem., Macromol. Symp.*, **1993**, *73*, 37.
78. N. Spassky, M. Wisniewski, C. Pluta and A. Le Borgne, *Macromol. Chem. Phys.*, **1996**, *197*, 2627.
79. M. Wisniewski, A. Le Borgne and N. Spassky, *Macromol. Chem. Phys.*, **1997**, *198*, 1227.
80. T. M. Ovitt and G. W. Coates, *J. Am. Chem. Soc.*, **1999**, *121*, 4072.
81. C. P. Radano, G. L. Baker and M. R. Smith III, *J. Am. Chem. Soc.*, **2000**, *122*, 1552.
82. T. M. Ovitt and G. W. Coates, *J. Polym. Sci., Part A: Polym. Chem.*, **2000**, *38*, 4686.
83. K. Majerska and A. Duda, *J. Am. Chem. Soc.*, **2004**, *126*, 1026.
84. Z. Zhong, P. J. Dijkstra and J. Feijen, *Angew. Chem., Int. Ed.*, **2002**, *41*, 4510.
85. Z. Zhong, P. J. Dijkstra and J. Feijen, *J. Am. Chem. Soc.*, **2003**, *125*, 11291.
86. H. Du, A. H. Velders, P. J. Dijkstra, J. Sun, Z. Zhong, X. Chen and J. Feijen, *Chem.–Eur. J.*, **2009**, *15*, 9836.
87. N. Nomura, R. Ishii, M. Akakura and K. Aoi, *J. Am. Chem. Soc.*, **2002**, *124*, 5938.
88. N. Nomura, R. Ishii, Y. Yamamoto and T. Kondo, *Chem.–Eur. J.*, **2007**, *13*, 4433.
89. P. Hormnirun, E. L. Marshall, V. C. Gibson, A. J. P. White and D. J. Williams, *J. Am. Chem. Soc.*, **2004**, *126*, 2688.
90. M. H. Chisholm, J. C. Gallucci, H. Zhen and J. C. Huffman, *Inorg. Chem.*, **2001**, *40*, 5051.

91. H. Y. Chen, H. Y. Tang and C. C. Lin, *Macromolecules*, **2006**, *39*, 3745.
92. W. C. Hung, Y. Huang and C. C. Lin, *J. Polym. Sci. Part A Polym. Chem.*, **2008**, *46*, 6466.
93. C. K. Williams, N. R. Brooks, M. A. Hillmyer and W. B. Tolman, *Chem. Commun.*, **2002**, 2132.
94. C. K. Williams, L. E. Breyfogle, S. K. Choi, W. Nam, V. G. Young, Jr., M. A. Hillmyer and W. B. Tolman, *J. Am. Chem. Soc.*, **2003**, *125*, 11350.
95. J. Ejfler, S. Szafert, K. Mierzwicki, L. B. Jerzykiewicz and P. Sobota, *Dalton Trans.*, **2008**, 6556.
96. W. H. Xie, D. P. Chen, X. H. Fan, J. Li, P. G. Wang, H. N. Cheng and R. G. Nickol, *J. Polym. Sci. Part A: Polym. Chem.*, **1999**, *37*, 3486.
97. H. R. Kricheldorf and K. Saunders, *Makromol. Chem.*, **1990**, *191*, 1057.
98. J. E. Kasperczyk and M. Bero, *Polymer* **2000**, *41*, 391.
99. J. E. Kasperczyk, *Macromolecules*, **1995**, *28*, 3937.
100. S. Dutta, W.-C. Hung, B.-H. Huang and C.-C. Lin, *Adv Polym Sci.*, **2012**, *245*, 219; B. T. Ko and C.-C. Lin, *J. Am. Chem. Soc.*, **2001**, *123*, 7973.
101. C.-A. Huang and C.-T. Chen, *Dalton Trans.*, **2007**, 5561.
102. C.-A. Huang and C.-T. Chen, *Dalton Trans.*, **2008**, 3502.
103. C.-T. Chen, C.-A. Huang and B.-H. Huang, *Dalton Trans.*, **2003**, 3799.
104. N. Nomura, T. Aoyama, R. Ishii and T. Kondo, *Macromolecules*, **2005**, *38*, 5363.
105. W. Li, W. Wu, Y. Wang, Y. Yao, Y. Zhanga and Q. Shen, *Dalton Trans.*, **2011**, *40*, 11378.
106. S. L. Hancock, M. D. Jones, C. J. Langridge and M. F. Mahon, *New J. Chem.*, **2012**, *36*, 1891.
107. C. M. Silvernail, L. J. Yao, L. M. R. Hill, M. A. Hillmyer and W. B. Tolman, *Inorg. Chem.*, **2007**, *46*, 6565.
108. D. J. Darensbourg and O. Karroonnirun, *Macromolecules*, **2010**, *43*, 8880.

109. J. B. L. Gallaway, J. R. K. McRae, A. Decken, and M. P. Shaver, *Can. J. Chem.*, **2012**, *90*: 419.
110. L.-C. Liang, S.-T. Lin, C.-C. Chien, *Polyhedron*, **2012**, <http://dx.doi.org/10.1016/j.poly.2012.06.069>.
111. H. Arakawa, M. Aresta, J.N. Armor, M. A. Barteau, E. J. Beckman, A. T. Bell, J. E. Bercaw, C. Creutz, E. Dinjus, D. A. Dixon, K. Domen, D. L. DuBois, J. Eckert, E. Fujita, D. H. Gibson, W. A. Goddard, D. W. Goodman, J. Keller, G. J. Kubas, H. H. Kung, J. E. Lyons, L. E. Manzer, T. J. Marks, K. Morokuma, K. M. Nicholas, R. Periana, L. Que, J. Rostrup-Nielson, W. M. H. Sachtler, L. D. Schmidt, A. Sen, G. A. Somorjai and P. C. Stair, *Chem. Rev.*, **2001**, *101*, 953.
112. T. Sakakura, J. C. Choi and H. Yasuda, *Chem. Rev.*, **2007**, *107*, 2365.
113. <http://www.chemicals-technology.com/projects/bayer-co2-plastics/>
114. E. B. Cole and A. B. Bocarsly, Photochemical, Electrochemical and Photoelectrochemical Reduction of Carbon Dioxide. In *Carbon Dioxide as Chemical Feedstock*; M. Aresta, Ed.; Wiley-VCH Verlag GmbH & Co. KGaA, Weinheim. **2010**, pp 291-329.
115. G. A. Olah, A. Goeppert and G.K.Surya Prakash, *Beyond Oil and Gas: The Methanol Economy*, Wiley-VCH, **2009**.
116. M. Aresta and A. Dibenedetto, *Dalton Trans.*, **2007**, 2975.
117. N. MacDowell, N. Florin, A. Buchard, J. Hallett, A. Galindo, G. Jackson, C. S. Adjiman, C. K. Williams, N. Shahb and P. Fennell, *Energy Environ. Sci.*, **2010**, *3*, 1645.
118. <http://www.chemicals-technology.com/projects/george-olah-renewable-methanol-plant-iceland/>
119. S. Inoue, H. Koinuma and T. Tsuruta, *J. Polym. Sci. Polym. Lett.*, **1969**, *7*, 287.
120. S. Inoue, H. Koinuma and T. Tsuruta, *Macromol. Chem.*, **1969**, *130*, 210.
121. G. Odian, Principles of polymerization, 4th ed. John Wiley & Sons Inc. New Jersey, **2004**, pp 79.
122. M. Kobayashi, S. Inoue and T. Tsuruta, *Macromolecules*, **1971**, *4*, 658.

123. M. Kobayashi, Y. L. Tang, T. Tsuruta and S. Inoue, *Makromol. Chem.*, **1973**, *169*, 69.
124. M. Kobayashi, S. Inoue and T. Tsuruta, *J. Polym. Sci. Polym. Chem. Ed.* **1973**, *11*, 2383.
125. S. Inoue, M. Kobayashi, H. Koinuma and T. Tsuruta, *Makromol. Chem.* **1972**, *155*, 61.
126. D. J. Darensbourg, J. C. Yarbrough, C. Ortiz, and C. C. Fang, *J. Am. Chem. Soc.* **2003**, *125*, 7586.
127. N. Takeda and S. Inoue, *Makromol. Chem.*, **1978**, *179*, 1377.
128. T. Aida and S. Inoue, *Macromolecules*, **1982**, *15*, 682.
129. T. Aida, M. Ishikawa and S. Inoue, *Macromolecules*, **1986**, *19*, 8.
130. W. Kuran, T. Listos, M. Abramczyk, and A. Dawidek, *J. Macromol. Sci. Pure Appl. Chem.*, **1998**, *35*, 427.
131. M. H. Chisholm and Z. Zhou, *J. Am. Chem. Soc.*, **2004**, *126*, 11030.
132. D. J. Darensbourg and D. R. Billodeaux, *Inorg. Chem.*, **2005**, *44*, 1433.
133. D. J. Darensbourg and M. W. Holtcamp, *Macromolecules*, **1995**, *28*, 7577.
134. D. J. Darensbourg, M. W. Holtcamp, G. E. Struck, M. S. Zimmer, S. A. Niezgoda, P. Rainey, J. B. Robertson, J. D. Draper and J. H. Reibenspies, *J. Am. Chem. Soc.* **1999**, *121*, 107.
135. D. J. Darensbourg, J. R. Wildeson, J. C. Yarbrough and J. H. Reibenspies, *J. Am. Chem. Soc.*, **2000**, *122*, 12487.
136. M. Cheng, E. B. Lobkovsky and G. W. Coates, *J. Am. Chem. Soc.* **1998**, *120*, 11018.
137. M. Cheng, D. R. Moore, J. J. Reczek, B. M. Chamberlain, E. B. Lobkovsky and G. W. Coates, *J. Am. Chem. Soc.*, **2001**, *123*, 8738.
138. D. R. Moore, M. Cheng, E. B. Lobkovsky and G. W. Coates, *Angew. Chem., Int. Ed.*, **2002**, *41*, 2599.
139. Y. L. Xiao, Z. Wang, K. L. Ding, *Chem. Eur. J.* **2005**, *11*, 3668.

140. M. R. Kember, P. D. Knight, P. T. R. Reung and C. K. Williams, *Angew. Chem. Int. Ed.* **2009**, *48*, 931.
141. M. R. Kember, A. J. P. White and C. K. Williams, *Inorg. Chem.*, **2009**, *48*, 9535.
142. F. Jutz, A. Buchard, M. R. Kember, S. B. Fredriksen and C. K. Williams, *J. Am. Chem. Soc.*, **2011**, *133*, 17395.
143. Y. L. Xiao, Z. Wang and K. L. Ding, *Macromolecules*, **2006**, *39*, 128.
144. S. Sujith, J. Min, J. Seong, S. Na and B. Y. Lee, *Angew. Chem., Int. Ed.*, **2008**, *47*, 7306.
145. J. K. Varghese, A. Cyriac and B. Y. Lee, *Polyhedron*, **2012**, *32*, 90.
146. X.-B. Lu, Y.-J. Zhang, B. Liang, X. Li and H. Wang, *J. Mol. Catal. A: Chem.*, **2004**, *210*, 31.
147. X.-B. Lu, Y.-J. Zhang, K. Jin, L.-M. Luo and H. Wang, *J. Catal.*, **2004**, *227*, 537.
148. J. Melendez, M. North and R. Pasquale, *Eur. J. Inorg. Chem.*, **2007**, 3323.
149. W. Clegg, R. W. Harrington, M. North and R. Pasquale, *Chem. Eur. J.* **2010**, *16*, 6828.
150. M. North and R. Pasquale, *Angew. Chem., Int. Ed.*, **2009**, *48*, 2946.
151. Y.-M. Shen, W.-L. Duan, M. Shi, *J. Org. Chem.*, **2003**, *68*, 1559.
152. T. Ema, Y. Miyazaki, S. Koyama, Y. Yano and T. Sakai, *Chem. Commun.*, **2012**, *48*, 4489.
153. E. N. Jacobsen, *Science*, **2003**, *299*, 1691.
154. Taden, H.-C. Kang, W. Massa, T. P. Spaniol and J. Okuda, *Eur. J. Inorg. Chem.* **2000**, 441.
155. T. M. Ovitt and G. W. Coates, *J. Am. Chem. Soc.* **2002**, *124*, 1316.
156. N. Nimitsiriwat, E. L. Marshall, V. C. Gibson, M. R. J. Elsegood and S. H. Dale, *J. Am. Chem. Soc.* **2004**, *126*, 13598.
157. J. Ejfler, M. Kobylka, L. B. Jerzykiewicz and P. Sobota, *Dalton Trans.* **2005**, 2047.

158. E. Y. Tshuva, M. Versano, I. Goldberg, M. Kol, H. Weitman and Z. Goldschmidt, *Inorg. Chem. Commun.*, **1999**, 2, 371.
159. E. Y. Tshuva, I. Goldberg, M. Kol, H. Weitman, and Z. Goldschmidt, *Chem. Commun.*, **2000**, 379.
160. E. Y. Tshuva, I. Goldberg, M. Kol and Z. Goldschmidt, *Inorg. Chem. Commun.*, **2000**, 3, 610.
161. E. Y. Tshuva, I. Goldberg, M. Kol and Z. Goldschmidt, *Organometallics*, **2001**, 20, 3017.
162. S. Groysman, E. Sergeeva, I. Goldberg, and M. Kol, *Inorg. Chem.* **2005**, 44, 8188

1.16 Co-Authorship Statement

This PhD thesis includes results of joint research that have been published in peer reviewed journals in the form of three full papers, as follows:

Chapter 3: Zinc Complexes of Piperazinyl-aminephenolate Ligands: Synthesis, Characterization and Ring-Opening Polymerization Activity

Authors: Nduka Ikpo, Lisa N. Saunders, Jillian L. Walsh, Jennifer M. B. Smith, Louise N. Dawe, and Francesca M. Kerton

Journal: *Eur. J. Inorg. Chem.*, **2011**, 5347–5359

The principal author (Nduka Ikpo) contributed to all aspects of the project as the main researcher including: literature review, performing 90% of all the experiments, collecting and analyzing the data, designing some of the experiments, presenting and discussing the data with the corresponding author, mentoring Lisa N. Saunders and Jillian L. Walsh as summer students and Jennifer M. B. Smith as a Women in Science and Engineering High-School Summer Student (WISE) and writing the first manuscript.

The co-authors (Lisa N. Saunders and Jillian L. Walsh and Jennifer M. B. Smith) ran around 10% of the experiments, particularly helping in the ligand synthesis.

The co-author (Dr. Louise Dawe) is a crystallographer at Memorial University of Newfoundland, who collected XRD data and solved the structures for the complexes and wrote the crystallographic procedure section.

The corresponding author (Dr. Francesca M. Kerton) was the principal investigator and developed the original ideas for this research. She oversaw all aspects of the project,

including supervision of the principal author (N. I.) and co-authors (the summer students) the design of experiments, data analysis, revision of the draft manuscript and submission to the journal, and responding to the questions and comments from the peer reviewers.

Chapter 4: Aluminum methyl and chloro complexes bearing monoanionic aminephenolate ligands: synthesis, characterization and use in polymerizations.

Authors: Nduka Ikpo, Stephanie M. Barbon, Marcus W. Drover, Louise N. Dawe, and Francesca M. Kerton

Journal: *Organometallics*, **2012**, *31*, 8145–8158.

The principal author (Nduka Ikpo) contributed to all aspects of the project as the main researcher including: literature review, performing 70% of all the experiments, collecting and analyzing the data, designing some of the experiments, presenting and discussing the data with the corresponding author, mentoring Stephanie M. Barbon, Marcus W. Drover as summer students and writing the first draft of the manuscript.

The co-authors (Stephanie M. Barbon, Marcus W. Drover) ran around 30% of the experiments, helping in the synthesis and growing crystals of the Al complexes.

The co-author (Dr. Louise Dawe) is a crystallographer at Memorial University of Newfoundland, who collected XRD data and solved the structures for the complexes and wrote the crystallographic procedure section.

The corresponding author (Dr. Francesca M. Kerton) was the principal investigator and developed the original ideas for this research. She oversaw all aspects of the project, including supervision of the principal author (N. I.) and co-authors (S. M. B and M.W.D)

the design of experiments, data analysis, revision of the draft manuscript and submission to the journal, and responding to the questions and comments from the peer reviewers.

Chapter 5: Ring-opening polymerization of ϵ -caprolactone by lithium piperazinyl-aminephenolate complexes: Synthesis, characterization and kinetic studies.

Authors: Nduka Ikpo, Christian Hoffmann, Louise N. Dawe, and Francesca M. Kerton

Journal: *Dalton Trans.*, **2012**, *41*, 6651–6660

The principal author (Nduka Ikpo) contributed to all aspects of the project as the main researcher including: literature review, performing 90% of all the experiments, collecting and analyzing the data, designing some of the experiments, presenting and discussing the data with the corresponding author, mentoring Christian Hoffmann as DAAD-RISE summer student and writing the first draft of the manuscript.

The co-authors (Christian Hoffmann) ran around 10% of the experiment, helping in conducting part of the polymerization experiments.

The co-author (Dr. Louise Dawe) is a crystallographer at Memorial University of Newfoundland, who collected XRD data and solved the structures for the complexes and wrote the single crystal X-ray diffraction studies section.

The corresponding author (Dr. Francesca M. Kerton) was the principal investigator and developed the original ideas for this research. She oversaw all aspects of the project, including supervision of the principal author (N. I.) and co-authors (C. H.) the design of

experiments, data analysis, revision of the draft manuscript and submission to the journal,
and responding to the questions and comments from the peer reviewers

CHAPTER 2

Synthesis and Characterization of Amine-Phenol Ligands

Chapter 2

Synthesis and Characterization of Amine-Phenol Ligands

This chapter will discuss the synthesis and characterizations of the ligands used throughout this thesis to prepare metal complexes that were subsequently investigated for catalytic ROP of cyclic esters. A series of methylpiperazinyl phenols, morpholinyl phenols, 2,4-dimethylmorpholinyl phenols and homopiperazinyl bis(phenols) were synthesized in one-pot Mannich condensation reactions in water. The formation of these compounds was confirmed by ^1H and $^{13}\text{C}\{^1\text{H}\}$ NMR spectroscopies, MALDI-TOF MS, melting point, elemental analysis and, in some cases, X-ray diffraction studies.

2.1 Introduction

In recent years, ligands based on a mixed set of N-,O-donor atoms have attracted a great deal of interest because of the appealing modular (sterics and electronics can be tailored) properties they exhibit. Oxygen is considered a hard donor atom, while nitrogen falls within the borderline region in the hard and soft acids and bases (HSAB) classification.¹ This implies the ability to bind to the oxophilic main group and early transition metals in a variety of coordination geometries. As discussed in Chapter 1 (section 1.4.3.2), control of the nuclearity of the metal species is a goal in the design of catalysts for polymerization reactions. Bulky ancillary ligands are very important to provide a steric barrier for prevention of undesired side reactions; however, the ligand should be small enough as to not excessively hinder the approach of the monomer to the

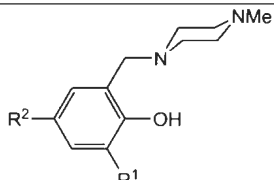
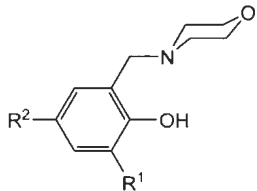
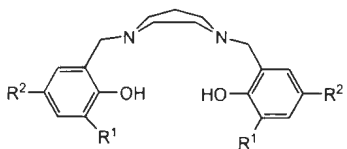
active site.² Thus, N-,O-mixed donor amine-phenol ligands would be reasonable candidates to meet the demands for steric and electronic tunability, since the *ortho* and *para* substituents (R) and the substituents on the amine unit can be conveniently varied. This can be achieved by selection of electron-withdrawing e.g. Cl, electron-donating e.g. methoxy, or bulkier e.g. *tert*-butyl substituents. Amine-phenol ligands are of particular interest because they can be easily synthesized from readily available starting materials, i.e., amines, formaldehyde, and substituted phenols, in a single-step Mannich condensation reaction.³

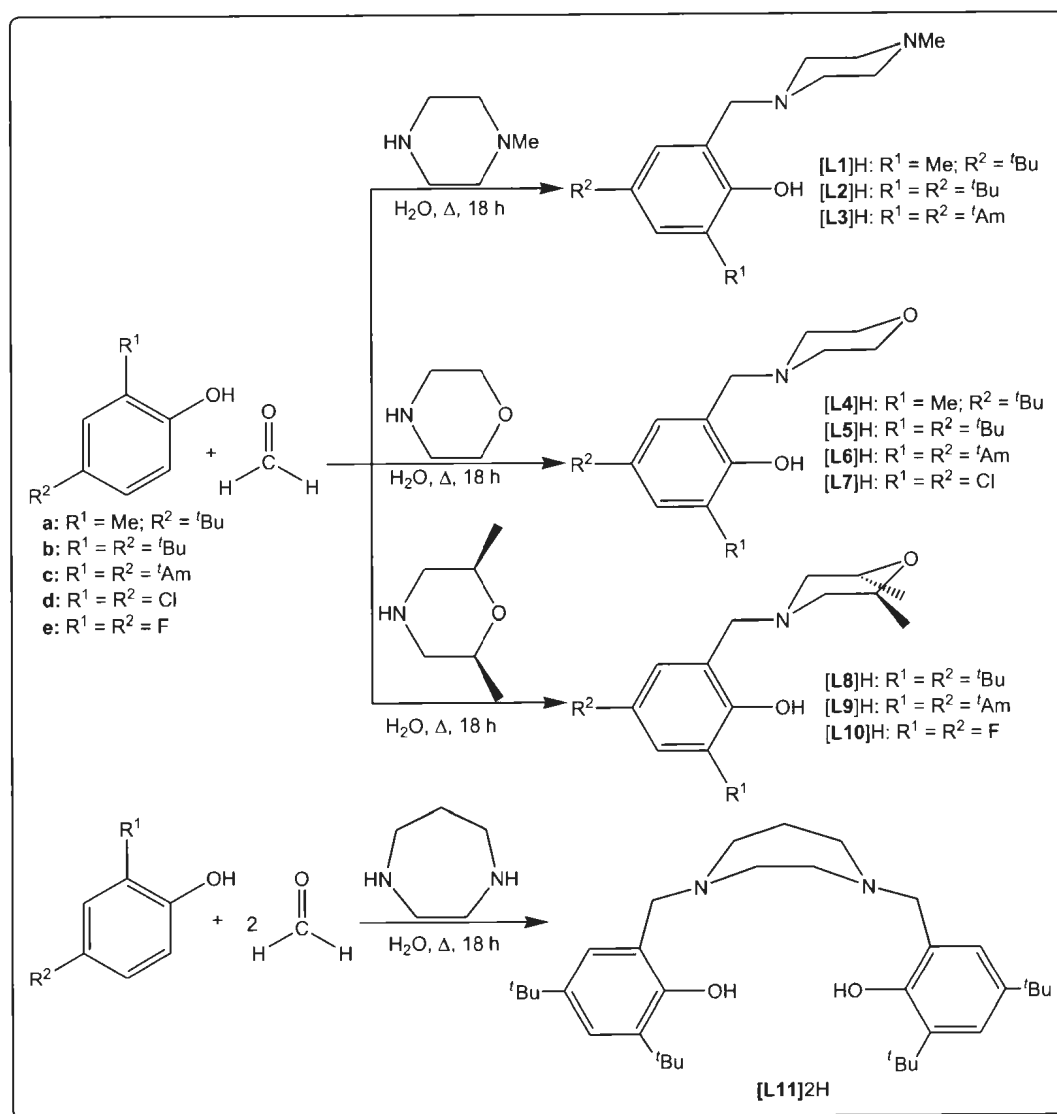
The Mannich reaction involves the combination of a compound containing active hydrogen atoms (enolizable carbonyl compound) with a non-enolizable aldehyde (commonly formaldehyde) and an amine, which can be ammonia, amide, or a primary or secondary amine.³ Burke *et al.* prepared a large number of amine mono- and bis-phenol ligands by reaction of *ortho* and *para* halogen substituted phenols with formaldehyde and primary amines in dioxane, affording 61-88% yields.⁴ Kol and co-workers reported the preparation of amine-phenol ligands using ether as a solvent and their coordination chemistry with Group IV transition metals.⁵⁻⁷ These complexes were employed as catalysts in ethylene and alpha-olefin polymerization. Because of the importance of these ligands, it is important to develop efficient methods to prepare them. Significant progress has been made with respect to this by Kerton and co-workers by the introduction of benign reaction conditions (using water as a medium) for the synthesis of amine-phenol ligands. Not only is this route greener, it also resulted in increased yields and better reproducibility of the Mannich condensation reaction.^{8,9}

2.2 Results and Discussion

A series of amine-mono(phenol) and amine-bis(phenol) ligands have been synthesized by Mannich reactions between formaldehyde, substituted phenols and various amines to obtain ligands of different sizes. Some of the amine-phenol ligands independently synthesised by other research groups during the course of this research are comparatively reported in Table 2.1. The reactions were carried out under reflux using water as a reaction medium, as shown in Scheme 2.1. Aqueous formaldehyde was used in all syntheses, while the amines and phenols were varied (*viz.* 1-methyl piperazine, morpholine, 2,4-dimethyl morpholine, homopiperazine). In addition, substituted phenols used include 2-*tert*-butyl-4-methylphenol, 2,4-di-*tert*-butylphenol, 2,4-dichlorophenol, 2,4-difluorophenol and 2,4-di-*tert*-amylphenol.

Table 2.1. Some amine-phenol ligands independently reported by other research groups

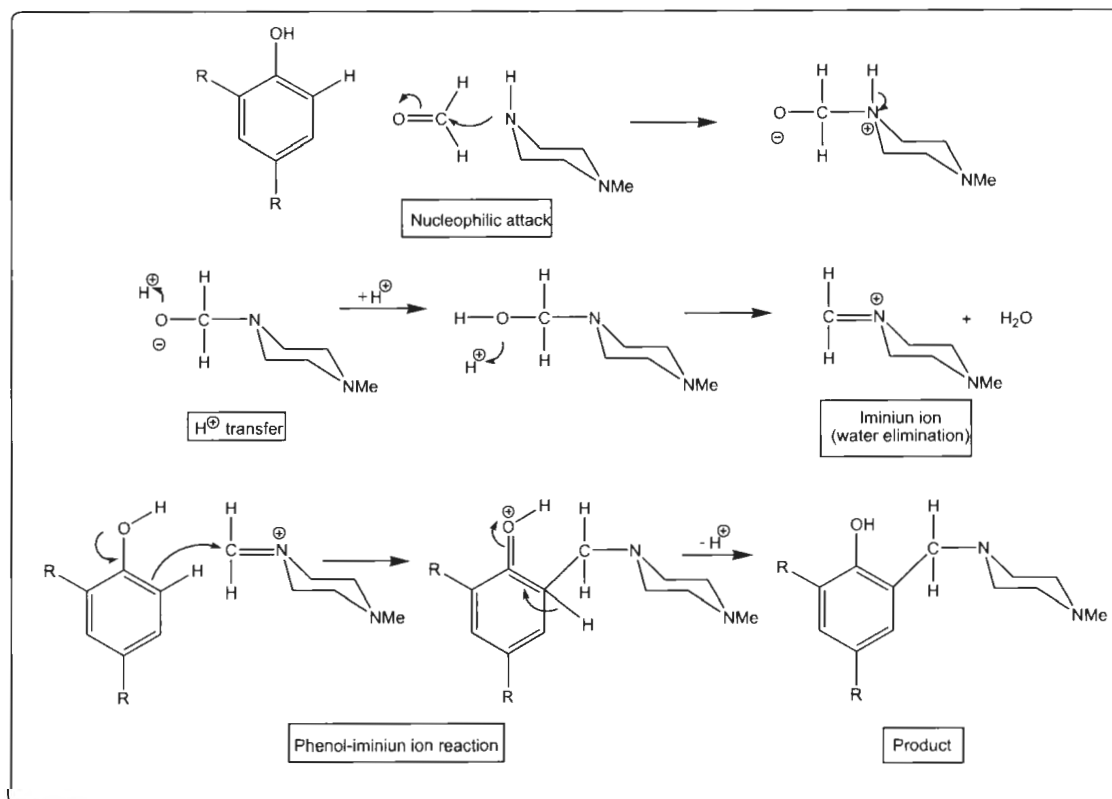
Ligand	Substituent	Solvent and reagents	Yield (%)	Ref
	$R^1 = \text{'Bu}, R^2 = \text{H}$	Ethanol	66	10
	$R^1 = \text{'Bu}, R^2 = \text{'Bu}$	Ethanol, HBr, Na[HCO ₃]	86	11
	$R^1 = \text{'Bu}, R^2 = \text{'Bu}$	Water	90	This work
	$R^1 = \text{'Bu}, R^2 = \text{H}$	Ethanol	50	10
	$R^1 = \text{'Bu}, R^2 = \text{'Bu}$	Dioxane,	94	12
	$R^1 = \text{'Bu}, R^2 = \text{Me}$	Water	88	This work
	$R^1 = \text{'Bu}, R^2 = \text{'Bu}$	Methanol, CH ₂ Cl ₂	72	13
	$R^1 = \text{'Bu}, R^2 = \text{'Bu}$	Water	95	This work



Scheme 2.1. Procedure for preparation of amine-phenol ligands.

The generally accepted mechanism of the Mannich reaction involves nucleophilic attack by the amine at the carbonyl C atom as the first step, followed by electrophilic addition of the iminium ion to the C—C double bond of the active hydrogen compound. This mechanism applied to the formation of the aminephenol ligands in the current research, is depicted in Scheme 2.2. The reaction is initiated by the attack of the

nucleophilic N atom of the amine to the carbonyl C atom of the formaldehyde, which forms the iminium ion with the elimination of water. The iminium ion subsequently reacts with the substituted phenol (active hydrogen compound) to generate the desired product.



Scheme 2.2. Proposed mechanism of Mannich condensation.

It is noteworthy that the preparation and characterization of [L1]H, [L2]H, [L3]H and [L5]H have been discussed in Chapter 3 with their zinc complexes. Generally, the formaldehyde and amine reagents are miscible in the aqueous phase, but the phenols are generally insoluble. With rapid stirring of the reaction mixture, however, an emulsion

forms, causing the reaction to occur at an aqueous-organic interface.⁷ By simple filtration or decanting of the resulting aqueous phase of the reaction mixture, the products of the ligand synthesis can be obtained in moderate to high yields.

2.2.1 Morpholinyl Phenol Ligands

The morpholinyl phenols [L4]H, [L6]H, and [L7]H were synthesized by condensation of one equivalent each of morpholine, formaldehyde and various phenols in water to afford the products shown in Scheme 2.1. The structures of these compounds were deduced from their ¹H NMR spectra and also from the X-ray crystal structure of [L5]H, which confirms connectivity of the compounds. For [L4]H with ^tBu and Me groups in the *ortho* and *para* positions of the phenol, respectively, the presence of 9 protons, 3 protons, and 2 protons at 1.40, 2.23 and 3.65 ppm as singlets correspond to the ^tBu, Me and CH₂ groups, respectively (Figure 2.1). Two broad signals at 2.54 ppm and 3.74 ppm corresponding to 4 protons were assigned to the two the sets of CH₂ hydrogens in the morpholine unit. The ligand identity was further confirmed by the ¹³C{¹H} NMR spectrum, in which all the characteristic peaks were observed and assigned. The MALDI-TOF MS spectrum of [L4]H exhibits a peak at *m/z* 262 {[M]⁺} (Figure 2.2), which is in good accordance with the composition of the ligand.

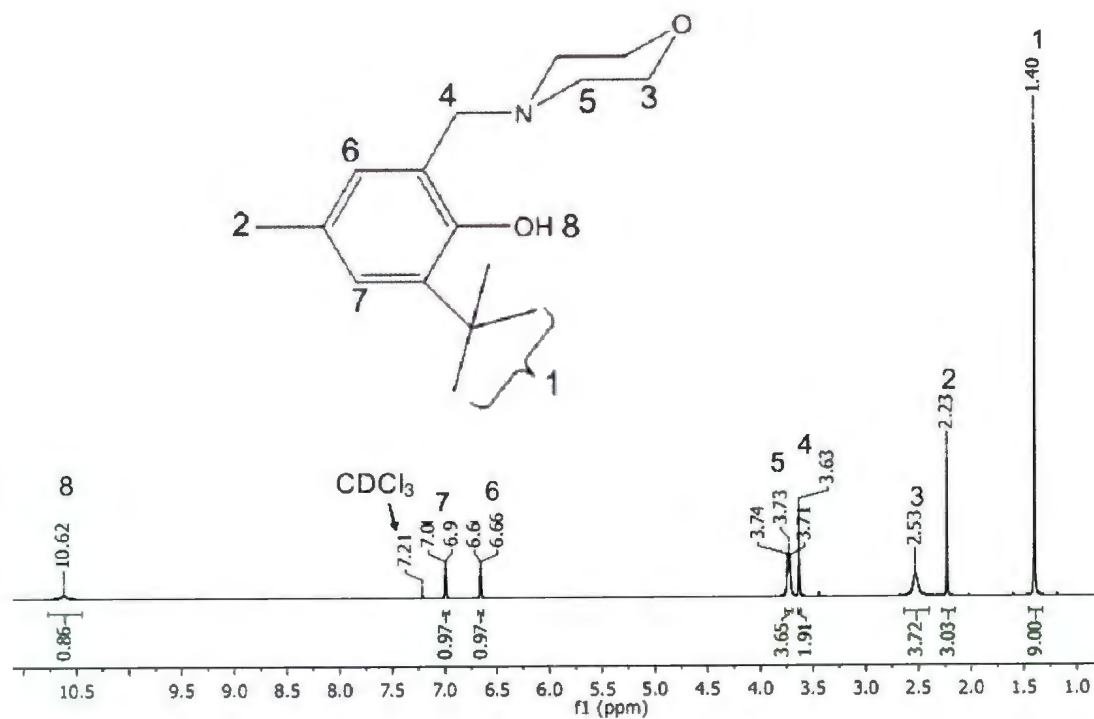


Figure 2.1. ¹H NMR spectrum of [L4]H

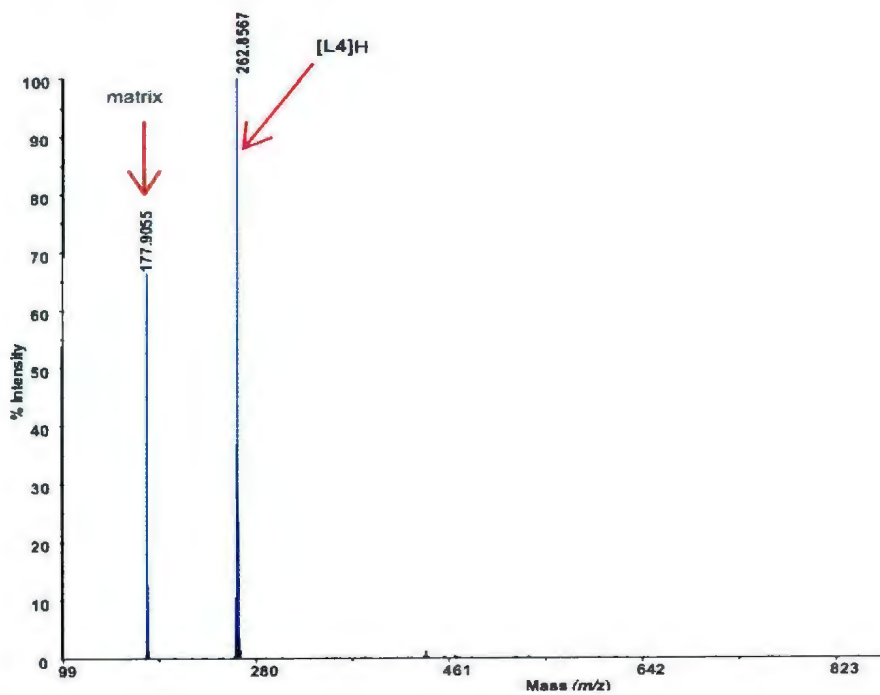


Figure 2.2. MALDI-TOF mass spectrum of [L4]H

The structure of the ligand [L6]H with ¹Am groups in the *ortho* and *para* positions was elucidated from the ¹H NMR spectrum, in which two overlapping triplets at 0.61-0.65 ppm, two sets of quartets at 1.54 ppm and 1.85 ppm, and two singlets at 1.35 ppm and 1.54 ppm were assigned to Me protons adjacent to the CH₂ group, the CH₂ protons adjacent to the Me group and two sets of Me protons of the ¹Am substituents in the *ortho* and *para* positions respectively. The CH₂ and the Me group in the ¹Am substituent coupled with each other, resulting in multiplicities of a quartet and triplet with *J* = 7.4 Hz. The structure was also confirmed by ¹³C{¹H} NMR and authenticated by the MALDI-TOF MS spectrum with a peak at *m/z* 333, which corresponds to the molecular weight of the ligand. The ¹H NMR spectrum of the ligand [L7]H, which contains electron withdrawing substituents in the *ortho/para* positions exhibited resonances for the methylene groups within the morpholine unit at 2.60 ppm and 3.77 ppm; the CH₂ protons connecting the morpholine and the phenol unit gave rise to a peak at 3.70 ppm, while the aromatic proton resonances occurred at 6.89 ppm and 7.28 ppm, integrating to 4, 4, 2, 1 and 1 protons, respectively.

2.2.2 2,6-Dimethyl Morpholinyl Phenol Ligands

The ligands with methyl groups in the 2- and 6- positions of the morpholine unit, [L8]H, [L9]H and [L10]H, were prepared in satisfactory yields in an analogous procedure to the unsubstituted analogs. All 3 ligands possessed similar NMR spectra and the ¹H NMR spectrum for [L8]H will be discussed in detail. Resonances in the ¹H NMR spectrum of compound [L8]H appeared at *ca.* 3.74, 1.90 and 1.16 ppm as triplets, quartets and doublets, which were attributed to the CH, CH₂ and CH₃ protons of the morpholine

unit, respectively. The MALDI-TOF MS spectra of the ligands were in agreement with the molecular weight of the proposed structures of the ligands. The structure of [L8]H was further established by its X-ray crystal structure (Figure 2.3). Table 2.2 summarizes crystal data for compounds [L8]H and [L11]H₂

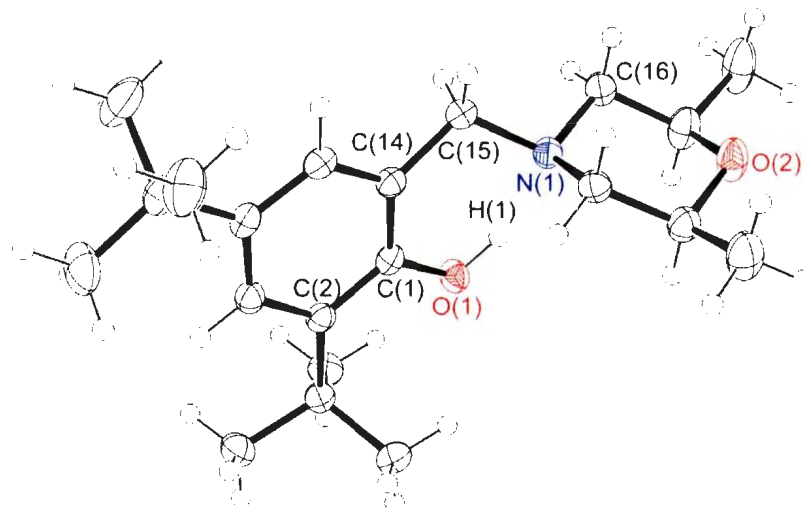


Figure 2.3. Molecular structure of [L8]H. (50% displacement ellipsoids). Selected bond lengths (Å) and bond angles (°): O(1)-C(1), 1.366(2); N(1)-C(15), 1.472(2); C(14)-C(15), 1.516(2); O(1)-C(1)-C(14), 119.73(14); O(1)-C(1)-C(2), 119.76(14); N(1)-C(15)-C(14), 113.72(14).

2.2.3 Homopiperazinyl Bis(phenol) Lgand

The homopiperazine ligand [L11]H₂ was prepared in high yield by the condensation reaction between 2 equivalents of both 2,4-di-*tert*-butyl phenol, and formaldehyde, and 1 equivalent of homopiperazine. The structure was elucidated by its ¹H NMR spectrum, which displayed two singlets at 1.27 and 1.42 ppm, a quintet at 1.92 ppm, a singlet at 2.77 ppm, a broad peak at 2.82 ppm, a singlet at 3.76 ppm and two aromatic resonances at 6.81 and 7.21 ppm. These peaks integrated to 2 × 18, 2, 4, 2 × 4 and 2 × 2 protons and were

attributed to the two sets of ^tBu groups, CH₂ of the amine, CH₂ linkage which couples the amine and the phenol, another CH₂ of the amine and the CH of the phenol, respectively. The structure was further confirmed by MALDI-TOF MS in which the peak at *m/z* 536 is consistent with the molecular weight of the desired product. In addition, X-ray diffraction studies authenticate the structure of the compound [L11]H₂. The Ortep structure (Figure 2.4) shows the ligand oriented such that the two phenol oxygens are *trans* to one another.

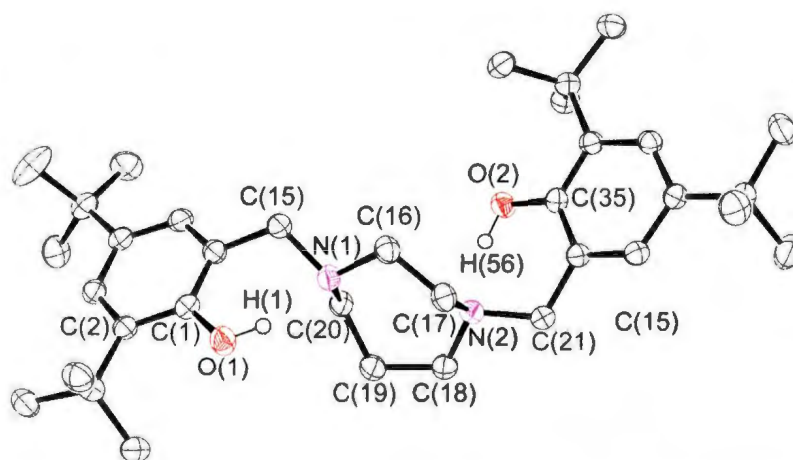


Figure 2.4. Molecular structure of [L11]H₂. The displacement ellipsoids are drawn at the 50% probability level; H atoms are excluded for clarity. Selected bond lengths [Å] and bond angles [°]: O(1)-C(1), 1.373(2); O(1)-H(1), 0.86(2); O(2)-C(35), 1.367(2); O(2)-H(56), 0.93(2); N(1)-C(16), 1.467(2); N(1)-C(20), 1.474(2); N(1)-C(15), 1.480(2); N(2)-C(18), 1.463(2); N(2)-C(21), 1.479(2); N(2)-C(17), 1.479(2); C(1)-O(1)-H(1), 104.6(16); C(35)-O(2)-H(56), 102.8(14); C(16)-N(1)-C(20), 113.25(13); C(16)-N(1)-C(15), 108.77(13); C(20)-N(1)-C(15), 110.23(13); C(18)-N(2)-C(21), 108.94(13); C(18)-N(2)-C(17), 113.56(14); C(21)-N(2)-C(17), 112.37(14); O(1)-C(1)-C(2), 120.05(15)

2.3 Conclusions

In conclusion, an array of N,O-mixed donor amine-phenol ligands have been successfully synthesized through one-pot reactions whose workups involved straightforward filtrations. By altering the amine precursors, combined with controlling of

the stoichiometry, ligands with different outersphere substituents (O and NMe), ranging from amine-mono(phenol)s up to amine-bis(phenol) were obtained. The general mechanism for Mannich condensation, which involves the formation of iminium ion intermediates is adopted for the reactions.

Interestingly, the synthesis of these amine-phenol ligands was carried out using water as the reaction medium. This method not only prevents the use of multiple steps, but improves the yields of the products compared to methods employing volatile organic compound solvents.

2.4 Experimental Section

2.4.1 General Procedures

All experiments involving ligands were performed on the bench. Deuterated chloroform (CDCl_3) was purchased from Cambridge Isotope Laboratories, Inc. 2,4-di(*tert*-butyl)phenol, 2-*tert*-butyl-4-methylphenol, 2,4-di(*tert*-amyl)phenol, 1-methyl piperazine, homopiperazine, morpholine and 2,6-dimethylmorpholine were purchased from Sigma-Aldrich or Alfa Aesar used as received. Elemental analyses were performed by Canadian Microanalytical Service Ltd., Delta, BC, Canada. ^1H and $^{13}\text{C}\{^1\text{H}\}$ NMR spectra were recorded on a Bruker Avance 300 or 500 MHz spectrometer at 25 °C (unless otherwise stated) and were referenced internally using the residual ^1H and ^{13}C resonances of the solvent. ^{13}C signals were assigned using heteronuclear single quantum coherence (HSQC) experiments. Matrix-assisted laser desorption/ionization time-of-flight mass spectrometry (MALDI-TOF MS) was performed using an Applied Biosystems Voyager

DE-PRO or an Applied Biosystems 4800 MALDI TOF/TOFTM Analyzer equipped with a reflectron, delayed ion extraction and high performance nitrogen laser (337 nm). Anthracene was used as the matrix.

2.4.2 Single Crystal X-ray Diffraction Studies

Crystals of [L8]H and [L11]H₂ were mounted on low temperature diffraction loops and measured on a Rigaku Saturn CCD area detector with graphite monochromated Mo-K α radiation. The structures were solved by direct methods¹⁴ and expanded using Fourier techniques.¹⁵ Neutral atom scattering factors were taken from Cromer and Waber.¹⁶ Anomalous dispersion effects were included in F_{calc}¹⁷; the values for $\Delta f'$ and $\Delta f''$ were those of Creagh and McAuley.¹⁸ The values for the mass attenuation coefficients are those of Creagh and Hubell.¹⁹ All calculations were performed using CrystalStructure^{20,21} except for refinement, which was performed using SHELXL-97.¹⁴ All non-hydrogen atoms were refined anisotropically, while hydrogen atoms were introduced in calculated positions and refined on a riding model.

Table 2.2. Summary of crystal data for compounds [L8]H and [L11]H₂

Compounds	[L8]H	[L11]H ₂
Formula	C ₂₁ H ₃₅ NO ₂	C ₃₅ H ₅₆ N ₂ O ₂
Formula Weight	333.51	536.84
Crystal System	Monoclinic	Triclinic
Space Group	P2 ₁ /C	P-1
<i>a</i> /Å	12.013(4)	10.054(2)
<i>b</i> /Å	17.863(6)	13.377(2)
<i>c</i> /Å	9.836(3)	14.313(4)
α /°	90	65.731(13)
β /°	101.484(5)	88.182(19)
γ /°	90	72.163(14)
<i>V</i> / Å ³	2068.5(12)	1660.7(6)
<i>T</i> /K	153	153
<i>Z</i>	4	2
<i>D</i> _c gcm ⁻³	1.071	1.073
<i>F</i> (000)	736	592
μ (MoK α) cm ⁻¹	0.67	0.65
Total reflections	21073	16049
Unique reflections	4291	6844
<i>R</i> _{int}	0.0239	0.0258
Reflections <i>I</i> > 2 σ (<i>I</i>)	4078	6051
No. of parameters	219	359
<i>R</i> , <i>wR</i> ₂ [<i>I</i> > 2 σ (<i>I</i>)]	0.0497, 0.1276	0.0639, 0.1831
GOF	1.112	1.094

2.4.3 Synthetic procedures

[ONO^{Me,tBu}] ([L4]H) Water (80 mL), 2-*tert*-butyl-4-methylphenol (13.0 g, 149 mmol) and formaldehyde, (37 wt.% in H₂O, 12.1 mL, 149 mmol) were added to a 250 mL round-bottom flask equipped with a stir bar and condenser. Morpholine (6.80 mL, 149 mmol) was added dropwise to the stirred solution. The resulting mixture was heated at

reflux for 18 h. Upon cooling to RT, a white precipitate formed and was isolated by filtration. Analytically pure product could be obtained by growing colorless crystals from a saturated MeOH solution. Yield: 34.4 g, 87.5%. mp 85-87 °C; MS (MALDI, matrix: anthracene) m/z 262 (M^+ , 100%); Anal. calcd. for $C_{16}H_{25}NO_2$: C, 72.96; H, 9.57; N, 5.32. Found: C, 71.70; H, 10.00; N, 5.19%. 1H NMR ($CDCl_3$, 300 MHz, 343 K) δ 10.62 (ArOH), 7.00 (1H, s, $J = 2.0$ Hz, ArH), 6.66 (1H, d, $J = 2.0$ Hz, ArH), 3.74 (4H, t, $J = 4.4$ Hz, O- C_2H_4 - C_2H_4 -N), 3.63 (2H, br, ArC- CH_2 -N), 2.53 (4H, br, O- C_2H_4 - C_2H_4 -N), 2.23 (3H, s, ArC- CH_3), 1.40 (18H, s, ArC-C{ CH_3 } $_3$), $^{13}C\{^1H\}$ NMR ($CDCl_3$, 125 MHz, 298 K) δ 153.7 (ArC-O), 136.0 (ArC-C{ CH_3 } $_3$), 127.1 (ArC- CH_3), 126.9 (ArC-H), 126.5 (ArC-H), 120.4 (ArC- CH_2 -N), 66.4 (ArC- CH_2 -N), 61.8 (O- C_2H_4 - C_2H_4 -N), 52.4 (O- C_2H_4 - C_2H_4 -N), 34.2 (ArC-C{ CH_3 } $_3$), 29.2 (ArC-C{ CH_3 } $_3$), 20.4 (ArC- CH_3).

[$ONO^{tAm,tAm}$] ([L6]H). Water (80 mL), 2,4-di-*tert*-amylphenol (18.8 g, 80.0 mmol) and formaldehyde (37 wt. % in H_2O , 6.50 mL, 80.0 mmol) were added to a 250 mL round-bottom flask equipped with a stir bar and condenser. Morpholine (6.97 mL, 80.0 mmol) was added dropwise to the stirred solution. The resulting mixture was heated at reflux for 18 h. Upon cooling to RT, a two-phase mixture was formed. The aqueous layer was decanted, while the oily, organic layer was washed with MeOH and dried under vacuum to remove any unreacted organic components. The resulting brown, sticky gel-like material was sonicated in an ultrasound bath to afford a white powder, which was recrystallized in MeOH to give a colorless solid. Yield: 25 g, 92%. mp 73-76 °C; MS (MALDI, matrix: anthracene) m/z 332 (M^+ , 100%); Anal. calcd for $C_{21}H_{35}NO_2$: C, 75.63; H, 10.58; N, 4.20. Found: C, 75.72; H, 10.73; N, 4.18%. 1H NMR ($CDCl_3$, 300 MHz, 298

K) δ 10.53 (1H, s, ArOH), 7.09 (1H, d, $J = 2.3$ Hz, ArH), 6.77 (1H, d, $J = 2.3$ Hz, ArH), 3.72 (4H, t, $J = 2.3$ Hz, O-C₂H₄C₂H₄-N), 3.66 (2H, s, ArC-CH₂-N), 2.52 (4H, br, O-C₂H₄C₂H₄-N), 1.93 (2H, q, $J = 7.4$ Hz, Ar-C{CH₂}CH₃), 1.61 (2H, q, $J = 7.4$ Hz, Ar-C{CH₂}CH₃), 1.36 (6H, s, ArC-C(CH₃)₂), 1.26 (6H, s, ArC-C(CH₃)₂), 0.68 (3H, t, $J = 7.4$ Hz, CH₂CH₃), 0.62 (3H, t, $J = 7.4$ Hz, CH₂CH₃). ¹³C{¹H} NMR (CDCl₃, 125 MHz, 298K): δ 153.5 (ArC-O), 138.4 (ArC-C{CH₃}₂), 133.4 (ArC-C{CH₃}₂), 124.8 (ArC-H), 123.8 (ArC-H), 119.4 (ArC-CH₂-N), 66.4 (O-C₂H₄-C₂H₄-N), 62.3 (ArC-CH₂-N), 52.0 (O-C₂H₄-C₂H₄-N), 38.0 (ArC-C{CH₃}₂CH₂), 36.8 (ArC-C{CH₃}₂CH₂), 32.6 (ArC-C{CH₃}₂CH₂), 28.2 (ArC-C{CH₃}₂CH₂), 27.3 (ArC-C{CH₃}₂CH₂), 9.2 (ArC-C{CH₃}₂CH₂CH₃), 8.8 (ArC-C{CH₃}₂CH₂CH₃).

[ONO^{Cl,Cl}] ([L7]H). A solution of formaldehyde (37 wt. % in H₂O, 8.10 mL, 100 mmol) and 2,4-dichlorophenol (16.3 g, 100 mmol) were added to a 500 mL round-bottom flask equipped with a stir bar, condenser and water (100 mL). Morpholine (8.65 mL, 100 mmol) was added dropwise to the stirred solution. The resulting mixture was heated at reflux for 18 h. Upon cooling to RT, a two-phase mixture was formed. The brown, oily organic layer was extracted from the aqueous layer using Et₂O in a separatory funnel. Et₂O was removed under reduced pressure to afford a brown, crystalline solid, and was recrystallized in MeOH to give an off-white, crystalline solid. Yield: 22.50 g, 86.2%. mp 87-90 °C; Anal. calcd. for C₁₁H₁₃Cl₂N₂O₂: C, 50.40; H, 5.00; N, 5.34. Found: C, 50.50; H, 5.06; N, 5.29%. ¹H NMR (CDCl₃, 500 MHz, 298 K) δ 11.46 (1H, s, ArOH), 7.25 (1H, s, $J = 2.4$ Hz, ArH), 6.88 (1H, s, $J = 2.4$ Hz, ArH), 3.74 (4H, $J = 4.4$ Hz, O-C₂H₄-C₂H₄-N), 3.67 (2H, s, Ar-CH₂-N), 2.56 (4H, br, O-C₂H₄-C₂H₄-N). ¹³C{¹H} NMR (CDCl₃, 125

MHz, 298K): δ 151.8 (ArC-OH), 128.1 (ArC-CH₂-N), 126.3 (ArCH), 122.8 (ArCH), 122.3 (ArC-Cl), 120.8 (ArC-Cl), 65.9 (O-C₂H₄-C₂H₄-N), 60.6 (ArC-CH₂-N), 52.1 (O-C₂H₄-C₂H₄-N).

[O^{Me,Me}NO^{tBu,tBu}] ([L8]H). [L8]H was prepared in analogous procedure to [L4]H, with H₂O (80.0 mL), 2,4-di-*tert*-butylphenol (6.19 g, 30.0 mmol), and formaldehyde (37 wt. % in H₂O, 2.44 mL, 30.0 mmol) and 2,6-di-methylmorpholine (3.70 mL, 30.0 mmol). [L8]H was obtained as a gray solid, which was recrystallized in MeOH to give a colourless, crystalline solid. Yield: 9.20 g, 92.0%. Crystals suitable for X-ray diffraction were grown from a saturated methanol solution at 0 °C. mp 133-135 °C; MS (MALDI, matrix: anthracene) *m/z* 332 (M⁺, 100%); Anal. calcd. for C₂₁H₃₅NO₂: C, 75.63; H, 10.58; N, 4.20. Found: C, 75.61; H, 10.73; N, 4.18%. ¹H NMR (CDCl₃, 500 MHz, 298 K) δ 10.78 (1H, s, ArOH), 7.24 (1H, d, *J* = 2.2 Hz, ArH), 6.84 (1H, d, *J* = 2.2 Hz, ArH), 3.74 (2H, m, O-C₂H₂{C₂H₆}C₂H₄-N), 3.65 (2H, s, Ar-CH₂-N), 2.84 (2H, d, *J* = 11.00 Hz, O-C₂H₂{C₂H₆}CH₂-N), 1.87 (2H, d, *J* = 11.00 Hz, O-C₂H₂{C₂H₆}CH₂-N), 1.41 (9H, s, ArC-C{CH₃}₃), 1.28 (9H, s, ArC-C{CH₃}₃), 1.17 (6H, d, *J* = 6.3 Hz, O-C₂H₂{C₂H₆}C₂H₄-N). ¹³C {¹H} NMR (CDCl₃, 125 MHz, 298 K) δ 154.0 (ArC-O), 140.5 (ArC-C{CH₃}₃), 135.4 (ArC-C{CH₃}₃), 123.4 (ArC-H), 123.0 (ArC-H), 120.0 (ArC-CH₂-N), 71.5 (O-C₂H₂{C₂H₆}C₂H₄-N), 62.2 (ArC-CH₂-N), 58.3 (O-C₂H₂{C₂H₆}C₂H₄-N), 34.7 (ArC-C{CH₃}₃), 34.0 (ArC-C{CH₃}₃), 31.6 (ArC-C{CH₃}₃), 29.5 (ArC-C{CH₃}₃), 18.9 (O-C₂H₂{C₂H₆}C₂H₄-N).

[O^{Me,Me}NO^{tAm,tAm}] ([L9]H). [L9]H was prepared analogously to [L6]H, with H₂O (80.0 mL), 2,4-di-*tert*-butylphenol (6.55 mL, 26.0 mmol), and formaldehyde (37 wt. % in

H₂O, 2.44 mL, 26.0 mmol) and 2,6-di-methylmorpholine (3.70 mL, 26.0 mmol). [L9]H was recrystallized in MeOH/pentane to give a colourless, crystalline solid. Yield: 8.00 g, 85.1%. mp 133-137 °C; MS (MALDI, matrix: anthracene) *m/z* 360 (M⁺, 100%); Anal. calcd. for C₂₃H₃₉NO₂: C, 76.40; H, 10.87; N, 3.87. Found: C, 76.44; H, 11.03; N, 4.38%. ¹H NMR (CDCl₃, 500 MHz, 298K) δ 10.66 (1H, s, ArOH), 7.09 (1H, d, *J*=1.4 Hz, ArH), 6.76 (1H, d, *J*=1.4 Hz, ArH), 3.74 (2H, m, O-C₂H₂{C₂H₆}C₂H₄-N), 3.63 (2H, s, Ar-CH₂-N), 2.80 (2H, d, *J* = 11.00 Hz, O-C₂H₂{C₂H₆}CH₂-N), 1.92 (2H, q, *J*=7.4 Hz, ArC-C-CH₂CH₃), 1.82 (2H, d, *J* = 11.00 Hz, O-C₂H₂{C₂H₆}CH₂-N), 1.61 (2H, q, *J*=7.4 Hz, ArC-C-CH₂CH₃), 1.37 (6H, s, ArC-C{CH₃}₂), 1.24 (6H, s, ArC-C{CH₃}₂), 1.16 (6H, d, *J* = 6.3 Hz, O-C₂H₂{C₂H₆}C₂H₄-N), 0.69 (3 H, t, *J* = 7.4 Hz, CH₂CH₃), 0.63 (3 H, t, *J* = 7.4 Hz, CH₂CH₃). ¹³C{¹H} NMR (CDCl₃, 125 MHz, 298K): δ 153.5 (ArC-O), 138.4 (ArC-C{CH₃}₂), 133.4 (ArC-C{CH₃}₂), 124.7 (ArC-H), 123.7 (ArC-H), 119.5 (ArC-CH₂-N), 71.3 (O-C₂H₄{C₂H₆}C₂H₄-N), 61.9 (ArC-CH₂-N), 58.0 (O-C₂H₂{C₂H₆}C₂H₄-N), 38.0 (ArC-C{CH₃}₂CH₂), 36.8 (ArC-C{CH₃}₂CH₂), 32.6 (ArC-C{CH₃}₂CH₂), 28.2 (ArC-C{CH₃}₂CH₂), 27.3 (ArC-C{CH₃}₂CH₂), 18.7 (O-C₂H₂{C₂H₆}C₂H₄-N), 9.1 (ArC-C{CH₃}₂CH₂CH₃), 8.8 (ArC-C{CH₃}₂CH₂CH₃).

[O^{Me,Me}NO^{F,F}] ([L10]H). [L10]H was prepared in similar fashion as described for [L7]H with water (100 mL), 2,4-difluorophenol (4.50 mL, 47.0 mmol), and formaldehyde (37 wt. % in water, 3.80 mL, 47.0 mmol) and 2,6-di-methylmorpholine (5.82 mL, 47.0 mmol). [L10]H was recrystallized in MeOH to give an off-white, crystalline solid. Yield: 6.45 g, 53.3%. mp 88-90 °C; ¹H NMR (CDCl₃, 300 MHz, 298K) δ 10.66 (1H, s, ArOH), 6.73-6.81 (1H, ddt, *J* = 2.0 Hz, ArH), 6.52-6.56 (1H, dd, *J* = 2.0 Hz, ArH), 3.75 (2H, m,

O-C₂H₂{C₂H₆}C₂H₄-N), 3.69 (2H, s, Ar-CH₂-N), 2.83 (2H, d, *J* = 11.00 Hz, O-C₂H₂{C₂H₆}CH₂-N), 1.92 (2H, d, *J* = 11.00 Hz, O-C₂H₂{C₂H₆}CH₂-N), 1.18 (6H, d, *J* = 6.3 Hz, O-C₂H₂{C₂H₆}C₂H₄-N). ¹³C{¹H} NMR (CDCl₃, 125 MHz, 298K): δ 155.8 (ArC-O), 152.6 (ArC-CF), 151.8 (ArC-CF), 148.5 (ArCH), 141.7 (ArCH), 122.8 (ArC-CH₂-N), 71.1 (O-C₂H₂{C₂H₆}C₂H₄-N), 60.5 (ArC-CH₂-N), 57.8 (O-C₂H₂{C₂H₆}C₂H₄-N), 18.7 (O-C₂H₂{C₂H₆}C₂H₄-N).

[ONNO^{*t*Bu,*t*Bu}] ([L11]H₂). [L11]H₂ was prepared in similar fashion as described for [L4]H with H₂O (80 mL), 2,4-di-*tert*-butylphenol (12.2 g, 61.5 mmol), and formaldehyde (37 wt. % in water, 5.00 mL, 61.5 mmol) and homopiperazine (3.08 g, 30.8 mmol). [L8]H was obtained as a gray/yellow solid, which was recrystallized in hexane to give a white powdery solid. Yield: 15.5 g, 95.4%. Crystals suitable for X-ray diffraction were grown from a saturated methanol/hexane solution at 0 °C; mp 188-191 °C; MS (MALDI, matrix: anthracene) *m/z* 536 (M⁺, 100%); Anal. calcd. for C₃₅H₅₆N₂O₂: C, 78.31; H, 10.51; N, 5.22. Found: C, 78.19; H, 10.33; N, 5.11%. ¹H NMR (CDCl₃, 500 MHz, 218 K) δ 11.03 (2H, s, ArOH), 7.21 (2H s, ArH), 6.81 (2H, s, ArH), 3.76 (4H, s, Ar-CH₂-N), 2.82 (4H, br, N-CH₂-CH₂-N), 2.77 (4H, br, N-CH₂{CH₂}CH₂-N), 1.90 (2H, m, N-CH₂{CH₂}CH₂-N), 1.42 (9H, s, Ar-C{CH₃}₃), 1.27 (9H, s, Ar-C{CH₃}₃), ¹³C{¹H} NMR (CDCl₃, 125 MHz, 298K): δ 154.2 (ArC-O), 140.5 (ArC-C{CH₃}₃), 135.7 (ArC-C{CH₃}₃), 123.3 (ArCH), 122.9 (ArCH), 121.1 (ArC-CH₂-N), 62.4 (ArC-CH₂-N), 54.3 (N-CH₂{CH₂}CH₂-N), 53.0 (N-CH₂CH₂-N), 34.7 (ArC-C{CH₃}₃), 34.0 (ArC-C{CH₃}₃), 31.6 (ArC-C-{CH₃}₃), 29.5 (ArC-C-{CH₃}₃), 26.6 (N-CH₂{CH₂}CH₂-N).

2.5 References

1. Crabtree, R. H. The organometallic chemistry of the transition metals, 3d ed; John Wiley and Sons: New York, **2001**.
2. G. W. Coates, Dalton Trans., 2002, 467; E. L. Marshall and V. C. Gibson, Metal Complexes as Catalysts for Polymerization Reactions. In *Comprehensive Coordination Chemistry II*; McCleverty, J. A., Meyer, T. J., Eds.; Elsevier: London **2004**; Vol. 9, pp 1-74.
3. C. S. Higham, D. P. Dowling, J. L. Shaw, A. Cetin, C. J. Ziegler and J. R. Farrell, Tetrahedron Lett., **2006**, 47, 4419.
4. W. J. Burke, E. L. M. Glennie and C. Weatherbee, *J. Org. Chem.*, **1964**, 29, 909.
5. E. Y. Tshuva, M. Versano, I. Goldberg, M. Kol, H. Weitman and Z. Goldschmidt, *Inorg. Chem. Commun.*, **1999**, 2, 371.
6. E. Y. Tshuva, I. Goldberg, and M. Kol. *Organometallics*, **2001**, 20, 3017.
7. S. Groysman, E. Sergeeva, I. Goldberg, and M. Kol, *Inorg. Chem.*, **2005**, 44, 8188.
8. K. L. Collins, L. J. Corbett, S. M. Butt, G. Madhurambal and F. M. Kerton, *Green Chem. Lett. Rev.*, **2007**, 1, 31.
9. F. M. Kerton, S. Holloway, A. Power, R. G. Soper, K. Sheridan, J. M. Lynam, A. C. Whitwood, C. E. Willans, *Can. J. Chem.* **2008**, 86, 435.
10. J.-T. Issenhuth, J. Pluvinage, R. Welter, S. Bellemin-Lapponnaz and S. Dagorne, *Eur. J. Inorg. Chem.*, **2009**, 4701.
11. J. D. Farwell, P. B. Hitchcock, M. F. Lappert, G. A. Luinstra, A. V. Protchenko, X.-H. Wei, *J. Organomet. Chem.*, **2008**, 693, 1861.
12. V. Poirier, T. Roisnel, J.-F. Carpentier, Y. Sarazin, *Dalton Trans.*, **2011**, 40, 523.
13. R. Mayilmurugan, H. Stoeckli-Evans, E. Sureshc and M. Palaniandavar, *Dalton Trans.*, **2009**, 5101.
14. SHELX97: G.M. Sheldrick, **1997**.
15. DIRDIF99: Beurskens, P.T., Admiraal, G., Beurskens, G., Bosman, W.P., de Gelder, R., Israel, R. and J. M. M. Smits, **1999**. *The DIRDIF-99 program system, Technical Report of the Crystallography Laboratory*, University of Nijmegen, The Netherlands.

16. Cromer, D. T. & Waber, J. T.; *International Tables for X-ray Crystallography*, The Kynoch Press, Birmingham, England, **1974**, Vol. IV, Table 2.2 A
17. J. A. Ibers and W. C. Hamilton, *Acta Crystallogr.*, **1964**, *17*, 781.
18. D. C. Creagh and W. J. McAuley, *International Tables for Crystallography*, ed., A. J. C. Wilson, Kluwer Academic Publishers, Boston, **1992**, Vol C, Table 4.2.6.8, pp 219.
19. D. C. Creagh and J. H. Hubbell, *International Tables for Crystallography*, ed., A. J. C. Wilson, Kluwer Academic Publishers, Boston, **1992**, Vol C, 200-206, Table 4.2.4.3.
20. CrystalStructure 3.7.0: Crystal Structure Analysis Package, Rigaku and Rigaku/MSK (2000-2005). 9009 New Trails Dr. The Woodlands TX 77381 USA.
21. CRYSTALS Issue 10: Watkin, D.J., Prout, C.K. Carruthers, J.R. & Betteridge, P.W. *Chemical Crystallography Laboratory*, Oxford, UK., **1996**.

CHAPTER 3

Zinc Complexes of Piperazinyl-Aminephenolate Ligands: Synthesis, Characterization and Ring-Opening Polymerization Activity

Chapter 3

Zinc Complexes of Piperazinyl-aminephenolate Ligands: Synthesis, Characterization and Ring–Opening Polymerization Activity

A version of this chapter has been published

Nduka Ikpo, Lisa N. Saunders, Jillian L. Walsh, Jennifer M. B. Smith, Louise N. Dawe
and Francesca M. Kerton

Eur. J. Inorg. Chem., **2011**, 5347–5359

Some modifications were made to the original paper for inclusion as a chapter in this thesis. For example, the ball and stick representation of ligand [L5]H in this chapter was not in the original version of the paper.

3.1 Introduction

As outlined in Chapter 1, amine-phenolate and related ligands possessing a mixed set of N- and O-donor atoms have attracted a great deal of interest over the past decade due to their ability to coordinate to a range of metal centres and the ease of systematic steric control by variation of the backbone and phenol substituents.¹⁻²³ Various ligands of this type have been used in main group and early transition metal chemistry (including lithium,^{2,3} magnesium,⁴⁻¹⁰ calcium,¹¹ rare-earths,^{12,13} zinc,^{1,14-16,19} aluminum,^{18,20}

zirconium^{21,22} and titanium²³). Many of these complexes have been reported to be excellent initiators for ring-opening polymerization (ROP) of cyclic esters. The quest is ongoing for new systems that can advance our understanding of this reaction and ultimately lead to a better-controlled performance in this and other polymerization reactions.

Recently, Issenhuth *et al.* reported the synthesis of cationic aluminum complexes supported by morpholine-derived aminephenolate ligands that act as efficient initiators for ROP of propylene oxide.²⁴ Of particular relevance to the current study, Carpentier and co-workers recently described the synthesis of zinc and magnesium complexes supported by ether-aminephenolate ligands, including those bearing morpholinyl side-arms, that are effective initiators for immortal ROP of cyclic esters.²⁵ Lappert and co-workers have reported zinc complexes stabilized by a piperazinylphenolate ligand,²⁶ and one such complex was found to uptake some CO₂ when cyclohexene oxide–CO₂ copolymerizations were attempted, although no polymer product was isolated.

In this Chapter the synthesis and structural characterization of a group of piperazinyl-phenol ligands and a morpholinyl phenol ligand, their coordination chemistry with Zn, and their use as single and/or binary component initiators for the ROP of lactide (LA) and ϵ -caprolactone (ϵ -CL) under various conditions are described, including under microwave (MW) irradiation. MW irradiation has not been used extensively in ROP of lactide facilitated by metal complexes.^{27,28} In the two examples reported to date simple tin initiators, e.g. stannous octoate, were used and the resulting polymers have broad polydispersities. High reaction temperatures are normally detrimental to achieving

controlled polymerization, however MW methods allow rapid heating of reaction mixtures. Sluggish initiators, e.g. those bearing ligands with sterically demanding groups, normally require heating to enable a worthwhile reaction rate to be obtained. In such cases, MW heating may lead to a reduction in the number of side reactions e.g. transesterification by reducing the overall reaction time. Also, MW heating could lead to more rapid screening of potential ROP initiators.

As many Zn phenolate and alkoxide complexes have shown good activity towards either copolymerization of CO₂ with epoxides or the formation of cyclic carbonates,^{29,30} preliminary studies of the activity of **3.6** and **3.7**/ROH towards coupling reaction of epoxide with carbon dioxide are also described in this chapter.

3.2 Results and Discussion

The protio ligands were synthesized from the appropriate phenol, formaldehyde, and 1-methylpiperazine *via* a modified Mannich condensation reaction, as discussed and shown in Chapter 2, Scheme 2.1. They were isolated in excellent yields. [L2]H has previously been prepared through a slightly different procedure that involved reduction with hydrobromic acid and neutralization with aqueous NaHCO₃,²⁶ however structural data for [L2]H have not been reported. The preparation of [L5]H through a Mannich condensation reaction in 1,4-dioxane under reflux has been reported previously.²⁵

The recently reported benign route (reaction in water)^{31,31,32} to amine-phenol ligands reduces the amount of reagents required relative to more traditional reaction routes and afforded high yields of [L1]H–[L5]H. These were recrystallized from methanol (cooled to 0 °C). Their characterization by ¹H- and ¹³C{¹H} NMR techniques afforded well

resolved resonances for all proton and carbon environments, while elemental analyses showed that the compounds were obtained in pure form. Single crystals of [L2]H suitable for X-ray crystallography were grown *via* slow evaporation of a saturated methanol solution of [L2]H at ambient temperature. The solid state structure of [L2]H shown in Figure 3.1 reveals intramolecular hydrogen bonding between the phenol and the proximal amine group. The *N*-methylpiperazine ring adopts the normal chair conformation. Table 3.5 and Table 3.6 summarize crystal data for all the structures reported in this article.

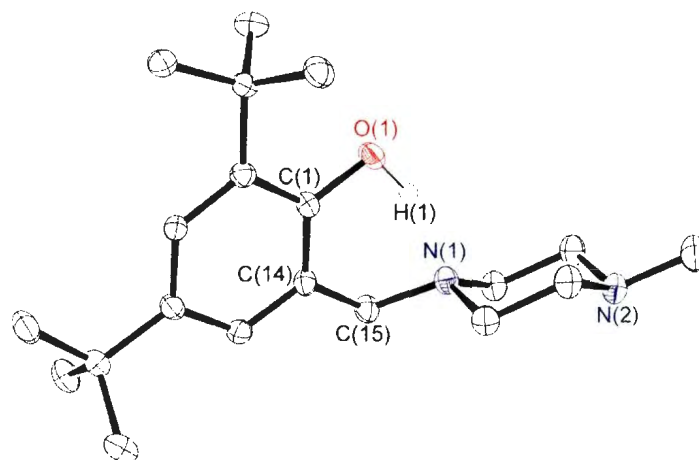


Figure 3.1. Molecular structure of [L2]H. (50% displacement ellipsoids; H atoms omitted for clarity except H1, which is involved in hydrogen bonding). Selected bond lengths (Å) and bond angles (°): O(1)-C(1), 1.366(2); N(1)-C(15), 1.472(2); C(14)-C(15), 1.516(2); O(1)-C(1)-C(14), 119.73(14); O(1)-C(1)-C(2), 119.76(14); N(1)-C(15)-C(14), 113.72(14)

The single crystal X-ray data for [L5]H were poor, but the ball and stick diagram as shown in Figure 3.2 confirms its connectivity and analogy to [L2]H.

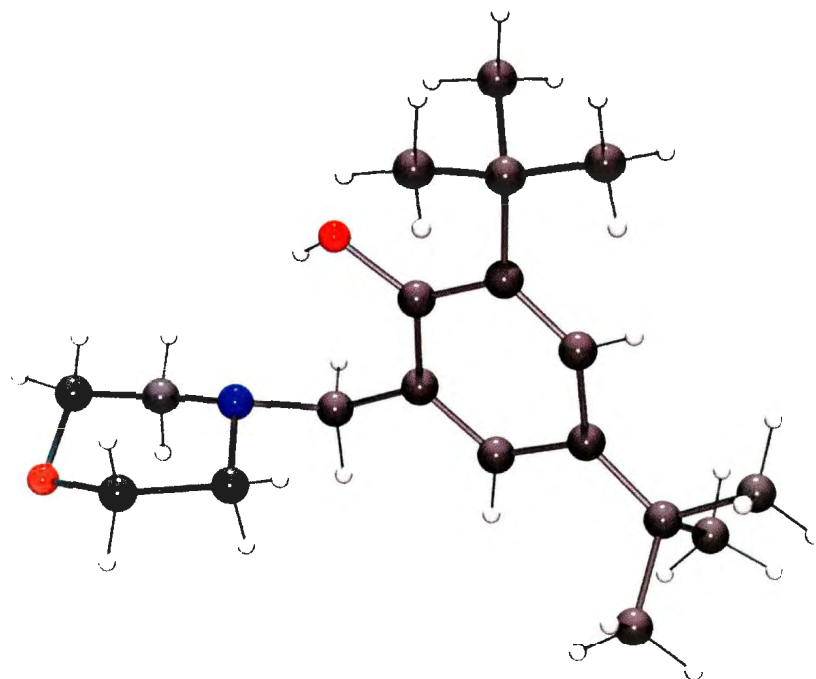
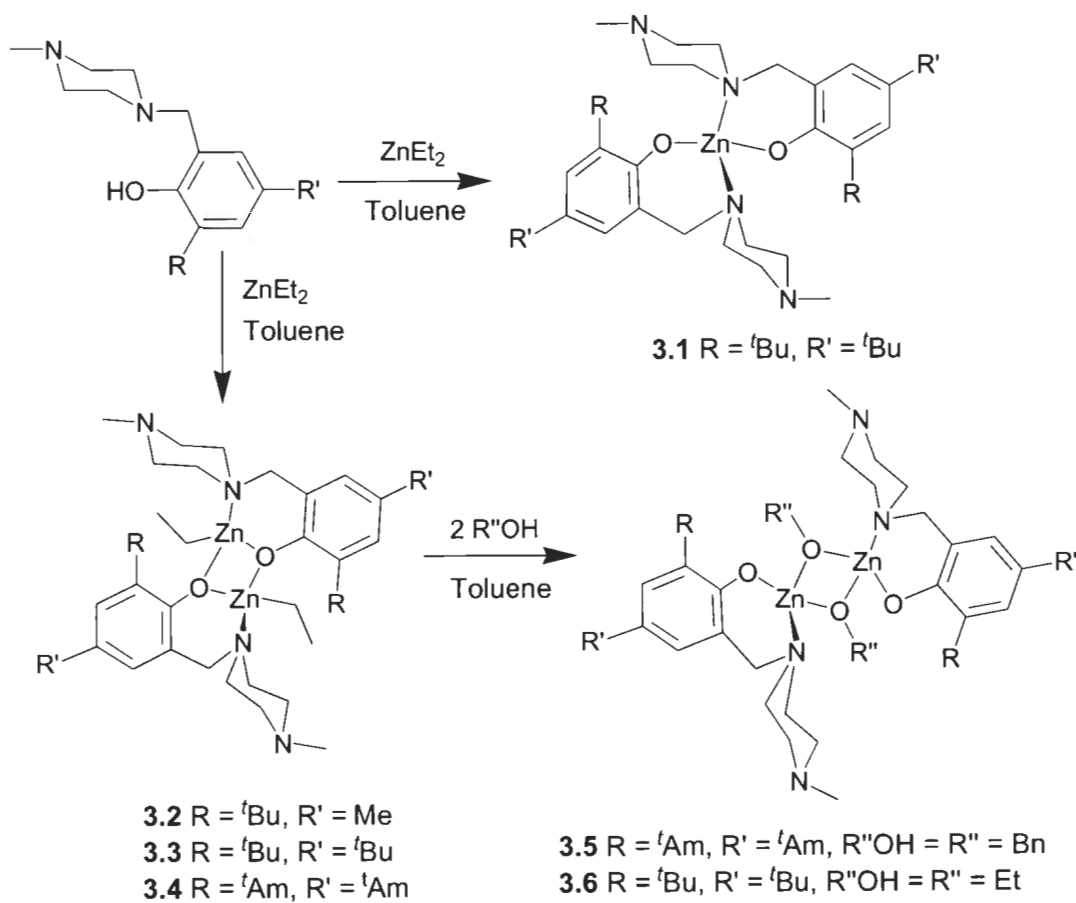


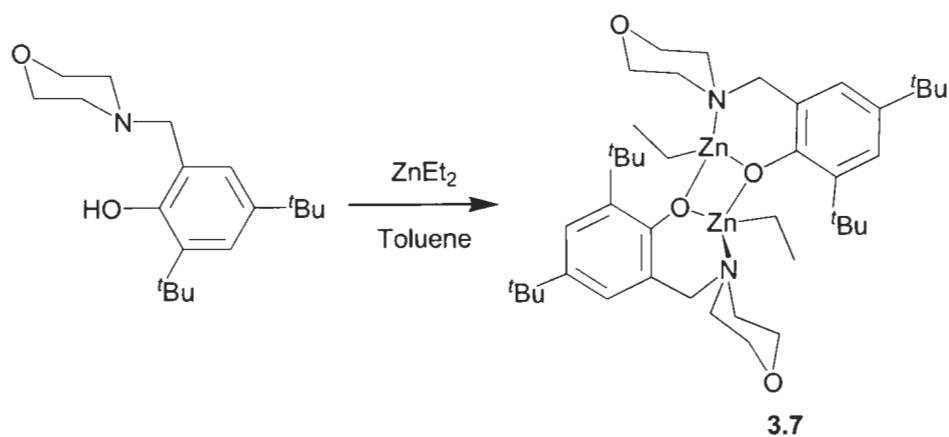
Figure 3.2. Ball and stick representation of [L5]H, based on poor quality X-ray diffraction results.

3.3 Synthesis and Characterization of Zinc Aminephenolate Complexes

Reactions of protio ligands $[\text{ONN}^{\text{R,R'}}]\text{H}$ with ZnEt_2 in toluene under ambient conditions led to the isolation of molecular zinc complexes $\text{Zn}[\text{ONN}^{\text{Bu,Bu}}]_2$ (**3.1**) and $\{[\mu\text{-ONN}^{\text{R,R'}}]\text{ZnEt}\}_2$ (**3.2–3.4**) in 56–96% yield (Scheme 3.1). Treatment of complexes **3.3** and **3.4** with two equivalents of benzyl alcohol and ethanol, respectively, in toluene at ambient temperature afforded **3.5** and **3.6** in 89% and 61% respectively. An equimolar reaction between [L5]H and ZnEt_2 afforded $\{[\mu\text{-ONO}^{\text{Bu,Bu}}]\text{ZnEt}\}_2$ (**3.7**) in 81% yield (Scheme 3.2).



Scheme 3.1. Synthetic procedure for the synthesis of piperazinyl amine-phenolate zinc complexes



Scheme 3.2. Synthesis of a morpholinyl amine-phenolate zinc complex

The synthesis of a monometallic zinc complex related to **3.1** has been reported by Lappert and co-workers; the synthesis proceeded *via* the indirect route of reacting a bimetallic phenolate-bridged ethylzinc complex with 2 equiv. of methanol.²⁶ Another similar monometallic zinc complex was reported by Sobota and co-workers, and was obtained from the reaction of 2 equiv. of an amine-phenol ligand with 1 equiv. of ZnEt₂.³³ In our case both the monometallic (**3.1**) and bimetallic (**3.2** and **3.4**) zinc complexes were synthesized by reaction of 1:1 ratio of ZnEt₂ with the corresponding ligands. Although all reactions were carried out under rigorous air- and moisture-free conditions, we cannot rule out the potential role of adventitious water in the preparation of **3.1**. In this regard, the preparation of **3.1** would proceed by a similar route to that reported by Lappert who used methanol as a proton source. Nevertheless, the reaction of [L**2**]H with an excess of ZnEt₂ in toluene did lead to the formation of the desired bimetallic zinc complex **3.2**. Treatment of complexes **3.3** and **3.4** with 2 equiv. of benzyl alcohol and ethanol, respectively, afforded alkoxy-bridged complexes **3.5** and **3.6**.

The zinc complexes **3.1–3.7** were characterized by elemental analyses, and ¹H and ¹³C{¹H} NMR spectroscopy. The ¹H NMR spectra of **3.1–3.7** in C₅D₅N solvent recorded at room temperature showed broad resonances in the methylene (PhCH₂N) and amine methyl regions, which prompted variable-temperature NMR studies of the complexes. A portion of a representative variable-temperature spectrum of **3.4** is shown in Figure 3.3. At elevated temperature (85 °C), sharp signals were discernable in the spectra that were very informative for establishing the formation of the complexes **3.1–3.7**. The spectrum of complex **3.1** exhibits three sharp singlets associated with the aromatic and methylene

protons. These signals occur at $\delta = 7.58$ ppm, 7.11 ppm and 4.07 ppm and are shifted from 7.26 ppm, 6.93 ppm and 3.75 ppm where they are observed in the spectrum of free ligand [L2]H. No Zn-ethyl resonances were observed in the spectrum of **3.1**. In contrast, the signals from the methylene (PhCH₂N) protons in **3.3** are observed at 3.65 ppm, and additional signals were observed at $\delta = 0.59$ ppm (quartet) and 1.57 ppm (triplet) that correspond to the ethyl group bound to the zinc ion. Similar resonances are observed in the spectra of complexes **3.2**, **3.4** and **3.7**. Upon lowering the temperature, the methylene signals became broader for all the complexes, which implied that at high temperature there is fast exchange on the NMR time scale of a coordinated pyridine or coordinated piperazine ligand and the free pyridine solvent. It should also be noted that in solution the bimetallic species (analogous to their solid state structures) are unlikely to exist in the presence of such a large quantity of Lewis base (C₅D₅N). However, use of this solvent was essential for gaining sufficient solubility for all samples studied, and to allow for direct comparison of their spectra.

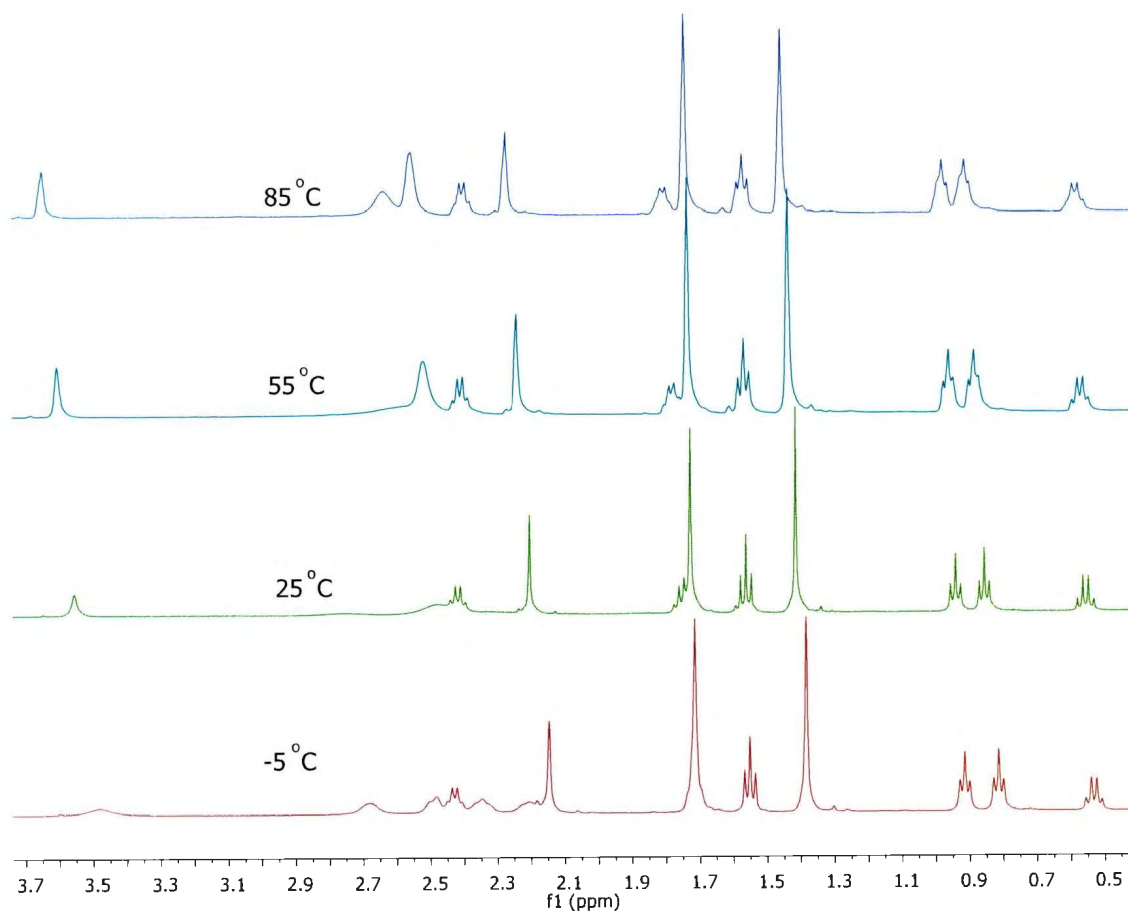


Figure 3.3. The methylene region of variable temperature ^1H NMR spectra of **3.4** in $\text{C}_5\text{D}_5\text{N}$

3.4 X-ray Crystallographic Analysis of Zinc Complexes

Crystal structures of complexes **3.1**–**3.7** were determined by X-ray diffraction analysis. The molecular structure of complex **3.1** is shown in Figure 3.4 along with selected bond lengths and angles. The central zinc atom adopts a distorted tetrahedral coordination geometry and is coordinated by four donor atoms from two (methylpiperazinyl)phenolate ligands. The fact that one of the amine nitrogen atoms remains pendant can be attributed to the restriction of the chair conformation adopted by the piperazinyl unit of the ligand that orientates N(2) away from the central metal atom.

Future studies will involve investigating the chemistry at this nitrogen centre. The structure of **3.1** is centrosymmetric (the zinc ion is located on a crystallographic inversion centre) with Zn–O and Zn–N distances within the normal ranges for related complexes.^{26,33} The smaller bond angles around Zn, O(1)–Zn(1)–N(1) 96.82(5)°, can most probably be associated with the bite of the six-membered C₃NZnO chelate ring. This ring adopts a legless chair³⁴ or slight sofa¹ conformation with the C(6) atom forming the back-rest and situated *ca.* 0.76 Å out of Zn(1)–O(1)–C(20)–C(7)–N(1) plane.

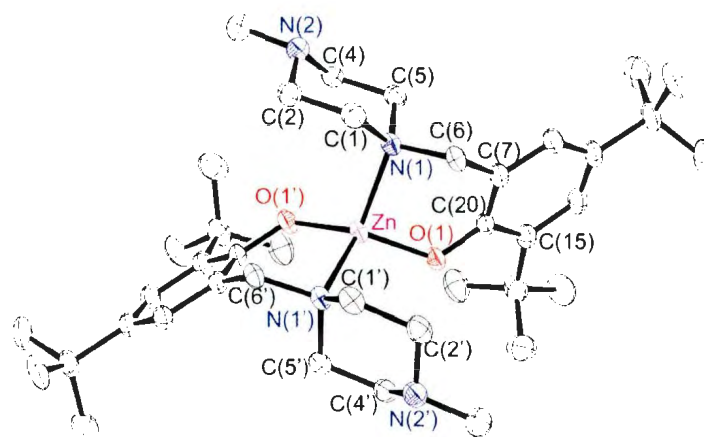


Figure 3.4. Molecular structure of **3.1**. The thermal ellipsoids are drawn at the 50% probability level; H atoms are excluded for clarity. The two halves of the molecule are symmetry related by inversion. Selected bond lengths [Å] and bond angles [°]: Zn(1)–O(1), 1.9008(11); Zn(1)–N(1), 2.1198(13); O(1)–C(20), 1.3357(17); N(1)–C(1), 1.4885(19); N(1)–C(5), 1.4909(19); N(1)–C(6), 1.4982(19); N(2)–C(2), 1.453(2); N(2)–C(3), 1.454(2); N(2)–C(4), 1.463(2); C(1)–C(2), 1.520(2); C(4)–C(5), 1.510(2); C(15)–C(20), 1.422(2); O(1)–Zn(1)–O(1'), 124.94(7); O(1)–Zn(1)–N(1), 110.52(5); O(1)–Zn(1)–N(1'), 96.82(5); C(20)–O(1)–Zn(1), 125.45(10); C(1)–N(1)–C(6), 108.82(12); C(1)–N(1)–Zn(1), 114.91(9); C(6)–N(1)–Zn(1), 102.40(9); N(1)–C(1)–C(2), 111.18(13).

An ORTEP drawing of **3.2** is presented in Figure 3.5 along with selected bond lengths and angles. The structure exhibits a butterfly-like arrangement with the two ethyl groups positioned on the same side with respect to the Zn₂O₂ core plane, while the two

piperazine units are situated on opposing sides of the Zn_2O_2 plane. This *cisoid* conformation of ethyl groups is rare in zinc ethyl chemistry. One other example has been reported to date.³⁵ Each zinc ion adopts a distorted tetrahedral coordination geometry consisting of two bridging phenolate oxygen atoms, one nitrogen donor and one ethyl group. The central metal ring, Zn_2O_2 , displays a twisted geometry with O(1) and O(2) *ca.* 0.54 and 0.55 Å from the O(2)–Zn(1)–Zn(2) and O(1)–Zn(1)–Zn(2) planes, respectively. The angles at the central atoms Zn(1) [O(1)–Zn(1)–O(2), 80.47(8)°] and Zn(2) [O(1)–Zn(2)–O(2), 80.89(8)°] are narrower than the corresponding angles for the bridging oxygen atoms O(1) [Zn(2)–O(1)–Zn(1), 97.75(9)°] and O(2) [Zn(1)–O(2)–Zn(2), 96.55(9)°]. The acute angles are likely a result of the six-membered chelate ring that is enforced by the ligand. The two C_3OZnN chelate rings adopt boat conformations with C(6) and O(1) *ca.* 0.62 and 0.71 Å from the Zn(1)–C(17)–C(7)–N(1) plane, while C(23) and O(2) are *ca.* 0.64 and 0.74 Å from the Zn(2)–C(34)–C(24)–N(2) plane. The Zn–C bond lengths in **3.2** are comparable to those in related complexes reported in the literature, where the mean Zn–C bond lengths in such species are 1.978 Å. Within those complexes that are bimetallic, the ethyl groups are transoidal.^{21,37,38} The Zn–O bond lengths in **3.2** are similar to the mean distance [2.039 Å] determined from a literature survey, and are comparable to those within related zinc complexes that are reported in the literature.^{26,35,38–41} The Zn(1)–Zn(2) distance [3.0527(6) Å] is close to that reported by Gibson [3.0276(5) Å], while the O(1)–O(2) separation distance [2.634(4) Å] is shorter [2.817(3) Å].¹

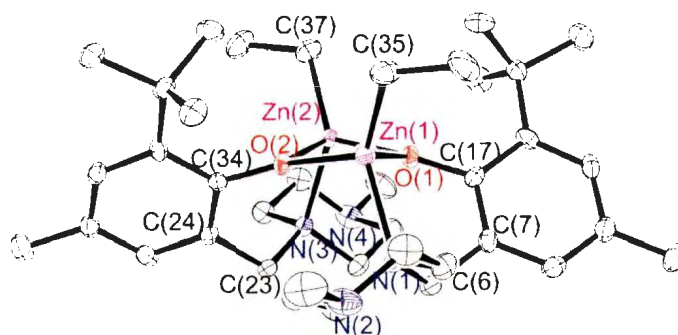


Figure 3.5. Molecular structure of **3.2**. The displacement ellipsoids are drawn at the 50% probability level; H atoms are excluded for clarity. Selected bond lengths [Å] and bond angles [°]: Zn(1)–C(35), 1.981(3); Zn(1)–O(1), 2.037(2); Zn(1)–O(2), 2.043(2); Zn(1)–N(1), 2.148(3); Zn(1)–Zn(2), 3.0527(6); Zn(2)–C(37), 1.991(3); Zn(2)–O(1), 2.015(2); Zn(2)–O(2), 2.047(2); Zn(2)–N(3), 2.143(3); O(1)–C(17), 1.361(3); O(2)–C(34), 1.353(3); C(35)–Zn(1)–O(1), 117.75(13); C(35)–Zn(1)–O(2), 124.72(12); C(35)–Zn(1)–N(1), 123.31(12); O(1)–Zn(1)–N(1), 93.77(9); O(2)–Zn(1)–N(1), 105.03(9); C(37)–Zn(2)–O(1), 123.41(12); C(37)–Zn(2)–O(2), 115.93(12); O(1)–Zn(2)–O(2), 80.89(8); Zn(2)–O(1)–Zn(1), 97.75(9); Zn(1)–O(2)–Zn(2), 96.55(9).

The single crystal structure of complex **3.3** depicted in Figure 3.6 reveals a centrosymmetric bimetallic complex with the zinc centres bridged through the oxygen atoms of the phenolate ligands. The coordination geometry at the zinc atom is a distorted tetrahedron. It should be noted that the bond angle O(1)–Zn(1)–O(1') [83.78(13)°] is wider than that in Bochmann's [EtZn(μ-OC₆F₅)(py)]₂ (py = pyridine) complex [78.00(5)°], which contains a *trans*-alkylzinc centre with a phenolate ligand and a nitrogen donor (in this case from pyridine).⁴² The similarities in the types of donors in the coordination spheres of Zn in each complex allows the difference in the bond angles to be attributed to the chelate bite angle of **L2** in complex **3.3**, whereas the donors in Bochmann's complex are not linked and are free to orientate themselves with minimal constraint. In **3.3**, C(15) and O(1) lie *ca.* 0.75 and 0.45 Å from the Zn(1)–N(1)–C(6)–C(1) mean plane, inducing the chelate ring to adopt a chair conformation, while the zinc atoms

lie *ca.* 0.58 Å above the plane defined by the coordinated N(1), C(21) and O(1) atoms. The central Zn₂O₂ ring is planar with the angle at Zn(1) being narrower than that at O(1). The Zn–C, Zn–N and Zn–O bond lengths are within the ranges previously reported for zinc complexes.^{1,26,39,43} The ethyl groups on each of the two metal centres lie *trans* to each other. Presumably, the large *tert*-butyl group in the 4-position of the phenolate donor in **3.3**, although distant from the metal coordination sphere, causes the ethyl groups to orientate themselves in a *trans* arrangement in contrast to the *syn-cis* arrangement in **3.2**, in which the 4-position of the phenolate ligand is occupied by a methyl group.

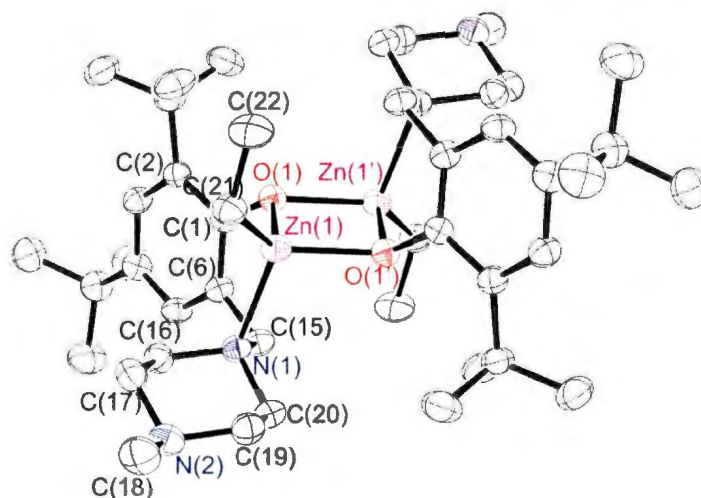


Figure 3.6. Molecular structure of **3.3**. The displacement ellipsoids are drawn at the 50% probability level; H atoms are excluded for clarity. The two halves of the molecule are symmetry related by inversion. Selected bond lengths [Å] and bond angles [°]: Zn(1)–C(21), 1.977(4); Zn(1)–O(1), 2.052(3); Zn(1)–N(1), 2.185(4); Zn(1)–Zn(1'), 3.068(5); O(1)–C(1), 1.362(3); N(1)–C(20), 1.479(4); N(1)–C(16), 1.483(4); N(1)–C(15), 1.498(4); N(2)–C(17), 1.457(4); N(2)–C(18), 1.458(4); N(2)–C(19), 1.460(4); C(1)–C(2), 1.416(4); C(21)–Zn(1)–O(1), 124.87(11); O(1)–Zn(1)–O(1'), 83.78(13); C(21)–Zn(1)–N(1), 118.53(16); O(1)–Zn(1)–N(1), 92.53(10); O(1)–Zn(1)–N(1'), 103.06(11); C(1)–O(1)–Zn(1), 117.95(18); C(1)–O(1)–Zn(1'), 123.86(17); Zn(1)–O(1)–Zn(1'), 96.22(13); C(20)–N(1)–C(16), 106.4(2); C(20)–N(1)–C(15), 107.5(2); C(16)–N(1)–C(15), 110.1(2); C(20)–N(1)–Zn(1), 113.99(18); C(16)–N(1)–Zn(1), 114.17(18).

The single-crystal X-ray data for **3.4** were of poor quality due to merohedral twinning of the crystals and their weak diffraction, however the structure and connectivity of **3.4** was confirmed and authenticates that it is structurally analogous to **3.3**. A ball and stick drawing of **3.4** is shown in Figure 3.7

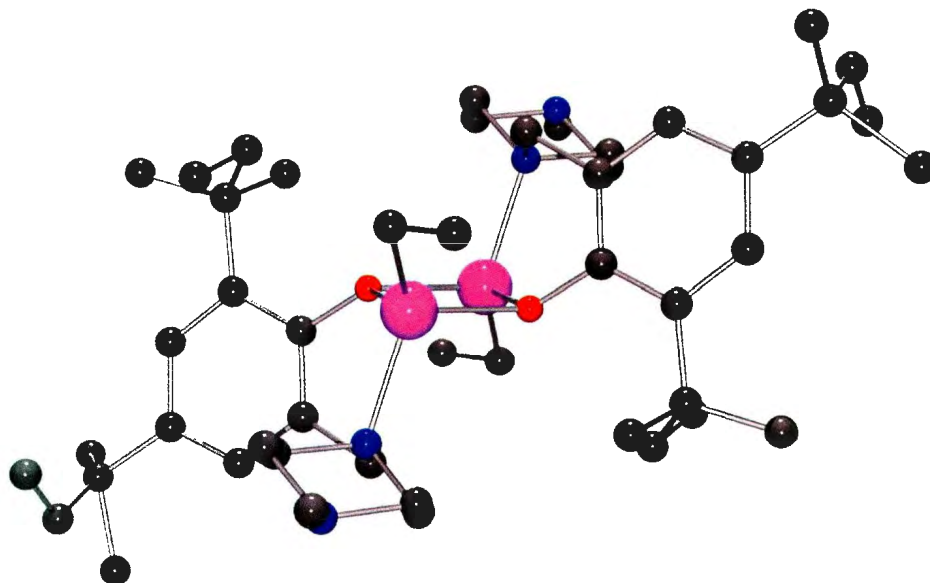


Figure 3.7. Ball and stick representation of **3.4**. (Weak diffraction and twinning yielded a data set containing severely disordered *para-t*-amyl group). This disorder and H-atoms have been omitted from this figure for clarity.

Reaction of the alkyl complexes with alcohols afforded alkoxy-bridged complexes. Suitable single crystals of these complexes were grown by the slow evaporation of a hexane/toluene mixture (**3.5**) and from a saturated toluene solution at $-35\text{ }^{\circ}\text{C}$ (**3.6**). The molecular structures of **3.5** and **3.6** reveal the bimetallic nature of these species. An ORTEP drawing of **3.5** is shown in Figure 3.8 and that of **3.6** is depicted in Figure 3.9, along with selected bond lengths and angles. The zinc centres in these complexes adopt distorted tetrahedral geometries and are bridged by the oxygen atoms of the benzyl

alkoxide or ethoxide groups to form planar Zn_2O_2 cores. Comparison of the angles within the Zn_2O_2 planar cores of complexes **3.5** and **3.6** reveals that the O–Zn–O bond angle in **3.6** is slightly narrower than that in complex **3.5**, while the Zn–O–Zn bond angle is wider in complex **3.6** than in complex **3.5**. The bond lengths within the two complexes are similar, and **3.6** contains bond lengths comparable to those in a related ethoxide-bridged zinc species.⁴⁴

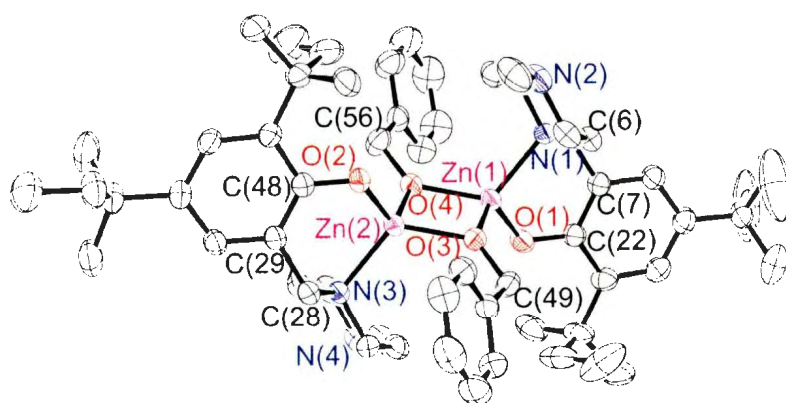


Figure 3.8. Molecular structure of **3.5**. (50% displacement ellipsoids; H atoms excluded for clarity). Selected bond lengths (Å) and bond angles (°): Zn(1)-O(1), 1.901(2); Zn(1)-O(4), 1.953(2); Zn(1)-O(3), 1.974(2); Zn(1)-N(2), 2.061(2); Zn(1)-Zn(2), 2.9459(5); Zn(2)-O(2), 1.900(2); Zn(2)-O(3), 1.954(2); Zn(2)-O(4), 1.970(2); Zn(2)-N(4), 2.059(2); O(1)-C(22), 1.342(3); O(2)-C(48), 1.346(4); O(3)-C(49), 1.411(3); O(4)-C(56), 1.414(3); N(1)-C(4), 1.454(4); N(1)-C(2), 1.459(4); O(1)-Zn(1)-O(4), 121.09(9); O(1)-Zn(1)-O(3), 115.98(9); O(4)-Zn(1)-O(3), 82.71(8); O(1)-Zn(1)-N(2), 101.29(9); O(4)-Zn(1)-N(2), 119.11(9); O(3)-Zn(1)-N(2), 117.34(9); O(1)-Zn(1)-Zn(2), 129.55(6); O(4)-Zn(1)-Zn(2), 41.56(6); O(3)-Zn(1)-Zn(2), 41.15(6); N(2)-Zn(1)-Zn(2), 128.95(7); O(2)-Zn(2)-O(3), 121.70(9); O(2)-Zn(2)-O(4), 116.84.

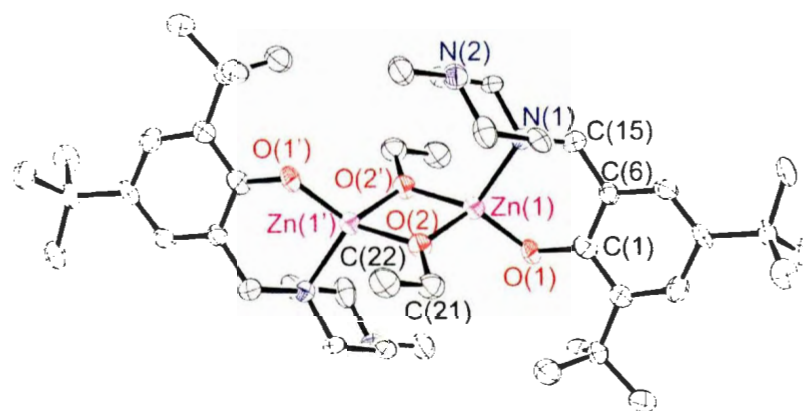


Figure 3.9. Molecular structure of **3.6**. The thermal ellipsoids are drawn at the 50% probability level; H atoms are excluded for clarity. Selected bond lengths [Å] and bond angles [°]: Zn(1)–N(1), 2.088(6); Zn(1)–Zn(1'), 2.954(2); O(1)–C(1), 1.330(8); O(2)–C(21), 1.404(8); O(2)–Zn(1), 1.957(5); O(2)–Zn(1)–O(2'), 82.0(2); O(1)–Zn(1)–N(1), 100.8(2); O(2)–Zn(1)–N(1), 117.4(2); C(21)–O(2)–Zn(1), 131.9(4); Zn(1)–O(2)–Zn(1'), 98.0(2).

Crystals of complex **3.7** were obtained by cooling a saturated toluene solution to -35 °C. The solid state structure of complex **3.7** (Figure 3.10), like the related piperazinyll complex **3.3**, contains zinc atoms coordinated by the phenolate oxygen atom and the proximal nitrogen atom of the ligand to form a planar Zn_2O_2 core. The bond angles and distances are in the range known for bimetallic zinc phenolate complexes, and comparable to those in **3.3**.^{1,26,39,43}

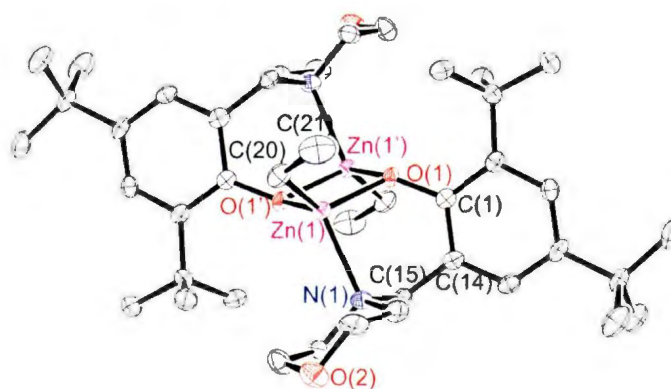


Figure 3.10. Molecular structure of **3.7**. The displacement ellipsoids are drawn at the 50% probability level; H atoms are excluded for clarity. The two halves of the molecule are symmetry related by inversion. Selected bond lengths [Å] and bond angles [°]: Zn(1)–C(20), 1.956(6); Zn(1)–O(1), 2.071(4); Zn(1)–N(1), 2.177(5); Zn(1)–Zn(1'), 3.0608(14); O(1)–C(1), 1.354(7); O(2)–C(17), 1.393(8); C(20)–Zn(1)–O(1), 128.8(2); C(20)–Zn(1)–O(1'), 115.6(2); O(1)–Zn(1)–O(1'), 82.87(17); C(20)–Zn(1)–N(1), 121.1(2); O(1)–Zn(1)–N(1), 92.70(18); C(1)–O(1)–Zn(1), 119.1(3).

3.5 Polymerization of Cyclic Esters

3.5.1 Ring-Opening Polymerization of *rac*-Lactide

The activities of complexes **3.2–3.5** and **3.7** as initiators for ROP of LA in toluene (Table 3.1 and Figure 3.11) and neat ester (Table 3.2) were examined. Compound **3.7** has been studied previously by Carpentier and co-workers but was not structurally characterized.²⁵ It is included here for comparative purposes and afforded a polymer with relatively narrow molecular weight distribution, M_w/M_n (M_w = weight averaged molecular weight, M_n = number average molecular weight). For the piperazinyll-derived initiators, M_w/M_n values for polylactide (PLA) were between 1.25 and 1.87. Reaction rates generally correlated with both the steric demands of the ligand and co-initiator (alcohol), with **3.2** and BnOH affording near quantitative conversions within shorter times than its 'Am and

^tBu analogues, and with activity comparable to that of compound **3.7**. Overall the M_n values of the polymer samples were lower than the expected values based on % conversion. This deviation likely implies that some transesterification reactions and/or a slow initiation step relative to propagation occurred. Both the broadening of the molecular weight distribution and the deviation from expected M_n increased with increasing $[LA]_0:[Zn]_0$ ratio (Table 3.1, entries 2 and 3, entries 6–8), and with increasing reaction time and temperature. These trends are frequently observed in ROP of cyclic esters.^{45–47} In an attempt to distinguish between less controlled polymerization due to slow initiation vs. transesterification, the single component initiator **3.5** was studied (Table 3.1, entry 12). The M_w/M_n for the resulting polymer was not significantly different to that obtained for PLA with **3.4**/BnOH under similar conditions (Table 3.1, entry 11). However, as expected, **3.5** did result in more rapid polymerization than **3.4**/BnOH. The difference in the rate of polymerization could be attributed to the time lapse required for the transformation of the precursor alkyl species, by alcoholysis, to the active alkoxide complex.

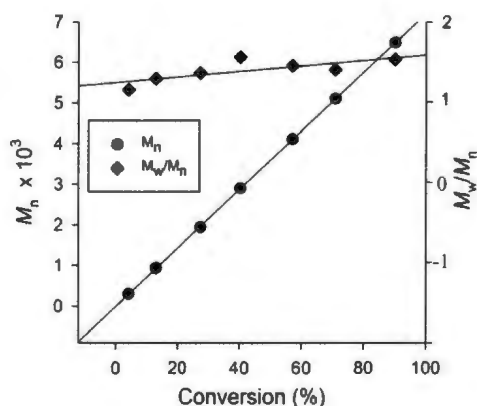


Figure 3.11. Plots of M_n and PDI (PDI = M_w/M_n and is determined by GPC) vs. monomer conversion for **3.3**/^tBuOH initiated ROP of LA. Conditions: $[LA]:[Zn]:[{}^t\text{BuOH}] = 50:1:1$,

$[Zn]_0 = 18.2 \text{ mM}$, toluene, $60 \text{ }^\circ\text{C}$, 0.1 mL aliquots taken at the given intervals. $\blacklozenge = M_w/M_n$ and $\bullet = M_n$.

Table 3.1. Ring-opening polymerization of *rac*-LA initiated by complexes **3.2-3.5, 3.7** in toluene

Entry	Initiator	[LA] ₀ /[Zn] ₀ /[ROH] ₀	t/min	T /°C	Conv (%) ^[d]	$M_{\text{ncal}}^{[e]} \times 10^3$	$M_n^{[f]} \times 10^3$	$M_w/M_n^{[f]}$	$P_r^{[g]}$
1	3.2	100/1/1 ^a	60	60	97.1	13.9	10.9	1.25	0.49
2	3.2	100/1/1 ^a	10	60	96.0	13.8	7.99	1.23	0.49
3	3.2	200/1/1 ^a	15	60	96.3	27.7	11.8	1.39	0.53
4	3.3	100/1/1 ^a	90	70	98.0	14.1	13.6	1.32	0.45
5	3.3	100/1/1 ^b	120	70	96.4	13.9	12.0	1.60	0.53
6	3.3	100/1/0	120	70	0.1	-	-	-	-
7	3.3	200/1/1 ^b	120	70	98.0	28.2	13.3	1.76	0.55
8	3.3	300/1/1 ^b	120	70	98.3	42.5	15.3	1.87	0.49
9	3.3	100/1/1 ^b	5	120 ^c	90.0	12.9	12.0	1.33	0.47
10	3.3	100/1/1 ^a	5	120 ^c	93.6	13.5	9.19	1.42	0.47
11	3.4	100/1/1 ^a	60	70	97.0	11.4	12.3	1.42	0.51
12	3.5	100/1/0	15	70	94.9	13.7	10.0	1.37	0.47
13	3.7	100/1/1 ^a	30	60	97.6	13.9	9.56	1.25	0.49

[a] In the presence of one equivalent of benzyl alcohol. [b] In the presence of one equivalent of *tert*-butyl alcohol. [c] Microwave reaction (MW). [d] Determined by ¹H NMR spectroscopy. [e] The M_{ncal} value of the polymer was calculated with $M_{\text{ncal}} = ([\text{rac-LA}]_0/[\text{Zn}]_0) \times 144.13$ (molecular weight of LA) \times conv. %/100. [f] The M_n value was calculated according to $M_n = 0.58M_{n\text{GPC}}$, where $M_{n\text{GPC}}$ is the value of M_n determined by GPC (chloroform) and is relative to polystyrene standards. [g] P_r is the probability of *racemic* enchainment of the monomers units, as determined by homodecoupled ¹H NMR spectroscopy according to the method reported by Coates *et al.*⁵¹

For the Zn-alkyl species the presence of alcohol was necessary to generate an efficient initiator system for the polymerization of LA, as has been reported in the literature. The use of BnOH and *t*-BuOH as coinitiators with **3.3** was studied in reactions conducted with conventional heating and MW irradiation. It was noted that conversions of 90% and 93% could be reached in 5 min with MW for *t*-BuOH and BnOH respectively (Table 3.1, entries 9 and 10), but similar conversions with conventional heating required significantly longer reaction times, particularly for *t*-BuOH when compared with BnOH (Table 3.1, entries 4 and 5). The M_n of the PLA prepared *via* a MW method showed good agreement with the theoretical values. These data imply that MW irradiation can be used to assist in the control of ROP when bulky co-initiators are used, as there is a smaller apparent difference in the initial reaction rate under such conditions compared with conventional heating methods. This could be useful particularly in the preparation of star-polymers and other systems where a sterically congested co-initiator is required. It should be noted that in the conventionally heated reactions, solutions of monomer and initiator were heated separately and then mixed once the desired reaction temperature was achieved.

Microstructural analyses of the resulting PLA were performed through inspection of the methine region of the homodecoupled ^1H NMR spectra (Figure 3.12). P_r values (probability of *racemic* enchainment of the monomer units) were generally close to 0.5 indicating that an atactic polymer was produced. Reactions with good initiation rates (Table 3.1, entries 4, 9, 10 and 12) afforded polymers with a very slight isotactic bias ($P_r = 0.45\text{--}0.47$) whereas long reaction times and high temperatures (excluding MW reactions) gave polymers with a very slight heterotactic bias ($P_r = 0.51\text{--}0.55$). The latter

polymers had, on average, broader molecular weight distributions than those with $P_r < 0.5$. Therefore, the apparent increase in heterotacticity is likely to be an artifact of transesterification reactions, and the small degree of isotacticity is probably induced through a chain-end control mechanism.

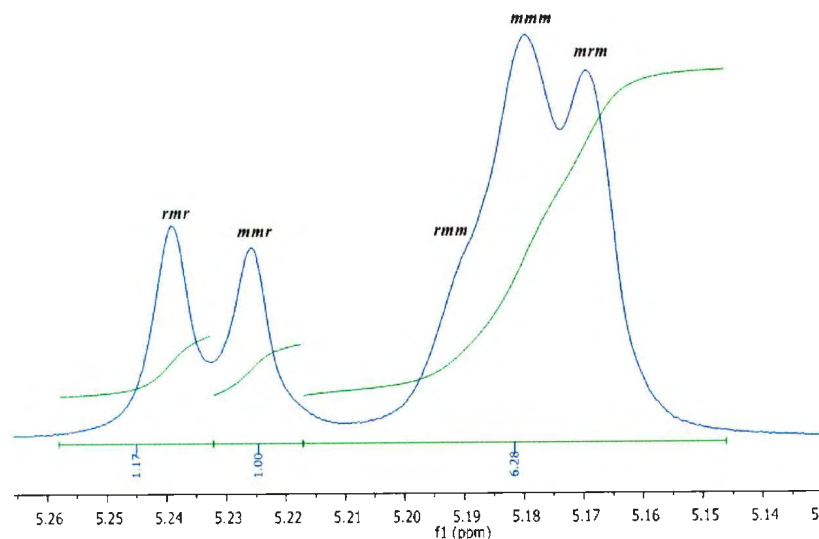


Figure 3.12. Typical homonuclear decoupled ^1H NMR spectrum of the methine region of PLA prepared by 3.3 t BuOH (500 MHz, CDCl_3).

Occurrence of transesterification was confirmed by matrix-assisted laser desorption ionisation time-of-flight mass spectrometry (MALDI-TOF MS) and ^1H NMR end-group analysis of the polymers. In the mass spectra, two main series of signals were observed that were separated by a difference of 72 in m/z . These were assigned to open chain (even mass) polymers and oligomers clustered with Na^+ and K^+ ions. Two less intense series of signals (80% less intense than the main series signals), separated by 72 in m/z , were also observed. These weaker signals were assigned to cyclic (odd mass) polymers and oligomers clustered with Na^+ and K^+ ions. ^1H NMR spectra of the polymers reported in

this paper all contained resonances attributable to OH end groups (Figure 3.13). However, integration of either the –OH or RO– end group resonances relative to the methine protons generally afforded higher molecular weights than those obtained through either gel permeation chromatography (GPC) or MALDI-TOF MS analysis. The values were up to three times higher for polymers with the broadest M_w/M_n values.

Therefore, the ^1H NMR end group analyses confirmed that intramolecular transesterification had occurred, which produced cyclic species and led to less intense end group resonances than predicted based on the M_n data. The results obtained in this study contrast with the previously reported work of Carpentier and co-workers where no transesterification was apparent (as indicated by narrower molecular weight distributions than seen for our polymers and by MALDI-TOF MS studies) and a heterotactic bias was observed in the resulting polymers ($P_r = 0.60$)²⁵ although to achieve this THF was used as the solvent, while in toluene a slight isotactic bias was observed ($P_r = 0.46$), in line with the results obtained with piperazinyl systems in this research project. For the single morpholinyl derived initiator, P_r value of 0.49 was found for the PLA formed in toluene (Table 3.1, entry 13).

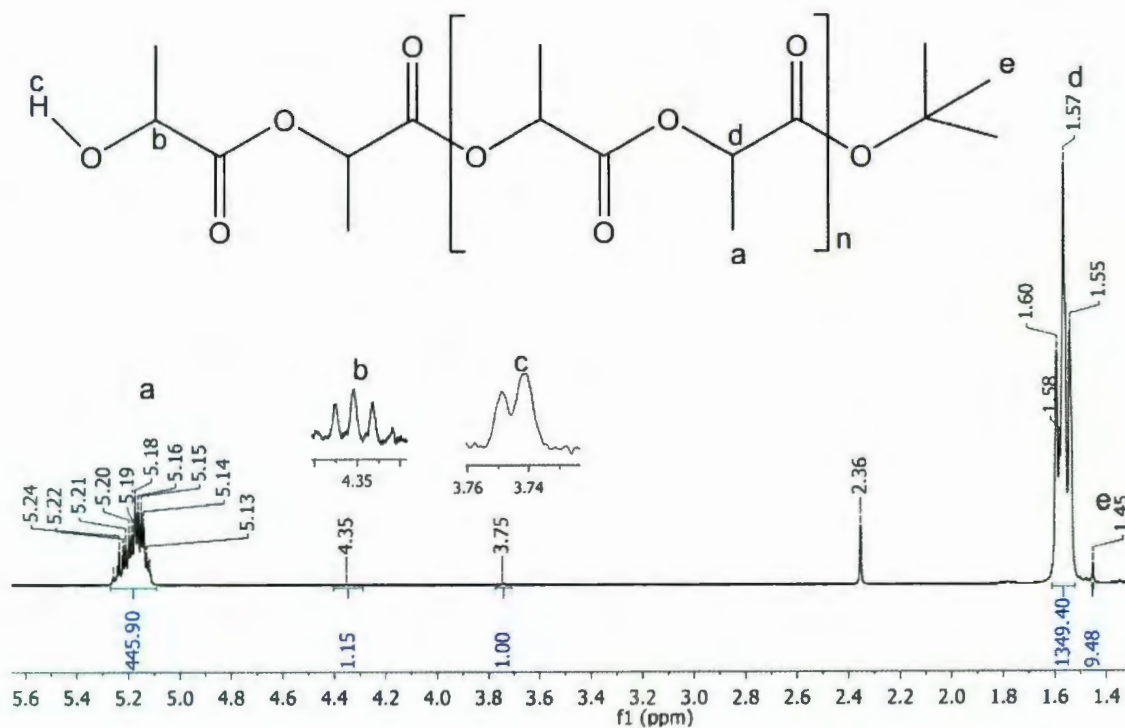


Figure 3.13. Section of the ^1H NMR spectrum (CDCl_3) of PLA sample prepared with **3.3**/ BuOH . Insets; (a) methyl resonance, (b) terminal methine resonance and (c) OH resonance

The first-order plot for solution polymerization with the initiator **3.7**/ BnOH (Figure 3.14) was linear with $k_{\text{app}} = 0.263 \text{ min}^{-1}$. The rate constants observed for the piperazinylderived species in this study were between 0.010 and 0.030 min^{-1} , both in toluene and in molten LA. These data suggest that the morpholinyl derived systems are superior initiators when compared with their piperazinyl analogues in terms of fast reaction rates and greater degree of control. This contrasts with related Al complexes described in chapter 4, in which the piperazinyl based initiators show good activity in ROP of ϵ -caprolactone than the morpholinyl analogues. We propose that the outersphere ether group in these systems may play a role in directing the incoming monomer for reaction at

the metal centre, and that the outersphere tertiary amine group is less efficient in this process.

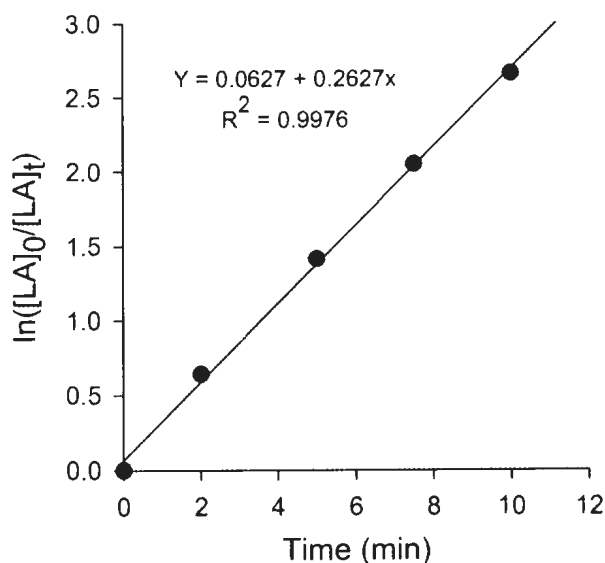


Figure 3.14. First-order plot of LA consumption in a reaction with **3.7**/BnOH conducted at 60 °C. Conditions: [LA]:[Zn]:[ROH] = 100:1:1, 10 mL of toluene, [Zn]₀ = 32.0 mM.

ROP reactions with the single component initiators **3.5** and **3.6** were also performed under solventless conditions at 130 °C (Table 3.2). Conversions reached more than 90% over 2 h (Table 3.2, entries 1 and 6), suggesting slow initiation compared with analogous solution phase polymerizations. The first-order plots for the bulk polymerization of LA with **3.5** and **3.6** as initiators (Figure 3.15) were linear with k_{app} values of 0.0179 and 0.0247 min⁻¹, respectively, albeit the linearity of the data using the complexes was not good. Bulk polymerization of LA in the presence of **3.6** (an ethoxide complex) is moderately faster than in the presence of **3.5** (a benzyl alkoxide species) due to the differences in the steric demands of the initiating alkoxide ligands. Complex **3.5** afforded

higher molecular weight polymers than **3.6**. The M_n values of these polymers were also significantly higher than the predicted values ($M_{n,cal}$), which might be attributed to decomposition of the initiators at the high temperatures required for melt polymerization. Initiator decomposition leading to higher than expected M_n values has been observed previously by Drouin *et al* in Zn diketiminate systems.⁵⁰ Both systems afforded predominantly atactic polymers under these reaction conditions due to the high temperatures used.

Table 3.2. Bulk polymerization of *rac*-LA initiated by **3.5** and **3.6** at 130 °C

Entry	Initiator	[LA] ₀ /[I] ₀	<i>t</i> /min	Conv. (%) ^[a]	<i>M</i> _{n,cal} ^[b] × 10 ³	<i>M</i> _n ^[c] × 10 ³	<i>M</i> _w / <i>M</i> _n ^[c]	<i>P</i> _r ^[d]
1	3.5	100/1	15	54.8	7.90	10.8	1.39	0.53
2	3.5	100/1	60	74	10.7	12.7	1.67	0.53
3	3.5	100/1	120	91.1	13.2	20.2	1.65	0.51
4	3.6	100/1	15	41.4	4.72	1.28	1.18	0.53
5	3.6	100/1	60	83.9	9.58	3.39	1.54	0.53
6	3.6	100/1	120	95.2	10.9	3.96	1.66	0.53

[a] Determined by ¹H NMR spectroscopy. [b] The *M*_{n,cal} value of the polymer was calculated with $M_n = ([LA]_0/[Zn]_0) \times 144.13$ (molecular weight of LA) × conversion %/100. [c] The *M*_n value was calculated according to $M_n = 0.58M_n^{GPC}$, where *M*_n^{GPC} is the value of *M*_n determined by GPC (chloroform) and is relative to polystyrene standards. [d] *P*_r is the probability of *racemic* enchainment of monomers units, as determined by homodecoupled ¹H NMR spectroscopy according to the method reported by Coates *et al.*⁵¹

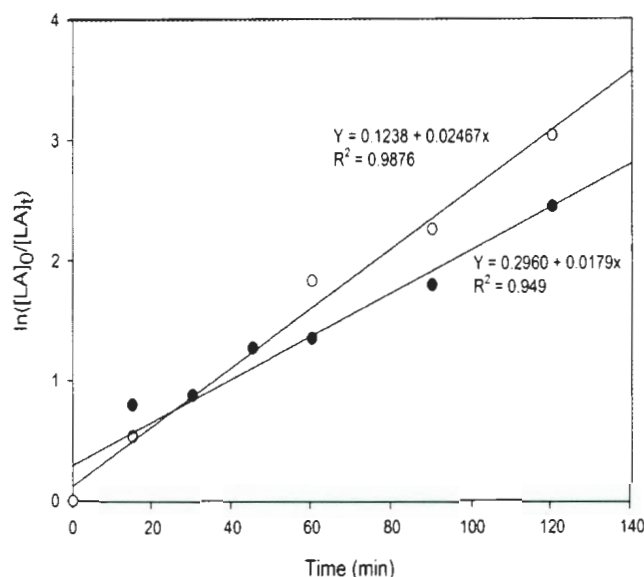


Figure 3.15. Plots of $\ln([LA]_0/[LA]_t)$ vs time for solventless polymerization of *rac*-LA initiated by **3.5** and **3.6**: $[LA]/[Zn] = 100$ at $130\text{ }^\circ\text{C}$, **3.5** = ● and **3.6** = ○

3.5.2 Ring-Opening Polymerization of ϵ -Caprolactone

Polymerization of ϵ -CL by complexes **3.2–3.5** and **3.7** was also assessed (Table 3.3). Similar trends in behaviour can be seen in the results from these reactions when compared to those of the ROP of LA study, e.g. slow initiation and reaction rates when t BuOH was used as the co-initiator (Table 3.3, entries 3 and 4). Molecular weight distributions were between 1.22 and 1.82. Conversions were generally higher when BnOH, which is less sterically demanding, was used in place of t BuOH. Of the complexes studied those containing the t Am substituted ligands afforded initiators with the greatest degree of reaction control for ROP of ϵ -CL, in that **3.4** and **3.5** afforded poly(ϵ -caprolactone) [P(ϵ -CL)] with narrow molecular weight distributions and molecular weights close to the expected values (Table 3.3, entries 7 and 8).

Table 3.3. Details of the ROP of ϵ -CL initiated by complexes **3.2-3.5** and **3.7** in toluene

Entry	Initiator	$[\epsilon\text{-CL}]_0/[\text{Zn}]_0/[\text{ROH}]_0$	t/min	T/°C	Conv. (%) ^[d]	$M_{\text{ncal}}^{\text{[e]}} \times 10^3$	$M_n^{\text{[f]}} \times 10^3$	$M_w/M_n^{\text{[f]}}$
1	2	100/1/1 ^b	15	60	74.4	8.49	5.69	1.27
2	2	200/1/1 ^b	60	60	94.5	21.4	9.72	1.34
3	3	100/1/1 ^a	120	70	17.1	-	-	-
4	3	200/1/1 ^a	270	70	76.3	17.4	14.6	1.82
5	3	100/1/1 ^a	5	130 ^c	50.0	5.71	12.2	1.37
6	3	100/1/1 ^b	5	130 ^c	98.3	11.2	7.70	1.46
7	4	100/1/1 ^b	40	70	99	11.3	8.56	1.22
8	5	100/1/0	60	70	95	10.8	9.03	1.30
9	7	100/1/1 ^b	30	70	88.5	20.2	17.5	1.21

[a] In the presence of one equivalent of *tert*-butyl alcohol. [b] In the presence of one equivalent of benzyl alcohol. [c] Microwave reaction (MW). [d] Determined by ¹H NMR spectroscopy. [e] The M_{ncal} value of the polymer was calculated with $M_{\text{ncal}} = ([\epsilon\text{-CL}]_0/[\text{Zn}]_0) \times 114.14$ (molecular weight of caprolactone) \times conv. %/100. [f] The M_n value was calculated according to $M_n = 0.56M_n^{\text{GPC}}$, where M_n^{GPC} was determined by GPC (chloroform), and is relative to polystyrene standards.

First-order plots of the consumption of ϵ -CL in ROP reactions conducted at 70 °C in the presence of **3.2**/BnOH and **3.7**/BnOH are shown in Figure 3.16. Comparisons with analogous Al complexes in this reaction are made in Chapter 4.

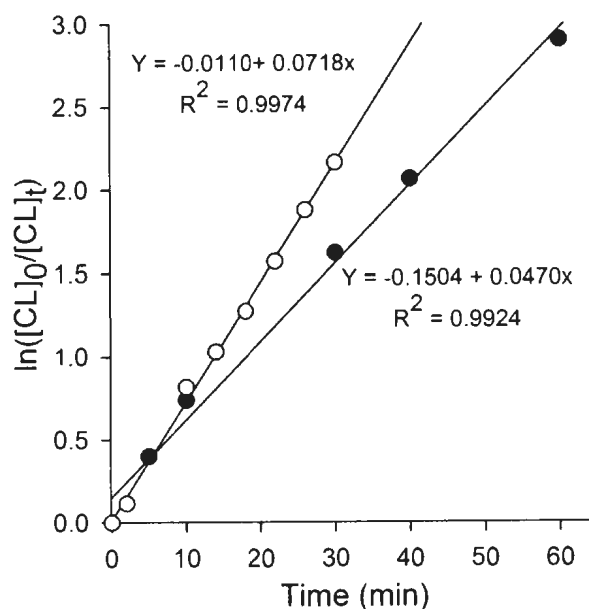


Figure 3.16. First-order plots of ϵ -CL consumption in ROP reactions conducted at 70 °C with **3.7**/BnOH (○) and **3.2**/BnOH (●). Conditions: $[\epsilon\text{-CL}]:[\text{Zn}] = 200:1:1$ $[\text{Zn}]_0 = 22.5$ mM (**3.7**) and 18.8 mM (**3.2**)

3.6 Reactivity of Complexes towards CO₂ and Cyclohexene Oxide Coupling

Amongst catalytic coordination complexes for CO₂/epoxide couplings and copolymerizations, zinc is central to many of the species studied.^{29,30,52–55} Therefore, studies were performed with **3.6** and **3.7**/ROH, with 4-(dimethylamino)pyridine (DMAP) and Bu₄NBr as cocatalysts (Table 3.4), to evaluate their activities in the reaction of CO₂ with

cyclohexene oxide. A control reaction was performed with Bu₄NBr alone as ionic salts such as this are known to catalyze the formation of cyclic carbonates (Table 3.4, entry 1).^{56,57} Compounds **3.6** and **3.7** exhibit some activity towards cyclic carbonate formation under high temperature and pressure conditions and in the presence of an ionic co-catalyst. Comparison of entries 1 and 5 (Table 3.4) indicates that the zinc complex does play a role in this reaction as the conversion increases by 18.1% when it is present in the reaction mixture and a small amount of *trans*-cyclic carbonate was observed. A **3.7**/EtOH/Bu₄NBr combination under the same conditions, entry 7, produced slightly less carbonate but with a larger amount of the *trans*-isomer than when only Bu₄NBr is present in the reaction mixture. The *cis*- and *trans*-isomers are likely formed through different mechanisms, with the *trans*-isomer probably formed through a back-biting reaction at the metal centre. Although conversions were modest and high temperatures and pressures were required, compared to state-of-the-art catalysts reported in the literature these results can act as a starting point for further studies, and also give some indication as to the reason for CO₂ uptake by the related Zn complexes reported by Lappert and co-workers.²⁶

Table 3.4. Reaction of cyclohexene oxide (CHO) with CO₂ in the presence of Zn complexes and co-catalysts

Entry	Catalyst	Co-catalyst	[CHO] ₀ /[Zn] ₀ /[Co-cat] ₀	t [h]	P [bar]	T [°C]	Conv. [%] ^[a]
1	-	Bu ₄ NBr	500/0/1	24	65	100	39.0 (100% <i>cis</i>)
2	3.6	-	500/1/0	18	45	70	0
3	3.6	DMAP	500/1/1	16	45	70	0
4	3.6	Bu ₄ NBr	500/1/1	18	45	70	4.8
5	3.6	Bu ₄ NBr	500/1/1	24	65	100	57.1 (96.2% <i>cis</i>)
6	3.7/BnOH	Bu ₄ NBr	500/1/1	18	45	70	8.3
7	3.7/EtOH	Bu ₄ NBr	500/1/1	24	65	100	45.1 (86.4% <i>cis</i>)

[a] Determined by the relative intensities of the methine protons in the ¹H NMR spectra.⁵⁸

3.7 Conclusions

Piperazinyl-derived amine-phenolate protio ligands can be prepared in excellent yields in water *via* a modified Mannich condensation reaction. As expected, these ligands readily react with diethylzinc and generally afford phenolate bridged Zn-Et dimers. These complexes readily undergo alcoholysis to yield alkoxide bridged species. A range of these complexes has been structurally characterized. The Zn-Et species in the presence of an alcohol, and the alkoxide complexes as single component initiators, are able to facilitate ring-opening polymerization of cyclic esters, however, no control of stereoselectivity is observed in ROP of LA and this is probably due to the solvent employed in these reactions. In comparison with morpholinyl derived complexes, the piperazinyl-derived species show slower ROP reaction rates. MW irradiation was used in some of the ROP reactions and was useful in reducing reaction times whilst maintaining control of the reaction (i.e. increased polydispersities that usually exist in polymers formed during high temperature ROP reactions were not observed). Both classes of complex show slight activity towards cyclic carbonate formation involving cyclohexene oxide and carbon dioxide. These studies suggest that an outersphere ligand group or base (ether or amine) within an initiating or catalytic species can affect the outcome of ROP and potentially other reactions. Further studies utilizing these interesting ligands are underway in the Kerton research group.

3.8 Experimental Section

3.8.1 General Considerations

All experiments involving metal complexes were performed in a nitrogen atmosphere with standard Schlenk and glovebox techniques. THF was distilled under nitrogen over sodium/benzophenone. Toluene and hexane were purified by an MBraun Solvent Purification System. Deuterated solvents (C_6D_6 , $CDCl_3$, C_5D_5N) were purchased from Cambridge Isotope Laboratories Inc., purified and dried before use. All solvents were degassed by freeze-vacuum-thaw cycles prior to use. 2,4-bis-(*tert*-butyl)phenol, 2-*tert*-butyl-4-methylphenol, 2,4-bis(*tert*-amyl)phenol, *n*-butyllithium, 1-methyl piperazine, morpholine, diethylzinc (15 wt.-% solution in hexane), LA, ϵ -CL and cyclohexene oxide were purchased from Sigma–Aldrich or Alfa Aesar. Monomers were dried and degassed prior to use. Elemental analyses were performed by Canadian Microanalytical Service Ltd., Delta, B.C. Canada. 1H and $^{13}C\{^1H\}$ NMR spectra were recorded on a Bruker Avance 500 MHz spectrometer at 25 °C (unless otherwise stated) and were referenced internally with respect to the residual proton and ^{13}C resonances of the solvent. ^{13}C signals were assigned by heteronuclear single quantum correlation spectroscopy (HSQC) experiments. MALDI-TOF MS measurements were performed with an Applied Biosystems Voyager DE-PRO equipped with a reflectron, delayed ion extraction and high performance nitrogen laser (337 nm). Anthracene was the matrix for the ligands and complexes.^{59–60} Mass spectra were also obtained by atmospheric pressure chemical ionization mass spectrometry (AP-CI MS) in positive mode (70 eV) with an Agilent 1100 LC mass spectrometer. GPC data were collected on a Viscotek GPCMax System

equipped with a Refractive Index Detector, and columns were purchased from Phenomenex (Phenogel 5 μ Linear/mixed bed 300 4.60 mm column in series with a Phenogel 5 μ , 100 Å, 300 4.60 mm column). Samples were run in chloroform at a concentration of 1 mg mL⁻¹, and at 35 °C. The instrument was calibrated against polystyrene standards (Viscotek) to determine the molecular weights (M_n and M_w) and the polydispersity index (M_w/M_n) of the polymers. For PLA samples, P_r were determined by analysis of the methine region of the homonuclear decoupled ¹H NMR spectra (CDCl₃). The equations used to calculate P_r were as described by Coates *et al.*⁵¹ The conversions were determined by integration of the relative intensities of the OCHMe resonances corresponding to the residual LA and poly(*rac*-lactide), and integration of the ϵ -methylene signals due to the residual ϵ -CL and poly(ϵ -caprolactone). Microwave heated polymerizations were performed with a Biotage Initiator™ eight microwave synthesizer.

3.8.2 Crystallographic Procedures

All crystals were mounted with paratone oil onto low temperature diffraction loops. Measurements were made on a Rigaku AFC8-Saturn 70 single-crystal X-ray diffractometer equipped with an X-stream 2000 low temperature system and a SHINE optic. Data were collected with Mo-K α radiation. Data were collected and processed with the CrystalClear software (Rigaku).^{61,62} Numerical absorption corrections were applied and the data were corrected for Lorentz and polarization effects. The structures were solved by direct methods ([L1]H, 3.1, 3.3-3.7),⁶³ (3.2)⁶⁴ and refined by Fourier techniques.⁶⁵ Neutral atom scattering factors were taken from those provided by Cromer and Waber.⁶⁶ Anomalous dispersion effects were included in F_{calc} ;⁶⁷ the values for $\Delta f'$

and $\Delta f''$ were those of Creagh and McAuley.⁶⁸ The values for the mass attenuation coefficients were those of Creagh and Hubbell.⁶⁹ All calculations were performed with the CrystalStructure^{70,71} crystallographic software package except for refinement, which was performed with SHELXL-97.⁶³ Hydrogen atoms were introduced in calculated positions and refined on a riding model, unless otherwise indicated. All non-hydrogen atoms were refined anisotropically. For [L2]H, **3.1**, **3.3**, **3.5** and **3.6**, data collections, structural solutions, and refinements proceeded normally. For [L2]H, atom H1 was introduced into the refinement model according to its position in the difference map, and initially the atomic x , y , z coordinates were refined, but finally the atom was refined with a riding model. Friedel mates were averaged and the absolute configuration was not determined. The asymmetric unit of **3.1** contained a half-occupancy toluene molecule that was disordered over two sites. The toluene protons could not be located from difference maps, and were omitted from the model. For **3.5**, one disordered amyl group was present (PART 1: [C32–35, C39] at 0.65 occupancy; PART 2: [C32A, C36–38, C40] at 0.35 occupancy). Hydrogen atoms on C33 and C36 were omitted from the model. Complexes **3.2** and **3.7** were refined as non-merohedral twins with 2 components #1 comprising 47.99% and 64.81% of the crystal, respectively (Table 3.5 and Table 3.6). For **3.2**, a large negative residual density peak was present in the difference map (1.82 Å from H5A) and is likely a result of twinning that was not accounted for; overlap from the second twin domain can cause errors in the intensities of some reflections. Complex **3.4** was refined as a merohedral twin, with component #1 comprising 19.60% of the crystal. The merohedral twin law was identified by the TwinRotMat function in the PLATON software.⁷²

Table 3.5. Summary of crystal data for compounds [L2]H, 3.1-3.5

Compounds	[L2]H	3.1	3.2	3.3	3.5
Formula	C ₂₀ H ₃₄ N ₂ O	C ₄₇ H ₇₄ N ₄ O ₂ Zn	C ₃₈ H ₆₄ N ₄ O ₂ Zn ₂	C ₅₈ H ₉₂ N ₄ O ₂ Zn ₂	C ₇₉ H ₁₁₂ N ₄ O ₄ Zn ₂
Formula Weight	318.50	792.51	739.71	1008.15	1312.54
Crystal System	Triclinic	Monoclinic	Triclinic	Triclinic	Monoclinic
Space Group	P-1	C2/c	P-1	P-1	P2/c
<i>a</i> / Å	6.1799(14)	10.0658(11)	9.6308(9)	9.206(14)	24.314(4)
<i>b</i> / Å	8.4415(18)	17.945(2)	11.0488(11)	11.540(19)	10.9529(17)
<i>c</i> / Å	10.081(2)	25.003(3)	19.6721(19)	13.902(20)	28.023(4)
α /°	67.242(7)	90	100.023(5)	92.493(13)	90
β /°	78.354(11)	99.377(3)	97.146(5)	93.888(18)	94.232(4)
γ /°	89.180(12)	90	108.791(4)	111.02(3)	90
<i>V</i> / Å ³	473.76(17)	4455.8(9)	1914.6(3)	1372(4)	7442.7(20)
<i>T</i> /K	153	153	153	153	153
<i>Z</i>	1	4	2	1	4
<i>D</i> _c g cm ⁻³	1.116	1.181	1.283	1.220	1.171
<i>F</i> (000)	176	1720	792	544	2824
μ (MoK α)/ cm ⁻¹	0.68	5.92	12.89	9.18	6.94
Total reflections	3883	28248	20078	14165	96494
Unique reflections	1914	4605	20078	5600	15414
<i>R</i> _{int}	0.0167	0.0216	0.0000	0.0314	0.0563
Reflections <i>I</i> > 2 σ (<i>I</i>)	1904	4503	18150	5239	14321
No. of variables	209	259	417	299	851
<i>R</i> , <i>wR</i> ₂ [<i>I</i> > 2 σ (<i>I</i>)]	0.0350, 0.0961	0.0344, 0.0924	0.0975, 0.2538	0.0573, 0.1280	0.0695, 0.1574
GOF	1.049	1.038	1.144	1.120	1.172

Table 3.6. Summary of crystal data for compounds **3.6** and **3.7**

Compounds	3.6	3.7
Formula	C ₄₄ H ₇₆ N ₄ O ₄ Zn ₂	C ₅₆ H ₈₆ N ₂ O ₄ Zn ₂
Formula Weight	855.87	982.07
Crystal System	Triclinic	Triclinic
Space Group	P-1	P-1
<i>a</i> / Å	8.960(3)	10.9384(15)
<i>b</i> / Å	9.099(3)	11.4289(15)
<i>c</i> / Å	14.779(6)	11.9898(16)
α /°	81.33(3)	102.923(8)
β /°	76.04(2)	106.541(7)
γ /°	76.04(2)	107.637(8)
<i>V</i> / Å ³	1123.8(7)	1288.1(3)
<i>T</i> /K	153	153
<i>Z</i>	1	1
<i>D</i> _c g cm ⁻³	1.265	1.266
<i>F</i> (000)	460	528
μ (MoK α)/ cm ⁻¹	11.11	9.77
Total reflections	8979	15846
Unique reflections	4141	15846
<i>R</i> _{int}	0.0939	0.0000
Reflections <i>I</i> > 2 σ (<i>I</i>)	2984	14915
No. of parameters	245	290
<i>R</i> , <i>wR</i> ₂ [<i>I</i> > 2 σ (<i>I</i>)]	0.1060, 0.2132	0.1061, 0.2854
GOF	1.149	1.248

3.8.3 Synthetic Procedures

[ONN^{Me,tBu}] ([L1]H): Water (80 mL), 2-*tert*-butyl-4-methylphenol (10.1 g, 61.5 mmol) and formaldehyde 37 wt. % in water (5.00 mL, 61.5 mmol) were added to 250 mL round-bottom flask equipped with a stir bar and a condenser. 1-Methylpiperazine (6.80 mL, 61.5 mmol) was added dropwise to the stirred solution. The resulting mixture was heated at reflux for 18 h. Upon cooling to room temperature a two phase mixture was formed. The organic layer (solid) was isolated, washed with methanol and dried under vacuum to remove any unreacted organic components. The resulting pale grey solid was recrystallized from methanol to give colourless crystals; yield 16.7 g, 98.0%. mp 90 °C. MS (AP-CI, MeOH): $m/z = 277$ (M^+ , 100%). Anal. calcd. for C₁₇H₂₈N₂O (276.42): C 73.87, H 10.21, N 10.13; found C 73.81, H 10.10, N 10.66%. ¹H NMR (CDCl₃, 500 MHz, 298 K): $\delta = 10.90$ (1H, s, ArOH), 6.99 (1H, s, ArH), 6.67 (1H, s, ArH), 3.65 (2H, s, Ar-CH₂-N), 2.51 (8H, br, N-C₂H₄-C₂H₄-N), 2.31 (3H, s, N-CH₃), 2.23 (3H, s, Ar-CH₃), 1.40 (9H, s, Ar-C{CH₃}₃) ppm. ¹³C{¹H} NMR (CDCl₃, 125 MHz, 298 K): $\delta = 154.7$ (ArC-OH), 136.6 (ArC-CH₃), 127.7 (ArCH), 127.5 (ArCH), 127.0 (ArC-C{CH₃}₃), 121.6 (ArC-CH₂-N), 62.1 (ArC-CH₂-N), 55.3 (N-C₂H₄-C₂H₄-N), 52.7 (N-C₂H₄-C₂H₄-N), 46.3 (N-CH₃), 35.0 (ArC-C{CH₃}₃), 30.0 (ArC-C{CH₃}₃), 21.2 (ArC-CH₃) ppm.

[ONN^{tBu,tBu}] ([L2]H): This compound was prepared in the same manner as described above for [L1]H with 2,6-di-*tert*-butylphenol (12.7 g, 61.5 mmol), formaldehyde 37 wt. % in water (5.00 mL, 61.5 mmol), and 1-methyl piperazine (6.80 mL, 61.5 mmol) as starting materials. The product was recrystallized to yield a colourless crystalline solid;

yield 17.7 g, 90.0%. mp 119 °C. MS (MALDI, anthracene matrix): $m/z = 381$ (M^+ , 100%). Anal. calcd. for $C_{20}H_{34}N_2O$ (318.50): C 75.42, H 10.76, N 8.80; found C 75.40, H 10.65, N 8.79%. 1H NMR ($CDCl_3$, 500 MHz, 298 K): $\delta = 11.49$ (1H, s, ArOH), 7.26 (1H, s, ArH), 6.93 (1H, s, ArH), 3.75 (2H, s, Ar- CH_2 -N), 2.98 (4H, d, $J = 10.2$ Hz, N- C_2H_4 - C_2H_4 -N), 2.86 (4H, d, $J = 10.3$ Hz, N- C_2H_4 - C_2H_4 -N), 2.35 (3H, s, N- CH_3), 1.42 (9H, s, ArC{ CH_3 } $_3$), 1.29 (9H, s, ArC(CH_3) $_3$) ppm. $^{13}C\{^1H\}$ NMR ($CDCl_3$, 125 MHz, 298 K): $\delta = 154.5$ (ArC-OH), 140.9 (ArC-C{ CH_3 } $_3$), 135.8 (ArC-C{ CH_3 } $_3$), 123.8 (ArCH), 123.3 (ArCH), 120.9 (ArC- CH_2 -N), 62.5 (ArC- CH_2 -N), 55.3 (N- C_2H_4 - C_2H_4 -N), 52.7 (N- C_2H_4 - C_2H_4 -N), 46.3 (N- CH_3), 35.2 (ArC-C{ CH_3 } $_3$), 34.5 (ArC-C(CH_3) $_3$), 32.1 (ArC-C{ CH_3 } $_3$), 30.0 (ArC-C{ CH_3 } $_3$) ppm.

[ONN^{tAm,tAm}] ([L3]H): Water (100 mL), 2,6-di-*tert*-amylphenol (19.0 g, 81.0 mmol) and formaldehyde 37 wt. % in water (6.60 mL, 81.0 mmol) were added to a 500 mL round-bottom flask equipped with a stir bar and a condenser. 1-Methyl piperazine (8.10 g, 81.0 mmol) was added dropwise to the stirred solution. The resulting mixture was heated at reflux for 18 h. Upon cooling to room temperature a two phase mixture formed. The organic material was extracted with diethyl ether and dried with magnesium sulfate. The solvent was removed by rotary evaporation to give a pale brown oil from which colourless crystals were obtained upon standing for several days under ambient conditions; yield 23.0 g, 82.0%. mp 82 °C. MS (AP-Cl, MeOH): $m/z = 347$ (M^+ , 100%). $C_{22}H_{38}N_2O$ (348.55): calcd. C 76.25, H 11.05, N 8.08; found C 76.36, H 10.80, N 8.04%. 1H NMR ($CDCl_3$, 500 MHz, 298 K): $\delta = 10.77$ (1H, s, ArOH), 7.07 (1H, d, $J = 2.2$ Hz, ArH), 6.75 (1H, d, $J = 2.2$ Hz, ArH), 3.67 (2H, s, Ar- CH_2 -N), 2.53 (8H, br, N- C_2H_4 -

C_2H_4-N), 2.30 (3H, s, $N-CH_3$), 1.88 (2H, q, $J = 7.4$ Hz, $ArC-C\{CH_2CH_3\}$), 1.56 (2H, q, $J = 7.4$ Hz, $ArC-C\{CH_2CH_3\}$), 1.36 (6H, s, $ArC-C\{CH_3\}_2$), 1.23 (6H, s, $ArC-C\{CH_3\}_2$), 0.65 (3H, t, $J = 7.4$ Hz, $ArC-C\{CH_2CH_3\}$), 0.64 (3H, t, $J = 7.4$ Hz, $ArC-C\{CH_2CH_3\}$), ppm. $^{13}C\{^1H\}$ NMR ($CDCl_3$, 500 MHz, 298 K): $\delta = 154.2$ ($ArC-OH$), 139.0 ($ArC-C\{CH_3\}_2$), 134.1 ($ArC-C\{CH_3\}_2$), 125.3 ($ArCH$), 124.4 ($ArCH$), 120.6 ($ArC-CH_2-N$), 62.5 ($ArC-CH_2-N$), 55.3 ($N-C_2H_4-C_2H_4-N$), 52.3 ($N-C_2H_4-C_2H_4-N$), 46.3 ($ArC-C\{CH_3\}_2$), 38.7 ($N-CH_3$), 37.6 ($ArC-C\{CH_2CH_3\}$), 37.5 ($ArC-C\{CH_2CH_3\}$), 33.4 ($ArC-C\{CH_3\}_2$), 28.9 ($ArC-C\{CH_3\}_2$), 28.0 ($ArC-C\{CH_3\}_2$), 9.8 ($ArC-C\{CH_2CH_3\}$), 9.5 ($ArC-C\{CH_2CH_3\}$) ppm.

[ONO^{tBu,tBu}] ([L5]H): Water (80 mL), 2-tert-butyl-4-methylphenol (16.5 g, 80.0 mmol) and formaldehyde 37 wt. % in water (6.50 mL, 80.0 mmol) were added to 250 mL round-bottom flask equipped with a stir bar and a condenser. Morpholine (6.97 mL, 80.0 mmol) was added dropwise to the stirred solution. The resulting mixture was heated at reflux for 18 h. Upon cooling to room temperature a two phase mixture was formed. The organic layer (solid) was isolated, washed with methanol and dried under vacuum to remove any unreacted organic components. The resulting brown gel-like solid was recrystallized from methanol to give a colourless solid; yield 21.2 g, 87.0%. mp 112 °C. MS (MALDI, anthracene matrix): $m/z = 305$ (M^+ , 100%). $C_{19}H_{31}NO_2$ (305.46): calcd. C 74.71, H 10.23, N 4.59; found C 74.66, H 10.27, N 4.52%. 1H NMR ($CDCl_3$, 500 MHz, 298 K): $\delta = 10.66$ (1H s, , $ArOH$), 7.23 (1H, d, $J = 2.2$ Hz, ArH), 6.84 (1H, d, $J = 2.2$ Hz, ArH), 3.75 (2H, s, $Ar-CH_2-N$), 3.68 (4H, br, $O-C_2H_4-C_2H_4-N$) 2.56 (4H, br, $O-C_2H_4-C_2H_4-N$), 1.41 (9H, s, $ArC-C\{CH_3\}_3$), 1.28 (9H, s, $ArC-C\{CH_3\}_3$) ppm. $^{13}C\{^1H\}$ NMR

(CDCl₃, 125 MHz, 298 K): δ = 154.4 (ArC–OH), 141.2 (ArC–C{CH₃}₃), 136.0 (ArC–C{CH₃}₃), 124.0 (ArCH), 123.6 (ArCH), 120.5 (ArC–CH₂–N), 67.2 (O–C₂H₄–C₂H₄–N), 63.1 (ArC–CH₂–N), 53.2 (O–C₂H₄–C₂H₄–N), 35.3 (ArC–C{CH₃}₃), 34.6 (ArC–C{CH₃}₃), 32.1 (ArC–C{CH₃}₃), 30.0 (ArC–C{CH₃}₃) ppm.

Zn[ONN^{tBu,tBu}]₂ (3.1): To a 50 mL flask containing diethylzinc (1.70 mL, 2.00 mmol, 15 wt. % in hexane) a solution of [L2]H (0.64 g, 2.00 mmol) in toluene (2.00 mL) that was cooled to –35 °C was added dropwise. The colourless mixture was warmed, while being stirred, to room temperature and then held at this temperature for 18 h. Volatiles were removed under vacuum to give a white residue, which was washed with hexane (2 × 4 mL) and dried in vacuo. **3.1** was obtained as a colourless crystalline solid; yield: 1.07 g, 77.0%. Crystals suitable for X-ray crystallography could be grown by slow evaporation, or by cooling at –35 °C of a saturated toluene/hexane solution. Anal. calcd. for C₄₇H₇₄N₄O₂Zn·(C₇H₈) (792.5 + 92.1 = 884.6): C 71.23, H 9.41, N 7.07; found C 71.10, H 9.49, N 7.05%. ¹H NMR (C₅D₅N, 500 MHz, 343 K): δ = 7.58 (1H, s, ArH), 7.11 (1H, s, ArH), 4.07 (2H, s, Ar–CH₂–N), 3.07 (4H, br, N–C₂H₄–C₂H₄–N), 2.83 (4H, s, N–C₂H₄–C₂H₄–N), 2.29 (3H, s, N–CH₃), 1.60 (9H, s, ArC–C{CH₃}₃), 1.44 (9H, s, ArC–C{CH₃}₃) ppm. ¹³C{¹H} NMR (C₅D₅N, 125 MHz, 298 K): δ = 165.3 (ArC–O), 137.8 (ArC–C{CH₃}₃), 134.5 (ArC–C{CH₃}₃), 129.6 (ArCH), 128.9 (ArCH), 122.1 (ArC–CH₂–N), 64.6 (ArC–CH₂–N), 55.1 (N–C₂H₄–C₂H₄–N), 53.5 (N–C₂H₄–C₂H₄–N), 46.1 (N–CH₃), 36.0 (ArC–C{CH₃}₃), 34.4 (ArC–C{CH₃}₃), 32.6 (ArC–C{CH₃}₃), 30.5 (ArC–C{CH₃}₃), ppm.

{[μ -ONN^{Me,Bu}]ZnEt}₂ (3.2): To a 50 mL flask containing diethylzinc (6.20 mL, 5.02 mmol, 15 wt. % in hexane) a solution of [L1]H (1.39 g, 5.02 mmol) in toluene (2.0 mL) that was cooled to -35 °C was added dropwise. The colourless mixture was warmed, while being stirred, to room temperature and then held at this temperature for 18 h. Volatiles were removed under vacuum to give a white residue, which was washed with hexane (2 × 4 mL) and dried in *vacuo*. The crude product was recrystallized from a saturated toluene solution held at -35 °C to give **3.2** as a colourless crystalline solid; yield 1.43 g, 77%. Anal. calcd. for C₃₈H₆₄N₄O₂Zn₂ (739.71): C 61.70, H 8.72, N 7.57; found C 62.02, H 9.13, N 7.98%. ¹H NMR (C₅D₅N, 500 MHz, 343 K): δ = 7.33 (1H, s, ArH), 6.84 (1H, s, ArH), 4.00 (2H, s, Ar-CH₂-N), 3.04 (4H, br, N-C₂H₄-C₂H₄-N), 2.83 (4H, br, N-C₂H₄-C₂H₄-N), 2.35 (3H, s, N-CH₃), 2.30 (3H, s, ArC-CH₃), 1.78 (2H, s, Zn-CH₂CH₃), 1.58 (9H, q, ArC-C{CH₃}₃), 0.91 (3H, t, Zn-CH₂CH₃) ppm. ¹³C{¹H} NMR (C₅D₅N, 125 MHz, 298 K): δ = 164.4 (ArC-O), 138.6 (ArC-{CH₃}), 130.4 (ArC-C{CH₃}₃), 128.7 (ArCH), 121.9 (ArCH), 120.8 (ArC-CH₂-N), 64.6 (ArC-CH₂-N), 55.4 (N-C₂H₄-C₂H₄-N), 53.0 (N-C₂H₄-C₂H₄-N), 45.9 (Ar-CH₂-N), 35.5 (N-CH₃), 30.6 (ArC-C{CH₃}₃), 30.4 (ArC-C{CH₃}₃), 21.4 (Zn-CH₂CH₃), 21.2 [ArC-(CH₃)], 14.1 (Zn-CH₂CH₃) ppm.

{[μ -ONN^{Bu,Bu}]ZnEt}₂ (3.3): To a 50 mL flask containing diethylzinc (3.3 mL, 4.0 mmol, 15 wt. % in hexane) a solution of [L2]H (0.64 g, 2.0 mmol) in toluene (2.0 mL) that was cooled to -35 °C was added dropwise. The colourless mixture was warmed, while being stirred, to room temperature and then held at this temperature for 18 h. Volatiles were removed under vacuum to give a white residue, which was washed with hexane (2 × 4 mL) and dried in *vacuo*; yield 0.92 g, 56%. Crystals suitable for X-ray

crystallography could be grown by slow evaporation, or by cooling at $-35\text{ }^{\circ}\text{C}$, of a saturated toluene/hexane solution. Anal. calcd. for $\text{C}_{44}\text{H}_{76}\text{N}_4\text{O}_2\text{Zn}_2$ (823.87): C 64.14, H 9.30, N 6.80; found C 63.72, H 9.21, N 6.10%. ^1H NMR ($\text{C}_5\text{D}_5\text{N}$, 500 MHz, 358 K): δ = 7.63 (1H, s, ArH), 7.10 (1H, s, ArH), 3.65 (2H, s, Ar-CH₂-N), 2.64 (4H, br, N-C₂H₄-C₂H₄-N), 2.54 (4H, br, N-C₂H₄-C₂H₄-N), 2.27 (3H, s, N-CH₃), 1.81 (9H, s, ArC-C{CH₃}₃), 1.57 (3H, t, J = 8.0 Hz, Zn-CH₂CH₃) 1.50 (9H, s, ArC-C{CH₃}₃), 0.59 (2H, q, J = 8.0 Hz, Zn-CH₂CH₃) ppm. $^{13}\text{C}\{^1\text{H}\}$ NMR ($\text{C}_5\text{D}_5\text{N}$, 125 MHz, 298 K): δ = 165.3 (ArC-O), 138.3 (ArC-C{CH₃}₃), 134.5 (ArC-C{CH₃}₃), 126.6 (ArCH), 126.0 (ArCH), 122.1 (ArC-CH₂N), 64.6 (ArC-CH₂-N), 55.2 (N-C₂H₄-C₂H₄-N), 53.5 (N-C₂H₄-C₂H₄-N), 46.1 (N-CH₃), 36.0 (ArC-C{CH₃}₃), 34.4 (ArC-C{CH₃}₃), 32.6 (ArC-C{CH₃}₃), 30.5 (ArC-C{CH₃}₃), 14.1 (Zn-CH₂CH₃), 1.5 (Zn-CH₂CH₃) ppm.

{[μ -ONN^{tAm,tAm}]ZnEt}₂ (3.4): To a 50 mL flask containing diethylzinc (6.20 mL, 5.02 mmol, 10 wt. % in hexane) a solution of [L3]H (1.74 g, 5.02 mmol) in toluene (2.0 mL) that was cooled to $-35\text{ }^{\circ}\text{C}$ was added dropwise. The colourless mixture was warmed, while being stirred, to room temperature and then held at this temperature for 18 h. Volatiles were removed under vacuum to give a white residue, which was washed with hexane (2×4 mL) and dried in *vacuo*. The crude product was recrystallized from a saturated toluene solution at $-35\text{ }^{\circ}\text{C}$ to give **3.4** as a colourless crystalline solid; yield 1.92 g, 87.0%. Anal. calcd. for $\text{C}_{48}\text{H}_{84}\text{N}_4\text{O}_2\text{Zn}_2$ (879.98): C 65.51, H 9.62, N 6.37; found C 65.47, H 10.89, N 6.28%. ^1H NMR ($\text{C}_5\text{D}_5\text{N}$, 500 MHz, 358 K): δ = 7.49 (1H, s, ArH), 7.04 (1H, s, ArH), 3.65 (2H, s, ArC-CH₂-N), 2.64 (4H, br, N-C₂H₄-C₂H₄-N), 2.56 (4H, s, N-C₂H₄-C₂H₄-N), 2.41 (2H, q, J = 7.4 Hz, ArC-C{CH₂CH₃}), 2.27 (3H, s, N-CH₃),

1.80 (2H, q, $J = 7.4$ Hz, ArC-C{CH₂CH₃}), 1.74 (6H, s, ArC-C{CH₃}₂), 1.59 (3H, t, $J = 8.0$ Hz, Zn-CH₂CH₃), 1.46 (6H, s, ArC-C{CH₃}₂), 0.98 (3H, t, $J = 7.4$ Hz, ArC-C{CH₂CH₃}), 0.91 (3H, t, $J = 7.4$ Hz, ArC-C{CH₂CH₃}), 0.61 (2H, q, $J = 8.0$ Hz, Zn-CH₂CH₃), ppm. ¹³C{¹H} NMR (C₅D₅N, 125 MHz, 298 K): $\delta = 165.2$ (ArC-O), 136.0 (ArC-C{CH₂CH₃}), 132.4 (ArC-C{CH₂CH₃}), 127.3 (ArCH), 126.4 (ArCH), 121.8 (ArC-CH₂-N), 64.5 (ArC-CH₂-N), 55.1 (N-C₂H₄-C₂H₄-N), 53.5 (N-C₂H₄-C₂H₄-N), 46.1 (N-CH₃), 39.42 (ArC-C{CH₂CH₃}), 37.9 (ArC-C{CH₂CH₃}), 37.5 (ArC-C{CH₂CH₃}), 33.3 (ArC-C{CH₂CH₃}), 29.6–28.5 ArC-C{CH₃}₂, 14.1 (Zn-CH₂CH₃) 10.7–9.9 (ArC-C{CH₂CH₃}), 1.6 (Zn-CH₂CH₃) ppm.

{[ONN^{rAm,Am}]Zn(μ -OBn)}₂ (3.5): To a solution of **3.4** (0.80 g, 0.91 mmol) in toluene (5.0 mL) that was cooled to -35 °C, BnOH (190 μ L, 1.80 mmol) was added dropwise. The reaction mixture was warmed, while being stirred, to room temperature and then held at this temperature for 3 h. The solvent was removed under vacuum to give a white residue, which was washed with cold hexane (2 \times 4 mL) and dried in *vacuo*. The crude product was recrystallized from toluene/hexane to give **3.5** as a colourless crystalline solid; yield 0.84 g, 89%. Anal. calcd. for C₅₈H₈₈N₄O₄Zn₂ (1036.12): C 67.23, H 8.56, N 5.41; found C 67.78, H 9.12, N 5.63%. ¹H NMR (C₅D₅N, 500 MHz, 343 K): $\delta = 7.69$ (1H, s, ArH), 7.51 (2H, s, ArH), 7.43 (1H, s, ArH), 7.37 (1H, s, ArH), 7.05 (2H, s, ArH), 5.11 (2H, br, OCH₂Ar), 4.09 (2H, s, ArC-CH₂-N), 2.60–3.05 (8H, br, overlapping, (N-C₂H₄-C₂H₄-N), 1.77 (4H, m, ArC-C{CH₂CH₃}), 1.58 (3H, s, N-CH₃), 1.41 (6H, s, ArC-C{CH₃}₂), 1.38 (6H, s, ArC-C{CH₃}₂), 0.87 (6H, m, ArC-C{CH₂CH₃}), ppm. ¹³C{¹H} NMR (C₅D₅N, 125 MHz, 298 K): $\delta = 163.8$ (ArC-O), 144.5 (ArC-CH₂-O),

133.6 ArC-C{CH₂CH₃}, 129.1 (ArC), 129.0 (ArC), 128.0 (ArCH), 127.3 (ArCH), 126.8 (ArC), 119.9 (ArC-CH₂-N), 69.4 (ArC-CH₂-O), 65.0 (ArC-CH₂-N), 55.3 (N-C₂H₄-C₂H₄-N), 54.2 (N-C₂H₄-C₂H₄-N), 45.9 (N-CH₃), 39.1 (ArC-C{CH₂CH₃}), 37.8 (ArC-C{CH₂CH₃}), 37.5 (ArC-C{CH₂CH₃}), 33.4 (ArC-C{CH₂CH₃}), 29.4–28.5 ArC-C{CH₃}₂, 10.4–9.9 (ArC-C{CH₂CH₃}). ppm.

{[ONN^{tBu,tBu}]Zn(μ-OEt)}₂ (3.6): To a 50 mL flask containing diethylzinc (7.8 mL, 6.3 mmol, 15 wt. % in hexane) a solution of [L2]H (2.00 g, 6.30 mmol) in toluene (2.0 mL) cooled to -35 °C was added dropwise. The colourless mixture was warmed, while being stirred, to room temperature and then held at this temperature for 3 h. Volatiles were removed under vacuum to give an off-white residue, which was washed with pentane (2 × 4 mL) and redissolved in toluene (2.0 mL). To this solution EtOH (366 μL, 6.30 mmol) was added dropwise, and the reaction mixture was stirred at room temperature for 18 h. The resulting mixture was filtered and the filtrate was concentrated under vacuum and cooled to -35 °C to afford **3.6** as a colourless crystalline solid; yield 1.65 g, 61.0%. Anal. calcd. for C₄₄H₇₆N₄O₄Zn₂ (855.87): C 61.75, H 8.95, N 6.55; found C 61.69, H 9.19, N 7.00%. ¹H NMR (C₅D₅N, 500 MHz, 358 K): δ = 7.72 (1H, s, ArH), 7.66 (1H, s, ArH), 4.04 (2H, br, O-CH₂CH₃), 3.83 (2H, s, Ar-CH₂-N), 3.00 (4H, br, N-C₂H₄-C₂H₄-N), 2.79 (4H, br, N-C₂H₄-C₂H₄-N), 2.53 (3H, s, N-CH₃), 1.92 (9H, s, ArC{CH₃}₃), 1.58 (9H, s, ArC{CH₃}₃), 1.55 (3H, t, O-CH₂CH₃), ppm. ¹³C{¹H} NMR (C₆D₆, 125 MHz, 298 K): δ = 163.9 (ArC-O), 138.1 (ArC-CH₂N), 135.5 (ArCH), 126.6 (ArCH), 119.6 (ArC-C{CH₃}₃), 119.3 (ArC-C{CH₃}₃), 65.5 (ArC-CH₂-N), 55.2 (N-C₂H₄-C₂H₄-N), 53.7 (N-C₂H₄-C₂H₄-N), 45.9 (N-CH₃), 45.6 (O-CH₂CH₃) 35.8 (ArC-

C{CH₃}₃), 35.5 (ArC–C{CH₃}₃), 34.1 (O–CH₂CH₃) 32.2 (ArC–C{CH₃}₃), 30.2 (ArC–C{CH₃}₃), ppm.

{[μ-ONO^{tBu,tBu}]ZnEt}₂ (3.7): To a 50 mL flask containing diethylzinc (6.20 mL, 5.02 mmol, 15 wt. % in hexane) a solution of [**L4**]H (1.53 g, 5.02 mmol) in toluene (2.00 mL) cooled at –35 °C was added dropwise. The colourless mixture was warmed, while being stirred, to room temperature and then held at this temperature for 18 h. Volatiles were removed under vacuum to give a white residue, which was washed with hexane (2 × 4 mL) and dried in *vacuo*; yield 1.62 g, 81.0%. Crystals suitable for X-ray crystallography could be grown by slow evaporation, or by cooling at –35 °C, of a saturated toluene solution. Anal. calcd. for C₄₂H₇₀N₄O₄Zn₂ (825.80): C 63.23, H 8.84, N 3.51; found C 63.16, H 8.55, N 3.60%. ¹H NMR (C₅D₅N, 500 MHz, 313 K): δ = 7.63 (1H, s, ArH), 7.10 (1H, s, ArH), 3.81 (4H, br, O–C₂H₄–C₂H₄–N), 3.59 (2H, s, Ar–CH₂–N), 2.50 (4H, br, O–C₂H₄–C₂H₄–N), 1.79 (9H, s, ArC–C{CH₃}₃), 1.59 (3H, t, *J* = 8.0 Hz, Zn–CH₂CH₃), 1.48 (9H, s, ArC–C{CH₃}₃), 0.58 (2H, q, *J* = 8.0 Hz, Zn–CH₂CH₃), ppm. ¹³C{¹H} NMR (C₅D₅N, 125 MHz, 298 K): δ = 165.35 (ArC–O), 141.2 (ArC–C{CH₃}₃), 137.93 (ArC–C{CH₃}₃), 126.73 (ArCH), 124.44 (ArCH), 121.57 (ArC–CH₂–N), 65.55 (ArC–CH₂–N), 65.45 (O–C₂H₄–C₂H₄–N), 65.13 (O–C₂H₄–C₂H₄–N), 36.01 (ArC–C{CH₃}₃), 34.41 (ArC–C{CH₃}₃), 32.60 (ArC–C{CH₃}₃), 30.48 (ArC–C{CH₃}₃), 13.98 (Zn–CH₂CH₃), 0.76 (Zn–CH₂CH₃) ppm.

3.8.4 Polymerization Procedures

Typical Solution Polymerization Procedure: The reaction mixtures were prepared in a glovebox and subsequent operations were performed with standard Schlenk

techniques. A monomer:initiator ratio of 100:1 was employed. A sealable Schlenk tube containing a stir bar and the monomer (0.05 mmol) in toluene (8.00 mL) was heated to the desired temperature, then the initiator solution (26.3 mm), which was taken from a stock solution containing a prescribed amount of ROH, was added to the tube. The mixture was stirred for the allotted time. An aliquot of the reaction solution was taken for NMR spectroscopic analysis, and the reaction was quenched immediately by the addition of methanol. The resulting solid was dissolved in dichloromethane and the polymer precipitated with excess cold methanol. The polymer was collected by filtration, washed with methanol to remove any unreacted monomer, and dried under reduced pressure.

Bulk Polymerization Procedure: For solvent free polymerizations of LA, the monomer:initiator ratio employed was 100:1 and the reactions were conducted at 130 °C. A Schlenk tube equipped with magnetic stir bar was charged in a glovebox with the required amount of LA (0.50 g, 3.5 mmol) and initiator (0.042–0.015 g). The reaction vessel was sealed, brought out of the glovebox and immersed in an oil bath that was preheated to 130 °C. At the desired time an aliquot (*ca* 0.3 mL) was withdrawn from the flask for ¹H NMR analysis to determine the monomer conversion. The reaction was quenched with methanol and the resulting solid was dissolved in dichloromethane, precipitated with excess cold methanol, then filtered and dried under reduced pressure.

Typical Microwave-Assisted Ring-Opening Polymerization: To a microwave vial charged with LA (576 mg, 5.27 mmol) or ϵ -CL (601 mg, 5.27 mmol) in toluene (10 mL), a toluene solution (2.00 mL) of the initiator containing a prescribed amount of benzyl or tert-butyl alcohol was added. The vial was sealed with a septum and the mixture was

irradiated to a constant required temperature for the desired amount of time. After irradiation, the vial was cooled to room temperature, an aliquot of the product was taken for NMR spectroscopic analysis, and the reaction was quenched immediately by the addition of methanol. The resulting solid was dissolved in dichloromethane and the polymer precipitated with excess cold methanol. A colourless product was collected by filtration, washed with methanol to remove any unreacted monomer, and dried under reduced pressure.

CO₂-Cyclohexene Oxide Reactions: The complex (0.2 mol-%) was dissolved in cyclohexene oxide (2.27 g, 23.2 mmol) that was held in a glovebox. The mixture and co-catalyst (0.2 mol-%) was placed in a predried autoclave equipped with a pressure gauge. The autoclave was sealed, removed from the glovebox and attached to an overhead magnetic stirrer. The system was pressurized to approx. 40 bar with CO₂ and heated (as with all processes under high pressure, appropriate safety precautions must be taken). The mixture was stirred for the desired amount of time and then the pressure was slowly released whilst the pressure vessel was cooled in an ice-bath. A small amount of the residue in the vessel was removed for ¹H NMR analysis.

3.9 References

1. D. J. Doyle, V. C. Gibson, A. J. P. White, *Dalton Trans.*, **2007**, 358.
2. C.-A. Huang, C.-L. Ho, C.-T. Chen, *Dalton Trans.*, **2008**, 3502.
3. C.-A. Huang, C.-T. Chen, *Dalton Trans.*, **2007**, 5561.
4. J. Ejfler, K. Krauzy-Dziedzic, S. Szafert, L. B. Jerzykiewicz, P. Sobota, *Eur. J. Inorg. Chem.*, **2010**, 3602.
5. X. Zhang, T. J. Emge, K. C. Hultsch, *Organometallics*, **2010**, *29*, 5871.
6. A. D. Schofield, M. L. Barros, M. G. Cushion, A. D. Schwarz, P. Mountford, *Dalton Trans.*, **2009**, 85.
7. W.-C. Hung, C.-C. Lin, *Inorg. Chem.*, **2009**, *48*, 728.
8. L. E. Breyfogle, C. K. Williams, J. V. G. Young, M. A. Hillmyer, W. B. Tolman, *Dalton Trans.*, **2006**, 928.
9. E. L. Marshall, V. C. Gibson, H. S. Rzepa, *J. Am. Chem. Soc.*, **2005**, *127*, 6048.
10. Y. Sarazin, V. Poirier, T. Roisnel, J.-F. Carpentier, *Eur. J. Inorg. Chem.*, **2010**, 3423.
11. D. J. Darensbourg, W. Choi, O. Karroonnirun, N. Bhuvanesh, *Macromolecules*, **2008**, *41*, 3493.
12. H. E. Dyer, S. Huijser, A. D. Schwarz, C. Wang, R. Duchateau, P. Mountford, *Dalton Trans.*, **2008**, 32.
13. A. Amgoune, C. M. Thomas, J.-F. Carpentier, *Macromol. Rapid Commun.*, **2007**, *28*, 693.
14. G. Labourdette, D. J. Lee, B. O. Patrick, M. B. Ezhova, P. Mehrkhodavandi, *Organometallics*, **2009**, *28*, 1309.
15. L. Wang, H. Ma, *Dalton Trans.*, **2010**, *39*, 7897.
16. C. K. Williams, L. E. Breyfogle, S. K. Choi, W. Nam, V. G. Young, M. A. Hillmyer, W. B. Tolman, *J. Am. Chem. Soc.*, **2003**, *125*, 11350.
17. M. H. Chisholm, J. C. Gallucci, H. Zhen, J. C. Huffman, *Inorg. Chem.*, **2001**, *40*, 5051.

18. M. H. Chisholm, Z. Zhou, *J. Mater. Chem.*, **2004**, *14*, 3081.
19. C. K. Williams, N. R. Brooks, M. A. Hillmyer, W. B. Tolman, *Chem. Commun.*, **2002**, 2132.
20. J. Lewinski, P. Horeglad, M. Dranka, I. Justyniak, *Inorg. Chem.*, **2004**, *43*, 5789.
21. S. Groysman, E. Sergeeva, I. Goldberg, M. Kol, *Inorg. Chem.*, **2005**, *44*, 8188.
22. S. Gendler, S. Segal, I. Goldberg, Z. Goldschmidt, M. Kol, *Inorg. Chem.*, **2006**, *45*, 4783.
23. L. M. Broomfield, Y. Sarazin, J. A. Wright, D. L. Hughes, W. Clegg, R. W. Harrington, M. Bochmann, *J. Organomet. Chem.*, **2007**, *692*, 4603.
24. J.-T. Issenhuth, J. Pluinage, R. Welter, S. Bellemin-Laponnaz, S. Dagorne, *Eur. J. Inorg. Chem.*, **2009**, 4701.
25. V. Poirier, T. Roisnel, J.-F. Carpentier, Y. Sarazin, *Dalton Trans.*, **2011**, *40*, 523.
26. J. D. Farwell, P. B. Hitchcock, M. F. Lappert, G. A. Luinstra, A. V. Protchenko, X.-H. Wei, *J. Organomet. Chem.*, **2008**, *693*, 1861.
27. L. Nikolic, I. Ristic, B. Adnadjevic, V. Nikolic, J. Jovanovic, M. Stankovic, *Sensors*, **2010**, *10*, 5063.
28. S. Jing, W. Peng, Z. Tong, Z. Baoxiu, *J. Appl. Polym. Sci.* **2006**, *100*, 2244.
29. M. R. Kember, A. Buchard, C. K. Williams, *Chem. Commun.*, **2011**, *47*, 141.
30. M. North, R. Pasquale, C. Young, *Green Chem.*, **2010**, *12*, 1514.
31. K. L. Collins, L. J. Corbett, S. M. Butt, G. Madhurambal, F. M. Kerton, *Green Chem. Lett. Rev.*, **2007**, *1*, 31.
32. F. M. Kerton, S. Holloway, A. Power, R. G. Soper, K. Sheridan, J. M. Lynam, A. C. Whitwood, C. E. Willans, *Can. J. Chem.*, **2008**, *86*, 435.
33. J. Ejfler, S. Szafert, K. Mierzwicki, L. B. Jerzykiewicz, P. Sobota, *Dalton Trans.*, **2008**, 6556.
34. A. Gao, Y. Mu, J. Zhang, W. Yao, *Eur. J. Inorg. Chem.*, **2009**, 3613.

35. K. Nakano, K. Nozaki, T. Hiyama, *J. Am. Chem. Soc.* **2003**, *125*, 5501.
36. I. J. Bruno, J. C. Cole, M. Kessler, J. Luo, W. D. S. Momerwell, L. H. Purkis, B. R. Smith, R. Taylor, R. I. Cooper, S. E. Harris, A. G. Orpen, *J. Chem. Inf. Comput. Sci.*, **2004**, *44*, 2133.
37. J. Hunger, S. Blaurock, J. Sieler, *Z. Anorg. Allg. Chem.*, **2005**, *631*, 472.
38. M. R. P. Van Vliet, J. T. B. H. Jastrzebski, G. Van Koten, K. Vrieze, A. L. Spek, *J. Organomet. Chem.*, **1983**, *251*, c17.
39. H.-Y. Chen, H.-Y. Tang, C.-C. Lin, *Macromolecules*, **2006**, *39*, 3745.
40. A. Banerjee, S. Ganguly, T. Chattopadhyay, K. S. Banu, A. Patra, S. Bhattacharya, E. Zangrando, D. Das, *Inorg. Chem.*, **2009**, *48*, 8695.
41. K. Nakano, T. Hiyama, K. Nozaki, *Chem. Commun.*, *2005*, 1871.
42. Y. Sarazin, J. A. Wright, D. A. J. Harding, E. Martin, T. J. Woodman, D. L. Hughes, M. Bochmann, *J. Organomet. Chem.*, **2008**, *693*, 1494.
43. A. R. F. Cox, V. C. Gibson, E. L. Marshall, A. J. P. White, D. Yeldon, *Dalton Trans.*, **2006**, 5014.
44. C. M. Silvernail, L. J. Yao, L. M. R. Hill, M. A. Hillmyer, W. B. Tolman, *Inorg. Chem.*, **2007**, *46*, 6565.
45. F. Qian, K. Liu, H. Ma, *Dalton Trans.*, **2010**, *39*, 8071.
46. L. F. Sanchez-Barba, C. Alonso-Moreno, A. Garces, M. Fajardo, J. Fernandez-Baeza, A. Otero, A. Lara-Sanchez, A. M. Rodriguez, I. Lopez-Solera, *Dalton Trans.*, **2009**, 8054.
47. A. Garcés, L. F. Sánchez-Barba, C. Alonso-Moreno, M. Fajardo, J. Fernández-Baeza, A. Otero, A. Lara-Sánchez, I. López-Solera, A. M. Rodríguez, *Inorg. Chem.*, **2010**, *49*, 2859.
48. C. Zhang, Z.-X. Wang, *Appl. Organomet. Chem.*, **2009**, *23*, 9.
49. H. Zhu, E. Y. X. Chen, *Organometallics*, **2007**, *26*, 5395.
50. F. Drouin, P. O. Oguadinma, T. J. J. Whitehorne, R. E. Prud'homme, F. Schaper, *Organometallics*, **2010**, *29*, 2139.

51. B. M. Chamberlain, M. Cheng, D. R. Moore, T. M. Ovitt, E. B. Lobkovsky, G. W. Coates, *J. Am. Chem. Soc.*, **2001**, *123*, 3229.
52. T. Sakakura, K. Kohno, *Chem. Commun.*, **2009**, 1312.
53. D. J. Darensbourg, S. J. Lewis, J. L. Rodgers, J. C. Yarbrough, *Inorg. Chem.*, **2003**, *42*, 581.
54. Y.-M. Shen, W.-L. Duan, M. Shi, *J. Org. Chem.*, **2003**, *68*, 1559.
55. F. Li, L. Xiao, C. Xia, B. Hu, *Tetrahedron Lett.*, **2004**, *45*, 8307.
56. V. Caló, A. Nacci, A. Monopoli, A. Fanizzi, *Org. Lett.*, **2002**, *4*, 2561.
57. J. Sun, J. Ren, S. Zhang, W. Cheng, *Tetrahedron Lett.*, **2009**, *50*, 423.
58. D. J. Darensbourg, J. L. Rodgers, R. M. Mackiewicz, A. L. Phelps, *Catal. Today*, **2004**, *98*, 485.
59. N. Ikpo, S. M. Butt, K. L. Collins, F. M. Kerton, *Organometallics*, **2009**, *28*, 837.
60. M. D. Eelman, J. M. Blacquiere, M. M. Moriarty, D. E. Fogg, *Angew. Chem.*, **2008**, *120*, 309; *Angew. Chem. Int. Ed.*, **2008**, *47*, 303.
61. CrystalClear, Rigaku Corporation, **1999**, CrystalClear Software User's Guide, Molecular Structure Corporation, **2000**.
62. J. W. Pflugrath, *Acta Crystallogr.*, Sect. D **1999**, *55*, 1718.
63. SHELX97: G. M. Sheldrick, *Acta Crystallogr.*, Sect. A **2008**, *64*, 112.
64. SIR92: A. Altomare, G. Cascarano, C. Giacovazzo, A. Guagliardi, M. Burla, G. Polidori, M. J. Camalli, *J. Appl. Crystallogr.*, **1994**, *27*, 435.
65. DIRDIF99: P. T. Beurskens, G. Admiraal, G. Beurskens, W. P. Bosman, R. de Gelder, R. Israel, J. M. M. Smits, The DIRDIF-99 program system, Technical Report of the Crystallography Laboratory, University of Nijmegen, The Netherlands, **1999**.
66. D.T.Cromer, J.T.Waber, International Tables for X-ray Crystallography, vol. IV, The Kynoch Press, Birmingham, England, Table 2.2A, **1974**.
67. J.A. Ibers, W. C. Hamilton, *Acta Crystallogr.*, **1964**, *17*, 781.

68. D. C. Creagh, W. J. McAuley, *International Tables for Crystallography*, vol. C (Eds.: A. J. C. Wilson), Kluwer Academic Publishers, Boston, **1992**, Table 4.2.6.8, p. 219.
69. D. C. Creagh, J. H. Hubbell, *International Tables for Crystallography*, vol. C (Eds.: A. J. C. Wilson), Kluwer Academic Publishers, Boston, **1992**, Table 4.2.4.3, p. 200.
70. CrystalStructure, v. 3.7.0, Crystal Structure Analysis Package, Rigaku and Rigaku/MSK, 9009 New Trails Dr., The Woodlands, TX 77381, U.S.A., **2000–2005**.
71. D. J. Watkin, C. K. Prout, J. R. Carruthers, P. W. Betteridge, *CRYSTALS Issue 10, Chemical Crystallography Laboratory*, Oxford, UK, **1996**.
72. A. L. Spek, *J. Appl. Crystallogr.*, **2003**, 36,7.

CHAPTER 4

Aluminum Methyl and Chloro Complexes Bearing Monoanionic Aminephenolate Ligands: Synthesis, Characterization and Use in Polymerizations.

Chapter 4

Aluminum Methyl and Chloro Complexes Bearing Monoanionic Aminephenolate Ligands: Synthesis, Characterization and Use in Polymerizations.

A version of this chapter has been published

Nduka Ikpo, Stephanie M. Barbon, Marcus W. Drover, Louise N. Dawe, and Francesca
M. Kerton

Organometallics, **2012**, *31*, 8145

Some modifications were made to the original paper for inclusion as a chapter in this
thesis.

4.1 Introduction

Biodegradable and biocompatible polyesters, such as poly(ϵ -caprolactone) (PCL), have attracted much attention due to their wide range of applications including environmentally friendly bulk packaging materials, implantable materials, sutures and as delivery media for controlled release of drugs.¹⁻⁴ Ring-opening polymerization (ROP) of cyclic esters is mainly mediated by metal complexes which afford faster polymerization

rates and greater control over molecular weight of the resulting polymers.⁵⁻⁸ Biocompatible metal complexes are important in the production of these polymers, where small amounts of catalyst may inevitably be incorporated.

Efforts by many research groups have focused on the development of biocompatible single-site metal initiators for ROP of ϵ -caprolactone and lactide with ligand design playing a profound role in this area. Well-designed ligands provide the ability to tune electronic and steric properties of the metal centres, which changes their reactivity. Thus, amine-phenolate and related ligands possessing a mixed set of N- and O- donor atoms have emerged as attractive candidates due to their ability to stabilize a wide range of metal centres and the ease of systematic steric manipulation by variation of the backbone and phenol substituents.⁹ A number of main-group and transition metal complexes including lithium,¹⁰⁻¹⁶ magnesium,¹⁷⁻²³ calcium,²⁴ rare-earths,^{25,26} zinc,²⁷⁻³⁶ aluminum,³⁷⁻⁴⁴ zirconium^{46,47} and titanium⁴⁸ complexes stabilized by these and related ligands have been prepared and some are effective initiators for ROP of cyclic esters such as lactide and ϵ -caprolactone (e.g., **I-IV**, Figure 4.1). Among the catalysts/initiators studied, aluminum complexes with N,O- chelate and related ligands have attracted much attention due to their high activity and good polymer molecular weight control.^{4,49} For example, Dagorne and co-workers reported four-coordinate aluminum alkyl cationic complexes stabilized by a piperazinyl aminephenolate ligand (e.g. Figure 4.1V) which was employed in a preliminary study of propylene oxide ROP.³⁹ Five-coordinate aluminum complexes supported by mono anionic bidentate ketimate ligands have been investigated as catalysts for ROP of ϵ -caprolactone.⁵⁰ However, neutral five-coordinate piperazinyl

aminephenolate aluminum species have not been reported in the literature for the polymerization of cyclic esters.

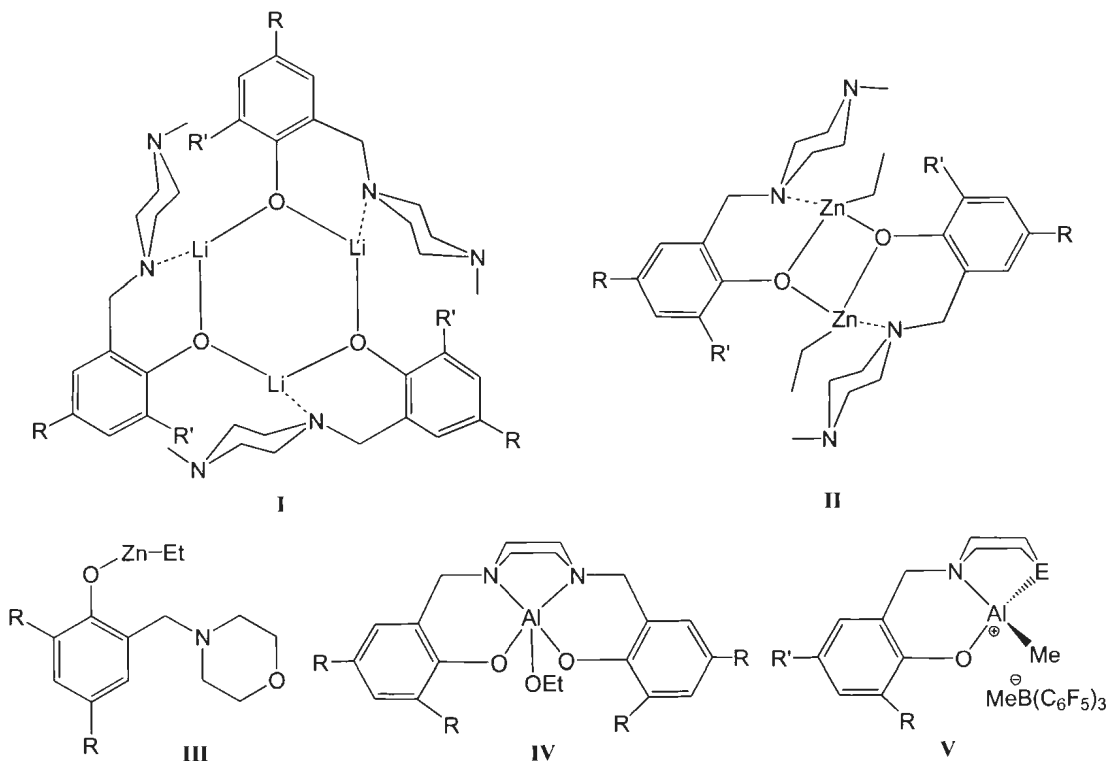


Figure 4.1. Some previously reported piperazinyll and morpholinyl aminephenolate based complexes ($R, R' = \text{alkyl or aryl}; E = \text{NMe or O}$).^{10,27,28,39,40}

Recently, we reported the synthesis of piperazinyll-aminephenolate zinc complexes (**II**), which showed good activity in ROP of *rac*-lactide and ϵ -caprolactone.²⁷ These zinc complexes, however, showed poor activity in the cycloaddition of carbon dioxide and epoxides. Lithium complexes (**I**) of the same ligand showed good activity in catalytic ROP of ϵ -caprolactone.¹⁰ Similarly, Carpentier, Sarazin and co-workers employed zinc complexes of a morpholinyl derived ligand (**III**) to achieve immortal ROP of cyclic esters.²⁸ The same group has investigated the reactivity of tin complexes of these ligands

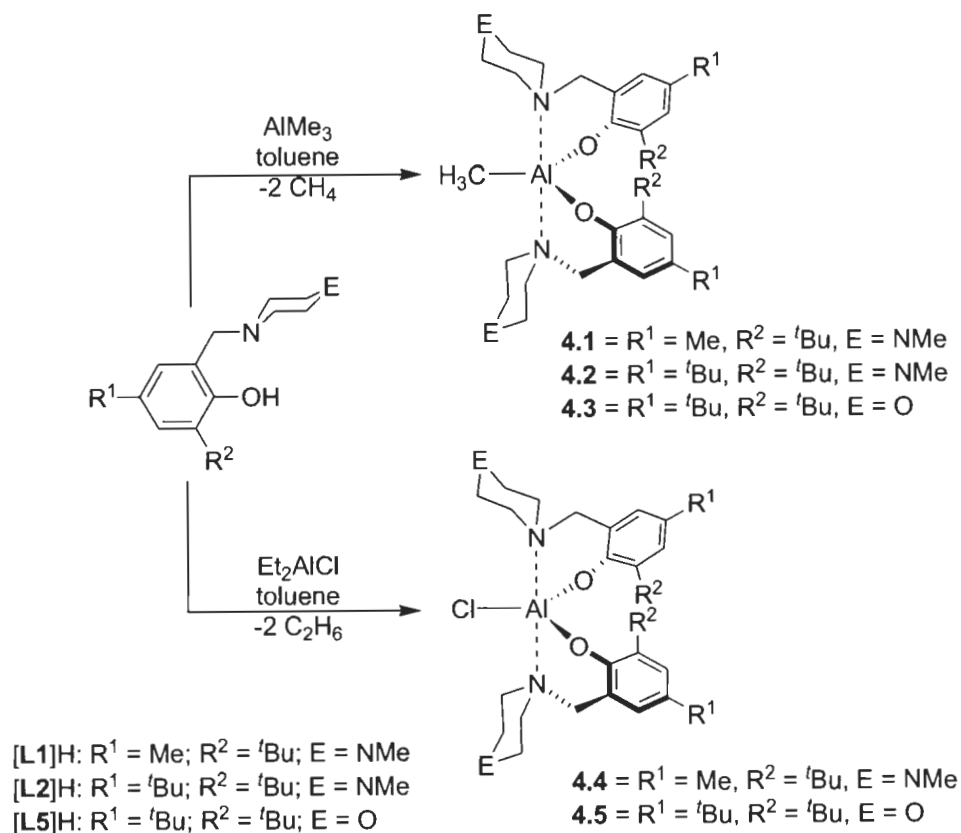
in immortal ROP of lactide and trimethylene carbonate.⁴⁵ In a recent study by Ma and Wang, aluminum complexes of quinoline-based ligands showed greater catalytic activity than corresponding Zn complexes in ROP of lactones,⁵¹ and therefore this research project intends to determine whether this was a general trend for bidentate ligand complexes of Al and Zn in ROP reactions. Also to be studied in this project is the effect of outersphere ligand substituents on polymerization reactions. In this chapter the synthesis and characterization of five-coordinate aluminum alkyl/halide complexes bearing piperazinyl-aminephenolate ligands and their catalysis in the ROP of ϵ -caprolactone and preliminary results in carbon dioxide-cyclohexene oxide copolymerizations are discussed.

4.2 Results and Discussion

4.2.1 Synthesis and solid-state structures

The protio ligands were synthesized from the appropriate phenol, formaldehyde and 1-methylpiperazine or morpholine *via* a modified Mannich condensation reaction in water as described previously.^{27,52,53} The piperazinyl and morpholinyl aminephenol ligands differ in the nature of the E substituent, which is a methylamine (NMe) or ether (O) group respectively. Some complexes of these ligands ([L1], [L2] and [L5]) have been reported by Kerton's group and others, and will allow the comparison of reactivity where data are available from these prior studies.^{10,27,28,31,32,39} Compounds **4.1-4.5** were synthesized through alkane elimination reactions using two equivalents of the appropriate protio ligands with the corresponding alkyl/halide aluminum precursors (AlMe₃ or Et₂AlCl) in

dry toluene as summarized in Scheme 4.1. Reactions of protio ligands $[\text{ONE}^{\text{R}^1\text{R}^2}]_2\text{H}$ with AlMe_3 in toluene under ambient conditions led to the isolation of monometallic aluminum complexes $[\text{ONE}^{\text{R}^1\text{R}^2}]_2\text{AlMe}$ (**4.1-4.3**) in 73-92% yield. Attempts to form $[\text{ONE}^{\text{R}^1\text{R}^2}]\text{AlMe}_2$ were not successful and **4.1-4.3** were isolated from reactions of two equiv. AlMe_3 with 1 equiv. aminephenol. Treatment of Et_2AlCl with two equiv. of the corresponding ligand in toluene at ambient temperature afforded (**4.4-4.5**) in 86-90% yield. In this manner, two types of aluminum aminephenolate complexes were prepared where the labile group was either a methyl (**4.1-4.3**) or chloride ligand (**4.4** and **4.5**).



Scheme 4.1. Synthesis of methyl and chloro Al aminephenolate complexes

All complexes were isolated as colorless crystalline solids and were characterized by elemental analysis and ^1H , $^{13}\text{C}\{^1\text{H}\}$ and ^{27}Al NMR spectroscopy. The ^1H NMR spectra of **4.1-4.3** confirmed that the complexes were monometallic with two coordinated aminophenolate ligands. The methyl group in **4.1-4.3** gave rise to sharp signals upfield between 0.12 and - 0.31 ppm. This signal was absent from the ^1H NMR spectra of **4.4-4.5** differentiating the alkyl complexes from those bearing chloride ligands. ^{27}Al NMR spectroscopy has been helpful in correlating chemical shift with coordination number and the ^{27}Al NMR shifts for compounds **4.1-4.5** (71-76 ppm, $w_{1/2} = 4010\text{-}3490$ Hz) fall within the range for five coordinate complexes.⁵⁴

Compounds **4.1-4.5** were characterized by single-crystal X-ray diffraction analysis and the crystallographic data are summarized in Table 4.9.⁵⁵ The τ (tau) value is a method of establishing the degree to which observed geometries for five coordinate compounds approaches either trigonal bipyramidal or square pyramidal geometry.⁵⁶ A value of zero describes a compound with perfectly square pyramidal parameters and a value of one is perfectly trigonal bipyramidal, while a value of 0.5 is intermediate between the two geometries. The τ values calculated for **4.1-4.4** are listed in Table 4.1. Compounds **4.1-4.3** are slightly distorted from trigonal bipyramidal, while compound **4.4** with a chloride group possesses a near to perfect trigonal bipyramidal geometry. This slight difference between the two compounds could be attributed to steric interactions of the bulkier alkyl and less bulky chloride groups within the Al coordination sphere.

Table 4.1. τ values for compounds **4.1-4.4**

Compound	τ value
$[\text{ONN}^{\text{Me,tBu}}]_2\text{AlMe}$ (4.1)	0.79
$[\text{ONN}^{\text{tBu,tBu}}]_2\text{AlMe}$ (4.2)	0.82
$[\text{ONO}^{\text{tBu,tBu}}]_2\text{AlMe}$ (4.3)	0.80
$[\text{ONN}^{\text{Mc,tBu}}]_2\text{AlCl}$ (4.4)	0.97

The ORTEP plot of **4.1** is shown in Figure 4.2 along with selected bond lengths and angles. Ligands are bound to the central metal in a bidentate manner with each of the methylamine groups orientated away from the Al centre. This phenomenon was also observed in related zinc²⁷ and aluminum complexes.³⁹ The central nitrogen atoms of each ligand are bound to the Al centre in the axial positions, with the equatorial sites occupied by the methyl group and two phenolate oxygen donors. These form two puckered six-membered rings (C_3NAIO). The bond angles around Al are O(1)-Al(1)-N(1), $90.33(5)^\circ$ and O(2)-Al(1)-N(1), $87.73(5)^\circ$ and the relative narrowness of the O(2)-Al(1)-N(1) bond angle can be attributed to the bite of the six-membered C_3NAIO chelate ring which possesses a torsion angle of $-15.9(2)^\circ$. This ring adopts a “legless” chair⁵⁷ conformation with N(1) and N(3) atoms forming the backrest and lie *ca.* 0.83 and 0.97 Å above the plane of Al-O(1)-C(1)-C(11)-C(12) and Al-O(2)-C(18)-C(28)-C(29) respectively. As expected, the two neutral nitrogen atoms occupying the axial sites exhibit longer contacts to the central Al (Al-N(1), 2.1612(14) Å and Al-N(3), 2.1567(14) Å) than the anionic equatorial contacts (Al(1)-C(35), 1.9901(18) Å, Al-O(1), 1.7898(12) Å and Al-O(2),

1.7911(12) Å). Al-O, Al-N and Al-C bond distances are comparable to related Al complexes reported elsewhere.⁵⁸⁻⁶⁰

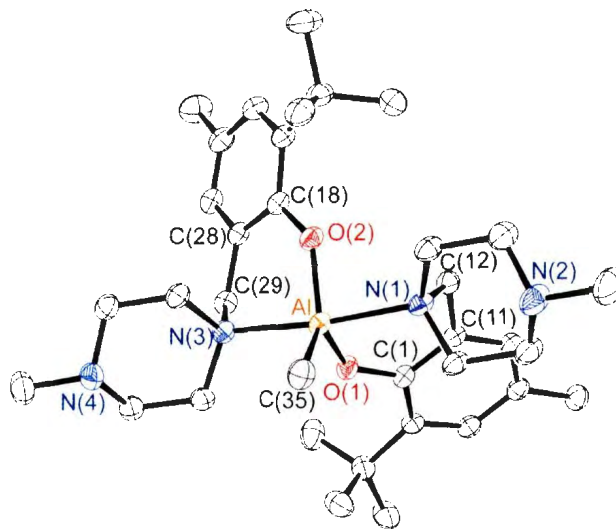


Figure 4.2. Molecular structure of **4.1** (50% displacement ellipsoids; H atoms excluded for clarity). Selected bond lengths (Å) and bond angles (°): Al(1)-O(1), 1.7898(12); Al(1)-O(2), 1.7911(12); Al(1)-C(35), 1.9901(18); Al(1)-N(3), 2.1567(14); Al(1)-N(1), 2.1612(14); O(1)-C(1), 1.3597(17); O(2)-C(18), 1.3564(18); N(3)-C(29), 1.491(2); C(1)-C(11), 1.405(2); C(11)-C(12), 1.500(2); N(1)-C(12), 1.498(2); C(18)-C(28), 1.412(2); C(28)-C(29), 1.506(2) O(1)-Al(1)-O(2), 115.61(6); O(1)-Al(1)-C(35), 117.72(7); O(2)-Al(1)-C(35), 126.67(7); O(1)-Al(1)-N(3), 91.21(5); O(2)-Al(1)-N(3), 86.27(5); C(35)-Al(1)-N(3), 92.88(7); O(1)-Al(1)-N(1), 90.33(5); O(2)-Al(1)-N(1), 87.73(5); C(35)-Al(1)-N(1), 91.64(7); N(3)-Al(1)-N(1), 173.89(5); C(1)-O(1)-Al(1), 134.43(10); C(18)-O(2)-Al(1), 134.51(10).

The structural features of complex **4.2** (Figure 4.3) are very similar to those in **4.1**, with the only significant difference being a more acute angle around the central Al atom [O(1)-Al-N(3)] in **4.2** than in **4.1**., possibly due to the greater steric demands of the *para* 'Bu group in **4.2** and resulting packing effects.

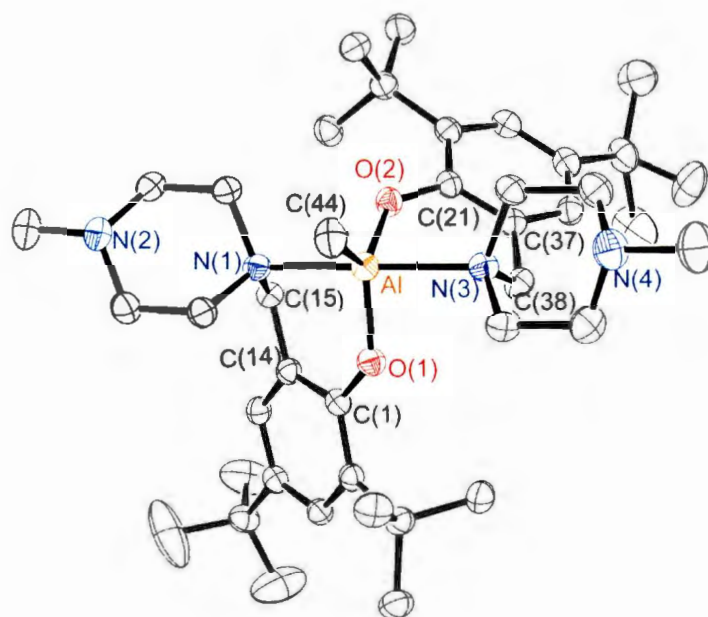


Figure 4.3. Molecular structure of **4.2** (50% displacement ellipsoids; H atoms excluded for clarity). Selected bond lengths (Å) and bond angles (°): Al(1)-O(1), 1.7875(13); Al(1)-O(2), 1.7903(14); Al(1)-C(44), 1.981(2); Al(1)-N(1), 2.1509(16); Al(1)-N(3), 2.1686(16); O(1)-C(1), 1.356(2); O(2)-C(21), 1.356(2); O(1)-Al(1)-O(2), 116.96(6); O(1)-Al(1)-C(44), 119.01(8); O(2)-Al(1)-C(44), 124.03(8); O(1)-Al(1)-N(1), 88.13(6); O(2)-Al(1)-N(1), 88.33(6); C(44)-Al(1)-N(1), 93.26(8); O(1)-Al(1)-N(3), 89.78(6); O(2)-Al(1)-N(3), 87.14(6); C(44)-Al(1)-N(3), 93.13(8); N(1)-Al(1)-N(3), 173.51(6); C(1)-O(1)-Al(1), 135.07(11); C(21)-O(2)-Al(1), 135.47(11).

Single crystal X-ray analysis shows that **4.3** crystallizes as a monometallic species in the orthorhombic space group *Pbca* and the ORTEP drawing is shown in Figure 4.4 along with selected bond lengths and angles. The structural features of **4.3** are similar to those of **4.1** and **4.2** with Al-N, Al-O and Al-C bond distances being within the range observed for **4.1**, **4.3** and other related complexes.⁵⁸⁻⁶⁰

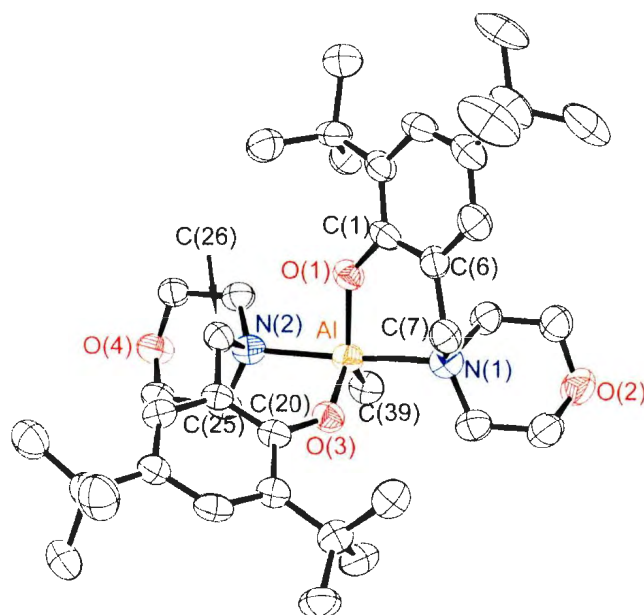


Figure 4.4. Molecular structure of **4.3** (50% displacement ellipsoids; H atoms excluded for clarity). Selected bond lengths (Å) and bond angles(°): Al(1)-O(3), 1.792(4); Al(1)-O(1), 1.793(4); Al(1)-C(39), 1.981(7); Al(1)-N(2), 2.148(5); Al(1)-N(1), 2.151(5); O(1)-C(1), 1.350(7); N(2)-C(26), 1.489(8); N(2)-C(27), 1.499(8); O(3)-Al(1)-O(1), 117.1(2); O(3)-Al(1)-C(39), 118.2(3); O(1)-Al(1)-C(39), 124.6(3); O(3)-Al(1)-N(2), 88.6(2); O(1)-Al(1)-N(2), 88.9(2); C(39)-Al(1)-N(2), 93.6(3); O(3)-Al(1)-N(1), 88.6(2); O(1)-Al(1)-N(1), 86.7(2); C(39)-Al(1)-N(1), 93.4(3); N(2)-Al(1)-N(1), 173.0(2); C(30)-N(2)-Al(1), 110.9(4); C(26)-N(2)-Al(1), 103.1(4).

The ORTEP drawing of **4.4** is depicted in Figure 4.5, along with selected bonds lengths and angles. Complex **4.4** crystallizes in the monoclinic space group $C2/c$. The Al-O [1.7721(10) Å] and Al-N [2.1033(12) Å] bond distances are shorter than the corresponding bond lengths in **4.1-4.3** but longer than those of a related aluminum piperazinyll aminephenolate complex (η^2 -*N,O*-[2-{CH₂N(C₄H₈NMe)}]-6-PhC₆H₃O]AlMe₂), having Al(1)-O(1) [1.761(1) Å] and Al(1)-N(1) [2.045(1) Å].³⁹

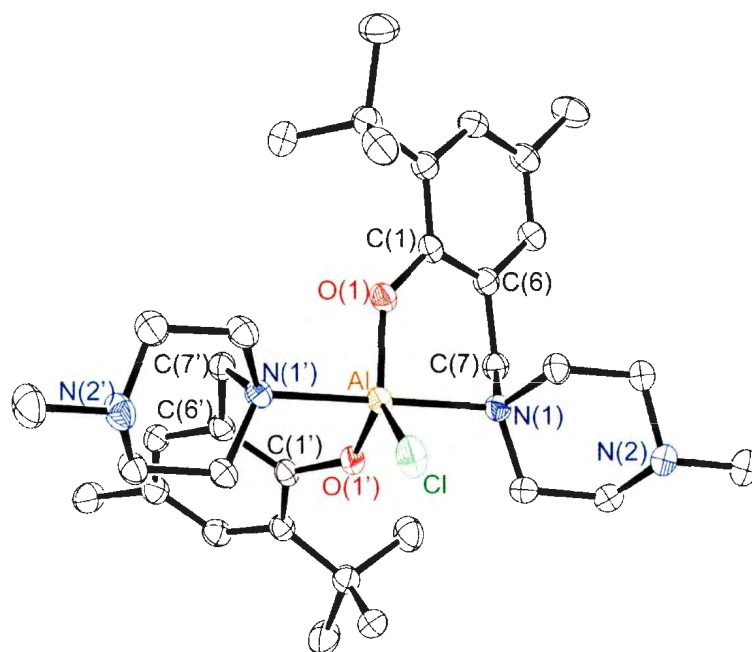


Figure 4.5. Molecular structure of **4.4** (50% displacement ellipsoids; H atoms excluded for clarity). Selected bond lengths (Å) and bond angles (°): Cl(1)-Al(1), 2.2102(9); Al(1)-O(1), 1.7721(10); Al(1')-O(1'), 1.7721(10); Al(1)-N(1), 2.1033(12); O(1)-C(1), 1.3628(15); N(1)-C(7), 1.5031(16); O(1)-Al(1)-O(1'), 118.27(7); O(1)-Al(1)-N(1), 90.73(4); O(1)-Al(1)-N(1'), 89.61(4); N(1)-Al(1)-N(1'), 179.35(6); O(1)-Al(1)-Cl(1), 120.87(3); N(1)-Al(1)-Cl(1), 89.67(3).

The single crystal X-ray data for complex **4.5** were poor and could not be fully refined as a result of merohedral twinning. However, these data were sufficient to confirm gross connectivity and structural analogy to **4.4**. The ball and stick drawing of **4.5** is depicted in Figure 4.6

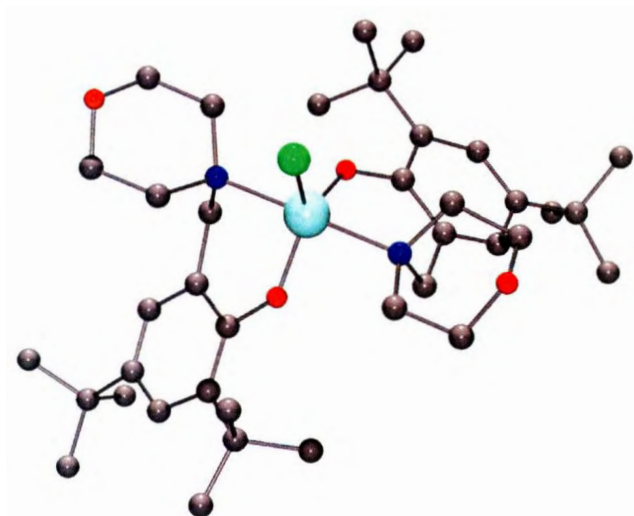


Figure 4.6. Ball and stick representation of compound **4.5**

4.3 Ring-Opening Polymerization of ϵ -Caprolactone

Ring-opening polymerization (ROP) catalysis of ϵ -CL was carried out using **4.1-4.3** in the presence and absence of BnOH (results are summarized in Table 4.2). Complexes **4.1-4.3** showed low catalytic activity in the absence of BnOH with conversions of 16, 27 and 22% respectively at 80 °C within 30 minutes (Table 4.2; entries 1, 9 and 21) and so no further studies were conducted in this fashion. This contrasts with the good activity observed for related piperazinyl aminophenolate lithium complexes in the absence of alcohols, which yielded cyclic polymers in the ROP of ϵ -CL.¹⁰ **4.1-4.3** exhibit efficient catalytic activity in the polymerization of ϵ -CL in the presence of BnOH under the reaction conditions studied. The *in situ* formation of an alkoxide species under the reaction conditions employed was confirmed by ¹H NMR spectroscopy for the 1:1 reaction of complex **4.2** with BnOH (Figure 4.7). The signal of the methyl ligand disappeared and new resonances for the alkoxide group grew in. The formation of an

alkoxide complex could also be seen in the ^1H spectra from a 1:1 reaction of **4.4** with BnOH . *In situ* formation of active Al alkoxide complexes for ROP have been reported recently by Redshaw and co-workers for dialkylaluminum amidates⁶¹ and other authors for various metal complexes.⁶²⁻⁶⁴ The formation of an alkoxide species suggests that the mechanism of polymerization is *via* coordination-insertion and that an activated-monomer mechanism is less plausible.⁶⁵ However, in order to fully rule out the latter mechanism, further studies involving installation of less potent nucleophiles on the Al center would be required, e.g. $-\text{OSiR}_3$.⁴⁵

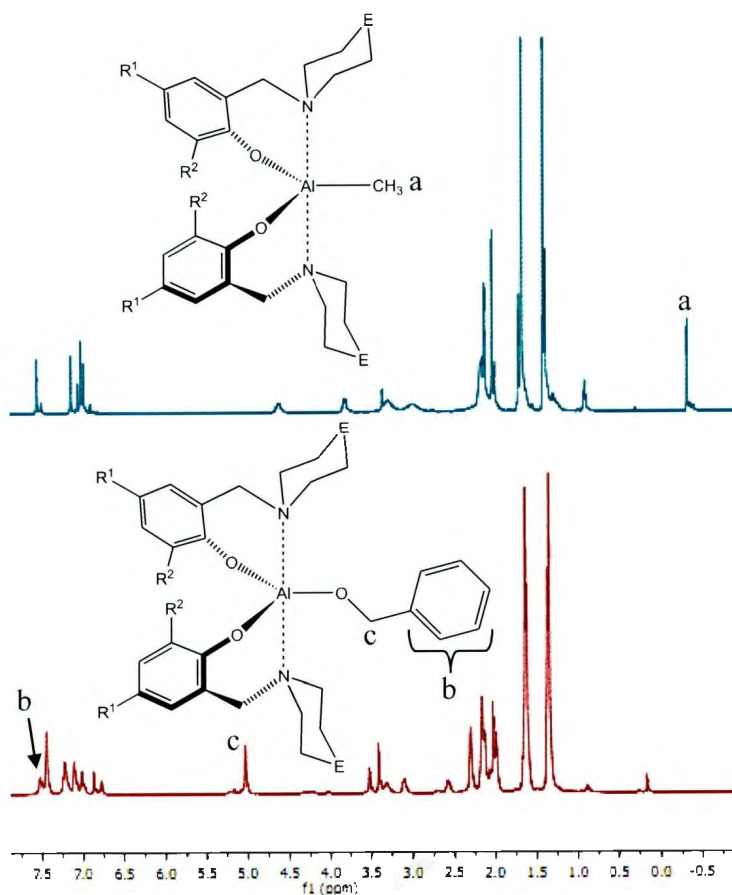


Figure 4.7. ^1H NMR spectra of **4.2** (top) and of a 1:1 reaction of **4.2** with BnOH in $\text{tol-}d_8$ (bottom)

Polymerizations were relatively slow at room temperature and 88, 96 and 78% monomer conversion were achieved in 150 minutes using **4.1**, **4.2** and **4.3** respectively (Table 4.2, entries 3,10 and 17), whereas similar conversions were obtained within 10 minutes at 80 °C. It should be noted that under identical conditions, **4.2**/BnOH did not facilitate ROP of *rac*-lactide (0% conv., 80 °C, 10 min). This is in stark contrast to the analogous Zn complex, EtZnL2, which in the presence of BnOH achieved quantitative conversion of *rac*-lactide at 70 °C after 90 min and measurable conversions after 10 minutes.²⁷ For ROP of ϵ -CL, it can be noticed that generally **4.2**/BnOH exhibits higher catalytic activity than **4.1**/BnOH and **4.3**/BnOH as it achieves higher conversions in a shorter time (Table 4.2, entries 7, 12, 19). However, **4.2**/BnOH produced polymers with lower molecular weights than those of **4.1**/BnOH, and the molecular weight distributions (M_w/M_n) of the polymers obtained using **4.1**/BnOH were narrower than those obtained using **4.2**/BnOH (Table 4.2, entries 2-8 and 10-16). This indicates that polymerization using **4.1**/BnOH is more controlled than that using **4.2**/BnOH. This is somewhat surprising given previous ROP reactions studied using Li and Zn complexes of these ligands,^{10,27} where narrower M_w/M_n polymers were obtained from complexes bearing more sterically demanding ligands.

Table 4.2. Polymerization of ϵ -CL initiated by 4.1-4.5 in the presence and absence of BnOH^[a]

Entry	Initiator	[CL] ₀ /[Al] ₀ /[BnOH] ₀	t/min	T /°C	Conv (%) ^[b]	$M_{n,cal}^{[c]} \times 10^3$	$M_n^{[d]} \times 10^3$	$M_w/M_n^{[d]}$
1	4.1	50/1/0	30	80	16.0	—	—	—
2	4.1	75/1/1	12	80	73.8	6.31	5.17	1.30
3	4.1	100/1/1	150	25	82.2	9.35	8.18	1.34
4	4.1	100/1/1	10	80	78.2	8.93	6.46	1.31
5	4.1	150/1/1	10	80	69.9	11.9	9.08	1.34
6	4.1	200/1/1	18	80	92.1	21.0	15.4	1.65
7	4.1	100/1/1	35	60	84.6	9.58	7.77	1.33
8	4.1	100/1/1	55	40	87.0	9.93	7.82	1.42
9	4.2	50/1/0	30	80	27.0	—	—	—
10	4.2	100/1/1	150	25	96.7	10.9	8.62	1.65
11	4.2	100/1/1	10	80	97.6	11.0	5.14	2.51
12	4.2	100/1/1	12	60	88.9	10.1	5.47	1.51
13	4.2	100/1/1	24	40	79.3	9.01	5.80	1.59
14	4.2	75/1/1	12	80	98.8	8.38	3.88	2.19
15	4.2	150/1/1	12	80	99.1	16.9	9.71	1.89
16	4.2	200/1/1	10	80	96.1	21.9	15.3	1.76

Table 4.2. Continued

Entry	Initiator	[CL] ₀ /[Al] ₀ /[BnOH] ₀	t/min	T /°C	Conv (%) ^[b]	$M_{\text{ncal}}^{[c]} \times 10^3$	$M_n^{[d]} \times 10^3$	$M_w/M_n^{[d]}$
17	4.3	100/1/1	150	25	78.8	8.90	4.12	1.69
18	4.3	100/1/1	54	40	54.8	6.16	4.96	1.47
19	4.3	100/1/1	24	60	83.4	9.47	5.91	1.42
20	4.3	100/1/1	12	80	95.9	10.8	5.70	1.96
21	4.3	50/1/0	30	80	22.3	—	—	—
22	4.3	75/1/1	12	80	91.0	7.79	4.49	1.88
23	4.3	150/1/1	10	80	89.0	15.2	8.54	2.23
24	4.3	200/1/1	10	80	88.0	20.0	14.3	1.91
25	4.4	100/1/1	12	80	83.0	9.47	6.27	1.30
26	4.4	100/1/0	24	80	92.9	10.6	12.3	1.73
27	4.4	100/1/0	30	60	50.5	5.76	52.7	2.4
28	4.5	100/1/0	10	80	41.1	4.69	10.3	1.99
29	4.5	100/1/0	14	60	28.1	3.20	13.5	2.21

[a] Reactions performed in toluene using the mole ratios, temperatures and reaction times indicated. [b] Determined by ¹H NMR spectroscopy. [c] The M_{ncal} value of the polymer was calculated with $M_{\text{ncal}} = ([\epsilon\text{-CL}]_0/[\text{Al}]_0) \times 114.14$ (molecular weight of CL) \times conv. %. [d] The M_n value was calculated according to $M_n = 0.56M_n^{\text{GPC}}$, where M_n^{GPC} was determined by GPC (chloroform), and is relative to polystyrene standards.

It was also observed that in all cases using **4.1-4.3**, the measured number average molecular weight of the polymers obtained *via* GPC were lower than the calculated values based on initial [Al]:[ϵ -CL] ratios. This suggests that transesterification has occurred during the polymerization process. It is worth noting that the effect of [BnOH] was investigated and it was found that an Al/BnOH molar ratio of 1:1 afforded the best activity whereas the presence of two or three equivalents of BnOH rendered the catalyst inactive. This observation is similar to that reported by Duda, wherein he used the aluminum isopropoxide trimer [Al(OⁱPr)₃] in the presence of diol {HO(CH₂)₅OH} and suggested that the alcohol reversibly coordinated to the active species leading to catalytic inhibition.^{66,67}

In the polymerization reactions initiated by **4.4** and **4.5**, gelation was observed for all reactions and conversion of ϵ -CL did not reach completion in 5.00 mL of toluene, the volume used in ROP using **4.1-4.3**/BnOH above, due to increased viscosity resulting from a rapid increase in molecular weight. However, in 10.00 mL of toluene the polymerization could proceed, albeit not to completion (Table 4.2; entries 26-29). For these reactions, the molecular weight data obtained by GPC for each of the polymerization runs were much higher than calculated theoretical values, while the molecular weight distributions (M_w/M_n) were rather broad. Zhang *et al.*^{68,69} reported similar observations with aluminum complexes of functionalized phenolate ligands, which he interpreted to arise from higher reaction temperatures resulting in transesterification.⁷⁰⁻⁷² However, it could also be that when **4.4** and **4.5** are used, initiation proceeds *via* acid-initiation (HCl generated *in situ*) and this reaction is less controlled

than in reactions catalyzed by an Al-alkyl/alcohol system. Another possibility is that the reaction may be proceeding *via* a reaction pathway involving insertion of the monomer into the Al-Cl bond. This has previously been suggested as a plausible mechanism for ROP of trimethylene carbonate using a chloro-aluminum salen complex.⁷³ Due to the broad polydispersity of the polymer produced using **4.4** and **4.5** without BnOH, the polymerization mechanism for these systems was not studied in detail. The resulting polymers were characterized using ¹H NMR spectroscopy and MALDI-TOF MS, as discussed below. No alkoxide end groups are seen in the polymers that were isolated from reactions using **4.4** or **4.5** when no BnOH was used as co-initiator. It should be noted that 1.0 M anhydrous HCl in ether has previously been reported to facilitate ROP of ϵ -CL to yield high molecular weight, polydisperse polymer,⁷⁴ and that under reaction conditions similar to those reported in this study using Al complexes, 16.7 mM HCl in toluene afforded 43% conversion of ϵ -CL at 80 °C in 15 min. Therefore, at this stage, both an acid catalyzed reaction and insertion of the monomer into the Al-Cl bond remain plausible mechanisms.

Polymers obtained using complexes **4.1-4.5** in the presence or absence of BnOH were characterized using GPC, MALDI-TOF MS, ¹H NMR spectroscopy, TGA and DSC.

4.4 End-group Analysis

4.4.1 NMR Spectroscopy

A ¹H NMR spectrum of a typical polymer sample obtained using **4.1-4.3** is shown in Figure 4.8. Methylene proton signals were assigned at 1.38, 1.65, 2.31 and 4.06 ppm. The

presence of aromatic benzyl protons at 7.35 ppm, and the benzyl and hydroxyl methylene signals at 5.12 and 3.65 ppm with an integral ratio close to 1 indicate the formation of linear polymers capped with a benzyloxy group at one end and a hydroxyl group at the other. $^{13}\text{C}\{^1\text{H}\}$ NMR analysis confirmed end-group assignments with resonances of CH_2OH and OCH_2Ph appearing at 62.58, 66.15 and 128.55 ppm respectively. These signal assignments are in good agreement with results reported previously.⁷⁵ This observation is consistent with acyl-oxygen bond cleavage of the $\epsilon\text{-CL}$, which would occur in ROP reactions occurring via either a coordination-insertion or activated monomer mechanism.

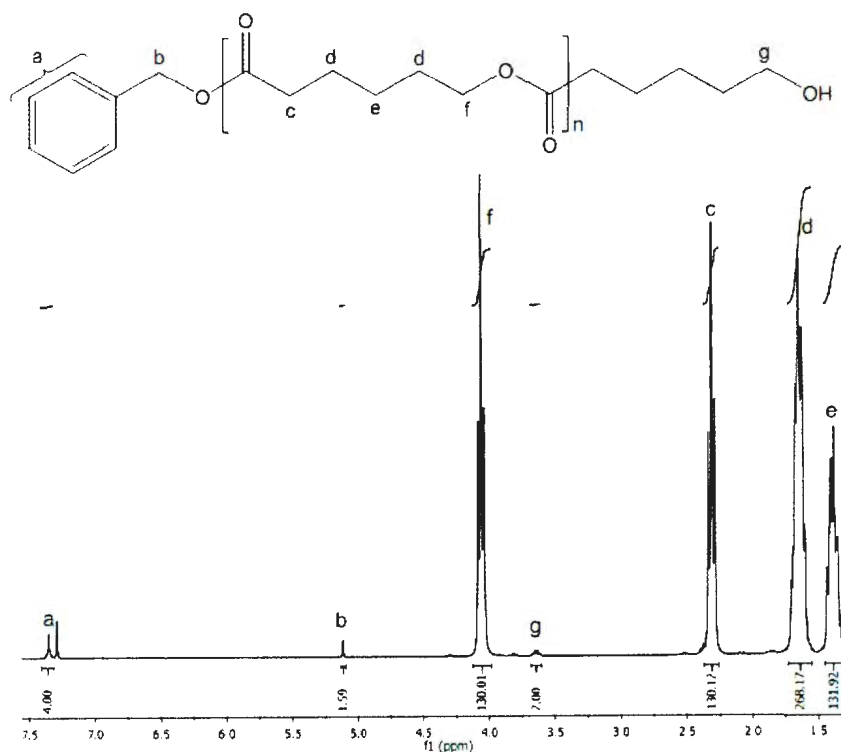


Figure 4.8. Typical ^1H NMR spectrum of PCL prepared using 4.1/BnOH

The ^1H NMR spectrum (Figure 4.9) of the polymers obtained with chloride complex **4.4** indicates that the polymer is a linear chain, evidenced by the resonance at 3.67 ppm, which corresponds to the terminal methylene proton (CH_2OH). However, no other assignable end-group resonances were located and as a result, information about the initiating group and the mechanism could not be obtained from ^1H NMR spectroscopy. However, it is clear that insertion in the Al-phenolate bond is not occurring.

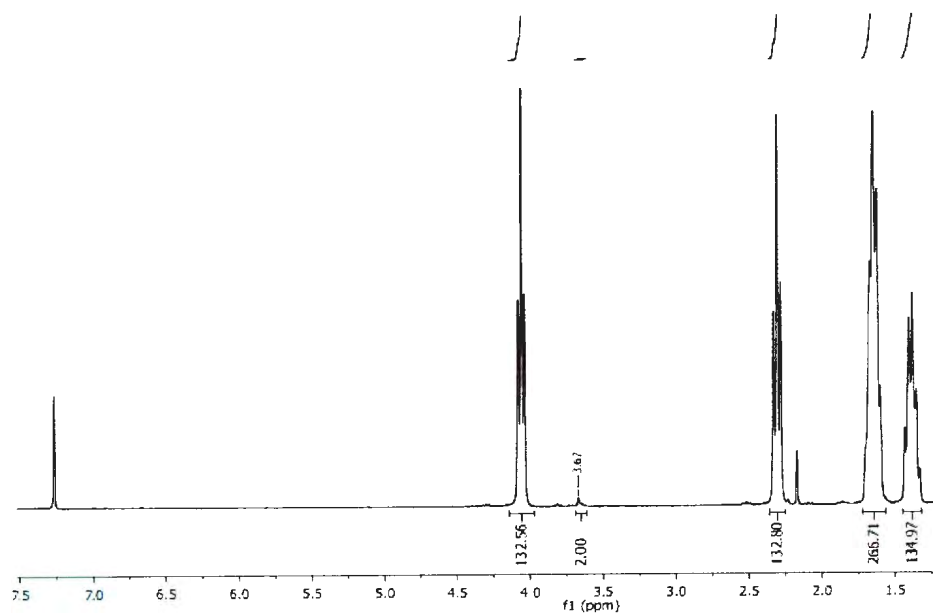


Figure 4.9. ^1H NMR spectrum of PCL prepared using **4.4**

4.4.2 MALDI-TOF Mass Spectrometry

Further end-group analyses were conducted through MALDI-TOF mass spectrometry. The mass spectrum of the polymer prepared with **4.2**/BnOH is depicted in Figure 4.10 (Table 4.2, entry 11) and revealed the presence of a single major peak series. Each successive group of peaks exhibits a mass difference of 114 Da corresponding to the

repeating unit of ϵ -caprolactone and is in agreement with polycaprolactone chains capped with benzyloxy groups clustered with sodium ions to give adducts: $(\text{BnO}\{\text{CL}\}_n\text{H})+\text{Na}$ [e.g. $n = 11$, m/z 1385.3376 (exp.), 1385.80 (calc.)]. In addition to the major peak population, minor sets of peaks at the low m/z region of the spectrum (inset) could be attributed to macromolecules associated with potassium ions rather than sodium [e.g. $n = 11$, m/z 1401.7856 (exp.), 1401.77(calc.)], similar to results observed by Mata *et al.*⁶² A second minor set of peaks, differing by 15 mass units from the first minor series, might possibly be assigned to a protonated methyl terminated polymer associated with potassium ions, $(\text{BnO}\{\text{Cl}\}_n\text{CH}_3)+\text{H}+\text{K}$ [e.g. $n = 11$, m/z 1416.9983 (exp.), 1416.79 (calc.)]. This minor series of peaks did not fit models for other possibilities including incorporation of the ligand and association with other metal ions including aluminum. How the methyl group proposed has been incorporated into or become associated with the polymer is not clear at this stage, especially as resonances for such a group were not observed in the ^1H NMR spectra of the polymer. It should be noted that MALDI-TOF MS is a more sensitive technique for detecting impurities and differences in end groups for polyesters than ^1H NMR and that reactions can also occur in the spectrometer leading to polymer modification.⁷⁶ The identification of PCL capped with benzyloxy and hydroxy end-groups as the main signals in the MALDI-TOF mass spectrum is in agreement with ^1H NMR analysis. There is little evidence for transesterification side reactions (either intra- or intermolecular) occurring from the mass spectra of this polymer, despite the lower than expected molecular weights indicated by GPC data.

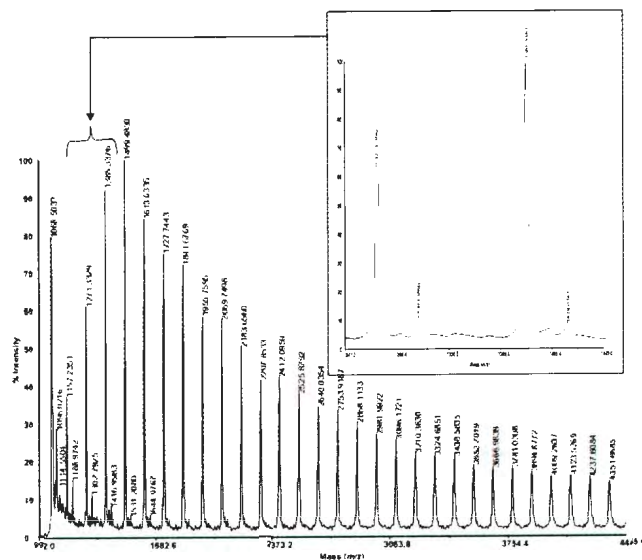


Figure 4.10. MALDI-TOF mass spectrum of PCL prepared using **4.2**/BnOH

The MALDI-TOF spectrum of PCL obtained using **4.4** as initiator (Figure 4.11) displays two sets of peak distributions. The major series of peaks (the most important) correspond to macromolecules capped on each end with chloride and hydroxyl groups ($\text{Cl}\{\text{CL}\}_n\text{OH}$) [e.g. $n = 12$, m/z 1420.69 (exp.), 1420.79 (calc.)]. The remaining minor series of peaks were assigned to macromolecules capped with hydroxyl groups, ($\text{H}\{\text{CL}\}_n\text{OH}$) [e.g. $n = 12$, m/z 1387.1106 (exp.), 1386.83 (calc.)]. Similar hydroxyl terminated macromolecules have been previously reported by others.^{62,77} The main chlorinated polymer product could be formed from either monomer insertion into the Al-Cl bond or initiation by HCl.

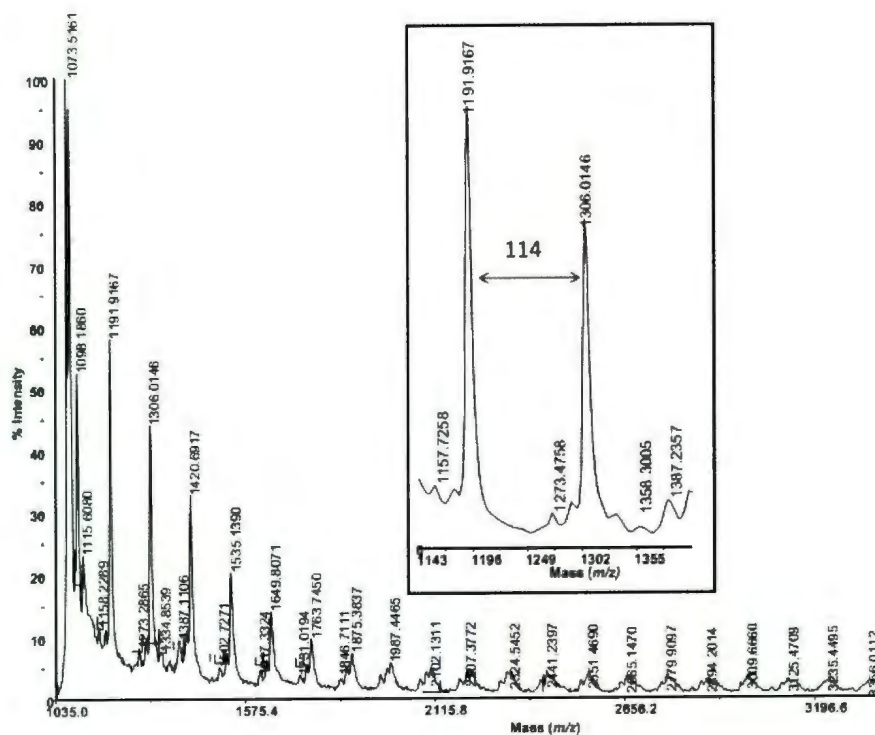


Figure 4.11. MALDI-TOF mass spectrum of PCL initiated by **4.4**

4.5 Kinetic Studies of ϵ -CL Polymerization

In order to better understand the nature of ϵ -CL polymerization initiated by **4.1-4.3** in the presence of BnOH, a series of polymerization reactions were conducted in toluene at 80 °C for various monomer to initiator [CL]/[Al] mole ratios to determine the effect of [CL] and [Al] on the catalytic activity. The conversion of ϵ -CL was monitored by ^1H NMR spectroscopy and semilogarithmic plots of $\ln[\text{CL}]_0/[\text{CL}]_t$ versus time for the polymerizations initiated by **4.2**/BnOH are shown in Figure 4.12. These plots revealed that reaction rates slightly decreased with increasing [CL]/[Al] molar ratio in all cases investigated.

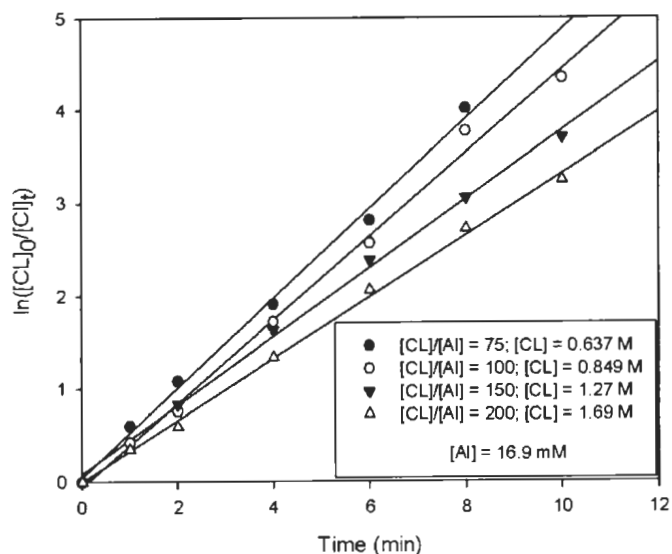


Figure 4.12. Semilogarithmic plots of $\ln[\epsilon\text{-CL}]_0/[\epsilon\text{-CL}]_t$ vs. time for the ROP of $\epsilon\text{-CL}$ at different monomer molar ratios initiated with **4.2**; $[\text{CL}]_0/[\text{4.2/BnOH}]_0 = 75$ (●), 100 (○), 150 (▼), 200 (▲), ($[\text{4.2}]_0 = 16.9$ mM, 80 °C)

In addition, it was observed that number average molecular weight M_n obtained by GPC increased linearly as monomer to initiator ratios $[\text{CL}]/[\text{Al}]$ were increased as shown in Figure 4.13, which demonstrates the “living character” of the polymerization process, implying that the growing polymer chain does not terminate as the polymerization progresses. Similar results have been previously reported by Wu and co-workers⁷⁸ and others for bridged bulky aluminum phenoxide initiator systems.^{79,80} However, it should also be noted that in the current study at higher $\epsilon\text{-CL}:\text{Al}$ ratios there is some deviation from this linearity towards formation of higher M_n polymer that potentially indicates occurrence of termination by chain-transfer under such conditions.

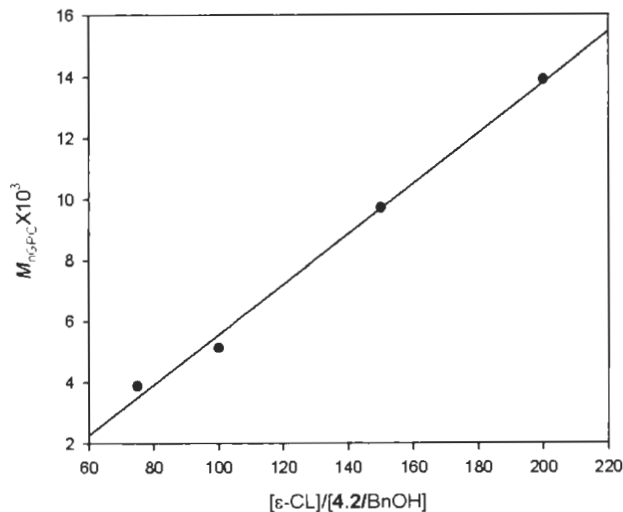


Figure 4.13. Relationship between M_n^{GPC} of the polymer and initial mole ratio $CL]_0/[4.2/BnOH]_0$ for the polymerization of ϵ -CL initiated by 4.2/BnOH in toluene at 80 °C. $R = 0.9974$, $R^2 = 0.9948$.

By conducting the reactions over a range of temperatures, it was observed that the overall polymerization rate (k_{obs}) increases with an increase in temperature as shown in Figure 4.14. The semilogarithmic plots shown herein are linear, indicating a first-order dependence of reaction rate with respect to monomer concentration and pass through the origin indicating the absence of an induction period,^{81,82} which is in contrast to some previous polymerization reactions using aluminum alkoxides where induction periods were observed.^{75,83} This might also imply that the reaction is proceeding *via* an activated monomer mechanism but it might also be an artifact of the temperatures at which reactions were studied. Greater linearity can be seen in the plots for reactions conducted at higher temperatures, where a shorter induction period would also be expected. It should be noted that the aluminum complex and BnOH were mixed and heated alone to the

reaction temperature (to allow the active alkoxide species to form) before mixing with the preheated monomer solution.

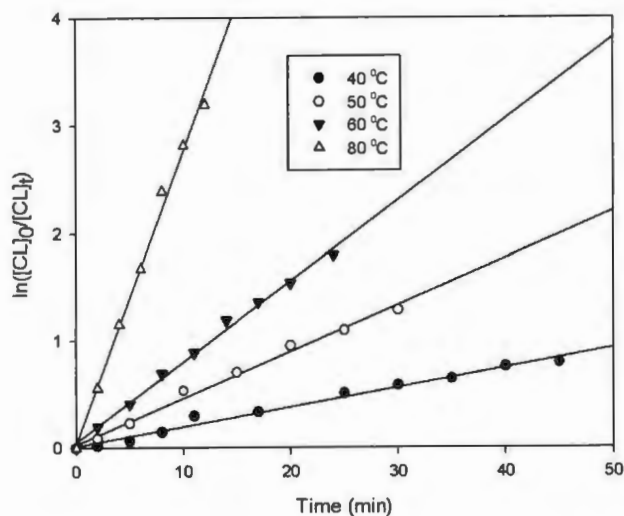


Figure 4.14. Semilogarithmic plots of $\ln[\epsilon\text{-CL}]_0/[\epsilon\text{-CL}]$ vs time for the ROP of $\epsilon\text{-CL}$ at different temperatures initiated with **4.3**/BnOH; $[\text{CL}]_0/[\text{4.3/BnOH}]_0 = 100$, $([\text{4.3/BnOH}]_0 = 16.9 \text{ mM}, [\epsilon\text{-CL}]_0 = 0.845 \text{ M})$; (●) = 40 °C, (○) = 50 °C, (▼) = 60 °C, (△) = 80 °C.

The observed rate constant (k_{obs}) for each catalyst was obtained from the slope of $\ln[\text{CL}]_0/[\text{CL}]_t$ versus time and are summarized in Table 4.3. It can be seen that the fastest polymerization was observed for **4.2**/BnOH. In comparison, the value determined for **4.2**/BnOH is about twice that of **4.1**/BnOH and only slightly higher than that of **4.3**/BnOH under similar reaction conditions, i.e. the rate of polymerization by **4.1-4.3** in the presence of BnOH follows the order **4.2**/BnOH \geq **4.3**/BnOH > **4.1**/BnOH. For further clarification, comparative semilogarithmic plots obtained for the polymerization of $\epsilon\text{-CL}$ by **4.1-4.3** in the presence of BnOH are shown in Figure 4.15. Therefore, it is hypothesized that the more bulky *tert*-butyl substituent in the *para* position of the ligand has some influence on the catalytic behavior of the complexes despite being somewhat

remote from the center of reactivity. This observation is similar to that reported by Chmura *et al.*⁸⁴ for Ti(IV) complexes of bis(phenolate)s, but in contrast to the aluminum systems reported by other authors where less sterically demanding ligands afforded more effective initiators.^{85,86} However, by comparing the activity of the methyl complexes with the chloride complexes, the latter showed lower activity and produced polymers with different properties. This trend has also been observed by others.⁵⁰

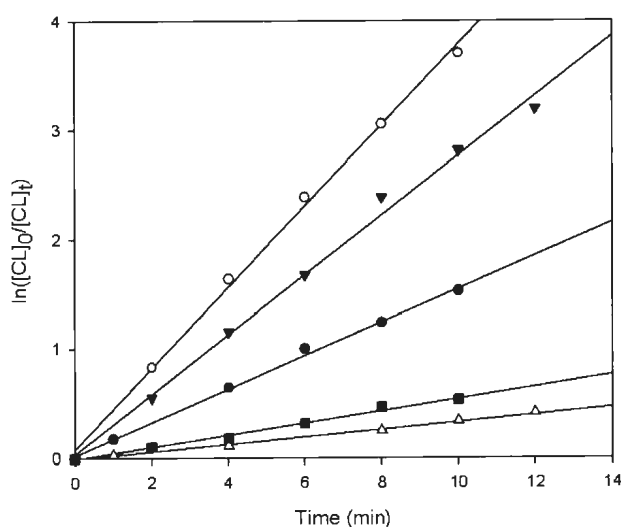


Figure 4.15. Semilogarithmic plots of $\ln[CL]_0/[CL]_t$ vs time for observed rate constant comparison between (4.1-4.3)/BnOH, 4.4 and 4.5 at 80 °C. (○) = 4.2/BnOH, $k_{obs} = 0.3708$; (▼) = 4.3/BnOH, $k_{obs} = 0.2731$; (●) = 4.1/BnOH, $k_{obs} = 0.1527$; (■) = 4.5, $k_{obs} = 0.0565$; (△) = 4.4, $k_{obs} = 0.0342 \text{ L mol}^{-1}\text{min}^{-1}$.

To draw comparisons to previously reported kinetic data for other initiators, some rate constant values are collected in Table 4.3. The values determined for 4.1 and 4.2 in the presence of BnOH are similar to the values observed in Chapter 5 for the piperazinyll aminephenolate lithium complexes with the same supporting ligand under similar reaction conditions but lower temperature.¹⁰ The k_{obs} values for 4.1-4.3/BnOH are significantly lower⁸⁷ but higher than those for some aluminum

and zinc alkoxides albeit at lower temperatures.^{88,89} Reaction rates obtained using analogous Zn complexes containing **L1** and **L5** are significantly lower than those obtained using the corresponding Al compounds.²⁷ This contrasts with the increased reactivity observed using the Zn complexes of the same ligands compared with Al derivatives in ROP of *rac*-LA. This implies that the choice of monomer has a significant influence on the relative reactivity of catalysts and this should be taken into account when designing new systems for ROP of cyclic esters. The Al complexes contain two ligands per metal center and this leads to a more sterically congested reaction site compared with the Zn compounds that contain only one amine-phenolate ligand per Zn. In ROP, *rac*-LA can be considered a more sterically demanding monomer than ϵ -CL. The methyl groups within the monomer and growing polymer chain would interact unfavorably with ligands that potentially block the binding site for the incoming monomer. In contrast, ϵ -CL polymerization is perhaps affected more strongly by the Lewis acidity of the metal center (electronics rather than sterics) and therefore, the Al complexes are more reactive than their Zn analogs.

The relationship between $\ln(k_{\text{obs}})$ and the reciprocal of polymerization temperature ($1/T$) is shown in Figure 4.16. According to the Arrhenius equation, the activation energies calculated for **4.1**/BnOH, **4.2**/BnOH and **4.3**/BnOH are shown in Table 4.4.

Table 4.3. A comparison of rate constants for the ROP of ϵ -CL initiated by various aluminum and metal complexes in toluene.

Entry	Initiator	T/ °C	k_{obs} (L mol ⁻¹ min ⁻¹)	Ref
1	Et ₂ AlOCH ₂ CH ₃	25	8.40	87
2	Al[O(CH ₂) ₃ NEt ₂] ₃	25	3.00	88
3	Et ₂ AlO(CH ₂) ₃ NEt ₂	25	0.030	88
4	Et ₂ AlO(CH ₂) ₃ CH=CH ₂	25	0.160	88
5	Me ₂ Al[O-2- ^t Bu-6{C ₆ F ₅ }N=CH}C ₆ H ₄]/BnOH	50	0.028	89
6	{Li[ONN ^{Me,tBu}]} ₂ /BnOH	40	0.133	10
7	{[ONN ^{Me,tBu}] ₂ AlMe}(4.1/BnOH)	80	0.153 ^a 0.129 ^b	This work
8	{[ONN ^{tBu,tBu}] ₂ AlMe}(4.2/BnOH)	80	0.371 ^a	This work
9	{[ONO ^{tBu,tBu}] ₂ AlMe}(4.3/BnOH)	80	0.274 ^a 0.221 ^c	This work
10	{[ONN ^{Me,tBu}]ZnEt}/BnOH	70	0.047 ^d	27
11	{[ONN ^{tBu,tBu}]ZnEt}/BnOH	70	0.072 ^e	27

^a[CL]/[Al] = 100, [Al] = 16.9 mM. ^b[CL]/[Al] = 150, [Al] = 16.9 mM. ^c[CL]/[Al] = 200, [Al] = 16.9 mM. ^d[CL]/[Al] = 200, [Al] = 22.5 mM. ^e[CL]/[Al] = 200, [Al] = 18.8 mM

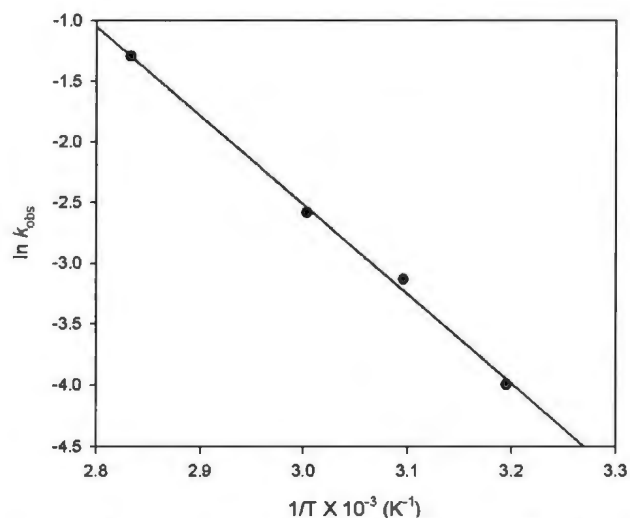


Figure 4.16. Arrhenius plot of $\ln(k_{\text{obs}})$ vs $1/T$ for the ROP of ϵ -CL initiated by 4.3/BnOH: [4.3/BnOH] = 16.9 mM; $[\text{CL}]_0/[\text{3/BnOH}]_0 = 100$. $R = 0.9984$, $R^2 = 0.9968$.

The activation energy for **4.3** is higher than those of **4.1** and **4.2** and this must be attributed to the difference in outersphere (E) substituents within the complexes. It is possible that the methylamine (NMe) group of **4.1** and **4.2**, which is a stronger base than the ether (O) group of **4.3**, activates the incoming monomer *via* non-covalent interactions. Another explanation could be that when E = O (**4.3**) the ether donor can coordinate temporarily with the Al centre and block the vacant coordination site from incoming monomer. In contrast, when E = NMe (**4.1** and **4.2**) the nitrogen would need to undergo inversion to coordinate to the metal centre and therefore, the coordination site for incoming monomer remains accessible. The activation energy values obtained for **4.1**/BnOH and **4.2**/BnOH were similar to those reported for $\text{Et}_2\text{AlO}(\text{CH}_2)_3\text{CH}=\text{CH}_2$, while the value for **4.3**/BnOH is similar to those given for $\text{Et}_2\text{AlO}(\text{CH}_2)_3\text{NEt}_2$.⁸⁸ It is worth noting that this last example also contains an amine group within the coordination sphere of the metal and although opposite to the trend we observe, this further indicates that outersphere heteroatoms can influence activation energies in ROP reactions. For the piperazinyll aminephenolate lithium complex/BnOH with the same supporting ligand as **4.1**/BnOH, a higher activation energy was measured compared with the aluminum system. This possibly indicates that the monomer is more activated by the highly Lewis acidic aluminum centre. Furthermore, more controlled ROP was demonstrated by the piperazinyll aminephenolate aluminum complexes and this might be due to less opportunity for competing side reactions in the aluminum-catalyzed process due to the presence of two ligands per metal center rather than one. In reactions using the lithium

complexes, ROP could be initiated by the phenolate nucleophile in addition to the alkoxide,¹⁰ whereas no evidence for this has been seen with the aluminum species discussed herein.

Table 4.4. A comparison of activation energy for the ROP of ϵ -CL initiated by various aluminum and metal complexes

Initiator	E_a (kJ mol ⁻¹)	Ref
{[ONN ^{Me./Bu}] ₂ AlMe}(4.1/BnOH)	39.7	This work
{[ONN ^{Bu./Bu}] ₂ AlMe}(4.2/BnOH)	31.8	This work
{[ONO ^{Bu./Bu}] ₂ AlMe}(4.3/BnOH)	61.0	This work
{Li[ONN ^{Me./Bu}]} / BnOH (5.1/BnOH)	53.4	10
Et ₂ AlO(CH ₂) ₃ CH=CH ₂	42.3	88
Et ₂ AlO(CH ₂) ₃ NEt ₂	57.3	88

The kinetic data were also subjected to Eyring analyses (Table 4.5). This shows that in terms of both enthalpy and entropy there are significant differences between 4.1/BnOH and 4.2/BnOH compared with 4.3/BnOH. However, the Gibbs energies of activation at 80 °C are all very similar (~ 90 kJ mol⁻¹) and comparable with a value recently reported for an Al half-salen complex for ROP of ϵ -CL (95 kJ mol⁻¹, 90 °C).⁹⁰ Computational studies are needed in order to determine the reasons behind the significant differences in the entropic and enthalpic components for the systems reported in the current study.

Table 4.5. A comparison of activation parameters for ϵ -CL polymerization initiated by Al complexes **4.1-4.3**

Initiator	$\Delta H^\ddagger/\text{kJ mol}^{-1}$	$\Delta S^\ddagger/\text{J mol}^{-1} \text{K}^{-1}$	$\Delta G^\ddagger/\text{kJ mol}^{-1}$ [a]
4.1/BnOH	36.9(\pm 0.7)	-150(\pm 1)	90
4.2/BnOH	29.0(\pm 0.1)	-180(\pm 1)	93
4.3/BnOH	58.2(\pm 0.2)	-92(\pm 1)	90

[a] T = 80 °C

4.6 Thermal Properties Studies

4.6.1 Thermalgravimetric Analysis (TGA)

The thermal properties of PCL samples were investigated using both thermalgravimetric analysis (TGA) and differential scanning calorimetry (DSC). Figure 4.17 shows TGA (and the derivative) for PCL prepared using **4.1/BnOH** and **4.4**. The TGA plots exhibited a one-step decomposition profile for PCL obtained by **4.1/BnOH** and **4.4**, which is similar to that reported by Gorrasi *et al.*⁹⁰ The initial thermal degradation for polymer obtained by **4.1/BnOH** and **4.4** was at 317.8 °C and 322.7 °C respectively, while the maximum degradation peak was at 329.4 °C for **4.1/BnOH** and was higher than that observed for PCL prepared using **4.4** (322.9 °C). The observed lower initial and higher maximum thermal degradation temperatures coupled with the weight loss differences for **4.1/BnOH** relative to **4.4** could be the result of different degradation mechanisms due to the difference in the end-groups of the two polymer samples.

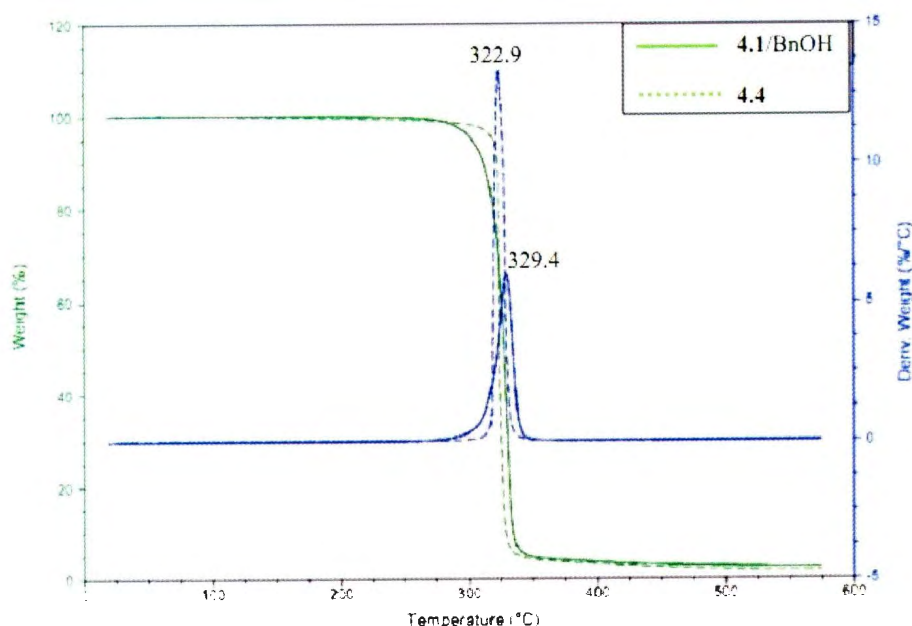


Figure 4.17. TGA thermogram of the PCL sampled obtained using **4.1/BnOH** and **4.4** in the temperature range 25-600 °C at 10 °C/min.

4.6.2 Differential Scanning Calorimetry (DSC)

The DSC traces for polymer samples obtained with **4.2/BnOH** and **4.4** are shown in Figure 4.18. The corresponding melting temperature (T_m), enthalpy heat of fusion (ΔH_m) and calculated weight percent crystallinity (X_c) are summarized in Table 4.6. The weight percent crystallinity was determined using the reported enthalpy of fusion (139.3 J g^{-1}) as a reference for completely crystalline PCL.⁹¹ As evidenced, the percent weight crystallinity (63%) for the sample obtained with **4.4** was lower than that for the sample obtained with **4.2/BnOH** (70%) (Table 4.6), which is consistent with the observations made with TGA. This is consistent with the more controlled polymerization achieved using **4.2/BnOH** compared with **4.4** in the absence of BnOH (where **4.4** possibly degrades through reaction with moisture to yield HCl, which performs the ROP reaction in an uncontrolled way). It is worth mentioning that the DSC measurements did not reveal a

glass-transition temperature (T_g) at low temperature due to inadequacies in the sensitivity of the instrument used.

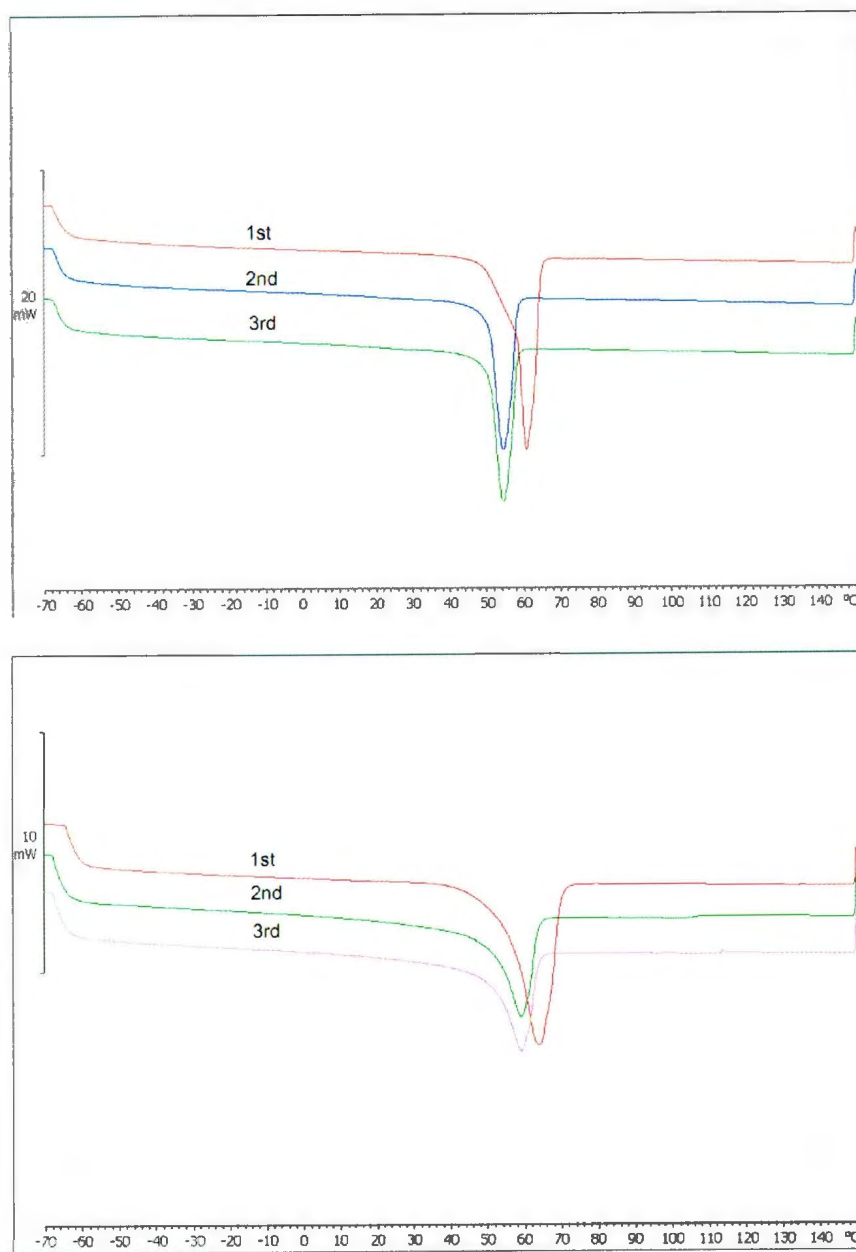


Figure 4.18. DSC thermogram of PCL samples obtained by 4.2/BnOH (Top, red = 1st heating curve, blue = 2nd heating curve, green = 3rd heating curve) and 4.4 (Bottom, red = 1st heating curve, green = 2nd heating curve, pink = 3rd heating curve) [Table 4.2, entries 12 and 27]

Table 4.6. Melting point, ΔH_m and crystallinity of PCL obtained with **4.2**/BnOH and **4.4**

Sample	Melting point (peak) $\{T_m\}$ ($^{\circ}\text{C}$)	Melting point (onset) $\{T_m\}$ ($^{\circ}\text{C}$)	Enthalpy of fusion ΔH_m (J g^{-1})	Crystallinity $\{X_c\}$ (%)
4.2 /BnOH	54.0	50.5	97.4	70 \pm 1
4.4	58.9	50.9	88.0	63 \pm 1

4.7 Copolymerization of Carbon Dioxide and Epoxides using Compounds **4.4** and **4.5**

Compound **4.5** with PPNCI(bis(triphenylphosphoranylidene)ammonium chloride) as co-catalyst was preliminarily screened for the reaction of styrene oxide (SO) and CO_2 . The results are summarized in Table 4.7, in which very low conversion to styrene carbonate (SC) was obtained with the combination of **4.5** and PPNCI for 3 h (Table 4.7, entry 1). However, when the time was increased to 24 h, the conversion improved about three fold (Table 4.7, entry 2). A control reaction using the co-catalyst alone was conducted and the activity was slightly less than that in the presence of **4.5** under similar reaction conditions (Table 4.7, entry 3). The observed decrease in activity confirms that **4.5** is a catalyst for the coupling reaction, albeit with low activity.

Table 4.7. Coupling reactions of SO and CO_2 using **4.5** and PPNCI^a

Entry	Catalyst	Co-catalyst	$[\text{SO}]_0/[\text{Al}]_0/$ $[\text{Co-cat}]_0$	t (h)	P [CO_2] (bar)	T ($^{\circ}\text{C}$)	SO conv. (%)
1	4.5	PPNCI	200/1/1	3	40	60	9.3
2	4.5	PPNCI	200/1/1	24	40	60	37.0
3	—	PPNCI	200/0/1	24	40	60	23.7

^aPPNCI = bis(triphenylphosphoranylidene)ammonium chloride

Table 4.8 contains data from attempted CHO/CO₂ copolymerization reactions using compounds **4.1**, **4.4** and **4.5** as catalysts. In all cases a [CHO]:[Al] ratio of 500:1 was used and CO₂ pressure of 40 bar unless otherwise indicated. It should be noted that in none of the reactions described here was polyether formation observed. This contrasts with related cationic Al complexes, which show good activity in ROP of epoxides.^{92,93} Compound **4.1** with tetrabutylammonium fluoride [Bu₄NF] was found to couple cyclohexene oxide (CHO) and CO₂ in neat CHO at 80 °C (Table 4.8, entry 1). Cyclohexene carbonate (CHC) at 38 % conversion levels was detected with 97% *cis* stereoselectivity. Reactions of CHO and CO₂ using compound **4.4** showed that it was inactive towards both copolymerization and cycloaddition reactions even in combination with PPNCI as a co-catalyst (Table 4.8, entries 2 and 3). Compound **4.5** was found to be active without a co-catalyst producing a copolymer (Table 4.8, entry 4). The resulting polymer was a polyethercarbonate, which consists of polyether (m) and polycarbonate (n) with 54% carbonate linkages. Both the polyether and polycarbonate portions were identified and quantified through ¹H NMR spectroscopy using the signal of methine hydrogen atoms as shown in the supporting information (Figure 4.19).

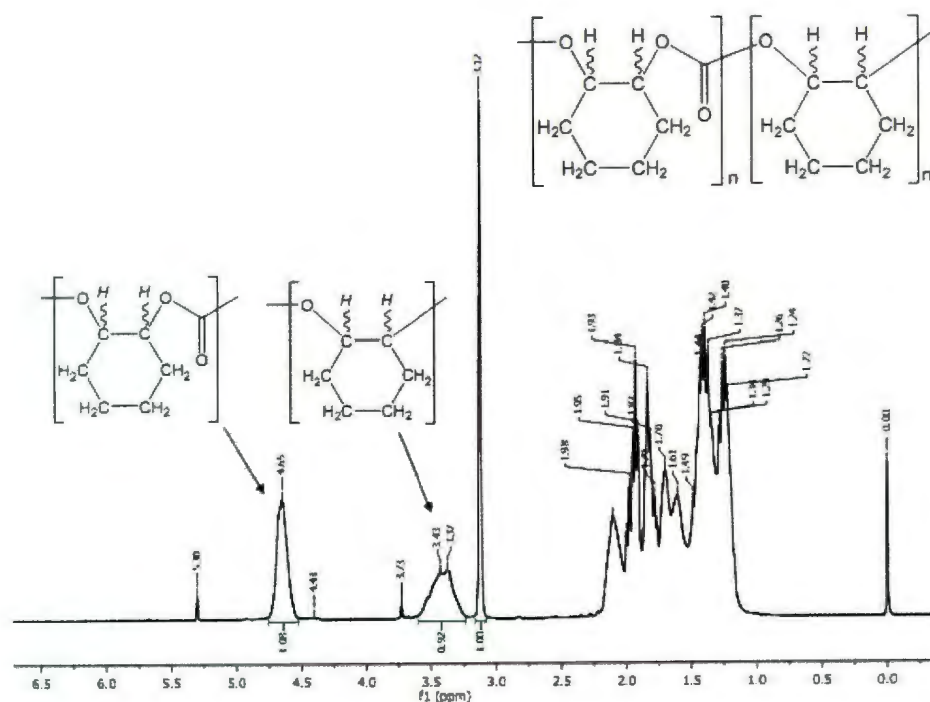


Figure 4.19. ^1H NMR spectrum of the copolymerization of CHO and CO_2 (MHz, CDCl_3)

Efforts to enhance the activity of **4.5** were attempted by adding PPNCl as a co-catalyst. However, this led to inactivity of **4.5**, possibly by the co-catalyst blocking the active site hindering monomer access to the metal centre. These preliminary results also demonstrate significant differences between **4.4** and **4.5**, which are probably due to the nature of the outer-sphere heteroatom. Therefore, it is proposed that **4.5** is better able than **4.4** to support the formation of an ionic complex, where the chloride is not closely associated with the aluminum center, Figure 4.20. The nucleophilic chloride ion would then be able to ring-open the epoxide, which could be bound to the aluminum center. It is suggested that the chloride ion dissociates more readily from the aluminum center in **4.5** because the metal can more readily coordinate the formally outer-sphere ethereal donor

atom compared with the amine donor atom in 4.4. The morpholinyl-oxygen in 4.5 possesses two lone pairs, is less sterically demanding and the morpholinyl-ring potentially undergoes conformational changes with less energy compared with the piperazinyl-ring in 4.4. Coordination of the nitrogen atom in 4.4 to the aluminum center in order to stabilize the ionic form of the complex would require stereochemical inversion of the nitrogen center. These initial results in the area of carbon dioxide activation are promising but further reaction optimization is required for 4.5 to be competitive with other copolymerization catalysts,^{94,95} and computational studies are needed in order to understand the difference in reactivity compared with 4.4.

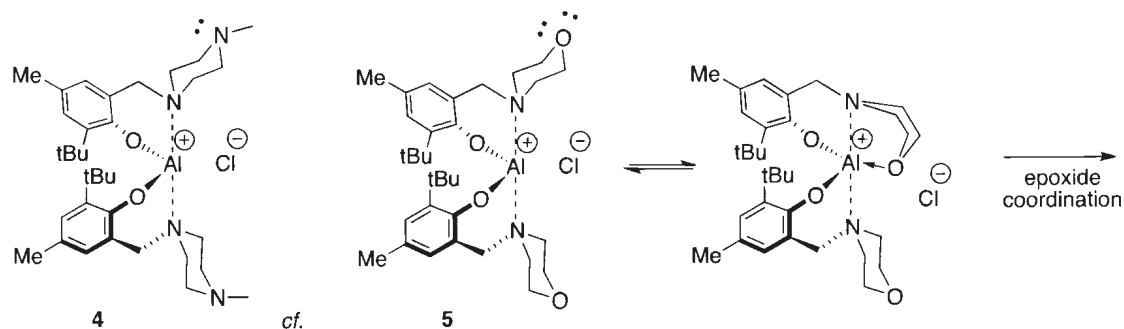


Figure 4.20. Possible key ionic intermediate in CO₂-epoxide copolymerization facilitated by 4.5

Table 4.8. Copolymerization of CHO/CO₂ using **4.1**, **4.4** and **4.5** as catalysts^[a]

Entry	Cat	Co-cat.	[Al] ₀ / [Co-cat] ₀	t (h)	% CHC ^[b]	% Polymer ^[b] [% Carbonate]	M _n ^[c] (kg mol ⁻¹)	M _w / M _n ^[c]
1 ^d	4.1	Bu ₄ NF	1/1	24	38.3 (97.0% <i>cis</i>)	0	–	–
2	4.4	–	1/0	24	0	0	–	–
3	4.4	PPNCl	1/1	24	0	0	–	–
4	4.5	–	1/0	16	0	66.7 [54.0]	29.0	3.16
5	4.5	PPNCl	1/1	24	0	0	–	–

[a] Reactions run neat at 60 °C with [CHO]:[Al] 500:1, CO₂ pressure of 40 bar. [b] Determined by ¹H NMR. [c] Determined by GPC calibrated with polystyrene standards in chloroform. [d] Run neat at 80 °C and CO₂ pressure of 65 bar.

4.8 Conclusions

In summary, aluminum alkyl and halide complexes supported by monoanionic piperazinyl- and morpholinyl-aminephenolate ligands were synthesized and fully characterized. Aluminum alkyl complexes **4.1-4.3** are efficient catalysts for the ROP of ϵ -CL in the presence of BnOH, and possess good activity (TOF ~ 1000 h⁻¹, 80 °C) for this reaction based on the reactivity scale developed by Redshaw and Arbaoui.⁴ In comparison with previously reported Zn analogs,²⁷ the Al complexes exhibit higher reactivity in ROP of ϵ -CL but lower (zero) reactivity in ROP of *rac*-LA. This study sheds some light on ways to develop active catalysts for ROP of lactones and demonstrates that significant differences in reactivity trends occur when studying different monomers. Based on the experimental data, the reactivity of the complexes has the order **4.2**/BnOH ≥ **4.3**/BnOH > **4.1**/BnOH. Polymerization kinetic studies revealed a first order dependence on monomer concentration. Comparison of the activation energies of polymerization for piperazinyl-

aminephenolate and morpholinyl-aminephenolate complexes revealed that the activation energy is lower for the piperazinyll-containing complexes than for the morpholinyl-containing complex, highlighting the effects of the outersphere (E) substituent groups on the resulting activity of complexes in ROP reactions. Differences were noted between the activation entropies and enthalpies for the reactions using these complexes. However, the Gibbs energies of activation for all three complexes were similar. **4.4** ($\{[\text{ONN}^{\text{tBu,tBu}}]_2\text{AlCl}\}$) was not active in the CHO/CO₂ copolymerization, in contrast, **4.5** ($[\text{ONO}^{\text{tBu,tBu}}]_2\text{AlCl}\}$) was active even without a co-catalyst. This shows that the E substituent once again impacted the activity of these complexes within a reaction. It is proposed that this is due to facile coordination of the ethereal morpholinyl oxygen atom to the metal center, which displaces the chloride ion which can then ring-open the epoxide. Further studies are required to understand the subtle differences in reactivity observed and build on these discoveries, particularly with regards to carbon dioxide copolymerization

4.9 Experimental Section

4.9.1 General Considerations

All experiments involving metal complexes were performed under a nitrogen atmosphere using standard Schlenk and glove-box techniques. Toluene, hexane and pentane were purified using an MBraun Solvent Purification System. Deuterated solvents (C₆D₆, CDCl₃, C₅D₅N, C₇D₈) were purchased from Cambridge Isotope Laboratories, Inc.,

purified and dried before use. All solvents were degassed using freeze-pump-thaw cycles prior to use. 2,4-di(*tert*-butyl)phenol, 2-*tert*-butyl-4-methylphenol, 1-methyl piperazine, morpholine, trimethylaluminum (25% w/w in hexane), diethylaluminum chloride (25% w/w in heptane), and ϵ -caprolactone were purchased from Sigma-Aldrich or Alfa Aesar. ϵ -Caprolactone was dried and degassed prior to use. Cyclohexene oxide (CHO) was refluxed over CaH₂, distilled and stored under nitrogen. CO₂ (99.99% purity) was used without further purification. Elemental analyses were performed by Canadian Microanalytical Service Ltd., Delta, B.C. Canada. ¹H and ¹³C{¹H} NMR spectra were recorded on a Bruker Avance 300 or 500 MHz spectrometer at 25 °C (unless otherwise stated) and were referenced internally using residual proton and ¹³C resonances of the solvent. ²⁷Al NMR spectra were recorded on a Bruker 300 MHz spectrometer and referenced externally to Al₂(SO₄)₃ in D₂O. For polymer MALDI-TOF MS analysis, an Applied Biosystems 4800 TOF-TOF instrument was used and the mass spectra were recorded in linear mode. 2-(4-hydroxyphenylazo)benzoic acid (HABA) was used as the matrix and purified tetrahydrofuran was used as the solvent for depositing analytes onto the instrument plate. GPC data were collected on a Viscotek GPCMax system equipped with a refractive index detector and columns purchased from Phenomenex (Phenogel 5 μ Linear/mixed bed 300 \times 4.60 mm column). Samples were run in chloroform at 35 °C at a concentration of 1 mg mL⁻¹. The instrument was calibrated against polystyrene standards (Viscotek) to determine the molecular weights (M_n and M_w) and the polydispersity index (M_w/M_n) of polymers. Conversions were determined by ¹H NMR integration of the ϵ -methylene of residual ϵ -caprolactone and poly(ϵ -caprolactone). TGA measurements were

obtained using a TGA Q500 Thermogravimetric Analyzer (TA Instruments). Approximately 4.8 mg of sample was loaded onto the open platinum pan. The samples were heated from 25 to 600 °C under dry nitrogen at a constant heating rate of 50 °C min⁻¹ using the high-resolution method (dynamic rate). The TGA data were plotted as temperature versus weight %, from which onset and final decomposition temperatures were obtained. Data were also plotted as temperature versus derivative of weight %, from which peak decomposition temperatures were obtained. Melting temperatures of PCL samples were obtained using a DSC1 STAR^e System (Mettler Toledo). The measurements were carried out at a scanning rate of 10 °C min⁻¹ and nitrogen gas flow rate of 50 ml min⁻¹ with approximately 4.0 mg of sample. Samples were heated from -70 to +150 °C and the melting point was determined at the maximum of the melting endotherm.

4.9.2 Single Crystal X-ray Diffraction Studies

Crystals of 4.1-4.4, and 4.5 were mounted on low temperature diffraction loops and measured on a Rigaku Saturn CCD area detector with graphite monochromated Mo-K α radiation. Structures were solved by direct methods^{96,97} and expanded using Fourier techniques.⁹⁸ Neutral atom scattering factors were taken from Cromer and Waber.⁹⁹ Anomalous dispersion effects were included in Fcalc¹⁰⁰; the values for $\Delta f'$ and $\Delta f''$ were those of Creagh and McAuley¹⁰¹ The values for the mass attenuation coefficients are those of Creagh and Hubbell.¹⁰² All calculations were performed using CrystalStructure^{103,104} except for refinement, which was performed using SHELXL-97.⁹⁶

All non-hydrogen atoms were refined anisotropically, while hydrogen atoms were introduced in calculated positions and refined on a riding model.

For **4.2**, one 'Bu group was disordered with two orientations (0.6 : 0.4-occupancy), and was modeled with angle restraints. Crystals of **4.3** were irregular and diffracted poorly leading to a high internal consistency of the reflection data. For **4.4**, one toluene molecule, disordered around a two-fold rotation axis, was present in the asymmetric unit. Protons could not be suitably fixed, and so they were omitted from the model, but included in the formula for the calculation of intensive properties.

Two full data collections were performed on different crystals of **4.5**, however, in both cases problems due to large structure size, weak diffraction (therefore, few high angle reflection/observations for refinement) and possible twinning were encountered. Due to poor internal consistency of data for the full collection, each of four scans was examined separately and only a single scan was used for solution and refinement. A second twin component, related to the first by a rotation of 2.88° around the normal to (-2.61, -3.89, 1.00) was identified, however, it was not found to be significant (BASF refined to 0.0003), and was therefore not included in this model. SHELXL SIMU restraints were applied to all bonds that did not involve Al, in order to increase the observation-to-parameters ratio.

Table 4.9. Summary of crystal data for compound 4.1-4.4^a

Compounds	4.1	4.2	4.3	4.4
Formula	C ₃₅ H ₅₇ AlN ₄ O ₂	C ₄₈ H ₇₇ AlN ₄ O ₂	C ₃₉ H ₆₃ AlN ₂ O ₄	C ₄₁ H ₆₂ AlClN ₄ O ₂
Formula Weight	592.84	769.14	650.92	705.40
Crystal System	Triclinic	Triclinic	Orthorhombic	Monoclinic
Space Group	<i>P-1</i>	<i>P-1</i>	<i>Pbca</i>	<i>C2/c</i>
<i>a</i> / Å	9.096(3)	11.663(3)	19.976(4)	17.093(5)
<i>b</i> / Å	13.328(4)	13.140(4)	13.016(3)	14.214(4)
<i>c</i> / Å	14.479(4)	17.086(5)	29.350(6)	16.467(5)
α / °	97.164(5)	100.407(3)	90	90
β / °	93.365(6)	108.304(4)	90	95.641(3)
γ / °	96.972(6)	105.925(3)	90	90
<i>V</i> / Å ³	1723.8(8)	2286.1(11)	7631(3)	3981(2)
<i>T</i> / K	153	153	153	153
<i>Z</i>	2	2	8	4
<i>D_c</i> g cm ⁻³	1.142	1.117	1.133	1.177
<i>F</i> (000)	648	844	2848	1528
μ (MoK α)/ cm ⁻¹	0.94	0.85	0.93	1.57
Total reflections	14082	20390	19498	19462
Unique reflections	7005	9356	6290	4095
<i>R</i> _{int}	0.0216	0.0267	0.1825	0.0352
Reflections <i>I</i> > 2 σ (<i>I</i>)	6409	8365	2818	3916
No. of parameters	380	524	428	246
<i>R</i> , <i>wR</i> ₂ [<i>I</i> > 2 σ (<i>I</i>)]	0.0490, 0.1251	0.0615, 0.1605	0.1224, 0.2881	0.0420, 0.1229
GOF	1.064	1.065	1.038	1.045

^a Data in common: graphite-monochromated via Rigaku SHINE Optic Mo-K α radiation, λ = 0.71073 Å; $R_1 = \Sigma ||F_o| - |F_c|| / \Sigma |F_o|$, $wR_2 = [\Sigma (w (F_o^2 - F_c^2)^2) / \Sigma w(F_o^2)^2]^{1/2} w^{-1} = [\sigma^2(F_o^2) + (aP)^2]$, $P = [\text{Max}(F_o^2, 0) + 2(F_c^2)]/3$

4.9.3 Synthetic Procedures

[ONN^{Me,^tBu}]₂AlMe (4.1). A solution of trimethylaluminum (25% w/w in toluene; 0.270 g 3.75 mmol) was added dropwise to a rapidly stirred solution of [L1]H (2.07 g, 7.49 mmol) in toluene (10.0) mL under nitrogen at 25 °C. This mixture was allowed to stir for 2 h at room temperature, yielding a yellow solution. All volatiles were removed under vacuum affording a white solid. Yield: 1.96 g, 91.6%. X-ray quality crystals were obtained through crystallization from a 50/50 toluene/hexane solution at -35 °C. After several days, clear, colorless crystals of **4.1** were obtained. Anal. calcd. for C₃₅H₅₇AlN₄O₂: C, 70.91; H, 9.69; N, 9.45. Found: C, 70.65; H, 9.83; N, 9.40%. ¹H NMR (C₅D₅N, 300 MHz, 298 K) δ 7.20 (2H s, ArH), 6.73 (2H, s, ArH), 3.58 (4H, s, Ar-CH₂-N), 2.35-2.59 (16H, br, N-C₂H₄-C₂H₄-N), 2.30 (6H, s, N-CH₃), 2.13 (6H, s, ArC-CH₃), 1.61 (18H, s, ArC-C{CH₃}₃), 0.12 (3H, s, Al-CH₃). ¹³C{¹H} NMR (C₇D₈, 125 MHz, 298 K) δ 157.2 (ArC-O), 155.5 (ArC-C{CH₃}₃), 138.1 (ArC-H), 136.8 (ArC-H), 123.9 (ArC-CH₂-N), 121.9 (ArC-CH₃), 62.4 (ArC-CH₂-N), 55.5 (N-C₂H₄-C₂H₄-N), 52.9 (N-C₂H₄-C₂H₄-N), 46.6 (N-CH₃), 46.2 (ArC-C{CH₃}₃), 35.3 (Al-CH₃) 31.0 (ArC-C{CH₃}₃) 30.4 (ArC-CH₃); ²⁷Al NMR (C₅D₅N, 78.22 MHz, 298 K) δ 74, ω_{1/2} = 4050 Hz.

[ONN^{tBu,^tBu}]₂AlMe (4.2). This compound was prepared in the same manner as described above for **4.1** with trimethylaluminum (25% w/w in toluene; 0.230 g 3.14 mmol) and [L2]H (2.00 g, 6.28 mmol) as starting materials. Compound **4.2** was obtained as a colorless crystalline solid. Yield: 1.07 g, 77%. Crystals suitable for X-ray crystallography could be grown by cooling a saturated toluene solution at -35 °C. Anal. calcd. for C₄₁H₆₉AlN₄O₂: C, 72.74; H, 10.27; N, 8.28. Found: C, 72.75; H, 10.14; N,

8.03%. ^1H NMR ($\text{C}_5\text{D}_5\text{N}$, 500 MHz, 328 K) δ 7.29 (2H, s, ArH), 7.08 (2H, s, ArH), 3.64 (4H, s, Ar- $\text{CH}_2\text{-N}$), 3.14 (8H, br, N- $\text{C}_2\text{H}_4\text{-C}_2\text{H}_4\text{-N}$), 2.43 (8H, br, N- $\text{C}_2\text{H}_4\text{-C}_2\text{H}_4\text{-N}$), 2.13 (6H, s, N- CH_3), 1.64 (18H, s, ArC-C $\{\text{CH}_3\}_3$), 1.40 (18H, s, ArC-C $\{\text{CH}_3\}_3$), -0.31 (3H, s, Al- CH_3); $^{13}\text{C}\{^1\text{H}\}$ NMR ($\text{C}_5\text{D}_5\text{N}$, 125 MHz, 298 K): δ 156.6 (ArC-O), 155.1 (ArC-C $\{\text{CH}_3\}_3$), 141.0 (ArCH), 139.9 (ArCH), 125.5 (ArC- CH_2N), 121.1 (ArC-C $\{\text{CH}_3\}_3$), 63.7 (ArC- CH_2N), 56.7 (N- $\text{C}_2\text{H}_4\text{-C}_2\text{H}_4\text{-N}$), 54.1 (N- $\text{C}_2\text{H}_4\text{-C}_2\text{H}_4\text{-N}$), 47.8 (N- CH_3), 36.9 (ArC-C $\{\text{CH}_3\}_3$), 36.0 (ArC-C $\{\text{CH}_3\}_3$), 33.6 (ArC-C $\{\text{CH}_3\}_3$), 32.1 (Al- CH_3), 31.5 (ArC-C $\{\text{CH}_3\}_3$); ^{27}Al NMR ($\text{C}_5\text{D}_5\text{N}$, 78.22 MHz, 298 K) δ 72, $\omega_{1/2} = 3490$ Hz.

[ONO^{tBu,tBu}]₂AlMe (4.3). Compound **4.3** was prepared in the same manner as described above for **4.2** with trimethylaluminum (25% w/w in toluene; 0.236 g, 3.27 mmol) and **[L5]H** (2.00 g, 6.55 mmol) as starting materials and **4.3** was obtained as a colorless crystalline solid. Yield: 1.92 g, 90.1%. Crystals suitable for X-ray crystallography could be grown by cooling a saturated toluene solution at -35 °C. Anal. calcd. for $\text{C}_{39}\text{H}_{63}\text{AlN}_2\text{O}_4$: C, 71.96; H, 9.76; N, 4.30. Found: C, 71.87; H, 9.77; N, 4.46%. ^1H NMR (C_6D_6 , 500 MHz, 343 K) δ 7.56 (2H, d, $J = 2.5$ Hz, ArH), 6.96 (2H, d, $J = 2.5$ Hz, ArH), 3.79 (4H, br, Ar- $\text{CH}_2\text{-N}$), 3.43 (8H, br, O- $\text{C}_2\text{H}_4\text{-C}_2\text{H}_4\text{-N}$), 2.91 (8H, br, O- $\text{C}_2\text{H}_4\text{-C}_2\text{H}_4\text{-N}$), 1.61 (18H, s, ArC-C $\{\text{CH}_3\}_3$), 1.40 (18H, s, ArC-C $\{\text{CH}_3\}_3$), -0.38 (3H, s, Al- CH_3). $^{13}\text{C}\{^1\text{H}\}$ NMR (C_6D_6 , 125 MHz, 298 K) δ 155.8 (ArC-O), 139.3 (ArC-C $\{\text{CH}_3\}_3$), 137.3 (ArC-C $\{\text{CH}_3\}_3$), 125.0 (ArC-H), 123.8 (ArC-H), 122.7 (ArC- $\text{CH}_2\text{-N}$), 61.3 (ArC- $\text{CH}_2\text{-N}$), 52.5 (O- $\text{C}_2\text{H}_4\text{-C}_2\text{H}_4\text{-N}$), 49.8 (O- $\text{C}_2\text{H}_4\text{-C}_2\text{H}_4\text{-N}$), 35.0 (ArC-C $\{\text{CH}_3\}_3$), 34.0, (ArC-C $\{\text{CH}_3\}_3$), 31.7 (ArC-C $\{\text{CH}_3\}_3$), 30.3 (ArC-C $\{\text{CH}_3\}_3$), 29.7 (Al- CH_3); ^{27}Al NMR (C_6D_6 , 78.22 MHz, 298 K) δ 70, $\omega_{1/2} = 4020$ Hz.

[ONN^{Me,tBu}]₂AlCl (4.4). Compound **4.4** was prepared in the same manner as described above for **4.2** with diethylaluminum chloride (25% w/w in toluene; 0.436 g, 3.62 mmol) and **[L1]H** (2.00 g, 7.23 mmol) as starting materials and **4.4** was obtained as a colorless crystalline solid. Yield: 1.67 g, 75.2%. Crystals suitable for X-ray crystallography could be grown by cooling a saturated toluene solution at -35 °C. Anal. calcd. for C₃₄H₅₄AlClN₄O₂: C, 66.59; H, 8.88; N, 9.14. Found: C, 66.32; H, 8.86; N, 8.97%. ¹H NMR (C₅D₅N, 300 MHz, 298 K) δ 7.20 (2H s, ArH), 6.73 (2H, s, ArH), 3.59 (4H, s, Ar-CH₂-N), 2.56 (8H, br, N-C₂H₄-C₂H₄-N), 2.48 (8H, br, N-C₂H₄-C₂H₄-N), 2.30 (6H, s, N-CH₃), 2.25 (6H, s, ArC-CH₃), 1.59 (18H, s, ArC-C{CH₃}₃). ¹³C{¹H} NMR (C₅D₅N, 125 MHz, 298 K) δ 153.3 (ArC-O), 136.4 (ArC-C{CH₃}₃), 128.8 (ArC-H), 128.0 (ArC-H), 127.2 (ArC-CH₂-N), 121.8 (ArC-CH₃), 61.6 (ArC-CH₂-N), 54.7 (N-C₂H₄-C₂H₄-N), 51.9 (N-C₂H₄-C₂H₄-N), 45.2 (N-CH₃), 35.0 (ArC-C{CH₃}₃), 30.0 (ArC-C{CH₃}₃) 21.0 (ArC-CH₃); ²⁷Al NMR (C₅D₅N, 78.22 MHz, 298 K) δ 71, ω_{1/2} = 4080 Hz.

[ONO^{tBu,tBu}]₂AlCl (4.5). Compound **4.5** was prepared in the same manner as described above for **4.4** with diethylaluminum chloride (25% w/w in toluene; 0.395 g, 3.27 mmol) and **[L5]H** (2.00 g, 6.28 mmol) as starting materials and **4.5** was obtained as a colorless crystalline solid. Yield: 1.89 g, 86.3%. Anal. calcd. for C₃₈H₆₀AlClN₂O₄: C, 67.99; H, 9.01; N, 4.17. Found: C, 67.54; H, 9.11; N, 4.58%. ¹H NMR (C₅D₅N, 300 MHz, 298 K) δ 7.52 (2H, d, *J* = 2.2 Hz, ArH), 7.09 (2H, d, *J* = 2.2 Hz, ArH), 3.67 (4H, s, Ar-CH₂-N), 3.65 (8H, br, O-C₂H₄-C₂H₄-N), 2.43 (8H, br, O-C₂H₄-C₂H₄-N), 1.64 (18H, s, ArC-C{CH₃}₃), 1.38 (18H, s, ArC-C{CH₃}₃); ¹³C{¹H} NMR (C₅D₅N, 125 MHz, 298 K) δ 154.9 (ArC-O), 141.2 (ArC-C{CH₃}₃), 139.3 (ArC-C{CH₃}₃), 124.4 (ArCH), 122.9

(ArCH), 121.1 (ArC-CH₂-N), 66.8 (ArC-CH₂-N), 62.5 (O-C₂H₄-C₂H₄-N), 53.0(O-C₂H₄-C₂H₄-N), 35.3 (ArC-C{CH₃}₃), 34.5, (ArC-C{CH₃}₃), 32.0 (ArC-C{CH₃}₃), 30.0 (ArC-C{CH₃}₃). ²⁷Al NMR (C₅D₅N, 78.22 MHz, 298 K) δ 73, ω_{1/2} = 3710 Hz.

4.10 Polymerization Procedures

4.10.1 Typical ROP of ε-CL Procedure

All manipulations were performed under an inert atmosphere. The reaction mixtures were prepared in a glove box and subsequent operations were performed using standard Schlenk techniques. A sealable Schlenk flask equipped with a stir bar was charged with a solution of complex **4.1** (20.0 mg, 33.7 μmol) in toluene (2.0 mL) with the prescribed amount of BnOH. Another Schlenk flask was charged with a toluene (4.0 mL) solution of ε-caprolactone (0.390 g, 3.37 mmol, 100 equiv). The two flasks were then attached to a Schlenk line and temperature equilibration was ensured in both Schlenk flasks by stirring the solutions for 10 minutes in a temperature controlled oil bath. The complex solution was transferred to the monomer solution, which was stirring rapidly, and polymerization times were measured from that point. At appropriate time intervals, aliquots of the reaction mixture were removed using a pipette for determining monomer conversion by ¹H NMR spectroscopy. The reaction was quenched with methanol once near-quantitative conversion had been obtained. The polymer was precipitated with an excess of cold methanol, isolated by filtration and dried under reduced pressure.

4.10.2 Representative Copolymerization Procedure

An autoclave (Parr) was heated to 80 °C under vacuum for 4 h, then cooled and moved to a glovebox. **4.5** (72.0 mg, 0.107 mmol) and cyclohexene oxide (5.26 g, 53.6 mmol) were placed into the autoclave, which was then sealed and removed from the glovebox. The autoclave was pressurized to 60 bar of CO₂ and was heated to the reaction temperature. After the stipulated reaction time, the reactor was cooled, vented and a small sample of the polymerization mixture was taken for ¹H NMR analysis. The remaining mixture was dissolved in dichloromethane (10 mL), quenched with methanol and then precipitated from cold methanol. The resultant polymer was collected and dried under vacuum. Characterization of polymer was performed by NMR and GPC. ¹H NMR (CDCl₃, 300 MHz, 298 K) δ 4.65 (br CH, polycarbonate), 3.43 (br CH, polyether), 2.2-1.1 (m CH₂, cyclohexyl).

4.11 References

1. R. Chandra and R. Rustgi, *Prog. Polym. Sci.*, **1998**, *23*, 1273.
2. D. R. Chen, J. Z. Bei and S. G. Wang, *Polym. Degrad. Stab.*, **2000**, *67*, 455.
3. Y. Ikada and H. Tsuji, *Macromol. Rapid Commun.*, **2000**, *21*, 117.
4. A. Arbaoui and C. Redshaw, *Polym. Chem.*, **2010**, *1*, 801.
5. B. J. O'Keefe, M. A. Hillmyer and W. B. Tolman, *J. Chem. Soc. Dalton Trans.*, **2001**, 2215.
6. J. Wu, T.-L. Yu, C.-T. Chen and C.-C. Lin, *Coord. Chem. Rev.*, **2006**, *250*, 602.
7. M. Labet and W. Thielemans, *Chem. Soc. Rev.*, **2009**, *38*, 3484.
8. N. Ajellal, J.-F. Carpentier, C. Guillaume, S. M. Guillaume, M. Helou, V. Poirier, Y. Sarazin and A. Trifonov, *Dalton Trans.*, **2010**, *39*, 8363.
9. O. Wichmann, R. Sillanpää and A. Lehtonen, *Coord. Chem. Rev.*, **2012**, *256*, 371.
10. N. Ikpo, C. Hoffmann, L. N. Dawe and F. M. Kerton, *Dalton Trans.*, **2012**, *41*, 665.
11. Y. Huang, Y.-H. Tsai, W.-C. Hung, C.-S. Lin, W. Wang, J.-H. Huang, S. Dutta and C.-C. Lin, *Inorg. Chem.*, **2010**, *49*, 9416.
12. L. Wang, X. Pan, L. Yao, N. Tang and J. Wu, *Eur. J. Inorg. Chem.*, **2011**, 632.
13. C.-A. Huang and C.-T. Chen, *Dalton Trans.* **2007**, 5561.
14. F. M. Kerton, C. M. Kozak, K. Luttmann, C. E. Willans, R. J. Webster and A. C. Whitwood, *Inorg. Chim. Acta.*, **2006**, *359*, 2819.
15. C.-A. Huang, C.-L. Ho and C.-T. Chen, *Dalton Trans.*, **2008**, 3502.
16. B.-T. Ko and C.-C. Lin, *J. Am. Chem. Soc.*, **2001**, *123*, 7973.
17. J. Ejfler, K. Krauzy-Dziedzic, S. Szafert, L. B. Jerzykiewicz and P. Sobota, *Eur. J. Inorg. Chem.*, **2010**, 3602.
18. X. Zhang, T. J. Emge and K. C. Hultsch, *Organometallics*, **2010**, *29*, 5871.

19. A. D. Schofield, M. L. Barros, M. G. Cushion, A. D. Schwarz and P. Mountford, *Dalton Trans.* **2009**, 85.
20. W.-C. Hung and C.-C. Lin, *Inorg. Chem.*, **2009**, *48*, 728.
21. L. E. Breyfogle, C. K. Williams, J. V. G. Young, M. A. Hillmyer and W. B. Tolman, *Dalton Trans.*, **2006**, 928.
22. E. L. Marshall, V. C. Gibson and H. S. Rzepa, *J. Am. Chem. Soc.*, **2005**, *127*, 6048.
23. Y. Sarazin, V. Poirier, T. Roisnel and J.-F. Carpentier, *Eur. J. Inorg. Chem.*, **2010**, 3423.
24. D. J. Darensbourg, W. Choi, O. Karroonnirun and N. Bhuvanesh, *Macromolecules*, **2008**, *41*, 3493.
25. H. E. Dyer, S. Huijser, A. D. Schwarz, C. Wang, R. Duchateau and P. Mountford, *Dalton Trans.*, **2008**, 32.
26. A. Amgoune, C. M. Thomas and J.-F. Carpentier, *Macromol. Rapid Commun.*, **2007**, *28*, 693.
27. N. Ikpo, L. N. Saunders, J. L. Walsh, J. M. B. Smith, L. N. Dawe and F. M. Kerton, *Eur. J. Inorg. Chem.*, **2011**, 5347.
28. V. Poirier, T. Roisnel, J.-F. Carpentier and Y. Sarazin, *Dalton Trans.*, **2011**, *40*, 523.
29. L. Wang and H. Ma, *Dalton Trans.*, **2010**, *39*, 7897.
30. G. Labourdette, D. J. Lee, B. O. Patrick, M. B. Ezhova and P. Mehrkhodavandi, *Organometallics*, **2009**, *28*, 1309.
31. J. D. Farwell, P. B. Hitchcock, M. F. Lappert, G. A. Luinstra, A. V. Protchenko and X.-H. Wei, *J. Organomet. Chem.*, **2008**, *693*, 1861.
32. J. Ejfler, S. Szafert, K. Mierzwicki, L. B. Jerzykiewicz and P. Sobota, *Dalton Trans.*, **2008**, 6556.
33. D. J. Doyle, V. C. Gibson and A. J. P. White, *Dalton Trans.*, **2007**, 358.
34. C. K. Williams, L. E. Breyfogle, S. K. Choi, W. Nam, V. G. Young, M. A. Hillmyer and W. B. Tolman, *J. Am. Chem. Soc.*, **2003**, *125*, 11350.

35. C. K. Williams, N. R. Brooks, M. A. Hillmyer and W. B. Tolman, *Chem. Commun.*, **2002**, 2132.
36. M. H. Chisholm, J. C. Gallucci, H. Zhen and J. C. Huffman, *Inorg. Chem.*, **2001**, *40*, 5051.
37. M. H. Chisholm and Z. Zhou, *J. Mater. Chem.*, **2004**, *14*, 3081.
38. J. Lewinski, P. Horeglad, M. Dranka and I. Justyniak, *Inorg. Chem.*, **2004**, *43*, 5789.
39. J.-T. Issenhuth, J. Pluvinage, R. Welter, S. Bellemin-Laponnaz and S. Dagorne, *Eur. J. Inorg. Chem.*, **2009**, 4701.
40. N. C. Johnstone, E. S. Aazam, P. B. Hitchcock and J. R. Fulton *J. Organomet. Chem.*, **2010**, *695*, 170.
41. H.-L. Chen, S. Dutta, P.-Y. Huang and C.-C. Lin, *Organometallics*, **2012**, *31*, 2016.
42. C. Bakewell, R. H. Platel, S. K. Cary, S. M. Hubbard, J. M. Roaf, A. C. Levine, A. J. P. White, N. J. Long, M. Haaf and C. K. Williams, *Organometallics*, **2012**, *31*, 4729.
43. M. Bouyahyi, T. Roisnel and J.-F. Carpentier, *Organometallics*, **2012**, *31*, 1458.
44. D. J. Darensbourg and O. Karroonnirun, *Organometallics*, **2010**, *29*, 5627.
45. V. Poirier, T. Roisnel, S. Sinbandhit, M. Bochmann, J.-F. Carpentier and Y. Sarazin, *Chem. Eur. J.* **2012**, *18*, 2998
46. S. Gendler, S. Segal, I. Goldberg, Z. Goldschmidt and M. Kol, *Inorg. Chem.*, **2006**, *45*, 4783.
47. S. Groysman, E. Sergeeva, I. Goldberg and M. Kol, *Inorg. Chem.*, **2005**, *44*, 8188.
48. L. M. Broomfield, Y. Sarazin, J. A. Wright, D. L. Hughes, W. Clegg, R. W. Harrington and M. Bochmann, *J. Organomet. Chem.*, **2007**, *692*, 4603.
49. R. H. Platel, L. M. Hodgson and C. K. Williams, *Polym. Rev.*, **2008**, *48*, 11.

50. R.-C. Yu, C.-H. Hung, J.-H. Huang, H.-Y. Lee and J.-T. Chen, *Inorg. Chem.*, **2002**, *41*, 6450.
51. W.-A. Ma and Z.-X. Wang, *Organometallics*, **2011**, *30*, 4364.
52. K. L. Collins, L. J. Corbett, S. M. Butt, G. Madhurambal and F. M. Kerton, *Green Chem. Lett. Rev.*, **2007**, *1*, 31.
53. F. M. Kerton, A. Power, R. G. Soper, K. Sheridan, J. M. Lynam, A. C. Whitwood and C. E. Willans, *Can. J. Chem.*, **2008**, *86*, 435.
54. J. J. Delpuech, in *NMR of Newly Accessible Nuclei*, P. Laszlo, Ed. Academic Press: New York, **1983**, Vol 2, Chapter 6.
55. The connectivity of complex 5 is supported by an X-ray diffraction study but the quality of this prevents its publication; Private Communication, F. M. Kerton, 2012, CCDC 904628.
56. A. W. Addison, T. N. Rao, J. Reedijk, J. van Rijn and G. C. Verschoor, *J. Chem. Soc., Dalton Trans.*, **1984**, 1349.
57. A. Gao, Y. Mu, J. Zhang and W. Yao, *Eur J. Inorg. Chem.*, **2009**, 3613.
58. M. P. Hogerheide, M. Wesseling, J. T. B. H. Jastrzebski, J. Boersma, H. Kooijman, A. L. Spek and G. van Koten, *Organometallics*, **1995**, *14*, 4483.
59. R. Kumar, M. L. Sierra and J. P. Oliver, *Organometallics*, **1994**, *13*, 4285.
60. C.-T. Chen, C.-A. Huang and B.-H. Huang, *Dalton Trans.*, **2003**, 3799.
61. W.-H. Sun, M. Shen, W. Zhang, W. Huang, S. Liu and C. Redshaw, *Dalton Trans.*, **2011**, *40*, 2645.
62. J. L. Mata-Mata, J. A. Gutiérrez, M. A. Paz-Sandoval, A. R. Madrigal and A. Martínez-Richa, *J. Polym. Sci. Part A: Polym. Chem.*, **2006**, *44*, 6926.
63. Y.-E. Tai, C.-Y. Li, C.-H. Lin, Y.-C. Liu, B.-T. Ko and Y.-S. Sun, *J. Polym. Sci. Part A: Polym. Chem.*, **2011**, *49*, 4027.
64. E. Martin, P. Dubois and R. Jerome, *Macromolecules*, **2000**, *33*, 1530.
65. M. Normand, E. Kirillov, T. Roisnel and J.-F. Carpentier, *Organometallics*, **2012**, *31*, 1448 and references therein.

66. A. Duda, *Macromolecules*, **1994**, *27*, 576.
67. A. Duda, *Macromolecules*, **1996**, *29*, 1399.
68. C. Zhang and Z.-X. Wang, *J. Organomet. Chem.*, **2008**, *693*, 3151.
69. C. Zhang and Z.-X. Wang, *Appl. Organometal. Chem.*, **2009**, *23*, 9.
70. A.-C.; Albertsson and I. K. Varma, *Biomacromolecules*, **2003**, *4*, 1466.
71. D. Takeuchi, T. Nakamura and T. Aida, *Macromolecules*. **2000**, *33*, 725.
72. P. Dubois, C. Jacobs, R. Jerome and P. Teyssie, *Macromolecules*, **1991**, *24*, 2266.
73. D. J. Darensbourg, P. Ganguly and D. Billodeaux, *Macromolecules*, **2005**, *38*, 5406.
74. F. M. Kerton, A. C. Whitwood and C. E. Willans, *Dalton Trans.*, **2004**, 2237.
75. W. Yao, Y. Mu, A. Gao, Q. Su, Y. Liu and Y. Zhang, *Polymer*, **2008**, *49*, 2486.
76. H. Luftmann, G. Rabani and A. Kraft, *Macromolecules*, **2003**, *36*, 6316.
77. Y. A. Piskun, I. V. Vasilenko, S. V. Kostjuk, K. V. Zaitsev, G. S. Zaitseva and S. S. Karlov, *J. Polym. Sci. Part A: Polym. Chem.*, **2010**, *48*, 1230.
78. X. Yang, L. Wang, L. Yao, J. Zhang, N. Tang, C. Wang and J. Wu, *Inorg. Chem. Commun.*, **2011**, *14*, 1711.
79. T.-C. Liao, Y.-L. Huang, B.-H. Huang and C.-C. Lin, *Macromol. Chem. Phys.*, **2003**, *204*, 885.
80. H.-L. Chen, B.-T. Ko, B.-H. Huang and C.-C. Lin, *Organometallics*, **2001**, *20*, 5076.
81. D. Dakshinamoorthy and F. Peruch, *J. Polym. Sci., Part A: Polym. Chem.*, **2011**, *49*, 5176.
82. Z. Zhong, P. J. Dijkstra, C. Birg, M. Westerhausen and J. Feijen, *Macromolecules*, **2001**, *34*, 3863.
83. A. Duda and S. Penczek, *Macromolecules*, **1995**, *28*, 5981.

84. A. J. Chmura, M. G. Davidson, M. D. Jones, M. D. Lunn, M. F. Mahon, A. F. Johnson, P. Khunkamchoo, S. L. Roberts and S. S. F. Wong, *Macromolecules*, **2006**, *39*, 7250.
85. W. Li, W. Wu, Y. Wang, Y. Yao, Y. Zhanga and Q. Shen, *Dalton Trans.*, **2011**, *40*, 11378.
86. Gong, S.; Ma, H. *Dalton Trans.* 2008, 3345.
87. A. Duda, Z. Florjanczyk, A. Hofman, S. Slomkowski and S. Penczek, *Macromolecules*, **1990**, *23*, 1640.
88. P. Dubois, N. Ropson, R. Jerome and P. Teyssie, *Macromolecules*, **1996**, *29*, 1965.
89. N. Iwasa, S. Katao, J. Liu, M. Fujiki, Y. Furukawa and K. Nomura, *Organometallics*, **2009**, *28*, 2179.
90. G. Gorrasi, L. Vertuccio, L. Annunziata, C. Pellicchia and D. Pappalardo, *React. Funct. Polym.*, **2010**, *70*, 151.
91. M. F. Koenig and S. J. Huang, *Polymer*, **1995**, *36*, 1877.
92. D. J. Darensbourg, O. Karroonnirun and S. J. Wilson, *Inorg. Chem.*, **2011**, *50*, 6775.
93. S. Dagorne, M. Bouyahyi, J. Vergnaud, and J.-F. Carpentier, *Organometallics*, **2010**, *29*, 1865.
94. Selected reviews: D. J. Darensbourg, *Chem. Rev.*, **2007**, *107*, 2388; M. R. Kember, A. Buchard and C. K. Williams, *Chem. Commun.*, **2011**, *47*, 141; X.-B. Lu and D. J. Darensbourg, *Chem. Soc. Rev.*, **2012**, *41*, 1462.
95. Selected papers on CO₂ copolymerization using Al complexes: D. J. Darensbourg and D. R. Billodeaux, *Inorg. Chem.*, **2005**, *44*, 1433; T. Aida and S. Inoue, *Acc. Chem. Res.*, **1996**, *29*, 39; T. Aida, M. Ishikawa and S. Inoue, *Macromolecules*, **1986**, *19*, 8.
96. SHELX97: G.M. *Sheldrick*, *Acta Cryst.*, **2008**, *A64*, 112.
97. SIR92: A. Altomare, G. Cascarano, C. Giacovazzo, A. Guagliardi, M. Burla, G. Polidori and M. Camalli, *J. Appl. Cryst.*, **1994**, *27*, 435.

98. DIRDIF99: P.T. Beurskens, G. Admiraal, G. Beurskens, W. P. Bosman, R. de Gelder, R. Israel and J. M. M. Smits, *The DIRDIF-99 program system, Technical Report of the Crystallography Laboratory*, University of Nijmegen, The Netherlands, **1999**.
99. D. T. Cromer and J. T. Waber, "*International Tables for X-ray Crystallography*", The Kynoch Press, Birmingham, England, **1974**, Vol. IV, Table 2.2 A.
100. J. A. Ibers and W.C. Hamilton, *Acta Cryst.*, **1964**, *17*, 781.
101. Creagh, D. C.; McAuley, E. W. J. *International Tables for Crystallography*, ed., A.J.C. Wilson, Kluwer Academic Publishers, Boston, **1992**, Vol C, Table 4.2.6.8, pp 219.
102. D. C. Creagh and J. H. Hubbell, *International Tables for Crystallography*, ed., A.J.C. Wilson, Kluwer Academic Publishers, Boston, **1992**, Vol C, Table 4.2.4.3, pp 200.
103. CrystalStructure 3.7.0: Crystal Structure Analysis Package, Rigaku and Rigaku/MSK (2000-2005). 9009 New Trails Dr. The Woodlands TX 77381 USA.
104. Watkin, D. J.; Prout, C. K.; Carruthers, J. R.; Betteridge, P. W. CRYSTALS Issue 10: Chemical Crystallography Laboratory, Oxford, UK. **1996**.

CHAPTER 5

Ring-Opening polymerization of ϵ -Caprolactone by Lithium Piperazinyli-Aminephenolate Complexes: Synthesis, Characterization and Kinetic Studies.

Chapter 5

Ring-Opening Polymerization of ϵ -Caprolactone by Lithium Piperazinyl-Aminephenolate Complexes: Synthesis, Characterization and kinetic Studies.

A version of this chapter has been published

Nduka Ikpo, Christian Hoffmann, Louise N. Dawe, and Francesca M. Kerton

Dalton Trans., **2012**, *41*, 6651–6660

Some modifications were made to the original paper for inclusion as a chapter in this thesis.

5.1 Introduction

N- and O- mixed donor amine phenolate and related ligands have received much interest recently due to their ability to stabilize a wide range of metal centres and their modular nature, which enables easy tailoring of steric and electronic properties resulting in metal complexes that often possess new and interesting properties.¹ Various ligands of this type have been used in main group and early transition metal chemistry (including

lithium,²⁻⁷ magnesium,⁸⁻¹⁴ calcium,¹⁵ rare-earths,^{16,17} zinc,¹⁸⁻²⁷ aluminum,²⁸⁻³⁰ zirconium^{31,32} and titanium³³). Many of these complexes have been reported to be active initiators for the ring-opening polymerization (ROP) of cyclic esters such as lactide and ϵ -caprolactone.

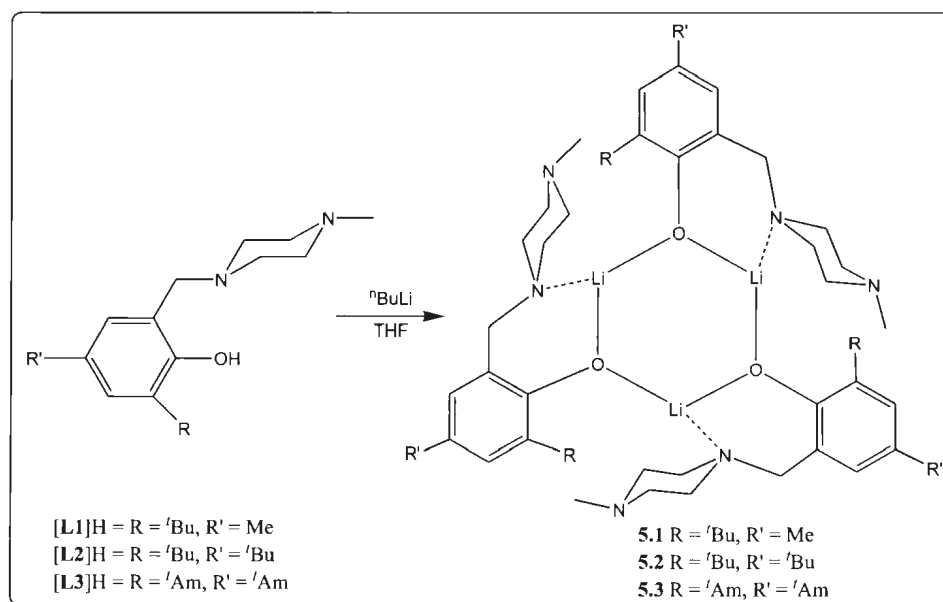
To date most well-characterized lithium aminephenolate complexes reported have contained bis(phenolate) ligands.^{2-5,34-36} This contrasts with related mono-anionic aminephenolate lithium complexes that still remain relatively unexplored.⁶ Furthermore, it has been established that lithium phenolates usually contain square Li_2O_2 dimers³⁷ or 'daisy-chain' Li_4O_4 tetramers with μ_2 -bridging-phenolate interactions.³⁸ In the literature, very few structurally characterized trimetallic lithium phenolate complexes have been reported: $[\text{LiOC}_6\text{H}_2(\text{CH}_2\text{NMe}_2)_{2-2,6-\text{Me}-4}]_3$,³⁹ $[\text{LiOC}_6\text{H}_3\{2,6(\text{Pr})_2\}(\text{THF})]_3$ ⁴⁰ and $[\{\text{Li}(\text{OC}_6\text{H}-3,5-\text{tBu}_2-2,6-\text{Ph}_2)\}_3]$.⁴¹

Following recently reported work by the Kerton group on zinc compounds of piperazinyll aminephenolate ligands,¹⁸ which efficiently initiated the ring-opening polymerization of rac-lactide and ϵ -caprolactone in a controlled manner, the chemistry of related Li complexes was studied. In this chapter, the synthesis and structural characterization of trimetallic lithium piperazinyll aminephenolate complexes are reported. Their catalytic activities in ring-opening polymerization of ϵ -caprolactone in the presence and absence of benzyl alcohol were also investigated.

5.2 Results and Discussion

5.2.1 Synthesis and Solid-State Structures

The reactions of 1.1 equiv. of *n*-butyllithium with the appropriate protio ligands in THF at $-78\text{ }^{\circ}\text{C}$ gave the corresponding lithium methylpiperazinyl aminephenolate complexes $\{\text{Li}[\text{ONN}^{\text{Me,tBu}}]\}_3$, **5.1**, $\{\text{Li}[\text{ONN}^{\text{tBu,tBu}}]\}_3$, **5.2** and $\{\text{Li}[\text{ONN}^{\text{tAm,tAm}}]\}_3$, **5.3** in high yield (Scheme 5.1). Of the alkyl groups on the aromatic rings, the *tert*-amyl groups, also known as *tert*-pentyl, were the most sterically demanding used in this study ($^{\text{t}}\text{Am} = \text{C}(\text{CH}_3)_2\text{CH}_2\text{CH}_3$).



Scheme 5.1. Synthesis of amine-phenolate lithium complexes

Single crystals of **5.1** suitable for X-ray diffraction analysis were obtained by cooling a saturated toluene/hexane solution to $-35\text{ }^{\circ}\text{C}$. The molecular structure shown in Figure 5.1 shows complex **5.1**, which is a trimetallic lithium complex with the lithium centres

bridged by phenolate oxygen atoms to form a Li_3O_3 six-membered ring. The bridging oxygen atoms are *ca.* 0.37 Å off the mean plane of the three central lithium ions. The central ring O(1)–Li(1)–O(1') and Li(1)–O(1)–Li(1') angles are 121.09(14) and 110.93(14)° respectively, which sum to 693.03° for all internal angles of the six-membered ring indicating a deviation from a perfect plane of 720° by 26.97°. The structure possesses a pseudo-threefold rotation axis with each of the three-coordinate lithium ions adopting a distorted trigonal planar geometry. The C_3NLiO six-membered chelate ring adopts a boat conformation with C(12) and O(1) situated *ca.* 0.66 and 0.52 Å off the mean plane of Li(1)–C(1)–C(11)–N(1) respectively. The phenolate rings are tilted with respect to the plane containing the lithium centres such that they display a propeller-like arrangement whose directions are controlled by the coordinated amine of the ligand. The bond lengths Li(1)–O(1) [1.844(3) Å], Li(1)–O(1) [1.832(3) Å], and Li(1)–N(1) [2.105(3) Å] are comparable to related trimetallic and bimetallic lithium complexes reported in the literature,^{5,33,39–41} but shorter than those (Li–O [1.938(3)–2.096(4) Å] and Li–N [2.158(3)–2.213(3) Å]) found for bridged phenoxide.³⁴

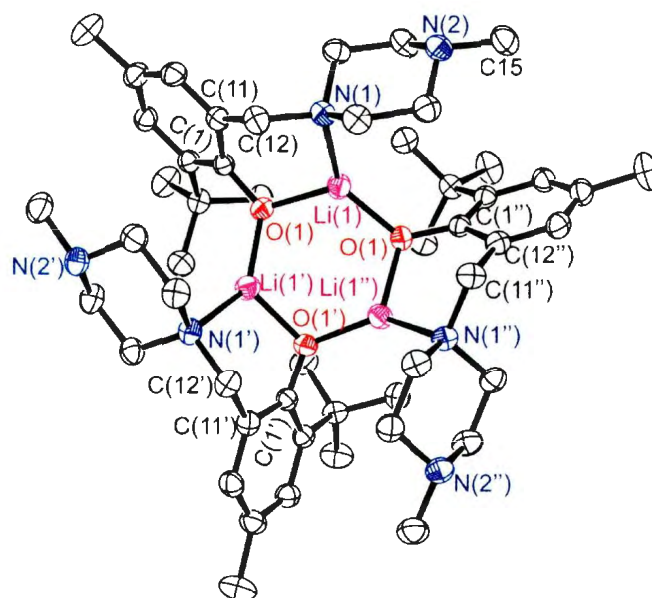


Figure 5.1. Molecular structure of **5.1** (50% displacement ellipsoids; H atoms excluded for clarity). Selected bond lengths (Å) and bond angles (°): O(1)–C(1), 1.3358(16); O(1)–Li(1), 1.832(3); O(1)–Li(1'), 1.844(3); N(1)–Li(1), 2.105(3); Li(1)–Li(1'), 3.028(4); C(1)–O(1)–Li(1), 128.70(11); C(1)–O(1)–Li(1'), 116.33(11); Li(1)–O(1)–Li(1'), 110.93(15); O(1)–Li(1')–O(1'), 121.09(14); O(1)–Li(1')–N(1'), 132.81(14); O(1)–Li(1)–N(1), 101.30(11).

Crystals of complex **5.3** were also grown from toluene/hexane at $-35\text{ }^{\circ}\text{C}$. The single crystal X-ray analysis shows that **5.3** (Figure 5.2) crystallizes as a trimetallic species in the triclinic space group P-1 and is slightly less symmetric than **5.1** due to the greater steric demands of **L3** compared with **L1**, and crystallographic disorder within the *tert*-amyl groups. The structural features of each Li atom in complex **5.3** are similar to those in complex **5.1**; each Li adopts a distorted trigonal planar geometry with the three-coordinate metal centre coordinated to two phenolate oxygen donors and an amine nitrogen atom of the piperazinyl group. The angles around the metal centre and the bond lengths from the Li to the oxygen and nitrogen atoms are similar to those of complex **5.1**.

Li(1), Li(2) and Li(3) are above the mean plane of O(1)-N(1)-O(3), O(1)-N(3)-O(2) and O(3)-N(5)-O(2) by *ca.* 0.27, 0.31 and 0.30 Å respectively.

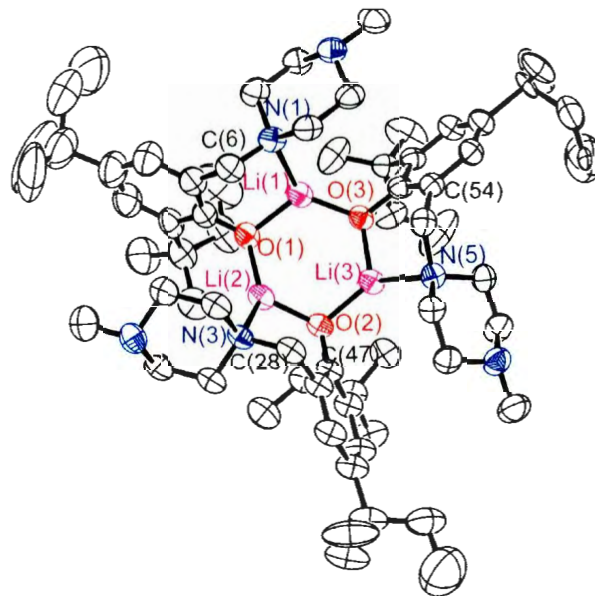


Figure 5.2. Molecular structure of **5.3** (50% displacement ellipsoids; H atoms excluded for clarity). Selected bond lengths (Å) and bond angles (°): O(1)-Li(1), 1.839(5); O(1)-Li(2), 1.862(5); O(2)-Li(2), 1.839(5); O(2)-Li(3), 1.845(5); O(3)-Li(1), 1.837(5); O(3)-Li(3), 1.857(5); N(1)-Li(1), 2.133(5); N(3)-Li(2), 2.138(5); N(5)-Li(3), 2.150(6); Li(1)-O(1)-Li(2), 112.1(2); Li(2)-O(2)-Li(3), 115.5(2); Li(1)-O(3)-Li(3), 110.4(2); O(3)-Li(1)-O(1), 121.9(2); O(2)-Li(2)-O(1), 119.5(3); O(2)-Li(3)-O(3), 120.1(3); O(3)-Li(1)-N(1), 132.3(3); O(1)-Li(1)-N(1), 99.7(2); O(2)-Li(2)-N(3), 101.0(2).

Attempts to grow crystals of complex **5.2**, however, led to amorphous white precipitates.

Complexes **5.1–5.3** were further characterized by elemental analysis, ^1H and $^{13}\text{C}\{^1\text{H}\}$ NMR spectroscopy. Variable temperature NMR studies of complexes **5.1–5.3** were recorded in $\text{C}_5\text{D}_5\text{N}$ from -35 to 70 °C and showed sharp, readily assignable peaks for the methylene (PhCH_2N , $\text{NCH}_2\text{CH}_2\text{N}$) and amine methyl groups at elevated temperature. When the temperature was slowly decreased to ambient, the methylene peaks broadened

and became indistinguishable from the spectral baseline. On further decreasing the temperature to below 0 °C, the methylene peaks became diastereotopic. The NMR spectral data for **5.1**–**5.3** are in good agreement with their formulations (Figure 5.3).

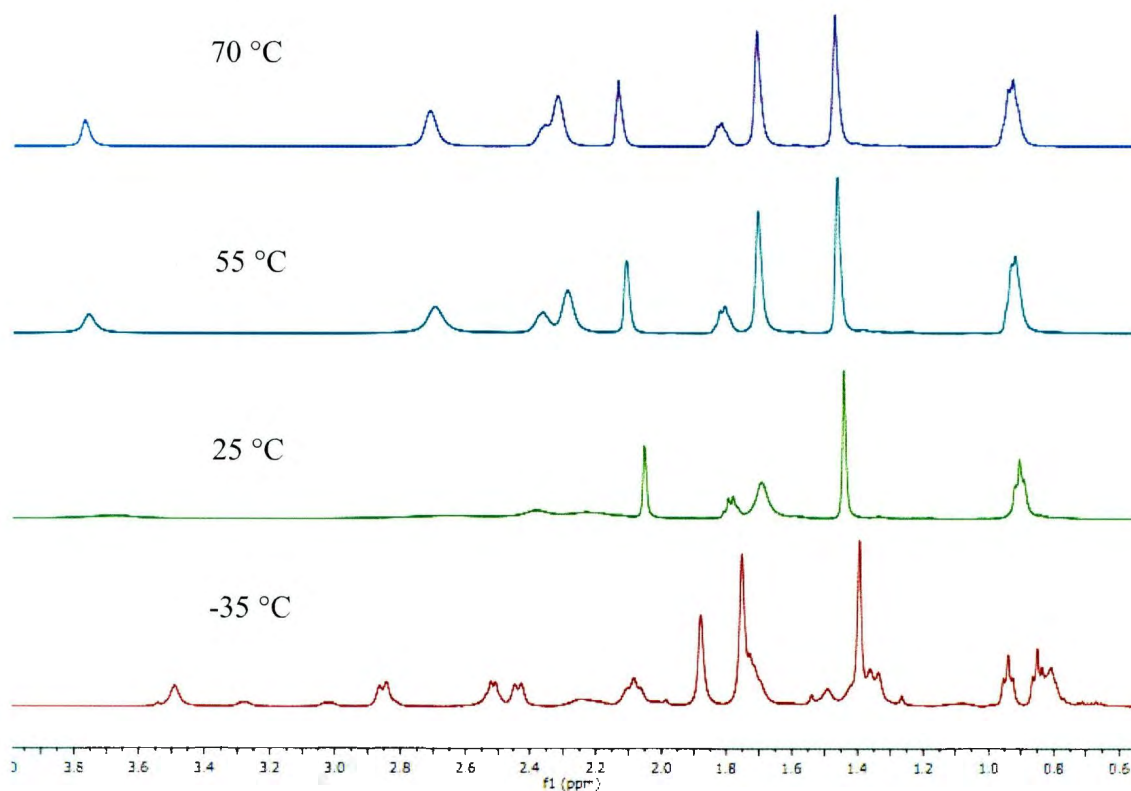


Figure 5.3. Variable temperature ^1H NMR spectrum of the methylene region of **5.3**

5.3 Polymerization Studies

5.3.1 Ring-Opening Polymerization of ϵ -Caprolactone

The ring opening polymerization (ROP) of ϵ -caprolactone (ϵ -CL) was performed using complexes **5.1**, **5.2** and **5.3** as catalysts in a toluene solution in the presence or absence of benzyl alcohol (BnOH). The complexes were highly reactive in the

polymerization of ϵ -caprolactone as summarized in Table 5.1. The choice of solvent was made by surveying the solvent effect on the ROP of ϵ -caprolactone using **5.1**, and it was observed that when tetrahydrofuran (THF) was used instead of toluene the ROPs proceeded slightly more slowly (Table 5.1, entries 1–3). This could be attributed to the coordinating nature of THF, which competes with the incoming monomer for coordination at the metal centre. The use of alcohols as activators has been reported to be necessary for ROPs of cyclic esters.^{2,4,6} In the current study, the polymerization time required in the absence of benzyl alcohol was longer than in the presence of benzyl alcohol as shown in Table 5.1, entries 9–18, 22–24. However, the reactions still proceeded. Theoretical number-average molecular weights (M_{ncal}) differed from the values obtained *via* GPC. Polydispersities increased with temperature (Table 5.1, entries 7, 8, 11, 12, 16, 17 and 21) and reaction time (Table 5.1, entries 6, 18, and 19). The polydispersity of all the polymerization reactions at or above 40 °C was high (>1.5), which suggests that transesterification had occurred. Also, it should be noted that the polydispersities are generally higher than those reported for poly(lactic acid) produced using lithium amine bis(phenolate) complexes.^{4,6}

Table 5.1. Polymerization of ϵ -CL using **5.1-5.3** in the presence and absence of BnOH^[a]

Entry	Complex	[CL] ₀ /[Li] ₀ /[BnOH] ₀	t/min	T/°C	Conv./% ^[c]	$M_{\text{ncal}}^{[d]}\times 10^3$	$M_n^{[e]}\times 10^3$	$M_w/M_n^{[e]}$
1	5.1	50/1/0 ^[b]	60	25	23.1	—	—	—
2	5.1	50/1/0 ^[b]	30	60	92.6	5.28	6.80	2.19
3	5.1	100/1/0 ^[b]	150	60	65.2	—	—	—
4	5.1	100/0/1	60	60	—	—	—	—
5	5.1	50/1/0	30	25	97.0	5.54	32.5	1.31
6	5.1	100/1/0	50	25	98.0	11.2	15.9	1.71
7	5.1	200/1/0	30	40	83.0	18.9	15.7	1.99
8	5.1	200/1/0	25	60	98.0	22.3	21.5	2.02
9	5.1	50/1/1	2	25	99.7	5.65	2.36	1.28
10	5.1	100/1/1	5	25	93.4	10.6	3.26	1.36
11	5.1	200/1/1	10	80	93.0	21.3	11.6	2.04
12	5.1	200/1/1	10	60	99.1	22.6	5.94	1.58
13	5.1	300/1/1	7	25	99.0	50.8	3.19	1.20
14	5.2	50/1/1	1	25	99.9	5.7	2.07	1.17
15	5.2	100/1/1	2	25	99.9	11.4	3.69	1.32
16	5.2	200/1/1	6	40	99.0	22.6	4.27	1.57
17	5.2	300/1/1	6	40	93.0	31.8	5.04	1.58
18	5.3	50/1/0	40	25	100	5.7	21.4	1.73
19	5.3	100/1/0	90	25	99.8	11.4	9.92	1.92
20	5.3	200/1/0	40	40	90.0	20.5	21.4	1.45
21	5.3	200/1/0	15	60	93.0	21.2	21.6	2.03
22	5.3	50/1/1	2	25	99.6	5.6	2.48	1.24
23	5.3	100/1/1	4	25	99.8	11.3	3.83	1.26
24	5.3	200/1/1	10	25	77.0	17.6	4.11	1.28

[a] Reactions performed in toluene using the mole ratios indicated at the temperature and for the time indicated above. [b] Reaction performed in THF. [c] Determined by ¹H NMR spectroscopy. [d] The M_{ncal} value of the polymer was calculated with $M_{\text{ncal}} = ([\epsilon\text{-CL}]_0/[\text{Li}]_0) \times 114.14$ (molar mass of $\epsilon\text{-CL}$) \times conv. %. [e] The M_n value was calculated according to $M_n = 0.56M_n^{\text{GPC}}$, where M_n^{GPC} was determined by GPC (chloroform), and is relative to polystyrene standards.

However, as it can be seen from Table 5.1, complex **5.3**, that contains the most sterically-demanding of the three ligands studied, in the presence of BnOH produces polymers with generally narrower polydispersity. This suggests that the polymerization reactions initiated by **5.3** proceeded in a more controlled fashion and that the ligand remains coordinated to the metal centre throughout the process.

It should also be noted that gelation was observed during the preliminary polymerization reactions. This led us to investigate the effects of monomer concentration (solvent volume) on the reactions. As one would expect, running the reaction at dilute monomer concentration levels lowered the rate of the reaction and afforded low conversions (Figure 5.4). A similar trend was also observed by Thibault and Fontaine.⁴²

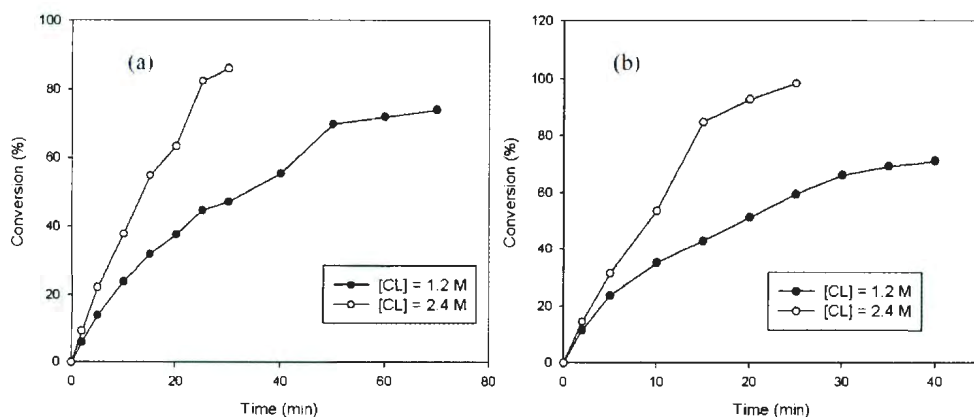


Figure 5.4. Effect of monomer concentration on the time of polymer conversion {Conditions: [5.1] = 17.7 mM in toluene, [ε-CL] = 1.2 M (●), [ε-CL] = 2.4 M (○)} at (a) 40 °C and (b) 60 °C.

5.3.2 Kinetic Studies of ϵ -Caprolactone Polymerization

In order to better understand the nature of these ϵ -caprolactone polymerizations, a series of reactions were conducted in toluene at ambient temperature for various monomer to lithium $[\text{CL}]/[\text{Li}]$ ratios. The conversion of ϵ -caprolactone was monitored by ^1H NMR analysis and semilogarithmic plots of $\ln([\text{CL}]_0/[\text{CL}]_t)$ versus time for two such polymerizations are shown in Figure 5.5. The plots revealed linear relationships in each case, indicating a first-order dependence of reaction rate on monomer concentration. In all semilogarithmic plots presented within this Chapter, $R \geq 0.98$. Data points for each line were obtained from a single experiment and if $R < 0.98$, the experiment was repeated with the aim of obtaining more accurate data. Deviations from linearity result from experimental error including catalyst decomposition and inhomogeneous heating of the reaction mixture.

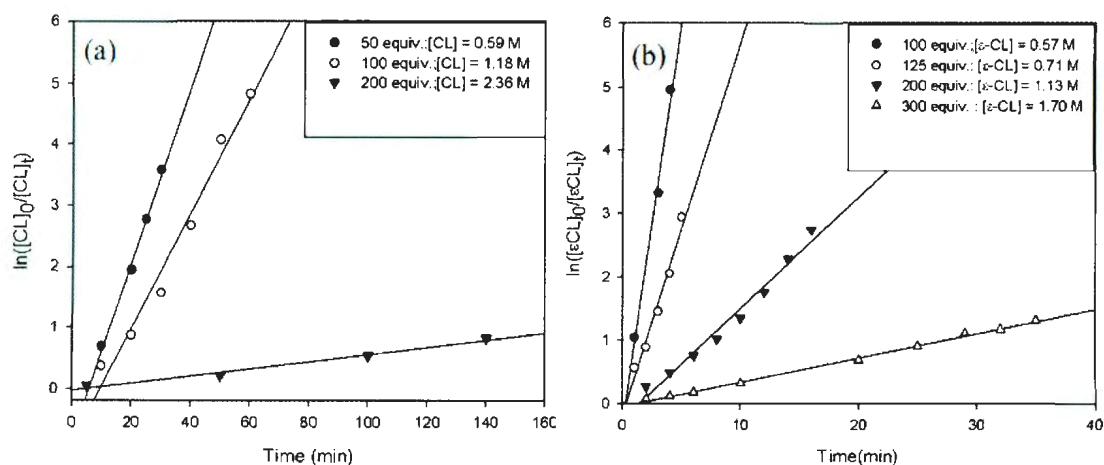


Figure 5.5. Semilogarithmic plots of $\ln([\epsilon\text{-CL}]_0/[\epsilon\text{-CL}]_t)$ vs time at different monomer molar ratios using: (a) **5.1**; $[\epsilon\text{-CL}]_0/[\mathbf{5.1}]_0 = 50$ (\bullet), 100 (\circ), 200 (\blacktriangledown); $[\mathbf{5.1}] = 17.7$ mM, 25 °C and (b) **5.3/BnOH**; $[\epsilon\text{-CL}]_0/[\mathbf{5.3/BnOH}]_0 = 100$ (\bullet), 125 (\circ), 200 (\blacktriangledown), 300 (\triangle), $[\mathbf{5.3/BnOH}]_0 = 17.7$ mM, 34 °C.

Further kinetic studies were carried out to determine the reaction rate (k_{obs}) and the effect of temperature at various reaction temperatures. It was observed that the overall polymerization rate increases with temperature (Figure 5.6). The semilogarithmic kinetic plots for ϵ -caprolactone polymerization using **5.1** and **5.1/BnOH** are depicted in Figure 5.6 and linear dependencies were found for $\ln[\epsilon\text{-CL}]_0/[\epsilon\text{-CL}]_t$ versus time for all polymerizations studied.

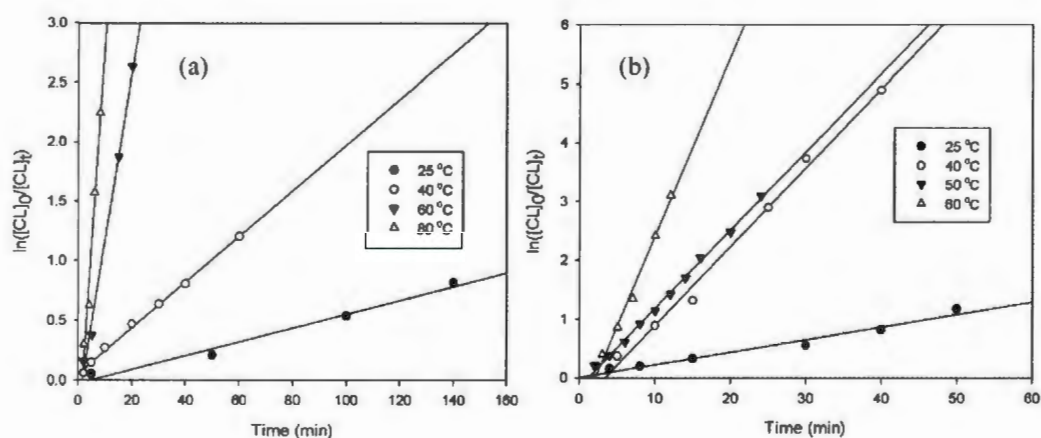


Figure 5.6. Semilogarithmic plots of $\ln[\epsilon\text{-CL}]_0/[\epsilon\text{-CL}]_t$ vs Time for the ROP of ϵ -CL at different temperatures using (a) **5.1**; $[\epsilon\text{-CL}]_0/[\mathbf{5.1}]_0 = 200$, ($[\mathbf{5.1}]_0 = 17.7$ mM, $[\epsilon\text{-CL}] = 1.18$ M); (●) = 25 °C, (○) = 40 °C, (▼) = 60 °C, (△) = 80 °C, and (b) **5.1/BnOH**; $[\epsilon\text{-CL}]_0/[\mathbf{5.1/BnOH}]_0 = 200$, ($[\mathbf{5.1}]_0 = 17.7$ mM, $[\epsilon\text{-CL}] = 1.18$ M); (●) = 25 °C, (○) = 40 °C, (▼) = 50 °C, (△) = 60 °C.

The values for the observed rate constant (k_{obs}) determined for **5.1** and **5.3** in the presence or absence of BnOH are summarized in Table 5.2 and are compared with values determined for various metal alkoxides. Unfortunately, for related amine-bis(phenolate) lithium complexes, and their activity in ROP of lactide and caprolactone, rate constants were not reported,^{4,6} and therefore, a direct comparison cannot be made. It can be seen that the fastest polymerization was observed for **5.3/BnOH**, which is twice that for

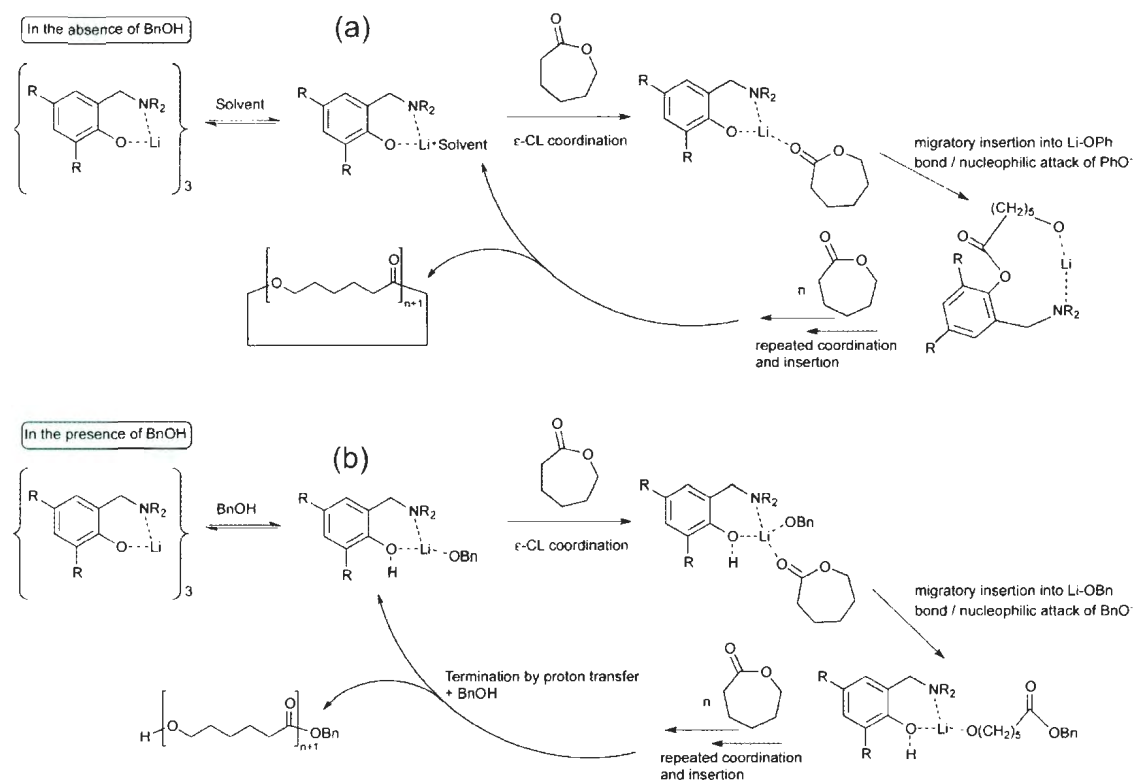
5.1/BnOH and lower than that of a yttrium phenolate complex (entry 5) and multi-metallic zinc species (entry 4), but is higher than that for the zinc, lanthanide and aluminum species (entries 1–3) shown in Table 5.2 for comparison.^{43–47} Solvent appears to have some impact on the reported rates in the literature with significantly higher rates for the reactions performed in CH₂Cl₂ (entries 4 and 5) compared with toluene. The rates for the reactions reported herein are therefore best compared with entries 1–3. It should be noted that the reactivity of 5.1–5.3 is compared with Al complexes of the same ligand in Chapter 4.

Table 5.2. A comparison of rate of constants for ϵ -CL polymerization by various metal alkoxides

Entry	Metal complex	Solvent	T/°C	k_{obs} /L mol ⁻¹ min ⁻¹	Ref
1	La(OTBP) ₃ ^[a]	Toluene	60	0.186	43
2	Me ₂ Al[O-2- ^t Bu-6{(C ₆ F ₅)N=CH}C ₆ H ₄]/BnOH	Toluene	50	0.028	44
3	Et ₂ AlO(CH ₂) ₃ CH=CH ₂	Toluene	0	0.16	45
4	[{(BDI-OMe)Zn(μ -OBn)} ₂ Zn(μ -OBn) ₂](RO) ₃ Y ^[b]	CH ₂ Cl ₂	25	97.2	46
5		CH ₂ Cl ₂	22	1.65	47
6	{Li[ONN ^{Me,tBu}]} ₃ (5.1)	Toluene	40	0.019	This work
7	{Li[ONN ^{Me,tBu}]} ₃ (5.1)/BnOH	Toluene	40	0.133	This work
8	{Li[ONN ^{tAm,tAm}]} ₃ (5.3)	Toluene	40	0.036	This work
9	{Li[ONN ^{tAm,tAm}]} ₃ (5.3)/BnOH	Toluene	40	0.273	This work

[a] lanthanum tris(4-*tert*-butylphenolate), [b] yttrium 2,6-di-*tert*-butylphenoxide and isopropanol.

The complexes used in entries 1–3 are known to perform ROP of lactones *via* coordination insertion mechanisms and the k_{obs} reported are of a similar order of magnitude to those seen in our studies. We propose that k_{obs} (entries 6 and 8) in the presence of BnOH were greater than in the absence of alcohol for two reasons. First, the resulting benzyl alkoxide group is a better nucleophile than the aryloxy ligand. This means that the ring-opening step (likely the rate-determining step) occurs more rapidly. Secondly, the presence of BnOH would assist in disassembly of Li-aggregates present in solution. As reaction rates are dependent on the ligand employed, the ligand must remain coordinated to the Li centre throughout the polymerization process, Scheme 5.2.



Scheme 5.2. Proposed mechanism for catalytic ROP of ϵ -CL using Li aminephenolate complexes. Ligand has been simplified for clarity. (a) in the absence of BnOH and (b) in the presence of BnOH.

An Arrhenius analysis showed that the relationship between the rate constants (k_{obs}) and the polymerization temperature was in good agreement with the Arrhenius equation. The activation energies (E_a) of ϵ -caprolactone polymerization by **5.1** and **5.3** in the absence and presence of BnOH were determined (Figure 5.7). Related reports of ROP reactions using lithium complexes could not be found in the literature and therefore, comparison is made with other discrete metal complexes used in ROP of ϵ -caprolactone. The value of E_a obtained for **5.1** in the absence of BnOH [$67.2 \pm 1.0 \text{ kJ mol}^{-1}$] is higher than those obtained for ROP of ϵ -caprolactone catalyzed by lanthanide tris-(4-*tert*-

butylphenolate) [51.9 kJ mol⁻¹],⁴³ scandium aryloxide [58.0 kJ mol⁻¹],⁴⁸ lanthanide tris(2,4,6-tri-*tert*-butylphenolate) [39.3 kJ mol⁻¹],⁴⁹ and titanium dialkanolateamine [48.5 kJ mol⁻¹].⁵⁰ However, in the presence of BnOH, the determined value [53.4 ± 4.1 kJ mol⁻¹] is similar to many of the values reported in the literature. The values determined for **5.3** in the absence of BnOH [56.8 ± 1.2 kJ mol⁻¹] and in the presence of BnOH [48.8 ± 4.0 kJ mol⁻¹] are lower than those determined for **5.1** and **5.1**/BnOH. Comparison of **5.1** and **5.3** using rate constants (Table 5.2) and activation energies indicate, under identical polymerization conditions, higher activity for **5.3** relative to **5.1**. These results indicate that changing the R substituents from *tert*-butyl (**5.1**) to the more sterically-demanding *tert*-amyl (**5.3**) enhanced the polymerization rate and lowered the activation energy of the ROP of ϵ -caprolactone. These data support the coordination of the aminephenol(ate) ligand to the metal centre throughout the polymerization process, Scheme 5.2. The lower E_a value for **5.3** might be indicative of easier dissociation of aggregated Li species in solution for the bulkier complexes but might also be the result of more electron rich Li centres for **5.3** compared with **5.1**.

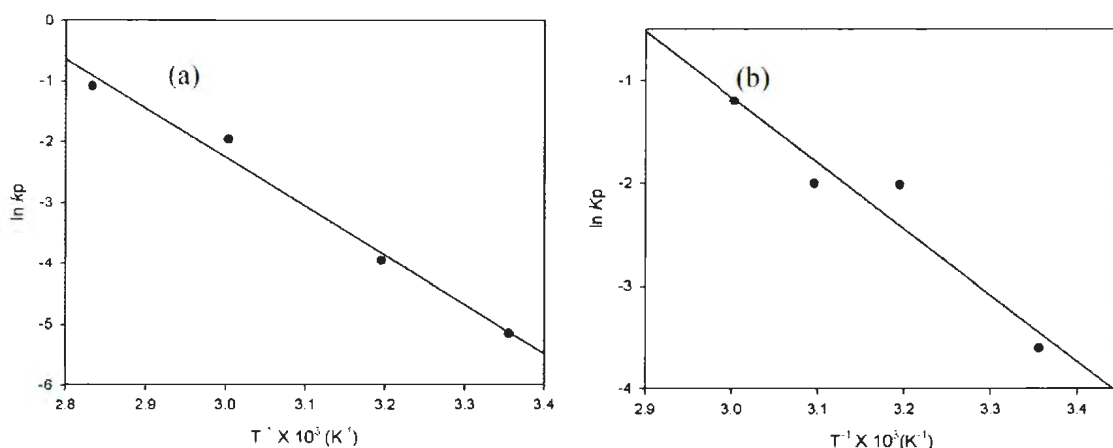


Figure 5.7. Arrhenius plots of $\ln(k_{\text{obs}})$ vs $1/T$ for the ROP of ϵ -CL using (a) $5.1:[5.1]_0 = 17.7 \text{ mM}$; $[CL]/[5.1] = 200$; $R = 0.9927$, $R^2 = 0.9855$, and (b) $5.1/\text{BnOH}$; $[5.1/\text{BnOH}]_0 = 17.7 \text{ mM}$; $[CL]/[5.1] = 200$; $R = 0.9609$, $R^2 = 0.9233$.

5.3.3 NMR Spectroscopy Analysis of Polycaprolactone

End-group analysis, by ^1H NMR spectroscopy, of the polymer obtained in the absence of BnOH shows typical polycaprolactone methylene proton signals at 1.38, 1.65, 2.31 and 4.06 ppm (Figure 5.8 (a)). However, no signals could be assigned to any end-group and this suggests that the polymers obtained were cyclic polycaprolactone (as shown in Scheme 5.2). Furthermore, the ^1H NMR spectrum of the polymers prepared in the presence of BnOH displayed characteristic signals of polycaprolactone methylene protons (c–f) (Figure 5.8 (b)). Alongside these were resonances at 7.35 ppm (a) and 5.12 ppm (b) assigned to the benzyl ester group, while the signal at 3.65 ppm corresponded to the hydroxymethylene ($-\text{CH}_2\text{OH}$) group (as shown in Scheme 5.2).

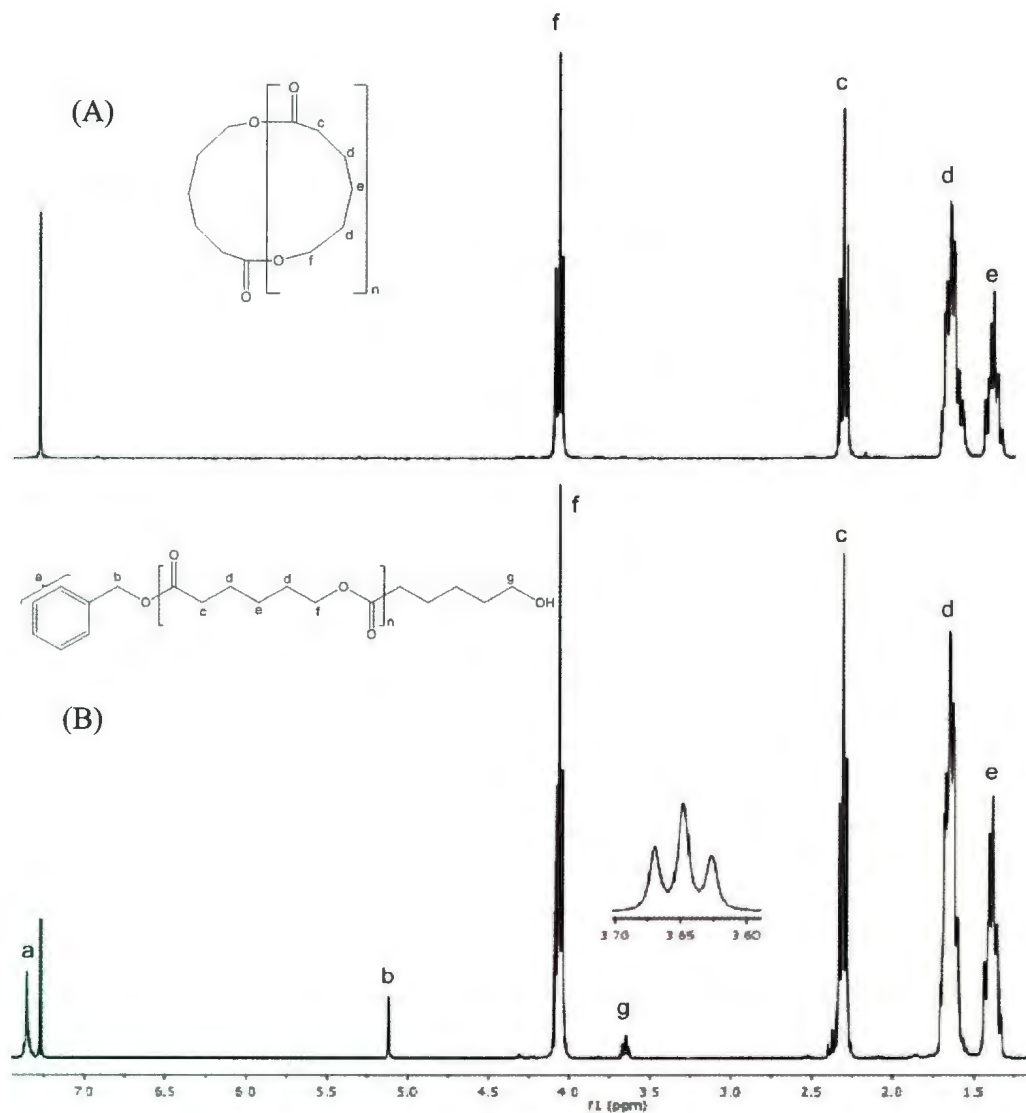


Figure 5.8. Typical ^1H NMR spectra of PCL synthesized with: (A) 5.3 (Table 5.1, entry 18) and (B) 5.2/BnOH (Table 5.1, entry 15).

^{13}C NMR analysis confirmed the end-group assignments with the resonances of CH_2OH and OCH_2Ph appearing at 62.65, 66.18 and 128.58 ppm respectively (Figure 5.9{B}). The signal assignments are in good agreement with previously reported results.⁵¹ The presence of terminal benzyloxy and hydroxyl groups indicates that the ring-opening

polymerization likely occurred through a coordination–insertion mechanism with the hydroxyl group introduced into the chain only at the termination stage. The proton could be transferred from the ligand (Scheme 5.2) or from the methanol used to quench the reaction.

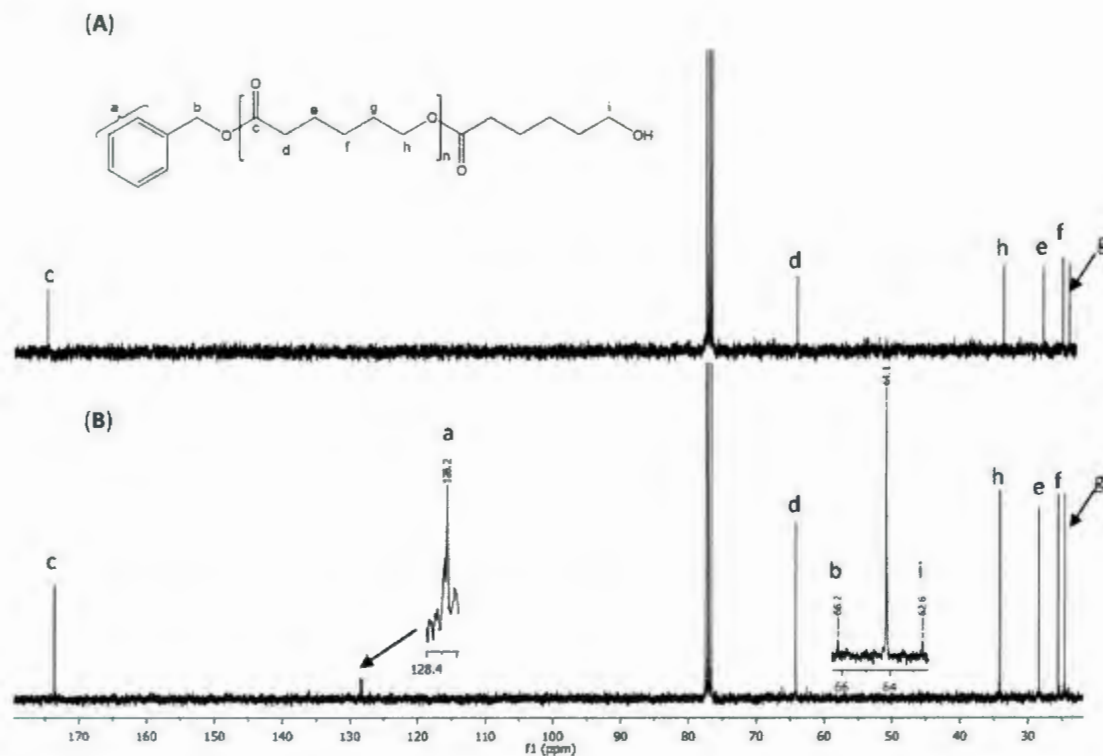


Figure 5.9. ^{13}C NMR spectra for PCL initiated by (A) **5.3** and (B) **5.2/BnOH**

5.3.4 MALDI-TOF MS Analysis

The MALDI-TOF mass spectrum of the polycaprolactone prepared using complex **5.3** in the absence of BnOH is shown in Figure 5.10 (Table 5.1, entry 18). Three series of signals can be distinguished from the spectrum. The first minor series of peaks starting at the m/z 1141.8, 1303.0 etc. were attributed to cyclic oligomers, while the second major series at the m/z of 1158.1, 1272.2, 1386.6 correspond to open chain oligomers with

hydroxy end group and the last minor peaks were assigned to cyclic oligomers clustered with Na^+ . The analysis of successive series shows that there is a difference of 114 in m/z between every neighbour in each series, which corresponds to the molecular weight of ϵ -caprolactone. It was also observed that successive peaks in the major series exhibit both even-membered and odd-membered oligomers. Interestingly, all the polymer samples obtained with **5.1**, **5.2** and **5.3** in the absence of BnOH showed similar series of species. It is well known that an odd–even distribution is a characteristic of intramolecular esterification (back-biting) reactions at long reaction times and at high conversion levels, and that this leads to the formation of cyclic oligomers.⁵² Therefore, the presence of the odd–even oligomers in the MALDI-TOF mass spectra indicate that transesterification occurred during the polymerization reactions reported herein.

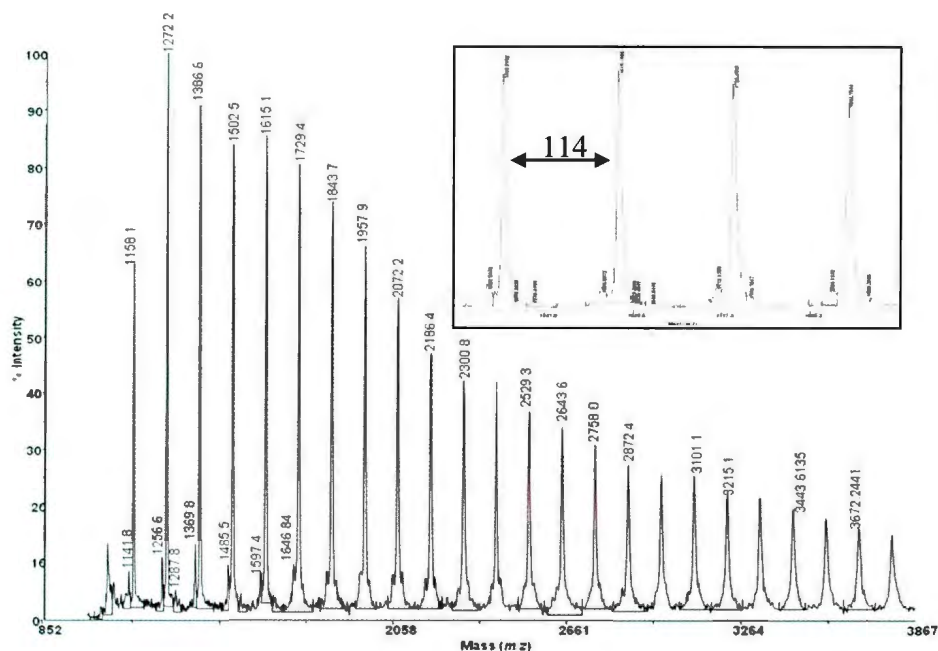


Figure 5.10. MALDI-TOF mass spectrum of PCL prepared using **5.3** in toluene at 40 °C, $[\text{CL}]/[\mathbf{5.3}] = 50$

Furthermore, the MALDI-TOF mass spectrum of the polymer prepared with **5.2** in the presence of BnOH as depicted in Figure 5.11 revealed the presence of four populations. Three minor peak populations of PCL with minimal intensity from the low m/z region of the spectrum were identified as related to macromolecules capped with (a) BnO group ($\text{BnO}\{\text{CL}\}_n\text{H}$), (b) clustered with Na^+ ($\text{BnO}\{\text{CL}\}_n\text{H}\text{Na}^+$) and (c) K^+ adducts ($\text{BnO}\{\text{CL}\}_n\text{H}\text{K}^+$) respectively. The main signals (most important signals) of the mass spectrum are separated by a caprolactone unit (114 g mol^{-1}) and correspond to polymer chain terminated with hydroxy and BnO end-groups, ($\text{BnO}\{\text{CL}\}_n\text{OH}$). The identification of PCL capped with BnO and hydroxyl end-groups as the main signals in the MALDI-TOF mass spectrum is in agreement with ^1H NMR analysis and confirms that the polymerization occurred through a coordination–insertion mechanism.

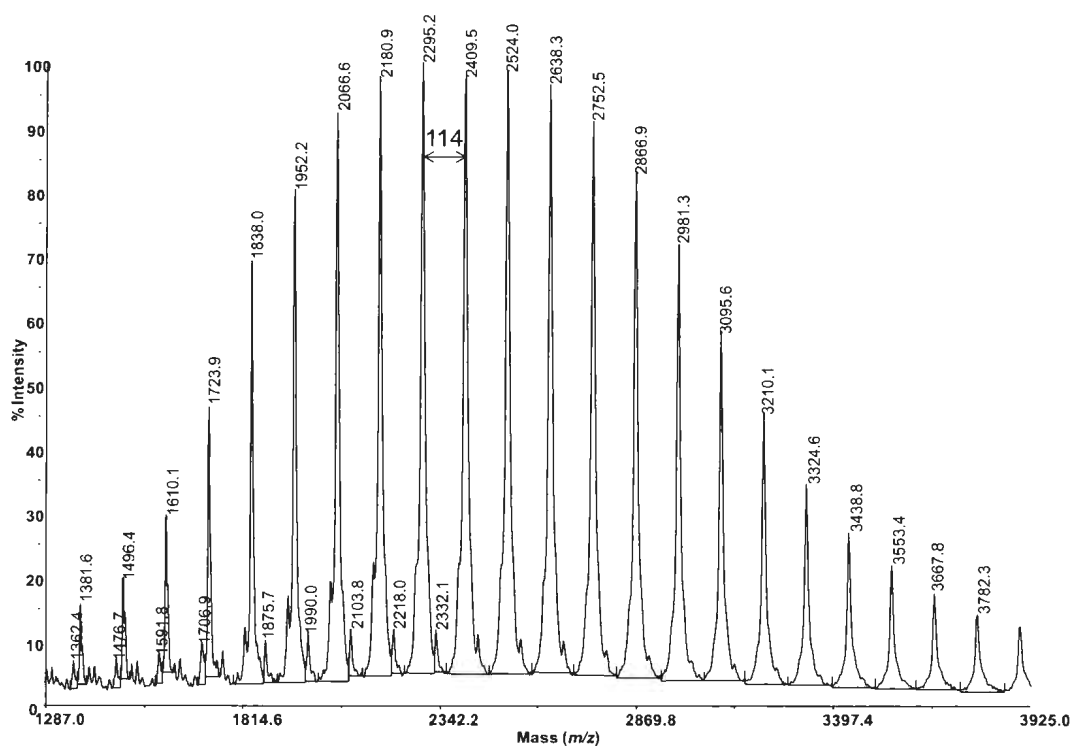


Figure 5.11. MALDI-TOF mass spectrum of PCL formed using **5.2**/BnOH at 25 °C

It is worth noting that even though the polydispersity seems not to be affected and remains fairly narrow in most cases, it can be seen that oligomers appear from the very start of the polymerization process, which is an indication of intermolecular transesterification. Dubois *et al.*⁵³ reported that the occurrence of inter- and intramolecular transesterification reactions can produce broadening of the polydispersity, a decrease in the average molecular weight and the appearance of a soluble low molecular weight fraction. This probably can explain the observed disparity in the calculated and experimental average molecular weight from both GPC and MALDI-TOF mass spectrometric data. MALDI-TOF mass spectra of polycaprolactone formed using Li-phenolate complexes have not been reported previously. Therefore, comparison was made with data reported using other metal complexes. In all the MALDI spectra of the polycaprolactone studied, the signals are similar to polymers obtained with tin(II) octoate or ammonium decamolybdate $(\text{NH}_4)_8[\text{Mo}_{10}\text{O}_{34}]$ in the presence of alcohol or water.⁵⁴⁻⁵⁶

5.4 Conclusions

Novel trimetallic lithium complexes supported by monoanionic piperazinyl aminephenolate ligands were synthesized and their structural features characterized by X-ray diffraction studies. Polymerization studies showed that the complexes could efficiently perform the ring-opening polymerization of ϵ -caprolactone. The results of kinetic studies revealed a first order dependence on monomer. Polymer end-group analysis by ^1H NMR, ^{13}C NMR and MALDI-TOF MS, when reactions had been conducted in the presence of BnOH, showed that the benzyloxy group was incorporated into the polycaprolactone growing chain. This supports the coordination–insertion

mechanism seen by others. In addition, polymerization in the absence of BnOH led to cyclic and open chain oligomer formation indicating that the ROPs were accompanied by transesterification reactions.

5.5 Experimental Section

5.5.1 General Considerations

All experiments involving metal complexes were performed under a nitrogen atmosphere using standard Schlenk and glovebox techniques. Solvents were distilled under nitrogen over sodium–benzophenone (THF, toluene, hexane) and degassed by freeze–vacuum–thaw cycles prior to use. Deuterated solvents (C_6D_6 , $CDCl_3$, C_5D_5N) were purchased from Cambridge Isotope Laboratories, Inc. and purified and dried before use. 2,4-di(*tert*-butyl)phenol, 2-*tert*-butyl-4-methylphenol, 2,4-di(*tert*-amyl) phenol, *n*-butyllithium and 1-methylpiperazine were purchased from Alfa Aesar. Elemental analyses were performed by Canadian Microanalytical Service Ltd., Delta, B.C. Canada. 1H and $^{13}C\{^1H\}$ NMR spectra were recorded on a Bruker Avance 500 or 300 MHz spectrometer at 25 °C (unless otherwise stated) and were referenced internally using the residual proton and ^{13}C resonances of the solvent. ^{13}C signals were assigned using HSQC experiments. 7Li NMR was recorded on a Bruker 300 MHz spectrometer and referenced externally to LiCl in D_2O . For the polymers, mass spectrometric measurements were performed using an Applied Biosystems 4800 TOF-TOF instrument and mass spectra were recorded in linear mode. 2-(4-Hydroxy-phenylazo)benzoic acid (HABA) was used as the matrix and purified tetrahydrofuran was used as the solvent for depositing analytes

onto the instrument's plate. GPC data were collected on a Viscotek GPCMax System equipped with a Refractive Index Detector (Phenogel 5 μ linear/mixed bed 300 \times 4.60 mm column in series with a Phenogel 5 μ , 100 \AA , 300 \times 4.60 mm column). Samples were run in chloroform at a concentration of 1 mg mL⁻¹ at 35 °C. The instrument was calibrated against polystyrene standards (Viscotek) to determine the molecular weights (M_n and M_w) and the polydispersity index (M_w/M_n) of the polymers. Conversions were determined by integration of the ϵ -methylene signals due to the residual ϵ -CL and poly-(ϵ -caprolactone).

5.5.2 Single Crystal X-ray Diffraction Studies

Crystals of **5.1** and **5.3** were mounted on low temperature diffraction loops and measured on a Rigaku Saturn CCD area detector with graphite monochromated Mo-K α radiation. Structures were solved by direct methods^{57,58} and expanded using Fourier techniques.⁵⁹ Neutral atom scattering factors were taken from Cromer and Waber.⁶⁰ Anomalous dispersion effects were included in F_{calc} ⁶¹ the values for $\Delta f'$ and $\Delta f''$ were those of Creagh and McAuley.⁶² The values for the mass attenuation coefficients are those of Creagh and Hubbell.⁶³ All calculations were performed using CrystalStructure^{64,65} except for refinement, which was performed using SHELXL-97.⁶⁶ Non-hydrogen atoms were refined anisotropically, unless otherwise indicated, while hydrogen atoms were introduced in calculated positions and refined on a riding model (Table 5.3). For **5.1**, the asymmetric unit contains a 1/6-occupancy methanol molecule adjacent to a special position. This molecule was refined isotropically, and the corresponding protons could not be located from difference maps, and were therefore omitted from the model. For **5.3**,

C(32A, 33–35 and 36A) (0.25 occupancy) and C(32B, 36B and 37–39) (0.75 occupancy) make up two parts of a disordered amyl group. Similarity restraints were applied to these disorder components, and sensible anisotropic convergence was achieved.

Table 5.3. Summary of crystal data for compounds **5.1** and **5.3**^a

Compounds	5.1	5.3
Formula	C _{51.50} H ₈₃ Li ₃ N ₆ O _{3.50}	C ₆₆ H ₁₁₁ Li ₃ N ₆ O ₃
Formula Weight	863.08	1057.46
Crystal System	Trigonal	Triclinic
Space Group	<i>R</i> -3	<i>P</i> -1
<i>a</i> /Å	19.315(2)	9.905(2)
<i>b</i> /Å	19.315(2)	18.234(5)
<i>c</i> /Å	24.872(3)	20.026(6)
α /°	90	107.574(3)
β /°	90	103.944(5)
γ /°	120	90.860(5)
<i>V</i> /Å ³	8036.0(17)	3331.4(15)
<i>T</i> /K	153	153
<i>Z</i>	6	2
<i>D</i> _c g cm ⁻³	1.070	1.054
<i>F</i> (000)	2826	1164
μ (MoK α)/cm ⁻¹	0.66	0.63
Total reflections	34847	32540
Unique reflections	3697	13769
<i>R</i> _{int}	0.0240	0.0313
Reflections <i>I</i> > 2 σ (<i>I</i>)	3630	11046
No. of parameters	198	749
<i>R</i> , <i>wR</i> ₂ [<i>I</i> > 2 σ (<i>I</i>)]	0.0589, 0.1677	0.1008, 0.2940
GOF	1.084	1.104

^aData in common: graphite-monochromated *via* Rigaku SHINE Optic Mo-K α radiation, $\lambda = 0.71073$ Å; $R_1 = \sum||F_o| - |F_c|| / \sum|F_o|$, $wR_2 = [\sum(w(F_o^2 - F_c^2)^2) / \sum w(F_o^2)^2]^{1/2}$ $w^{-1} = [\sigma^2(F_o^2) + (aP)^2]$, $P = [\text{Max}(F_o^2, 0) + 2(F_c^2)]/3$

5.5.3 Synthetic procedures

$\{\text{Li}[\text{ONN}^{\text{Me},\text{Bu}}]\}_3$ (**5.1**). A solution of *n*-butyllithium (6.50 mL, 10.0 mmol) in hexane was added dropwise to a stirred solution of [L1]H (2.5 g, 9.0 mmol) in THF (60.00 mL) at -78 °C. After stirring for 3 h, the solution was allowed to warm up to room temperature and stirred for a further 15 h. The solvent was then removed under vacuum to give a white residue. The residue was washed with cold pentane (20.00 mL), filtered and dried under vacuum to afford a white powder. Yield (2.46 g, 96.0%). Anal. calcd. for $\text{C}_{51}\text{H}_{81}\text{Li}_3\text{N}_6\text{O}_3$: C, 72.32; H, 9.64; N, 9.92. Found: C, 72.10; H, 10.08; N, 9.30%. ^1H NMR ($\text{C}_5\text{D}_5\text{N}$, 500 MHz, 348 K) δ 7.35 (1H, s, ArH), 7.00 (1H, s, ArH), 3.75 (2H, s, Ar-CH₂-N), 2.69 (4H, s, N-C₂H₄-C₂H₄-N), 2.45 (3H, s, N-CH₃), 2.30 (4H, s, N-C₂H₄-C₂H₄-N), 2.12 (3H, s, ArC-CH₃), 1.76 (9H, s, ArC-C{CH₃})₃. $^{13}\text{C}\{^1\text{H}\}$ NMR ($\text{C}_5\text{D}_5\text{N}$, 125 MHz, 298 K): δ 150.4 (ArC-O), 136.0 (ArC-C{CH₃})₃, 129.7 (ArCH), 128.9 (ArCH), 126.0 (ArC-CH₃), 124.0 (ArC-CH₂N), 63.5 (ArC-CH₂-N), 54.5 (N-C₂H₄-C₂H₄-N), 54.4 (N-C₂H₄-C₂H₄-N), 46.2 (N-CH₃), 35.8 (ArC-C{CH₃})₃, 31.0 (ArC-C{CH₃})₃, 21.5 (ArC-CH₃). ^7Li NMR ($\text{C}_5\text{D}_5\text{N}$, 116 MHz, 298 K) δ 8.27.

$\{\text{Li}[\text{ONN}^{\text{rBu},\text{Bu}}]\}_3$ (**5.2**). This compound was prepared in the same manner as described above for **5.1** with [L2]H (2.50 g, 7.85 mmol) and *n*-butyllithium (5.40 mL, 8.63 mmol) as starting materials. The product (2.30 g, 90.0%) was isolated as a white solid. Anal. calcd. for $\text{C}_{60}\text{H}_{99}\text{Li}_3\text{N}_6\text{O}_3$: C, 74.04; H, 10.25; N, 8.63. Found: C, 74.24; H, 10.04; N, 8.82%. ^1H NMR ($\text{C}_5\text{D}_5\text{N}$, 500 MHz, 328 K) δ 7.62 (1H, s, ArH), 7.14 (1H, s, ArH), 3.69 (2H, s, Ar-CH₂-N), 2.65 (4H, s, N-C₂H₄-C₂H₄-N), 2.30 (4H, s, N-C₂H₄-C₂H₄-N), 2.10 (3H, s, N-CH₃), 1.83 (9H, s, ArC-C{CH₃})₃, 1.52 (9H, s, ArC-C{CH₃})₃;

$^{13}\text{C}\{^1\text{H}\}$ NMR ($\text{C}_5\text{D}_5\text{N}$, 125 MHz, 298 K): δ 150.5 (ArC–O), 136.8 (ArC–C{CH₃}₃), 129.9 (ArC–C{CH₃}₃), 128.5 (ArCH), 127.6 (ArCH), 124.0(ArC–CH₂–N), 63.7 (ArC–CH₂–N), 54.5 (N–C₂H₄–C₂H₄–N), 54.4 (N–C₂H₄–C₂H₄–N), 46.2 (N–CH₃), 36.1(ArC–C{CH₃}₃), 34.3 (ArC–C{CH₃}₃), 32.7 (ArC–C{CH₃}₃), 31.0 (ArC–C{CH₃}₃). ^7Li NMR ($\text{C}_5\text{D}_5\text{N}$, 116 MHz, 298 K) δ 8.22.

$\{\text{Li}[\text{ONN}^{r\text{Am},r\text{Am}}]\}_3$ (**5.3**). This compound was prepared in the same manner as described above for **5.1** with [L3]H (2.80 g, 8.10 mmol) and *n*-butyllithium (5.60 mL, 8.90 mmol) as starting materials. The product (2.75 g, 97.0%) was obtained as a white solid. Anal. Calcd. for $\text{C}_{66}\text{H}_{111}\text{Li}_3\text{N}_6\text{O}_3$: C, 74.96; H, 10.58; N, 7.95. Found: C, 75.25; H, 10.38; N, 7.96%. ^1H NMR ($\text{C}_5\text{D}_5\text{N}$, 500 MHz, 328 K) δ 7.47 (1H, s, ArH), 7.15 (1H, s, ArH), 3.76 (2H, s, ArC–CH₂–N), 2.70 (4H, br, N–C₂H₄–C₂H₄–N), 2.37 (4H, br, N–C₂H₄–C₂H₄–N), 2.29 (2H, br, ArC–C{CH₂CH₃}), 2.11 (3H, s, N–CH₃), 1.82 (2H, br, ArC–C{CH₂CH₃}), 1.71 (6H, s, ArC–C{CH₃}₂), 1.47 (6H, s, ArC–C{CH₃}₂), 0.94 (3H, br, ArC–C{CH₂CH₃}), 0.85 (3H, br, ArC–C{CH₂CH₃}). $^{13}\text{C}\{^1\text{H}\}$ NMR ($\text{C}_5\text{D}_5\text{N}$, 125 MHz, 298 K): δ 150.5 (ArC–O), 135.0 (ArC–C{CH₂CH₃}), 128.4 (ArC–C{CH₂CH₃}), 126.1 (ArCH), 124.3(ArCH), 124.0 (ArC–CH₂–N), 63.1 (ArC–CH₂–N), 54.2(N–C₂H₄–C₂H₄–N), 54.1 (N–C₂H₄–C₂H₄–N), 46.2 (N–CH₃), 39.3 (ArC–C{CH₂CH₃}), 38.1 (ArC–C{CH₂CH₃}), 37.4 (ArC–C{CH₃}₂), 33.6 (ArC–C{CH₃}₂), 29.7 (ArC–C{CH₂CH₃}), 28.7 (ArC–C{CH₂CH₃}), 10.5 (ArC–C{CH₂CH₃}), 10.0 (ArC–C{CH₂CH₃}). ^7Li NMR ($\text{C}_5\text{D}_5\text{N}$, 116 MHz, 298 K) δ 8.19.

5.5.4 Polymerization Procedure

Typical Polymerization Procedure: All manipulations were performed under an inert atmosphere. The reaction mixtures were prepared in a glove box and subsequent operations were performed using standard Schlenk techniques.

A sealable Schlenk flask equipped with a stir bar was charged with a solution of complex 1 (10.0 mg, 35.4 μmol) in toluene (2.0 mL). Another Schlenk flask was charged with a toluene (6.0 mL) solution of ϵ -caprolactone (0.40 g, 3.54 mmol, 100 equiv.). The two flasks were then attached to a Schlenk line and temperature equilibration was ensured in both Schlenk flasks by stirring the solutions for 10 min in a temperature controlled oil bath. The complex solution was transferred to the monomer solution that was stirring rapidly and polymerization times were measured from that point. At appropriate time intervals, aliquots of the reaction mixture were removed using a pipette for determining monomer conversion by ^1H NMR spectroscopy. The reaction was quenched with methanol once near-quantitative conversion had been obtained. The polymer was precipitated with an excess of cold methanol. The polymer was isolated by filtration and dried under reduced pressure.

5.6 References

1. O. Wichmann, R. Sillanpää and A. Lehtonen, *Coord. Chem. Rev.*, **2012**, *256*, 371.
2. Y. Huang, Y.-H. Tsai, W.-C. Hung, C.-S. Lin, W. Wang, J.-H. Huang, S. Dutta, and C.-C. Lin, *Inorg. Chem.*, **2010**, *49*, 9416.
3. L. Wang, X. Pan, L. Yao, N. Tang, and J. Wu, *Eur. J. Inorg. Chem.*, **2011**, 632.
4. C.-A. Huang and C.-T. Chen, *Dalton Trans.*, **2007**, 5561.
5. F. M. Kerton, C. M. Kozak, K. Luttgen, C. E. Willans, R. J. Webster and A. C. Whitwood, *Inorg. Chim. Acta.*, **2006**, 2819.
6. C.-A. Huang, C.-L. Ho and C.-T. Chen, *Dalton Trans.*, **2008**, 3502.
7. B. Ko and C. Lin, *J. Am. Chem. Soc.*, **2001**, *123*, 7973.
8. J. Ejfler, K. Krauzy-Dziedzic, S. Szafert, L. B. Jerzykiewicz and P. Sobota, *Eur. J. Inorg. Chem.*, **2010**, 3602.
9. X. Zhang, T. J. Emge and K. C. Hultsch, *Organometallics*, **2010**, *29*, 5871.
10. A. D. Schofield, M. L. Barros, M. G. Cushion, A. D. Schwarz and P. Mountford, *Dalton Trans.*, **2009**, 85.
11. W.-C. Hung and C.-C. Lin, *Inorg. Chem.*, **2009**, *48*, 728.
12. L. E. Breyfogle, C. K. Williams, J. V. G. Young, M. A. Hillmyer and W. B. Tolman, *Dalton Trans.*, **2006**, 928.
13. E. L. Marshall, V. C. Gibson and H. S. Rzepa, *J. Am. Chem. Soc.*, **2005**, *127*, 6048.
14. Y. Sarazin, V. Poirier, T. Roisnel and J.-F. Carpentier, *Eur. J. Inorg. Chem.*, **2010**, 3423.
15. D. J. Darensbourg, W. Choi, O. Karroonnirun and N. Bhuvanesh, *Macromolecules*, **2008**, *41*, 3493.
16. H. E. Dyer, S. Huijser, A. D. Schwarz, C. Wang, R. Duchateau and P. Mountford, *Dalton Trans.*, **2008**, 32.
17. A. Amgoune, C. M. Thomas and J. Carpentier, *Macromol. Rapid Commun.*, **2007**, *28*, 693.

18. N. Ikpo, L. N. Saunders, J. L. Walsh, J. M. B. Smith, L. N. Dawe and F. M. Kerton, *Eur. J. Inorg. Chem.*, **2011**, 5347.
19. V. Poirier, T. Roisnel, J. Carpentier and Y. Sarazin, *Dalton Trans.*, **2011**, 40, 523.
20. L. Wang and H. Ma, *Dalton Trans.*, **2010**, 39, 7897.
21. G. Labourdette, D. J. Lee, B. O. Patrick, M. B. Ezhova and P. Mehrkhodavandi, *Organometallics*, **2009**, 28, 1309.
22. J. D. Farwell, P. B. Hitchcock, M. F. Lappert, G. A. Luinstra, A. V. Protchenko and X. Wei, *J. Organomet. Chem.*, **2008**, 693, 1861.
23. J. Ejfler, S. Szafert, K. Mierzwicki, L. B. Jerzykiewicz and P. Sobota, *Dalton Trans.*, **2008**, 6556.
24. D. J. Doyle, V. C. Gibson and A. J. P. White, *Dalton Trans.*, **2007**, 358.
25. C. K. Williams, L. E. Breyfogle, S. K. Choi, W. Nam, V. G. Young, M. A. Hillmyer and W. B. Tolman, *J. Am. Chem. Soc.*, **2003**, 125, 11350.
26. C. K. Williams, N. R. Brooks, M. A. Hillmyer and W. B. Tolman, *Chem. Commun.*, **2002**, 2132.
27. M. H. Chisholm, J. C. Gallucci, H. Zhen and J. C. Huffman, *Inorg. Chem.*, **2001**, 40, 5051.
28. M. H. Chisholm and Z. P. Zhou, *J. Mater. Chem.*, **2004**, 14, 3081.
29. J. Lewinski, P. Horeglad, M. Dranka and I. Justyniak, *Inorg. Chem.* **2004**, 43, 5789.
30. J.-T. Issenhuth, J. Pluvinage, R. Welter, S. Bellemin-Laponnaz, and S. Dagorne, *Eur. J. Inorg. Chem.*, **2009**, 4701.
31. S. Gendler, S. Segal, I. Goldberg, Z. Goldschmidt and M. Kol, *Inorg. Chem.*, **2006**, 45, 4783.
32. S. Groysman, E. Sergeeva, I. Goldberg and M. Kol, *Inorg. Chem.*, **2005**, 44, 8188.
33. L. M. Broomfield, Y. Sarazin, J. A. Wright, D. L. Hughes, W. Clegg, R. W. Harrington and M. Bochmann, *J. Organomet. Chem.*, **2007**, 692, 4603.

34. Z. Janas, T. Nerkowski, E. Kober, L. B. Jerzykiewicz and T. Lis, *Dalton Trans.*, **2012**, *41*, 442.
35. R. K. Dean, S. L. Granville, L. N. Dawe, A. Decken, K. M. Hattenhauer and C. M. Kozak, *Dalton Trans.*, **2010**, *39*, 548.
36. W. Clegg, M. G. Davidson, D. V. Graham, G. Griffen, M. D. Jones, A. R. Kennedy, C. T. O'Hara, L. Russoa and C. M. Thomson, *Dalton Trans.*, **2008**, 1295.
37. D. J. MacDougall, B.C. Noll, A. R. Kennedy and K. W. Henderson, *Dalton Trans.*, **2006**, 1875.
38. M. L. Cole, P. C. Junk, K. M. Proctor, J. L. Scott and C. R. Strauss, *Dalton Trans.*, **2006**, 3338.
39. P. A. van der Schaaf, M. P. Hogerheide, D. M. Grove, A. L. Spek and G. van Koten, *J. Chem. Soc., Chem. Commun.*, **1992**, 1703.
40. T. J. Boyle, D. M. Pedrotty, T. M. Alam, S. C. Vick and M. A. Rodriguez, *Inorg. Chem.*, **2000**, *39*, 5133.
41. J. S. Vilaro, P. E. Fanwick and I. P. Rothwell, *Polyhedron*, **1998**, *17*, 769.
42. M.-H. Thibault and F.-G. Fontaine, *Dalton Trans.*, **2010**, *39*, 5688.
43. C. Yu, L. Zhang and Z. Shen, *Eur. Polym. J.*, **2003**, *39*, 2035.
44. N. Iwasa, S. Katao, J. Liu, M. Fujiki, Y. Furukawa, and K. Nomura, *Organometallics*, **2009**, *28*, 2179.
45. Ph. Dubois, N. Ropson, R. Jerome, and Ph. Teyssie, *Macromolecules*, **1996**, *29*, 1965.
46. H.-Y. Chen, B.-H. Huang, and C.-C. Lin, *Macromolecules*, **2005**, *38*, 5400.
47. W. M. Stevels, M. J. K. Ankone, P. J. Dijkstra, and J. Feijen, *Macromolecules*, **1996**, *29*, 8296.
48. W. Zhu, J. Ling and Z. Shen, *Polymer Bulletin*, **2004**, *52*, 185.
49. L. Zhang, Y. Niu, Y. Wang, P. Wang and L. Shen, *J. Mol. Catal. A: Chem.*, **2008**, *287*, 1.

50. Y. A. Piskun, I. V. Vasilenko, S. V. Kostjuk, K. V. Zaitsev, G. S. Zaitseva and S. S. Karlov, *J. Polym. Sci., Part A: Polym. Chem.*, **2010**, *48*, 1230.
51. W. Yao, Y. Mu, A. Gao, Q. Su, Y. Liu, and Y. Zhang, *Polymer*, **2008**, *49*, 2486.
52. A. Kowalski, A. Duda, and S. Penczek, *Macromolecules*, **2000**, *33*, 689.
53. Ph. Dubois, R. Jacobs and R. Jerome, *Macromolecules*, **1991**, *24*, 2266.
54. A. Kowalski, A. Duda, and S. Penczek, *Macromolecules*, **2000**, *33*, 689.
55. M. Sobczak and W. Kolodziejcki, *Molecules*, **2009**, *14*, 621.
56. J. E. Baez, A. M.-Richa and A. M.-Fernandez, *Macromolecules*, **2005**, *38*, 1599.
57. SHELX97: G.M. Sheldrick, *Acta Cryst.*, **2008**, *A64*, 112.
58. SIR92: A. Altomare, G. Cascarano, C. Giacovazzo, A. Guagliardi, M. Burla, G. Polidori, and M. Camalli, *J. Appl. Cryst.*, **1994**, *27*, 435.
59. DIRDIF99: P.T. Beurskens, G. Admiraal, G. Beurskens, W. P. Bosman, R. de Gelder, R. Israel and J. M. M. Smits, *The DIRDIF-99 program system*, Crystallography Laboratory, University of Nijmegen, The Netherlands, **1999**.
60. D. T. Cromer and J. T. Waber, *International Tables for X-ray Crystallography*, The Kynoch Press, Birmingham, England, **1974**, Vol. IV, Table 2.2 A.
61. J. A. Ibers and W.C. Hamilton, *Acta Cryst.*, **1964**, *17*, 781.
62. D. C. Creagh and W. J. McAuley, *International Tables for Crystallography*, ed. A. J. C. Wilson, Kluwer Academic Publishers, Boston, **1992**, Vol C, Table 4.2.6.8, pp 219.
63. D. C. Creagh and J. H. Hubbell, *International Tables for Crystallography*, ed. A. J. C. Wilson, Kluwer Academic Publishers, Boston, **1992**, Vol C, Table 4.2.4.3, pp 200.
64. CrystalStructure 3.7.0: Crystal Structure Analysis Package, Rigaku and Rigaku/MSO (2000-2005). 9009 New Trails Dr. The Woodlands TX 77381 USA.
65. CRYSTALS Issue 10: D. J. Watkin, C. K. Prout, J. R. Carruthers and P. W. Betteridge, Chemical Crystallography Laboratory, Oxford, UK., **1996**.
66. A. L. Spek, *J. Appl. Cryst.*, **2003**, *36*, 7-13.

CHAPTER 6

Synthesis and Structure of Lithium, Titanium, Zirconium and Zinc Aminephenolate Complexes

Chapter 6

Synthesis and Structure of Lithium, Titanium, Zirconium and Zinc Aminephenolate Complexes

6.1 Introduction

In this chapter, some coordination chemistry of a range of metals with amine-phenolate ligands is presented and provides scope for future investigations within the Kerton research group. As discussed in Chapter 1, Group IV metal phenolates are attracting a great deal of interest in several fields. For example, they can be used for oxidation catalysis¹ and in the ring-opening polymerization (ROP) of cyclic esters, such as ϵ -caprolactone and lactides.^{2,3} Structures of several Group IV amine-phenolate complexes have been reported; most pertinent to this particular study are those stabilized by tetradentate amine mono(phenolate) ligands bearing two side arm donors reported by Kol *et al.*⁴ However, these reported Group IV complexes are supported by tridentate or tetradentate ligands whereas bidentate piperazinyl base analogues are very rare.⁵⁻⁸ Furthermore, a literature search for lithium aggregates shows that various types of aggregation have been found in the solid state, but tetrameric Li_4O_4 cubane or ladder and Li_2O_2 ring dimers are the most common motifs.⁹⁻¹³ Although multimeric ladder structures have been proposed, structurally characterized hexametallc ladder complexes are rare in lithium amine-phenolate chemistry.^{14,15}

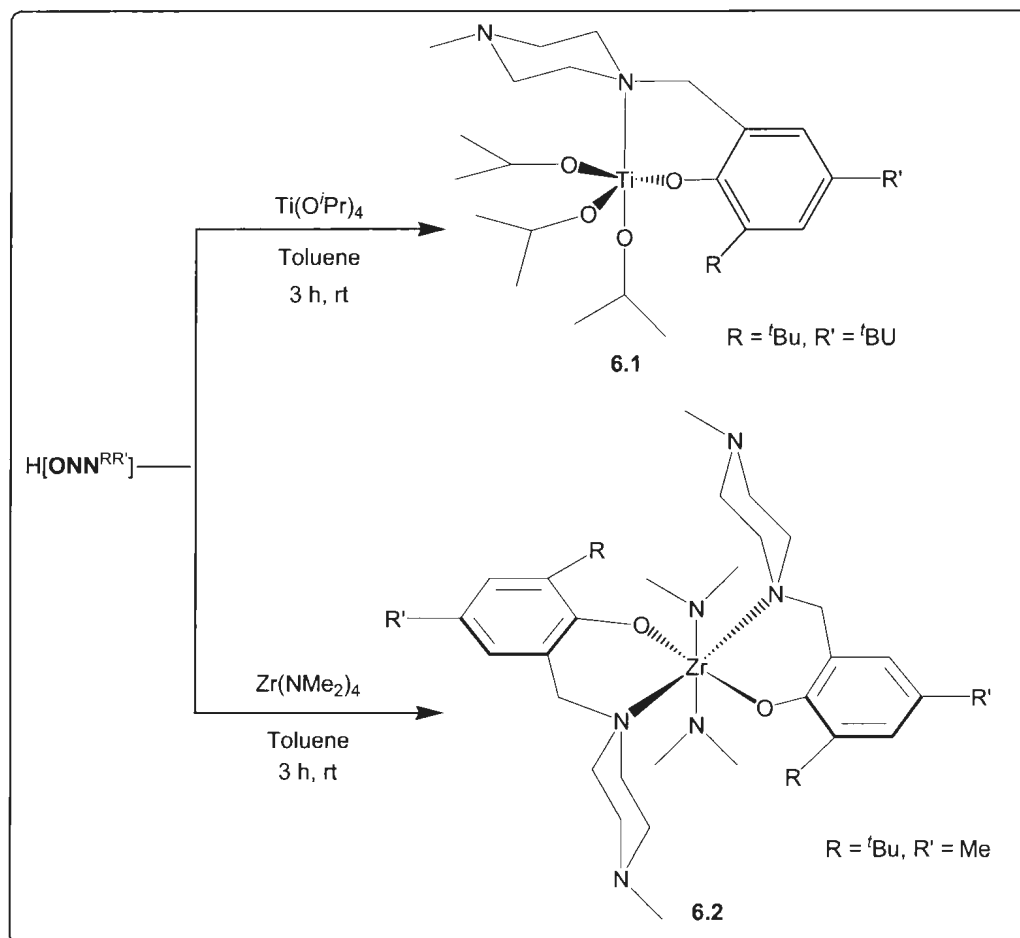
During the past two decades, weakly coordinating anions have been shown to play a vital role in the generation of reactive cationic complexes, and, among these anions, tetrakis{3,5-bis(trifluoromethyl)phenyl}borate anion has been recognised as an extremely important species. The growing interest in these weakly coordinating anions is a result of their stability toward oxidation and acidic media.^{16,17} Group IV metal complexes, associated with weakly coordinating anions, successfully mediated the polymerization of α -olefins.¹⁸⁻²⁰ A growing interest in cationic metal complexes as alternative catalysts has emerged in the development of discrete initiators for controlled ROP of cyclic esters. Thus, a series of well-defined cationic zinc complexes have been reported in the literature.²¹⁻²⁵ As part of studies targeted at developing zinc-based catalysts for the ROP of cyclic esters, cationic zinc complexes bearing piperazinyl-phenolate ligands have been prepared and characterized in this chapter.

6.2 Results and Discussion

6.2.1 Synthesis of amine-phenolate titanium alkoxide

The amine-mono(phenolate) titanium complex **6.1** was prepared in high yield as shown in Scheme 6.1, using a similar method method to that used by Kol and co-workers to prepare amine-bis(phenolate) Ti complexes.²⁶ The structure of the complex was established by ¹H NMR spectroscopy and its structural features confirmed by X-ray crystallography. The ¹H NMR spectrum of **6.1** in C₆D₆ at room temperature exhibits a doublet and septet resonances at 1.33 and 4.99 ppm, respectively, which corresponded to the methine and two methyl groups of the isopropoxide ligands coordinated to the metal

centre. The methylene groups ($\text{NCH}_2\text{CH}_2\text{N}$) of the piperaziny unit appeared as broad resonances at 2.25 and 3.23 ppm, while that of ($\text{ArCH}_2\text{-N}$) appeared as a sharp singlet at 4.06 ppm.



Scheme 6.1. Synthetic procedure for the synthesis of amine-phenolate titanium and zirconium complexes.

X-ray quality single crystals were grown from a saturated toluene/hexane solution at $-35\text{ }^\circ\text{C}$. The molecular structure is shown in Figure 6.1 with some selected bond lengths and angles. The complex is monomeric with a distorted trigonal bipyramidal Ti centre

($\tau = 0.87$)²⁷ bound by one phenolate ligand. The Ti ion is coordinated at the equatorial sites by the O atom of the phenolate ligand and two O atoms of OⁱPr groups. The axial positions are occupied by an OⁱPr oxygen and a N atom of the ligand. The Ti ion is located 0.26 Å above the plane of O(1)-O(2)-O(4) and the bond angles at Ti sum to 354.14°, indicating a deviation from a perfect trigonal equatorial plane by 5.86°. The Ti-O (1.797-1.8631 Å) and Ti-N (2.372 Å) bond distances are comparable to those in other reported Ti(IV) alkoxide complexes.^{28,29} Table 6.3 summarizes structural data for all the complexes reported in this Chapter.

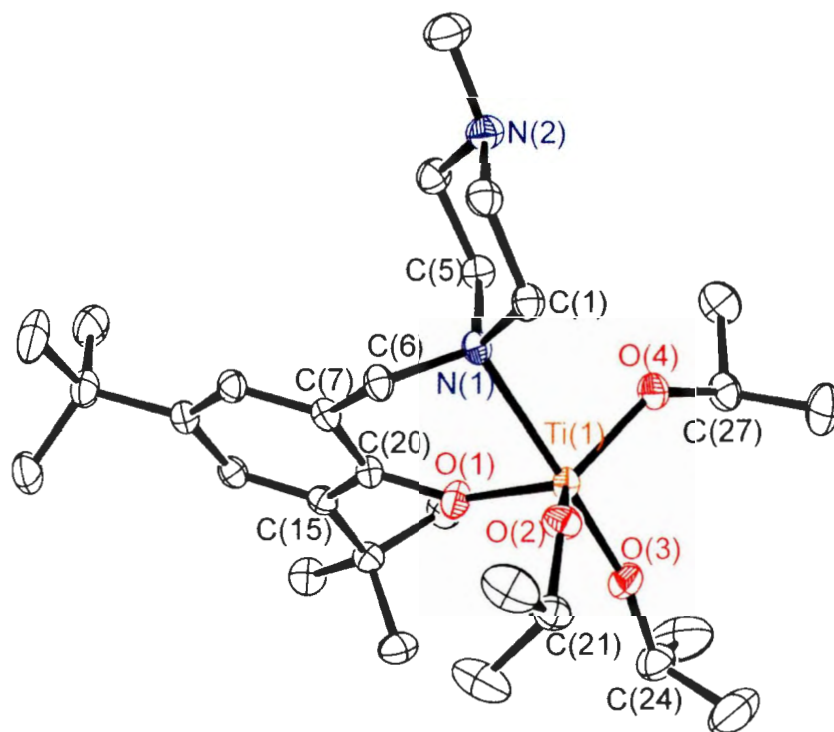


Figure 6.1. Molecular structure of **6.1** (50% displacement ellipsoids; H atoms excluded for clarity). Bond lengths (Å) and bond angles (°): Ti(1)-O(3), 1.7897(13); Ti(1)-O(2), 1.8111(12); Ti(1)-O(4), 1.8351(12); Ti(1)-O(1), 1.8631(12); Ti(1)-N(1), 2.3712(16); O(3)-Ti(1)-O(2), 101.51(5); O(3)-Ti(1)-O(4), 98.05(5); O(2)-Ti(1)-O(4), 116.06(5); O(3)-Ti(1)-O(1), 94.89(5); O(2)-Ti(1)-O(1), 116.24(5); O(4)-Ti(1)-O(1), 121.84(6); O(3)-Ti(1)-N(1), 174.04(4); O(2)-Ti(1)-N(1), 83.803(5); O(4)-Ti(1)-N(1), 81.77(5); O(1)-Ti(1)-N(1), 80.26(5).

6.2.2 Synthesis of Amine-Phenolate Zirconium Amide Complex

The treatment of $\text{Zr}(\text{NMe}_2)_4$ with 1 equiv. of the corresponding ligand gave the zirconium amine phenolate complex **6.2** as a white solid (Scheme 6.1). Single crystals of **6.2** could be grown by slow evaporation and cooling of a saturated toluene/pentane solution. The molecular structure of **6.2** is shown in Figure 6.2 with salient bond distances and angles. The structure consists of a Zr centre bound by two phenolate ligands in a near perfect octahedral geometry, as most *trans* L-Zr-L angles are close to 180° . In the view shown in Figure 6.2, the equatorial positions contain two *trans* phenolato O atoms and two *trans* piperazinyl N atoms, while the axial positions are occupied by the amido donors. The equatorial *cis* angles range from $81.70(7)^\circ$ to $99.25(25)^\circ$. The most narrow angles O(2)-Zr(1)-N(3) and O(1)-Zr(1)-N(1) are associated with the bite of the C_3NZrO six-membered chelate ring. C(6) and C(23) are off the mean plane of C(17)-C(7)-N(1)-O(1)-Zr(1) and C(34)-C(24)-N(3)-O(2)-Zr(1) by 0.72 \AA and 0.69 \AA , respectively, thereby inducing a “legless” chair conformation in each ring. The bond lengths around Zr lie within the ranges for related zirconium complexes.^{4,26,30}

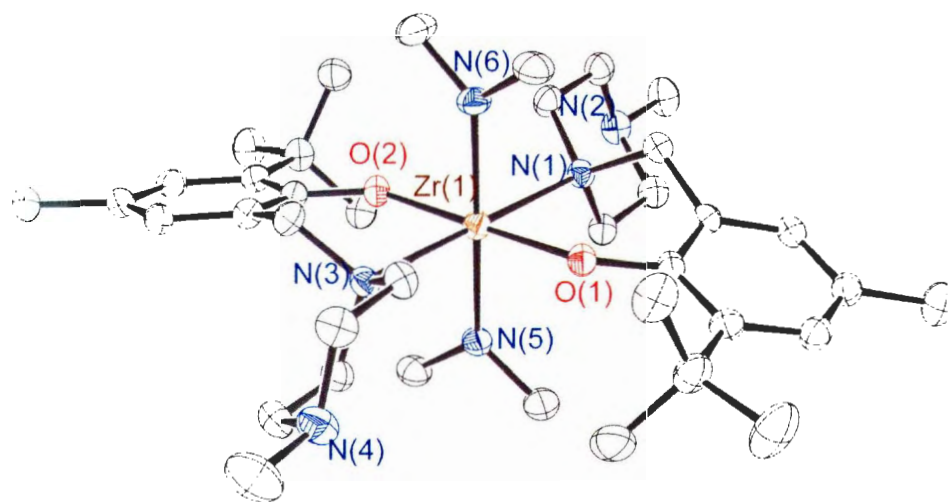
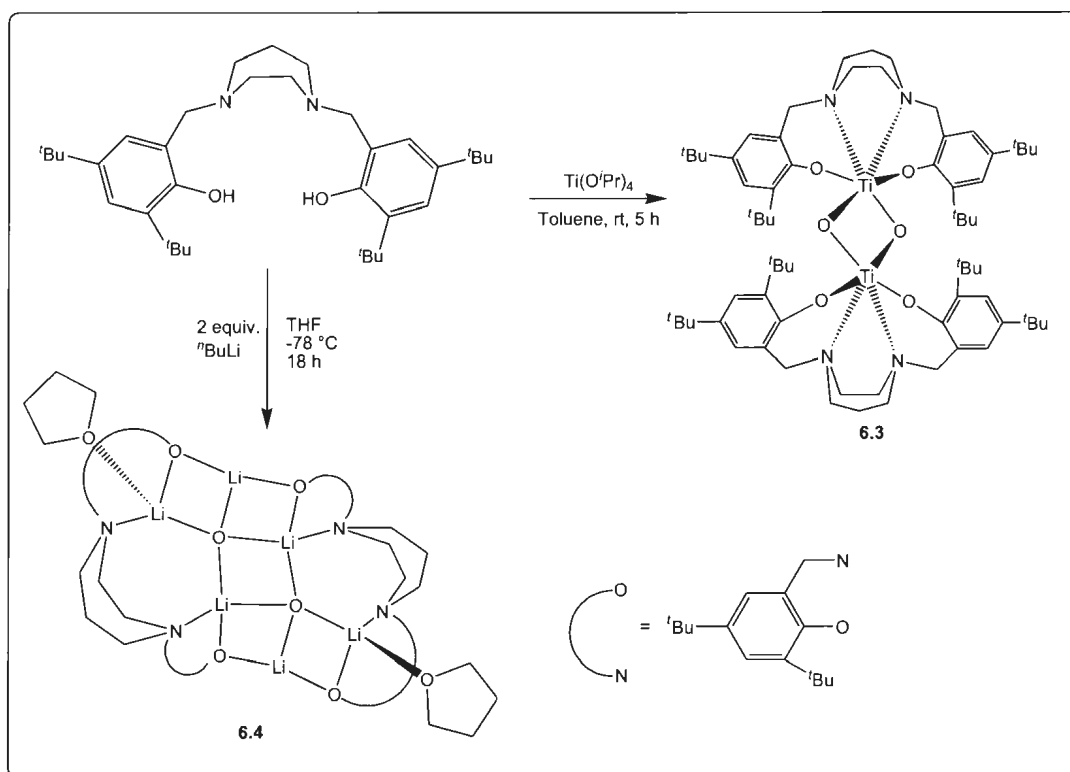


Figure 6.2. Molecular structure of **6.2** (50% displacement ellipsoids; H atoms excluded for clarity). Bond lengths (Å) and bond angles (°): Zr(1)-O(2), 2.0260(17); Zr(1)-O(1), 2.0409(17); Zr(1)-N(5), 2.128(2); Zr(1)-N(6), 2.150(2); Zr(1)-N(3), 2.431(2); Zr(1)-N(1), 2.434(2); O(2)-Zr(1)-O(1), 176.61(7); O(2)-Zr(1)-N(5), 90.68(8); O(1)-Zr(1)-N(5), 91.79(8); O(2)-Zr(1)-N(6), 88.51(8); O(1)-Zr(1)-N(6), 88.99(8); N(5)-Zr(1)-N(6), 179.08(8); O(2)-Zr(1)-N(3), 81.70(7); O(1)-Zr(1)-N(3), 96.02(7); N(5)-Zr(1)-N(3), 89.36(8); N(6)-Zr(1)-N(3), 90.07(8); O(2)-Zr(1)-N(1), 99.25(7); O(1)-Zr(1)-N(1), 83.01(7); N(5)-Zr(1)-N(1), 91.35(8); N(6)-Zr(1)-N(1), 89.23(8); N(3)-Zr(1)-N(1), 178.81(6).

6.2.3 Synthesis of Amine-Bis(phenolate) Titanium Complex

The 1:1 stoichiometric reaction of 2,2'-*N,N*-homopiperaziny-bis(2-methylene-4,6-*tert*-butyl-phenol){[L11]H₂} with [Ti(OiPr)₄], after workup gave **6.3** as a yellow precipitate in high isolated yield, as shown in Scheme 6.2. The composition of the complex was confirmed by elemental analysis and X-ray structure determination. During the course of these studies, it was discovered that Baldamus *et al.*,³¹ had independently reported the structure of compound **6.3**, however, there is difference in terms of solvent contents between the structures.



Scheme 6.2. Synthetic procedure for Ti and Li amine-bis(phenolate) complexes

The ORTEP diagram of complex **6.3**, shown in Figure 6.3, reveals a bimetallic Ti complex with highly distorted six-coordinate geometry at the Ti(1) site. Each Ti is coordinated to two phenolate oxygen atoms [O(1) and O(2)], two nitrogen atoms [N(1) and N(2)] from the ligand backbone and two bridging oxygen atoms [O(3)], leading to a planar Ti_2O_2 core (sum of the internal core angles is 360.0°). Ti-L (L = ligand) bond distances range from 1.8452(15) - 2.3365(18) Å (Table 6.1), while the juxtaposed L-Ti-L angles deviate significantly from the expected octahedral values of 180° , and instead vary between $140.33(6)$ - $157.20(6)^\circ$. The resulting geometry appears intermediate between

octahedral and trigonal prismatic. Additionally, coordination in this environment leads to a very short Ti-Ti separation of 2.8495(10) Å.

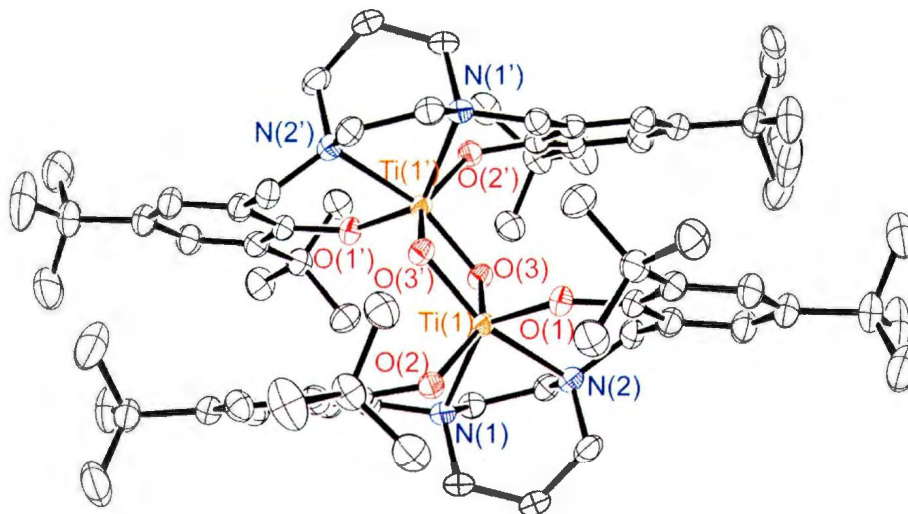


Figure 6.3. Molecular structure of **6.3**(50% displacement ellipsoids; H atoms excluded for clarity).

Table 6.1. Selected bond lengths (Å) and angles (°) for compound **6.3**

Ti(1)-O(3')	1.8452 (15)	O(3)-Ti(1)-O(2)	115.00 (6)
Ti(1)-O(3)	1.8707 (14)	O(3)-Ti(1)-N(2)	83.43 (7)
Ti(1)-O(2)	1.8861 (15)	O(3)-Ti(1)-N(1)	79.38 (6)
Ti(1)-O(1)	1.9369 (15)	O(2)-Ti(1)-O(3')	99.42 (6)
Ti(1)-N(2)	2.2881 (18)	O(2)-Ti(1)-O(1)	96.91 (6)
Ti(1)-N(1)	2.3365 (18)	O(2)-Ti(1)-N(1)	81.04 (6)
Ti(1)-Ti(1')	2.8495 (10)	O(1)-Ti(1)-O(3')	87.39 (7)
		O(1)-Ti(1)-N(2)	76.40 (6)
O(2)-Ti(1)-N(2)	140.33 (6)	O(1)-Ti(1)-N(1)	115.28 (6)
O(1)-Ti(1)-O(3)	147.06 (6)	N(2)-Ti(1)-O(3')	118.92 (6)
O(3)-Ti(1)-N(1')	157.20 (6)	N(2)-Ti(1)-N(1)	67.69 (6)
O(3)-Ti(1)-O(3')	79.86 (7)		

6.2.4 Synthesis of Amine-Bis(phenolate) Lithium Complex

As shown in Scheme 6.2, the reaction of 2,2'-*N,N'*-homopiperazinyl-bis(2-methylene-4,6-*tert*-butyl-phenol) with 2 equivalents of ${}^n\text{BuLi}$ after workup afforded **6.4**, a THF-coordinated lithium aggregate in high yield. The ${}^1\text{H}$ NMR spectrum exhibits two sets of singlets for the phenolate ${}^t\text{Bu}$ groups, two doublets for the phenolate protons, and a multiplet corresponding to the homopiperazine methylene protons. The integral of THF signals relative to that of the [ONNO] ligand unit confirms the presence of two coordinated THF molecules in the bis-ligand species. The ${}^7\text{Li}\{{}^1\text{H}\}$ NMR spectrum (Figure 6.4) shows a broad peak at 1.63 ppm with two shoulders; this suggests the presence of three Li centres for the complex in solution. This is consistent with the solid-state structure, which contains three different Li environments (Figure 6.5 and Figure 6.6). Only the frequency of the peak maximum was recorded, while detailed peak deconvolution was not pursued.

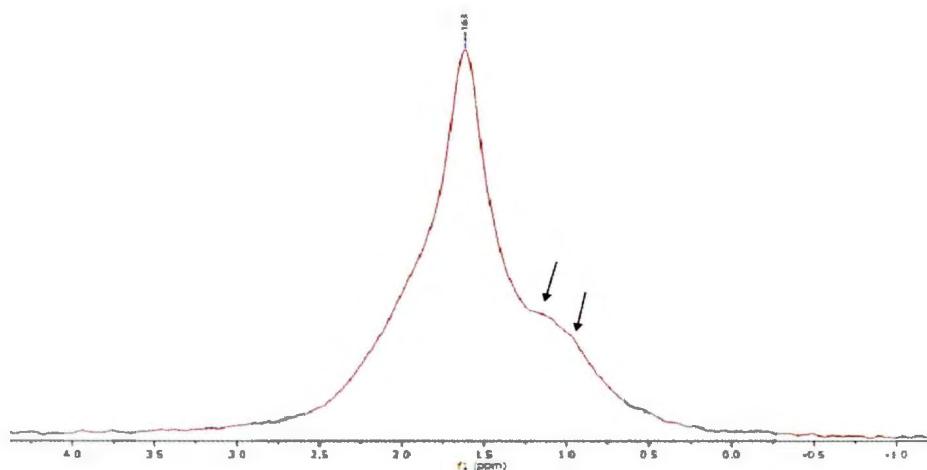


Figure 6.4. Solution-state ${}^7\text{Li}$ NMR spectrum of **6.4** in C_6D_6

The X-ray structure of **6.4** is depicted in Figure 6.5, with bond distances and angles summarized in Table 6.2. The complex exists as a solvated hexalithium dimer composed of two $\{[\text{ONNO}^{\text{Bu},\text{Bu}}]\text{Li}_3(\text{THF})(\mu\text{-O})\}$ units bridged by two phenolate moieties and one O (O4) atom trapped by three Li atoms from each monomeric $\{[\text{ONNO}^{\text{Bu},\text{Bu}}]\text{Li}_3(\text{THF})(\mu\text{-O})\}$. As a result, the Li_6O_6 core in $\{[\text{ONNO}]\text{Li}_3(\text{THF})(\mu\text{-O})\}_2$ adopts a ladder-like conformation with the coordinated THF molecules, exhibiting *transoid* geometry relative to each other (Figure 6.6). The ladder-like arrangement is comprised of five fused Li_2O_2 rungs (labelled **a-e**), in which the central rung (**c**) is planar while the others (**a**, **b**, **d** and **e**) are twisted, as evidenced by the corresponding torsion angles (**a** = 15.70°, **b** = -12.89°, **c** = 0°, **d** = -11.80°, **e** = 16.39°) and the sum of the internal angles (**a** = 355.69°, **b** = 357.47° and **c** = 360°). The central three-rung ladder adopts *transoid* geometry with a contiguous *cisoid* rung on both ends (**a** and **e**). This arrangement has been noted to minimize the steric congestion and impart a gentle undulation to the structure as a whole.³² The Li atoms which occupy positions in the outer rings; viz, Li(2) and Li(2'), are four-coordinate, being bonded by one N(1) atom from the ligand backbone, one $\mu_3\text{-O}$ [O(4)], one $\mu_2\text{-O}$ [O(1)] from the ligand, and one O [O(3)] atom from the THF molecule. The resulting geometry around the Li centres is distorted tetrahedral. Of the four Li ions occupying the central rings, Li(1) and Li(1') are four-coordinate, bonded by two $\mu_3\text{-O}$ [O(4) and O(4')], one N(2) atom from the ligand backbone, and one $\mu_2\text{-O}$ (O2) from one of the phenolate ligands, while Li(3) and Li(3') are three-coordinate, bonded by one $\mu_3\text{-O}$ [O(4)] and two $\mu_2\text{-O}$ [O(1) and O(2)] from each of the two phenolate ligands. The

average Li-O_{phenolate} and Li-O_{THF} bond distances are 1.8595(7) Å and 1.944(8) Å, respectively. In the case of the trapped O atom, the Li-O bond distance is 1.941(7) Å, while the mean Li-N bond distance is 2.1275(7) Å. These bonds are within the range of those reported for related phenolate lithium complexes.^{9,10,12,33,34} The origin of O(4) is likely either the result of adventitious water or from Li₂O impurities within the BuLi used.

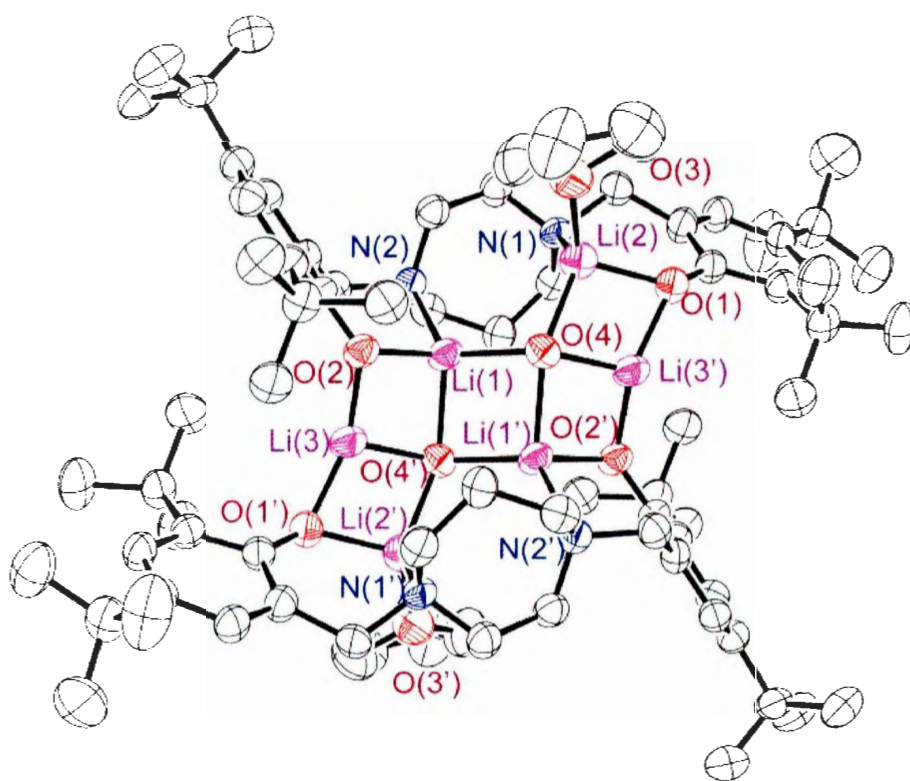


Figure 6.5. ORTEP structure of **6.4** (50% displacement ellipsoids; H atoms excluded for clarity.)

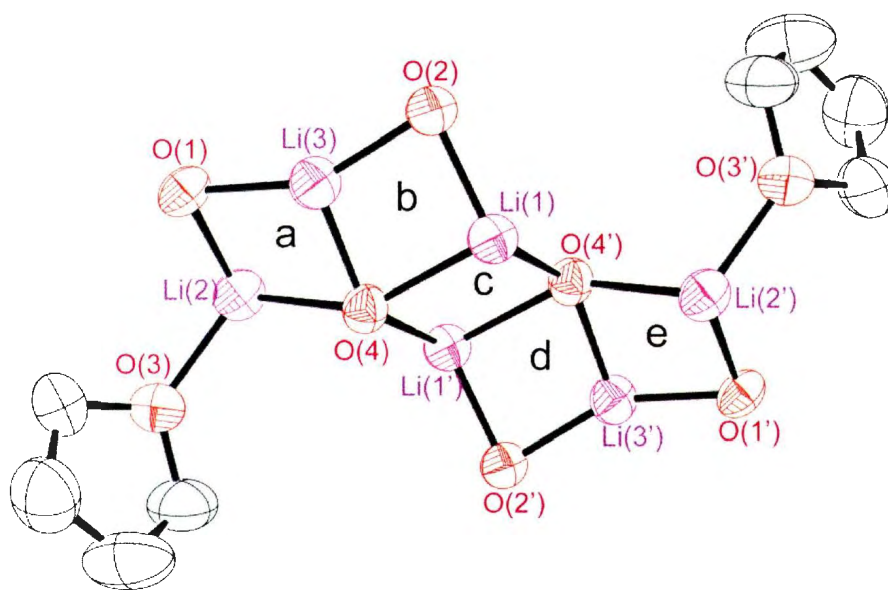


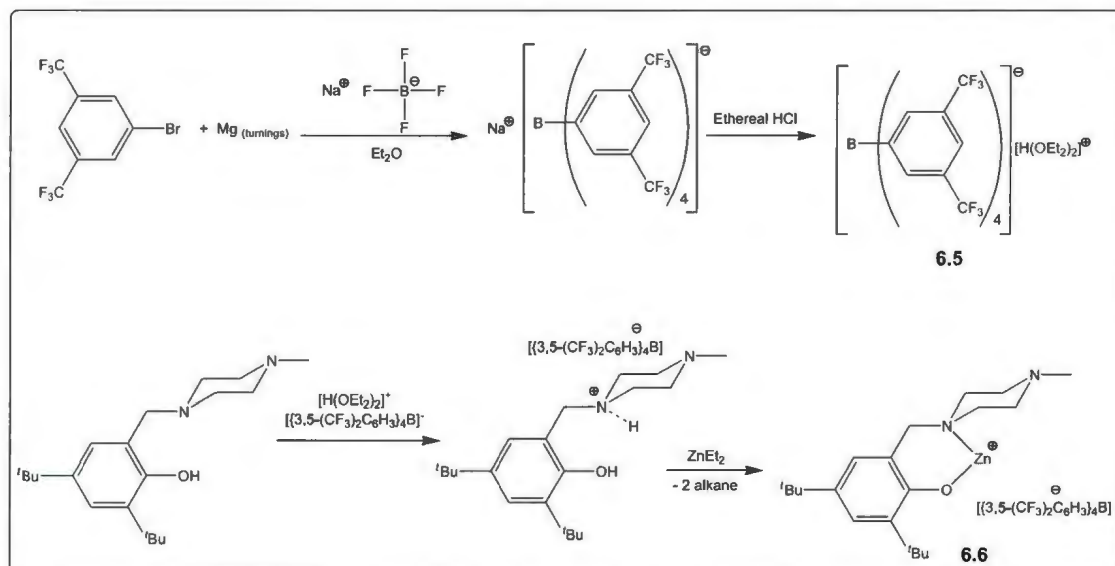
Figure 6.6. The ladder-like core of **6.4** showing its transoid-cisoidal geometry of the rungs

Table 6.2. Selected bond lengths (Å) and angles (°) for compound **6.4**

O(1)-Li(3)	1.825(7)	Li(3)-O(4')-Li(1)	78.1(3)
O(1)-Li(2)	1.873(7)	Li(1)-O(4)-Li(1')	82.0(3)
O(2)-Li(3)	1.837(7)	Li(1)-O(4')-Li(2')	146.9(3)
O(2)-Li(1)	1.903(7)	O(2)-Li(2)-O(4)	125.6(4)
O(3)-Li(2)	1.944(8)	O(2)-Li(1)-O(4')	94.1(3)
O(4)-Li(3)	1.916(7)	O(4)-Li(1)-O(4')	98.0(3)
O(4)-Li(1)	1.952(7)	O(2)-Li(1)-N(2)	96.5(3)
O(4)-Li(2)	1.972(7)	O(4')-Li(1)-N(2)	120.0(3)
O(4)-Li(1)	2.057(7)	O(1)-Li(2)-O(3)	112.4(4)
N(1)-Li(2)	2.090(7)	O(1)-Li(2)-O(4)	99.3(3)
N(2)-Li(1)	2.165(7)	O(3)-Li(2)-O(4)	115.5(3)
		O(3)-Li(2)-N(1)	111.2(3)
Li(2)-O(1)-Li(3')	78.9(3)	O(4)-Li(2)-N(1)	119.3(4)
Li(1)-O(2)-Li(3)	84.1(3)	O(1)-Li(3')-O(2')	151.6(4)
Li(1)-O(4)-Li(3')	134.1(3)	O(1)-Li(3')-O(4)	103.2(3)
Li(3)-O(4')-Li(2')	74.3(3)	O(2)-Li(3')-O(4')	101.2(3)
Li(1)-O(4)-Li(2)	104.6(3)		

6.2.5 Synthesis of Cationic Zinc Complex

Adopting the procedure described by Brookhart and co-workers,³⁵ compound **6.5** ($[\text{Na}]^+[\{3,5\text{-(CF}_3)_2\text{C}_6\text{H}_3\}_4\text{B}]^-$) was prepared by reaction of 3,5-bis(trifluoromethyl) bromobenzene $[3,5\text{-(CF}_3)_2\text{C}_6\text{H}_3\text{Br}]$, Mg and $\text{Na}^+[\text{BF}_4]^-$ in diethyl ether. The resultant compound was then reacted with ethereal HCl to precipitate NaCl and afford the desired product $[\text{H}(\text{OEt}_2)_2]^+[\{3,5\text{-(CF}_3)_2\text{C}_6\text{H}_3\}_4\text{B}]^-$ (**6.5**) in high yield (Scheme 6.3).



Scheme 6.3. Synthesis of cationic amine-phenolate zinc complex (**6.6**)

The solution ^1H NMR spectrum (Figure 6.7) exhibits two peaks at 7.73 ppm and 7.58 ppm, which integrate in an 8:4 ratio respectively, and correspond to the aryl protons. In addition, a broad singlet, a quartet, and a triplet were observed at 11.63, 3.84 and 1.31 ppm, which are respectively, attributed to the signals of the oxygen bound proton (H^+), and the CH_2 and CH_3 protons of diethyl ether.

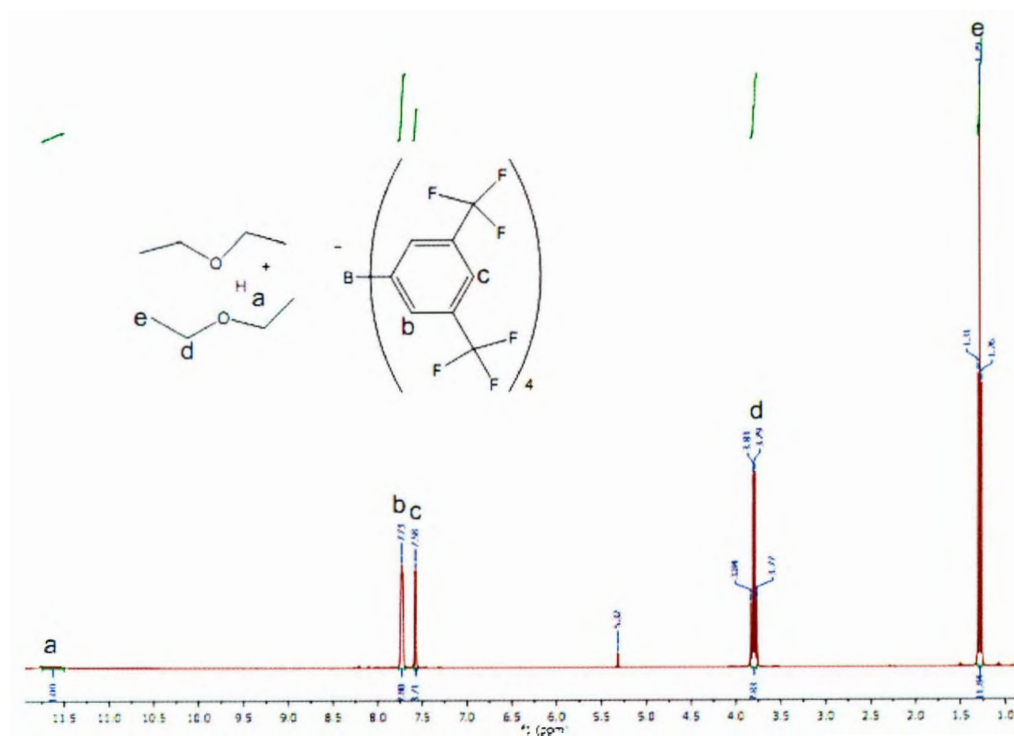


Figure 6.7. ^1H NMR spectrum of $[\text{H}(\text{OEt}_2)_2]^+[\{3,5\text{-(CF}_3)_2\text{C}_6\text{H}_3\}_4\text{B}]^-$

The cationic complex **6.6** was prepared by the reaction of the appropriate ligand $[\text{L}2]\text{H}$ with Brookhart's acid ($[\text{H}(\text{OEt}_2)_2]^+[\{3,5\text{-(CF}_3)_2\text{C}_6\text{H}_3\}_4\text{B}]^-$) to afford $[\{\text{H-ONN}^{\text{tBu, tBu}}\}\text{H}]^+[\{3,5\text{-(CF}_3)_2\text{C}_6\text{H}_3\}_4\text{B}]^-$, the subsequent reaction of the protonated ligand with alkyl zinc in toluene yielded the desired product in high yield (Scheme 6.3). The ^1H NMR spectrum shows two signals for the aryl protons and the characteristic resonances of the piperazinyl-based phenolate ligand (Figure 6.8). The ^{11}B and ^{19}F NMR spectra consist of peaks at -6.58 and -62.90 ppm, respectively, which implies no significant interaction between the anion and cation in solution.³⁶ This indicates that the compound exists in solution as charge-separated ion pairs. The spectroscopic data are consistent with

the proposed compound, however, attempts to grow single crystals proved futile. Thus, the solid-state structure of the compound could not be determined.

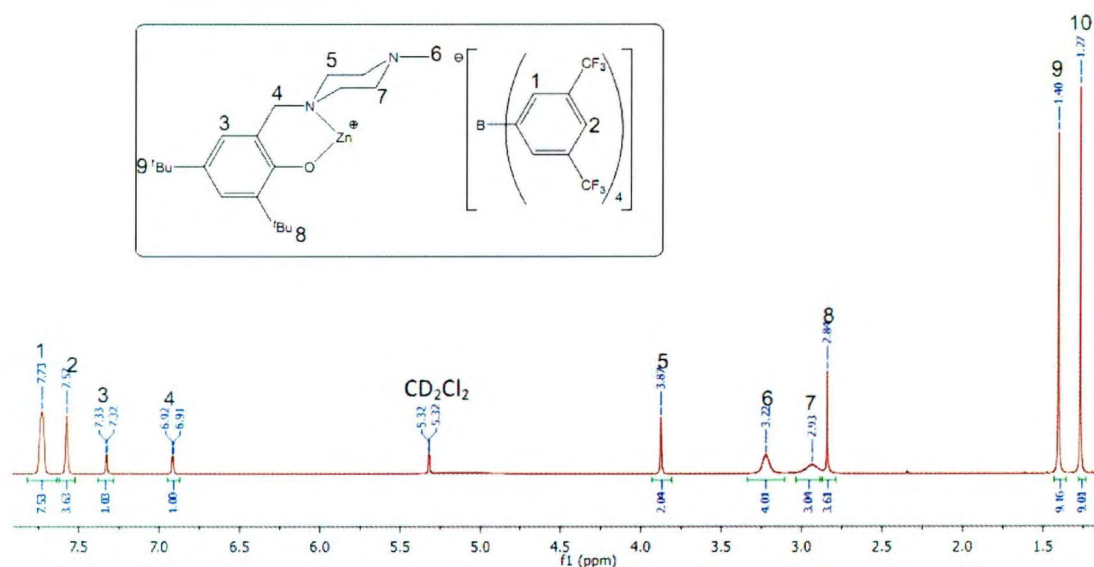


Figure 6.8. ^1H NMR spectrum of compound **6.6**

6.3 Conclusion

In conclusion, mononuclear Ti(IV) and Zr(IV) complexes supported by amine-phenolate ligands have been synthesized and fully characterized by NMR spectroscopy and X-ray diffraction studies. The structural features show that the Ti complex was coordinated by one aminephenolate ligand while the Zr complex was coordinated by two amine-phenolate ligands. In addition, Li and Ti metal complexes of an amine-bis(phenolate) ligand were prepared and structural features established by solution NMR spectroscopy and X-ray crystallography. The dimeric Ti complex was bridged by two O atom probably from adventitious moisture. Of particular note in the Li complex is the

construction of a ladder-like structure made up of five fused Li_2O_2 tetragons in $\{[\text{ONNO}]\text{Li}_3(\text{THF})(\mu\text{-O})\}_2$. Finally, Brookhart's acid was prepared and used to stabilize a cationic zinc complex of an amine-mono(phenolate) ligand. The zinc complex was characterized by NMR spectroscopy, but unfortunately efforts to obtain crystals for X-ray diffraction study were unsuccessful.

6.4 Experimental Section

6.4.1 General Considerations

All experiments involving metal complexes were performed under a nitrogen atmosphere using standard Schlenk and glove-box techniques. Solvents were distilled under nitrogen over sodium/benzophenone (THF, toluene, hexane) and degassed by freeze-thaw-vacuum cycles prior to use. Deuterated solvents (C_6D_6 , CDCl_3 , CD_2Cl_2 , $\text{C}_5\text{D}_5\text{N}$) were purchased from Cambridge Isotope Laboratories, Inc. and were purified and dried before use. Sodium tetrafluoroborate and 3,5-bis(trifluoromethyl)bromobenzene were obtained from SynQuest Labs Inc. and used as received. $\text{Ti}(\text{O}^i\text{Pr})_4$ and $\text{Zr}(\text{NMe}_2)_4$ were purchased from Aldrich, Alfa Aesar or Strem and used as received. Elemental analyses were performed by Canadian Microanalytical Service Ltd., Delta, BC, Canada. ^1H and $^{13}\text{C}\{^1\text{H}\}$, ^7Li , ^{11}B and ^{19}F NMR spectra were recorded on a Bruker Avance 300 MHz spectrometer at 25 °C (unless otherwise stated) and were referenced internally using the residual proton and ^{13}C resonances of the solvent. ^{13}C signals were assigned using HSQC experiments.

6.4.2 X-ray Crystallographic Studies

Crystals of **6.1–6.4** were mounted on a low temperature diffraction loop. All measurements were performed on a Rigaku-Saturn70 CCD diffractometer using graphite monochromated Mo-K α radiation equipped with a SHINE optic. Data were collected and processed using CrystalClear (Rigaku).^{37,38} Numerical absorption corrections were applied and data were corrected for Lorentz and polarization effects. The structures were solved by direct methods (**6.1**, **6.3**)³⁹ (**6.2**)⁴⁰ (**6.4**)⁴¹ and expanded using Fourier techniques.⁴² Neutral atom scattering factors were taken from Cromer and Waber.⁴³ Anomalous dispersion effects were included in F_{calc} ⁴⁴; the values for $\Delta f'$ and $\Delta f''$ were those of Creagh and McAuley.⁴⁵ The values for the mass attenuation coefficients are those of Creagh and Hubbell.⁴⁶ All calculations were performed using the CrystalStructure⁴⁷ crystallographic software package except for refinement, which was performed using SHELXL-97.³⁹ Hydrogen atoms were introduced in calculated positions and refined on the riding model. All non-hydrogen atoms were refined anisotropically.

Table 6.3. Summary of crystal data for compounds 6.1-6.4

Compounds	6.1	6.2	6.3	6.4
Formula	C ₂₉ H ₅₄ N ₂ O ₄ Ti	C ₃₈ H ₆₆ N ₆ O ₂ Zr	C ₇₀ H ₁₀₈ N ₄ O ₆ Ti ₂ ·4(C ₇ H ₈)	C ₁₁₃ H ₁₆₄ Li ₆ N ₄ O ₈
Formula Weight	542.66	730.20	1566.01	1748.21
Crystal System	Triclinic	Triclinic	Triclinic	Triclinic
Space Group	<i>P</i> -1	<i>P</i> -1	<i>P</i> -1	<i>P</i> -1
<i>a</i> / Å	10.879(5)	11.919(3)	11.052(3)	11.704(8)
<i>b</i> / Å	11.032(5)	12.483(3)	13.151(4)	14.470(11)
<i>c</i> / Å	14.425(6)	13.949(3)	16.791(5)	18.429(12)
α /°	71.622(13)	85.879(13)	100.967(5)	102.953(6)
β /°	73.474(17)	68.793(8)	96.234(4)	93.888(5)
γ /°	78.520(17)	88.513(12)	106.440(5)	110.311(11)
<i>V</i> /Å ³	1563.6(12)	1929.8(7)	2263.6(12)	2816(3)
<i>T</i> /K	153	153	153	153
<i>Z</i>	2	2	1	1
<i>D</i> _c g cm ⁻³	1.153	1.257	1.149	1.031
<i>F</i> (000)	592	784	848	952
μ (MoK α)/cm ⁻¹	3.07	3.24	2.30	0.62
Total reflections	12234	15785	21240	9785
Unique reflections	6314	7845	9286	9785
<i>R</i> _{int}	0.0199	0.0353	0.0469	0.0795
Reflections <i>I</i> > 2 σ (<i>I</i>)	6097	7161	8440	6250
No. of parameters	325	425	587	587
<i>R</i> ₁ , <i>wR</i> ₂ [<i>I</i> > 2 σ (<i>I</i>)]	0.0396, 0.1082	0.0494, 0.1200	0.0655, 0.1850	0.1091, 0.3185
GOF	1.031	1.061	1.063	1.062

^aData in common: graphite-monochromated via Rigaku SHINE Optic Mo-K α radiation, λ = 0.71073 Å; $R_1 = \sum ||F_o| - |F_c|| / \sum |F_o|$, $wR_2 = [\sum (w (F_o^2 - F_c^2)^2) / \sum w(F_o^2)^2]^{1/2} w^{-1} = [\sigma^2(F_o^2) + (aP)^2]$, $P = [\text{Max}(F_o^2, 0) + 2(F_c^2)]/3$

6.4.3 Synthetic Procedures

$[\text{ONN}^{t\text{Bu},t\text{Bu}}]\text{Ti}(\text{O}^i\text{Pr})_3$ (**6.1**). A toluene solution (10 mL) of $[\text{L2}]\text{H}$ (3.18 g, 10.0 mmol) was added to $\text{Ti}(\text{O}^i\text{Pr})_4$ (1.42 g, 5.00 mmol) in a 150 mL flask equipped with a stir bar. The mixture turned yellow upon the addition of the ligand. The reaction mixture was stirred for 3 h at room temperature (RT) and the solvent removed under vacuum. The resulting yellow, oily material was washed with hexane and dried under vacuum. $[\text{ONN}^{t\text{Bu},t\text{Bu}}]\text{Ti}(\text{O}^i\text{Pr})_3$ was obtained as a yellow solid in 90.4% yield (2.46 g). It should be noted that small quantities of $[\text{ONN}^{t\text{Bu},t\text{Bu}}]_2\text{Ti}(\text{O}^i\text{Pr})_2$ could also be isolated: Anal. calcd. for $\text{C}_{29}\text{H}_{54}\text{N}_2\text{O}_4\text{Ti}$: C, 68.97; H, 10.07; N, 6.99. Found: C, 69.14; H, 10.32; N, 7.52%. ^1H NMR (C_6D_6 , 500 MHz, 298 K) δ 7.51 (1H, d, $J = 2.3$ Hz, *ArH*), 7.06 (1H, d, $J = 2.2$, *ArH*), 4.98 (3H, sep, $J = 6.1$ Hz, $\text{O}-\text{CH}\{\text{CH}_3\}_2$), 4.06 (2H, s, $\text{Ar}-\text{CH}_2-\text{N}$), 3.23 (4H, br, $\text{N}-\text{C}_2\text{H}_4-\text{C}_2\text{H}_4-\text{N}$), 2.24 (4H, t, $J = 4.6$ Hz, $\text{N}-\text{C}_2\text{H}_4-\text{C}_2\text{H}_4-\text{N}$), 2.05 (3H, s, $\text{N}-\text{CH}_3$), 1.70 (9H, s, $\text{ArC}-\text{C}\{\text{CH}_3\}_3$), 1.39 (9H, s, $\text{ArC}-\text{C}\{\text{CH}_3\}_3$), 1.33 (18H, d, $J = 6.1$ Hz, $3 \text{ O}-\text{CH}\{\text{CH}_3\}_2$).

$[\text{ONN}^{\text{Me},t\text{Bu}}]_2\text{Zr}(\text{NMe}_2)_2$ (**6.2**). Solution of $[\text{L1}]\text{H}$ (1.1 g, 4.0 mmol) in toluene (2.0 mL) was cooled to -35 °C and added dropwise to a stirred toluene solution (4.0 mL) of $\text{Zr}(\text{NMe}_2)_4$ (1.1 g, 4.0 mmol). The resulting colourless solution was stirred for 3 h at RT. The solvent was removed in vacuo to give a white residue, which was washed with cold pentane (2×4 mL). Yield: 1.90 g, 65.0%. X-ray quality crystals could be grown by slow evaporation or cooling of a toluene/pentane solution at -35 °C. Anal. calcd. for $\text{C}_{26}\text{H}_{51}\text{N}_4\text{OZr}(\text{C}_5\text{H}_{12})$: C, 59.26; H, 9.76; N, 10.63. Found: C, 59.05; H, 9.11; N, 10.60%. ^1H NMR ($\text{C}_5\text{D}_5\text{N}$, 500 MHz, 313 K) δ 7.49 (1H s, *ArH*), 7.27 (1H, s, *ArH*), 4.06 (2H, s,

Ar-CH₂-N), 3.06 (6H, s, N{CH₃}₂), 2.85 (4H, br, N-C₂H₄-C₂H₄-N), 2.47 (4H, br, N-C₂H₄-C₂H₄-N), 2.35 (3H, s, N-CH₃), 2.22 (3H, s, ArC-CH₃) 1.59 (9H, s, ArC-C{CH₃}₃).

{[ONNO^{tBu,tBu}]Ti(μ-O)}₂ (6.3). A toluene solution (10 mL) of 2,2'-N,N'-homopiperazinyl-bis(2-methylene-4,6-*tert*-butyl-phenol) (2.68 g, 5.00 mmol) was added to Ti(OⁱPr)₄ (1.42 g, 5.00 mmol) in a 150 mL flask equipped with a stir bar. The mixture turned yellow upon the addition of the ligand. The reaction mixture was stirred for 5 h at RT and the solvent removed under vacuum. The resulting yellow, oily material was washed with pentane and dried under vacuum. Di-μ-oxo-bis[2,2'-N,N'-homopiperazine-bis(2-methylene-4,6-*tert*-butyl phenolate)titanium(IV)] (**6.3**) was obtained as a yellow solid. Crystals were grown by slow evaporation or by cooling a saturated toluene/heptane solution containing a few drops of hexamethyldisiloxane at -35 °C. Anal. calcd. for C₇₀H₁₀₈N₄O₆Ti₂ (C₇H₈) C, 71.72; H, 9.07; N, 4.34. Found: C, 71.79; H, 9.56; N, 4.58%.

{[ONNO^{tBu,tBu}]Li₃(THF)(μ-O)}₂ (6.4). A solution of ⁿBuLi (6.40 mL, 10.3 mmol, 1.6 M in hexane) was added dropwise to a stirred solution of [ONNO^{tBu,tBu}][L11]2H (2.5 g, 4.6 mmol) in THF (60.0 mL) at -78 °C. After stirring for 3 h, the solution was allowed to warm to RT and was stirred for a further 15 h. The solvent was then removed under vacuum to give a white residue. The residue was washed with cold pentane (20.0 mL), filtered and dried under vacuum to afford a white powder. Yield (2.20 g). Anal. calcd. for C₇₈H₁₂₄N₄O₈Li₆: C, 72.76; H, 9.71; N, 4.35. Found: C, 72.91; H, 10.01; N, 4.63%. Clear, colorless crystals suitable for X-ray diffraction were obtained from the slow evaporation of a saturated toluene/pentane solution (at -35 °C) under inert atmosphere. ¹H NMR (C₆D₆, 500 MHz, 298 K) δ 7.62 (4H, d, *J* = 2.6 Hz, ArH), 7.09 (4H, d, *J* = 2.6, ArH), 3.60

(8H, s, Ar-CH₂-N), 3.43 (8H, br, THF), 2.73 (8H, br, N-CH₂-CH₂-N), 1.98 (4H, br, N-CH₂{CH₂}CH₂-N), 1.82 (8H, br, N-CH₂{CH₂}CH₂-N), 1.68 (36H, s, Ar-C{CH₃}₃), 1.49 (36H, s, Ar-C{CH₃}₃), 1.40 (8H, br, THF). ¹³C{¹H} NMR (C₆D₆, 125 MHz, 298K): δ 136.2 (ArC-O), 133.4 (ArC-C{CH₃}₃), 129.2 (ArC-C{CH₃}₃), 126.7 (ArCH), 125.6 (ArCH), 123.2 (ArC-CH₂-N), 67.8 (THF), 62.0 (ArC-CH₂-N), 52.9 (N-CH₂-CH₂-N), 50.2 (N-CH₂{CH₂}CH₂-N), 35.0 (ArC-C{CH₃}₃), 33.8 (ArC-C{CH₃}₃), 32.1 (ArC-C{CH₃}₃), 30.2 (ArC-C-{CH₃}₃), 25.1 (THF), 24.4 (N-CH₂{CH₂}CH₂-N).

[Na]⁺[[3,5-(CF₃)₂C₆H₃]₄B]⁻.³⁵ In a 1 L round-bottom flask, a solution of 3,5-bis(trifluoromethyl) bromobenzene (25.0 g, 85.3 mmol) in diethyl ether (130.0 mL) was slowly added (*ca* 2 h) to magnesium turnings (2.55 g, 10.5 mmol) in Et₂O (75.0 mL).⁴⁸ The mixture was refluxed for 30 minutes to give a brown solution of the aryl Grignard reagent. Sodium tetrafluoroborate (1.70 g, 15.5 mmol) was added and the resulting mixture was stirred for 48 h during which the mixture became dark brown with some precipitate formed. The workup of the reaction mixture which did not involve inert atmosphere procedures were carried out by adding the reaction mixture to a saturated solution of Na₂CO₃ (37.5 g) in H₂O (500 mL). The mixture was stirred for 20 minutes, filtered and the filtrate and the aqueous phase were extracted with Et₂O (4 × 200 mL). The deep brown extracts were combined and dried over Na₂SO₄ and decolourizing charcoal. After 18 h, the solution was filtered and the solvent was removed under vacuum to afford a brown solid. The solid was washed with cold dichloromethane to remove traces of coloured impurities, and was dried overnight to give a grey solid. Yield: 9.18 g, 66.8%.

$[\text{H}(\text{OEt}_2)_2]^+[\{3,5\text{-(CF}_3)_2\text{C}_6\text{H}_3\}_4\text{B}]^-$ (**6.5**).³⁵ In a Schlenk tube, $[\text{Na}]^+[\{3,5\text{-(CF}_3)_2\text{C}_6\text{H}_3\}_4\text{B}]^-$ (3.0 g, 3.39 mmol) was dissolved in Et₂O (75.0 mL), and the solution was allowed to stand for 18 h upon the addition of 4-Å molecular sieves. The $[\text{Na}]^+[\{3,5\text{-(CF}_3)_2\text{C}_6\text{H}_3\}_4\text{B}]^-$ solution was transferred to a flask containing ethereal HCl (3.0 mL) cooled to 0 °C, which resulted in the precipitation of NaCl. The mixture was then filtered into another flask, using stick filtration, as well as the Et₂O washings of the precipitate (2 × 20 mL). The solution was concentrated to 10.0 mL, chilled to -78 °C, and was allowed to stand for 1 h, during which crystals began to form. Pentane (20.0 mL) was slowly added to the crystals to further precipitate the product. The supernatant was decanted and the residual solvent removed under vacuum to afford **6.5** as off-white solid. Yield: 3.3 g, 96.3%. ¹H NMR (CD₂Cl₂, 300 MHz, 298 K): δ 11.63 (1H, br, {Et₂O}H), 7.73 (8H, s, *o*-ArH), 7.58 (4H, s, *p*-ArH), 3.84 (8H, q, *J* = 7.1 Hz, OCH₂CH₃), 1.31 (12 H, t, *J* = 7.1, OCH₂CH₃). ¹³C {¹H} NMR (CD₂Cl₂, 125 MHz, 298 K): δ 161.3-163.3 (B-C), 135.4 (*p*-ArC), 129.1-130.6 (*m*-ArC), 127.0 (*o*-ArC), 123 (*o*-ArC), 118.1 (*m*-ArC-CF₃), 68.6 (OCH₂CH₃), 14.5 (OCH₂CH₃). ¹⁹F NMR (188.31 MHz, CD₂Cl₂, 298 K): δ = -62.90. ¹¹B NMR (96.29 MHz, CD₂Cl₂, 298 K): δ = -6.58.

$[\{\text{ONN}^{\text{Bu},\text{Bu}}\}\text{Zn}]^+[\{3,5\text{-(CF}_3)_2\text{C}_6\text{H}_3\}_4\text{B}]^-$ (**6.6**). To a vial equipped with a stir bar was added $[\text{H}(\text{Et}_2\text{O})_2]^+[\{3,5\text{-(CF}_3)_2\text{C}_6\text{H}_3\}_4\text{B}]^-$ (635 mg, 0.627 mmol) and toluene (2.0 mL). A solution of $[\text{NNO}^{\text{Bu},\text{Bu}}]\text{H}$ (**L2**H) (200 mg, 0.628 mmol) in toluene (2.0 mL) was added to the vial and the mixture was stirred for 1 h, after which ZnEt₂ (516 μL, 0.627 mmol, 15 wt.-% in hexane) was added and the reaction mixture stirred for an additional 1 h. The solvent was removed under vacuum to give a brown, oily liquid, which was triturated

with pentane (3×10 mL). The solvent was removed under reduced pressure to afford $[\{\text{ONN}^{i\text{Bu},t\text{Bu}}\}\text{Zn}]^+[\{3,5\text{-(CF}_3)_2\text{C}_6\text{H}_3\}_4\text{B}]^-$ as an off-white solid. Yield: 0.63 g, 81%. ^1H NMR (CD_2Cl_2 , 300 MHz, 298 K) δ 7.73 (8H, s, *o*-ArH), 7.57 (4H, s, *p*-ArH), 7.33 (1H, d, $J = 2.3$, ArH), 6.92 (1H, d, $J = 2.3$, ArH), 3.87 (2H, s, Ar-CH₂-N), 3.22 (4H, br, N-C₂H₄-C₂H₄-N), 2.93 (3H, br, N-CH₃), 2.84 (4H, s, N-C₂H₄-C₂H₄-N), 1.40 (9H, s, ArC-C{CH₃}₃), 1.27 (9H, s, ArC-C{CH₃}₃); $^{13}\text{C}\{^1\text{H}\}$ NMR (CD_2Cl_2 , 125 MHz, 298 K): δ 161.2-163.1 (B-C), 153.1 (ArC-O), 142.9 (ArC-C{CH₃}₃), 136.5 (ArC-C{CH₃}₃), 135.2 (*p*-ArC), 129.5-130.4 (*m*-ArC), 126.8 (*o*-ArC), 125.2 (ArCH), 124.9 (ArCH), 123.2 (*o*-ArC), 118.4 (ArC-CH₂N), 117.9 (*m*-ArC-CF₃), 61.4 (ArC-CH₂N), 55.1 (N-C₂H₄-C₂H₄-N), 50.4 (N-C₂H₄-C₂H₄-N), 45.0 (N-CH₃), 35.1(ArC-C{CH₃}₃), 34.5 (ArC-C{CH₃}₃), 31.6 (ArC-C{CH₃}₃), 29.8 (ArC-C{CH₃}₃). ^{19}F NMR (188.31 MHz, CD_2Cl_2 , 298 K): $\delta = -62.70$. ^{11}B NMR (96.29 MHz, CD_2Cl_2 , 298 K): $\delta = -6.58$.

6.5 References

1. E. N. Jacobsen, *Science*, **2003**, *299*, 1691.
2. T. M. Ovitt and G. W. Coates, *J. Am. Chem. Soc.*, **2002**, *124*, 1316.
3. J. Ejfler, M. Kobylka, L. B. Jerzykiewicz and P. Sobota, *Dalton Trans.*, **2005**, 2047.
4. S. Groysman, E. Sergeeva, I. Goldberg, and M. Kol, *Inorg. Chem.*, **2005**, *44*, 8188.
5. Y. Kim, G. K. Jnaneshwara, and J. G. Verkade, *Inorg. Chem.*, **2003**, *42*, 1437.
6. S. E. Reybuck, A. L. Lincoln, S. Ma, and R. M. Waymouth, *Macromolecules*, **2005**, *38*, 2552.
7. J. D. Chartres, A. Dahir, P. A. Tasker and F. J. White, *Inorg. Chem. Commun.*, **2007**, *10*, 1154.
8. S. H. Kima, J. Lee, D. J. Kima, J. H. Moon, S. Yoon, H. J. Oh, Y. Do, Y. S. Ko, J.-H. Yimd and Y. Kima, *J. Organomet. Chem.*, **2009**, *694*, 3409.
9. T. J. Boyle, D. M. Pedrotty, T. M. Alam, S. C. Vick and M. A. Rodriguez, *Inorg. Chem.*, **2000**, *39*, 5133.
10. F. M. Kerton, C. M. Kozak, K. Luttgen, C. E. Willans, R. J. Webster and A. C. Whitwood, *Inorg. Chim. Acta.*, **2006**, *2819*.
11. D. J. MacDougall, B. C. Noll, A. R. Kennedy and K. W. Henderson, *Dalton Trans.*, **2006**, 1875.
12. R. K. Dean, S. L. Granville, L. N. Dawe, A. Decken, K. M. Hattenhauer and C. M. Kozak, *Dalton Trans.*, **2010**, *39*, 548.
13. M. L. Cole, P. C. Junk, K. M. Proctor, J. L. Scott and C. R. Strauss, *Dalton Trans.*, **2006**, 3338.
14. R. E. Mulvey, *Chem. Soc. Rev.*, **1991**, *20*, 167.
15. B. W. F. Gordon, M. J. Scott, *Inorg. Chim. Acta.*, **2000**, *297*, 206.
16. H. Nishida, N. Takada, M. Yoshimura, T. Sonoda and H. Kobayashi, *Bull. Chem. Soc. Jpn.*, **1984**, *57*, 2600.

17. H. Sinn, W. Kaminsky, H. J. Vollmer and R. Woldt, *Angew. Chem. Int. Ed. Engl.*, **1980**, *19*, 390.
18. R. F. Jordan, *Adv. Organomet. Chem.*, **1991**, *32*, 325.
19. E. Y.-X. Chen and T. J. Marks, *Chem. Rev.*, **2000**, *100*, 1391.
20. M. Bochmann, *J. Organomet. Chem.*, **2004**, *689*, 3982.
21. M. D. Hannant, M. Schormann, M. Bochmann, *J. Chem. Soc., Dalton Trans.*, **2002**, 4071.
22. Y. Sarazin, M. Schormann, M. Bochmann, *Organometallics*, **2004**, *23*, 3296.
23. M. D. Hannant, M. Schormann, D. L. Hughes, M. Bochmann, *Inorg. Chim. Acta.*, **2005**, *358*, 1683.
24. C. A. Wheaton, B. J. Ireland, P. G. Hayes, *Organometallics*, **2009**, *28*, 1282.
25. C. A. Wheaton, P. G. Hayes, *Dalton Trans.*, **2010**, *39*, 3861.
26. S. Gendler, S. Segal, I. Goldberg, Z. Goldschmidt and M. Kol, *Inorg. Chem.*, **2006**, *45*, 4783.
27. A. W. Addison, T. N. Rao, J. Reedijk, J. Vanriijn and G. C. Verschoor, *J. Chem. Soc., Dalton Trans.*, **1984**, 1349.
28. Y. Kim and J. G. Verkade, *Organometallics*, **2002**, *21*, 2395.
29. A. L. Johnson, M. G. Davidson and M. F. Mahon, *Dalton Trans.*, **2007**, 5405.
30. A. Cohen, J. Kopilov, I. Goldberg and M. Kol, *Organometallics*, **2009**, *28*, 1391.
31. J. Baldamus and E. Hecht. *Z. Anorg. Allg. Chem.*, **2003**, *629*, 188.
32. D. Bond, *Chem.–Eur. J.*, **2004**, *10*, 1885.
33. D. J. MacDougall, B.C. Noll, A. R. Kennedy and K. W. Henderson, *Dalton Trans.*, **2006**, 1875.
34. W. Clegg, M. G. Davidson, D. V. Graham, G. Griffen, M. D. Jones, A. R. Kennedy, C. T. O'Hara, L. Russoa and C. M. Thomson, *Dalton Trans.*, **2008**, 1295.
35. M. Brookhart, B. Grant, and A. F. Volpe, Jr., *Organometallics*, **1992**, *11*, 3920.

36. A. D. Horton, *Organometallics*, **1996**, *15*, 2675.
37. CrystalClear: Rigaku Corporation, **1999**. CrystalClear Software User's Guide, Molecular Structure Corporation, **2000**.
38. J. W. Pflugrath, *Acta Cryst.*, **1999**, *D55*, 1718.
39. SHELX97: G.M. Sheldrick, **1997**; G.M. Sheldrick, *Acta Cryst.*, **2008**, *A64*, 112.
40. SIR92: A. Altomare, G. Cascarano, C. Giacovazzo, A. Guagliardi, M. Burla, G. Polidori and M. Camalli, *J. Appl. Cryst.*, **1994**, *27*, 435.
41. SIR2004: M. C. Burla, M. Camalli, B. Carrozzini, G. L. Cascarano, C. Giacovazzo, G. Polidori, and R. Spagna, *J. Appl. Cryst.*, **2003**, *36*, 1103.
42. DIRDIF99: Beurskens, P.T., Admiraal, G., Beurskens, G., Bosman, W.P., de Gelder, R., Israel, R. and J.M.M. Smits, **1999**. The DIRDIF-99 program system, Crystallography Laboratory, University of Nijmegen, The Netherlands.
43. D. T. Cromer, and J. T. Waber, *International Tables for X-ray Crystallography*, The Kynoch Press, Birmingham, England, **1974**, Vol. IV, Table 2.2 A.
44. J. A. Ibers and W. C. Hamilton, *Acta Crystallogr.*, **1964**, *17*, 781.
45. D. C. Creagh, and W. J. McAuley, *International Tables for Crystallography*, ed. A. J. C. Wilson, Kluwer Academic Publishers, Boston, **1992**, Vol C, Table 4.2.6.8, pp 219.
46. D. C. Creagh, and J. H. Hubbell, *International Tables for Crystallography*, ed. A. J. C. Wilson, Kluwer Academic Publishers, Boston, **1992**, Vol C, Table 4.2.4.3, pp 200.
47. CrystalStructure 4.0: Crystal Structure Analysis Package, Rigaku and Rigaku Americas (**2000-2010**). 9009 New Trails Dr. The Woodlands TX 77381 USA.
48. Caution! The mixture became so hot that it started to boil vigorously and generated a lot of pressure.

Chapter 7

Conclusion

7.1 Summary

Interest in aliphatic polyesters and polycarbonates has increased significantly over the past several decades as a result of the biorenewable source of many of the monomers, in addition to their biodegradable properties. The uses of these polymeric materials in modern society range from medicinal to commodity and textiles. Aliphatic polyesters are currently more expensive than polyolefins; however their commercial potential should increase with the development of more active catalysts for the ROP of cyclic esters and copolymerization of epoxides with CO₂ by reducing their costs. Moreover, their environmental impact is low compared to traditional non-degradable plastics based on fossil fuels. In light of this, the synthesis of inexpensive, more active catalysts based on biocompatible metals stabilized by monoanionic amine-mono(phenolate) ligands is the main focus of this research.

Chapter 1 of this thesis presented a brief introduction to PLA and PCL, and gave a literature overview on the advancement in single-site biocompatible catalysts for the ROP of cyclic esters and coupling/copolymerization of epoxides with CO₂. A series of amine-phenol ligands synthesised using modified Mannich condensation was described in Chapter 2. This method of three-component condensation, which utilises water as the reaction medium, offers the advantage of increased product yields and avoids the use of volatile organic compounds (VOCs) as solvents, which are detrimental to the

environment. Thus, this approach falls within the context of Green Chemistry. For the syntheses of these ligands, variations of the amine unit were undertaken by introducing ether (O) or methyl amine (NMe). In addition, the sterics and electronics were varied through the introduction of various groups on the phenol (e.g., Me, ^tBu, ^tAm, F, Cl).

A series of zinc alkyl and alkoxide complexes ligated by monoanionic amine-mono(phenolate) ligands that efficiently initiated the ROP of *rac*-LA and ϵ -CL were described in Chapter 3. The structural features of these complexes in solution and solid-state were established by NMR measurements and X-ray diffraction studies. The polymerization data indicate that reaction rates generally correlate with both the steric demands of the ligands and the co-initiator. The less bulky methyl substituent with BnOH afforded faster rates than its bulkier tert-butyl and tert-amyl analogues with ^tBuOH. The activities of the alkyl complexes show that the presence of alcohol was necessary to generate an efficient initiator system. In addition, the use of microwave irradiation for the polymerization of *rac*-LA and ϵ -CL indicates that more sterically demanding co-initiators (alcohols) can be used without increasing reaction time significantly. However, microanalyses show that the polymers formed in the ROP of *rac*-LA are predominantly atactic. Furthermore, preliminary studies indicate that the alkyl and alkoxide complexes have slight activity towards cyclic carbonate formation in the coupling reaction of cyclohexene oxide with CO₂. It would be interesting to study the effects of varying the ratio of the initiator:co-initiator system as well as the following reaction conditions: temperature, pressure, monomer ratio, and time. This would allow the determination of the appropriate (optimized) reaction conditions for significant product formation.

In Chapter 4, the synthesis and characterization of a series of aluminum methyl and chloro complexes was described. The aluminum methyl complexes efficiently initiated the ROP of ϵ -CL in the presence of benzyl alcohol (BnOH) through in situ formation of alkoxide species, while the chloro analogues initiated the reaction through the formation of HCl. Insight into the aluminum methyl/BnOH catalyzed ROP of ϵ -CL was gained through kinetic studies. The kinetic analysis revealed that the ϵ -CL polymerization using these initiator systems are first-order with respect to monomer concentration, which demonstrated the living character of the polymerization. Furthermore, observed rate constants (k_{obs}) show that the polymerization rate of **4.2**/BnOH is higher than that of **4.3**/BnOH and **4.1**/BnOH, which indicates that the rate of aluminum complex (**4.1**) with the less bulky Me substituent at the ortho position of the phenolate may be slower than its *t*-Bu analogues. However, **4.1** exhibited a more controlled reaction than its analogues. The activation parameters (E_a , ΔH^\ddagger and ΔS^\ddagger) obtained from Arrhenius and Eyring plots suggest that reaction rates are generally faster for the methyl aluminum complexes bearing piperazinyl (NMe)-based ligand than that supported by a morpholinyl (O)-based ligand. This indicates that there may be some structure-activity relationship with the outersphere substituent groups on the complexes. The end-group analysis conducted on the polymer using NMR spectroscopy and MALDI-TOF MS reveals that the polymers are capped at both ends with BnO and OH groups, indicating that the polymerization proceeded through a coordination-insertion mechanism. Preliminary study shows that complex **4.5** was active for the copolymerization of cyclohexene oxide with CO₂ without co-catalyst, affording polyethercarbonate. In contrast, complex **4.4** was inactive towards

both cycloaddition and copolymerization reactions. This further highlights the probable effect of outersphere substituents on the complexes. Further optimization of the copolymerization reaction conditions would likely favour formation of perfect alternating copolymers. Further studies would enable the evaluation of the activity of the complexes for a better understanding of the difference in their reactivity.

Trimetallic lithium complexes supported by monoanionic mono(phenolate) ligands were reported in Chapter 5. The solid-state structural features of the complexes were determined by X-ray diffraction studies. In the presence and absence of BnOH, the complexes efficiently initiated the ROP of ϵ -CL. Detailed kinetic studies revealed first-order dependence with respect to monomer concentration, and the k_{obs} values were greater in the presence of BnOH than in its absence. Comparative analysis of the kinetics showed that a change in the *ortho* substituent on the phenolate from ^tBu to the more sterically hindered ^tAm enhanced the polymerization rate. Furthermore, end-group analysis revealed that polymers prepared in the presence of BnOH are linear chains capped on both ends with benzyloxide and hydroxy groups, while in the absence of BnOH, cyclic and open chain oligomers were obtained, indicating the occurrence of a transesterification reaction (in the absence of BnOH).

Finally, Chapter 6 discussed the successful syntheses and characterization of Group IV complexes supported by monoanionic amine-mono(phenolate) ligands, Ti and Li complexes bearing amine-bis(phenolate) ligand, and a cationic Zn complex. The structural features of the complexes (**6.1-6.4**) were elucidated using X-ray diffraction studies and NMR spectroscopy. The crystal structures revealed complex **6.1** to be a

monometallic Ti alkoxide, **6.2** as a monometallic Zr amide, while **6.3** and **6.4** were dimeric Ti and Li amine-bis(phenolate) complexes respectively. Several related Li and Group IV metal phenolates and cationic Zn complexes are known to initiate catalytic ROP of cyclic esters. Therefore, it would be interesting to determine the activity of these complexes towards polymerization reactions and also to establish the solid state structure of **6.6**.

Appendix A: NMR Spectroscopy

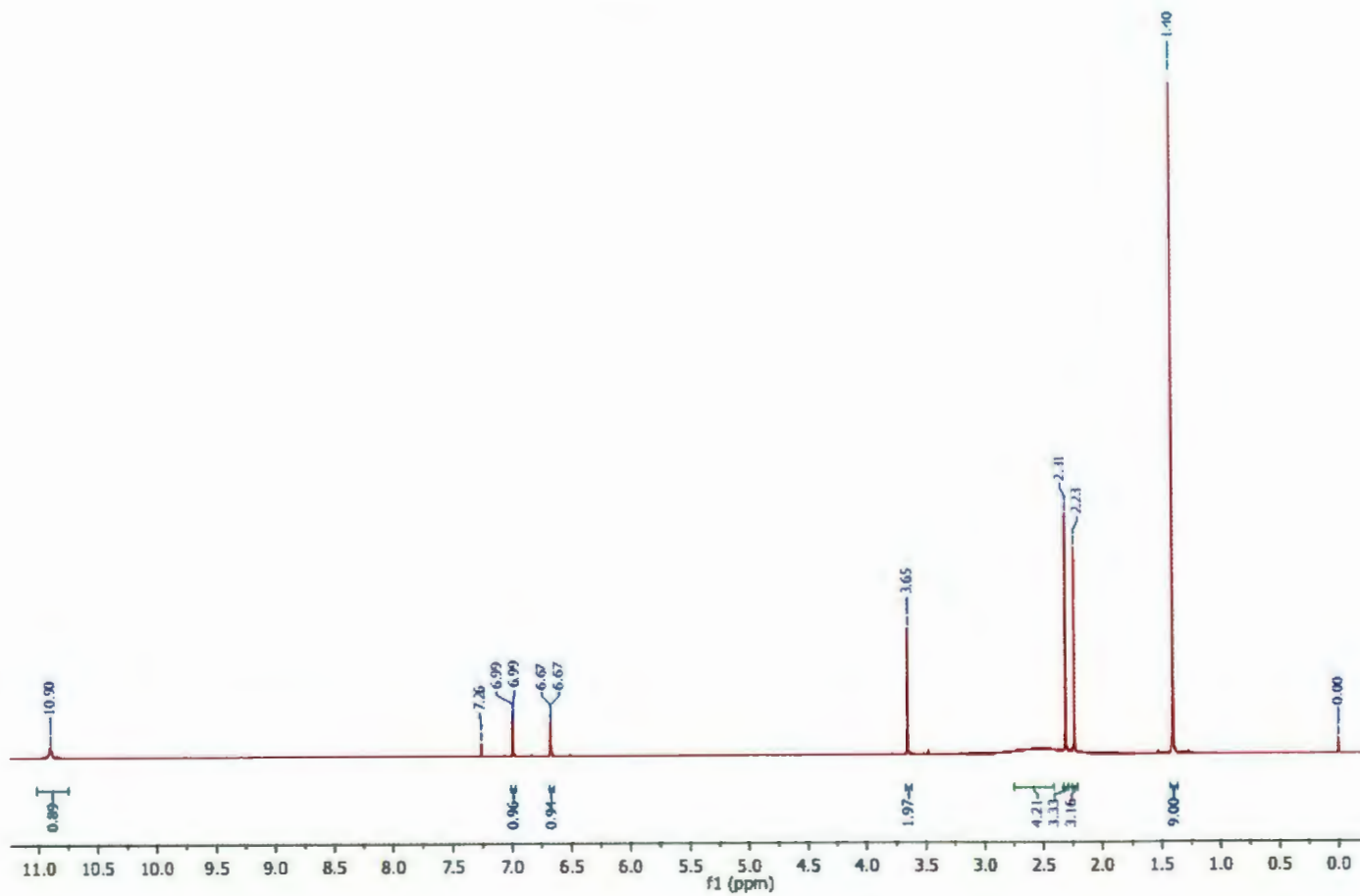


Figure A1.1. ^1H NMR spectrum of [L1]H

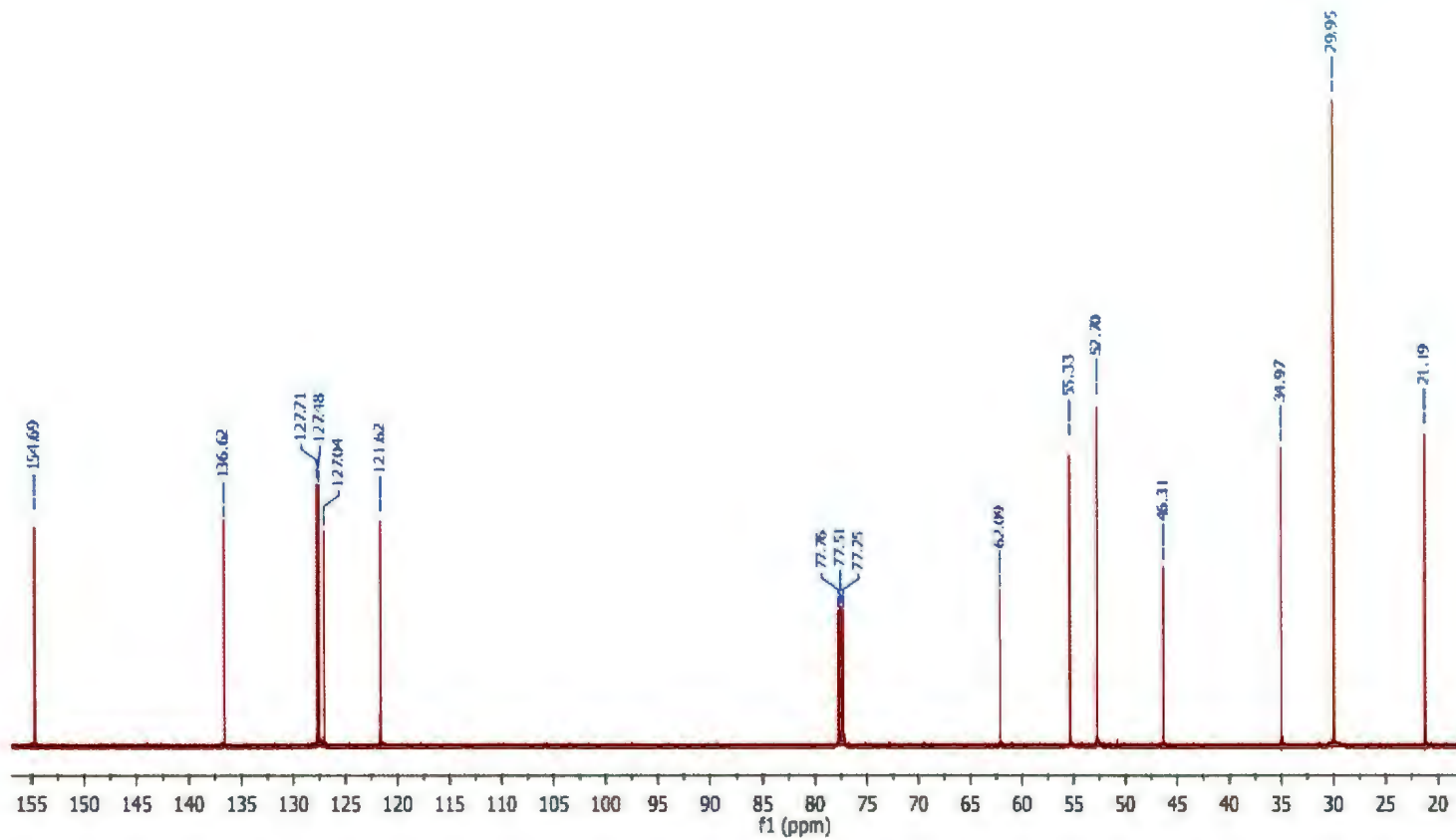


Figure A1.2. ^{13}C NMR spectrum of [L1]H

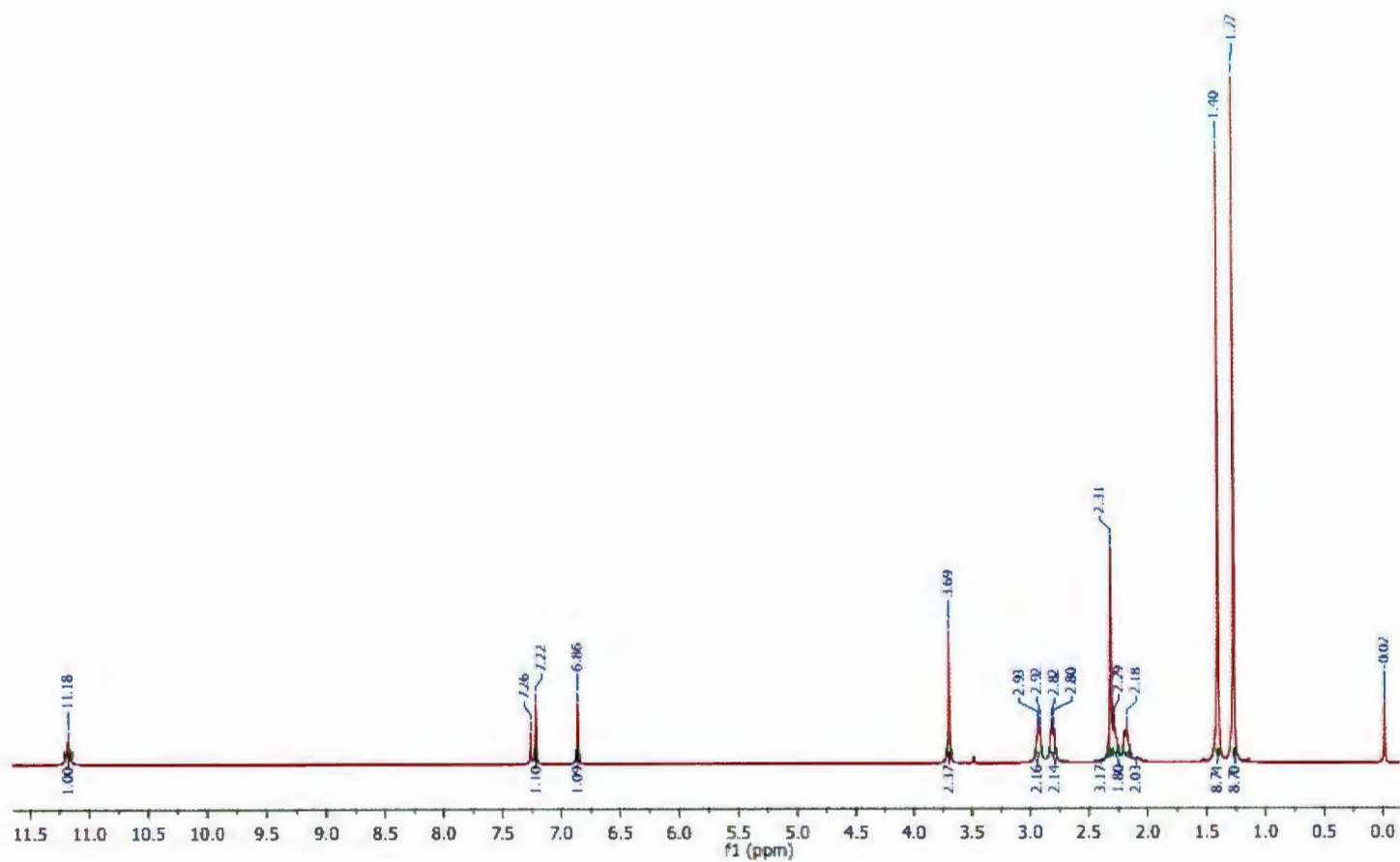


Figure A1.3. ^1H NMR spectrum of [L2]H

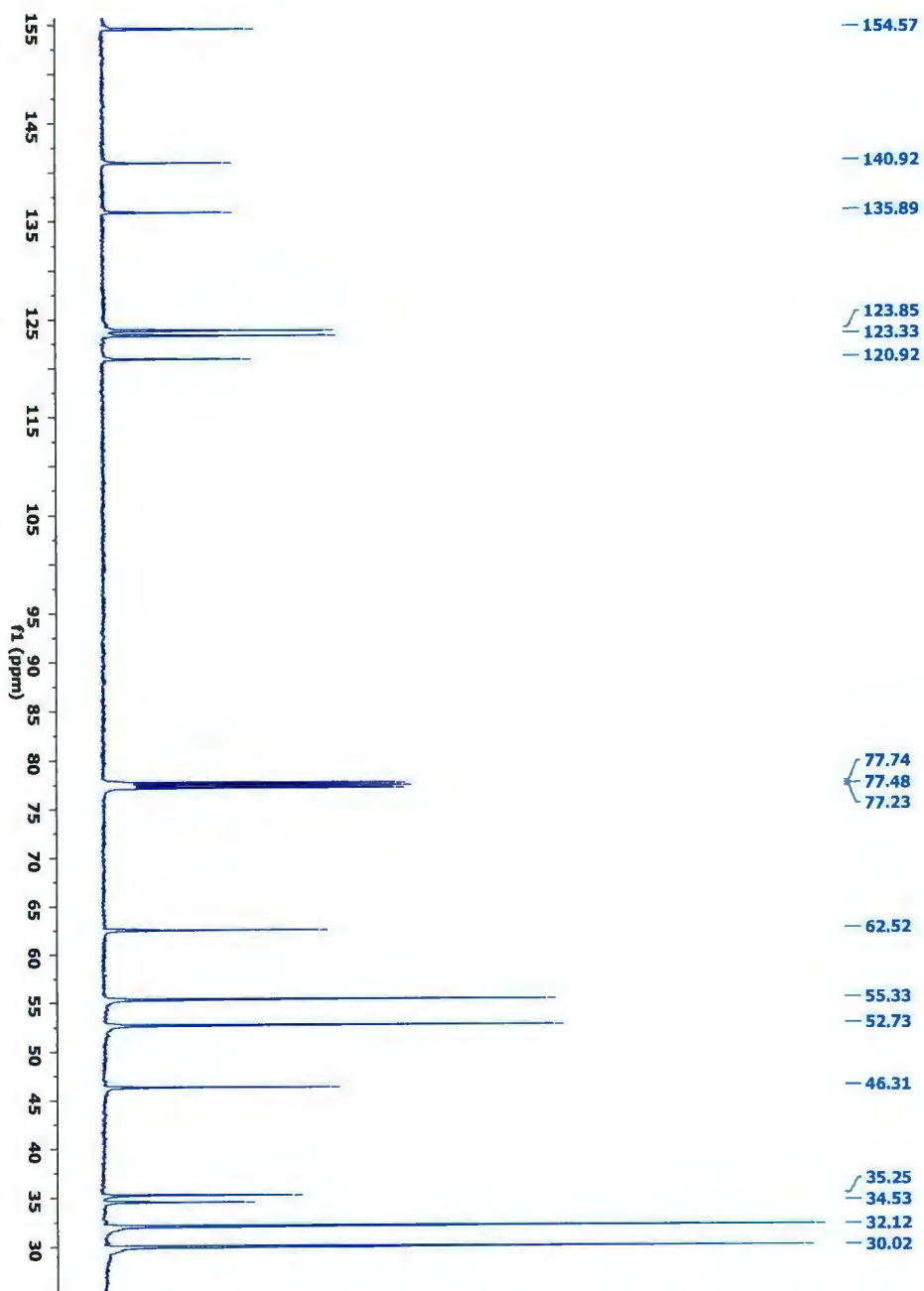


Figure A1.4. ^{13}C NMR spectrum of [L2]H

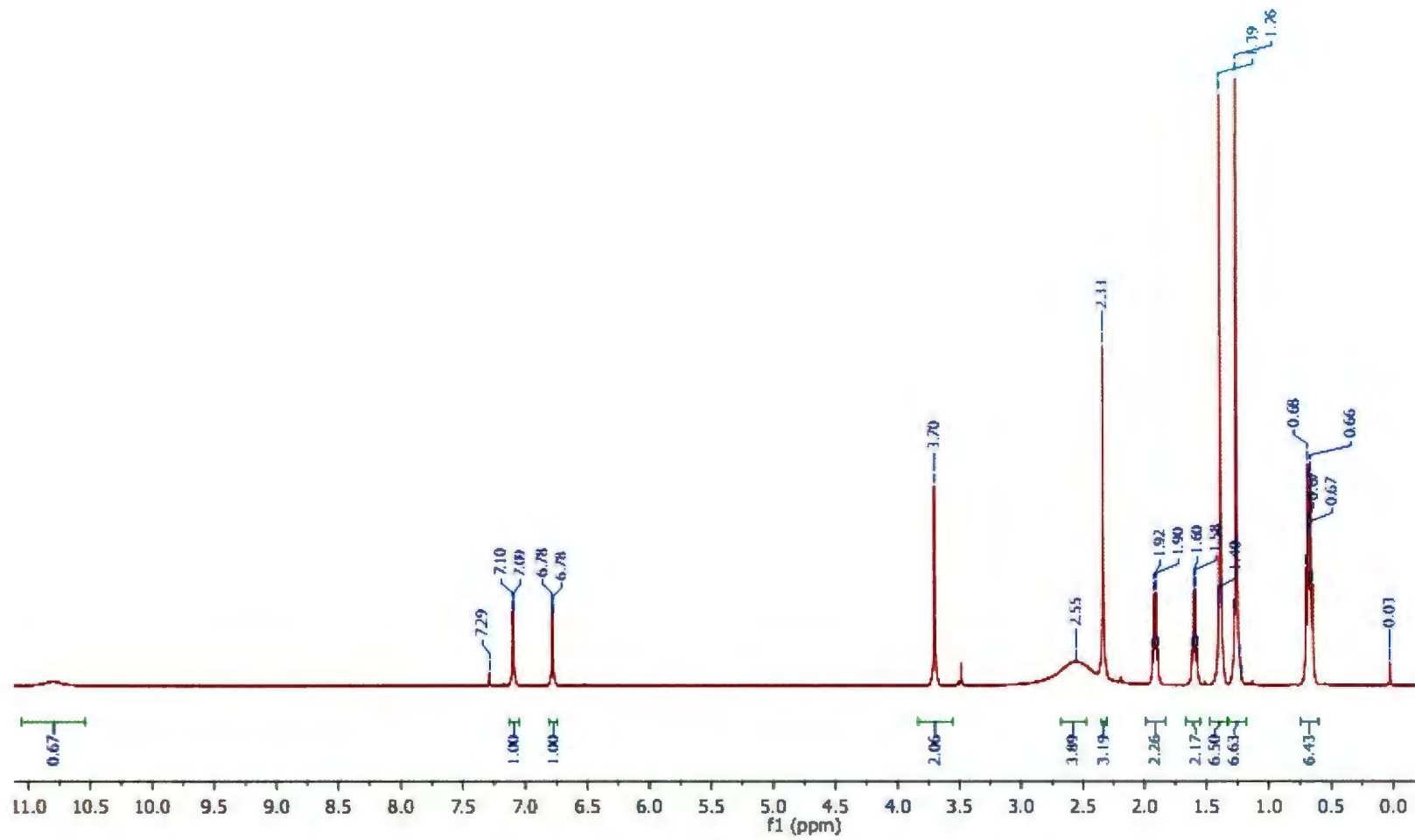


Figure A1.5. ¹H NMR spectrum of [L3]H

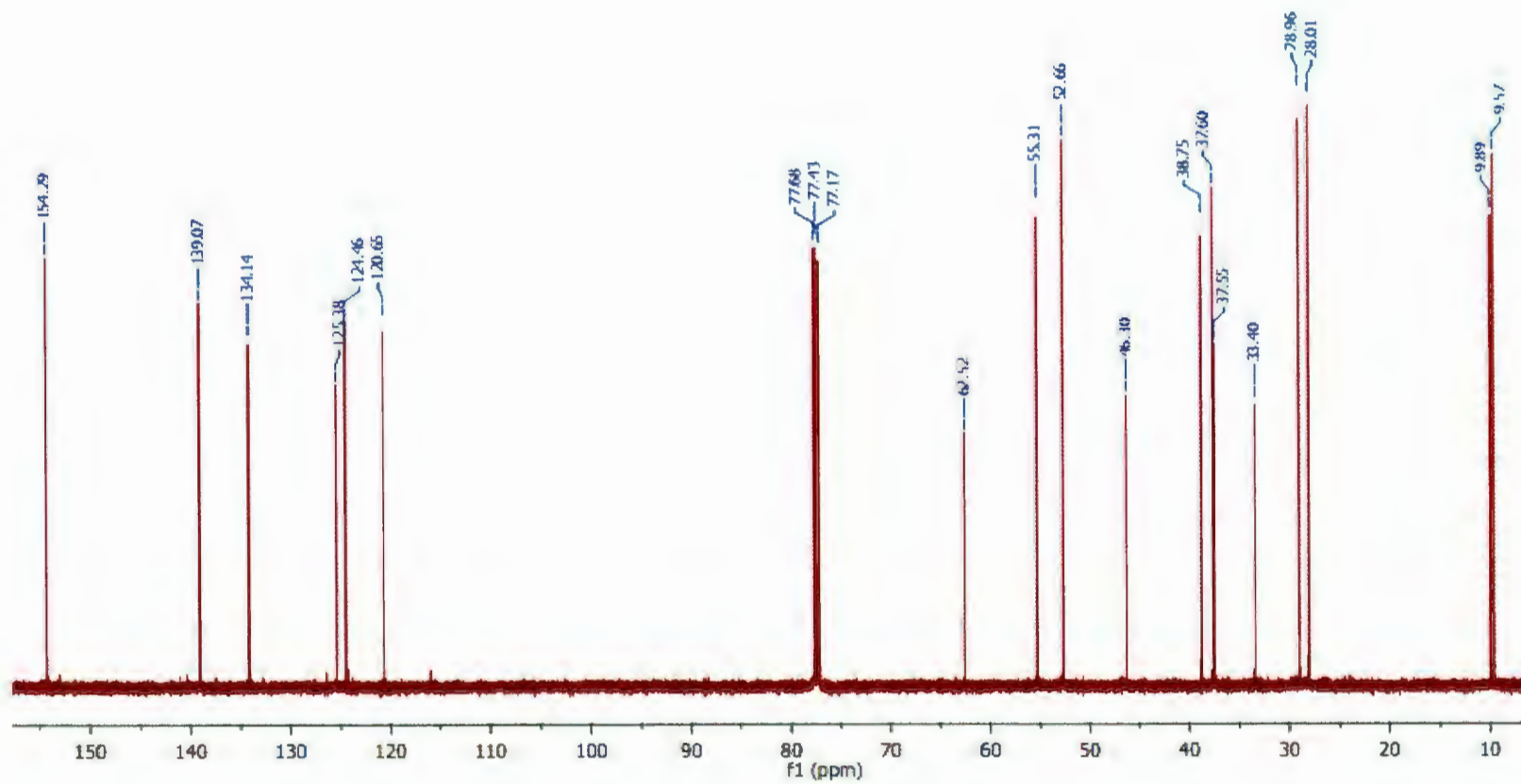


Figure A1.6. ^{13}C NMR spectrum of [L3]H

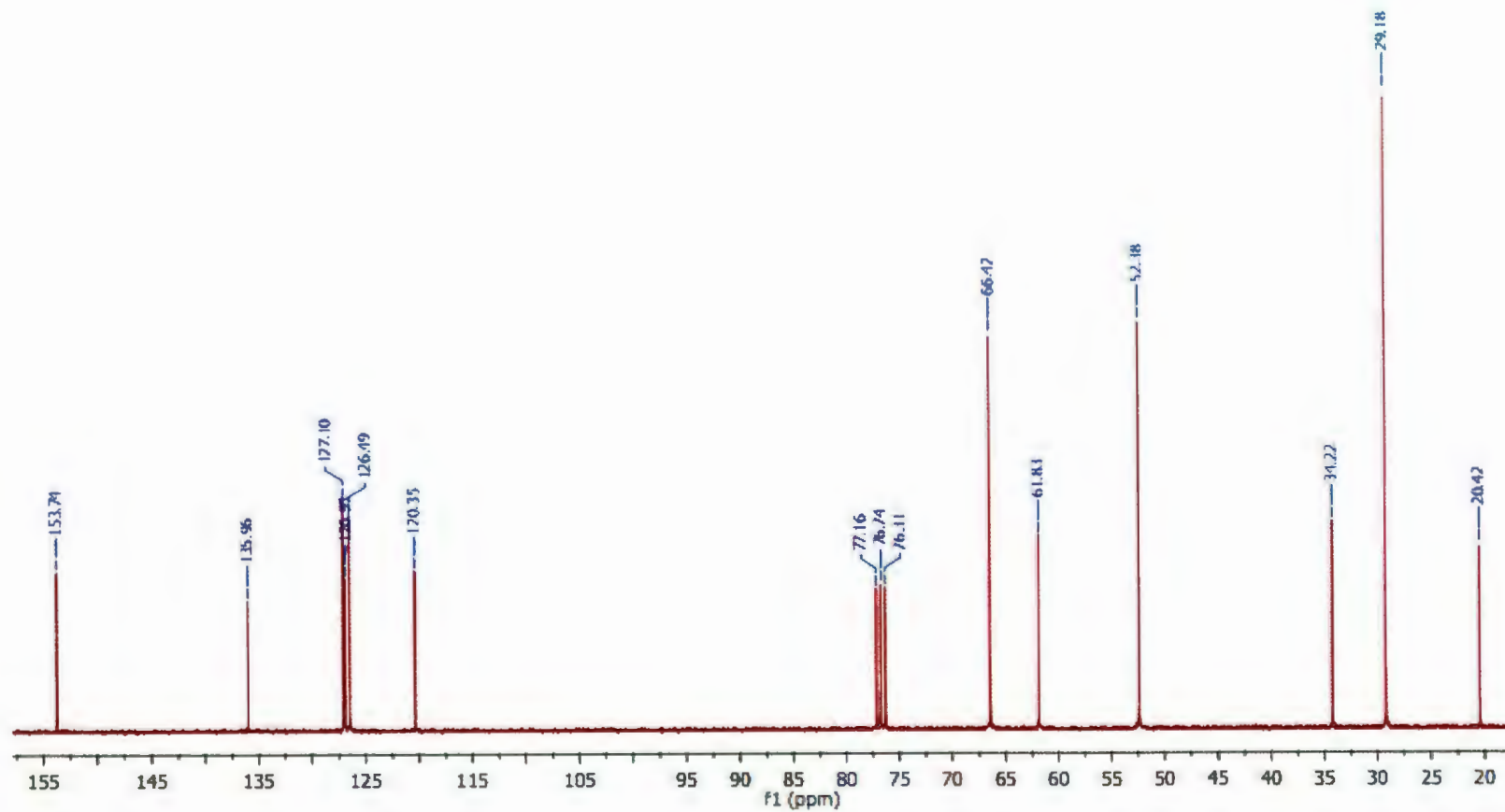


Figure A1.7. ^{13}C NMR spectrum of [L4]H

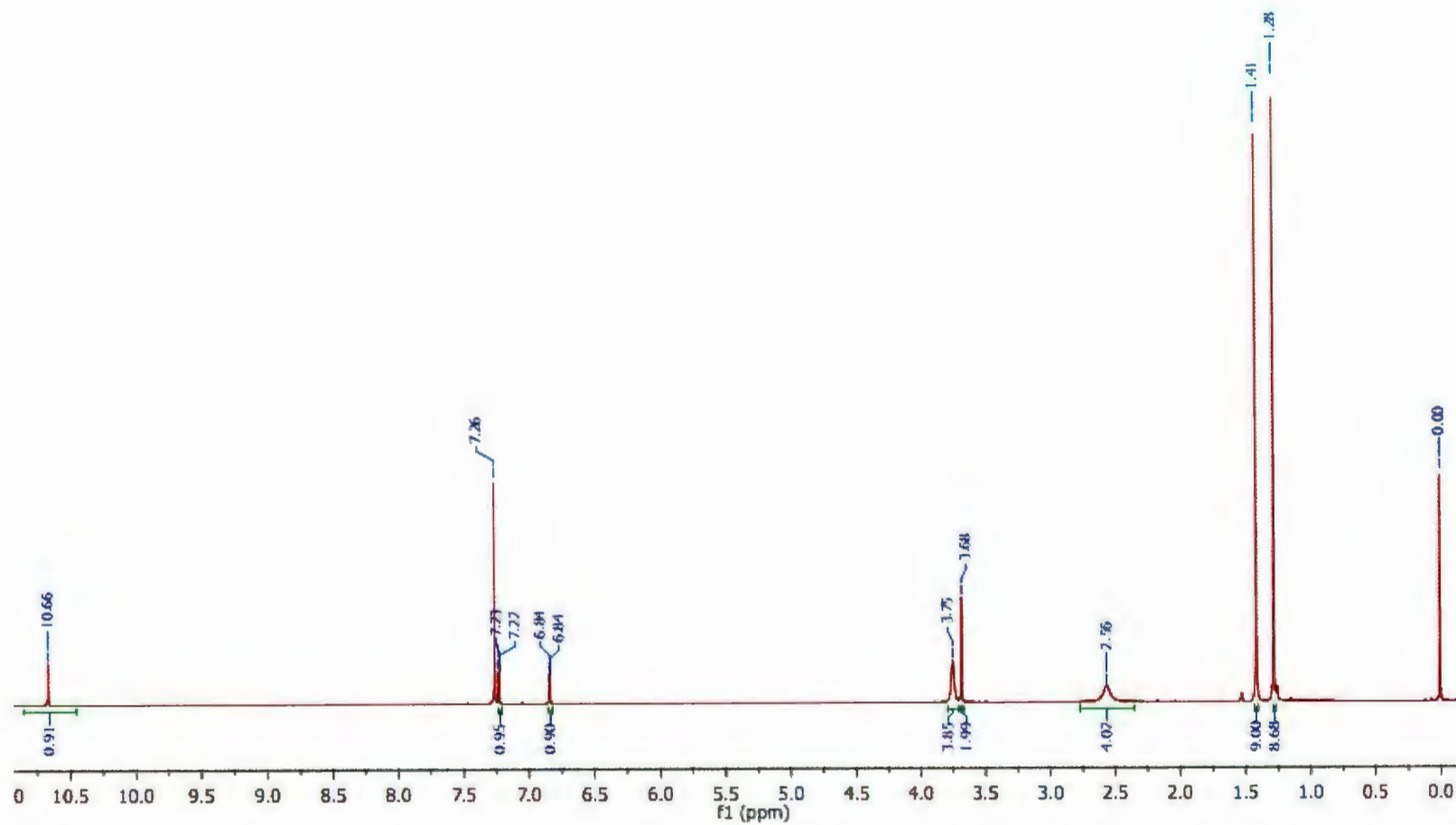


Figure A1.8. ^1H NMR spectrum of [L5]H

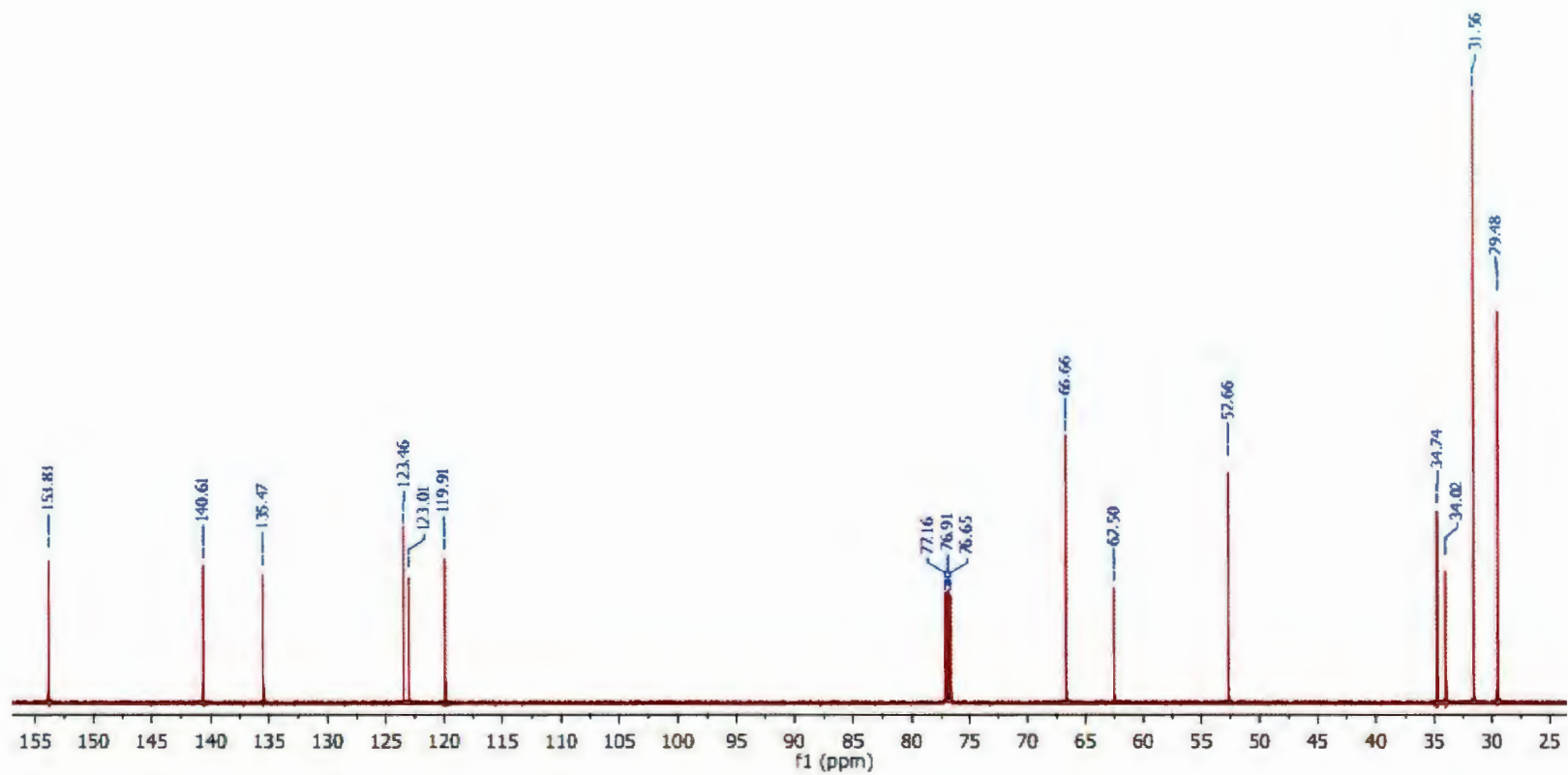


Figure A1.9. ^{13}C NMR spectrum of [L5]H

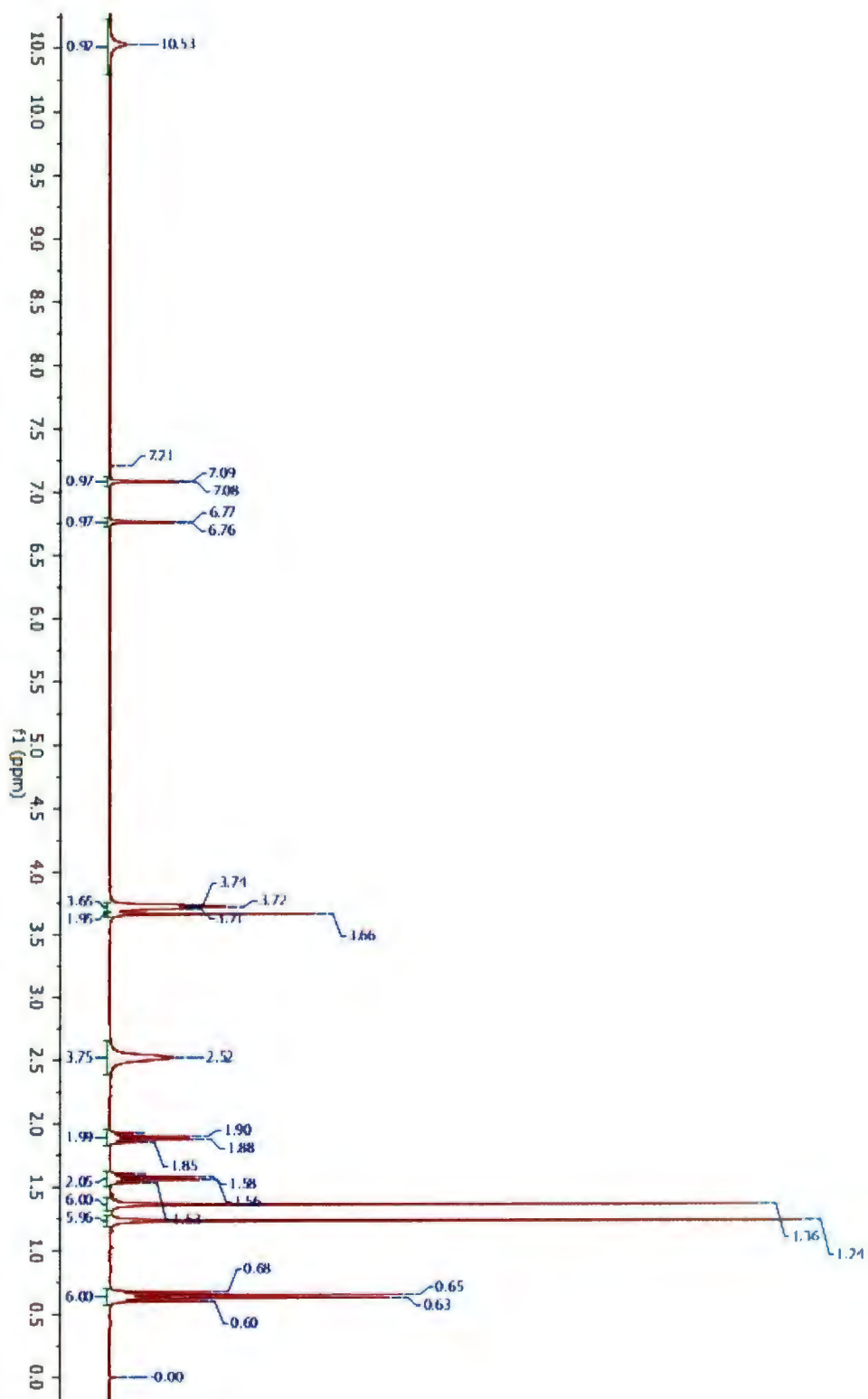


Figure A1.10. ^1H NMR spectrum of [L6]H

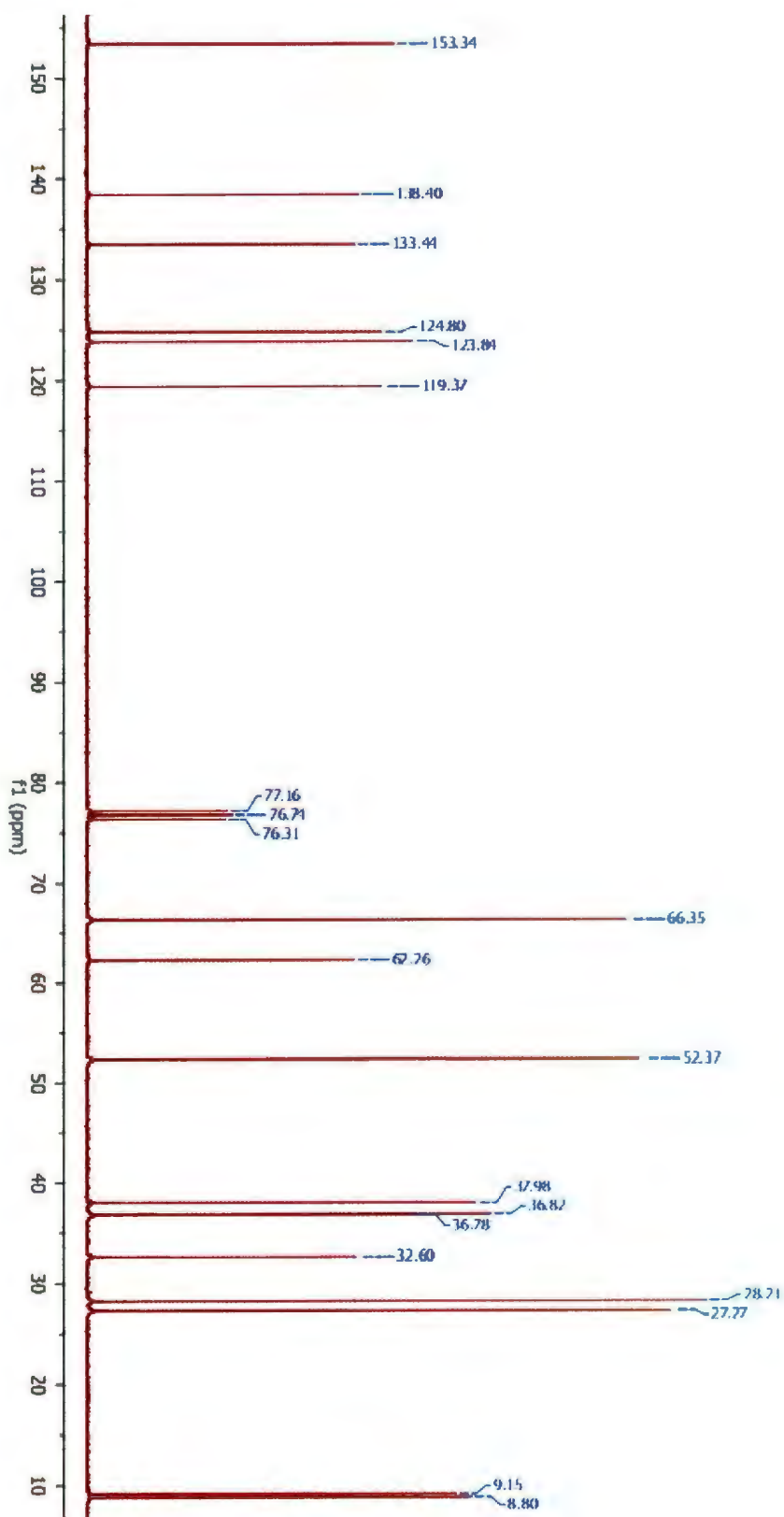


Figure A1.11. ^{13}C NMR spectrum of [L6]H

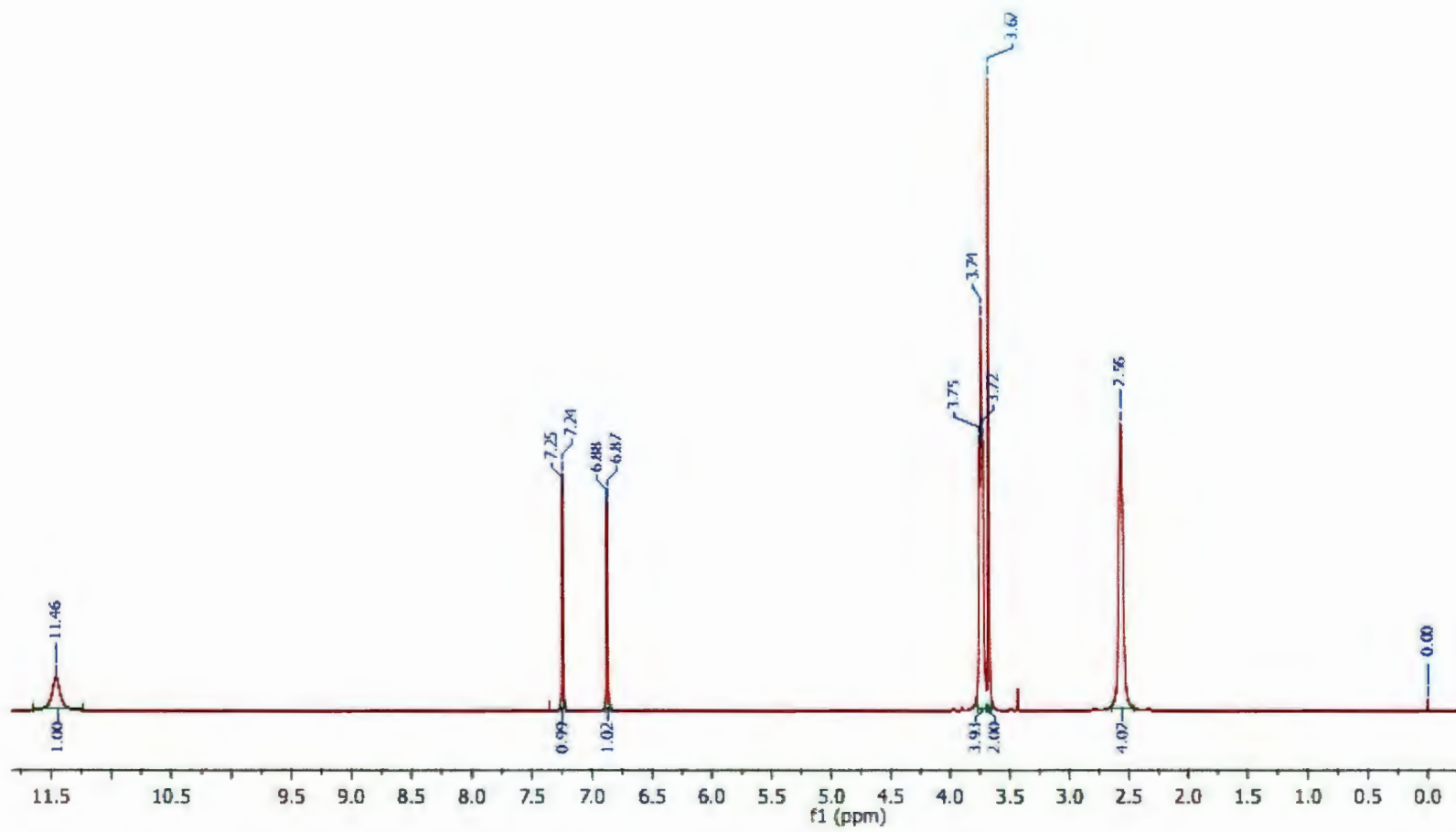


Figure A1.12. ^1H NMR spectrum of [L7]H

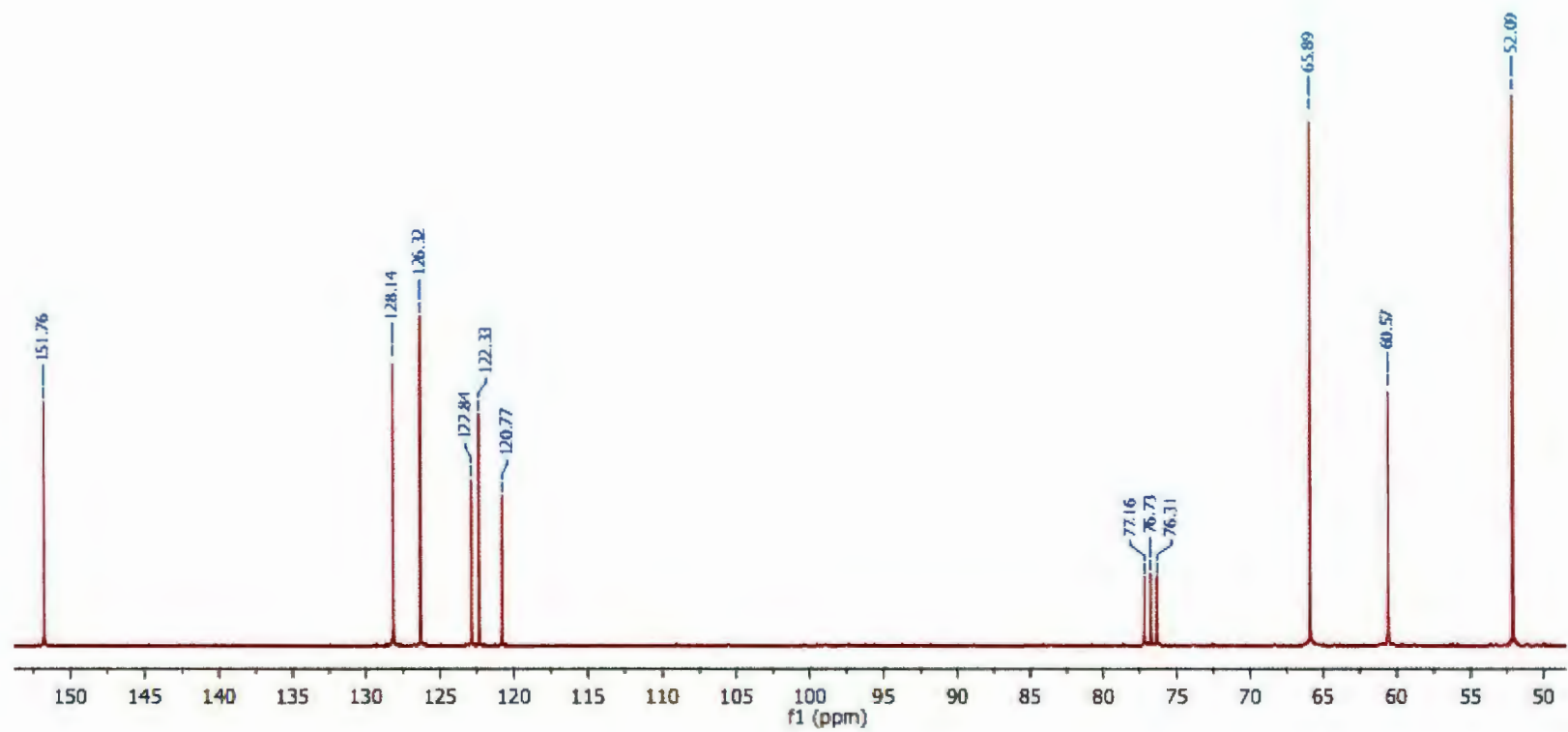


Figure A1.13. ^{13}C NMR spectrum of [L7]H

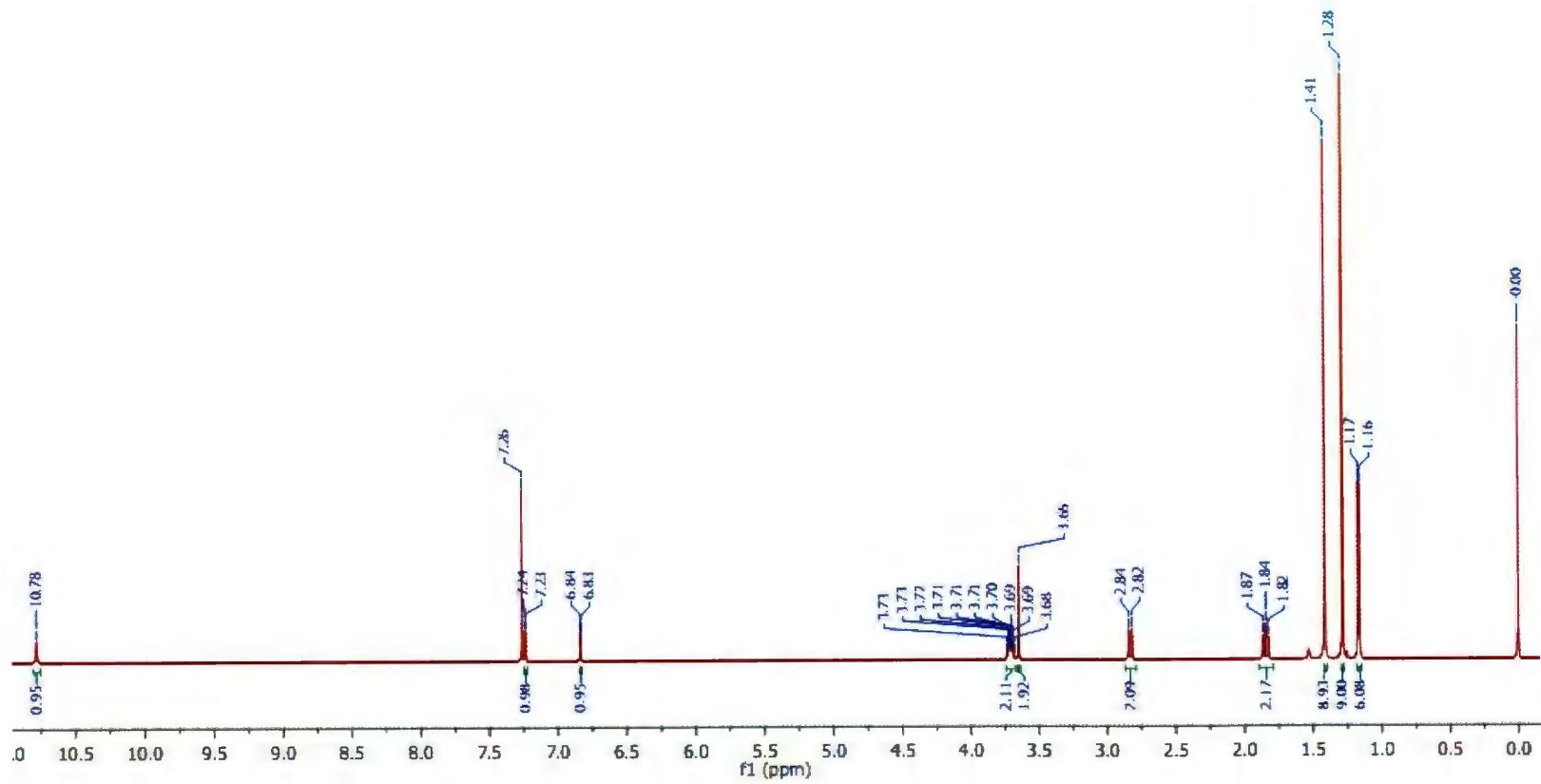


Figure A1.14. ¹H NMR spectrum of [L8]H

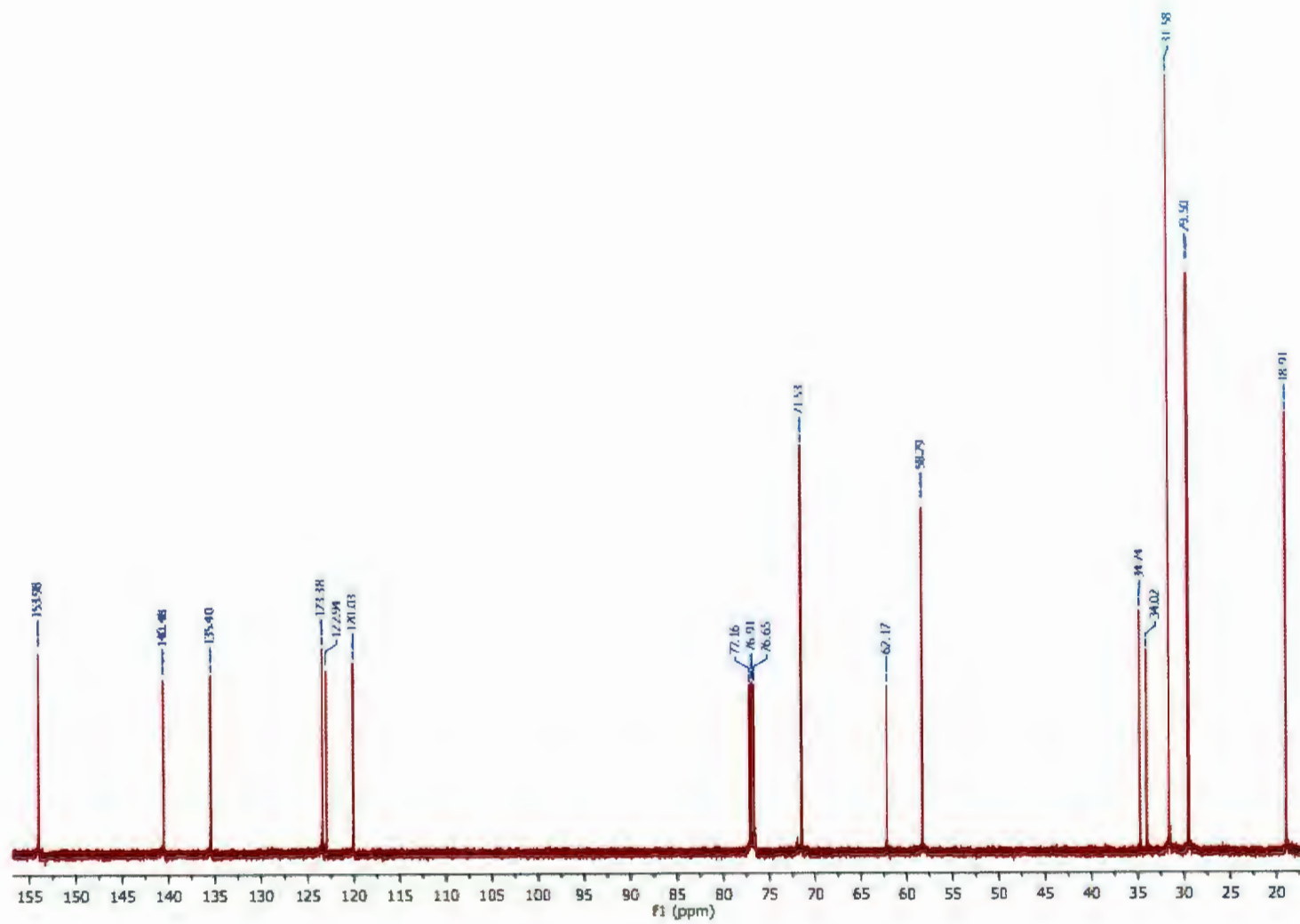


Figure A1. 15. ^{13}C NMR spectrum of [L8]H

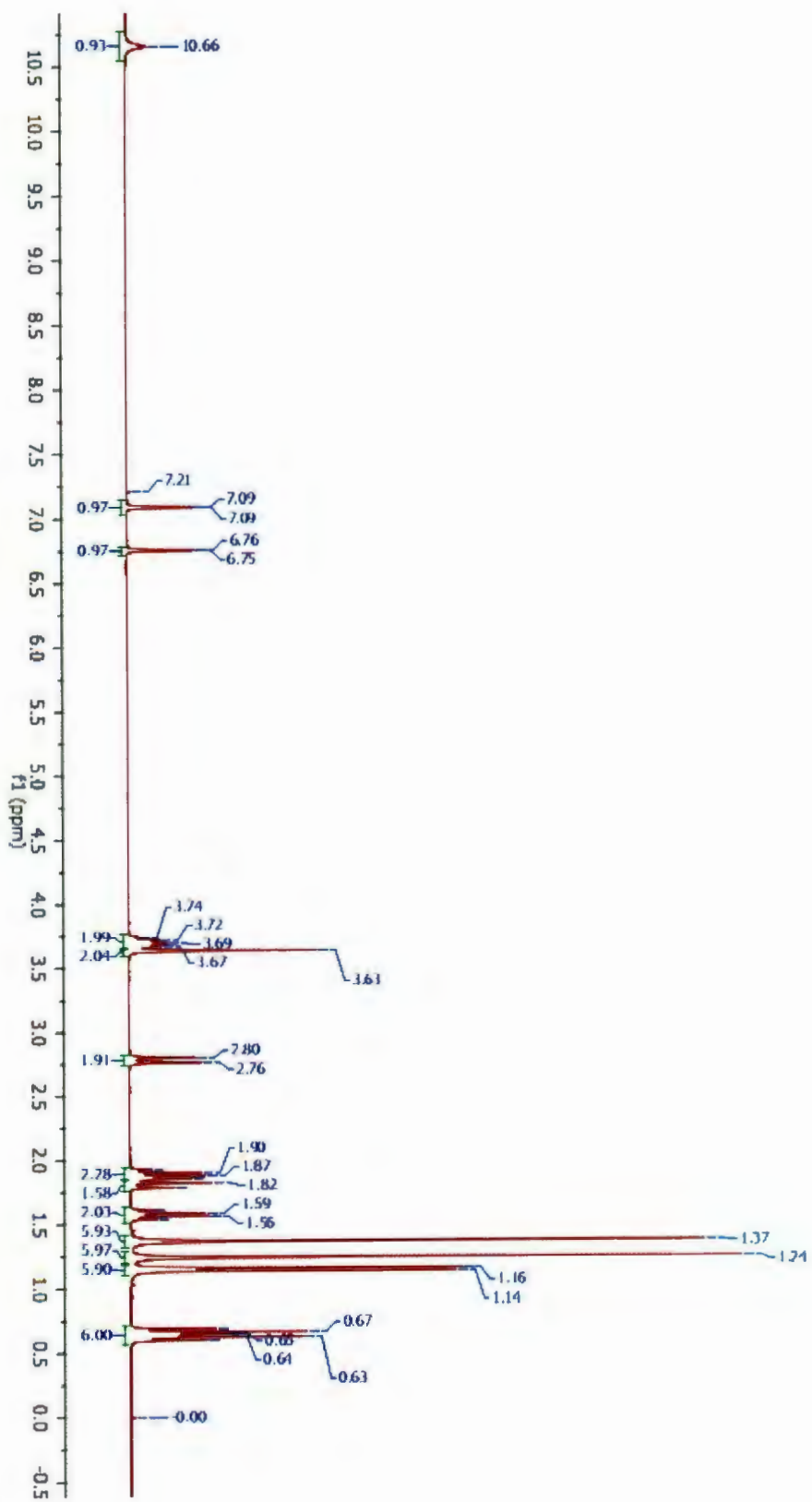


Figure A1.16. ^1H NMR spectrum of [L9]H

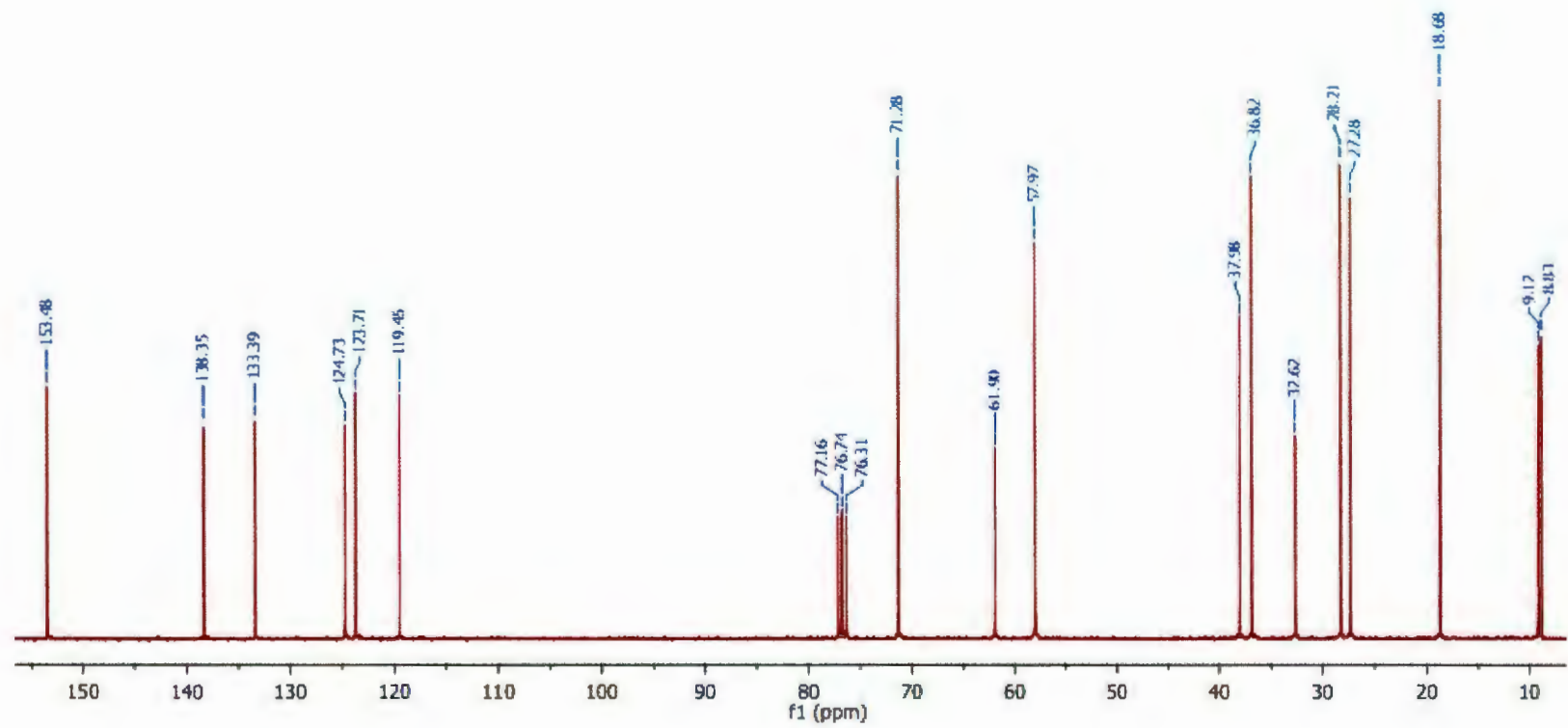


Figure A1.17. ^{13}C NMR spectrum of [L9]H

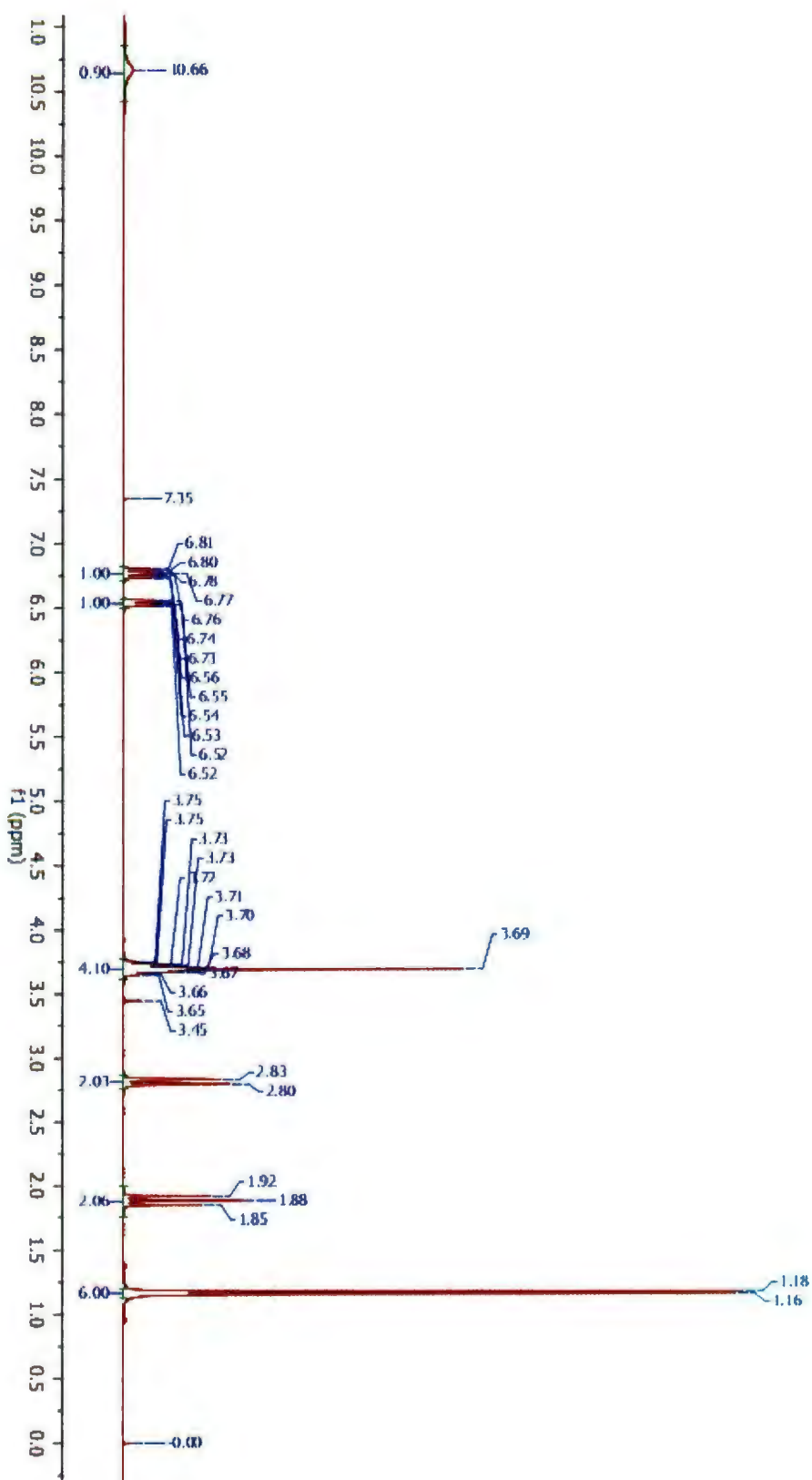


Figure A1.18. ^1H NMR spectrum of [L10]H

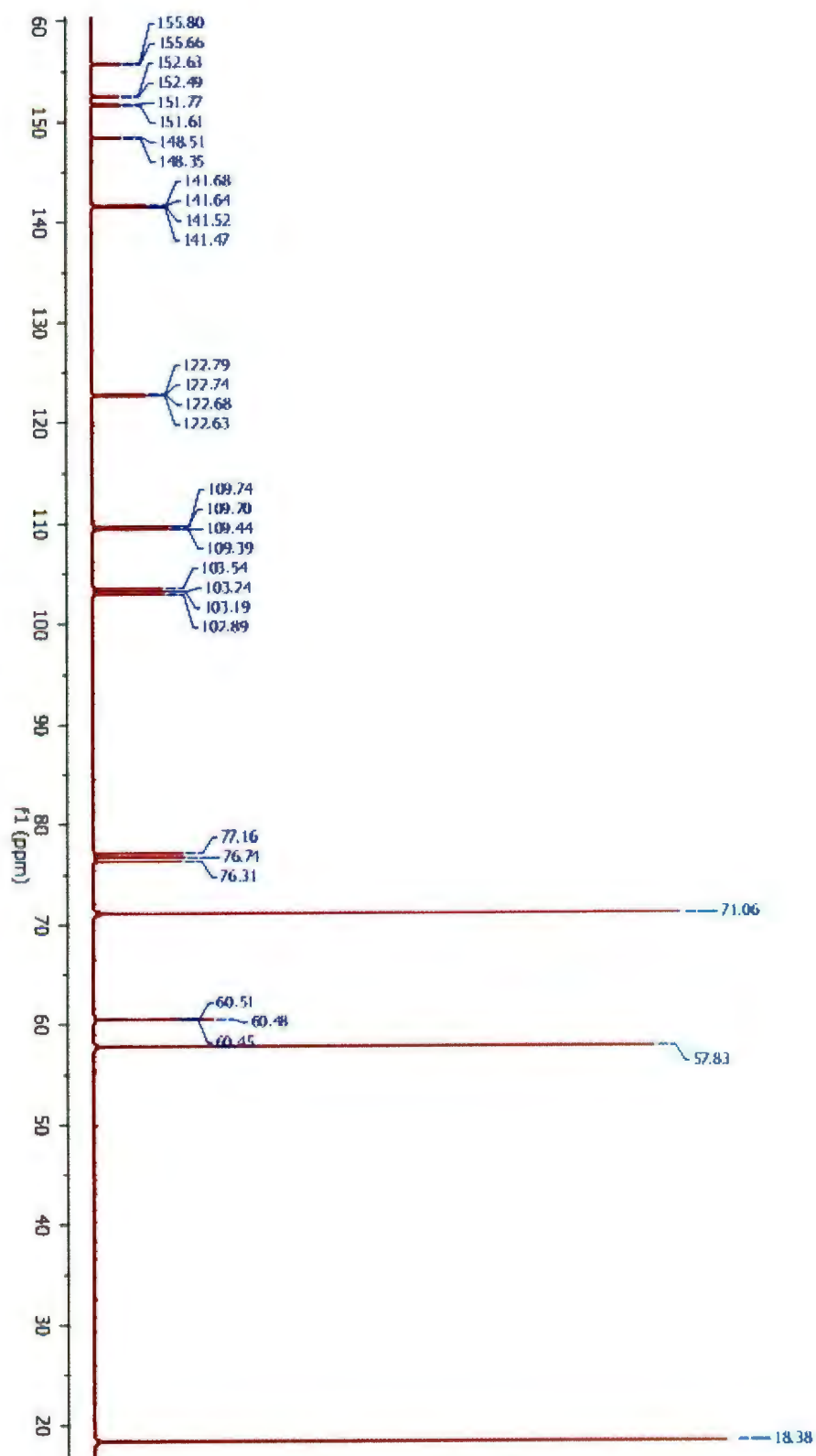


Figure A1.19. ¹³C NMR spectrum of [L10]H

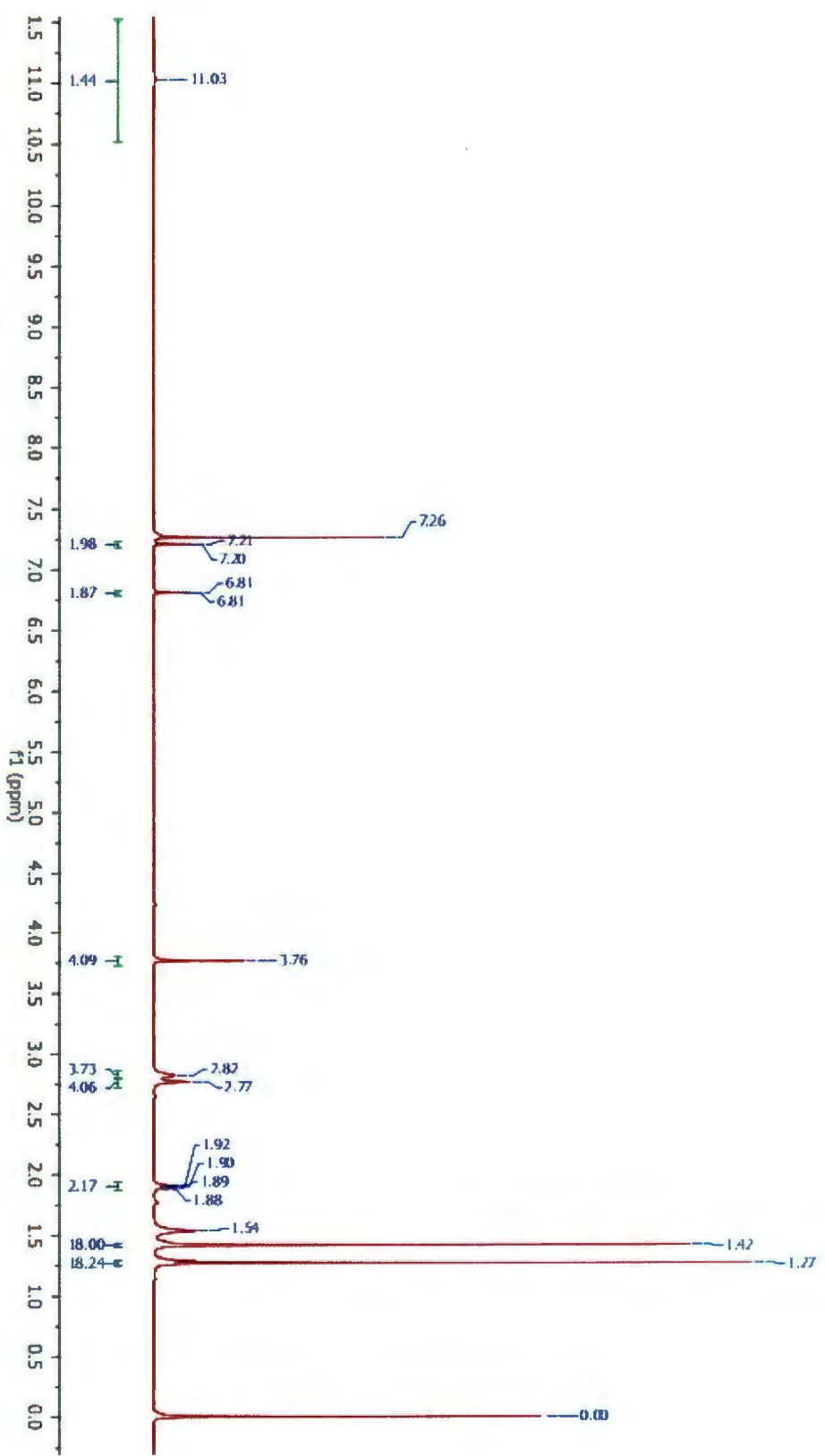


Figure A1.20. ¹H NMR spectrum of [L11]H₂

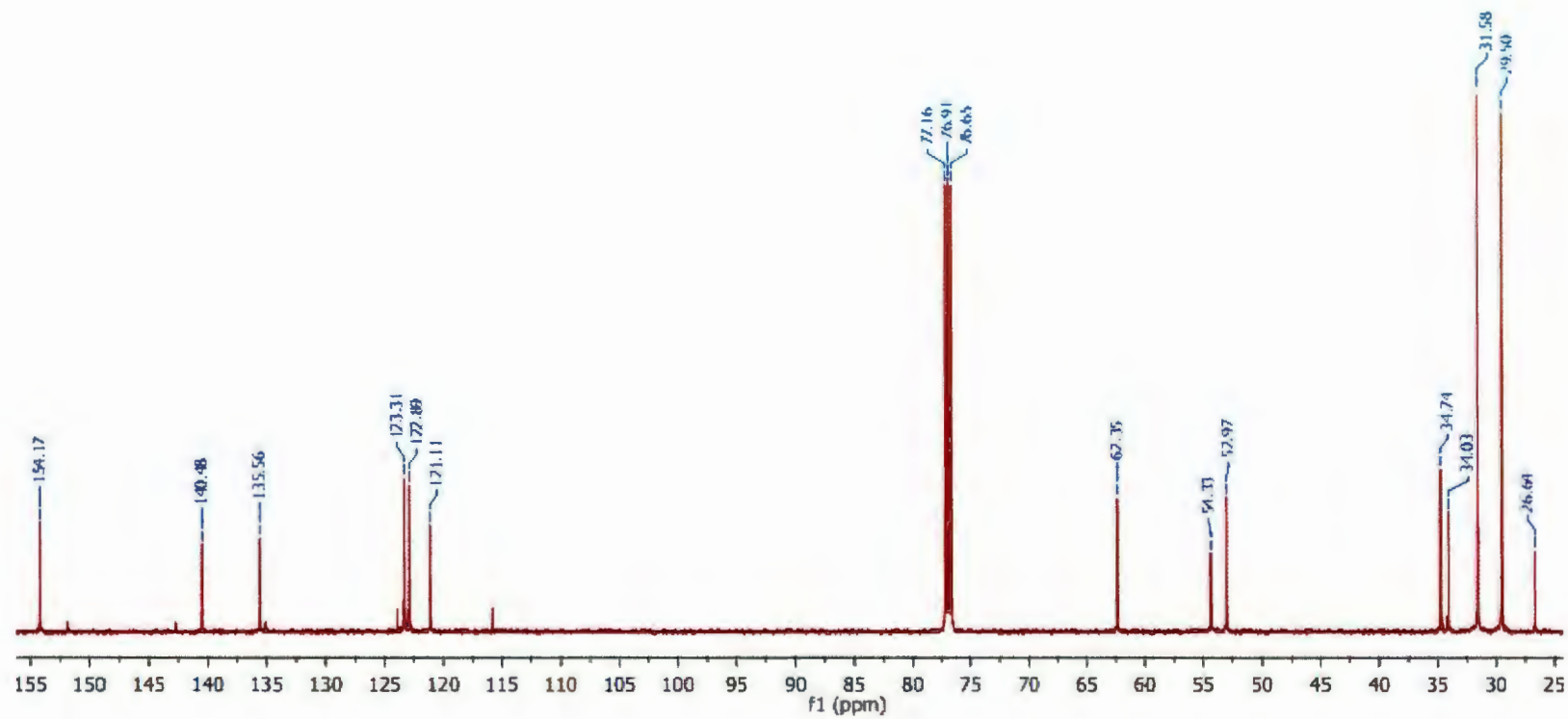


Figure A1.21. ^{13}C NMR spectrum of [L11]2H

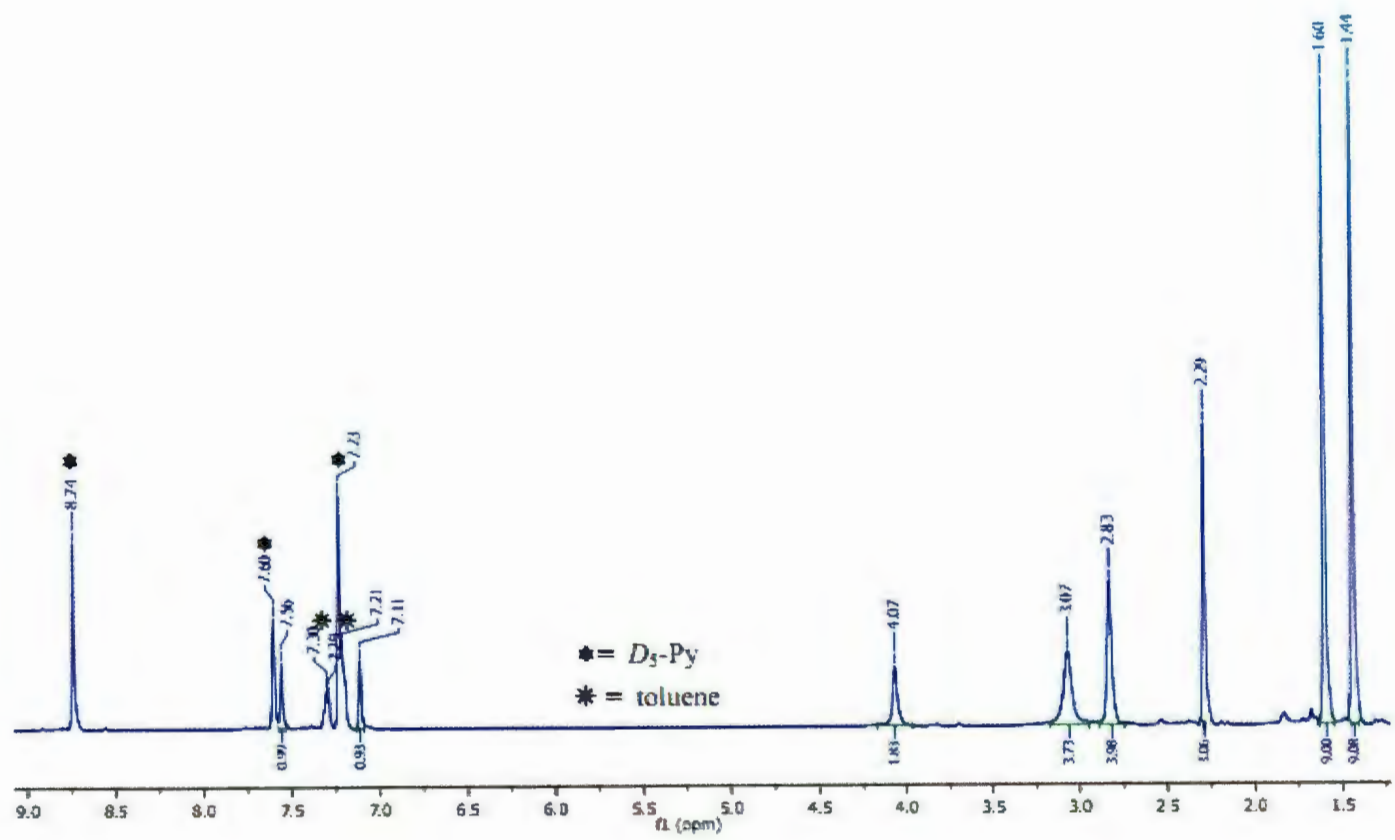


Figure A1.22. ^1H NMR spectrum of **3.1** ($\text{C}_5\text{D}_5\text{N}$, 500 MHz, 343 K)

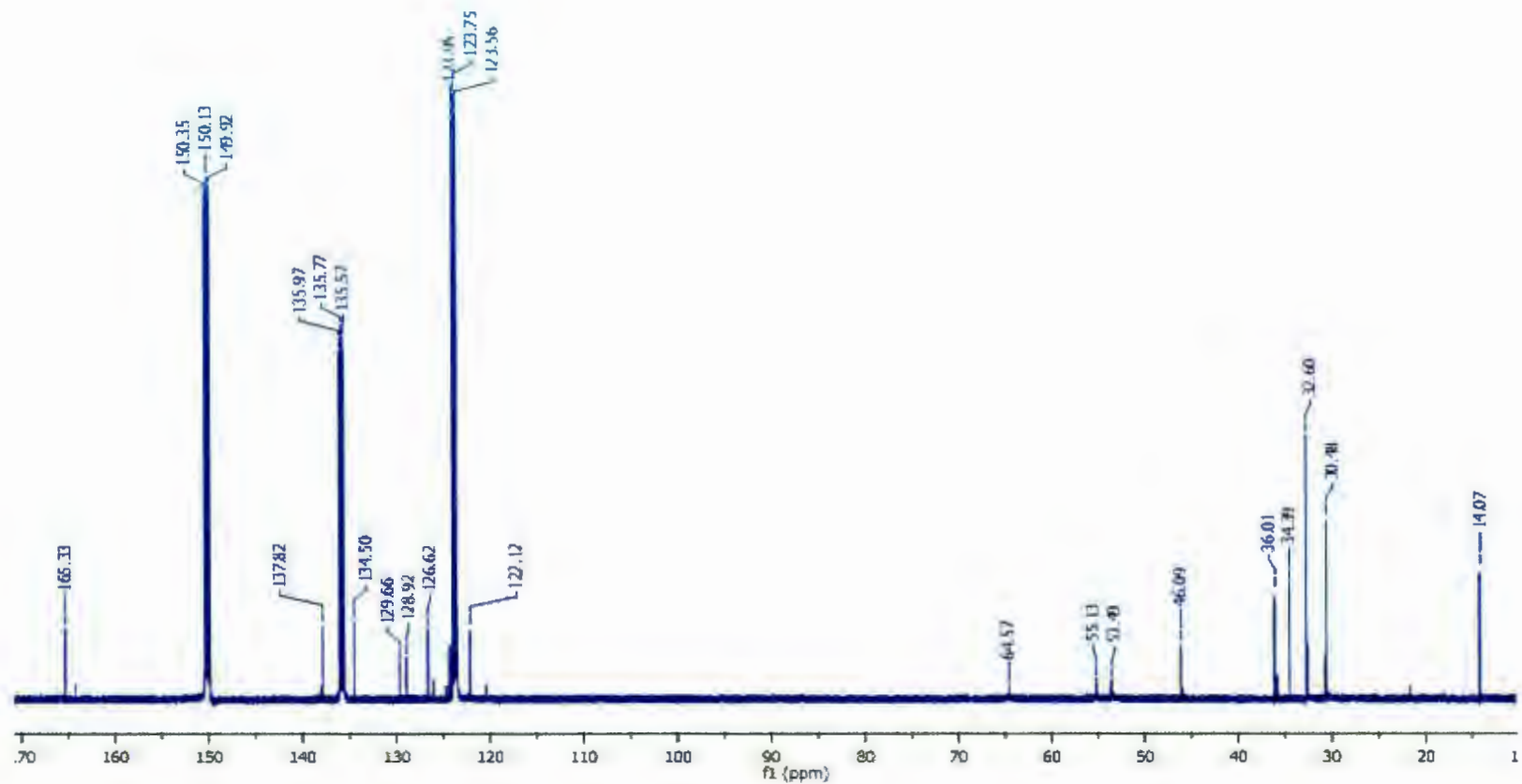


Figure A1.23. ^{13}C NMR spectrum of 3.1 ($\text{C}_5\text{D}_5\text{N}$, 125 MHz, 298 K)

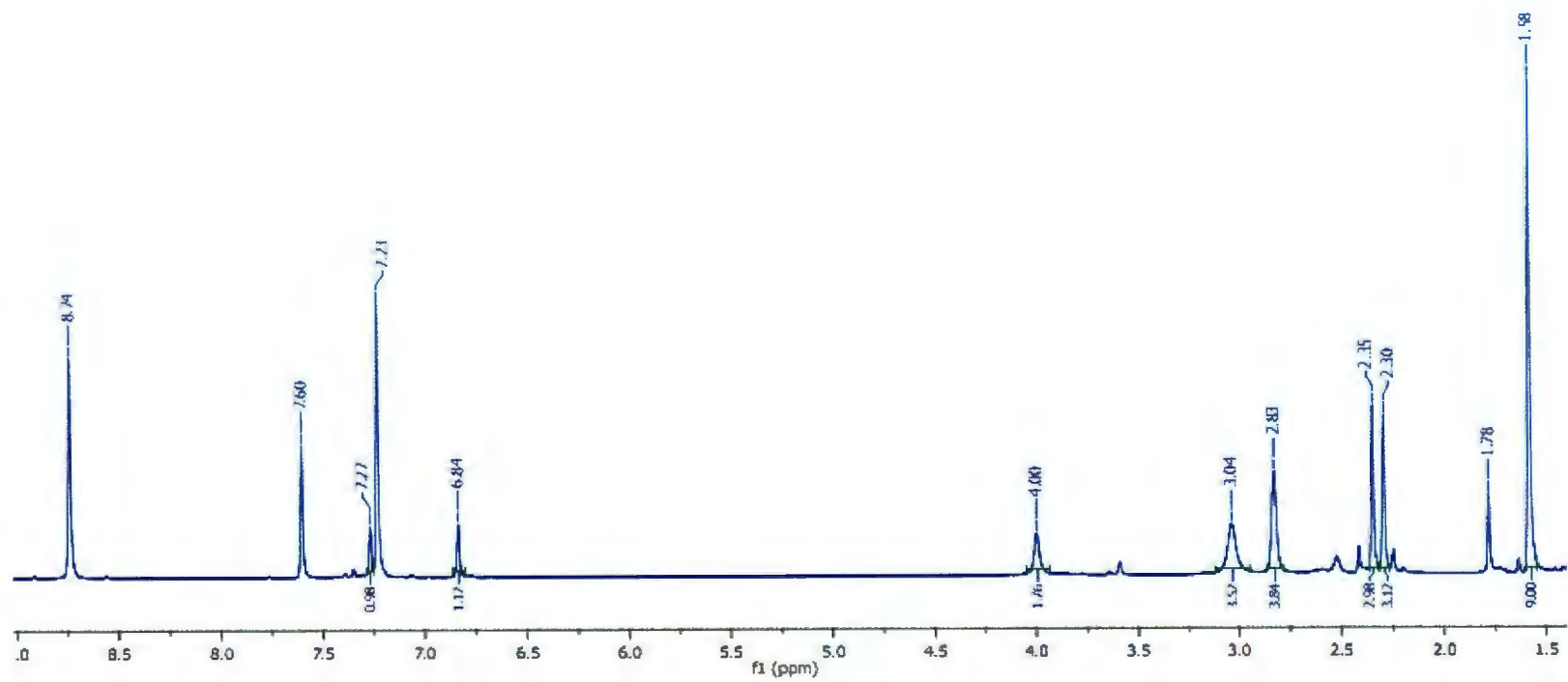


Figure A1.24. ^1H NMR spectrum of 3.2 ($\text{C}_5\text{D}_5\text{N}$, 500MHz, 343 K)

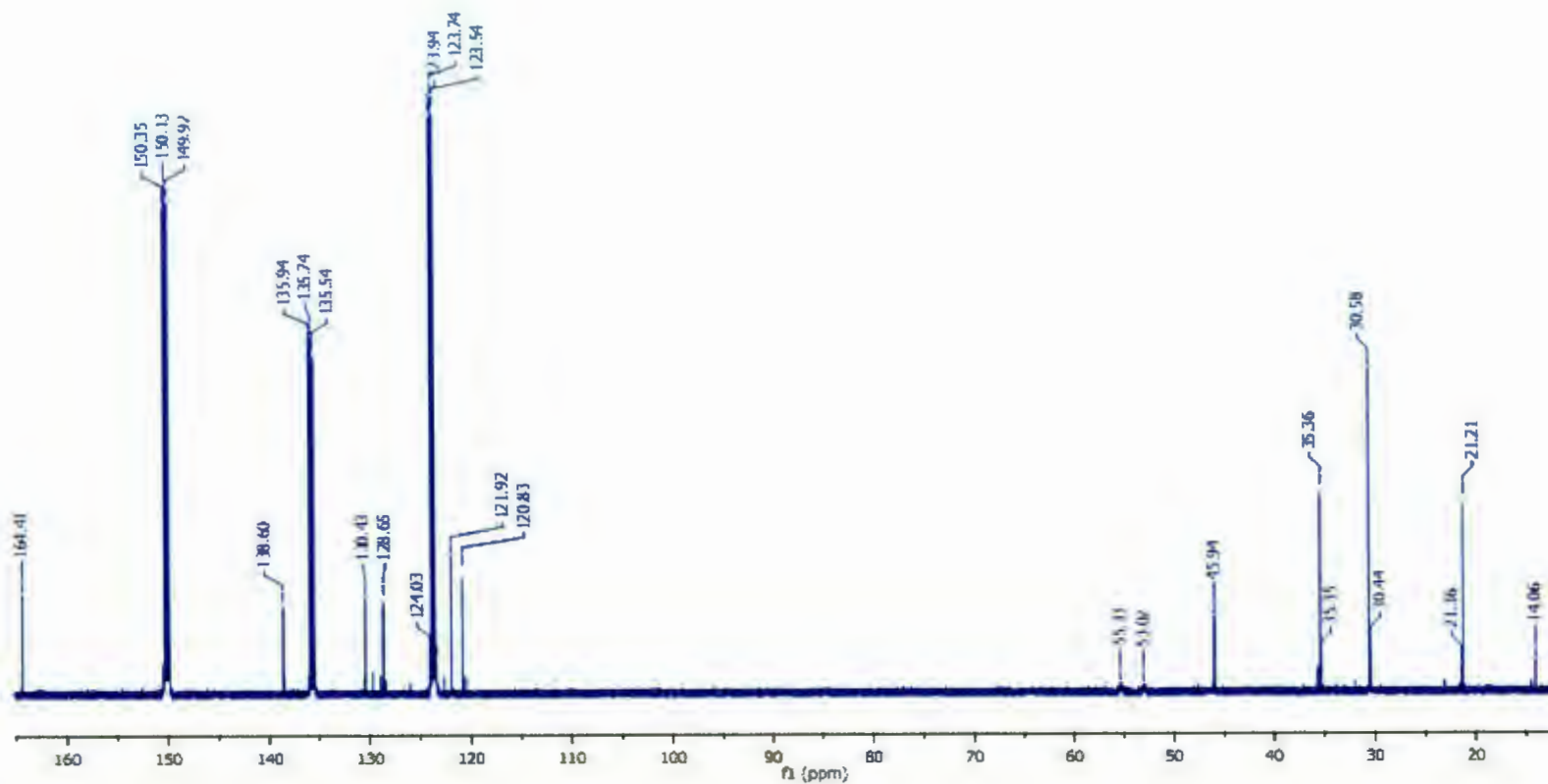


Figure A1.25. ^{13}C NMR spectrum of **3.2** ($\text{C}_5\text{D}_5\text{N}$, 125MHz, 298 K)

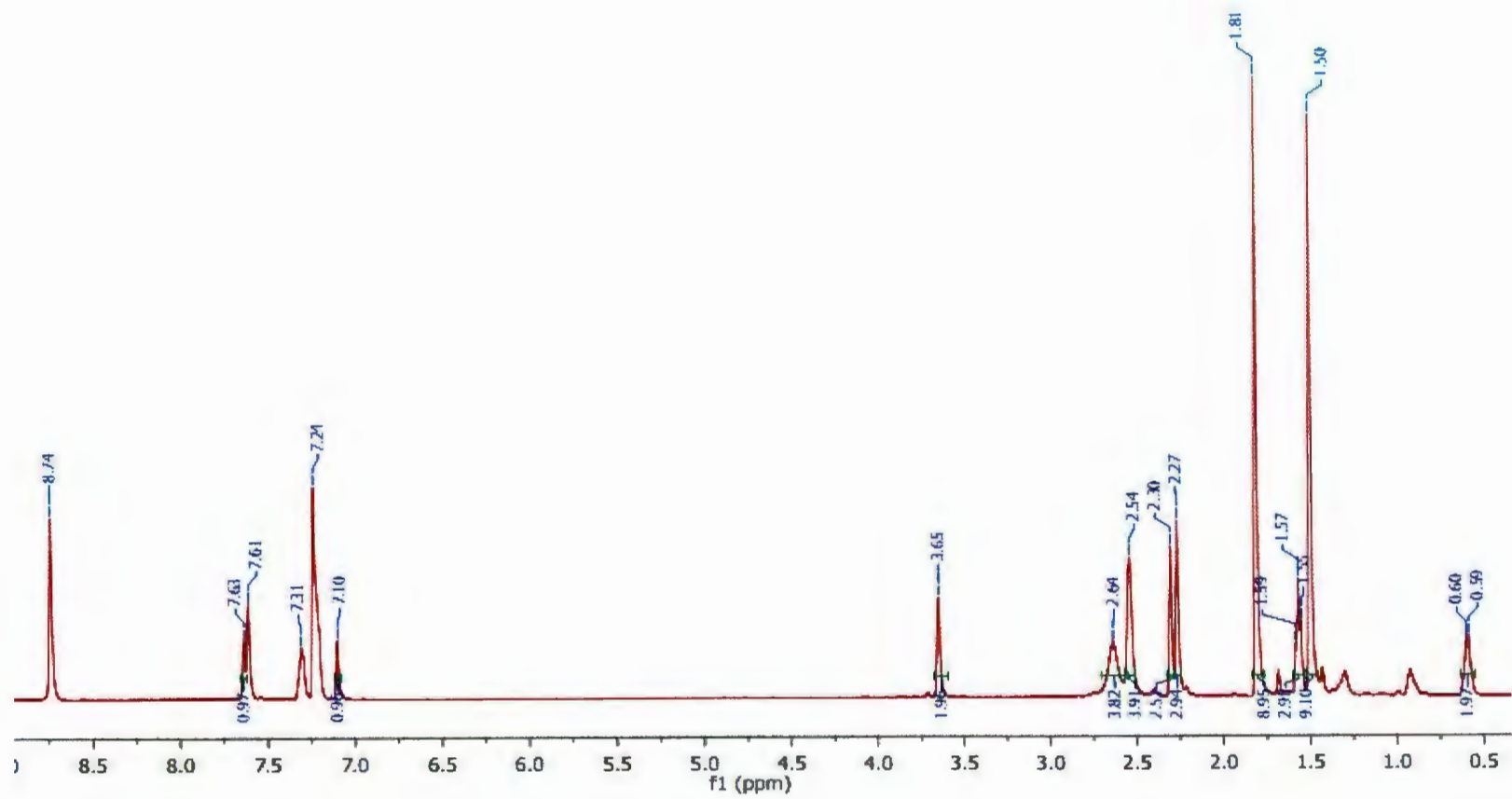


Figure A1.26. ^1H NMR spectrum of 3.3 ($\text{C}_5\text{D}_5\text{N}$, 500 MHz, 358 K)

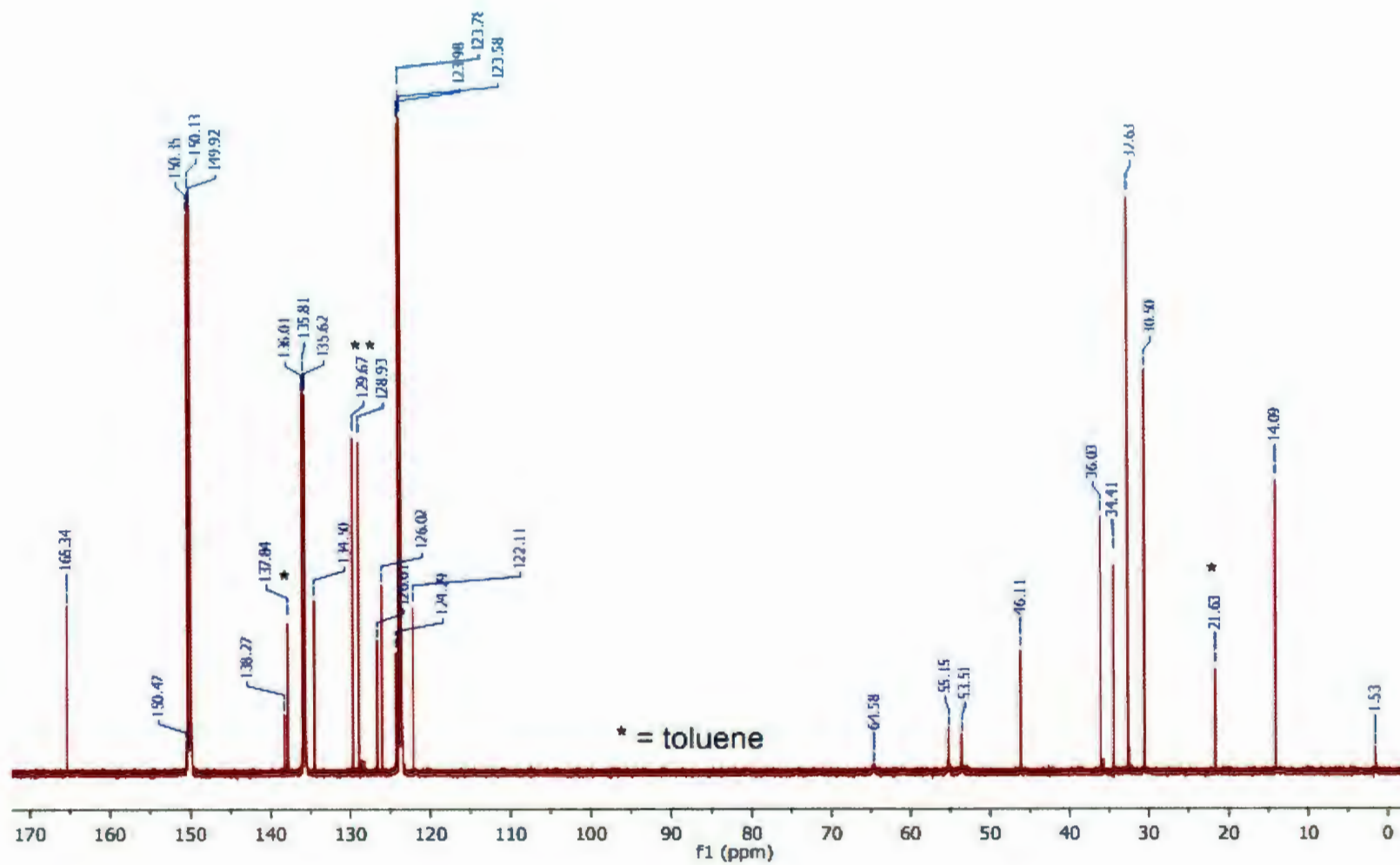


Figure A1.27. ^{13}C NMR spectrum of 3.3 ($\text{C}_5\text{D}_5\text{N}$, 125 MHz, 298K)

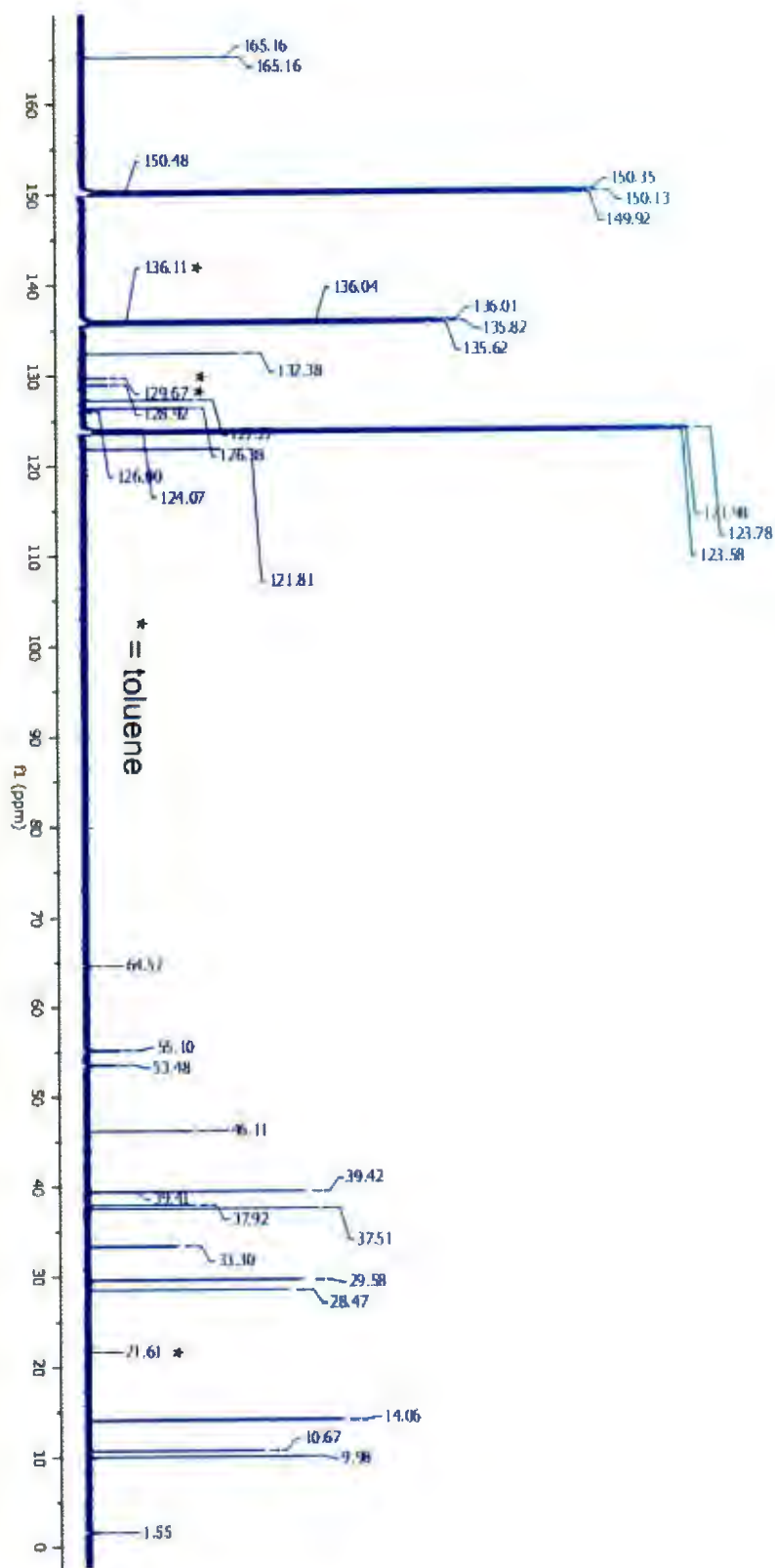


Figure A1.28. ^{13}C NMR spectrum of 3.4 ($\text{C}_5\text{D}_5\text{N}$, 125 MHz, 298 K)

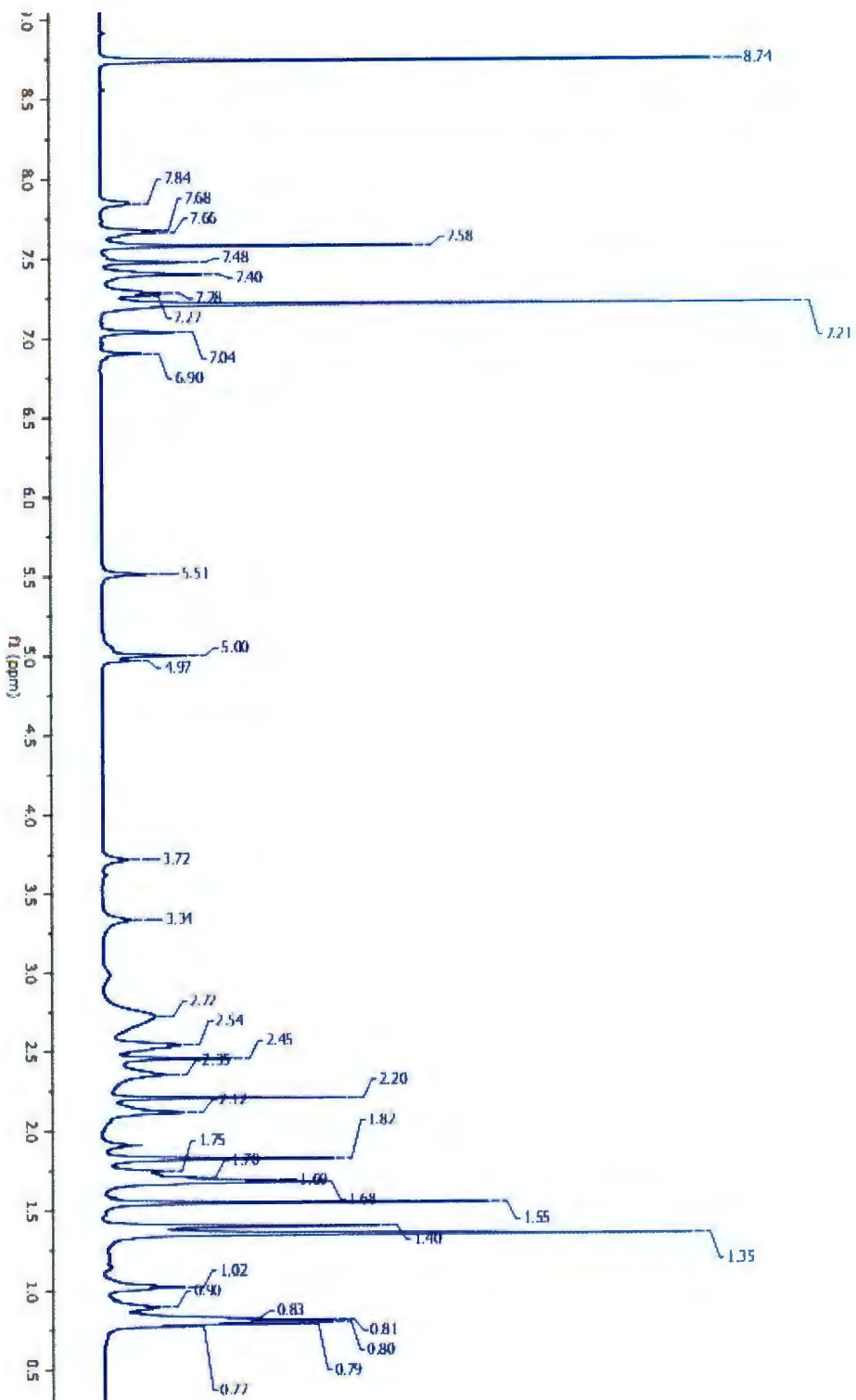


Figure A1.29. ^1H NMR spectrum of 3.5 ($\text{C}_5\text{D}_5\text{N}$, 500 MHz, 343 K)

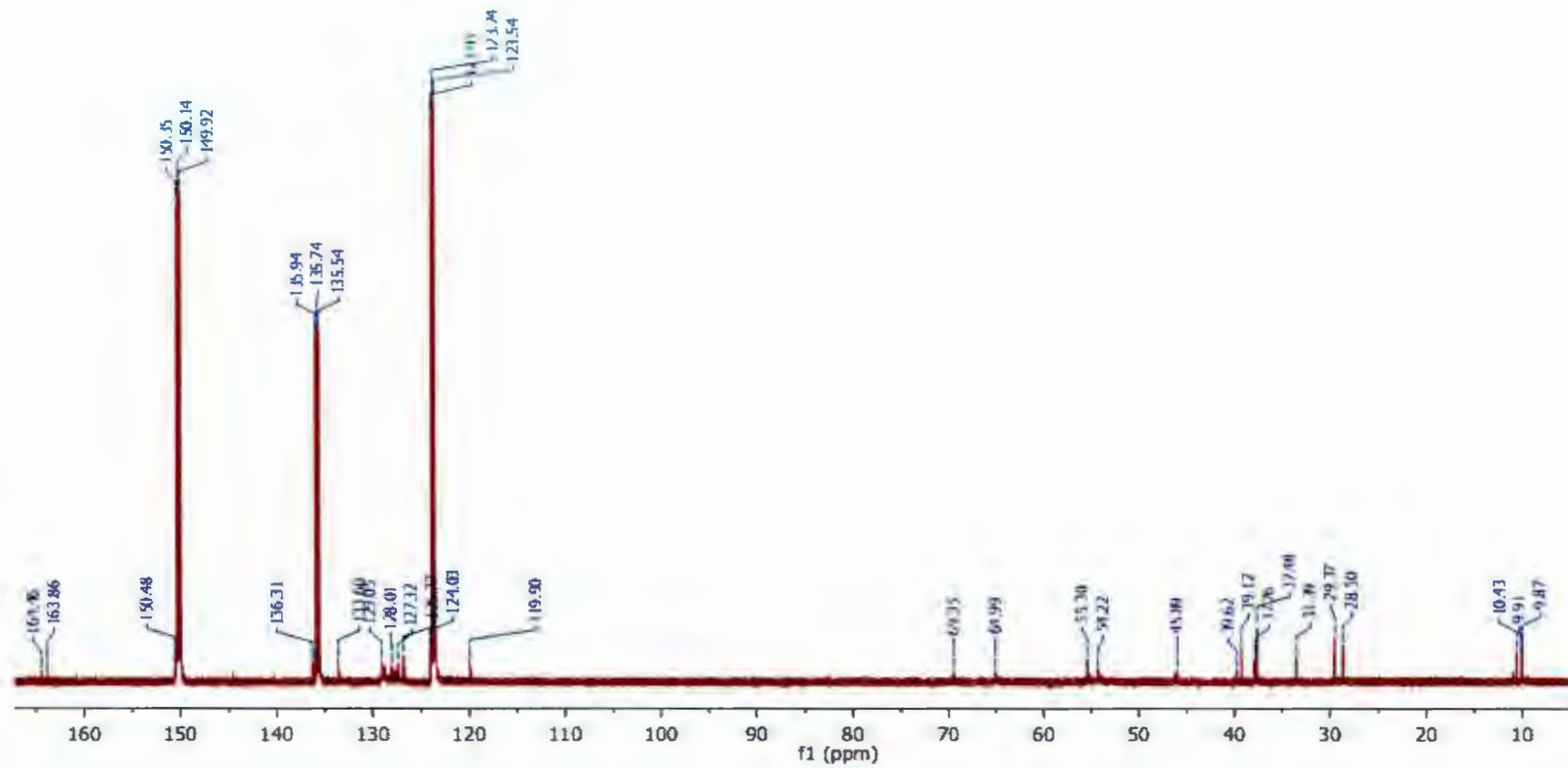


Figure A1.30. ^{13}C NMR spectrum of 3.5 ($\text{C}_5\text{D}_5\text{N}$, 125 MHz, 298 K)

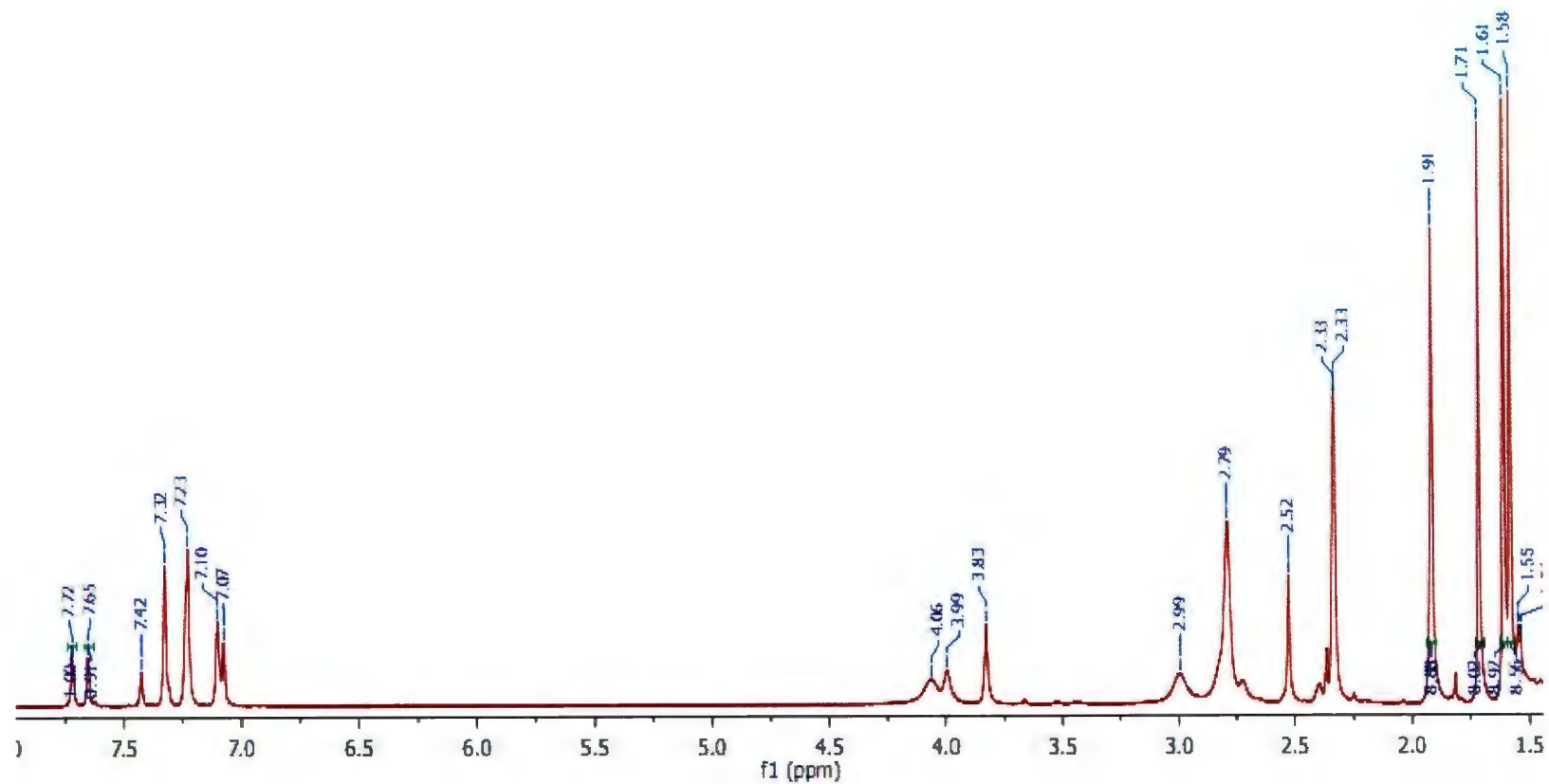


Figure A1.31. ^1H NMR spectrum of **3.6** ($\text{C}_5\text{D}_5\text{N}$, 500 MHz, 358 K)

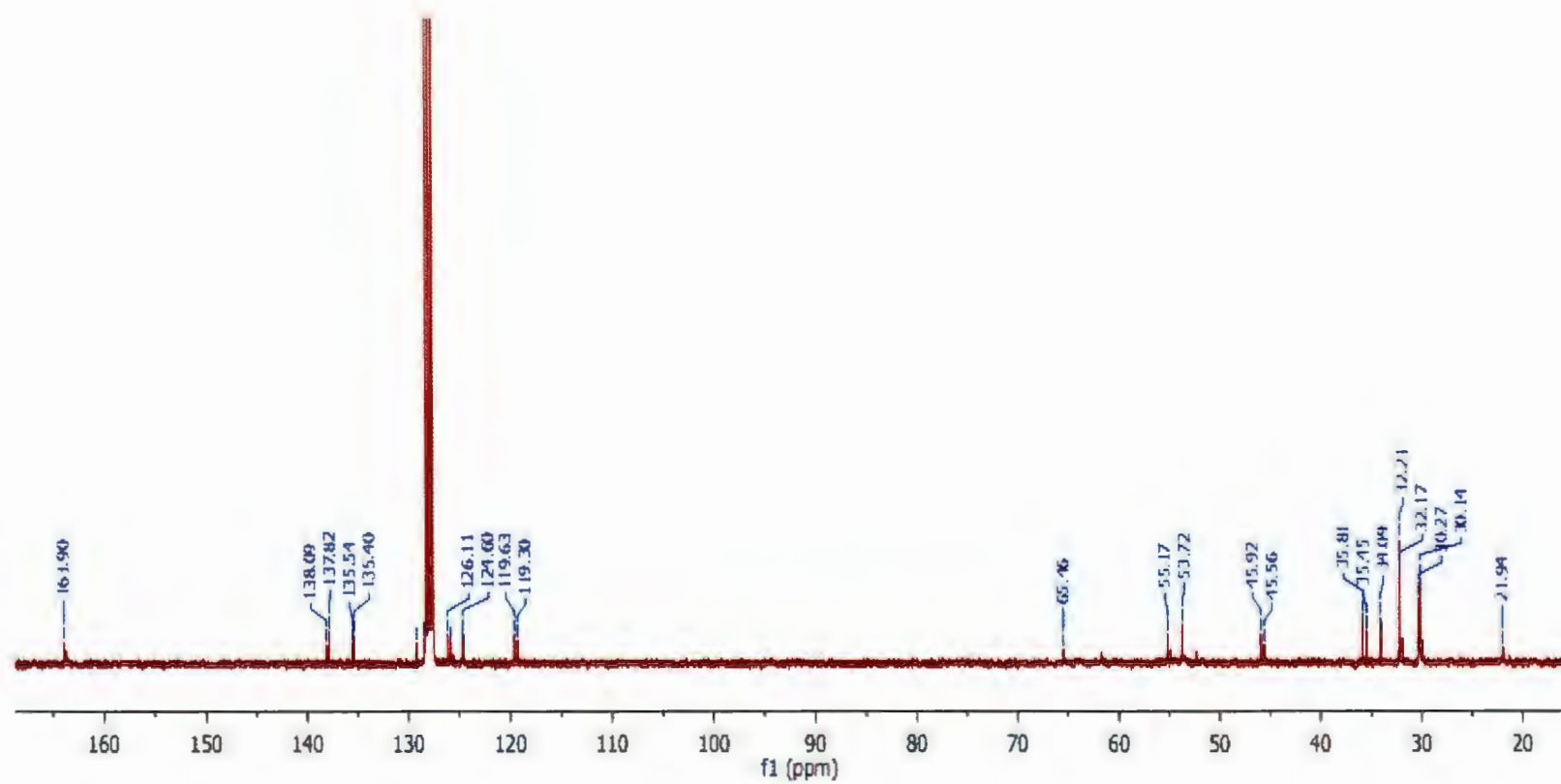


Figure A1.32. ^{13}C NMR spectrum of 3.6 (C_6D_6 , 125 MHz, 298 K)

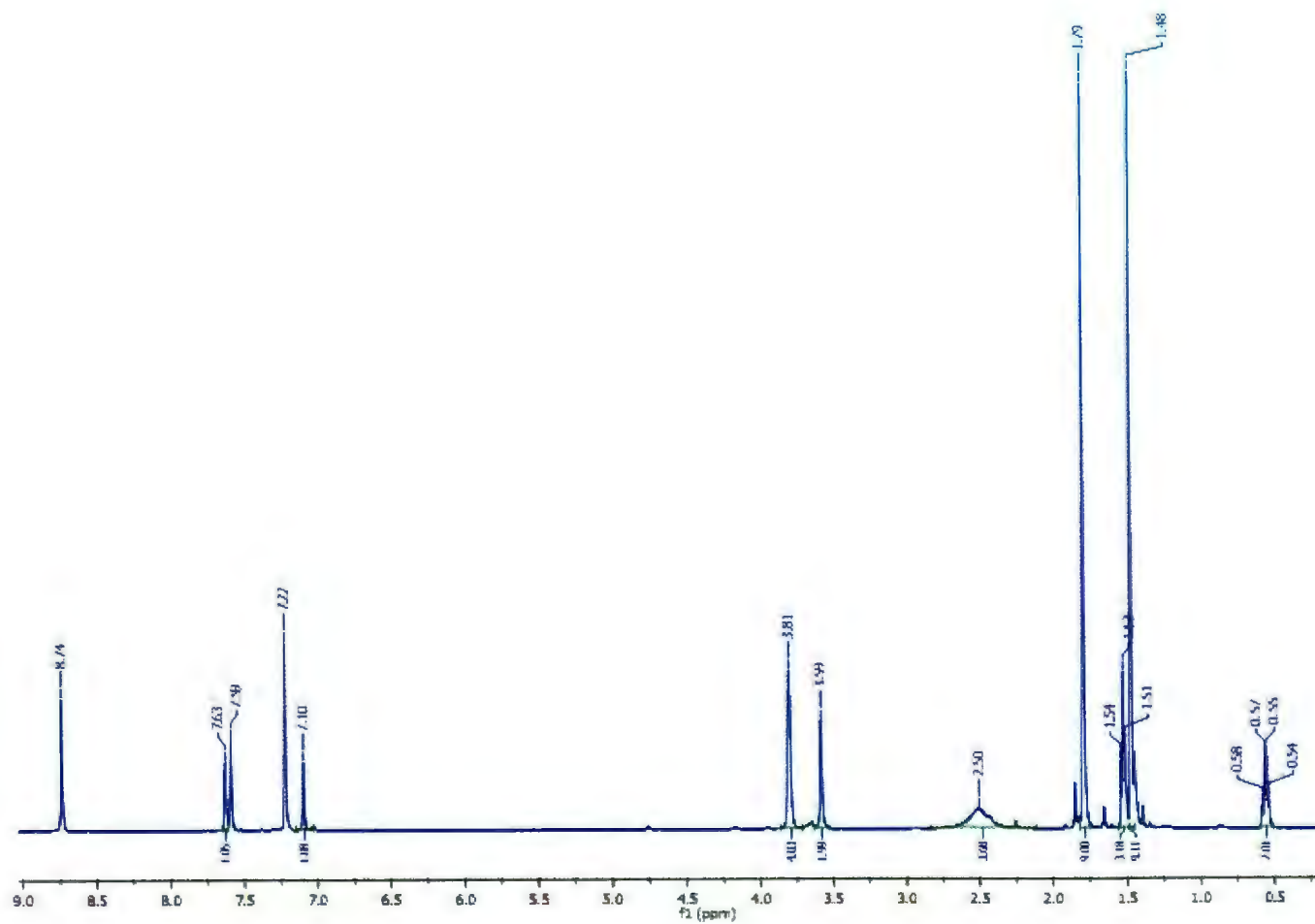


Figure A1.33. ^1H NMR spectrum of 3.7 ($\text{C}_5\text{D}_5\text{N}$, 500 MHz, 313 K)

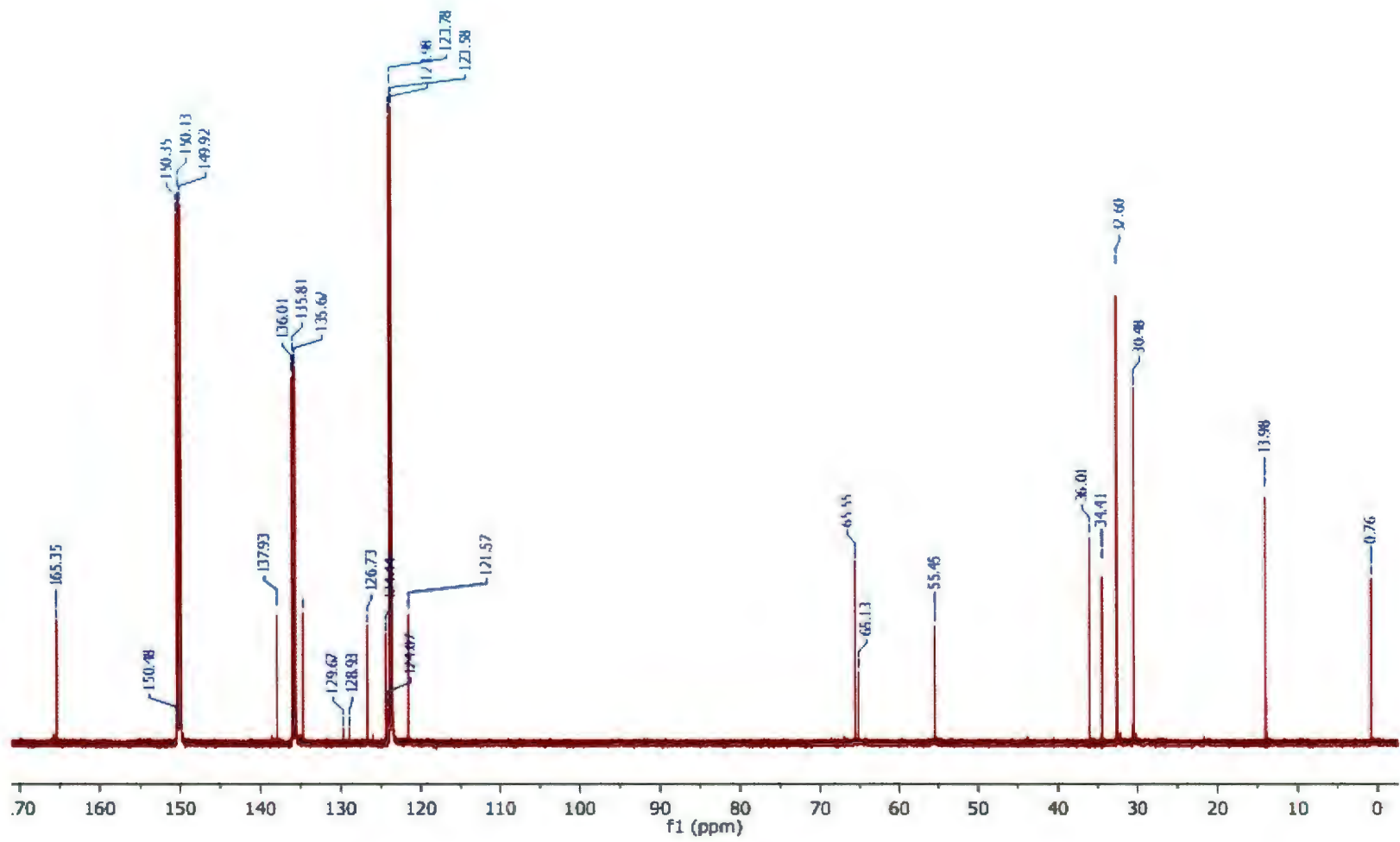


Figure A1.34. ^{13}C NMR spectrum of 3.7 ($\text{C}_5\text{D}_5\text{N}$, 125 MHz, 298 K)

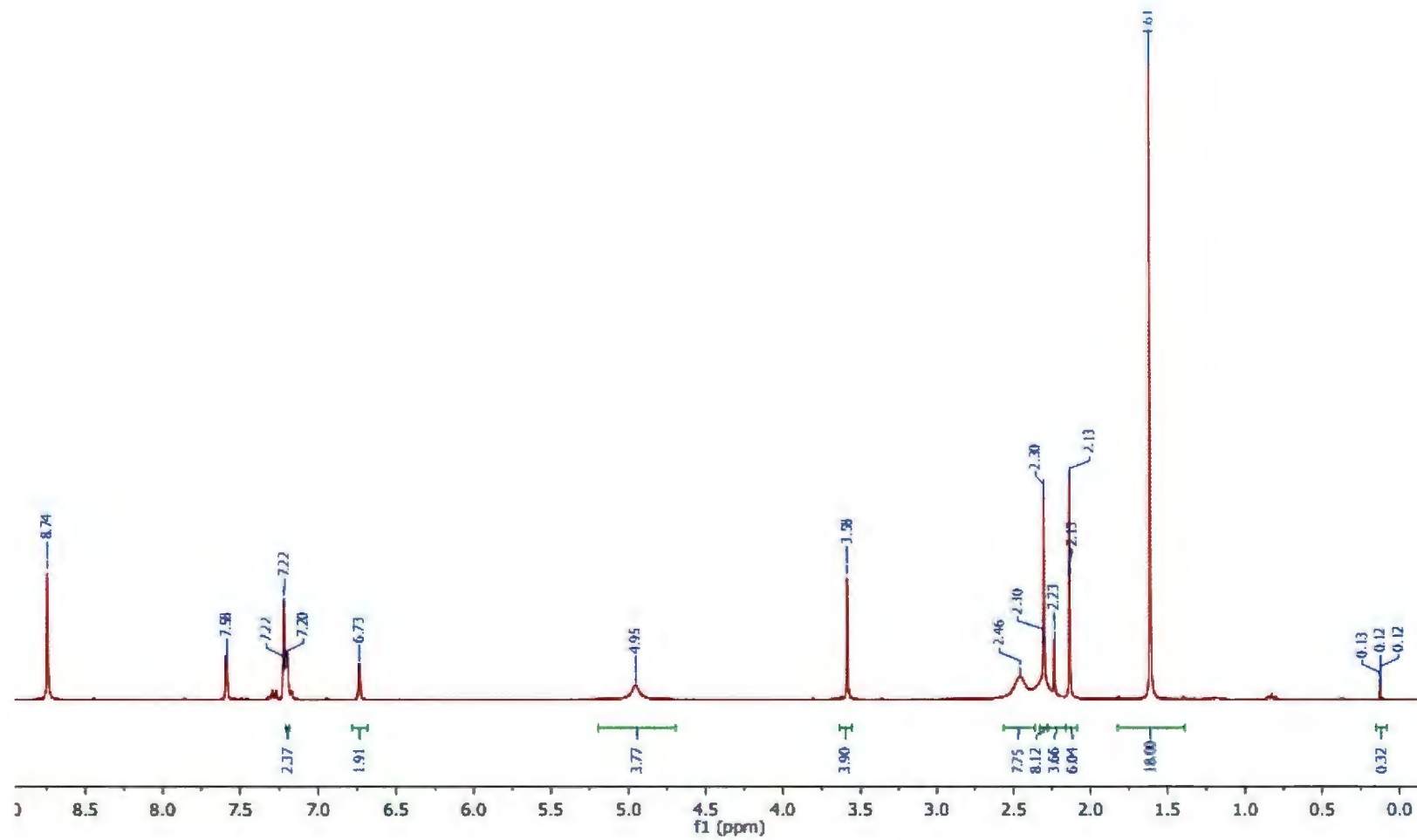


Figure A1.35. ^1H NMR spectrum of **4.1** ($\text{C}_5\text{D}_5\text{N}$, 300 MHz, 298 K)

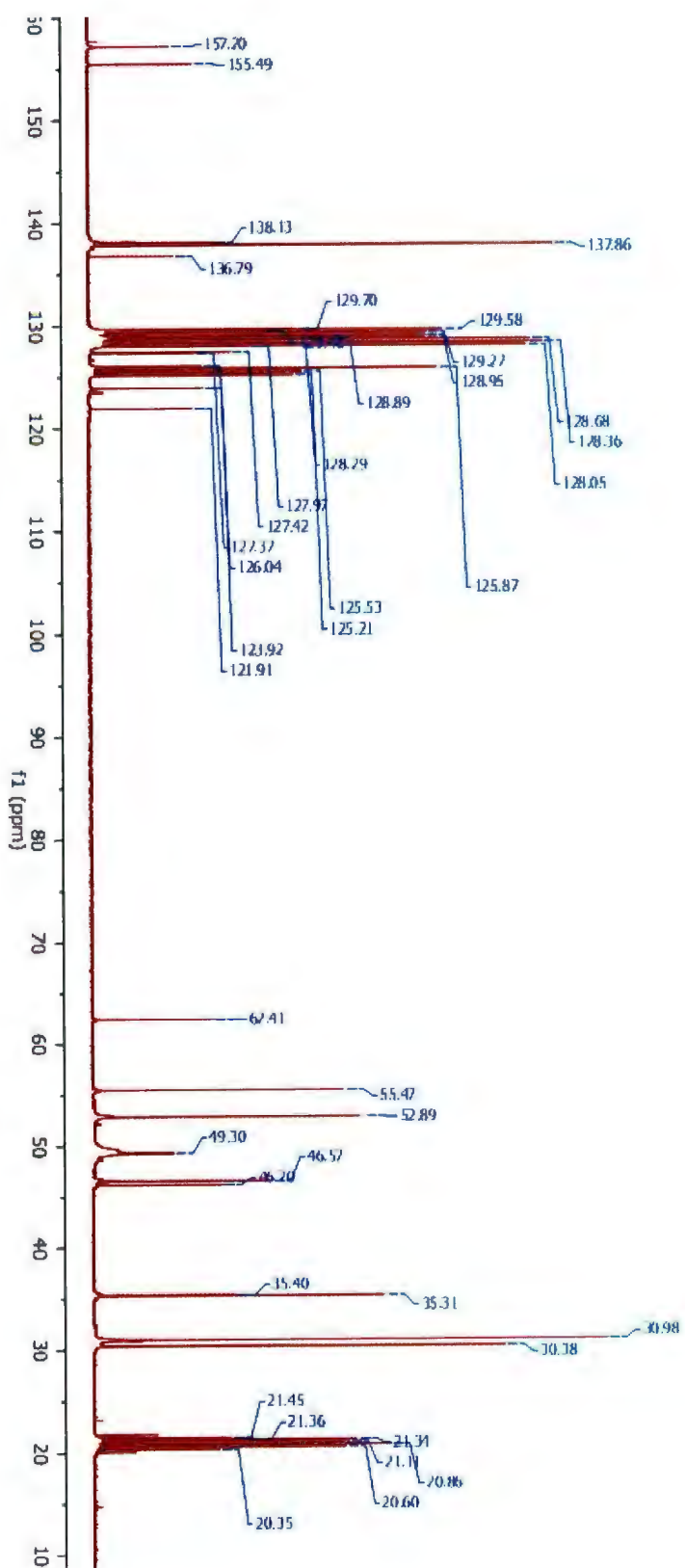


Figure A1.36. ^{13}C NMR spectrum of 4.1 (C_7D_8 , 125 MHz, 298 K)

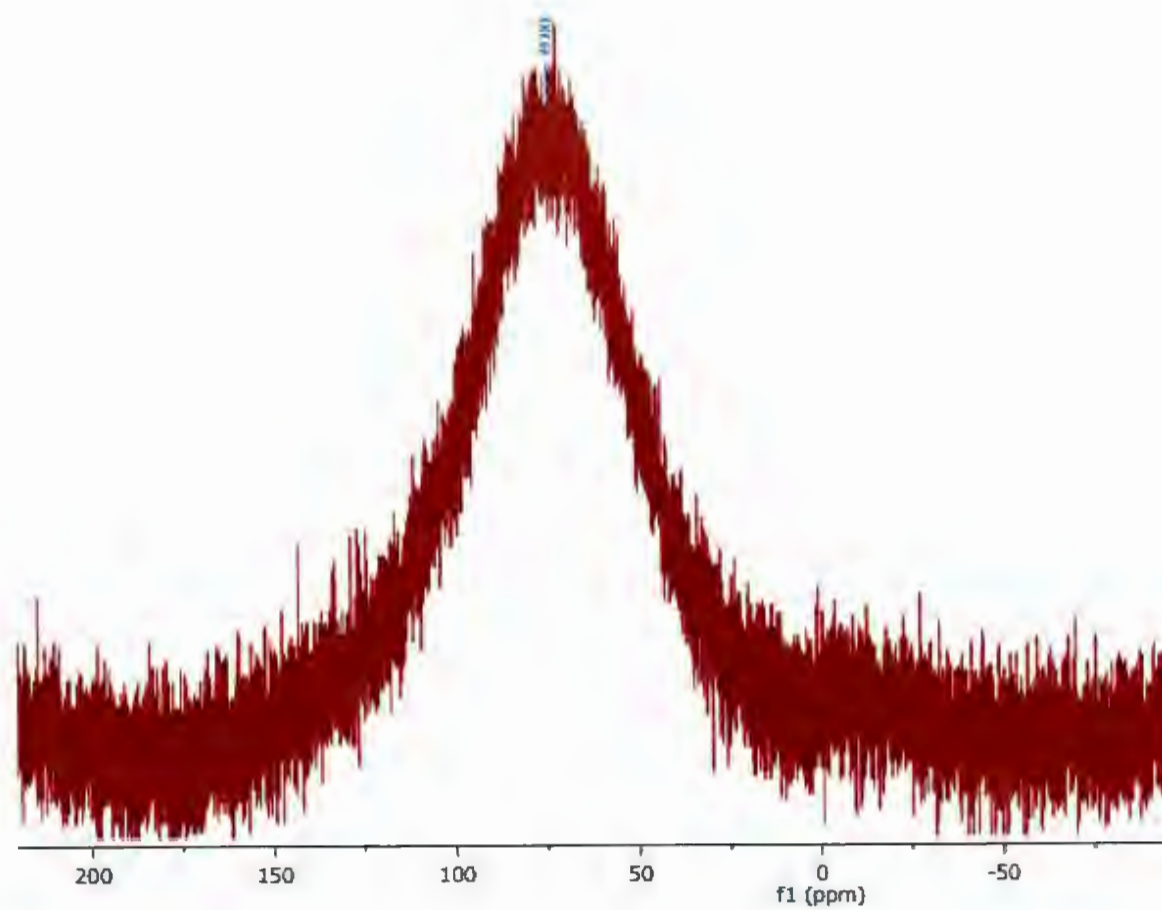


Figure A1. 37. ^{27}Al NMR spectrum of **4.1** ($\text{C}_5\text{D}_5\text{N}$, 78.22 MHz, 298 K)

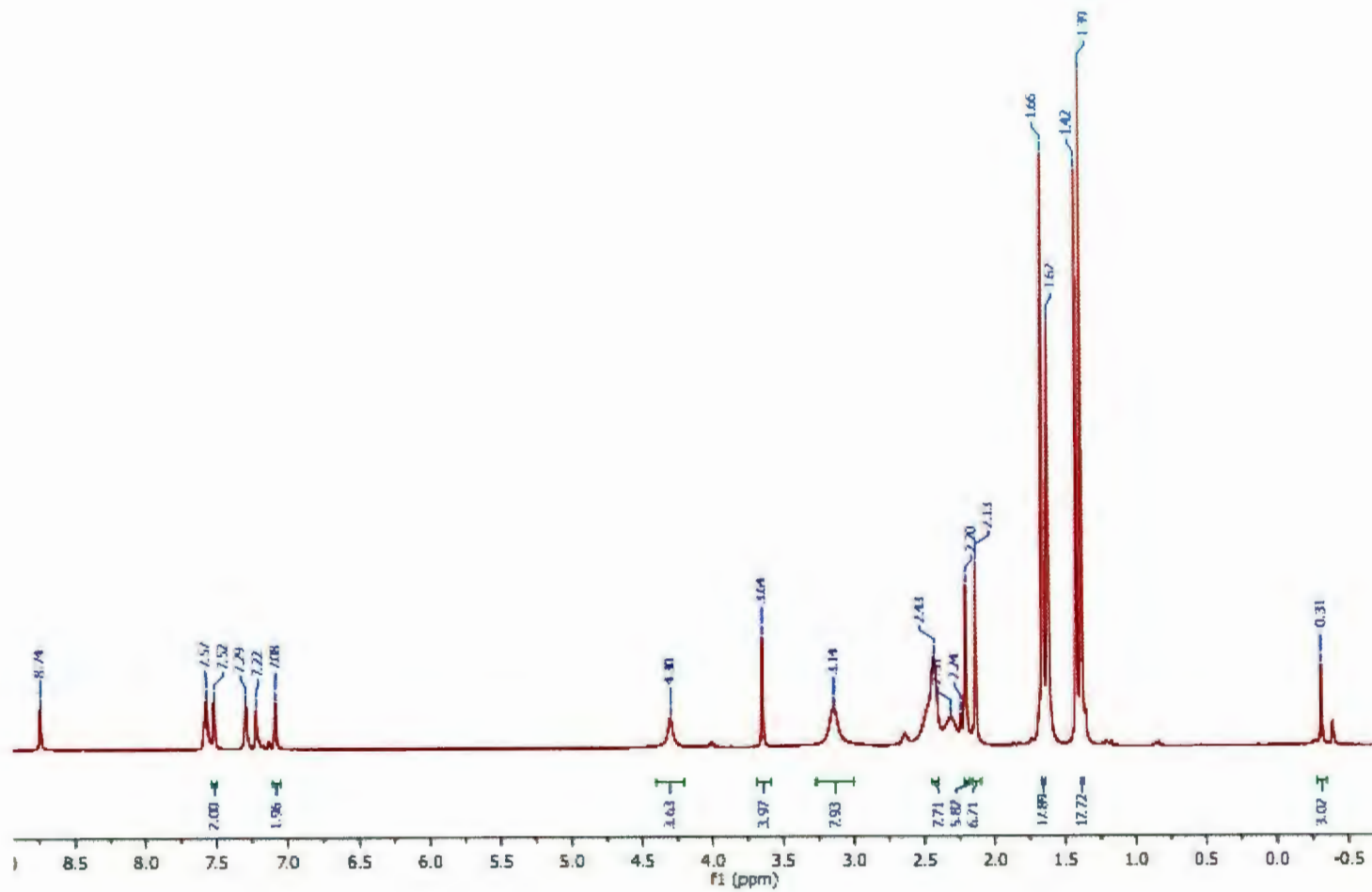


Figure A1.38. ^1H NMR spectrum of **4.2** ($\text{C}_5\text{D}_5\text{N}$, 500 MHz, 328 K)

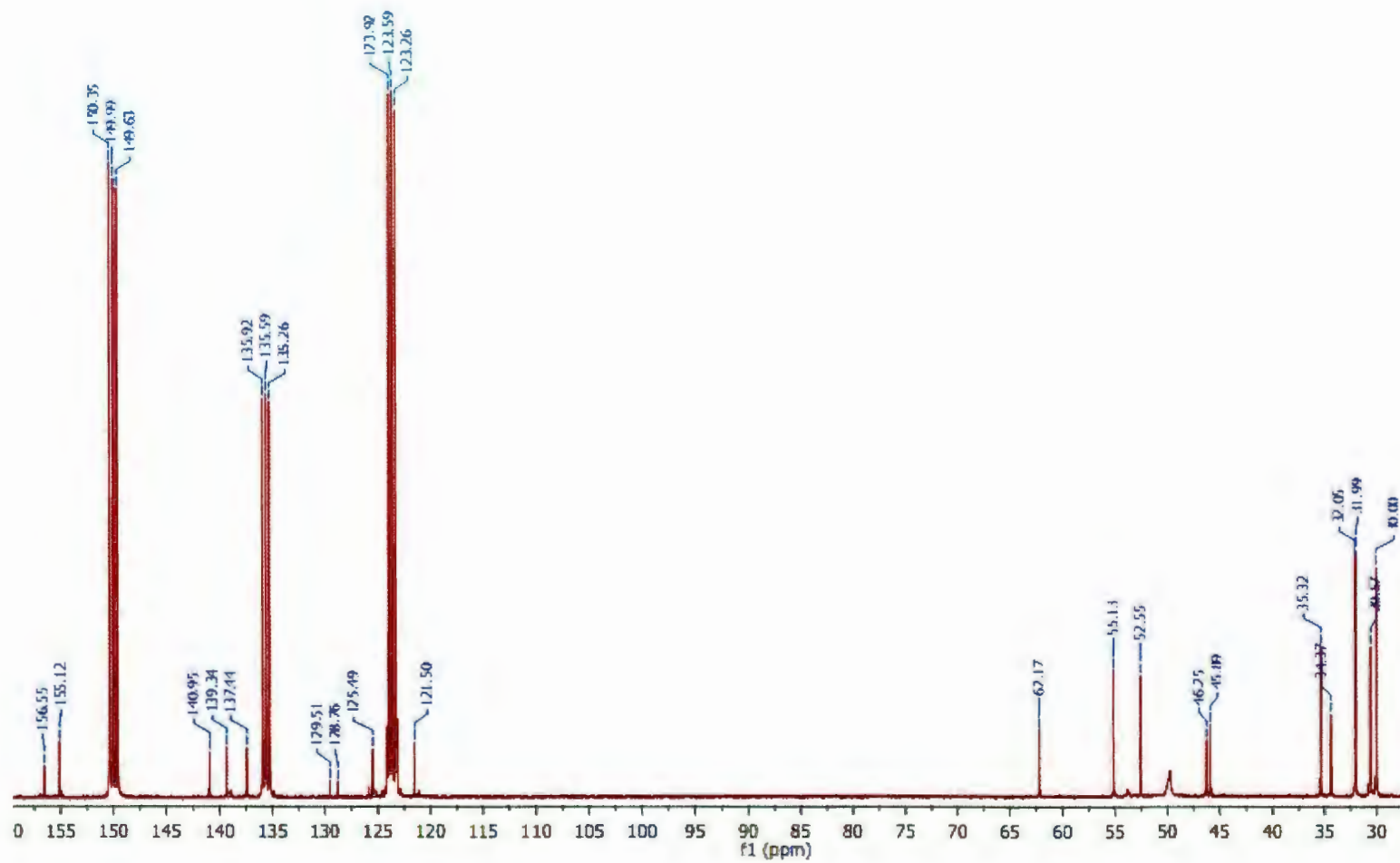


Figure A1.39. ^{13}C NMR spectrum of **4.2** ($\text{C}_5\text{D}_5\text{N}$, 125 MHz, 298 K)

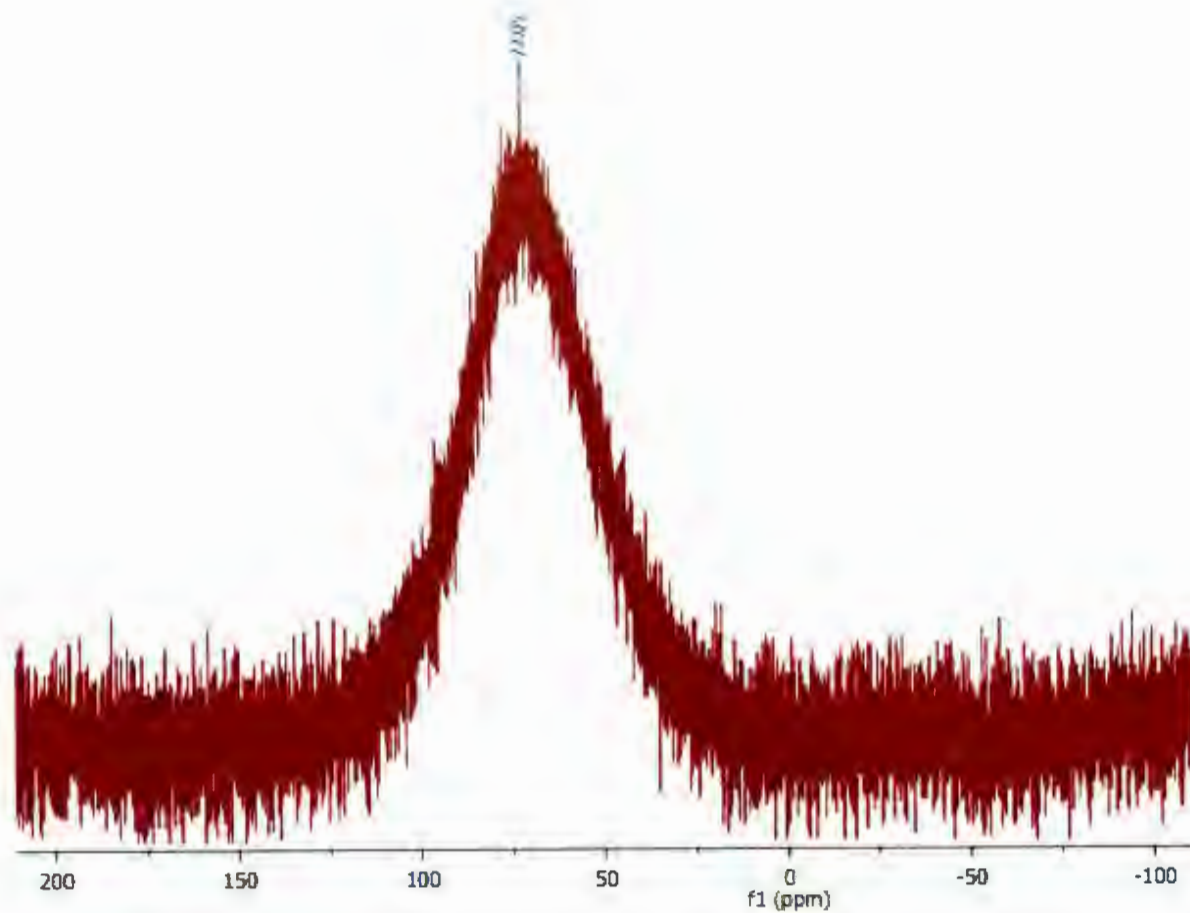


Figure A1.40. ^{27}Al NMR spectrum of **4.2** ($\text{C}_5\text{D}_5\text{N}$, 78.22 MHz, 298 K)

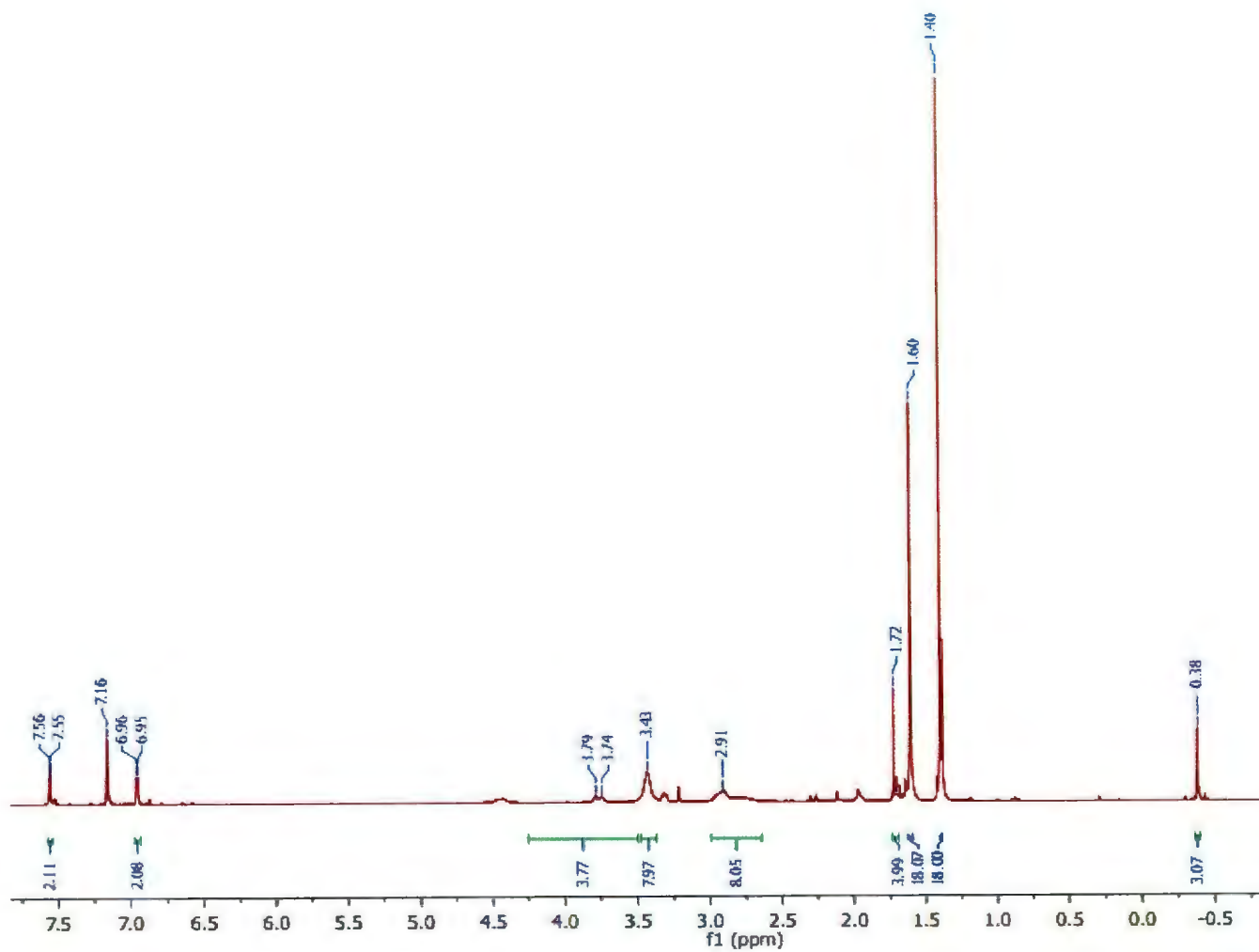


Figure A1.41. ^1H NMR spectrum of 4.3 (C_6D_6 , 500 MHz, 343 K)

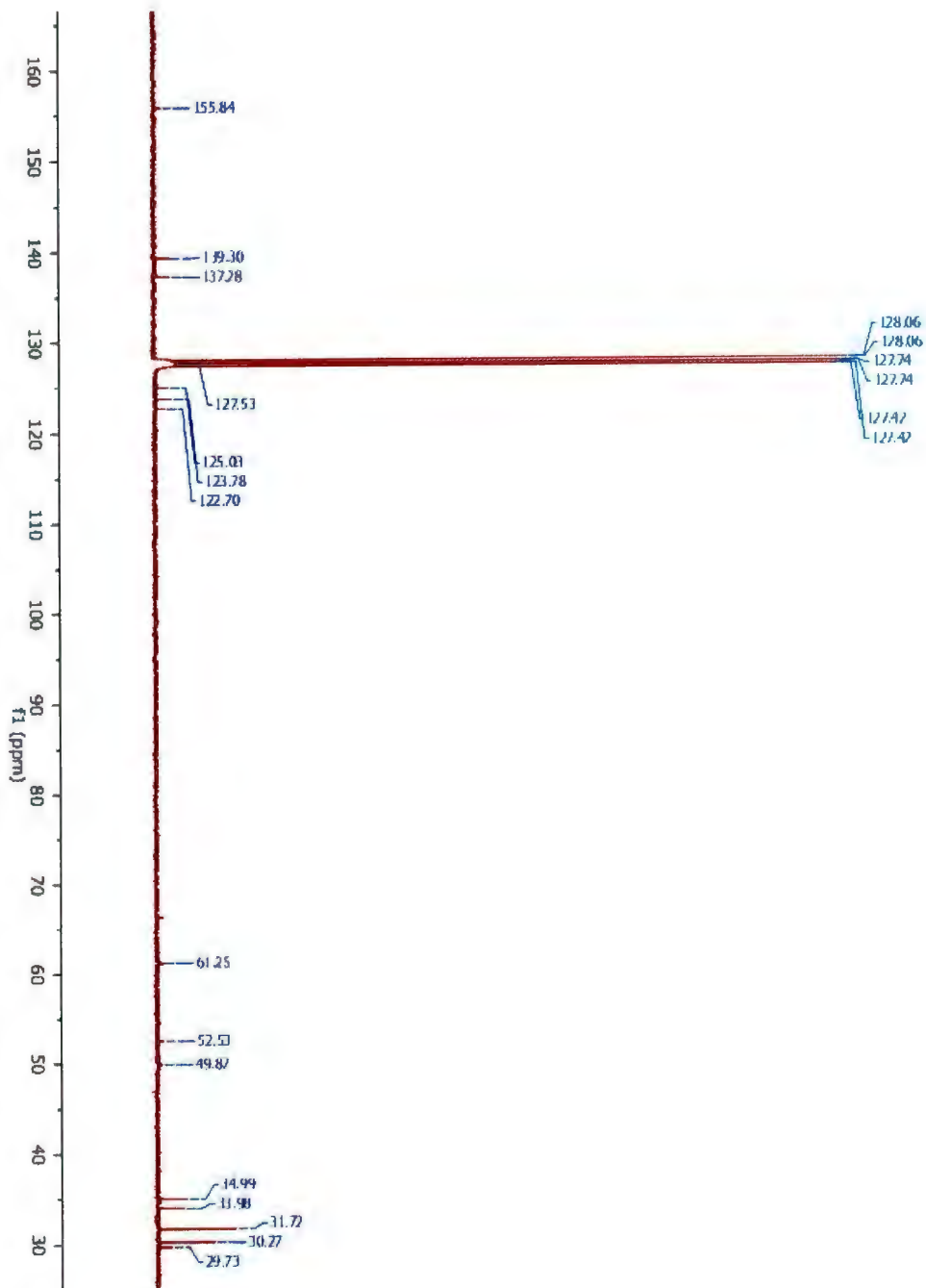


Figure A1.42. ^{13}C NMR spectrum of **4.3** (C_6D_6 , 125 MHz, 298 K)

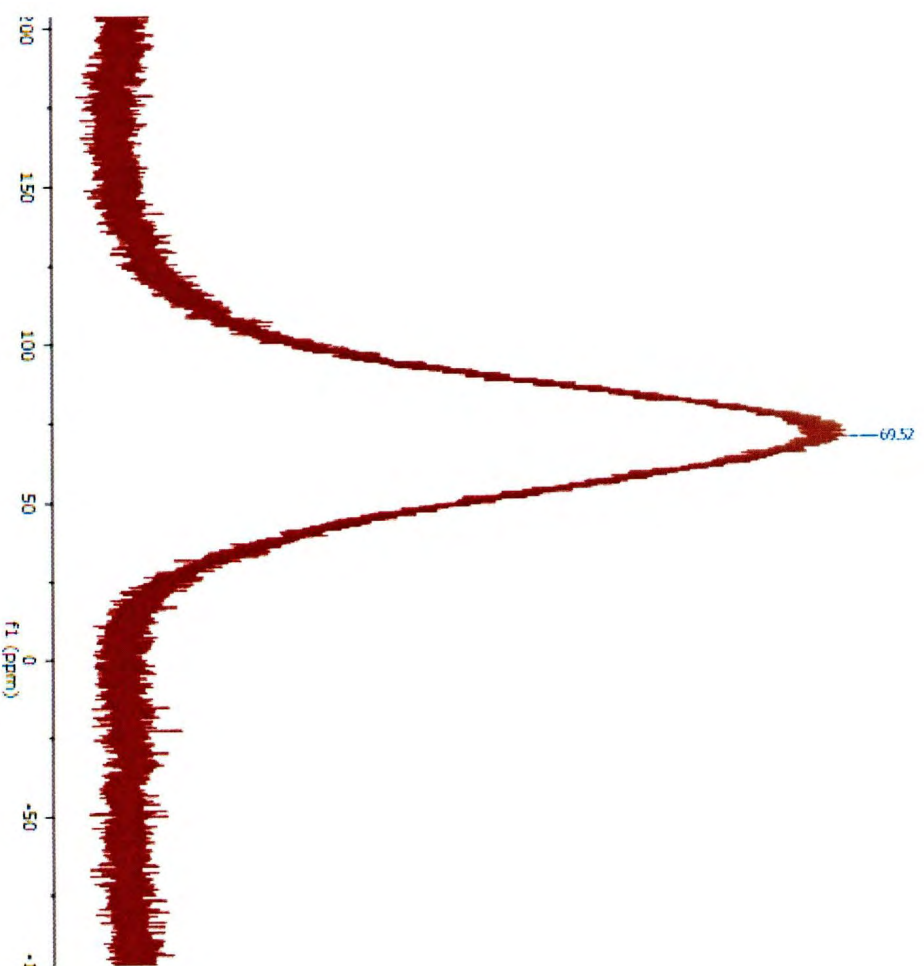


Figure A1.43. ^{27}Al NMR spectrum of **4.3** (C_6D_6 , 78.22 MHz, 298 K)

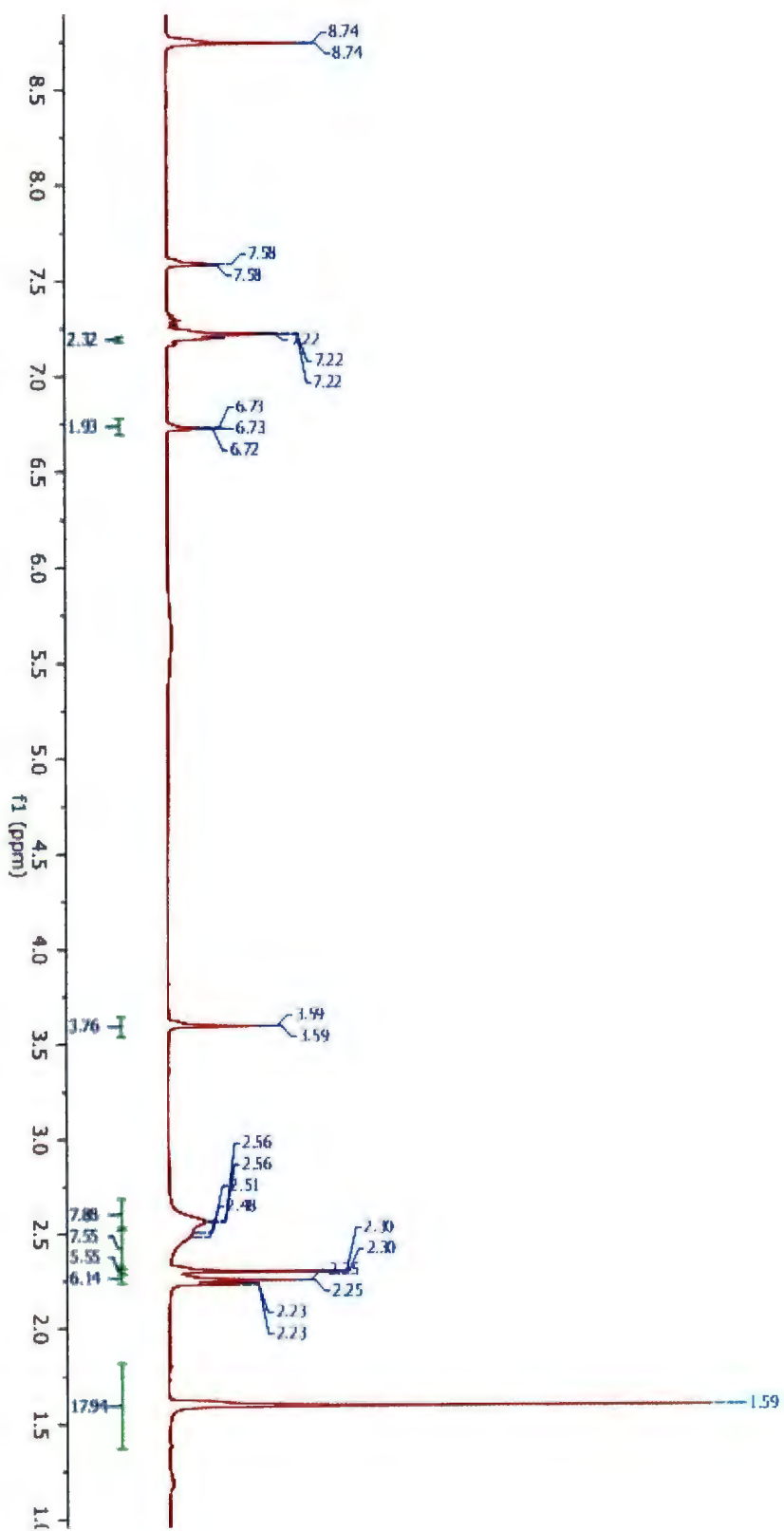


Figure A1.44. ^1H NMR spectrum of 4.4 ($\text{C}_5\text{D}_5\text{N}$, 300 MHz, 298 K)

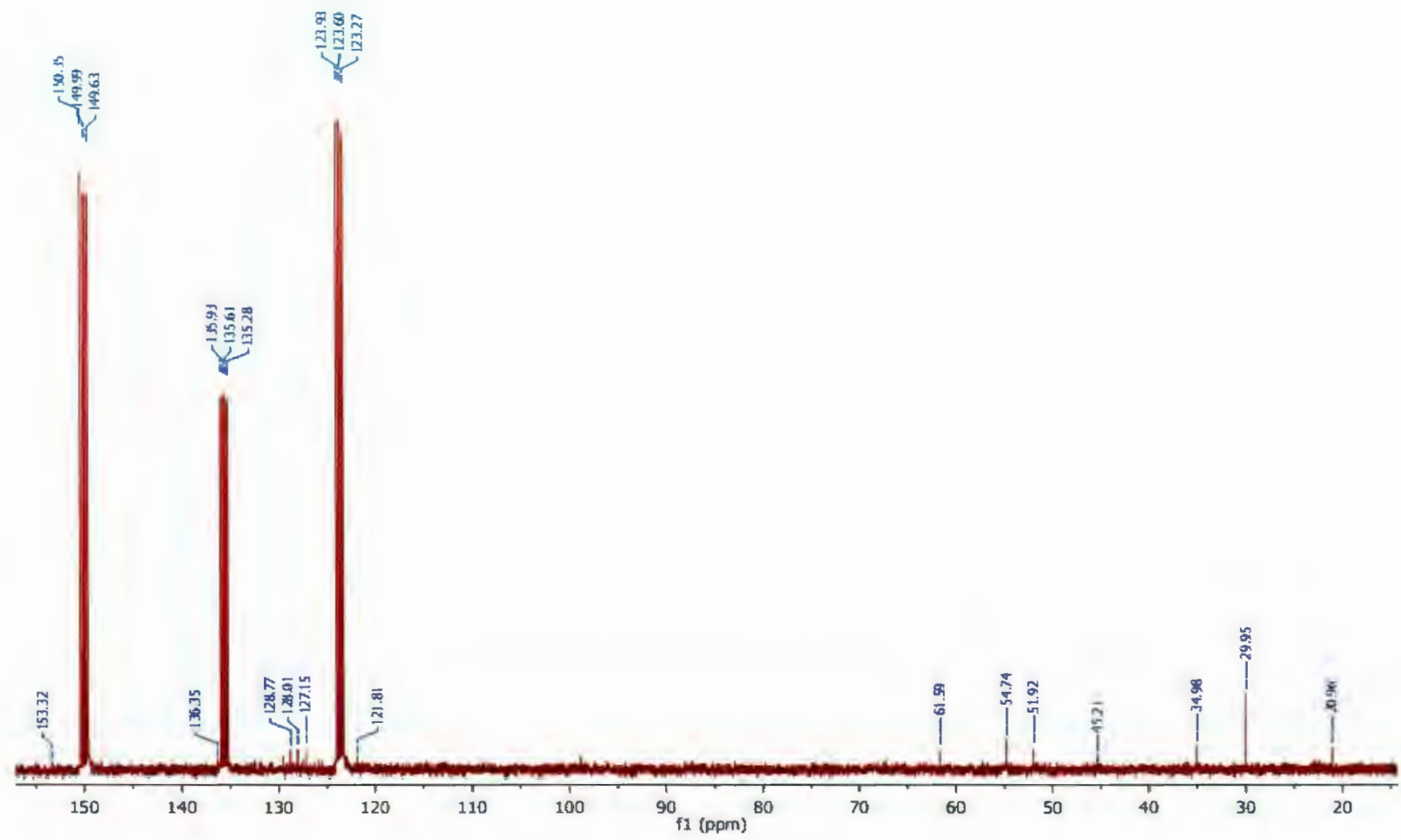


Figure A1.45. ^{13}C NMR spectrum of 4.4 ($\text{C}_5\text{D}_5\text{N}$, 125 MHz, 298 K)

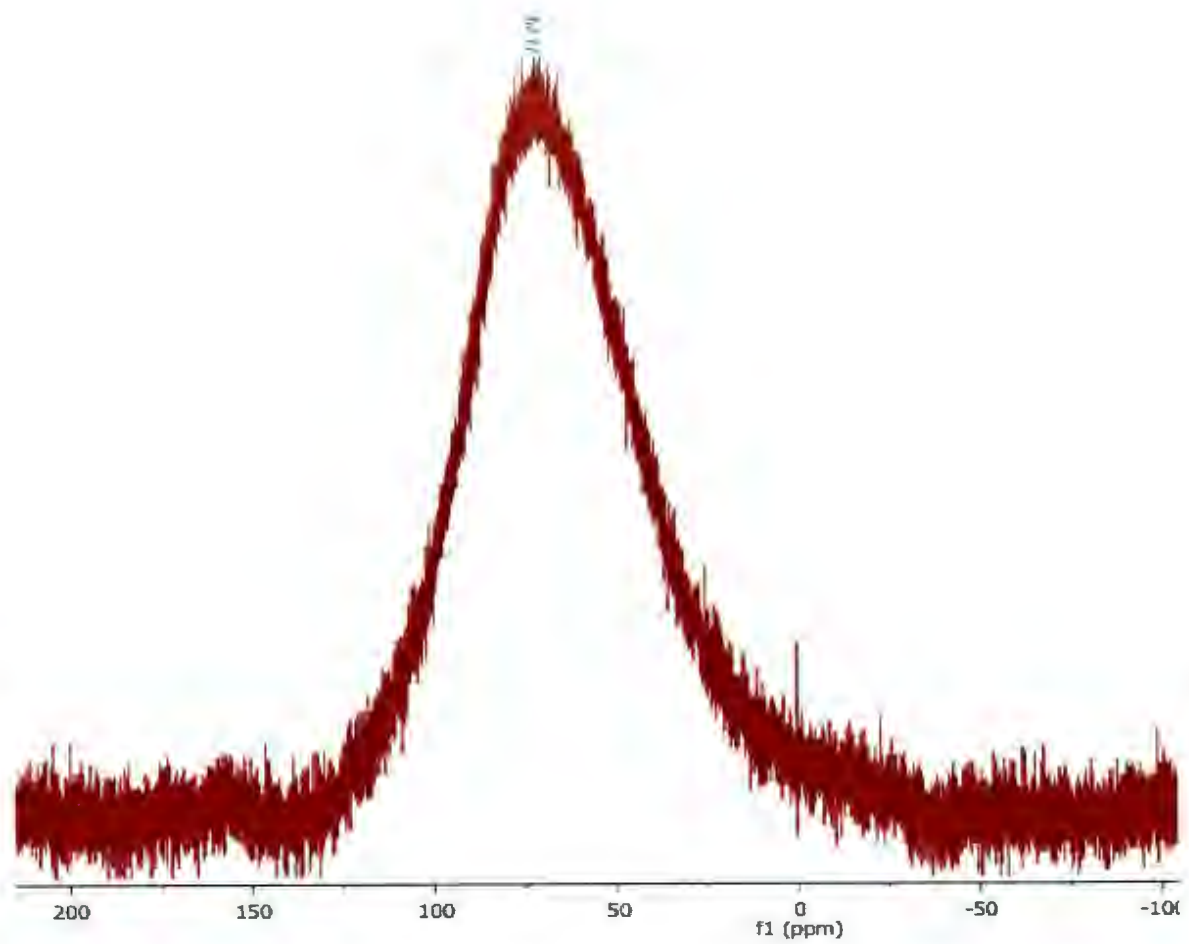


Figure A1.46. ^{27}Al NMR spectrum of **4.4** ($\text{C}_5\text{D}_5\text{N}$, 78.22 MHz, 298 K)

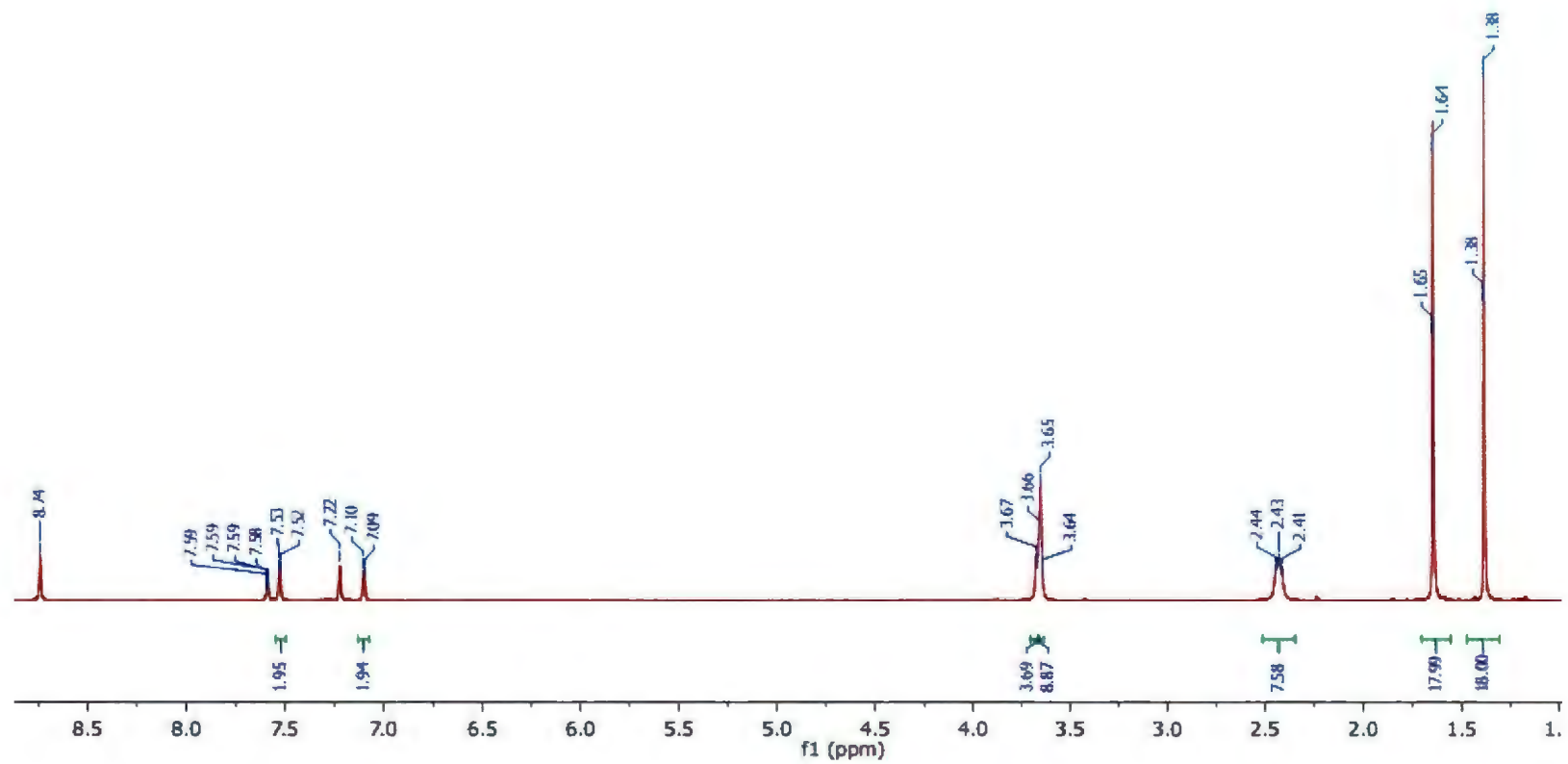


Figure A1.47. ^1H NMR spectrum of **4.5** ($\text{C}_5\text{D}_5\text{N}$, 300 MHz, 298 K)

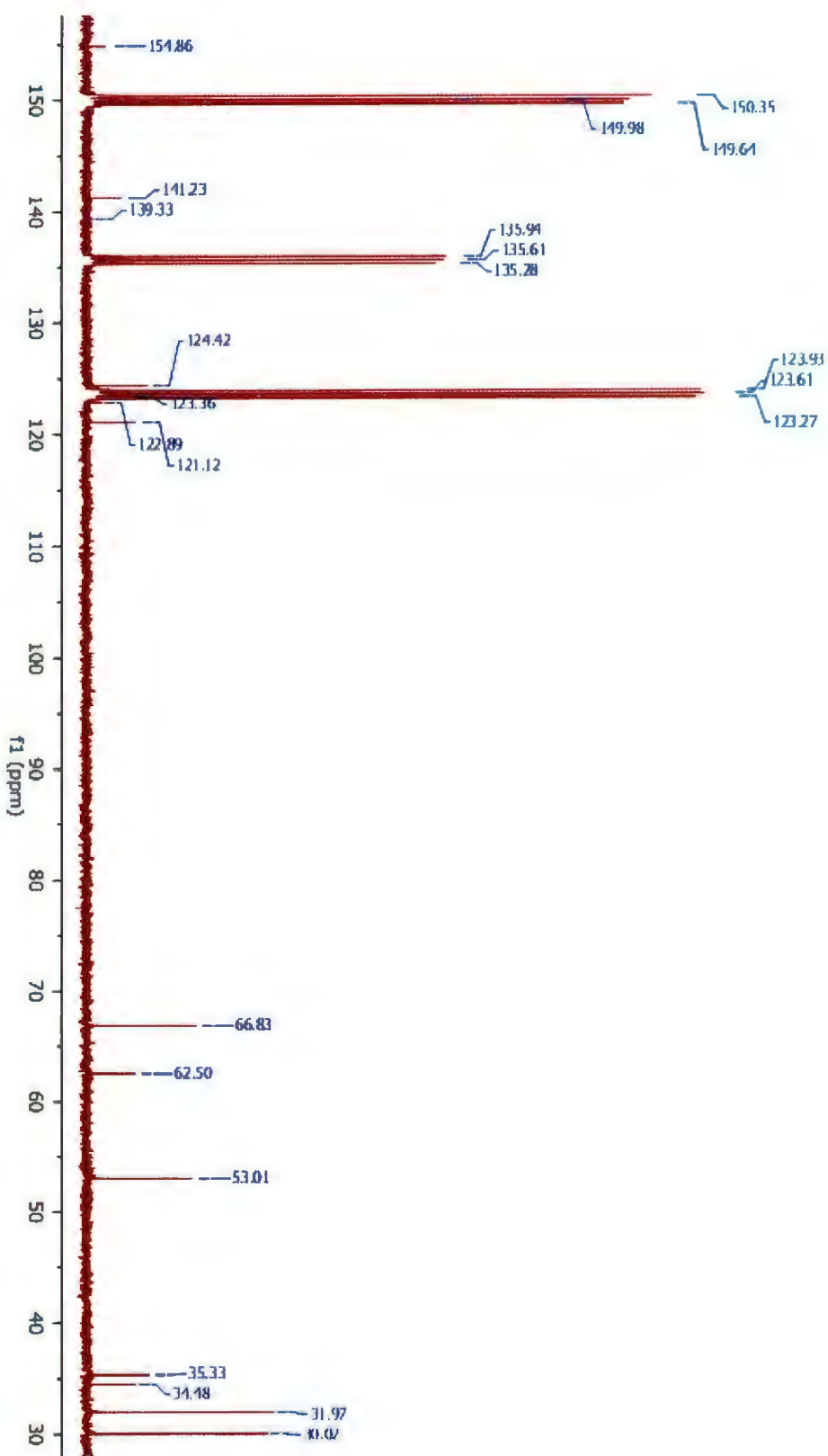


Figure A1.48. ^{13}C NMR spectrum of **4.5** ($\text{C}_5\text{D}_5\text{N}$, 125 MHz, 298 K)

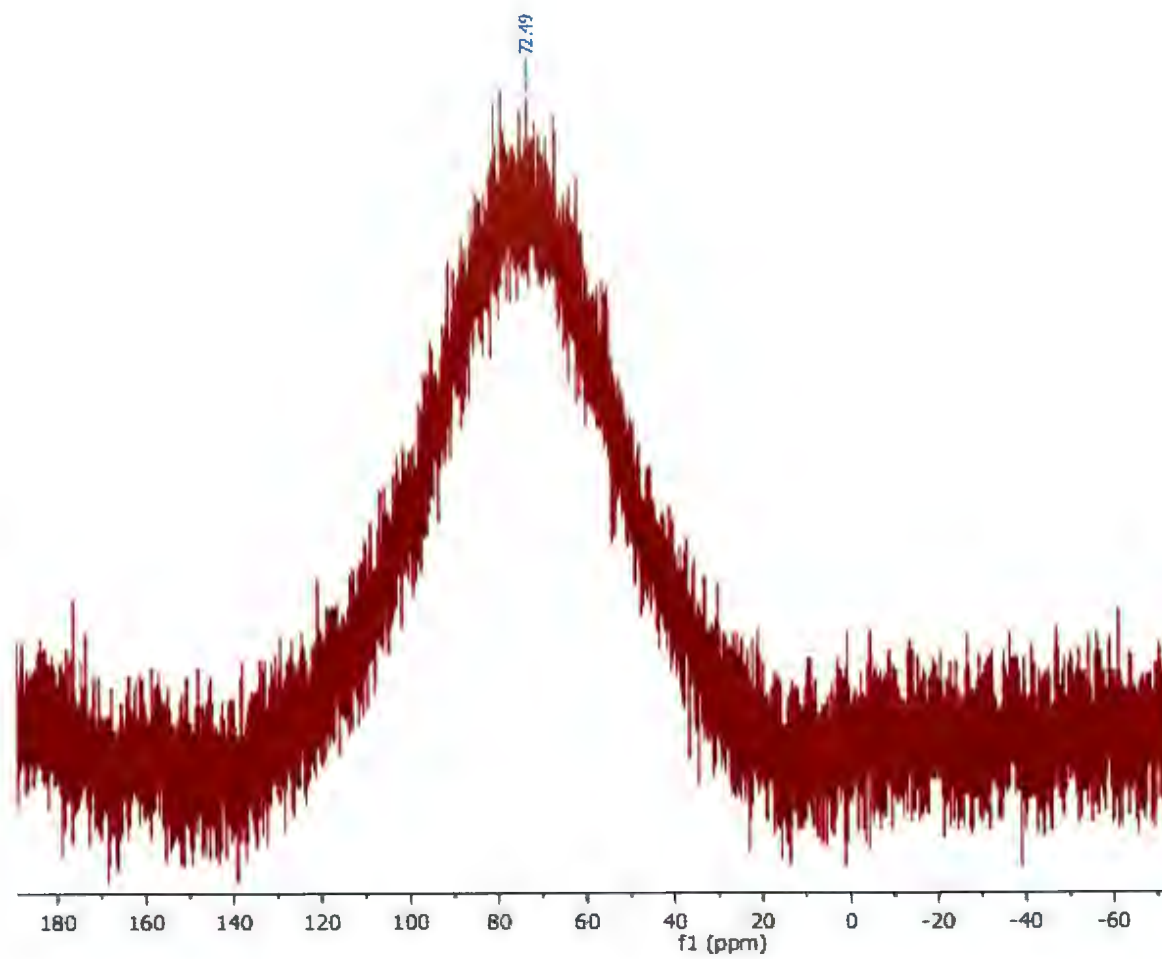


Figure A1.49. ^{27}Al NMR spectrum of 4.5 ($\text{C}_5\text{D}_5\text{N}$, 78.22 MHz, 298 K)

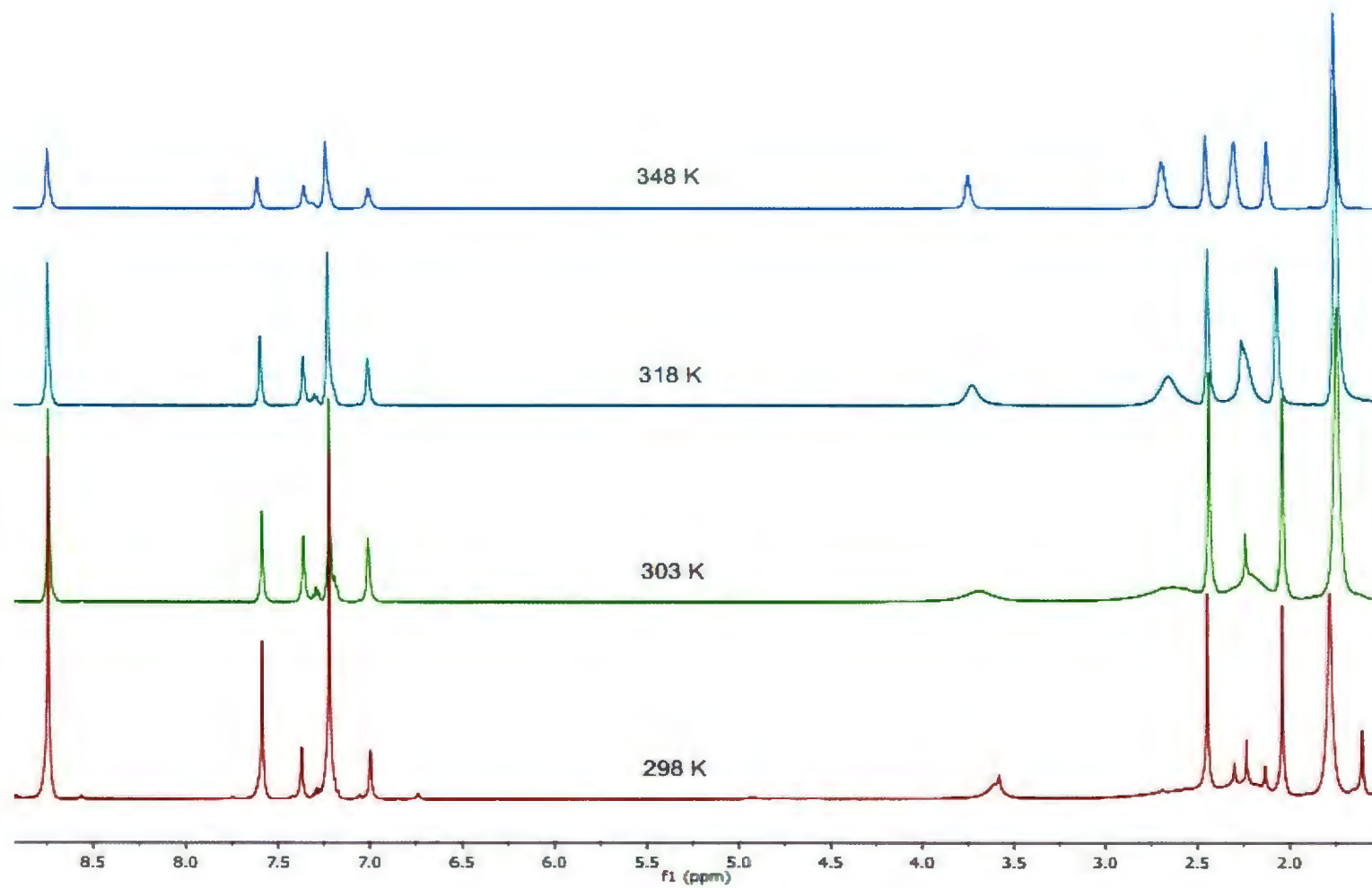


Figure A1.50. Variable temperature ¹H NMR spectra of **5.1** (C₅D₅N, 500 MHz)

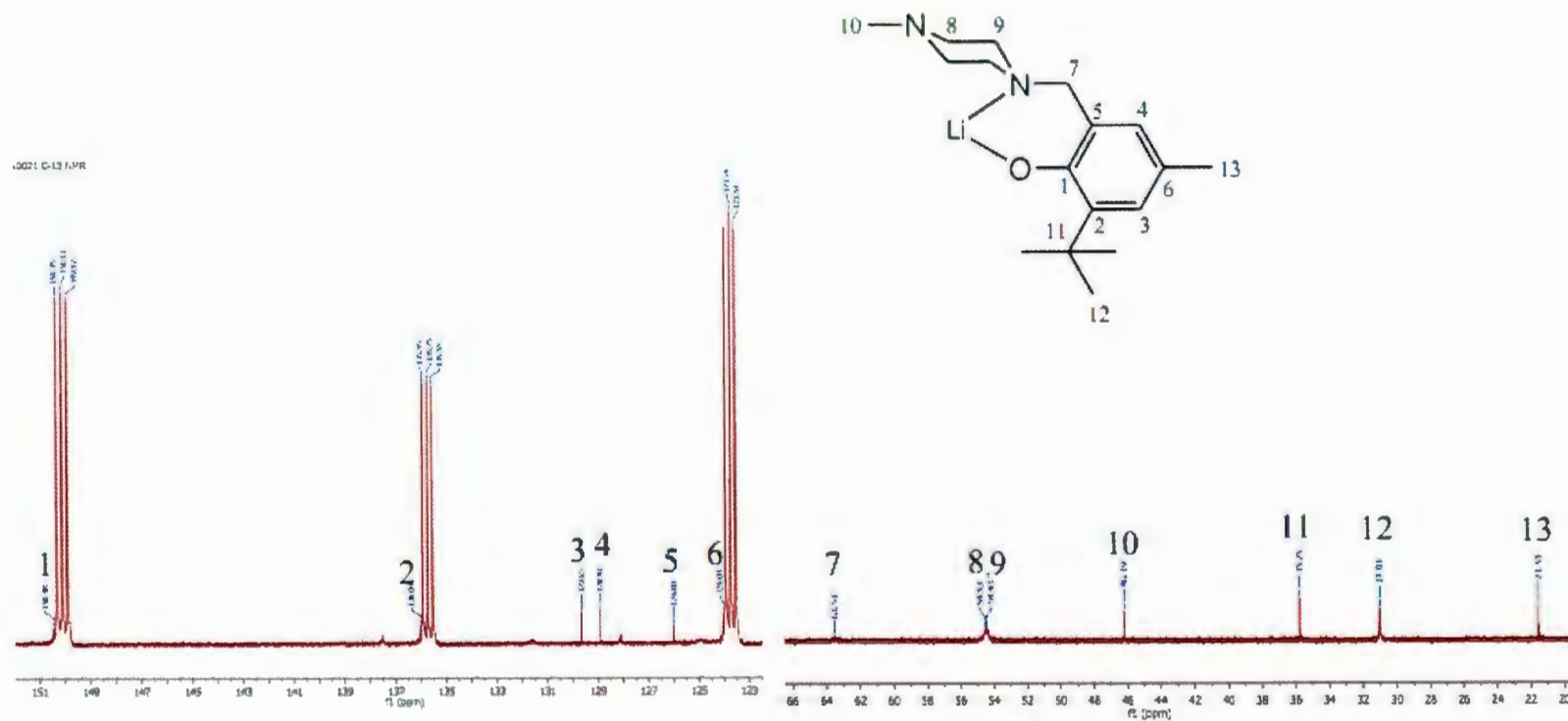


Figure A1.51. ^{13}C NMR spectrum of **5.1** ($\text{C}_5\text{D}_5\text{N}$, 125 MHz, 298K)

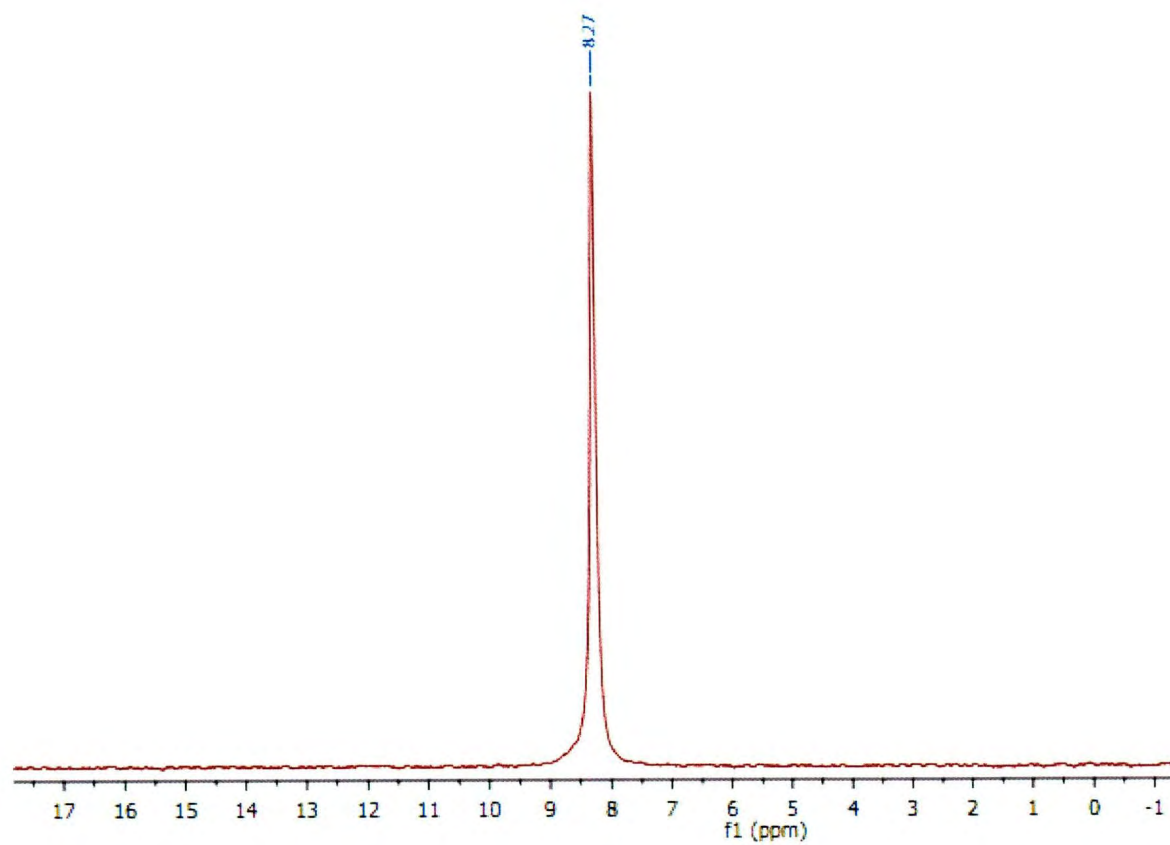


Figure A1. 52. ^7Li NMR spectrum of **5.1** ($\text{C}_5\text{D}_5\text{N}$, 116 MHz, 298 K)

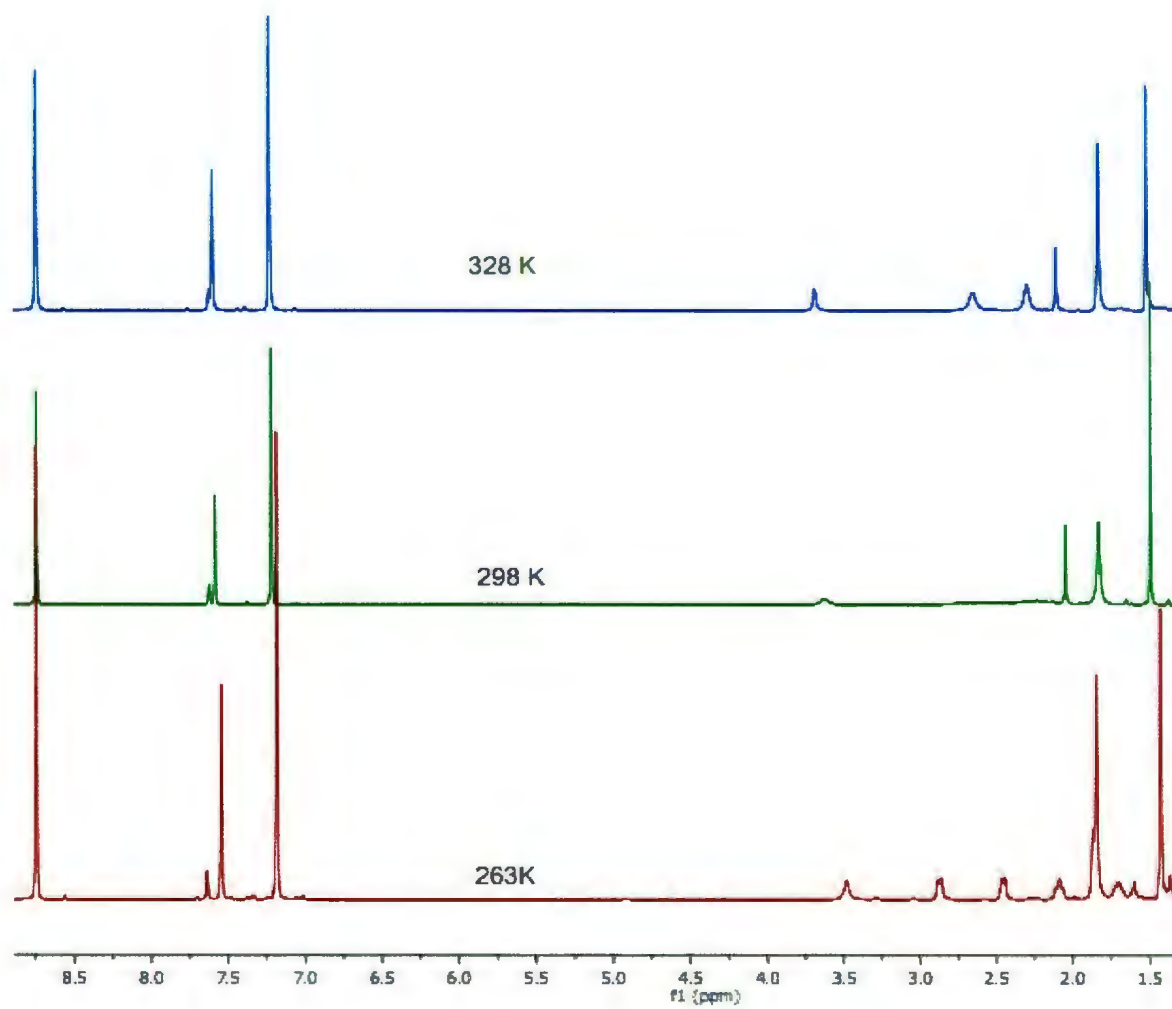


Figure A1.53. Variable temperature ^1H NMR spectra of **5.2** ($\text{C}_5\text{D}_5\text{N}$, 500MHz)

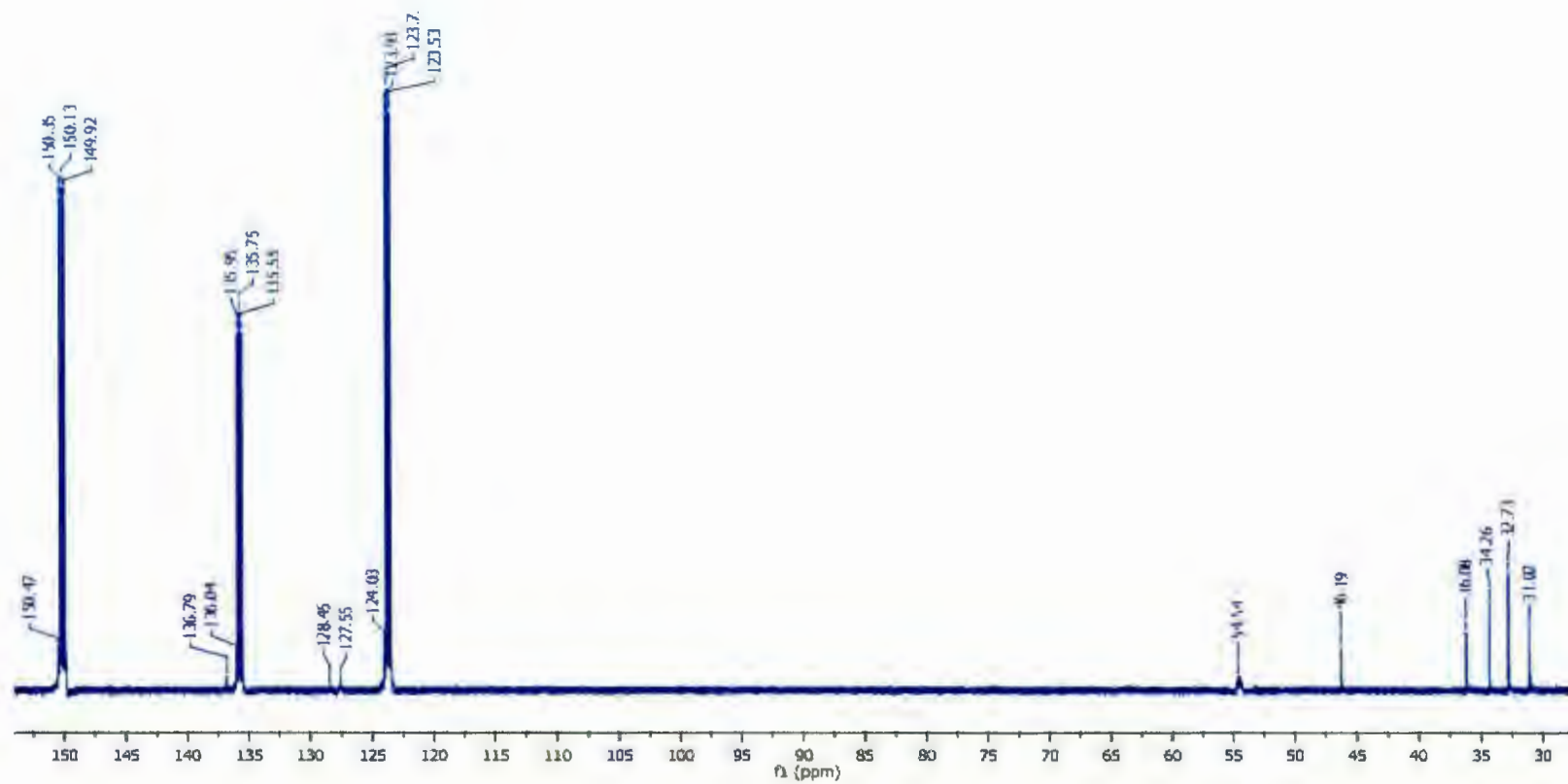


Figure A1.54. ^{13}C NMR spectrum of **5.2** ($\text{C}_5\text{D}_5\text{N}$, 125 MHz, 298 K)

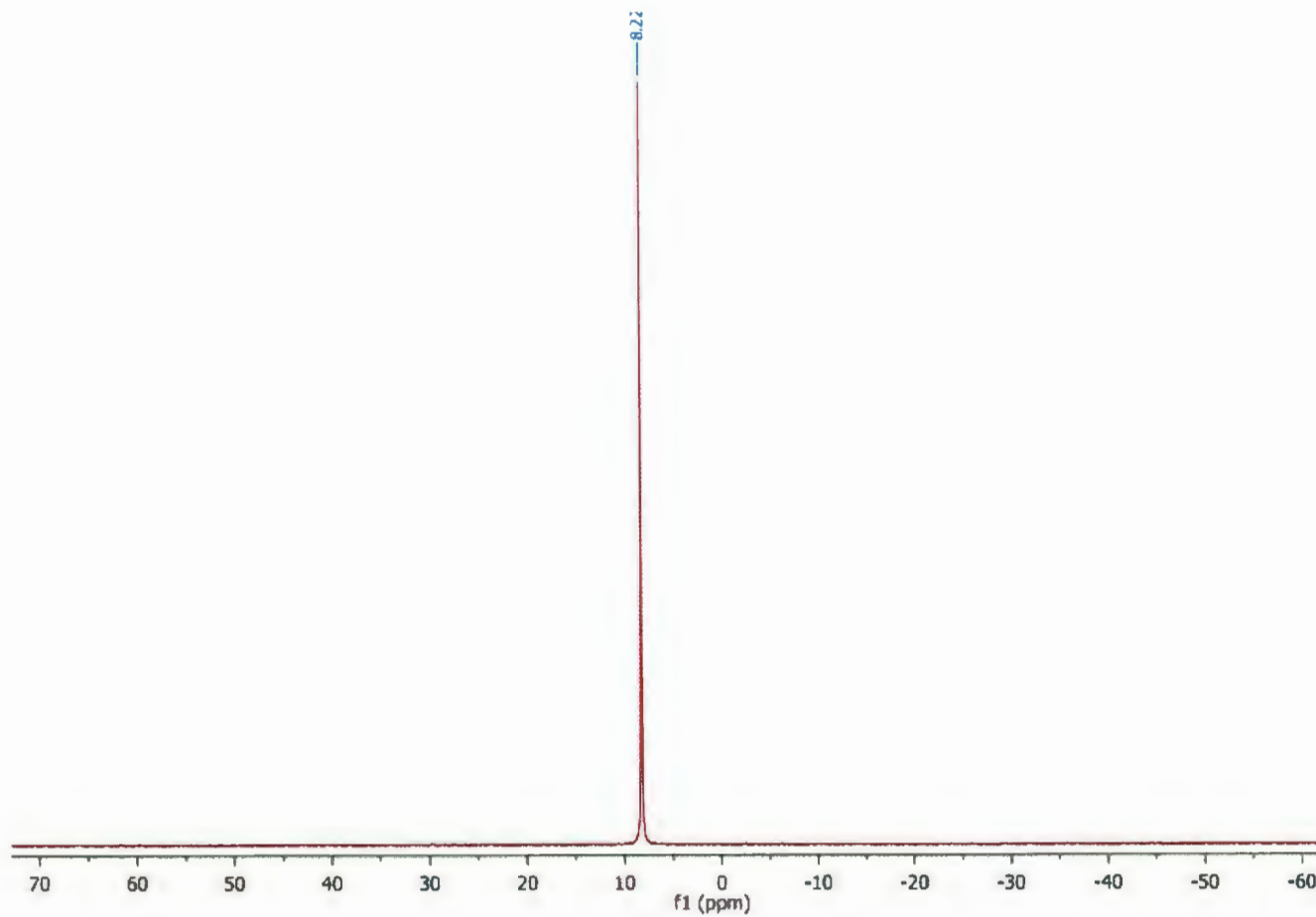


Figure A1.55. ${}^7\text{Li}$ NMR spectrum of **5.2** ($\text{C}_5\text{D}_5\text{N}$, 116 MHz, 298 K)

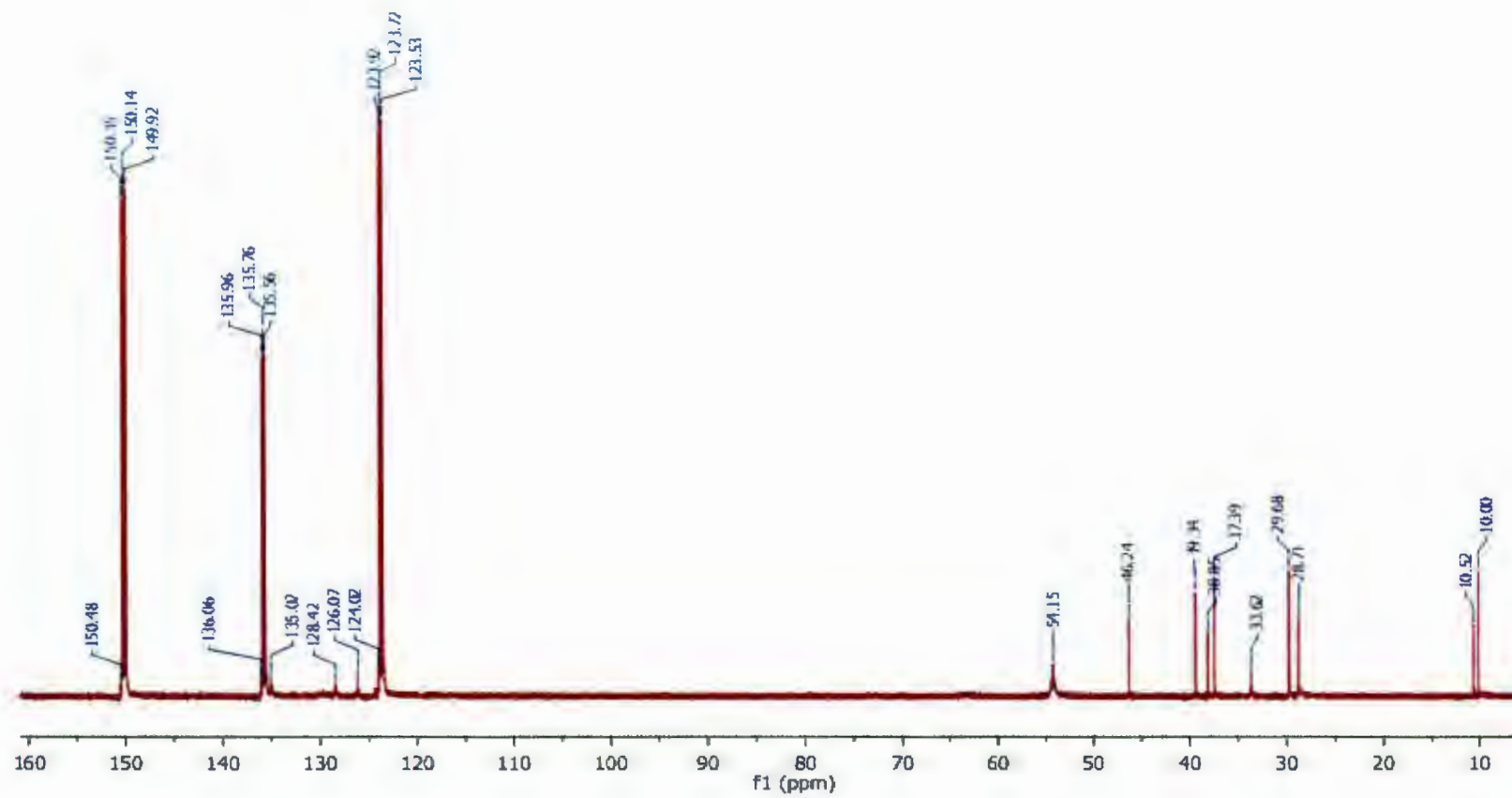


Figure A1.56. ^{13}C NMR spectrum of 5.3 ($\text{C}_5\text{D}_5\text{N}$, 125 MHz, 298 K)

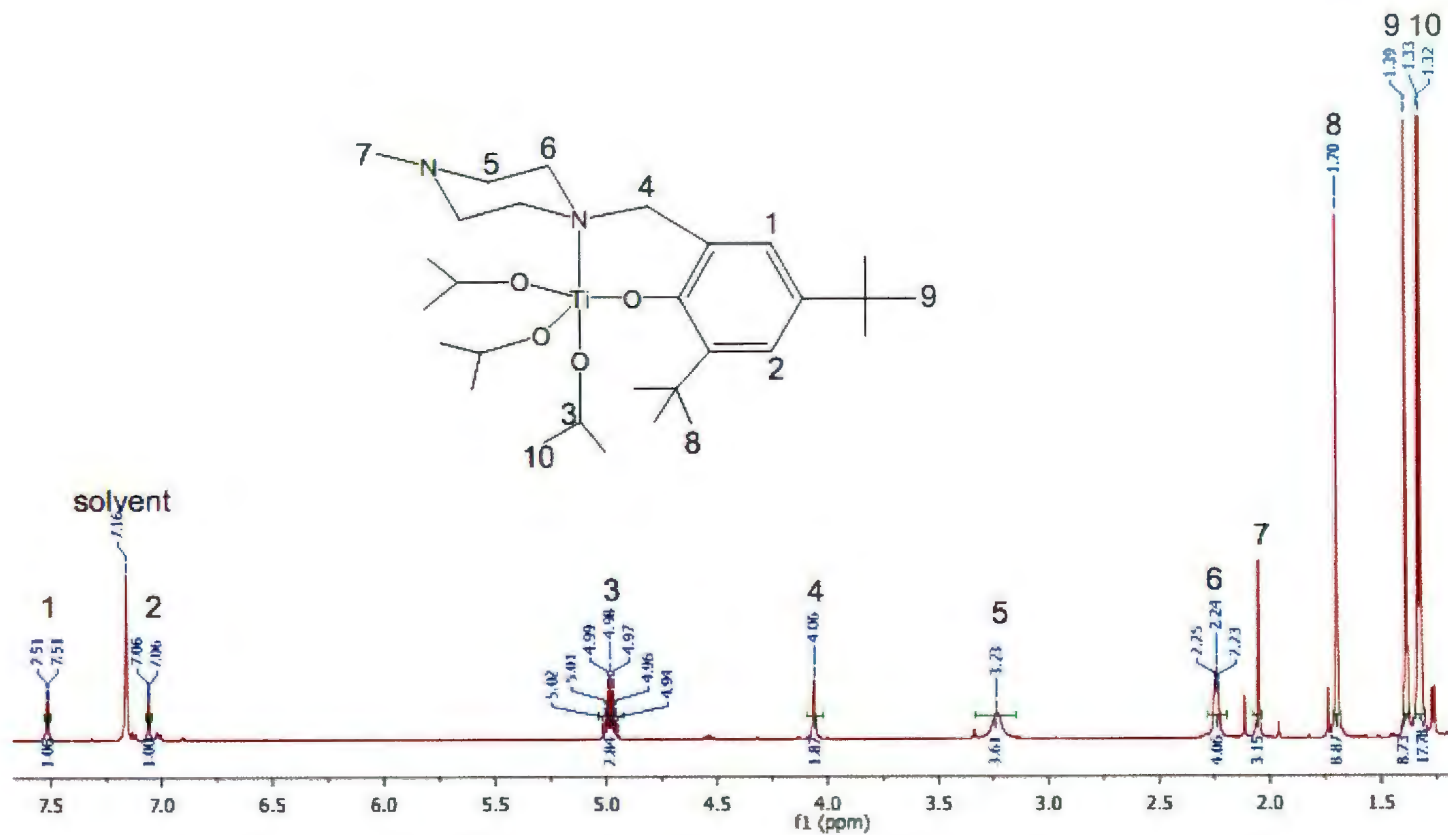


Figure A1.57. ^1H NMR spectrum of **6.1** (C_6D_6 , 500 MHz, 298 K)

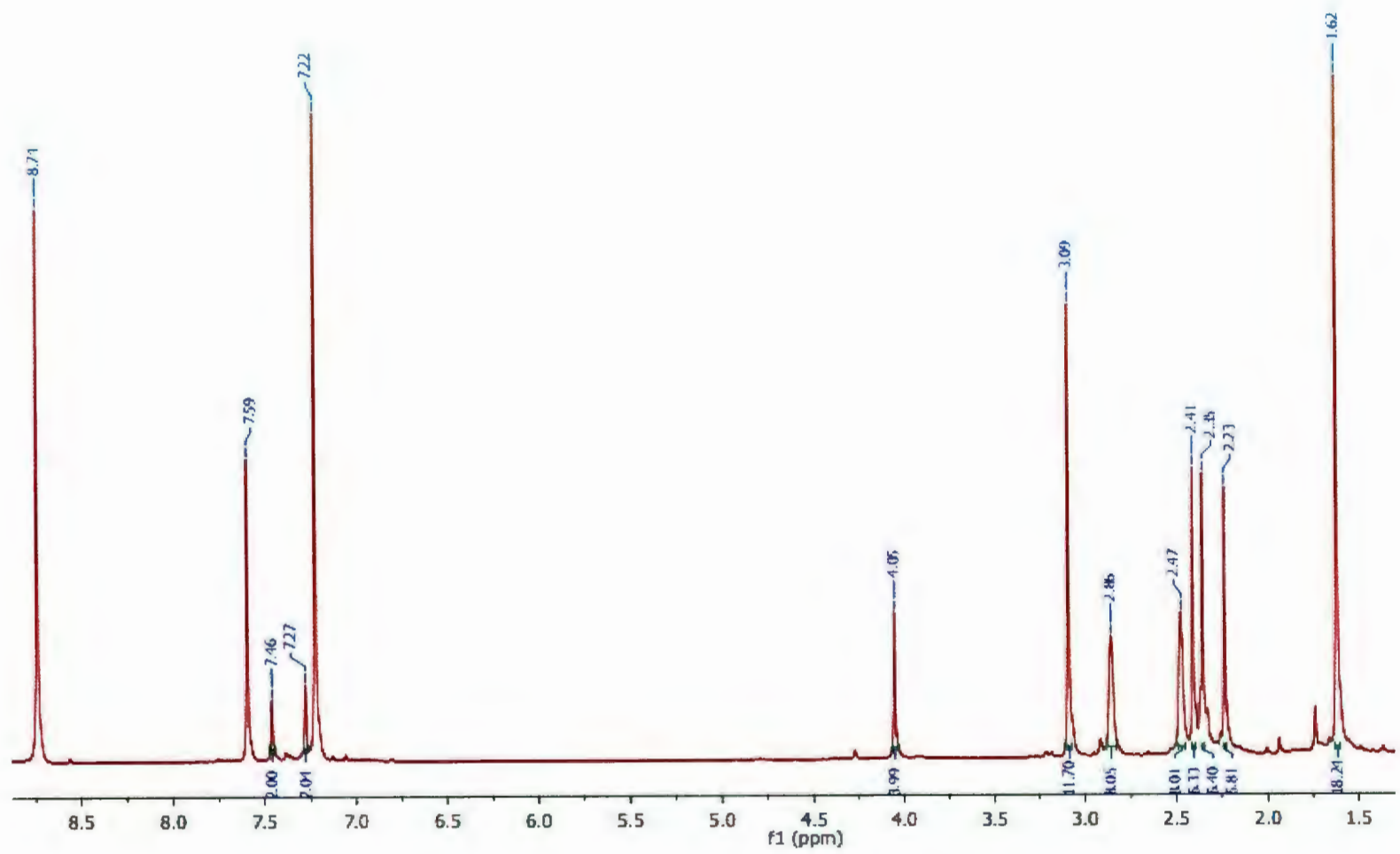


Figure A1.58. ^1H NMR spectrum of **6.2** ($\text{C}_5\text{D}_5\text{N}$, 500 MHz, 313 K)

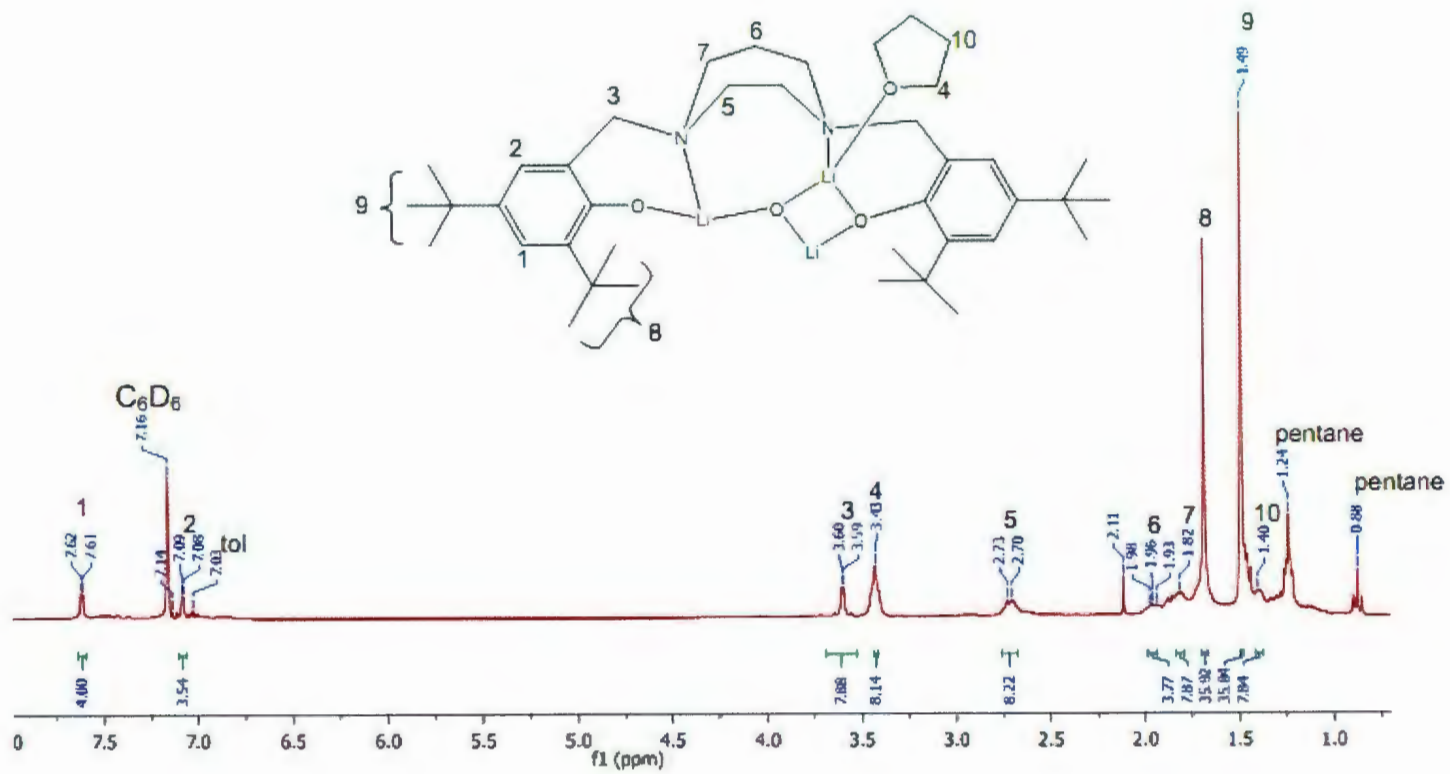


Figure A1.59. ¹H NMR spectrum of 6.4 (C₆D₆, 500 MHz, 298 K)

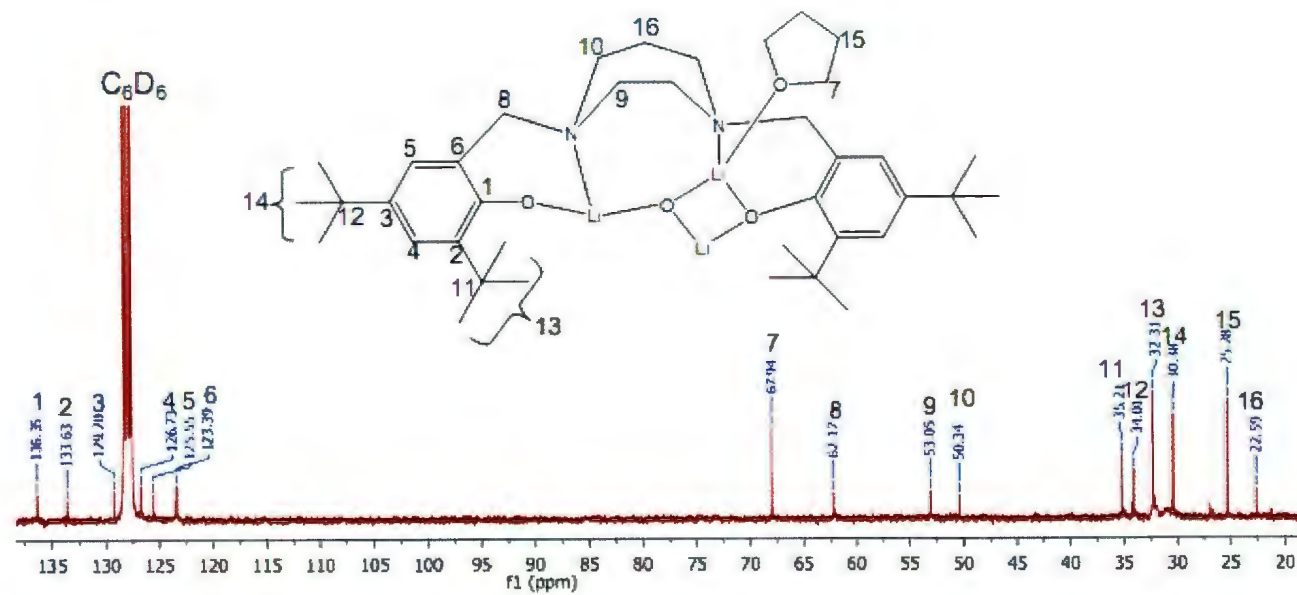


Figure A1.60. ^{13}C NMR spectrum of **6.4** (C_6D_6 , 125 MHz, 298 K)

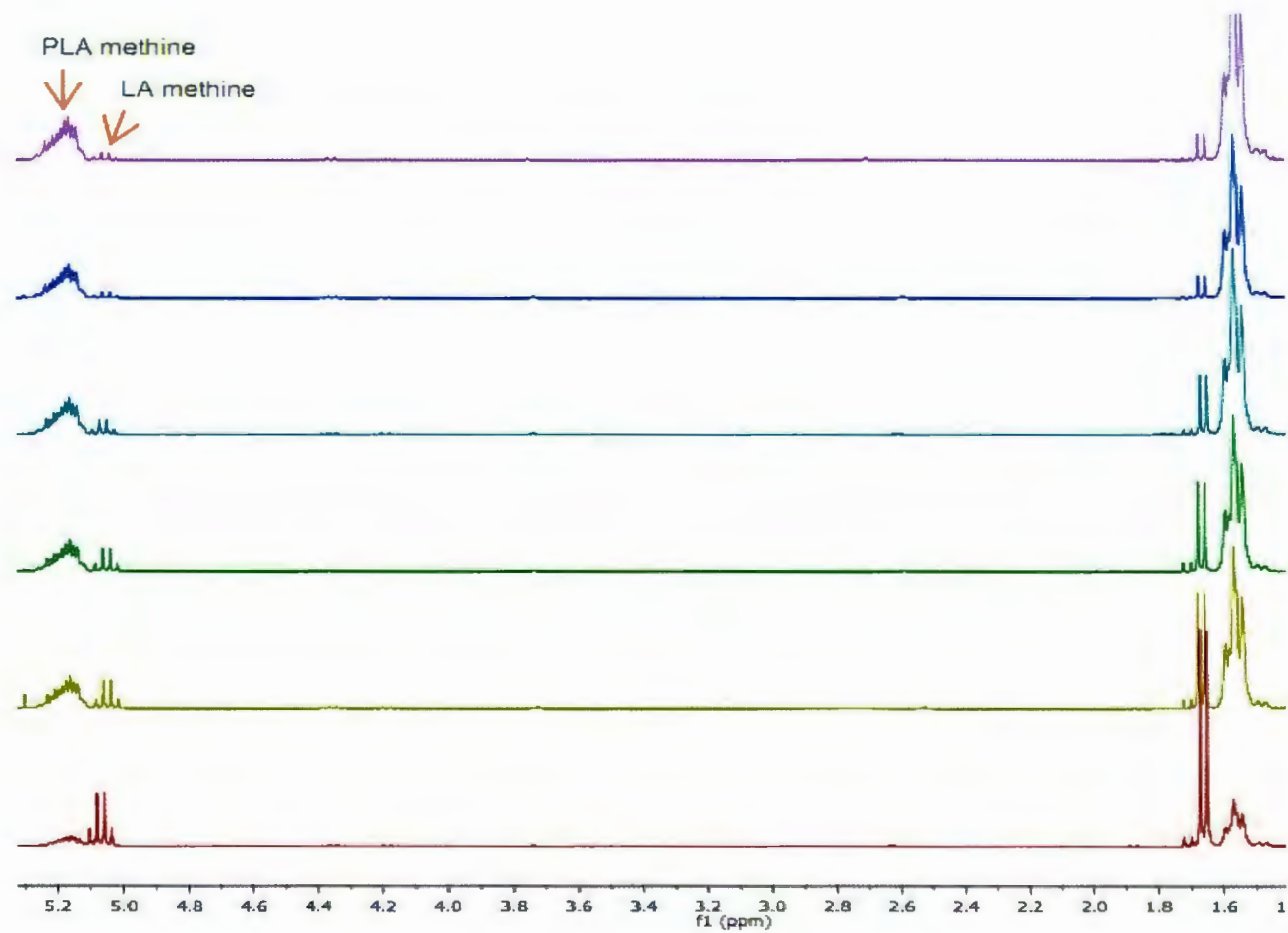


Figure A1.61. Typical ^1H NMR spectra showing the conversion of LA to PLA with time mediated by 5.6 at 130°C (Bulk polymerization)

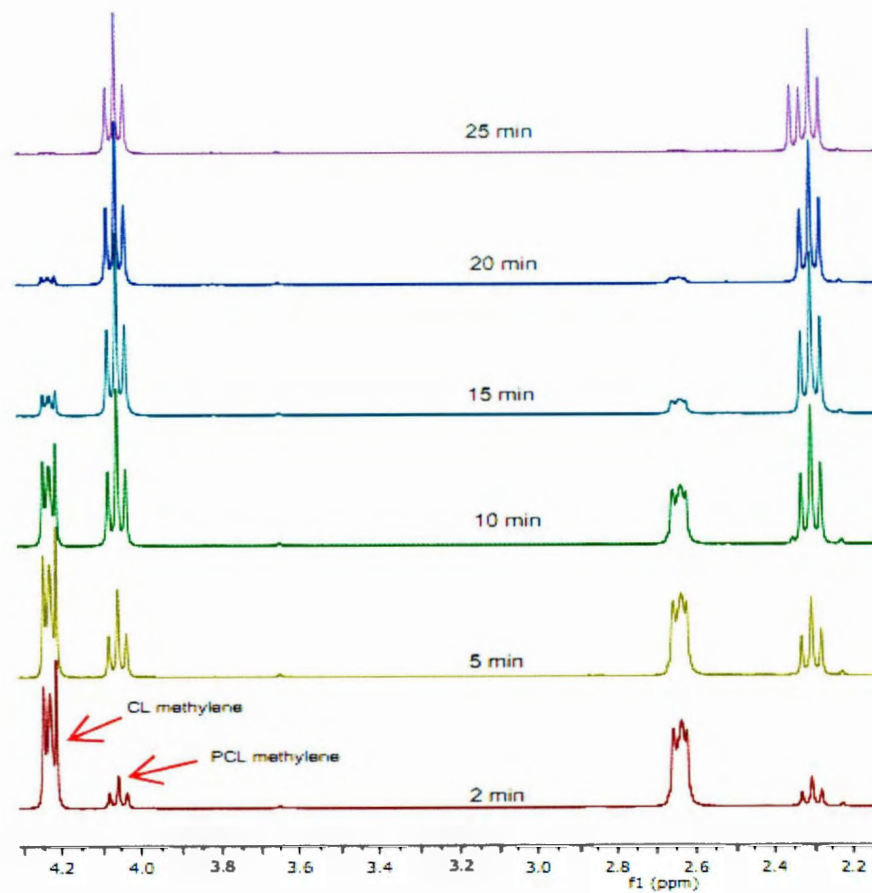


Figure A1.62. Typical ^1H NMR spectra showing the conversion of CL to PCL mediated by 5.1 at 60 °C

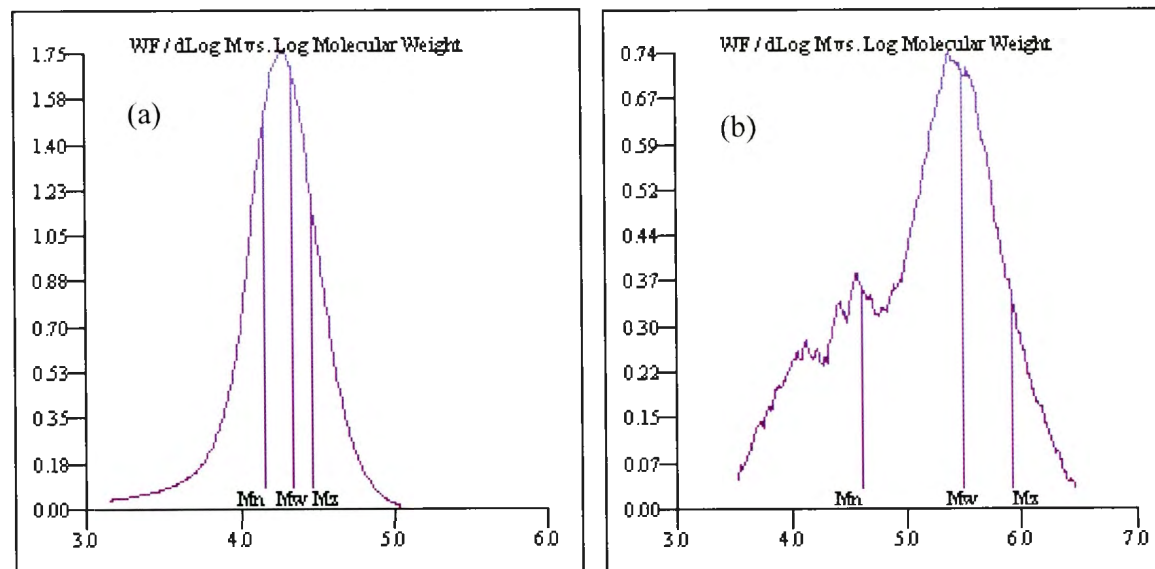


Figure A1.63. GPC traces of polymer samples prepared using (a) 4.1/BnOH (Table 4.2, entry 5) and (b) 4.4 (Table 4.2, entry 26)

Appendix B: MALDI-TOF Mass Spectrometry

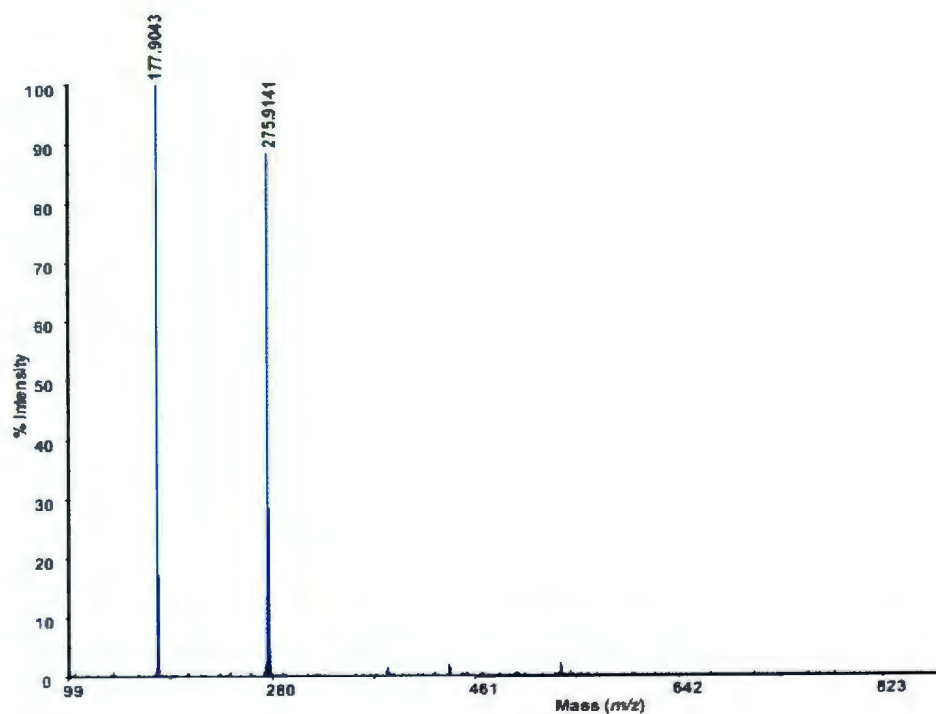


Figure B1.1. MALDI-TOF mass spectrum of [L1]H

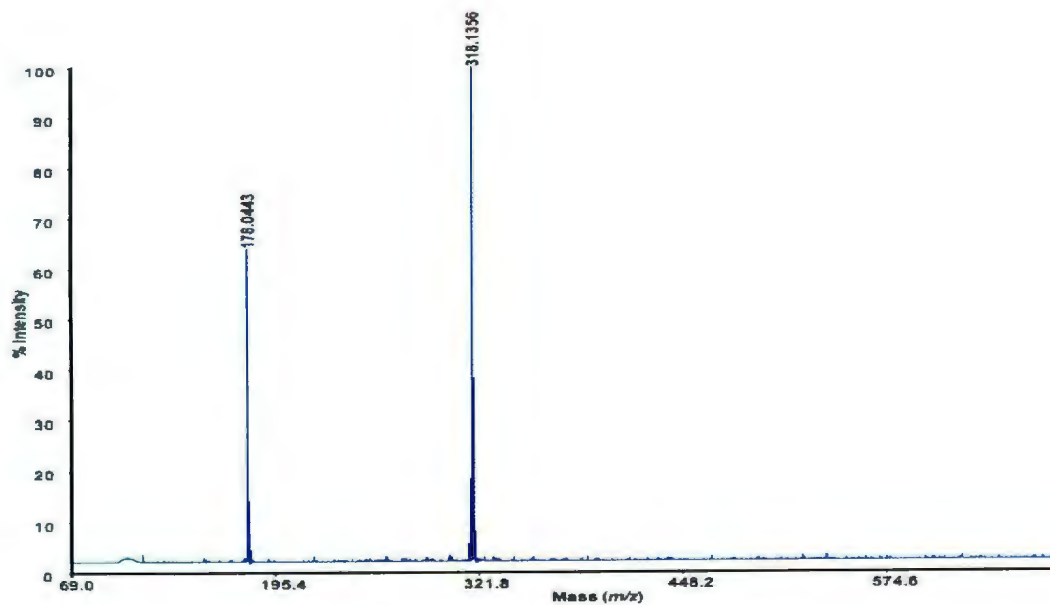


Figure B1.2. MALDI-TOF mass spectrum of [L2]H

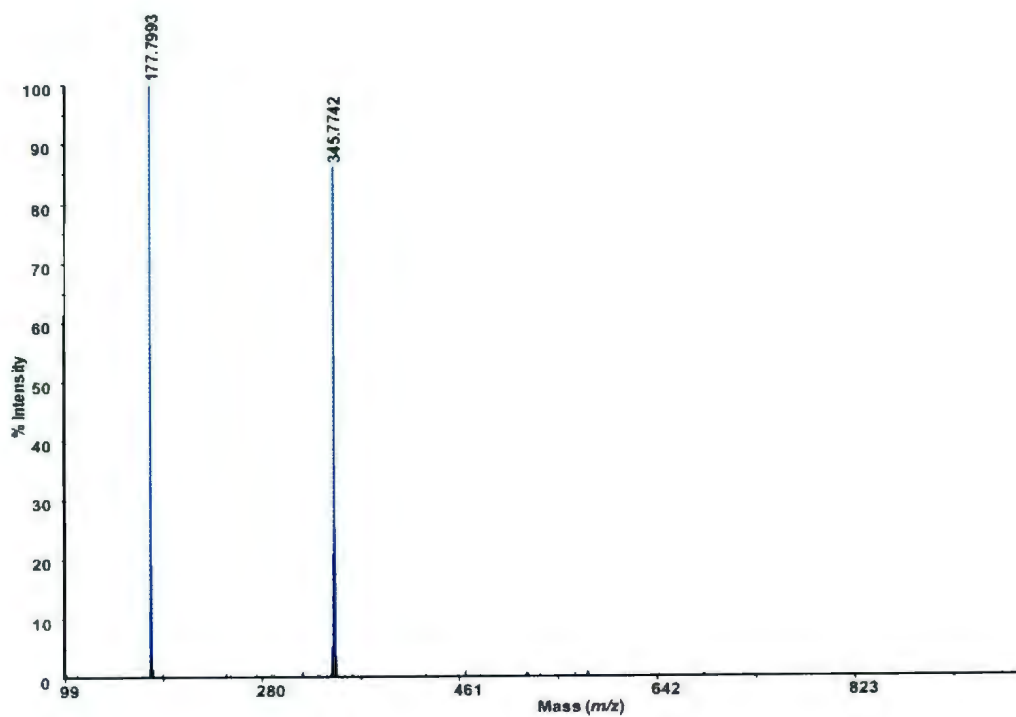


Figure B1.3. MALDI-TOF mass spectrum of [L3]H

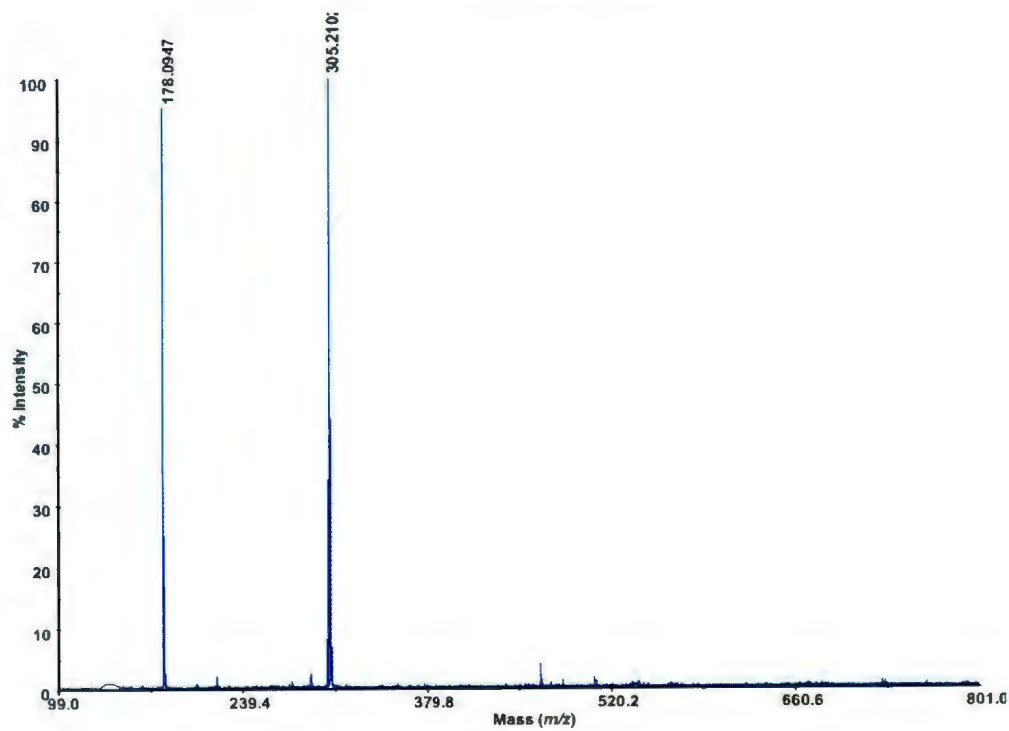


Figure B1.4. MALDI-TOF mass spectrum of [L5]H

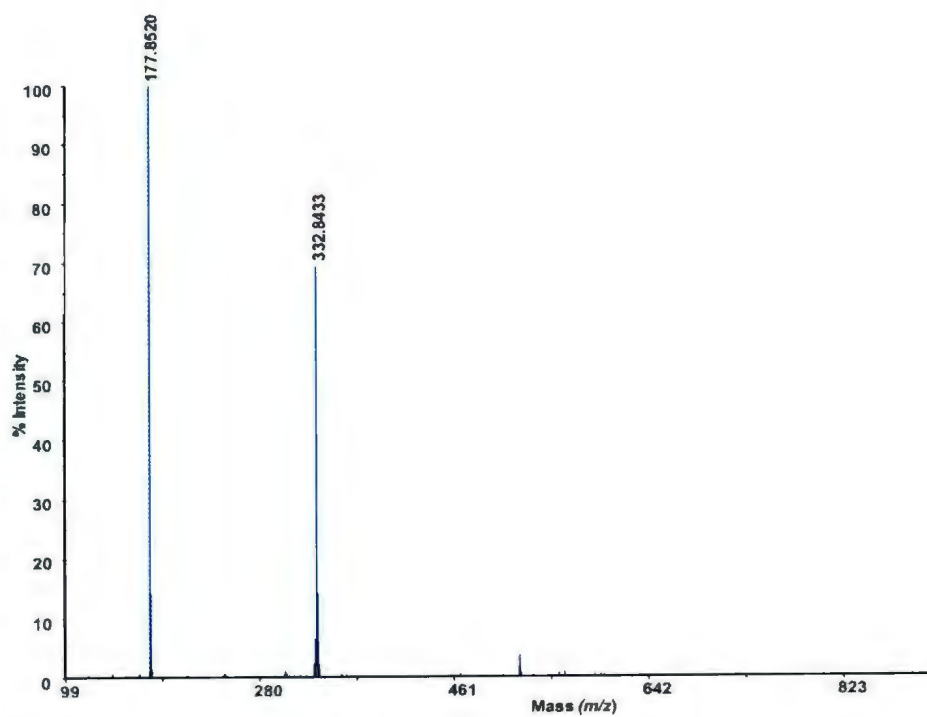


Figure B1.5. MALDI-TOF mass spectrum of [L6]H

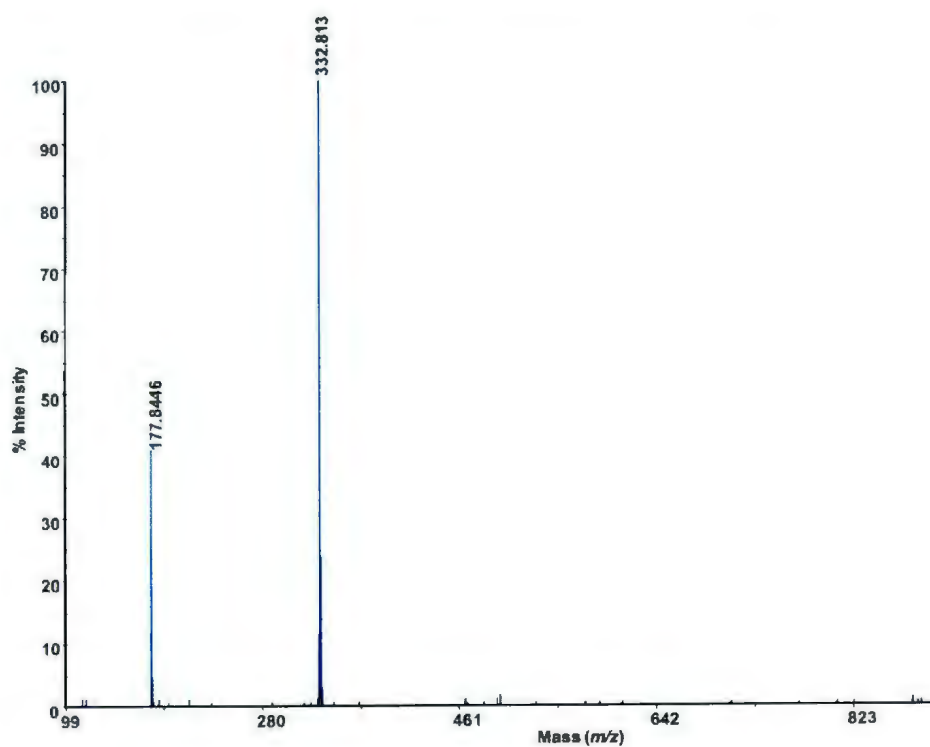


Figure B1.6. MALDI-TOF mass spectrum of [L8]H

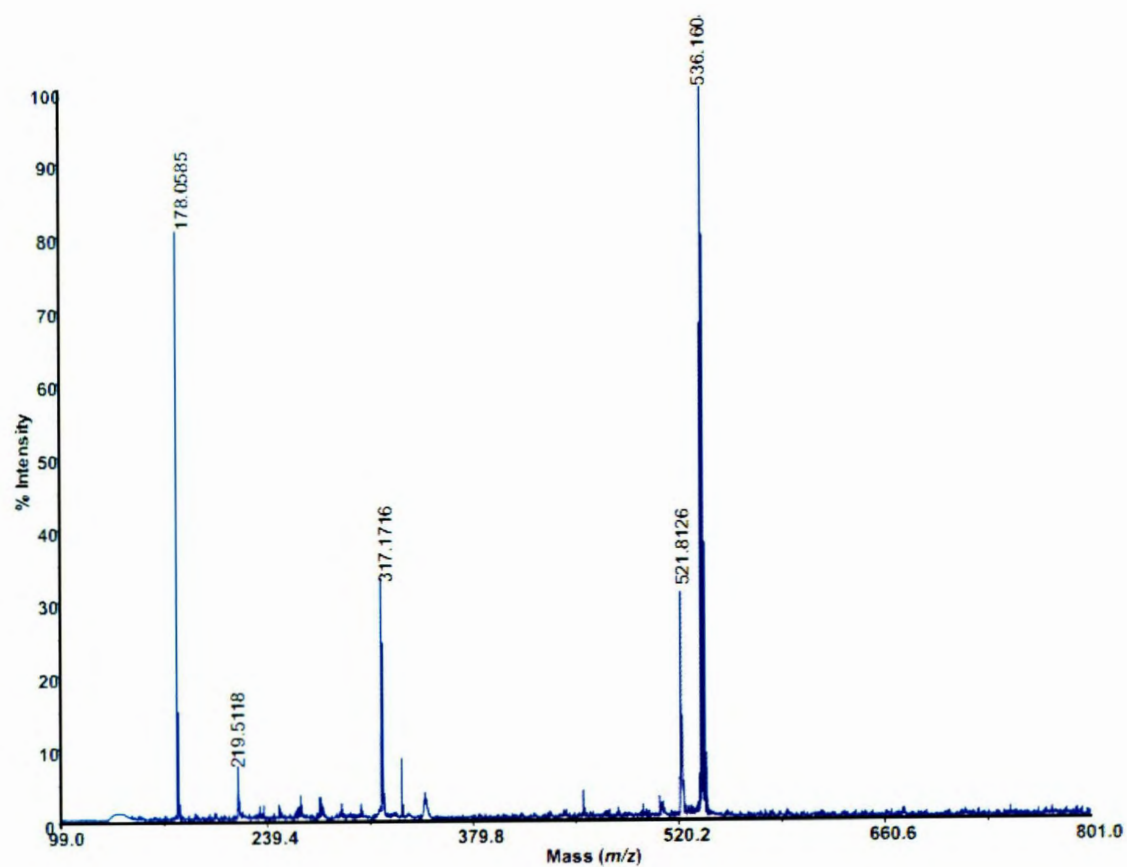


Figure B1.7. MALDI-TOF mass spectrum of [L11]H₂

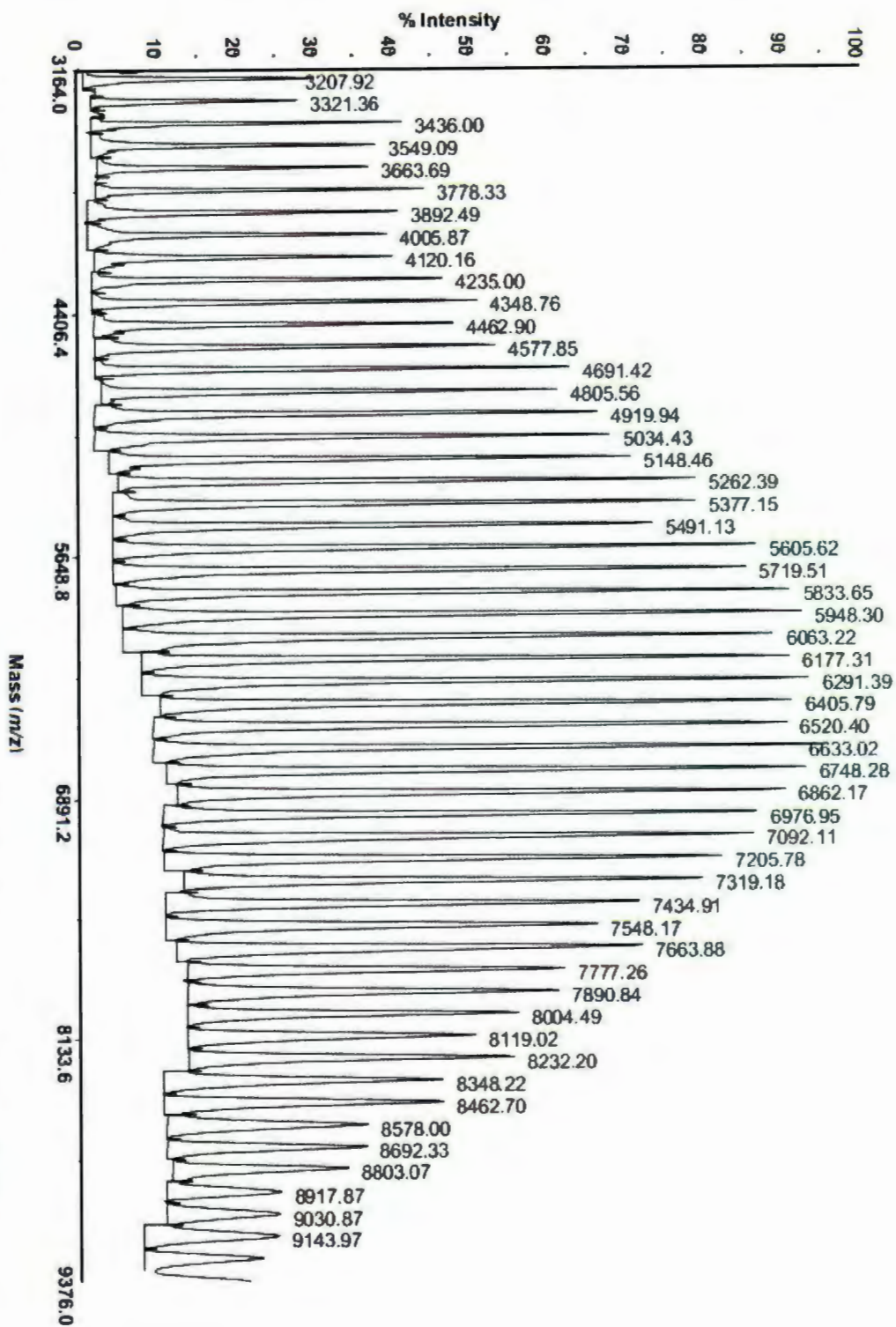


Figure B1.8. MALDI-TOF mass spectrum of PCL prepared using 4.1/BnOH at 80 °C [CL]/[4.1/BnOH] = 100 (Table 4.2, entry 4)

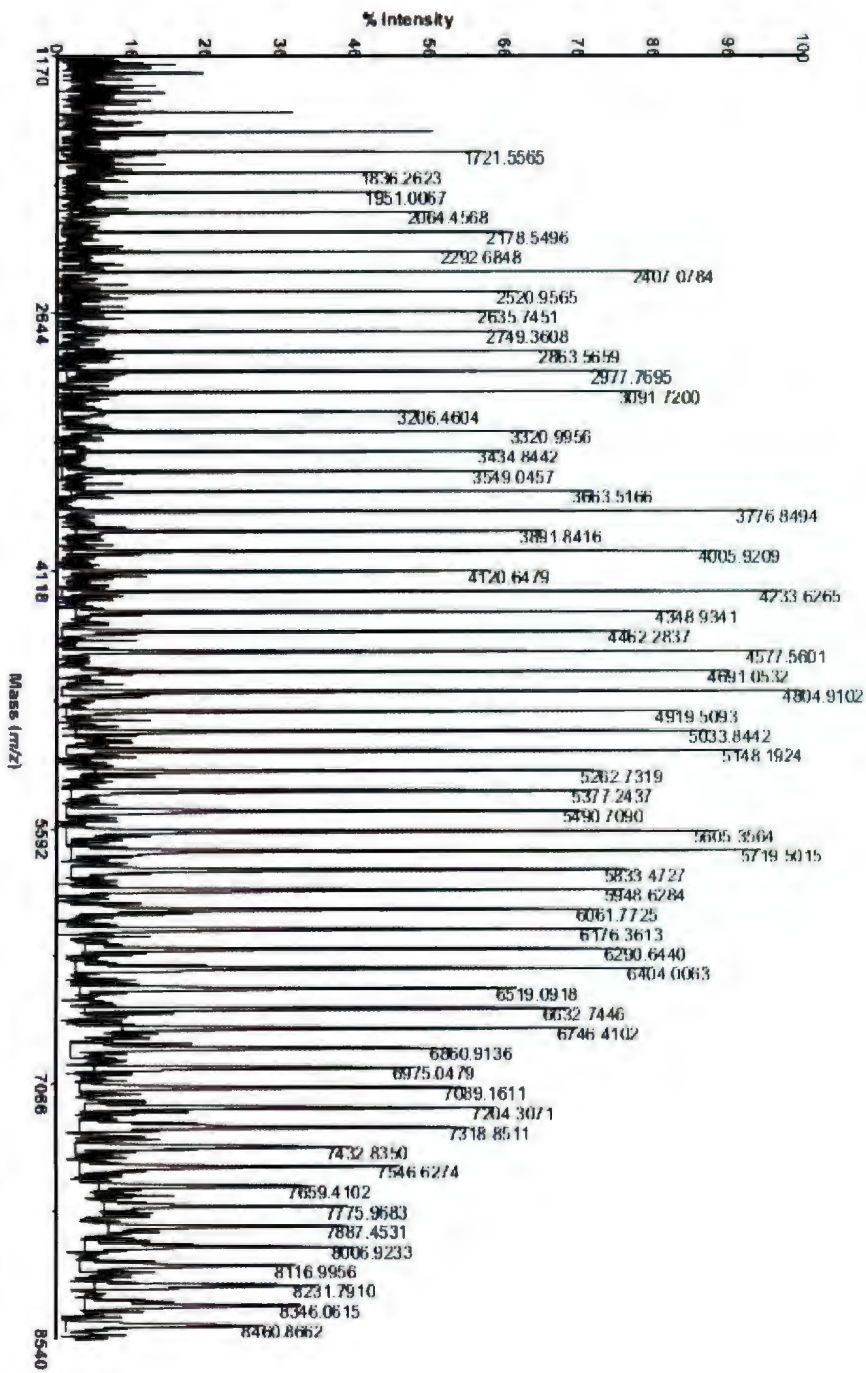


Figure B1.9. MALDI-TOF mass spectrum of PCL prepared using 4.3/BnOH at 40 °C [CL]/[4.3/BnOH] = 100 (Table 4.2, entry 18)

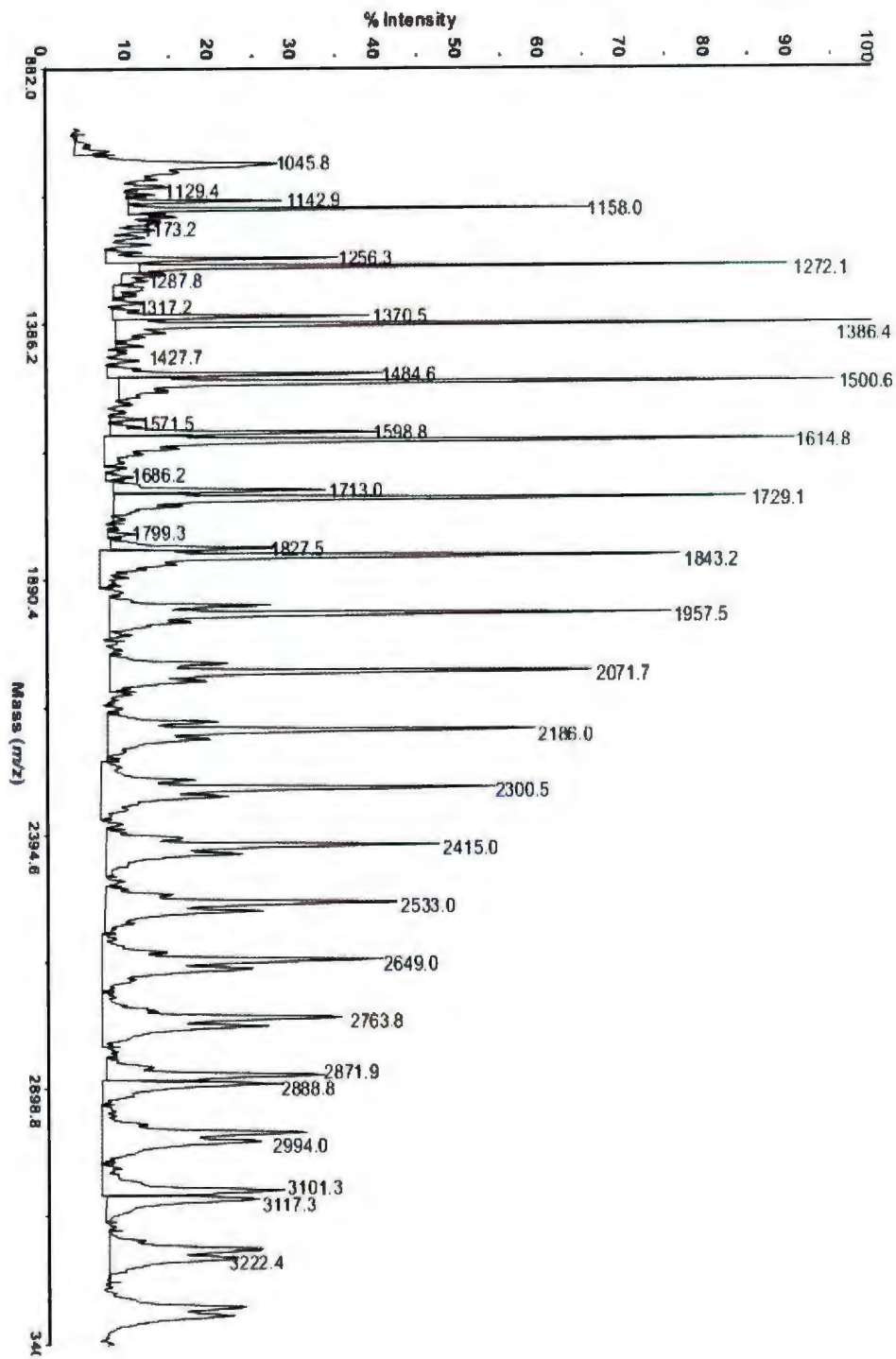


Figure B1.10. MALDI-TOF mass spectrum of PCL initiated by 5.1 in THF at 60 °C, [CPL]/[5.1] = 50 (Table 5.1, entry 2)

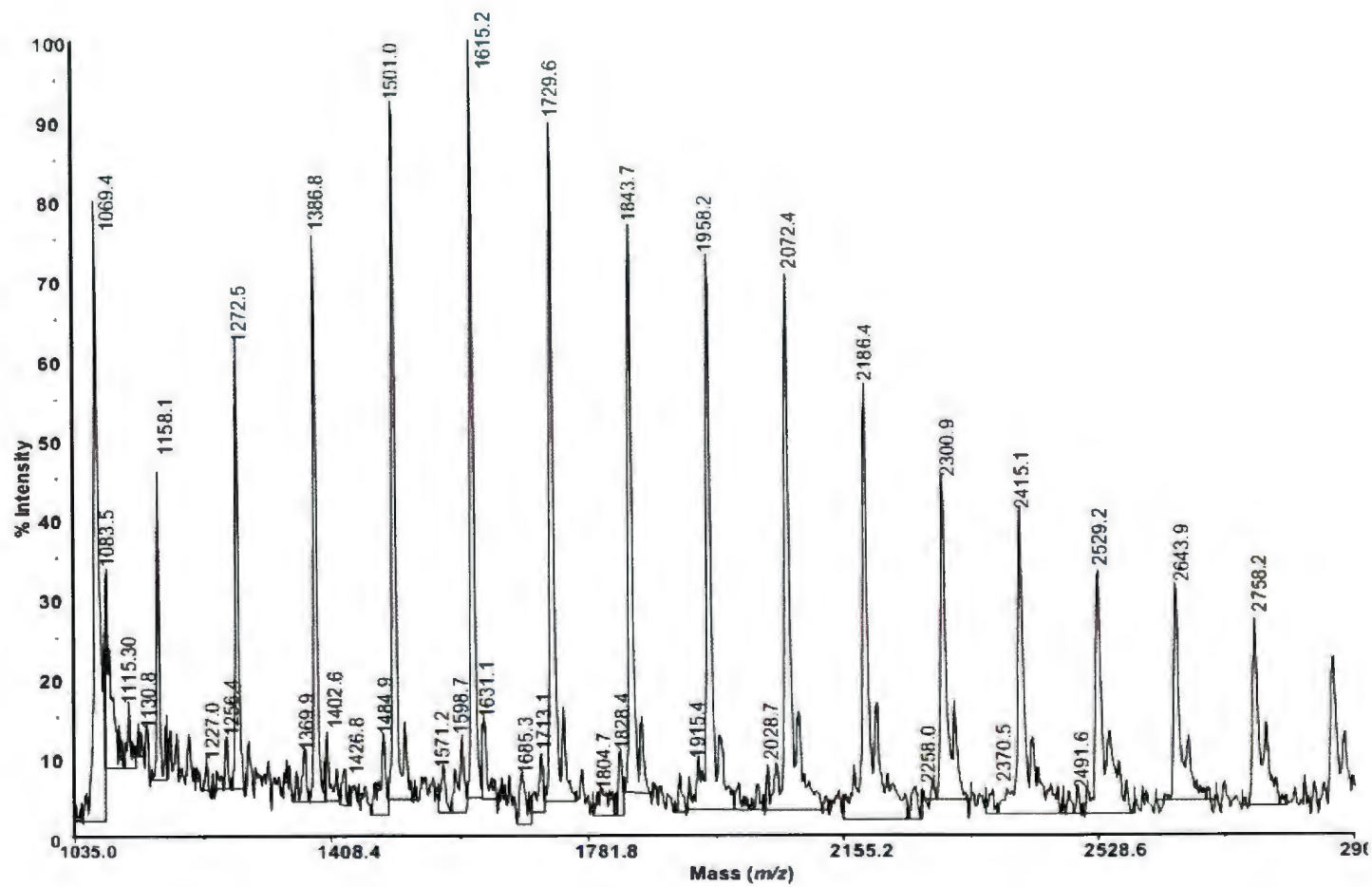


Figure B1.11. MALDI-TOF mass spectrum of PCL initiated by **5.1** in toluene at 25 °C [CL]/[**5.1**] = 50 (Table 5.1, entry 5)

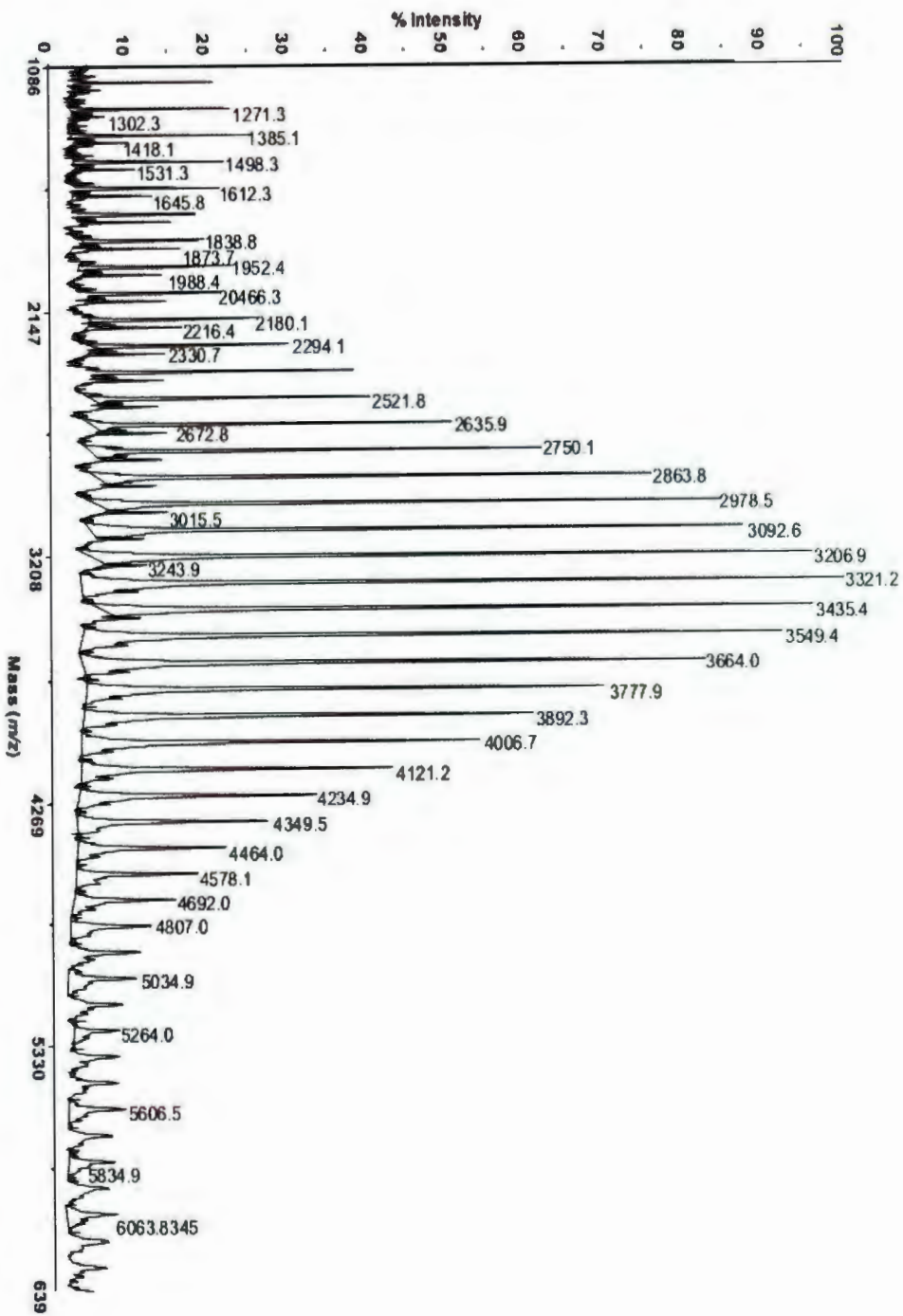


Figure B1.12. MALDI-TOF mass spectrum of PCL initiated by 5.1/BnOH in toluene at 60 °C, [CL]/[5.1/BnOH] = 200 (Table 5.1, entry 12)

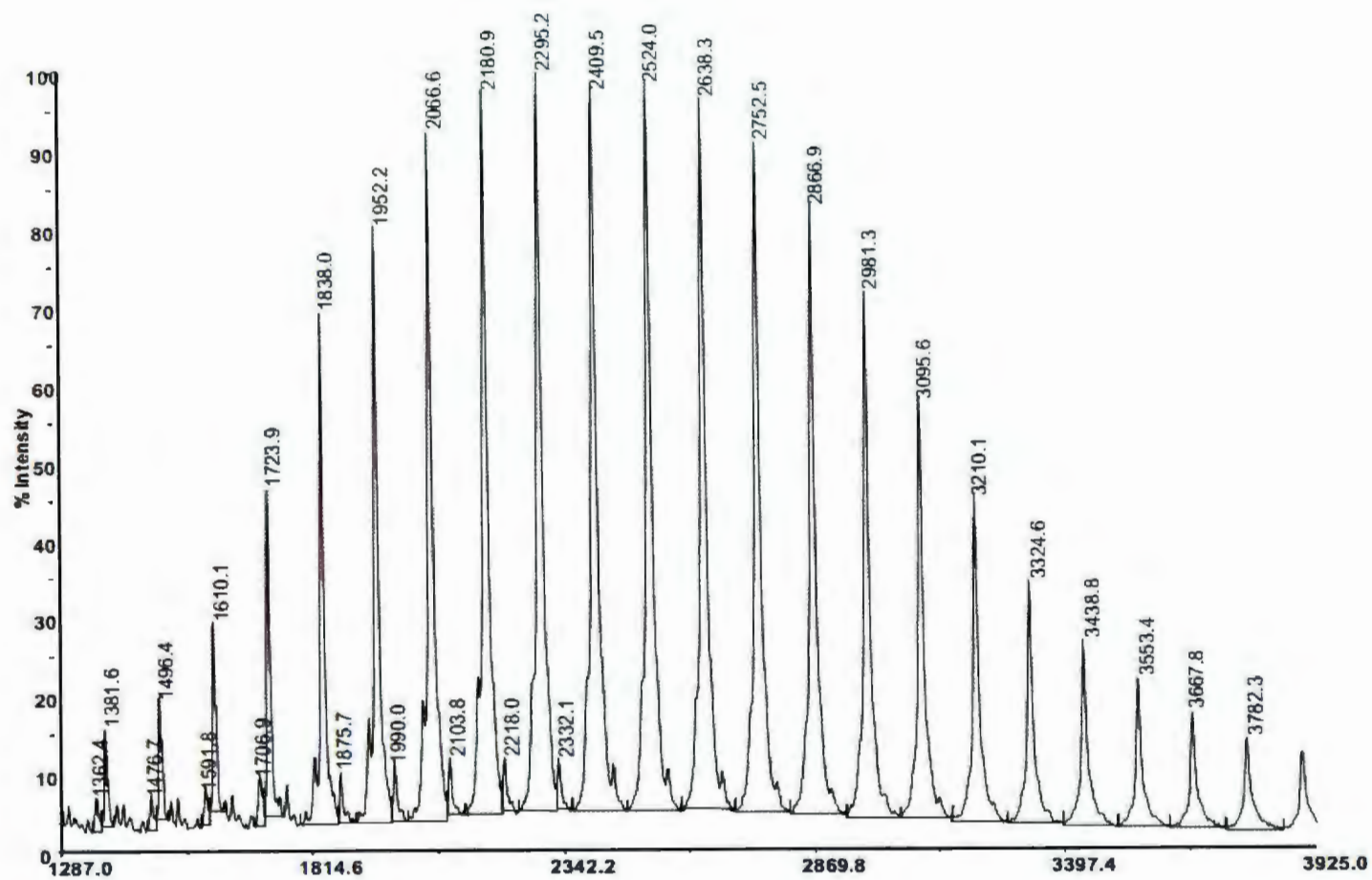


Figure B1.13. MALDI-TOF mass spectrum OF PCL initiated by **5.2**/BnOH in toluene at 25 °C, [CL]/[**5.2**/BnOH] = 100 (Table 5.1, entry 15)

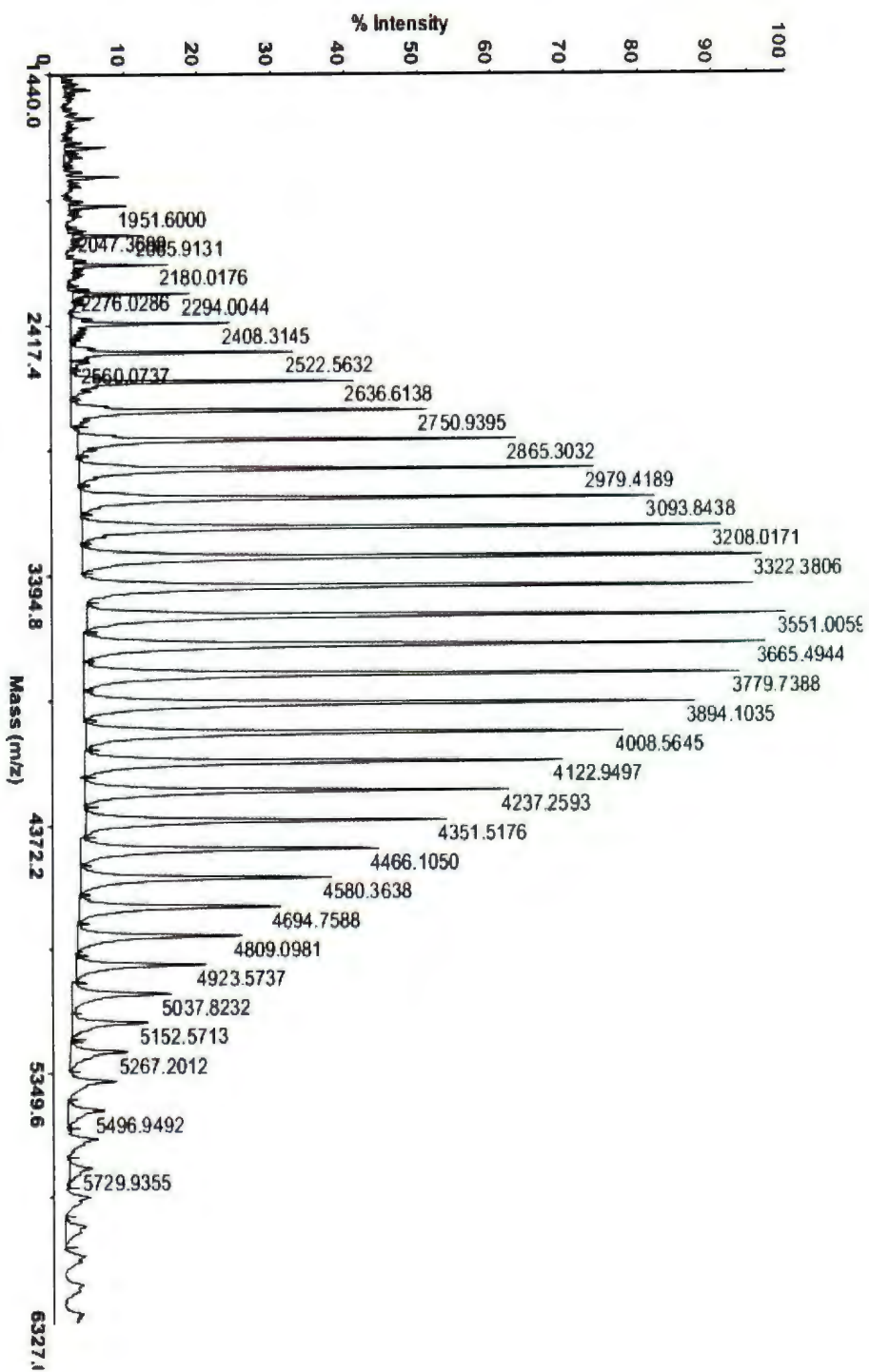


Figure B1.14. MALDI-TOF mass spectrum of PCL prepared using 5.3/BnOH in toluene at 25 °C, [CL]/[5.3/BnOH] = 200 (Table 5.1, entry 24)

Appendix C: Kinetic Plots

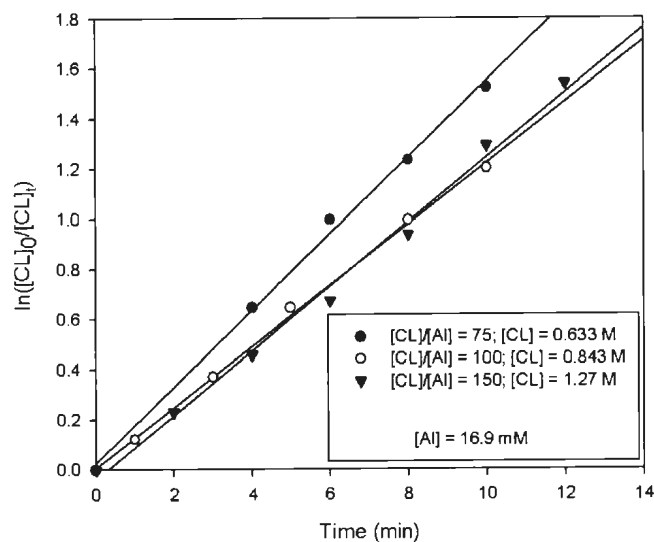


Figure C1.1. Semilogarithmic plots of $\ln[CL]_0/[CL]_t$ vs time for ROP of CL at different monomer molar ratios initiated with 4.1/BnOH; $[CL]_0/[4.1/BnOH]_0 = 75$ (●), 100 (○), 150 (▼), ($[4.1/BnOH]_0 = 16.9$ mM, 80 °C).

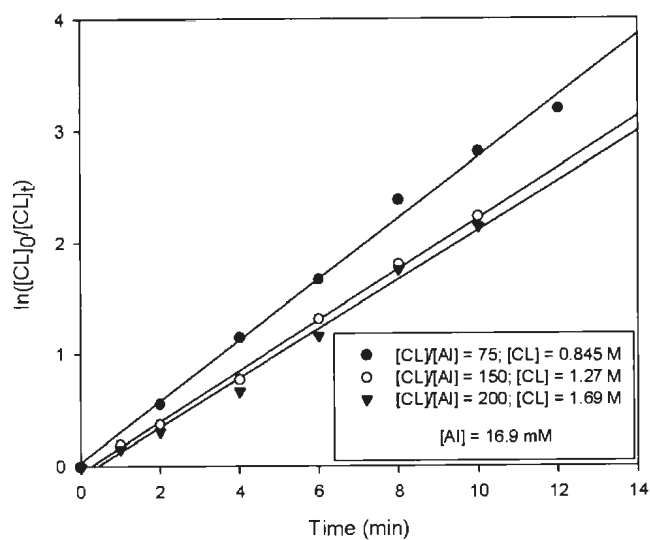


Figure C1.2. Semilogarithmic plots of $\ln[CL]_0/[CL]_t$ vs time for ROP of CL at different monomer molar ratios initiated with 4.3/BnOH; $[CL]_0/[4.3/BnOH]_0 = 75$ (●), 150 (○), 200 (▼), ($[4.3/BnOH]_0 = 16.9$ mM, 80 °C).

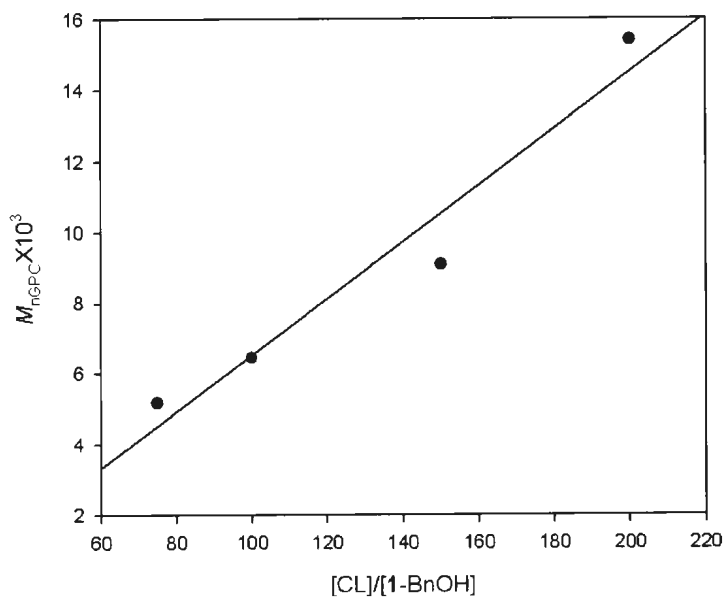


Figure C1.3. Plot of M_n^{GPC} of polymer vs initial mole ratio $[CL]_0/[4.1/BnOH]_0$ for ROP of CL initiated by 4.1/BnOH at 80 °C.

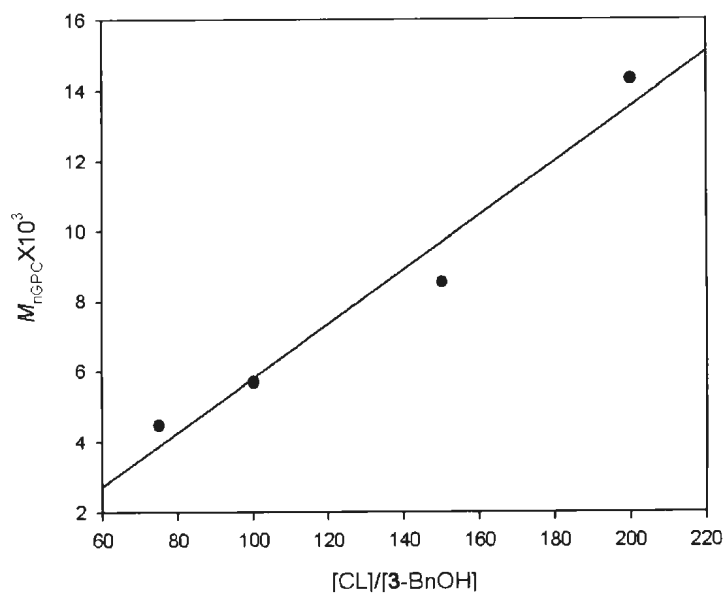


Figure C1.4. Plot of M_n^{GPC} of polymer vs initial mole ratio $[CL]_0/[4.3/BnOH]_0$ for ROP of CL initiated by 4.3/BnOH at 80 °C.

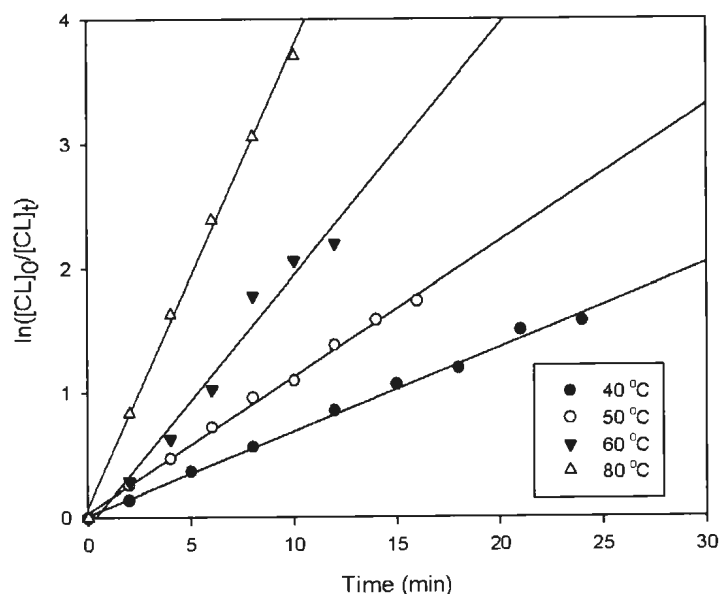


Figure C1.5. Semilogarithmic plots of $\ln[\text{CL}]_0/[\text{CL}]_t$ vs time for ROP of CL initiated with 4.1/BnOH at different temperature; $[\text{CL}]_0/[\text{4.1/BnOH}]_0 = 100$ ($[\text{4.1/BnOH}]_0 = 16.9$ mM, $[\text{CL}]_0 = 0.843$ M)

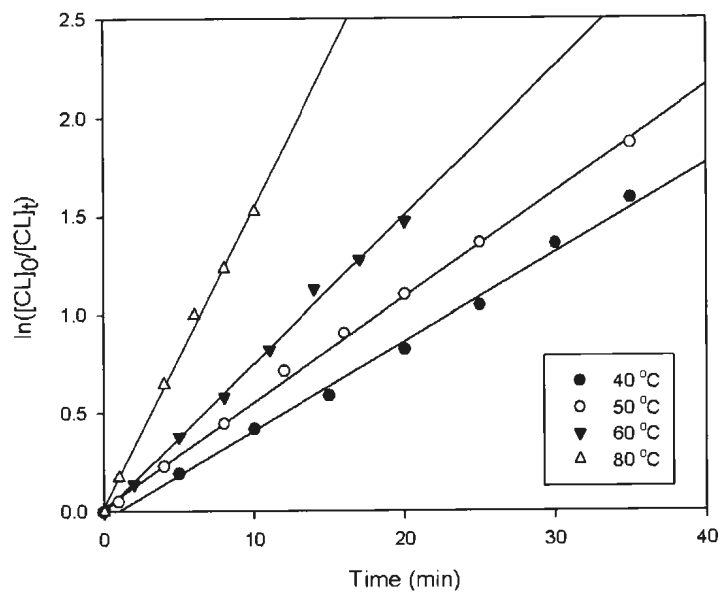


Figure C1.6 Semilogarithmic plots of $\ln[\text{CL}]_0/[\text{CL}]_t$ vs time for ROP of CL initiated by 4.2/BnOH at different temperature; $[\text{CL}]_0/[\text{4.2/BnOH}]_0 = 100$, ($[\text{4.2/BnOH}]_0 = 16.9$ mM, $[\text{CL}]_0 = 0.849$ M).

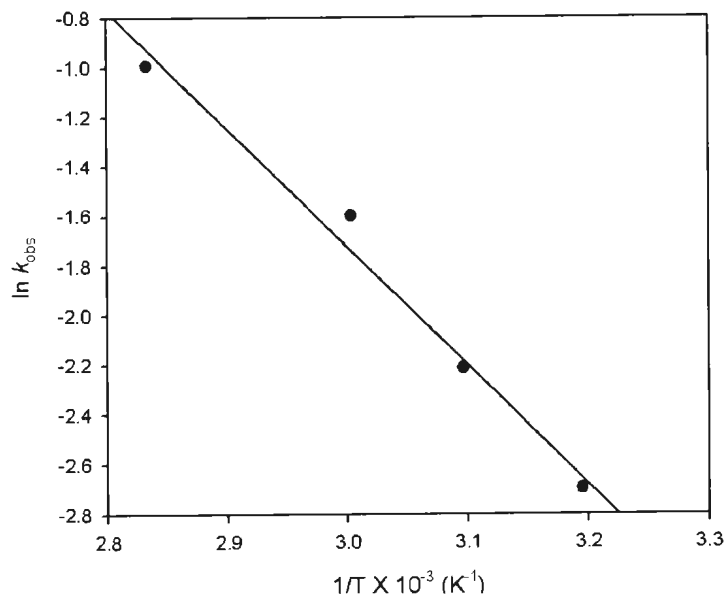


Figure C1.7. Arrhenius plot of $\ln(k_{\text{obs}})$ vs $1/T$ for ROP of CL initiated by 4.1/BnOH; $[\mathbf{4.1/BnOH}]_0 = 16.9 \text{ mM}$; $[\text{CL}]/[\mathbf{4.1/BnOH}] = 100$.

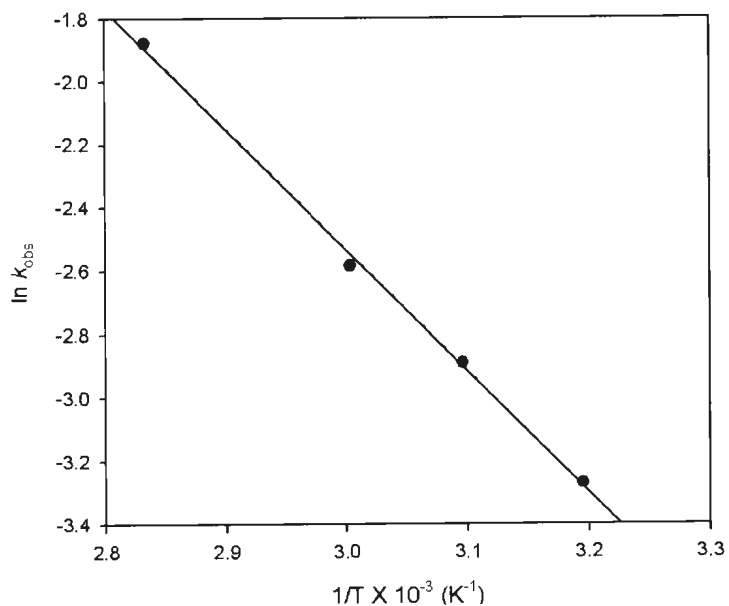


Figure C1.8. Arrhenius plot of $\ln(k_{\text{obs}})$ vs $1/T$ for ROP of CL initiated by 4.2/BnOH; $[4.2/\text{BnOH}]_0 = 16.9 \text{ mM}$; $[\text{CL}]/[4.2/\text{BnOH}] = 100$

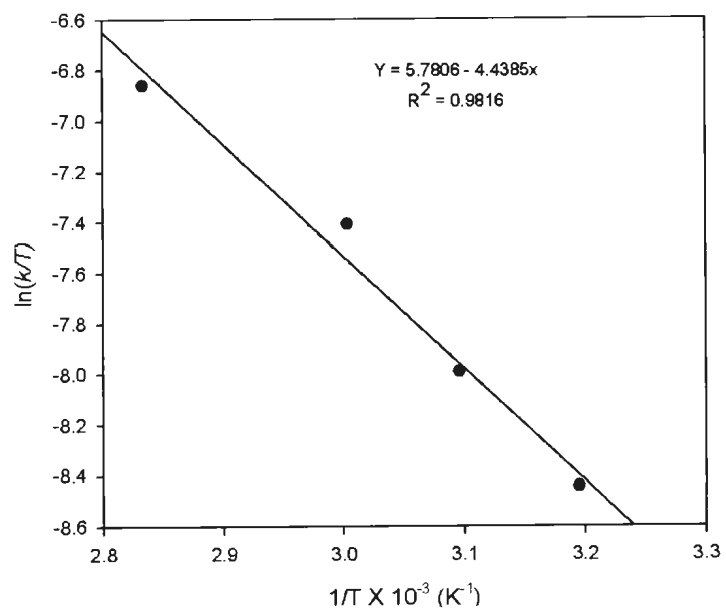


Figure C1.9. Eyring plot of $\ln(k_{\text{obs}}/T)$ vs $1/T$ for ROP of CL initiated by 4.1/BnOH

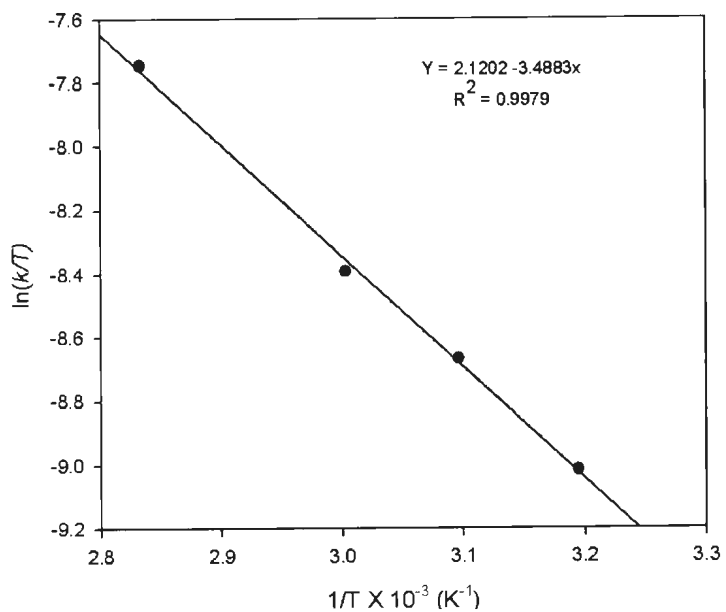


Figure C1.10. Eyring plot of $\ln(k_{\text{obs}}/T)$ vs $1/T$ for ROP of CL initiated by 4.2/BnOH

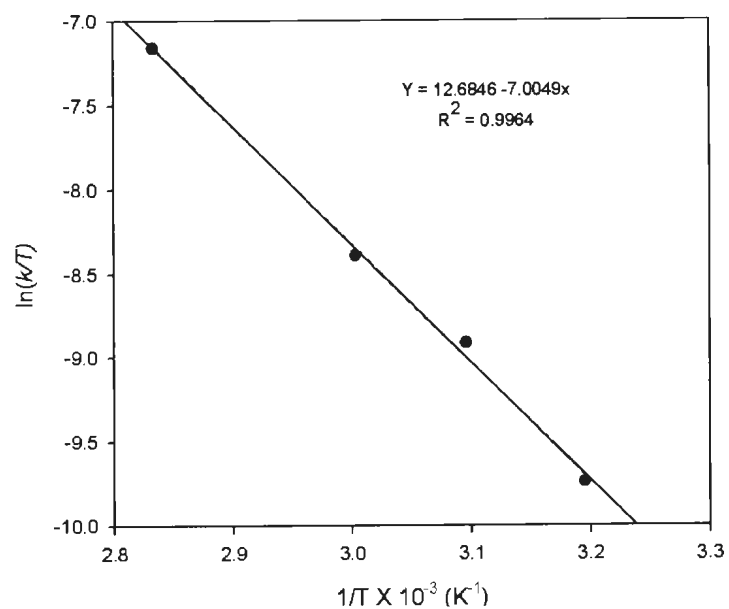


Figure C1.11. Eyring plot for $\ln(k_{\text{obs}}/T)$ vs $1/T$ for ROP of CL initiated by 4.3/BnOH

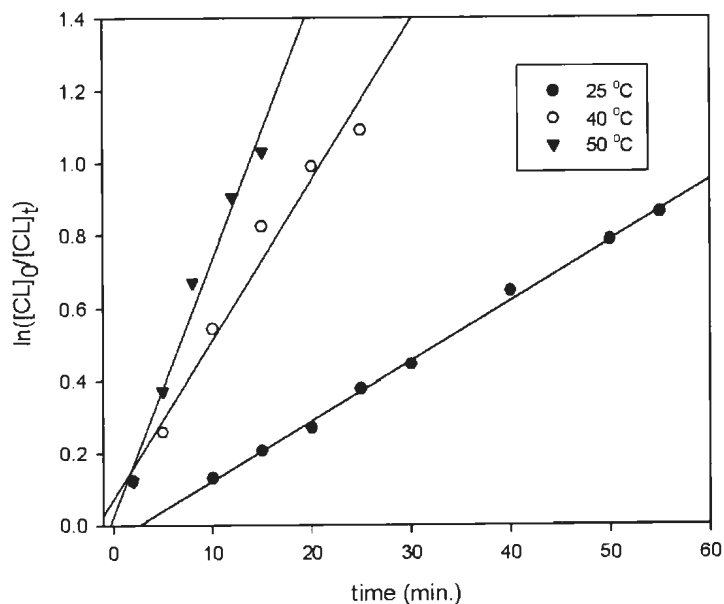


Figure C1.12. Semilogarithmic plot of $\ln[CL]_0/[CL]_t$ vs time for ROP OF CL initiated by 5.3 at different temperature; $[CL]_0/[5.3]_0 = 200$, ($[5.3]_0 = 17.7$ mM, $[CL]_0 = 1.52$ M).

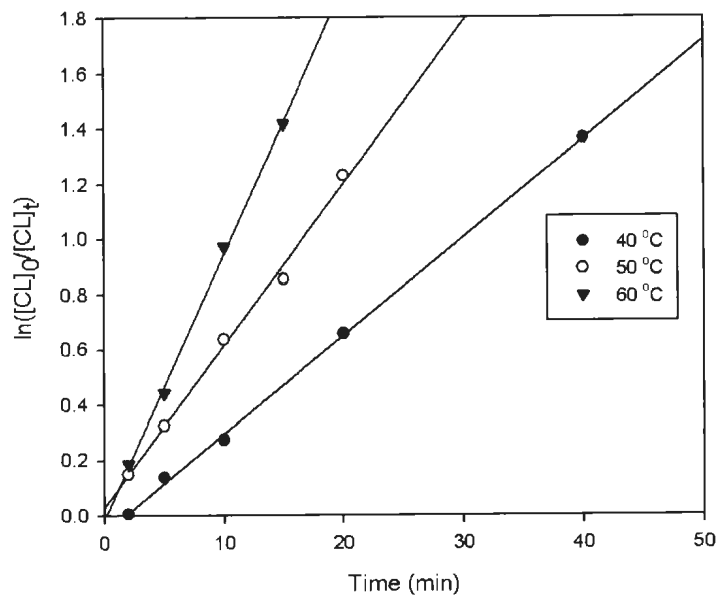


Figure C1.13. Semilogarithmic plot of $\ln[CL]_0/[CL]_t$ vs time for ROP of CL initiated by 5.3/BnOH at different temperature; $[CL]_0/[5.3/BnOH]_0 = 200$, ($[5.3/BnOH]_0 = 17.7$ Mm, $[CL]_0 = 1.52$ M)

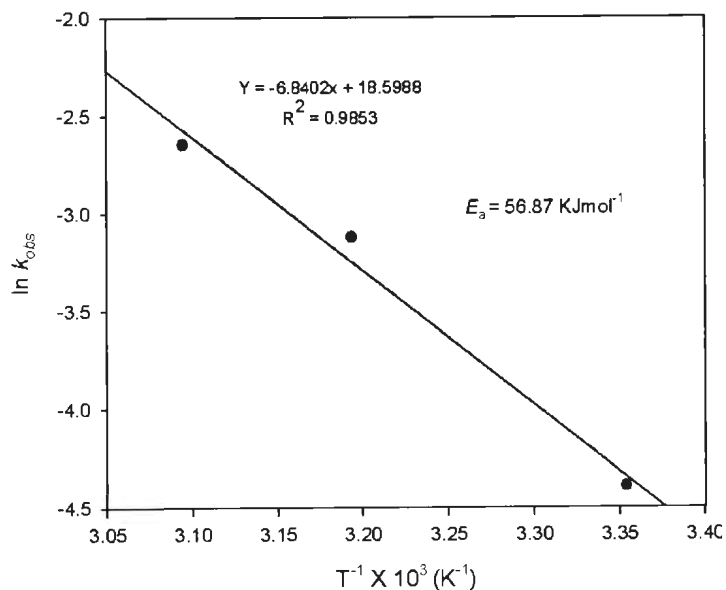


Figure C1.14. Arrhenius plot of $\ln(k_{\text{obs}})$ vs time for ROP of CL initiated by **5.3**; $[\mathbf{5.3}]_0 = 17.7$; $[\text{CL}]/[\mathbf{5.3}] = 200$

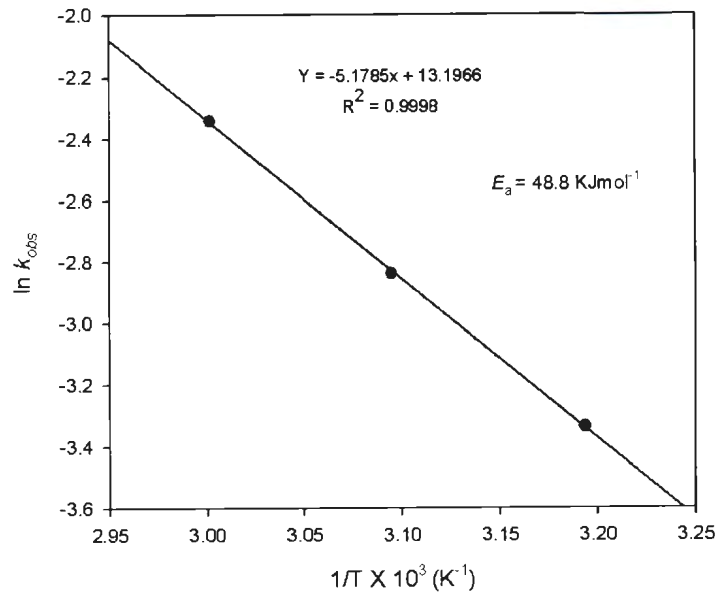


Figure C1.15. Arrhenius plot of $\ln(k_{\text{obs}})$ vs time for ROP of CL initiated by **5.3/BnOH**; $[\mathbf{5.3/BnOH}]_0 = 17.7$; $[\text{CL}]/[\mathbf{5.3/BnOH}] = 200$

Appendix D: Summary of R and R^2 Values

Table D1. 1. Activation parameters obtained from polymerization initiated by Al methyl complexes

	$\Delta H^\ddagger/\text{kJ mol}^{-1}$	$\Delta S^\ddagger/\text{J mol}^{-1} \text{K}^{-1}$	$\Delta G^\ddagger/\text{J mol}^{-1}{}^a$
4.1/BnOH	36.9(\pm 0.7)	-150(\pm 1)	90
4.2/BnOH	29.0(\pm 0.2)	-180(\pm 1)	93
4.3/BnOH	58.2(\pm 0.2)	-92(\pm 1)	90

^a T = 80 °C

Table D1.2. Summary of R and R^2 values of polymerization initiated by 4.1/BnOH

4.1/BnOH					
[CL]/[Al]	ln[CL] ₀ /[CL] _t vs time		Kinetics	ln[CL] ₀ /[CL] _t vs time	
	R	R^2		R	R^2
75 equiv	0.9969	0.9938	40 °C	0.9976	0.9953
100 equiv	0.9987	0.9973	50 °C	0.9984	0.9967
150 equiv	0.9992	0.9985	60 °C	0.9866	0.9733
			80 °C	0.9987	0.9974
<u>M_n vs ratio</u>	0.9733	0.9473	<u>E_a</u>	0.9921	0.9843

Table D1.3. Summary of R and R^2 values of polymerization initiated by 4.2/BnOH

4.2/BnOH					
[CL]/[Al]	ln[CL] ₀ /[CL] _t vs time		Kinetics	ln[CL] ₀ /[CL] _t vs time	
	R	R^2		R	R^2
75 equiv	0.9979	0.9959	40 °C	0.9972	0.9943
100 equiv	0.9987	0.9974	50 °C	0.9970	0.9941
150 equiv	0.9977	0.9953	60 °C	0.9983	0.9966
200 equiv	0.9990	0.9980	80 °C	0.9987	0.9973
<u>M_n vs ratio</u>	0.9974	0.9948	<u>E_a</u>	0.9991	0.9982

Table D1.4. Summary of R and R^2 values of polymerization initiated by 4.3/BnOH

4.3-BnOH					
[CL]/[Al]	ln[CL] ₀ /[CL] _t vs time		Kinetics	ln[CL] ₀ /[CL] _t vs time	
	R	R²		R	R²
75 equiv	0.9934	0.9868	40 °C	0.9922	0.9845
100 equiv	0.9973	0.9946	50 °C	0.9959	0.9918
150 equiv	0.9985	0.9969	60 °C	0.9972	0.9945
200 equiv	0.9952	0.9905	80 °C	0.9973	0.9935
<u>M_n vs ratio</u>			<u>E_a</u>		
	0.9802	0.9608		0.9984	0.9968

